Technical Report SL-99-9
September 1999

**US Army Corps of Engineers**
Engineer Research and Development Center

# Durability of Fiber-Reinforced Concrete Under Flexural Stress in a Severe Marine Environment

*by Edward F. O'Neil, ERDC*
*Jack T. Devlin, University of New Brunswick*





Prepared for Headquarters, U.S. Army Corps of Engineers

The contents of this report are not to be used for advertising, publication, or promotional purposes. Citation of trade names does not constitute an official endorsement or approval of the use of such commercial products.

The findings of this report are not to be construed as an official Department of the Army position, unless so designated by other authorized documents.

Technical Report SL-99-9
September 1999

# Durability of Fiber-Reinforced Concrete Under Flexural Stress in a Severe Marine Environment

by Edward F. O'Neil

U.S. Army Engineer Research and Development Center
Waterways Experiment Station
3909 Halls Ferry Road
Vicksburg, MS 39180-6199

Jack T. Devlin

Department of Civil Engineering
University of New Brunswick
P.O. Box 4400
Fredericton, N.B. Canada E3B 5A3

Final report

Approved for public release; distribution is unlimited

Prepared for U.S. Army Corps of Engineers
Washington, DC 20314-1000

Under Work Unit 31132

**Engineer Research and Development Center Cataloging-in-Publication Data**

O'Neil, Edward F.

Durability of fiber-reinforced concrete under flexural stress in a severe marine environment / by Edward F. O'Neil, Jack T. Devlin ; prepared for U.S. Army Corps of Engineers ; monitored by Structures Laboratory, U.S. Army Engineer Research and Development Center.

211 p. : ill. ; 28 cm. — (Technical report ; SL-99-9)

Includes bibliographic references.

1. Reinforced concrete, Fiber — Testing. 2. Reinforced concrete — Testing. I. Devlin, Jack T. II. United States. Army. Corps of Engineers. III. U.S. Army Engineer Research and Development Center. IV. Structures Laboratory (U.S.) V. Title. VI. Series: Technical report SL ; 99-9.

TA7 W34 no.SL-99-9

# Contents

# List of Figures

## List of Tables

# Preface

This report was prepared for Headquarters, U.S. Army Corps of Engineers (HQUSACE), by the U.S. Army Engineer Research and Development Center (ERDC), Structures Laboratory (SL), Waterways Experiment Station, Vicksburg, MS, under the Civil Works Research and Development Program, Work Unit 31132, "Field Exposure Durability Studies." The HQUSACE Technical Monitor was Dr. Tony C. Liu, CERD-C.

The study reported herein was conducted by the University of New Brunswick (UNB), Fredericton, N.B. Canada, under a BAA contract to SL. Contract Representative and Principal Investigator for the project was Mr. Edward F. O'Neil, Acting Chief, Engineering Mechanics Branch, SL. This report is a synthesis of the final report prepared by Mr. Jack T. Devlin under the direction of Professor Theodore W. Bremner, UNB, as the final product of that contract.

The investigation was conducted under the general supervision of Dr. Bryant Mather, Director, SL, and Mr. John Q. Ehrgott, Assistant Director, SL, and under the direct supervision of Dr. Paul F. Mlakar, Chief, Concrete and Materials Division, SL. Messrs. O'Neil and Devlin were the authors of this report.

At the time of publication of this report, Dr. Lewis E. Link was Acting Director of ERDC, and COL Robin R. Cababa, EN, was Commander.

# 1 Introduction

## Background

The concept of using distributed fibers to reinforce concrete has been considered since the beginning of this century (Porter 1910). The use of fiber reinforcement as an alternative or supplement to conventional mild steel reinforcement has been employed periodically since that time. It was only in the early 1970's that serious attempts were made to use them as components of concrete building materials.

In 1972, the U.S. Army Engineer Waterways Experiment Station (WES) received inquiries from field elements as to the feasibility of using fiber-reinforced concrete (FRC) in areas of hydraulic structures where cavitation, erosion, and durability problems are serious considerations. Problems in spillways near the ogee crest and in certain areas near the entrance to the stilling basin where serious loss of concrete was occurring from water-borne forces were the center of interest. Previous studies of the impact resistance of FRC suggested that this type of concrete could offer substantial benefits from a maintenance and repair point of view. At the time, however, little information was known about the long-term durability of concrete reinforced with distributed fibers.

As a result of this inquiry, a project plan for the determination of the feasibility of using FRC in selected hydraulic structures was submitted with the objectives of studying the durability of FRC in environments of near 100-percent saturation, cyclic saturation, and drying in fresh and salt water under severe climatic conditions, and high-velocity flows.

At the time of the development of this project plan, there were a number of different distributed fibers available from the commercial marketplace. In an effort to evaluate all existing types of fibers, a comprehensive study of four fiber types was proposed. Multiple series of FRC beams ranging in size from 82.5- by 114- by 406-mm (3 1/4- by 4 1/2- by 16-in.) to 229- by 229- by 1,143-mm (9- by 9- by 45-in.) laboratory freezing and thawing specimens were to be loaded in the field. These specimens were proposed to be fabricated and sent to the WES Severe Weather Exposure Station for long-term durability experiments. In October 1974, a research program to address these durability issues was funded and the project was initiated in the spring of 1975.

## WES severe weather exposure station

WES has maintained a marine exposure station for the study of concrete and related materials under severe weather conditions since 1936 when the first series of specimens were installed to support research into concrete materials for the Passamaquoddy Tidal Power Project. At that time, it was believed that exposure of concrete specimens made using the materials which would be used in the Passamaquoddy Tidal Power structure would provide valuable data on the durability of the concrete in the environment in which the structure was to serve. The project was never carried out, but the concept of a severe weather exposure station for evaluating the durability of concrete in the severe marine environment was kept and the exposure station has been maintained to this day.

The exposure station is located on 1.24 hectares (3.06 acres) of the northwest shore of Treat Island which is located in Cobscook Bay near Eastport, ME. Figure 1 shows the general and specific location of the facility, while Figure 2 shows the general layout of the exposure wharf and the beach exposure area. The station consists of two exposure locations for small- and medium-size specimens and a beach area which can accommodate large specimens. The 31- by 7-m (101- by 24-ft) pier has its deck at an elevation of 10 m (33 ft) above mean tide elevation and is always out of the water. It allows exposure of specimens to rainwater, saltwater spray, and the daily temperature fluctuations. The 37- by 12-m- (120- by 40-ft-) low wharf is constructed with its deck at the mean-tide elevation so that specimens exposed there will experience wetting and drying twice daily from the tidal range in the area, as well as thermal changes from the range of temperatures. The normal tidal range in this part of Cobscook Bay is 5.5 m (18 ft) with a maximum of 8 m (26 ft) and a minimum of 4 m (13 ft).

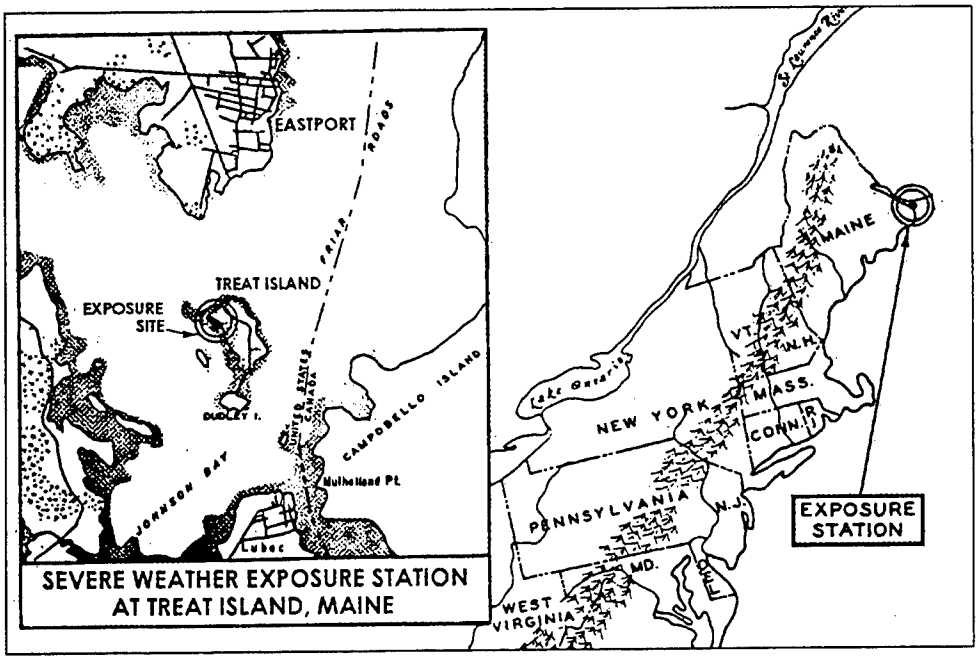


Figure 1. Location of exposure station within the state of Maine

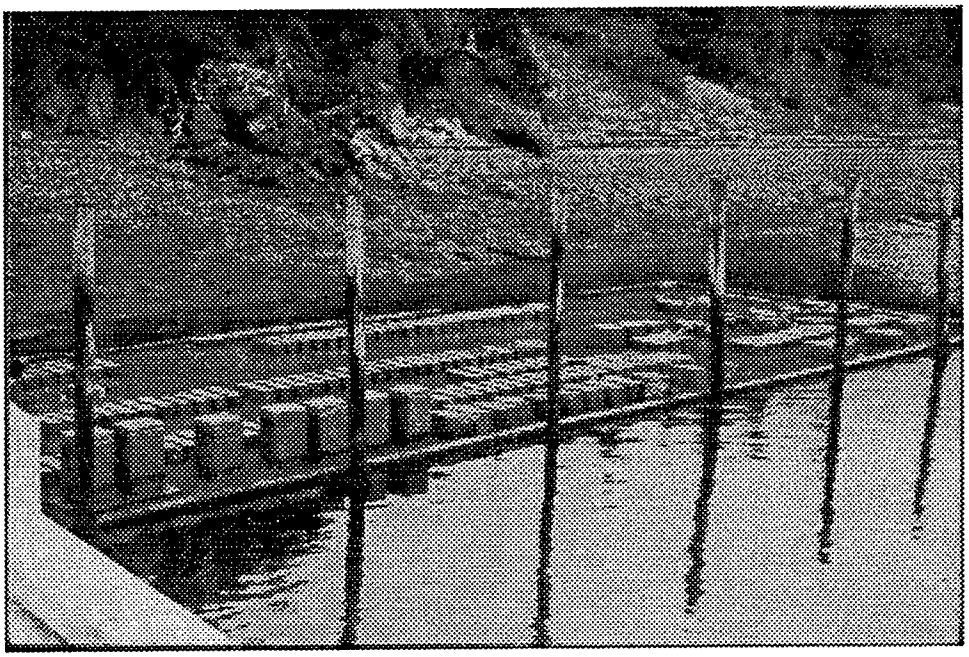

Figure 2. General layout of exposure wharf and beach area

### Environment

The summers are short, extending from late June through August. During this time, the air temperatures range from approximately 12 to 27 °C (54 to 80 °F), while the water temperature remains mostly below 4.5 °C (40 °F). The winters extend from early November through mid-March, the air temperatures range from -23 to 2 °C (-10 to 36 °F), and the water temperature remains at approximately 3 °C (37 °F).

The relatively cool summers provide an environment where chemical processes in the concrete are slowed and autogenous healing of cracked surfaces is retarded. The winter environment provides a combination of air and water temperatures which expose the specimens at mean-tide elevation to freezing between -23 and -2 °C (-10 and 28 °F) in the cold air and thawing to about 3 °C (37 °F) when covered with water. The alternate exposures in seawater and air result in rapid temperature changes in the specimens as well as changes from the frozen to thawed condition and visa versa. During an average winter, the specimens are subjected to about 125 cycles of freezing and thawing.

## Description of the Program

### Scope of the overall program

The overall scope of the WES fiber-reinforced concrete program encompassed a study of concrete using four types of fibers subjected to laboratory and long-term field durability studies of both loaded and unloaded specimens.

The field-exposure studies consisted of 50 fiber-reinforced concrete beams, small, medium, and large, which were installed in June 1975. The beams consisted of twelve 152- by 152- by 762-mm (6- by 6- by 30-in.), twenty-one 152- by 152- by 914-mm (6- by 6- by 36-in.), and seventeen 229- by 229- by 1,143-mm (9- by 9- by 45-in.) specimens. Sixteen of the 229- by 229- by 1,143-mm (9- by 9- by 45-in.) beams were yoked in pairs and stressed in third-point bending. One of the 17 beams was not loaded. It was to be an unreinforced control beam. The applied long-term load was kept at 35 percent of the short-term strength. This load was calculated to be 9.65 kN (2,170 lbf) and was adjusted annually to this value for the first 10 years to compensate for the relaxation of stress.

The laboratory work consisted of specimens cast and evaluated to measure the underwater abrasion resistance of FRC for potential use in stilling basins at Corps of Engineers dams; and the placement of a roadway slab approximately 6.1 by 30.5 m by 127 mm (20 by 100 ft by 5 in.) to study the suitability of FRC as a pavement material.

## Scope of the study in this report

This report covers details of work performed on the 12 surviving 229- by 229- by 1,143- mm (9- by 9- by 45-in.) beams which were removed from the WES severe weather exposure station in July 1993. The purpose of terminating the exposure of these beams and conducting laboratory study was to evaluate the results of 18 years of exposure of loaded beams containing the four types of fibers studied in the overall program. The scope of the work under this report included: determining the remaining load on the 12 surviving beams; photographing their postexposure condition; evaluating their condition by pulse-velocity and resonant-frequency measurements and comparing those to the 18-year history of these measurements; investigating the residual flexural strength and toughness of the full beams; examining uniaxial, compressive, and indirect-tensile strength of cores taken from the beams; and performing measurements for carbonation. The effect of the direction of stress during exposure was also examined. The condition of the fibers after 18 years of exposure was also studied. The nature and degree of the deterioration was investigated by scanning-electron microscope (SEM) techniques.

# 2 Measurements Apparatus, and Procedures

## Fibers

Four types of fibers were evaluated, and each fiber type was represented in the beams evaluated in this report. Each fiber was manufactured for use with concrete and each producer claimed advantages of their fiber over those of the competition. Table 1 gives details of the fibers. Seven mixtures used in the study contained fibers, while two control mixtures contained no fibers. Brass-coated 19-mm (3/4-in.) steel fibers; chopped steel 25.4-mm (1-in.) fibers; and alkali-resistant 25.4-mm (1-in.) glass fibers were used in two mixtures each, while stainless steel 25.4 mm (1-in.) fibers were used in one mixture. The chopped steel fibers were rectangular in cross section and all other fiber types were circular in cross section.

**Table 1**
**Physical Data of Fibers Used in the Study**

| Fiber Type | Manufacturer | Length, mm (in.) | Cross Section, mm (in.) |
|---|---|---|---|
| Brass-coated steel | National Standard | 19 (0.75) | 0.41 (0.016) diameter |
| Stainless steel | U.S. Steel | 25.4 (1.0) | 0.33 (0.013) diameter |
| Chopped steel | U.S. Steel | 25.4 (1.0) | 0.25 by 0.56 (0.01 by 0.02) |
| Fiberglass | Owens-Corning | 25.4 (1.0) | Not available |

## Mixtures

There were nine concrete mixtures used in the overall study. Each mixture was represented in the 12 surviving 229- by 229- by 1,143-mm (9- by 9- by 45-in.) beams evaluated in this report. The mixtures were designated H through P inclusively and are described in Table 2. Fine aggregate used in the concrete consisted of manufactured limestone sand from Vulcan Materials Quarry, Hermitage, TN, while the coarse aggregate was 19-mm (3/4-in.) maximum size limestone from Vulcan Materials Quarry, Calera, AL. Five of the mixtures (J, K, M, O, and P) had a neutralized vinsol resin air-entraining admixture added. The air contents for the remaining four (H, I, L, and N) mixtures were measured values on nonair-entrained concrete.

All mixtures contained 467 kg/m$^3$ (789 lb/yd$^3$) of type II portland cement, except the glass-fiber reinforced mixtures (N and O) which contained 651 kg/m$^3$ (1,100 lb/yd$^3$). The water-to-cement ratio (w/c) was maintained at 0.45 for all mixtures, which resulted in greater slump measurements for the nonfiber-reinforced mixtures H and J. A water-reducing admixture (1.5 percent by mass of concrete) was also added to mixtures N and O.

**Table 2**
**Mixture Data**

| Mixture | Fiber Type | Fiber Ratio by mass | Air Content, % | Slump, mm (in.) |
|---|---|---|---|---|
| H | None | — | 2.5 | 146 (5.8) |
| I | Brass-coated steel | 0.04 | 1.8 | 64 (2.5) |
| J | None | — | 8.5 | 178 (7) |
| K | Brass-coated steel | 0.04 | 8.5 | 102 (4) |
| L | Chopped steel | 0.04 | 1.9 | 51 (2) |
| M | Chopped steel | 0.04 | 7.0 | 76 (3) |
| N | Fiberglass | 0.01 | 3.6 | 26 (1.2) |
| O | Fiberglass | 0.01 | 7.0 | 51 (2) |
| P | Stainless steel | 0.04 | 7.0 | 70 (2.8) |

# Measurements

## Remaining load on the beams

At the conclusion of the exposure of the 12 remaining beams, the remaining load on the beams was measured at Treat Island by using a pair of calibrated hydraulic jacks to unload the coil springs. When the nuts become loose, the jack load was assumed to be the actual remaining long-term load on the beam. After the magnitude of the load was recorded, all load was removed from the beams and they were transported to the laboratory.

## Photographic record

An annual photographic record of the condition of the beams was kept from 1983 to the time of their removal in 1993. Photographs of the surviving beams as they appeared on the rack at Treat Island before removal for evaluation in 1993 are shown in Appendix A. When received in the laboratory, photographs showing the condition of all four faces (top-exposure face, bottom-exposure face, loaded-compression face, and loaded-tension face) of the beams as they appeared prior to evaluation were taken and are shown in Appendix B.

## Ultrasonic pulse-velocity measurements

Ultrasonic pulse-velocity measurements were made annually during exposure as well as in the laboratory at the conclusion of the exposure period. Measurements were conducted according to American Society for Testing and Materials (ASTM) C 597-83 (ASTM 1993f). A reference bar was used to calibrate the meter at the beginning of and at intervals throughout the measurement procedure. Fifty-millimetre (1.97-in.) transducers were used with a coupling medium made of kaolinite and glycerol.

## Flexural-toughness measurements

Flexural-toughness and first-crack strength measurements were conducted on all beams returned to the laboratory according to ASTM C 78-84 and C 1018-89 (ASTM 1993c, g). The one exception to this was one of the four nonfiber-reinforced beams which broke at Treat Island before being returned to the laboratory and, hence, was not tested. The loading machine used in the flexural-toughness measurements was a Baldwin model 200 BTE. Displacements of the beam during measurements were measured with linear variable differential transducers (LVDTs) located at the supports and at midspan to enable calculation of net midspan deflection. Load and displacement measurements were recorded at half-second intervals with a Sciemetric data-acquisition system.

For all beams the first-crack load, first-crack net deflection, modulus of elasticity, first-crack strength, and first-crack toughness were determined. When the beams did not have an instant brittle failure at first crack, a number of toughness indices (ratios) were determined to identify the postcrack behavior of the concrete. Toughness indices $I_5$, $I_{10}$, and $I_{20}$ were determined by dividing the area under the load vs deflection curve at deflections of 3.0, 5.5, and 10.5 times the first-crack deflection respectively, by the area under the curve for the first-crack deflection. Values of $I_5 = 5.0$, $I_{10} = 10.0$, and $I_{20} = 20.0$ correspond to linear elastic material behavior up to first crack and perfectly plastic behavior thereafter.

Two residual strength factors ($R_{5,10}$ and $R_{10,20}$) were also calculated from the toughness indices. The $R_{5,10}$ factor is defined as 20 ($I_{10}$ -$I_5$) and the $R_{10,20}$ factor as 10 ($I_{20}$-$I_{10}$). Therefore, the value of both these factors would be 100 if the beam failed in perfectly plastic behavior. In addition, the modulus of elasticity was calculated for each beam.

## Sawed-beam measurements

After the beams were evaluated for flexural toughness, the effect of the type of stress the beam experienced during long-term loading and exposure was examined. By sawing the longest remaining half of each beam along its neutral axis and conducting a second series of flexural-toughness measurements on the two beams so created, the effect of a beam face being under tension, compression, or being a neutral-axis face could be examined. Figure 3 shows the procedure used to create

four half-beams from the longest remaining halves of a pair of yoked beams. Previous tension, compression, and neutral stress zones from each mixture were evaluated in both positive and negative bending as the beams had originally been stressed in pairs. By preparing the beams in this manner, an additional 24 flexural measurements were conducted. These loading situations created the stress conditions shown in Table 3.

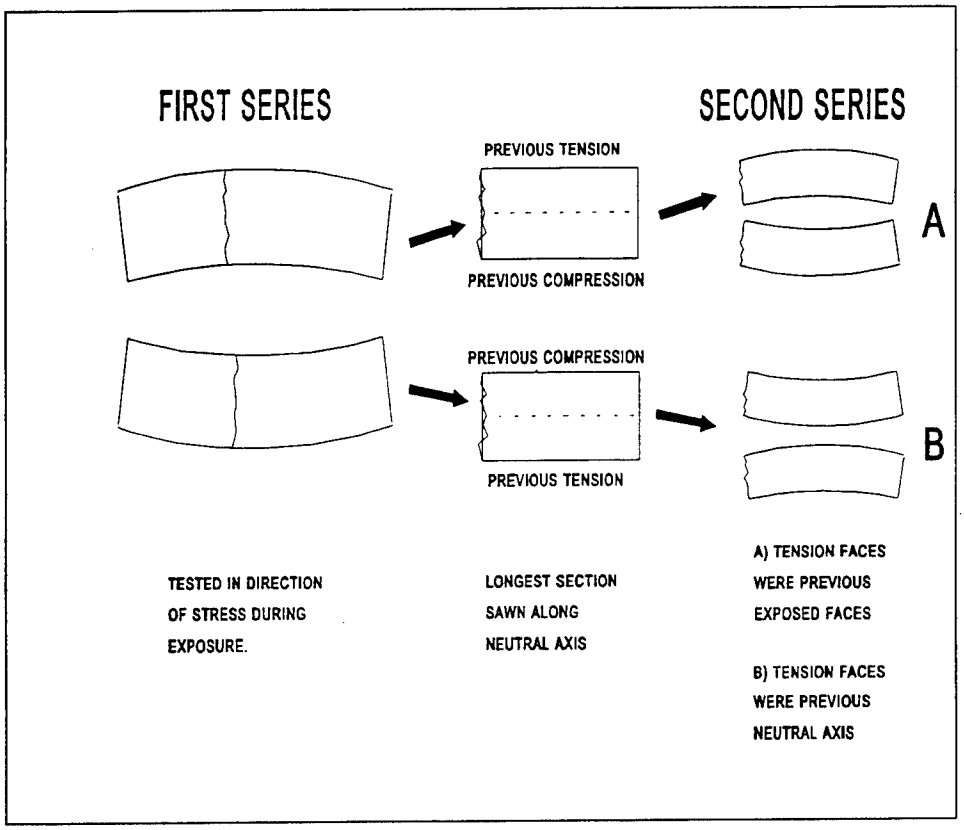


Figure 3. Direction of bending during flexural measurements for the first series of whole beams and the second series of sawed half-beams

**Table 3**
**Stress Conditions Created by Second Series of Flexure Measurements**

| Stress Condition during Exposure | Stress Condition of Sawed Face during Second Measurements |
|---|---|
| Face in tension | Evaluated in tension |
| At neutral axis | Evaluated in compression |
| Face in compression | Evaluated in tension |
| Face in compression | Evaluated in compression |
| At neutral axis | Evaluated in tension |
| Face in tension | Evaluated in compression |

## Compression measurements

After the whole-beam and half-beam flexural measurements were complete, three 102-mm (4-in.) cores were taken from the smallest remaining section of each beam. The cores were drilled from the original tension face through to the compression face. This direction of core drilling was used so the ends of the cores would be from the less exposed faces of the beam. Since the tension and compression faces of the beams were vertical faces when exposed, they suffered less surface deterioration from freezing and thawing than would surfaces that could collect water.

Core drilling was done in accordance to ASTM C 42-90 (ASTM 1993b). Core drill patterns and codes are presented in Appendix C. Because the beams were yoked and exposed in pairs, there were six cores from each study mixture. Three of the cores from each mixture were tested in compression according to ASTM C 39-93a (ASTM 1993a). From the six cores that were obtained from each type of mixture, the three cores with the smoothest cylinder sides were set aside for later use in the indirect-tension measurement and the remaining three were used in the compression testing.

A cylinder height-to-diameter ratio of 2:1 was obtained by sawing 12.7 mm (1/2 in.) from each end of the cores. The compression tests were performed on a 1,334-kN (300,000-lbf) capacity Riehle Universal Testing Machine.

## Indirect-tension measurement

American Society for Testing and Materials Standard C 496-90 (ASTM 1993e) determines splitting tensile strength of concrete by the application of a diametral compressive force on a cylindrical concrete specimen placed with its axis horizontal between the platens of a testing machine. As a means of determining the true tensile strength of the concrete, research has shown that the splitting tensile strength can be difficult to perform consistently and often produces results that are high compared to direct tensile strength measurements (Richart, Brandtzaeg, and Brown 1928). For these reasons, a new method of tensile strength measurement for cylindrical specimens was employed under this research project.

## Alternative-tension measurement

The tensile measurement method used is one which was developed in Great Britain (Clayton 1978). It makes use of axisymmetric pressure on the outer curved surface of the cylinder being evaluated. A schematic of the measurement apparatus is shown in Figure 4. In this method the cylinder is prepared by soaking it for 40 hr in a saturated lime water. The specimen is then sealed in an open-ended steel sleeve so that the ends of the cylinder are exposed to normal atmospheric conditions and a pressure cavity is formed between the steel sleeve and the cylinder as shown in Figure 4. The ends of the pressure cavity are maintained by means of rubber o-ring seals. Nitrogen gas is then pumped into the sleeve at a loading rate of 2.5 MPa

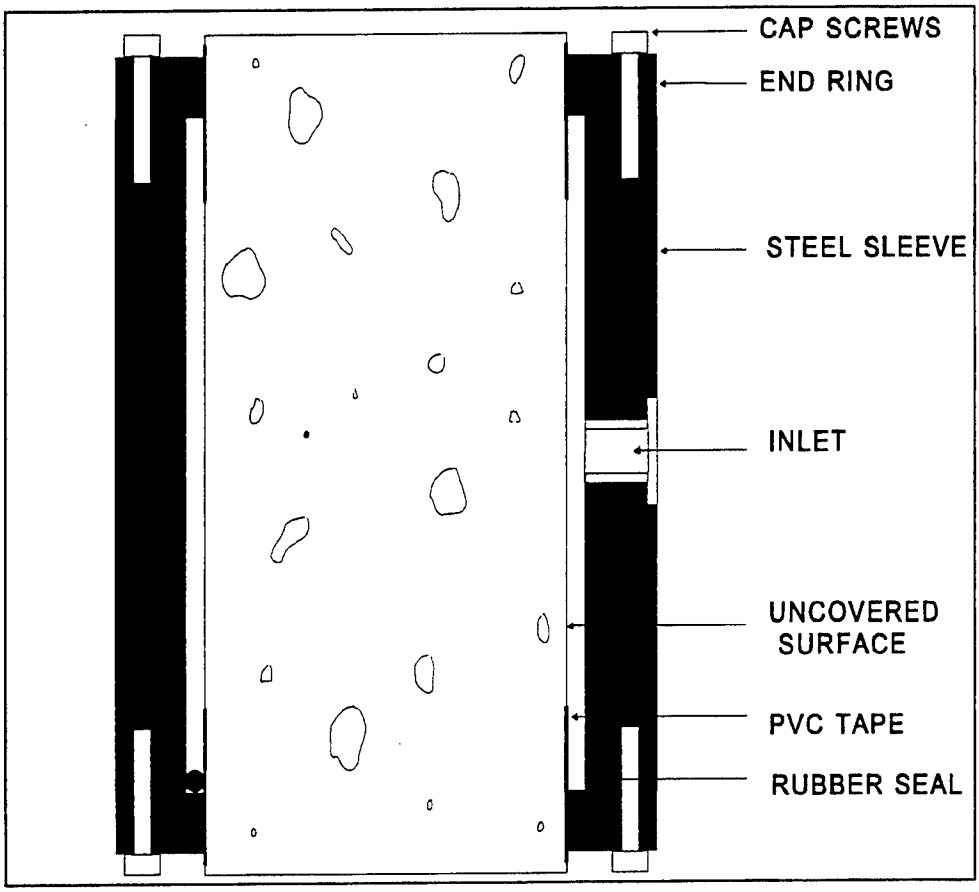


Figure 4. Indirect-tension measurement setup (Clayton 1978) (Reproduced by permission of the Building Research Establishment, United Kingdom)

(360 psi) per 100 sec. The external pressure on the sides of the cylinder cause an increase in pressure on the pore solution in the pores of the cylinder. The nature of fluids ensures that this pore pressure acts in all directions within the pore space and therefore produces a tensile stress on the cylinder cross section when the internal pressure exceeds atmospheric pressure. Explosive failure occurs when this net tensile pressure reaches the maximum tensile strength of the concrete. Results obtained with this method are lower than those of the splitting tensile measurement and are of the same order of magnitude as the conventional tensile strength.

## Carbonation

Broken surfaces of the beams were measured for the presence of calcium carbonate in the concrete by painting the surfaces with the end-point indicator phenolphthalein. A color change of the concrete from normal grey to reddish purple indicates that the pH of the concrete is above 8.5, which indicates that there is little carbonation. If the concrete remains its normal color, then the presence of carbonation is indicated.

## Resonant-frequency measurements

All resonant-frequency measurements were conducted in accordance with ASTM C 215-91 (ASTM 1993d). Alternative procedure number two, the impact resonance method, was used. An SA-77 signal analyzer manufactured by RION Co. Ltd. of Japan was used to record accelerometer data and produce amplitude versus frequency graphs of the resonant vibrations. The resulting data were stored in the unit and downloaded to a computer through a built in RS-232-C interface.

Transverse frequencies were measured on all four faces of the beams (top as exposed, bottom as exposed, tension, and compression). Longitudinal frequencies were measured twice, once with the accelerometer at the same end of the beam which was struck with the hammer, and once at the opposite end. One torsional-frequency measurement was made on each beam as well.

Specimen mass, fundamental frequencies, and dimensions were used to calculate dynamic Young's modulus of elasticity (E), dynamic modulus of rigidity (G), and dynamic Poisson's ratio ($\mu$).

## Scanning-electron microscope measurements

An SEM slide was prepared from the tension zone of one beam from each of the mixtures represented in the study. The slide was prepared such that one edge of the thin section was at the exterior tension fiber of the beam and the other was a location inward from the extreme tension face. The SEM was used to probe the surface of the concrete matrix over a range of locations on the slide to determine the percent mass concentrations of a number of elements. These data were used to create graphs showing concentrations of various elements versus depth from the tension face of the beam. Elements included in the scan were aluminum (Al), iron (Fe), magnesium (Mg), potassium (K), sulphur (S), chlorine (Cl), silicon (Si), and calcium (Ca).

The SEM used was a JEOL JSM-6400 equipped with a Link Pentafet energy dispersive detector and a Link EXL X-ray analyzer. Fifteen kV accelerating voltage and 2.5 nA of beam current were used with a spectrum collection time of 100 sec. To ensure that the analyzer focused on the maximum percentage of concrete and not on the air voids and other irregularities in the concrete, the smallest possible area was used for point analysis of the matrix. The resolution of the equipment limited this area to 15 $\mu$m square.

# 3 Results

## Remaining Beams

At the completion of the exposure period, 12 beams were still in a condition that would allow them to be removed and examined. Two beams from each of the original mixtures were available for analysis, including two that contained no fibers. The beam which was originally intended to be used as a control and which was left unloaded during the exposure period only contained 2.5 percent entrained air and failed within 8 years of the beginning of the exposure. As a result, the loaded pair of beams in mixture J which also contained no fibers were used as the control.

### Remaining load on the beams

The process of jacking a load onto the beams until the nuts holding the yoked pairs together became loose and then recording that as the remaining load on the beams revealed a residual load of approximately 5.4 kN (1,200 lbf) on all of the beams.

### Condition upon removal from the exposure station

Of the 17 original 229- by 229- by 1,143-mm (9- by 9- by 45-in.) beams, only 12 remained in 1993 after 18 years of exposure. All beams with less than 3 percent air content (those that were nonair-entrained, (mixtures H, I, and L)), regardless of fiber type, deteriorated quickly and failed within 8 years of the beginning of their exposure. The remaining 12 beams consisted of 2 beams from each of mixtures J, K, M, N, O, and P. These consisted of two beams containing brass-coated steel fibers, two with chopped steel fibers, four with alkali-resistant glass fibers, two with stainless steel fibers, and two control beams with no fibers. One of the two nonfiber-reinforced beams from mixture J (beam J-1) failed while still at Treat Island. Even though it was failed at the time of removal, it was returned and included in the results as part of the control.

**Visual evaluation.** The photographs of the beams while still under load at Treat Island, shown in Appendix A, and those taken in the laboratory before evaluation, shown in Appendix B, provide a valuable aide in evaluating the

condition of the beams at the conclusion of the exposure. The condition of the surfaces of the surviving beams varied with mixture type and the relative exposure of the particular face. The yoked-beam pairs were laid on their sides during exposure with one side described as the top and the other side as the bottom. The remaining faces of the beams were the tension or compression faces of the beams, and these faces of the beams were perpindicular to the surface of the water during exposure.

The glass-fiber-reinforced beams (mixtures N and O in Appendixes A and B) exhibited the greatest deterioration of the beams surviving in 1993, while the steel-fiber beams (mixtures K, M, and P) and nonreinforced beams (mixture J) suffered less significant damage, occurring mostly along the edges and corners of the beams.

The photographs in Appendix B show the condition of all faces of the beams at the end of the exposure. With respect to position of a face during exposure, in most cases, the bottom face of the beam suffered the least deterioration and the top surface the most. There was slightly more deterioration as revealed by visual inspection on the tension faces than the compression faces; however, this may have been more a function of the relative exposure than the direction of stress.

**Pulse-velocity evaluation.** The results of annual pulse-velocity measurements over the exposure life of the beams are plotted in Figures 5 through 8, and tabulated as $\%V^2$ in Appendix D. Deterioration information from these measurements is nonconclusive and tended to be erratic over the life of the beams. The measurements often would indicate an improved condition from 1 year to the next which is contrary to the normal progression of deterioration from freezing and thawing as time progresses. The measurements taken in 1983 appear to be low values in relation to those in other years. No significant difference in performance among fiber type is apparent from these data with the possible exception that the trend for the glass-fiber-reinforced beams (Figure 7) and the nonfiber/stainless-steel fiber beams (Figure 8) appear to show some slight decrease in $\%V^2$ over the years of exposure.

## Flexural Toughness

### Whole-beam measurements

Figures 9 and 10, as well as Table D-1 in Appendix E, summarize the first-crack strength (FCS), first-crack toughness (FCT), modulus of elasticity (E), and postcrack toughness indices $I_5$ and $I_{10}$ of the whole-beam flexural toughness measurements. The beams with carbon-steel fibers had the greatest first-crack strength, with the brass-coated 19-mm (3/4-in.) steel-fiber-reinforced beams (mixture K) reaching an average of 6.13 MPa (889 psi) and the chopped 25.4 mm (1 in.) steel-fiber-reinforced beams (mixture M) reaching an average of 6.56 MPa (951 psi) at first crack.

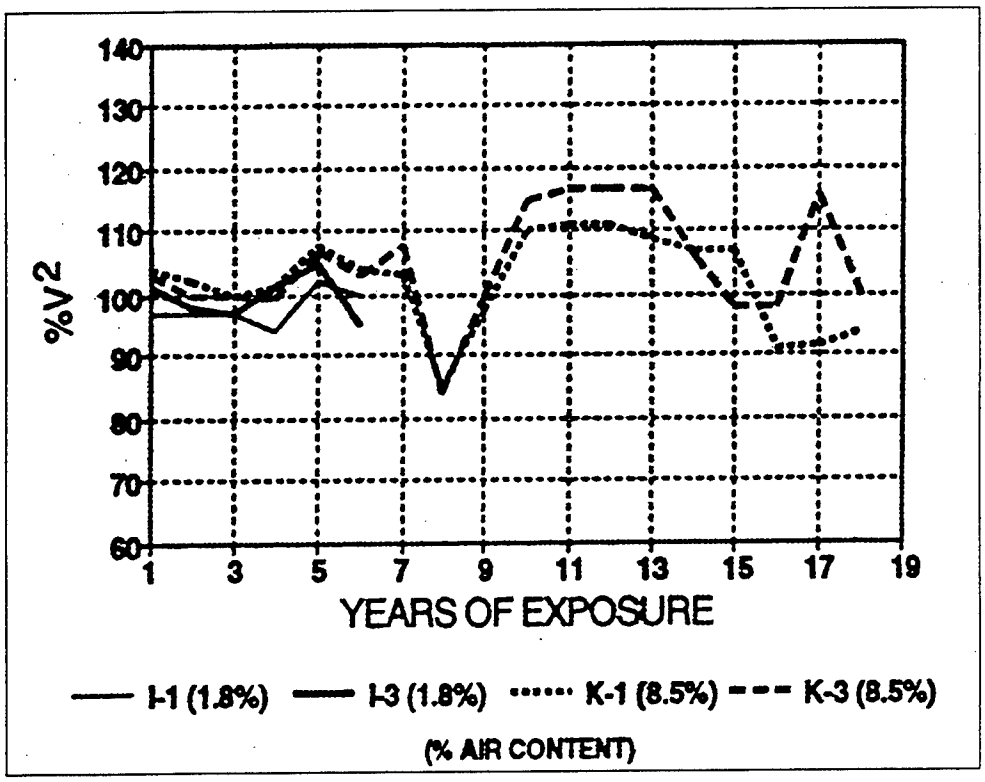


Figure 5. Pulse-velocity results for brass-coated steel-fiber-reinforced beams

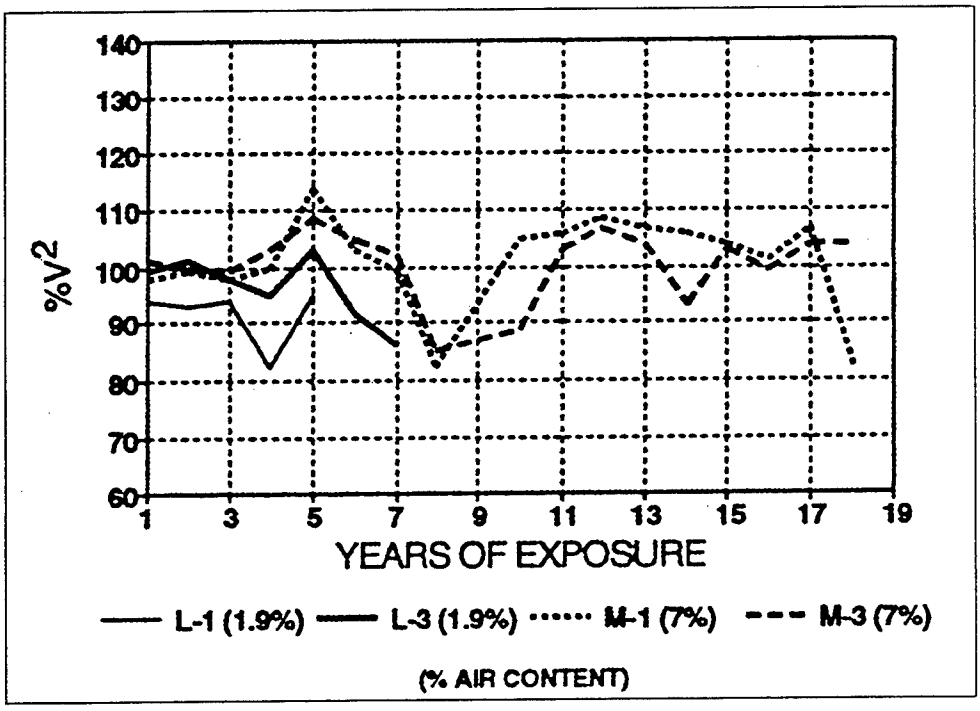


Figure 6. Pulse-velocity results for chopped steel-fiber-reinforced beams

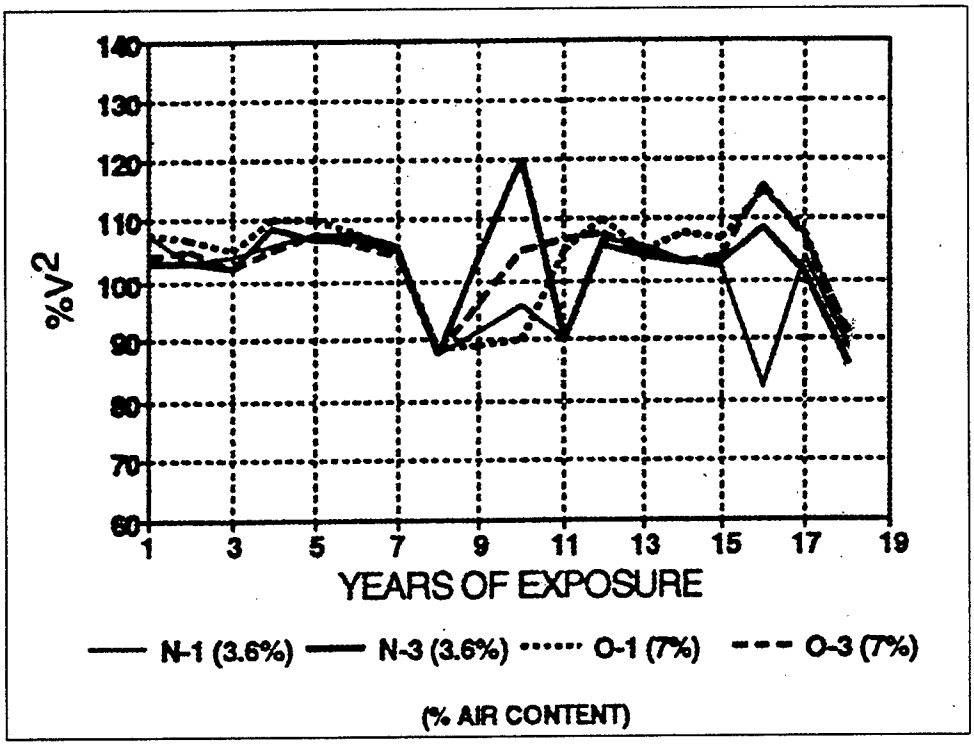


Figure 7. Pulse-velocity results for glass-fiber-reinforced beams

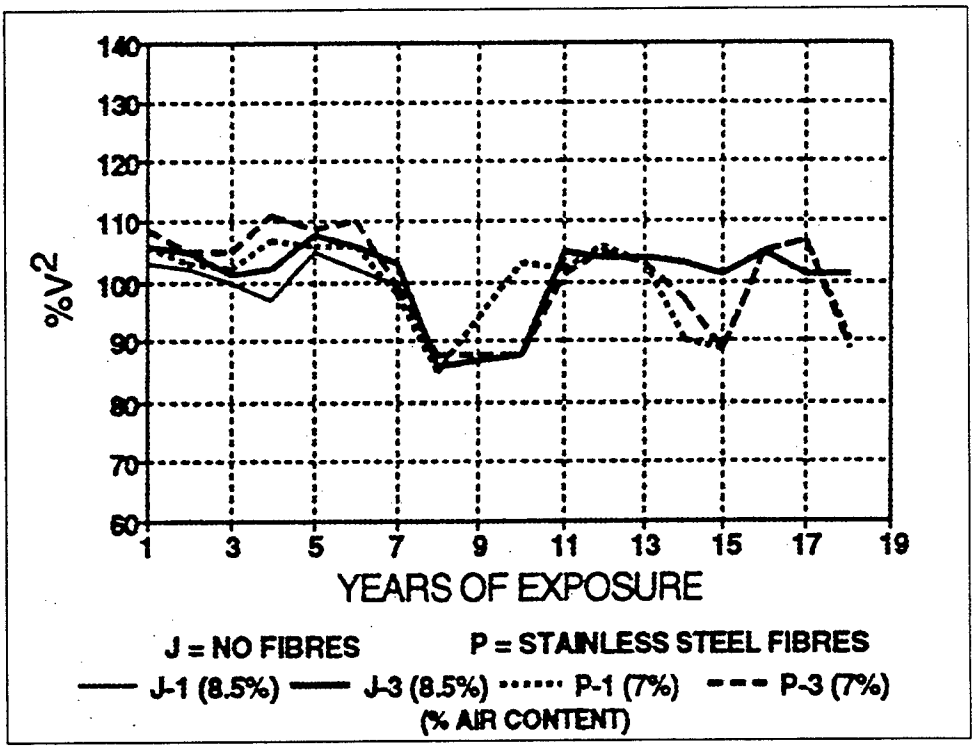


Figure 8. Pulse-velocity results for nonfiber- and stainless-steel-fiber-reinforced beams

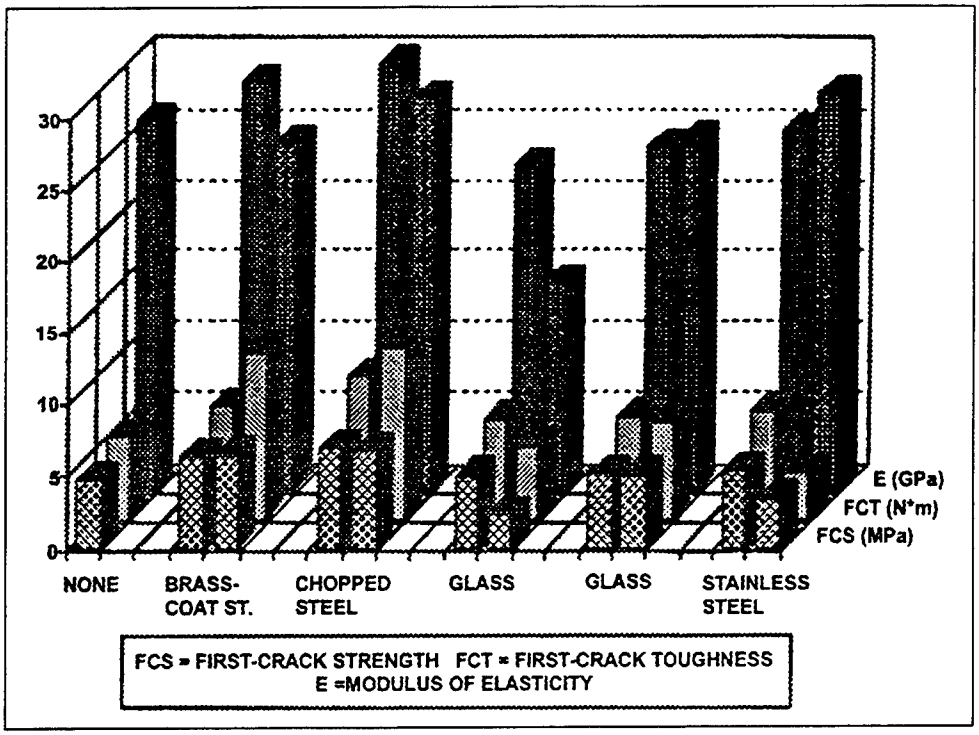


Figure 9. First-crack strength, toughness, and modulus of elasticity as calculated from flexural measurements

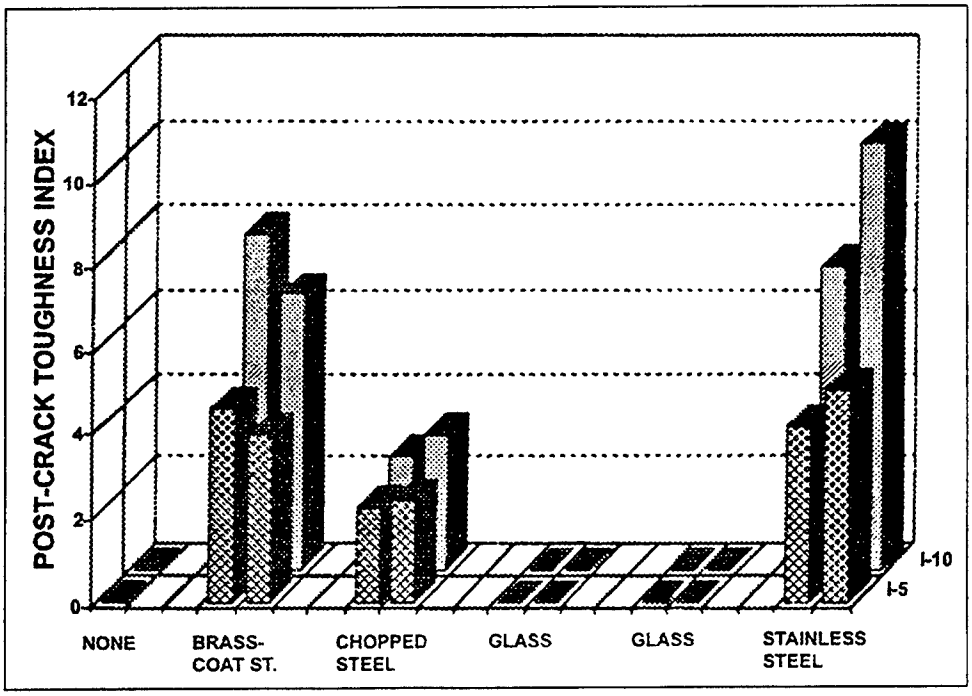


Figure 10. Postcrack-toughness indices $I_5$ and $I_{10}$ from flexural measurements

Glass-fiber beams from mixtures N and O had an average FCS of 4.84 MPa (702 psi) excluding the result of beam N-3 which exhibited a first crack at 2.21 MPa (321 psi). This beam had severe freezing and thawing deterioration on one face (see tension face of beam N-3 in Appendix B) and therefore failed at a low tensile strength. FCS of the stainless-steel-fiber beams from mixture P averaged 4.22 MPa (612 psi). In comparison, the FCS of the nonfiber-reinforced beam was 4.54 MPa (658 psi).

In a similar manner to FCS, the chopped-steel-fiber beams (mixture M) and the brass-coated-fiber beams (mixture K) had the highest FCT averaging 10.7 N-m (7.89 ft-lb) and 9.49 N-m (7.00 ft-lb), respectively. Conversely, the stainless-steel-fiber-beams had the lowest FCT, measuring 5.13 N-m (3.78 ft-lb). The glass-fiber beams had average FCT values of 5.76 N-m (4.25 ft-lb) (mixture N) and 6.75 N-m (4.98 ft-lb) (mixture O). The nonfiber-reinforced control mixture J had an FCT of 5.54 N-m (4.09 ft-lb).

The moduli of elasticity were also greater for the beams with carbon-steel fibers. The brass-coated, chopped-steel, and stainless-steel-fiber beams had moduli of 26.4 GPa (3,830 ksi), 28.5 GPa (4,130 ksi), and 26.5 GPa (3,840 ksi), respectively. The glass-fiber beams had the lowest moduli of elasticity averaging 21.4 GPa (3,100 ksi).

Although the stainless-steel-fiber beams (mixture P) had lower FCS and FCT values than the other carbon-steel-fiber beams, their toughness indices were greater, averaging 4.52, 8.64, and 16.68 for $I_5$, $I_{10}$, and $I_{20}$, respectively. Consequently, the residual-strength factors $R_{5,10}$ and $R_{10,20}$ were greater, averaging 82.5 and 80.5, respectively. The brass-coated 19-mm (3/4-in.) steel-fiber-reinforced beams (mixture K) had greater toughness indices and residual-strength factors than the chopped-steel 25.4-mm (1-in.) fiber-reinforced beams of mixture M. The control beam, mixture J, and both glass-fiber mixtures (mixtures N and O) failed in a brittle manner immediately after first crack and therefore had no postcrack-toughness indices.

### Sawed-beam flexural toughness

A second series of flexural-failure and toughness data were collected on sawed portions of the beams to determine if condition of stress during exposure would have an effect on first cracking and toughness. Beam numbering codes for these specimens are presented in Appendix C. The detailed results of the measurements are presented in Appendix F. Figure 11 shows the results of first crack flexural strength on sawed beams in which the faces were exposed either in tension or compression and tested a second time as shown in set A in Figure 3. In Figure 11 a bar designated C represents the FCS of the one-half of the beam that was in compression during the years of exposure. A designation of T indicates the concrete was in tension during exposure. While there are differences in the FCS, there is no apparent trend for any of the four fiber types in the comparison of previous tension

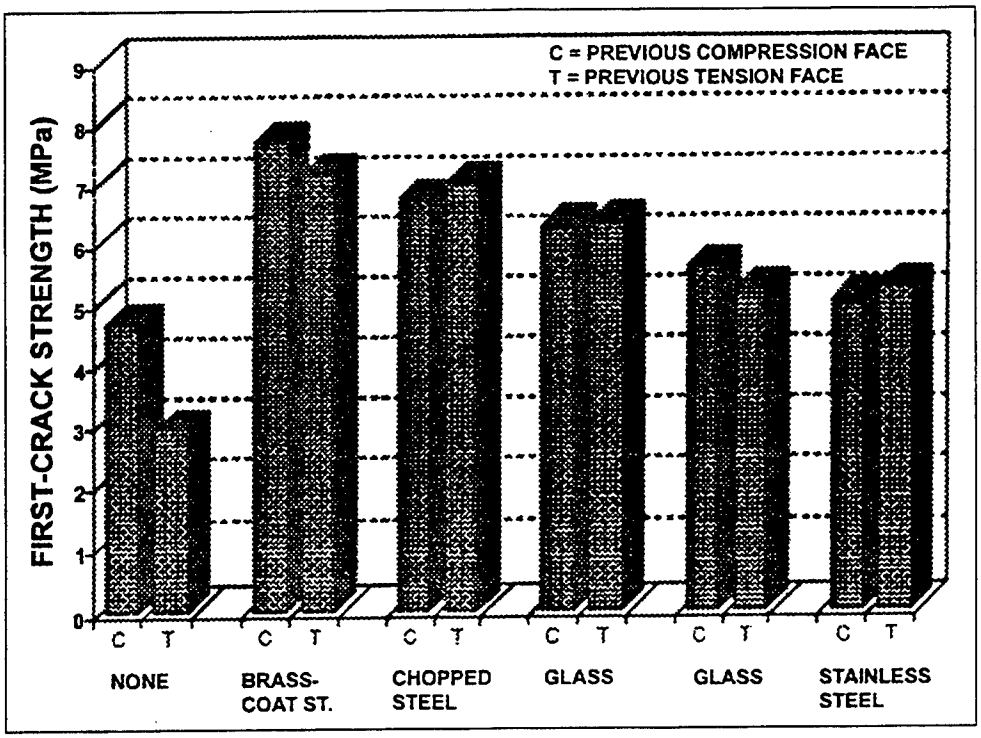


Figure 11. First-crack strength comparison of previous tension and previous compression faces

versus previous compression faces when evaluated in flexure in the second series of failures, i.e., when comparing the two beams within set (A) in Figure 3.

Similarly, there was no difference for any of the fiber types in the comparison of previous tension and compression zones when they were evaluated with the previous neutral axis as the new tension face, i.e., when comparing the two beams within set (B) in Figure 3.

Figure 12 compares the average of the FCS of faces either in tension or compression during exposure with the average of the FCS of the neutral axis during exposure as the tensile face, i.e., a comparison of the averages of set A versus set B in Figure 3. In this comparison, the previous exposed faces were stronger than the previous neutral axis for the brass-coated steel, chopped-steel, and glass-fiber-reinforced beams.

The first-crack toughness results of the second series of flexural-toughness measurements were similar to the first-crack strength results. There was no difference between previous tension and previous compression zones when placed in flexural tension. Similarly, there appeared to be some difference between the previous exposed faces and the previous neutral axis for the brass-coated steel, chopped steel, and alkali-resistant glass fibers.

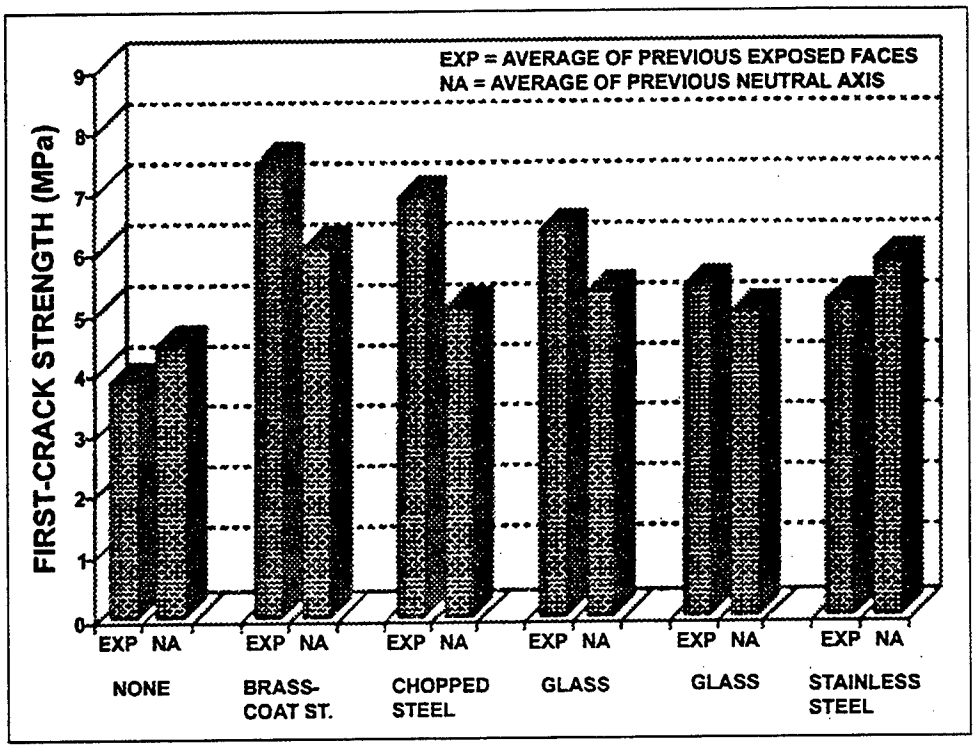


Figure 12. First-crack-strength comparison of previous exposed faces and previous neutral-axis faces

All second series beams that did not have brittle failure (mixtures K, M, and P) had higher toughness indices and residual-strength factors than whole beams (see Appendix F).

## Compression measurements

Table 4 gives the results of the uniaxial-compression measurements and Figure 13 graphically displays these data. The average compressive strength of the cores ranged from 41.9 MPa (6,080 psi) for the cores with no fiber reinforcement (mixture J) to 55.4 MPa (8,360 psi) for one set of the glass-fiber-reinforced cores (mixture N). The compressive strength of cores with any type of fiber reinforcement were very consistent. The strength of the cores from the nonfiber-reinforced beams (mixture J) were 20 percent lower than the average strength of the fiber-reinforced cores (Figure 13).

There was no apparent trend regarding the relative location along the beam from which the cores were taken (see insert in Figure 13) and the compressive strength of the individual cores.

**Table 4**
**Uniaxial-Compression Measurement Results**

| Fiber Type | Core Number | Strength, MPa (psi) | Avg Strength, MPa (psi) | Coefficient of Variation |
|---|---|---|---|---|
| None | J-3-1<br>J-3-2<br>J-1-3 | 41.2 (5,970)<br>44.3 (6,420)<br>40.2 (5,830) | 41.9 (6,080) | 5.1 |
| Brass-coated steel | K-1-1<br>K-3-2<br>K-1-3 | 50.4 (7,310)<br>50.7 (7,350)<br>53.1 (7,700) | 51.4 (7,450) | 2.9 |
| Chopped steel | M-1-1<br>M-3-1<br>M-3-2 | 51.2 (7,430)<br>53.9 (7,820)<br>51.4 (7,450) | 52.2 (7,570) | 2.9 |
| Glass mixture N | N-1-2<br>N-3-2<br>N-1-3 | 60.0 (8,710)<br>55.5 (8,050)<br>50.4 (8,330) | 55.4 (8,360) | 8.6 |
| Glass mixture O | O-1-1<br>O-1-2<br>O-3-3 | 48.5 (7,040)<br>49.0 (7,100)<br>59.3 (8,600) | 52.3 (7,580) | 11.7 |
| Stainless steel | P-2-1<br>P-1-2<br>P-1-3 | 49.5 (7,180)<br>54.2 (7,860)<br>49.7 (7,210) | 51.1 (7,420) | 5.2 |

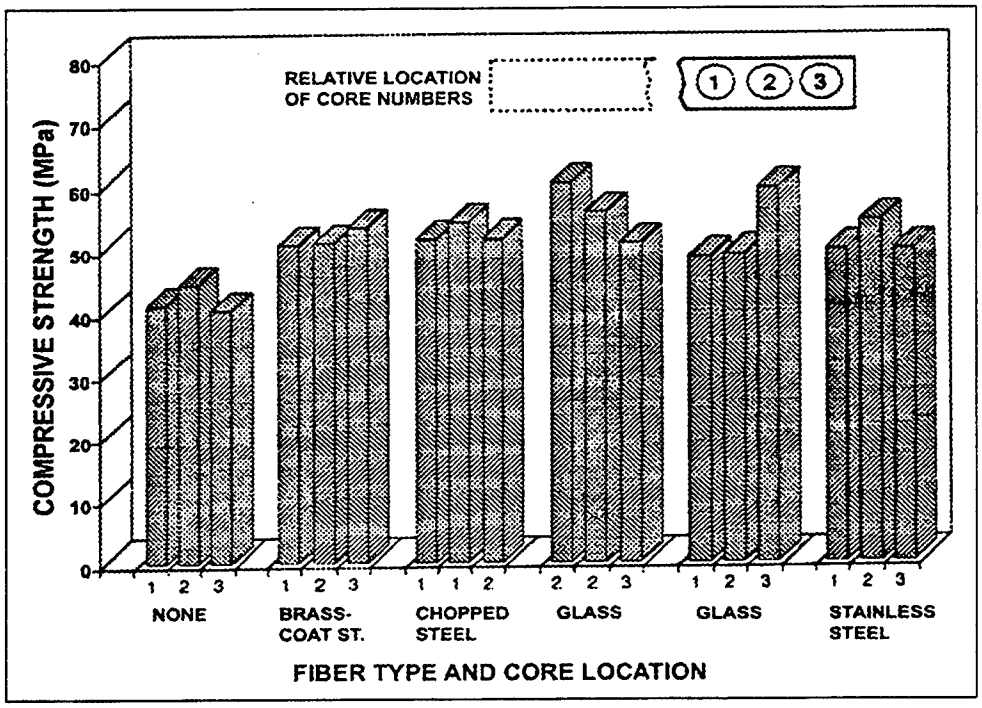


Figure 13. Ultimate compressive strength of cores by fiber type and relative location

### Indirect-tension measurement

Average tensile strength of the mixtures ranged from 3.16 MPa (459 psi) for mixture N, which was glass-fiber-reinforced, to 6.87 MPa (996 psi) for mixture M, which was reinforced with chopped-steel fibers (Appendix G). The second strongest cores were from the brass-coated carbon-steel fiber-reinforced beams (mixture K) which averaged 5.86 MPa (850 psi).

It was noted that among all the cores which had fiber reinforcement (mixtures K to P), there was a decrease in tensile strength of the individual cores as the drilling location progressed from the center to the end of the beam (Figure 14).

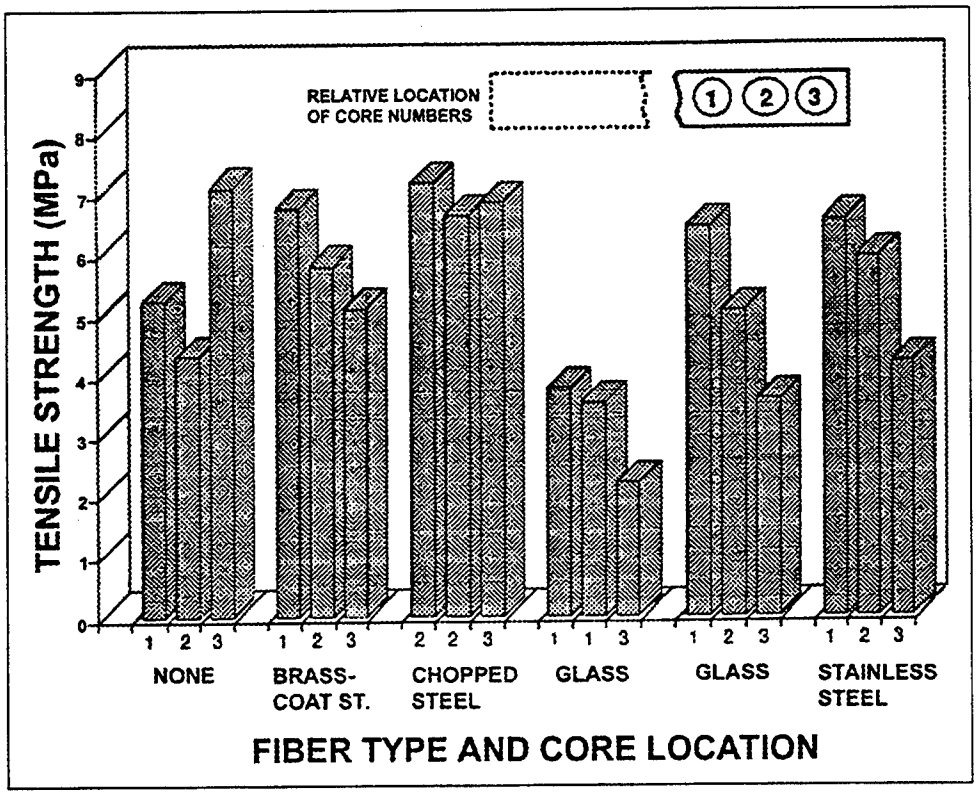


Figure 14. Indirect-tensile strength measurement results

The ratio of indirect-tensile strength to the uniaxial-compressive strength was computed for all mixtures. The carbon-steel-fiber mixtures and the nonreinforced mixture had the greatest ratio (Figure 15). The chopped-steel-fiber mixture and the nonreinforced mixture both measured 13.2 percent while the brass-coated steel fiber cores measured 11.4 percent. The ratios for the two sets of glass-fiber mixtures were lowest at 5.7 percent and 9.6 percent. The overall average ratio of tensile-to-compressive strength for all measurements was 10.7 percent, well within the accepted range of 8 to 12 percent (Kosmatka et al. 1991).

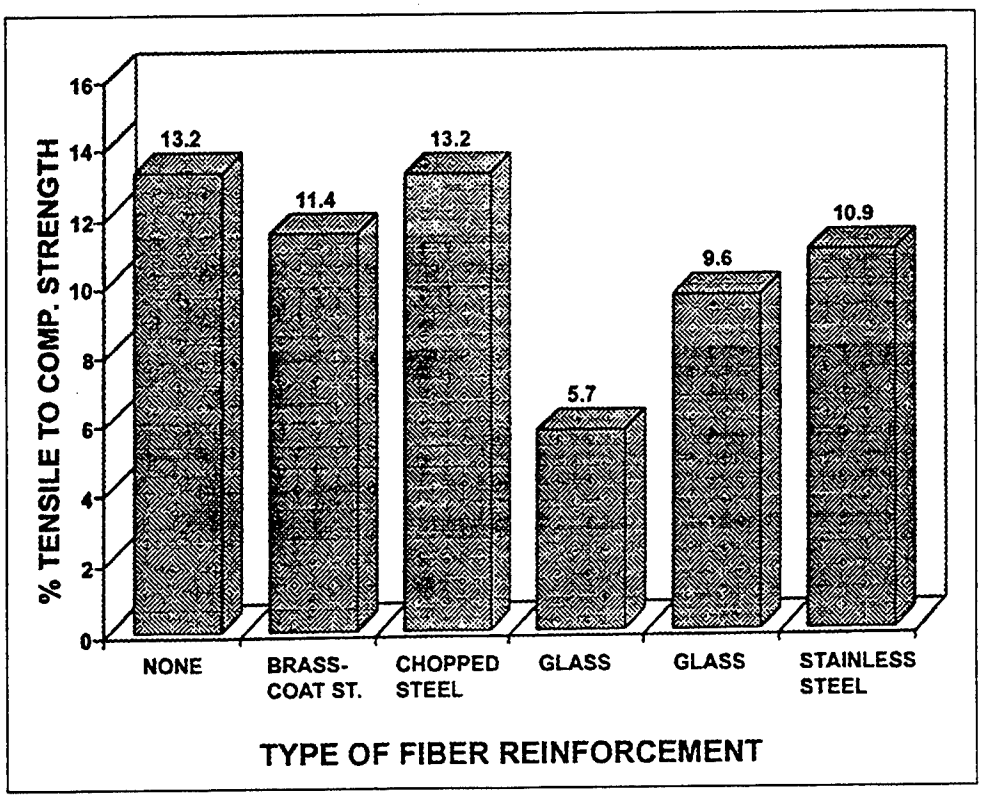


Figure 15. Indirect-tensile strength as a percent of uniaxial-compressive strength

### Carbonation

Phenolphthalein measurements showed no significant carbonation in any of the 12 beams after 18 years of exposure.

### Resonant frequency

Transverse frequencies of the four faces were consistent among individual beams (Table 5 and Appendix H). Readings taken from the top and bottom faces were the same in all cases. Compression and tension faces of the whole beams had slight differences of 1 percent or less in 4 of the 11 measurements.

When comparing the transverse frequencies of the stressed (i.e., compression and tension) faces with the top and bottom faces, the stressed faces averaged 1.2 percent less than the top and bottom faces. The average transverse frequency of the four faces was used to calculate the dynamic Young's modulus of the individual beams.

The longitudinal frequencies were identical, whether the accelerometer and hammer impact were at the same or opposite ends of the beam.

**Table 5**
**Resonant Frequencies of Whole Beams**

| Fiber Type | Beam | Resonant Frequency (hz) | | | | | | | Mass (kg) | Length (mm) |
|---|---|---|---|---|---|---|---|---|---|---|
| | | Transverse | | | | Longitudinal | | | | |
| | | Top | Botto m | Comp. | Tens. | Both Ends | Same End | Tor- sional | | |
| None | J1 LARGE | 1,562.5 | 1,562.5 | 1,531.2 | 1,531.2 | 2,893.7 | 2,893.7 | 1,693.7 | 78.2 | 26.5 |
| | J1 SMALL | 2,612.5 | 2,618.7 | 2,581.2 | 2,600.0 | 4,062.5 | 4,062.5 | 2,375.0 | 54.5 | 18.5 |
| | J3 | 631.2 | 631.2 | 612.5 | 612.5 | 1,718.7 | 1,718.7 | 612.5 | 143.6 | 1,143 |
| Brass-coat'd st. | K1 | 650.0 | 656.2 | 643.7 | 643.7 | 1,787.5 | 1,787.5 | 1,037.5 | 139.1 | 1,143 |
| | K3 | 625.0 | 625.0 | 631.2 | 631.2 | 1,768.7 | 1,768.7 | 1,018.7 | 139.1 | 1,143 |
| Chopped steel | M1 | 650.0 | 650.0 | 631.2 | 631.2 | 1,768.7 | 1,768.7 | 1,018.7 | 140 | 1,143 |
| | M3 | 637.5 | 637.5 | 631.2 | 625.0 | 1,787.5 | 1,787.5 | 1,043.7 | 142.3 | 1,143 |
| Glass | N1 | 606.2 | 606.2 | 612.5 | 612.5 | 1,668.7 | 1,668.7 | 612.5 | 141.8 | 1,143 |
| | N3 | 562.5 | 562.5 | 562.5 | 562.5 | 1,625.0 | 1,625.0 | 925.0 | 134.5 | 1,143 |
| Glass | O1 | 600.0 | 600.0 | 587.5 | 587.5 | 1,612.5 | 1,656.2 | 962.5 | 130.5 | 1,143 |
| | O3 | 612.5 | 612.5 | 602.5 | 600.0 | 1,662.5 | 1,662.5 | 975.0 | 130.9 | 1,143 |
| Stainless steel | P1 | 625.0 | 625.0 | 612.5 | 618.7 | 1,743.7 | 1,743.7 | 1,012.5 | 141.4 | 1,143 |
| | P2 | 631.2 | 631.2 | 631.2 | 625.0 | 1,762.5 | 1,762.5 | 1,012.5 | 142.7 | 1,143 |

Dynamic Young's moduli (E) values were determined for both transverse and longitudinal frequencies (Table 6). The moduli values from the longitudinal measurements were on average 2.7 percent greater than the values determined from the transverse-resonant frequencies. The moduli of elasticity values determined from resonant frequencies were on average 36 percent greater than those determined from the flexural toughness measurements or approximately 9.4 GPa (1,360 ksi) higher.

The brass-coated-steel- (mixture K) and chopped-steel-fiber beams (mixture M) had the greatest moduli of elasticity averaging 37.6 GPa (5,440 ksi) and 38.5 GPa (5,570 ksi), respectively (Figure 16). Stainless-steel-fiber beam (mixture P) results were slightly greater than the no-fiber beam (mixture J) results. As with the moduli of the glass-fiber-reinforced beams measured under the whole-beam flexural-toughness results, mixtures N & O were lowest in resonant-frequency measurements at 31.8 GPa (4,600 ksi) and 30.9 GPa (4,470 ksi), respectively.

Dynamic Poisson's ratio was calculated using the equation $\mu = (E/2G)-1$. Although no trend among the various fiber types was visible from the results, the average value was 0.23, which was well within the expected range.

### Sawed-beam results

Results of all resonant-frequency measurements on the sawed beams are presented in Table 7 and Appendix I. The transverse frequencies of all four faces (top, bottom, neutral, and previous compression or tension) were recorded as described in Figure 17. Measurements taken on the previous top or bottom faces are perpendicular to the direction of stress on the beams during the first series of

**Table 6**
**Modulus and Poisson's Ratio Values from Resonant Frequencies**

| Fibre Type | Beam | Dynamic Young's Modulus E | | | | | | Modulus of Rigidity G From Torsional | | Poisson's Ratio μ |
|---|---|---|---|---|---|---|---|---|---|---|
| | | From Avg. Transverse | | From Avg. Longitudinal | | From Overall Average | | | | |
| | | GPa | ksi | GPa | ksi | GPa | ksi | GPa | ksi | |
| None | J1 L | 34.3 | 4,975 | 33.6 | 4,873 | 34.0 | 4,924 | 13.6 | 1,972 | 0.25 |
| | J1 S | 31.6 | 4,583 | 32.3 | 4,685 | 32.0 | 4,634 | 13.1 | 1,900 | 0.22 |
| | J3 | 37.3 | 5,410 | 37.0 | 5,366 | 37.2 | 5,388 | 5.6 | 812 | - |
| Brass-coat'd st. | K1 | 38.3 | 5,555 | 38.8 | 5,627 | 38.6 | 5,591 | 15.5 | 2,248 | 0.24 |
| | K3 | 35.4 | 5,134 | 38.0 | 5,511 | 36.7 | 5,323 | 14.9 | 2,161 | 0.23 |
| Chopped steel | M1 | 38.5 | 5,584 | 38.2 | 5,540 | 38.4 | 5,562 | 15.0 | 2,175 | 0.28 |
| | M3 | 37.7 | 5,468 | 39.6 | 5,743 | 38.7 | 5,606 | 16.0 | 2,321 | 0.21 |
| Glass | N1 | 33.9 | 4,917 | 34.5 | 5,004 | 34.2 | 4,960 | 5.5 | 798 | - |
| | N3 | 27.7 | 4,017 | 31.0 | 4,496 | 29.4 | 4,257 | 11.9 | 1,726 | 0.23 |
| Glass | O1 | 30.6 | 4,438 | 29.6 | 4,293 | 30.1 | 4,365 | 12.5 | 1,813 | 0.20 |
| | O3 | 32.0 | 4,641 | 31.6 | 4,583 | 31.8 | 4,612 | 12.8 | 1,856 | 0.24 |
| Stainless Steel | P1 | 36.0 | 5,221 | 37.5 | 5,439 | 36.8 | 5,330 | 15.0 | 2,175 | 0.22 |
| | P2 | 37.0 | 5,366 | 38.7 | 5,613 | 37.9 | 5,489 | 15.7 | 2,277 | 0.20 |

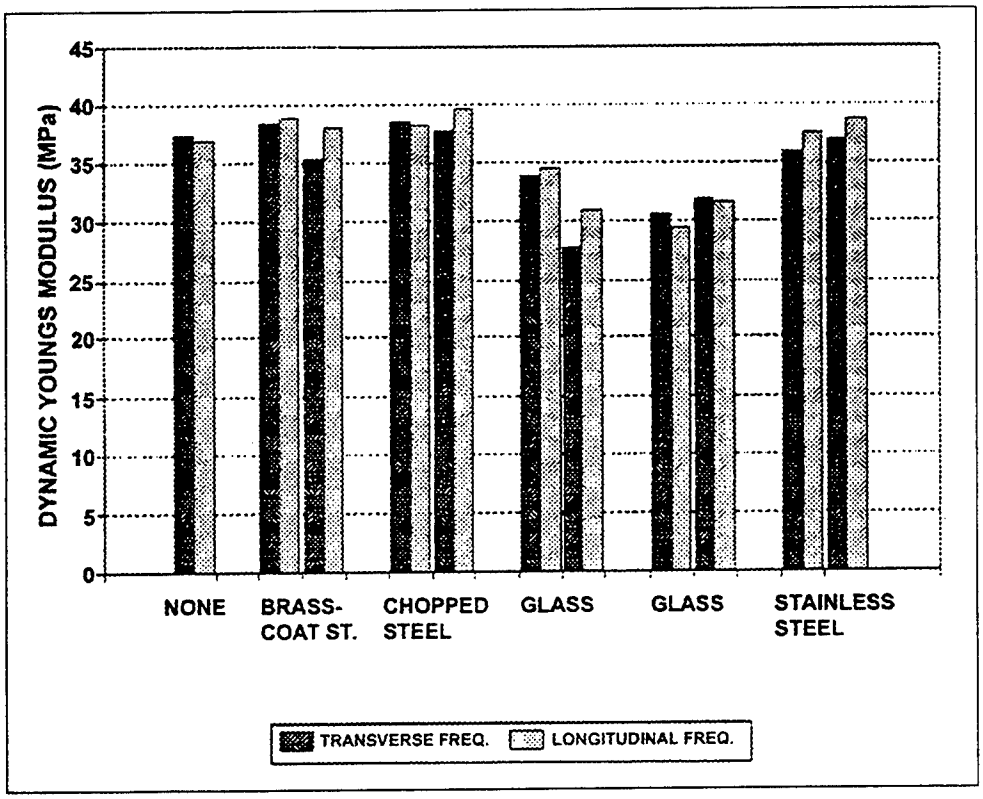


Figure 16. Dynamic Young's modulus of whole beams

**Table 7**
**Resonant Frequencies of Sawed Beams**

| Beam | Resonant Frequency (Hz) | | | | | | | Length (mm) | Mass (kg) |
|---|---|---|---|---|---|---|---|---|---|
| | Tansverse | | | | Longitudinal | | | | |
| | Top | Bottom | Comp. or Tens. | Neutral | Both Ends | Same End | Torsional | | |
| J1C | 1,581 | 1,594 | 931 | 919 | 2,994 | 2,956 | 1,356 | 673 | 38.6 |
| J1T | 1,613 | 1,606 | 3,931 | 913 | 2,963 | 2,983 | 1,356 | 673 | 39.4 |
| J3C | 1,700 | 1,706 | 1,000 | 1,000 | 3,088 | 3,088 | 1,438 | 642.5 | 40.3 |
| J3T | 1,694 | 1,688 | 956 | 969 | 3,063 | 3,063 | 1,375 | 642.5 | 40.4 |
| K1C | 1,800 | 1,788 | 1,056 | 1,056 | 3,238 | 3,238 | 1,781 | 635 | 38.1 |
| K1T | 1,731 | 1,731 | 1,025 | 1,025 | 3,144 | 3,144 | 1,719 | 635 | 39.0 |
| K3C | 1,588 | 1,575 | 956 | 950 | 3,019 | 3,013 | 1,575 | 673 | 40.4 |
| K3T | 1,588 | 1,569 | 2,281 | 3,894 | 3,025 | 3,031 | 1,388 | 673 | 41.3 |
| M1C | 1,813 | 1,800 | 1,063 | 1,069 | 3,219 | 3,219 | 1,469 | 622.3 | 38.2 |
| M1T | 1,794 | 1,800 | 1,094 | 1,081 | 3,194 | 3,194 | 1,819 | 622.3 | 38.1 |
| M3C | 1,719 | 1,719 | 1,025 | 1,019 | 3,181 | 3,163 | 1,719 | 647.7 | 40.2 |
| M3T | 1,719 | 1,719 | 1,013 | 1,013 | 3,150 | 3,150 | 1,706 | 647.7 | 40.2 |
| N1C | 1,594 | 1,588 | 956 | 956 | 2,950 | 2,931 | 3,181 | 660.4 | 39.0 |
| N1T | 1,594 | 1,575 | 1,006 | 988 | 3,006 | 2,988 | 1,588 | 660.4 | 39.1 |
| N3C | 1,888 | 1,888 | 1,206 | 1,206 | 3,325 | 3,331 | 1,613 | 591.8 | 34.8 |
| N3T | 1,956 | 1,938 | 1,181 | 1,169 | 3,313 | 3,313 | 1,913 | 591.8 | 34.8 |
| O1C | 1,456 | 1,444 | 3,556 | 3,350 | 2,763 | 2,750 | 1,281 | 685.8 | 39.0 |
| O1T | 1,406 | 1,413 | 3,537 | 3,512 | 2,731 | 2,713 | 1,281 | 685.8 | 39.0 |
| O3C | 1,669 | 1,694 | 969 | 969 | 3,063 | 3,063 | 1,400 | 635 | 36.4 |
| O3T | 1,694 | 1,700 | 1,019 | 1,019 | 3,063 | 3,044 | 1,425 | 635 | 36.3 |
| P1C | 1,813 | 1,819 | 1,113 | 1,100 | 3,300 | 3,281 | 1,819 | 617.2 | 38.2 |
| P1T | 1,838 | 1,838 | 1,081 | 1,100 | 3,256 | 3,256 | 1,500 | 617.2 | 38.2 |
| P2C | 1,869 | 1,856 | 1,188 | 1,181 | 3,356 | 3,356 | 1,900 | 609.6 | 38.0 |
| P2T | 1,763 | 1,781 | 1,081 | 1,075 | 3,231 | 3,244 | 3,244 | 609.6 | 38.0 |

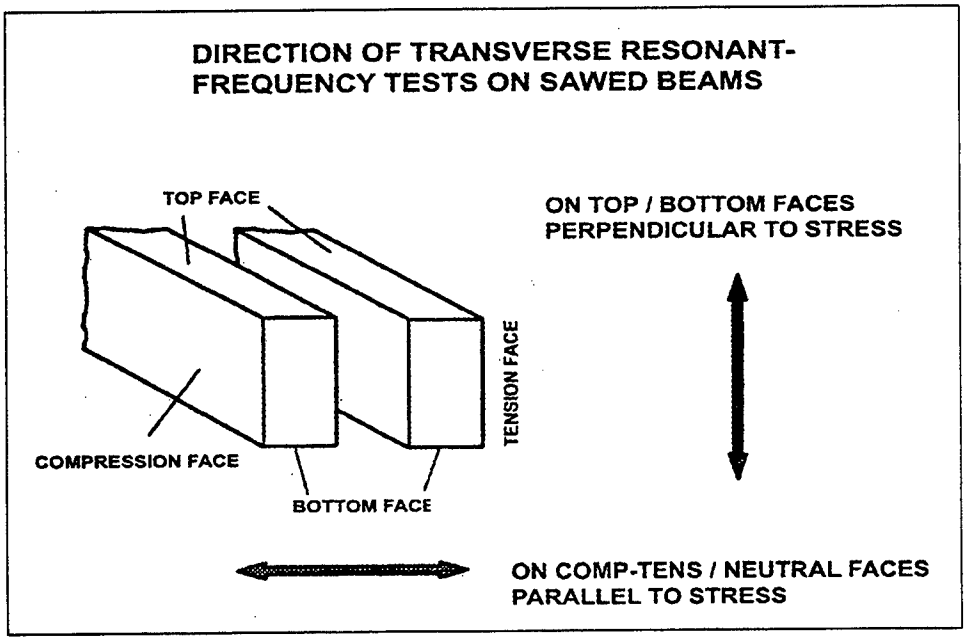


Figure 17. The direction of transverse-resonant-frequency measurements on the sawed beams

flexural-toughness measurements. Similarly, resonant-frequency measurements taken on the previous tension or compression face and the now exposed neutral axis are parallel to the direction of stress.

For individual beams, there was no significant difference between transverse resonant-frequency measurements of the top and bottom (T-B) faces, and all the measurements on these faces were in the expected range. However, four of the transverse-resonant frequencies taken on the previous compression or tension and neutral axis faces (T/C-N) of beams J1T, K3T, O1C, and O1T were well above the expected range.

The dynamic moduli of elasticity calculated from the transverse-resonant frequencies of the T-B faces agreed well with the values calculated from C/T-N faces as long as the fundamental frequency was in the true or expected range (Figure 18).

In the comparison of whole and sawed-beam results there was less than a 3-percent difference between the dynamic Young's modulus (from the average top/bottom face transverse and longitudinal resonant frequencies), even though the sawed beams had been previously stressed to failure in the first series of flexural-toughness measurements (Figure 19). Again, the steel-fiber-reinforced beams (mixtures K, M, and P) had the highest moduli values and the glass-fiber-reinforced beams (mixtures N and O) had the lowest.

### Scanning electron microscope results

All mixtures and fiber types displayed a peak concentration of magnesium (5 to 14 percent weight Mg) at or next to the surface of the beam, which declined quickly to an average of approximately 2 percent, within 1 mm of depth into the beam. A typical plot of scanning results is shown in Figure 20, while all plots are presented in Appendix J. In the figure and the appendix, all elemental concentrations are expressed as oxides.

Mixtures with no fibers (J) as well as the brass-coated and chopped-steel-fiber mixtures (K and M) displayed the greatest surface concentrations of magnesium while the stainless steel-fiber mixture (P) and glass-fiber mixtures (N and O) had lower surface concentrations. All six mixtures displayed a reduction in calcium (Ca) concentration near the surface (Figure 21). Additionally, any change in calcium concentration appeared to be mirrored by an opposite change in silicon (Si) concentration for the chopped-steel-fiber- (mixture M), glass-fiber- (mixtures N and O), and stainless-steel-fiber- (mixture P) reinforced beams.

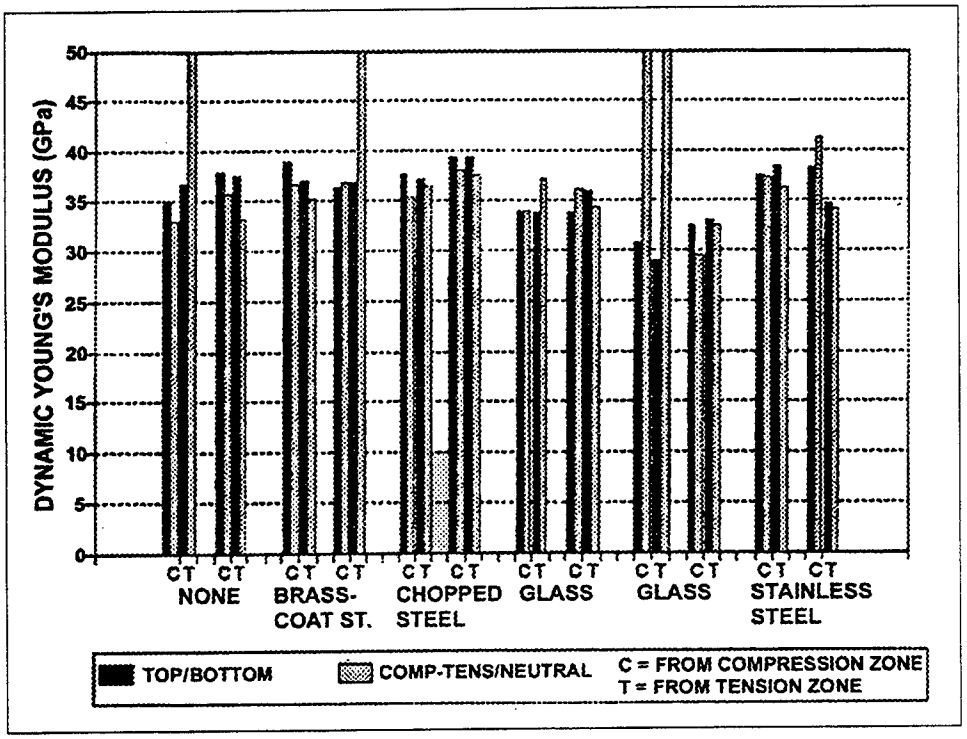


Figure 18. Comparison of dynamic Young's modulus from average top/bottom and compression-tension/neutral face transverse-resonant frequency

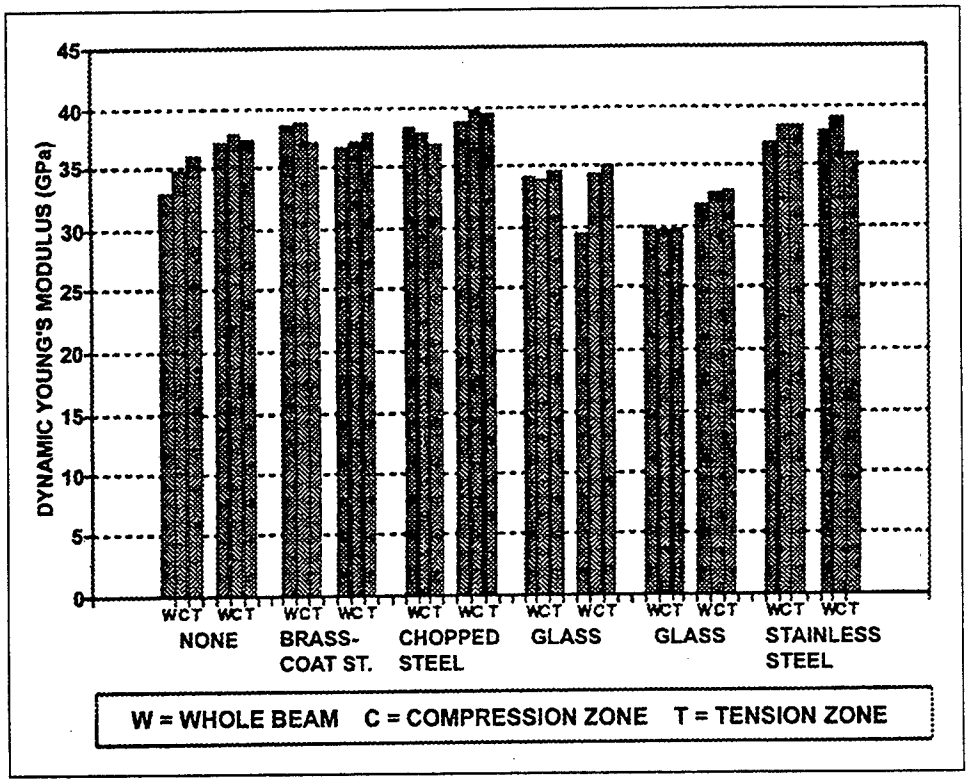


Figure 19. Comparison of dynamic Young's modulus of whole and sawed beams

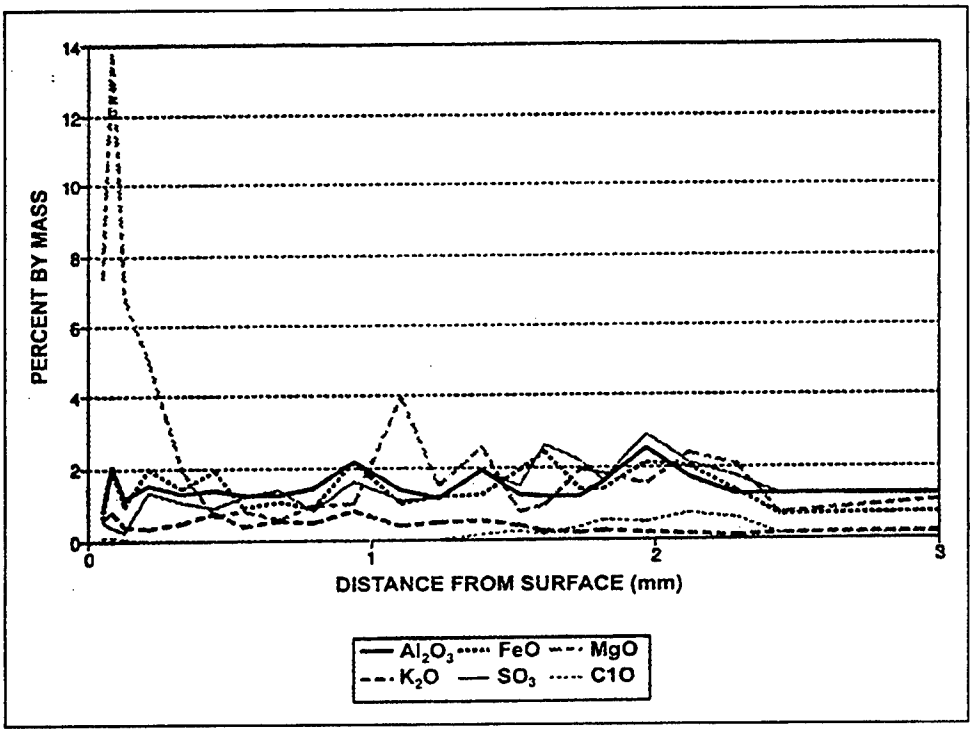


Figure 20. Electron microscope scan results for brass-coated steel-fiber-reinforced beam K-1

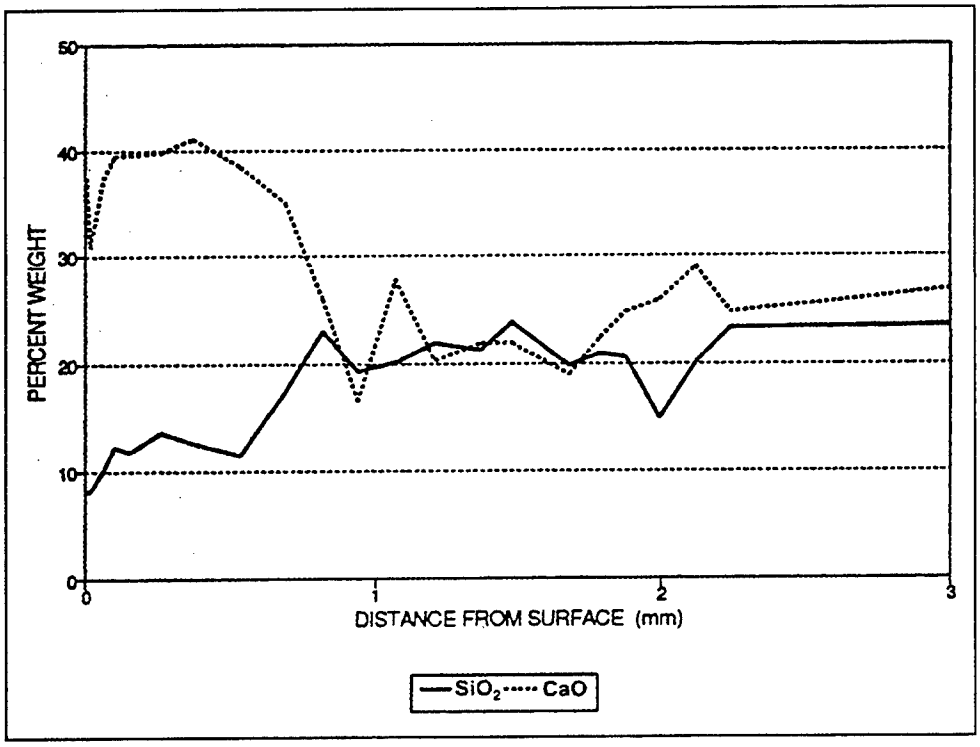


Figure 21. Electron microscope scan results for glass-fiber-reinforced beam O-3

# 4 Discussion

## Remaining Load on the Beams

The load on the beams at the time they were removed from the exposure station was recorded at 5.4 kN (1,200 lbf) which was only 55 percent of the original 9.65-kN (2,170-lbf) loading which was maintained on the beams for the first 10 years of their exposure. Subsequent to 1985, the load was no longer maintained due to deterioration of the mild-steel springs of the loading yokes. While relaxation of the intended loading reduces the stress level, the beams were still under tensile load for 18 years. Since all beams experienced approximately the same level of stress while the load was maintained and they all had approximately the same remaining load just before removal from the exposure station, the reduction in load in the last 8 years affected all beams similarly and should not be a major detriment to the study.

## Effect of Air Entrainment

The rapid deterioration of all beams which had less than 3 percent air content indicates that the use of fiber reinforcement does not minimize the need for proper air entrainment to ensure freezing and thawing resistance. After 7 years of exposure, the two beams with the lowest air content which were still surviving were the two glass-fiber beams from mixture N with 3.6 percent entrained air. These glass-fiber beams survived the full 18 years; however, they suffered greater general deterioration than all other remaining beams which had air contents between 7.0 and 8.5 percent. This was an indication that the minimum air content desired in this type of environment is greater than 3.6 percent. The higher cement content in the glass-fiber beams may have also contributed to their 18-year longevity with only 3.6 percent air. The two sets of glass-fiber beams (mixtures N and O) had 651 Kg/m$^3$ (1,100 lb/yd$^3$), where all other beams had only 467 Kg/m$^3$ (789 lb/yd$^3$).

### Visual evaluation of the beams

With respect to position of a face during exposure, in most cases, the bottom face of the beam suffered the least deterioration since it was better protected from the elements. The tops of the beams tended to suffer more deterioration due to the greater relative exposure. Marine growths form on the beams between each

evaluation period, and the growth helps hold moisture in the pores of the concrete by blocking evaporative drying. Since the bottom surface is shaded from the sun more than the top surface, it would experience fewer wetting and drying cycles than the top.

The degree of deterioration on the tension faces was slightly greater than on the compression face. This is most likely due to freezing and thawing effects in the greater network of small cracks in the tension face created by the tensile load. While the compressive faces would have just as many voids and pore spaces, they would not have cracks from the applied loads.

Visual evaluation of the beams both before measurement and after revealed that the corrosion of the carbon-steel fibers in the beams was limited about a 2-mm depth below the surface after 18 years of exposure under sustained load. The alkaline environment of the concrete below several millimetres of depth was sufficiently high to prevent the chopped and brass coated mild steel fibers from corroding. The stainless steel did not corrode. As the concrete at the surface of these beams deteriorated, the stainless steel fibers were exposed but remained uncorroded. Instead, the surface was covered with needle-like stainless steel fibers which made the beams difficult to handle and to collect pulse velocity data. The use of stainless steel fibers in concrete with which people will come in contact should be avoided because of this sharp-protrusion condition.

### Pulse-velocity evaluation of the beams

The pulse-velocity data taken over the 18 years of exposure did not produce information that could be used to determine trends in deterioration of the beams with any level of confidence. Figures 5 through 8 show pulse velocities that increase and decrease from year to year. In most cases, at some point in the time-history of the beams the velocities increased rather than decreased, indicating that the condition of the beams was improving rather than deteriorating. Several explanations for the insufficiency of these data can be presented. Over the 18 years that data were collected, different technicians were used to collect the data. Variation in reading technique, placement of the transmitters and receivers on the beams, and differences in temperature and humidity surrounding the beams at the time of reading could have produced great variation in the readings.

One other possibility for the increase in velocities could relate to increased strength of the concrete as time progressed. Percent $V^2$ data are given as a percentage of the initial pulse-velocity reading. This initial reading is taken when the concrete is less than 1 year old. As the concrete matures and gains strength over the years, pulse-velocity readings could have increased with the increasing strength of the concrete. This could offset some of the deterioration due to weathering and help to give false readings.

The beams with the lowest air contents showed the most rapid decrease in $\%V^2$ as a result of increased deterioration due to lower resistance to freezing and thawing. All beams with air content less than 3.6 percent failed and were removed from the

program within 7 years of exposure. Two of the glass-fiber-reinforced beams with marginal entrained air (mixture N, beams N-1 and N-3) showed a pulse-velocity trend which was slightly downward as time progressed. The photographs of the beams also showed these beams as the most deteriorated even though they had elevated cement contents.

Due to the scatter of the pulse-velocity readings taken over the exposure life of the specimens, no trends could be found in these data. To improve this condition, measurement procedures should be examined to determine if steps can be taken to reduce the variability in data gathering technique. Evaluations of the deterioration of the beams should be made from the other measurements and observations of the beams.

# Flexural Measurements

## Whole-beam measurements

The importance of monitoring the deflection of the supports as well as the center line during the flexural loading sequence was noted by the magnitude of the support movement. Figure 22 shows a representative graph of the raw data. This figure shows one of the glass-fiber mixtures which broke in a brittle manner after first crack but illustrates the magnitude of the end deflections. Deflections of the end supports were often on the order of 60 to 70 percent of the measured center-line deflection due to the relatively massive and stiff nature of the beams.

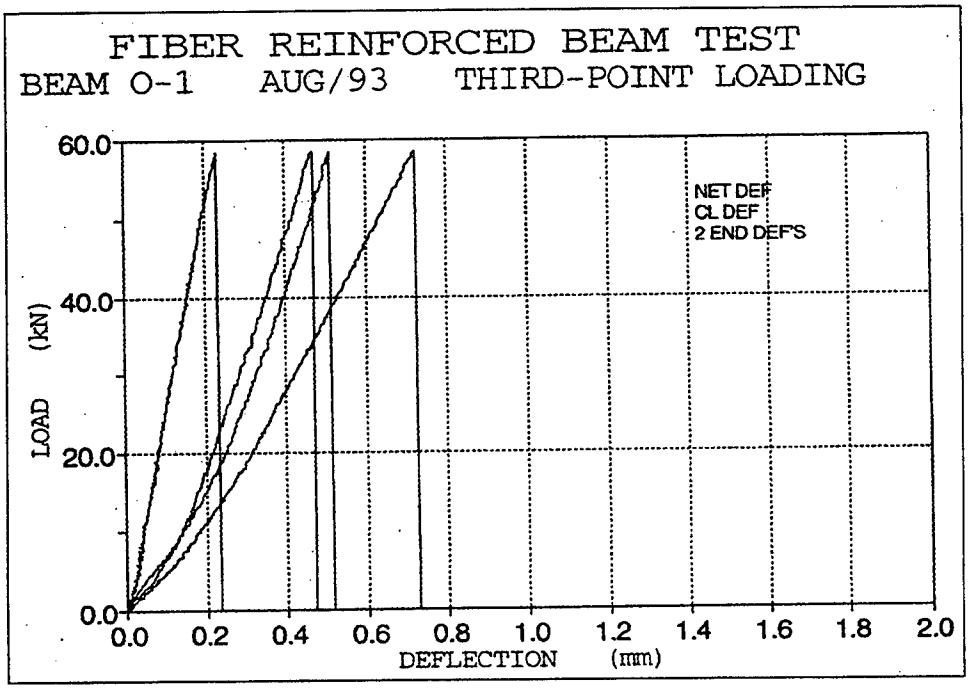


Figure 22. Load-deflection graph of whole-beam third-point flexural failure showing center-line and support-point deflections

Reference to Figure 9 shows that the carbon-steel-fiber mixtures provided greater first-crack strength, first-crack toughness, and flexural modulus than the glass-fiber mixtures or the control. The best performance was from the 25-mm (1-in.) chopped-steel fibers. All other parameters being considered equal, the first-crack strength and first-crack toughness results reflect the ability of the fibers to distribute the tensile load in the concrete and to delay the onset of tensile cracking in the matrix. In the load-deflection curves of flexural-toughness evaluations, the load-carrying capacity up to first-crack strength is a function of the concrete tensile strength and the bond between the cement paste and the fibers. Both glass-fiber mixtures and the stainless-steel-fiber mixture had FCS approximately equal to the control with no fiber. The lowest FCS occurred in mixture N which had the lowest entrained air content of 3.5 percent which probably accounts for its low first-crack strength. The glass-fiber mixture O was 7 percent higher in FCS than the control. In all mixtures except the glass-fiber mixtures, the mixture parameters were kept the same. In the glass-fiber mixtures, the cement content was elevated. This 7-percent difference can probably be attributed to the increased cement content in these mixtures. The fact that the fibers did not improve the first-crack strength over the control with no fibers indicates that the bond between the fibers and the cement matrix was very small or absent. The bond between glass fibers and cement is weaker than that between steel and cement. The results of first-crack strength of the concrete with stainless-steel fibers is of interest since there are very few published data on concrete made using these fibers.

The beams containing 19-mm (3/4-in.) brass-coated steel fibers had an average FCS of 6.13 MPa (889 psi), while the beams with 25.4-mm (1-in.) chopped-steel fibers achieved an average of 6.56 MPa (951 psi) at first crack. These represented 35- and 44.5-percent increases over the control. The chopped-fiber beams were 7 percent greater than the brass-coated-fiber beams.

Their first crack strengths indicate that the presence of these fibers controlled the initial cracking of the concrete much better than the glass or the stainless steel fibers. Perhaps the explanation of the additional 7-percent increase in FCS of the chopped fiber compared to the brass-coated steel fibers can be related to the length of the fiber. The chopped-steel fibers are 33 percent longer than the brass-coated steel fibers and can distribute the stresses away from a potential crack plane better than the shorter fibers. Additionally, the cross-sectional area of the chopped-steel fibers is also larger than the brass-coated steel by 9.4 percent. For a given load, the stress on the chopped-steel fiber would be less than on a brass-coated fiber.

The control beam failed instantly at first crack, since it had no fibers to prolong the ultimate failure. However, the two glass-fiber mixtures also failed instantly at first-crack strength. This again indicates the low or absent bond between the fiber and paste matrix. Of the three mixtures which had some postcrack toughness, the stainless-steel and the brass-coated-fiber mixtures out performed the chopped-steel fibers even though the chopped-steel-fiber mixture had the highest first-crack strength and toughness. The amount of postcrack toughness is an indication of the tortuosity of separating the debonded fiber from the matrix. If the surface of the fiber breaks smoothly from the paste and the fiber is straight, the chore of pulling the fiber out of the matrix will be easy. If there is paste bonded to the fiber or the

path is not straight, there will be additional energy required to pull the fiber from the matrix. The most likely explanation for these results is that the chopped-steel fibers debonded from the paste in a smooth manner while some paste stuck to the surface of the brass-coated and stainless-steel fibers. Observations of the surface condition of the fibers after the beams broke were not made in this study; however, research (Chan and Li 1997) has shown that a brass coating on steel fibers produces a debonding in the matrix rather than at the fiber/paste interface.

### Sawed-beam measurements

The series of flexural measurements on the sawed beams had some unexpected results when no difference was found between the first-crack strength of zones previously in tension and in compression. It had been hypothesized that microcracking in beams taken from the tension zone of the first series of measurements would have reduced the flexural strength and toughness to a level less than beams taken from the compression zone. However, this was not the case.

One possible explanation for this outcome is that the beams evaluated in the second series of measurements were from an area of the beam which had not been stressed to the point of producing microcracks or had cracking which was not severe enough to make a difference in the FCS or toughness in the second series of measurements. The data from Table F-1 in Appendix F and summarized in Figure 11 show that the FCS results of previous compression zone beams and previous tension zone beams are nearly the same and their differences are attributable to data scatter.

In general, the second series beams had higher FCS than the first series and all second series beams that did not have brittle failure (mixtures K, M, and P) had higher toughness indices and residual strength factors than the whole beams. This improved postcrack toughness may be attributed to the fact that the beam depth of the second series was only one-half that of the whole beams and therefore the ratio of length of the fiber to the depth of beams was greater.

Similarly, it was expected that the previously exposed and stressed faces would have lower FCS and toughness than those that had been at the neutral axis. Most measurement results indicated that the exposed faces had a larger modulus of rupture or first-crack strength greater than the previous neutral axis face.

## Compression and Tension Measurements

The compressive strength of all mixtures was very high. No significant difference was found among any of the mixtures which contained fiber reinforcement as they all measured between 51.1 and 55.4 MPa (7,410 and 8,030 psi). The absence of fiber reinforcement did appear to reduce the compressive strength as the plain concrete mixture had an average compressive strength of 41.9 MPa (6,078 psi) 20 percent lower than the average compressive strength of fiber-reinforced mixtures. However, it is not certain that the absence of

fibers is the controlling cause of this long compressive strength. The glass-fiber beams with the highest average compressive strength were from mixture N which had the 3.6 percent air content. The low air content apparently did not reduce its compressive strength.

The indirect-tensile strength of the concrete cores was on average 10.6 percent of the compressive strength. The brass-coated steel, chopped-steel and nonfiber-reinforced cores had above average percent tensile strength (11.4 percent to 13.2 percent), while the glass-fiber-reinforced cores were below average (5.7 percent to 9.6 percent). The actual tensile strengths agreed well with the first-crack strength results from the flexural toughness results both in magnitude and in ranking of the fiber type. Both series of measurements showed the beams with the chopped-steel fibers were strongest followed closely by the brass-coated steel fibers. Similarly, the glass-fiber and nonfiber reinforced beams had the lowest results in both measurements. These results help validate the usefulness of the alternative-tensile-evaluation method of obtaining tensile strength of concrete.

## Resonant-Frequency Measurements

### Whole-beam measurements

The resonant-frequency measurements revealed a number of valuable results. The fact that the transverse frequencies were nearly the same regardless of the face on which the measurement was taken indicates that the beams were in good condition with no localized deterioration that might affect the fundamental frequency. This was additionally reinforced with the results of the longitudinal frequencies being the same regardless of the location of the accelerometer and hammer.

Dynamic Young's modulus of elasticity (E) values were determined for both transverse and longitudinal frequencies. These values were given in Table 6. The moduli calculated in this manner were higher than those determined from the flexural toughness measurements. However, this difference is expected when using dynamic methods to determine moduli of elasticity. The ranking of the moduli of the mixtures remained essentially the same regardless of the type of method used in the calculations. The steel-fiber mixtures had the highest moduli followed by the control with the glass-fiber mixtures having the lowest modulus.

The modulus of rigidity, G, for each mixture was calculated from the torsional-frequency measurements. These values followed the ranking found for the dynamic Young's modulus with the chopped-steel-fiber mixture having the highest modulus and the glass mixture with the 3.6 percent entrained air having the lowest. Dynamic Poisson's ratio was also calculated using these data. No trend among mixtures using the various fiber types was visible from the Poisson's ratio results; however, the average value was 0.23 which was well within the expected range.

## Sawed-beam measurements

The transverse resonant-frequency measurements taken on the sawed-beam series clearly showed the effect of stress from the whole-beam flexural-toughness measurements. By using a RION signal analyzer, the response of each beam over a broad spectrum of frequencies was plotted (see Appendix I). These plots enabled a visual comparison to be made between the transverse resonant frequencies taken on the previous tension or compression faces (parallel to the bending stress direction) and the transverse frequencies taken on the top or bottom faces (perpendicular to the bending stress).

The plots of the amplitudes of the transverse vibrations over a wide range of frequencies showed multiple secondary peaks on the T/C-N faces, even if the transverse resonant frequencies were within the expected range. When a comparison was made of the frequency plots of the T-B faces (perpendicular to previous stress) and the T/C-N faces (parallel to the previous stress), in 20 out of 24 cases the T/C-N faces had far more irregular plots containing secondary peaks as a result of the previous stress (compare Figures 23 and 24). Multiple secondary peaks in the frequency data are found, as well as greater background vibrations across the spectrum in relation to fundamental frequency when the readings were taken parallel to the previous stress direction. No visible cracks were found on any of these beams.

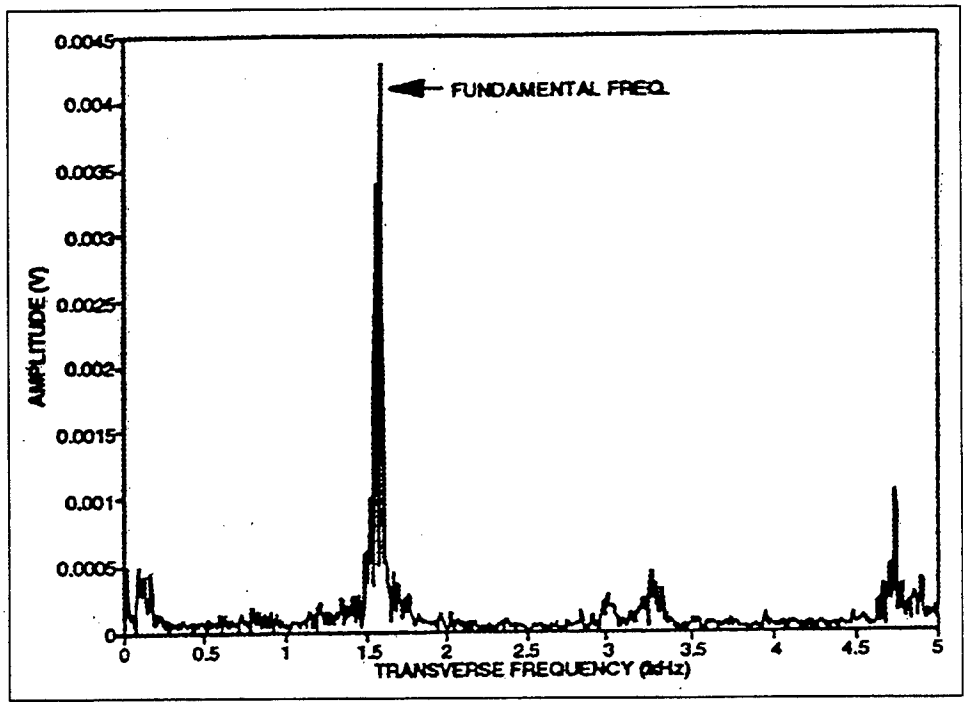


Figure 23. Frequency response of the top/bottom faces of beam K3C which were perpendicular to the direction of bending in flexural-toughness measurements

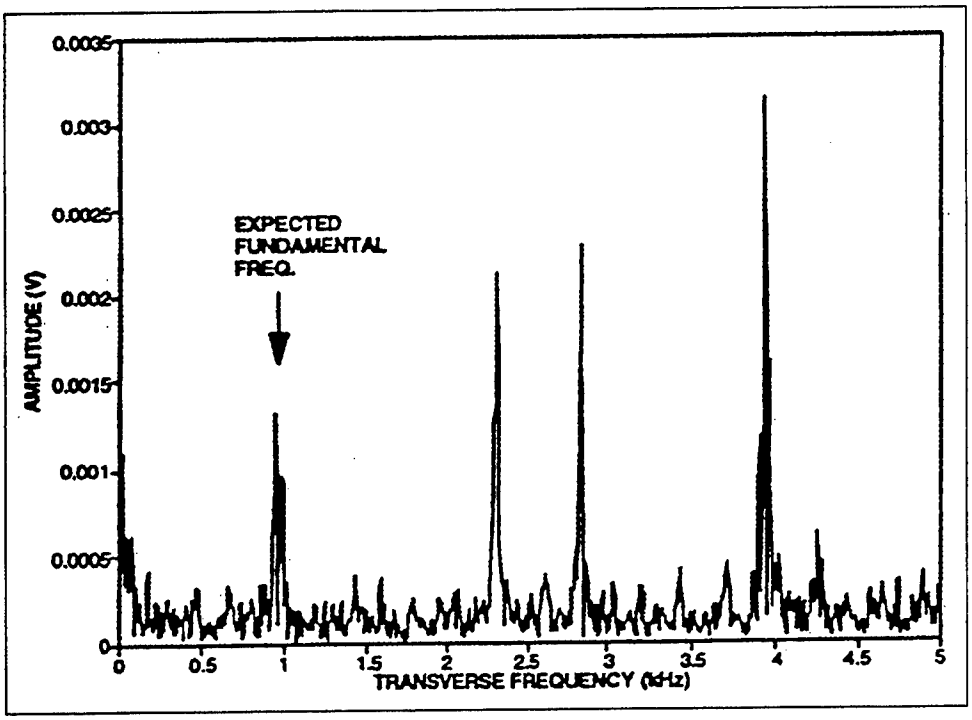


Figure 24. Frequency response of the tension-compression/neutral faces of beam K3C which were parallel to the direction of bending in flexural-toughness measurements

Although it was not the purpose of this investigation to do so, these results indicate that resonant-frequency plots can be used to examine not only the condition of a concrete beam but also the direction of stress which the beam may have undergone. Further investigation in this matter may result in the expanded use of resonant-frequency measurements as an investigative tool.

## Scanning-Electron Microscope

The X-ray analyzer could scan an area no smaller than 15 μm sq. Even at this small area, microscopic voids resulted in some variability in the total percent mass scanned by the electron microscope. However, the data collected were of interest concerning the reactions potentially formed and the depth to which these reactions were valid

The concentration of magnesium and reduction in calcium concentration near the surface of the beam is probably due to a reaction between the calcium hydroxide in the portland cement and the magnesium sulfate in the seawater. The reaction would produce magnesium hydroxide and calcium sulfate as follows:

$$Ca(OH)_2 + MgSO_4 \rightarrow Mg(OH)_2 + CaSO_4$$

The magnesium hydroxide is insoluble and would accumulate near the surface while the calcium sulfate is soluble and would be leached away over time.

The effects of any reactions between the constituents of the concrete and the seawater appear to be limited to about a 2-mm depth into the concrete as the mass percentages tend to a constant and lower percentage as the measurements are taken farther and farther away from the surface of the specimen.

# 5 Conclusions and Recommendations

## Conclusions

As documented by the rapid deterioration of all beams with less than 3 percent air, the use of fiber reinforcement in concrete does not reduce the need for air entrainment to resist the effects of freezing and thawing in concrete exposed to severe environments.

From the variability of the ultrasonic pulse-velocity measurement results over the years of exposure, drawing of any conclusions from these data regarding the relative performance of the different fiber types was not possible.

From the laboratory evaluations performed on the beams after being removed from the exposure station, it can be concluded that the chopped-steel and brass-coated-steel-fiber-reinforced concrete beams have greater flexural strength, toughness, modulus of elasticity, and indirect-tensile strength than glass-fiber, stainless-steel fiber-, and nonfiber-reinforced beams under sustained load in a severe marine environment.

From the resonant-frequency measurements conducted on the whole and sawed portions of the beams it can be concluded that the direction of stress does not appear to have an effect on the flexural strength or durability of fiber-reinforced concrete beams even when exposed to severe weathering. Similarly, the exposed surfaces of a beam do not appear to lose flexural strength when compared to the strength of the concrete at the neutral axis of the beam.

Resonant-frequency measurements which determine the response of a beam over a broad spectrum of frequencies can be used to determine the condition of a beam through discovery of its fundamental frequency, and it is believed that the technique can be used to determine the direction of major stress the beam may have undergone in the past.

From the results of the energy-dispersive X-ray analysis used in conjunction with the scanning electron microscope, it can be concluded that any microchemical reactions between the components of fiber-reinforced concrete and the seawater are limited to a depth of a few millimetres below the surface of the concrete. These

microchemical changes do not appear to have any detrimental effect on the durability and performance of the concrete under sustained load in a severe marine environment.

## Recommendations

For applications in a severe marine environment, carbon-steel-fiber reinforcement for concrete should be used in preference to glass-fiber, stainless-steel fiber, or no fiber reinforcement when improved flexural toughness, tensile strength, and/or compressive strength are desired.

Stainless-steel fibers should not be used in concrete in a severe marine environment where people will be in close proximity to the exposed surfaces. If the concrete deteriorates and leaves the fibers protruding from the surface, they become a hazard.

The use of a resonant-frequency signal analyzer as a tool for investigating the condition of concrete and its use in determining the effect of previous stress on concrete could be examined through further research.

# References


American Society for Testing and Materials. (1993). *1993 annual book of ASTM standards.* Philadelphia, PA.

a. Designation C 39-93a. "Standard test method for compressive strength of cylindrical concrete specimens."

b. Designation C 42-90. "Standard test method for obtaining and testing drilled cores and sawed beams of concrete."

c. Designation C 78-84. "Standard test method for flexural strength of concrete (using simple beam with third point loading)."

d. Designation C 215-91. "Standard test method for fundamental transverse, longitudinal, and torsional frequencies of concrete specimens."

e. Designation C 496-90. "Standard test method for splitting tensile strength of cylindrical concrete specimens."

f. Designation C 597- 83 (1991). "Standard test method for pulse velocity through concrete."

g. Designation C 1018-89. "Test method for flexural toughness and first-crack strength of fiber-reinforced concrete (using beam with third-point loading)."

Chan, V., and Li, V. C. (1997). "Effects of transition zone densification on fiber/cement paste bond strength improvement," *Journal of Advanced Cement Based Materials* 5(1), 8-17.

Clayton, N. (1978). "Fluid-pressure testing of concrete cylinders," *Magazine of Concrete Research* 30(102), 26-30.

Kosmatka, S. H., Panarese, W. C., et al. (1991). *'Design and control of concrete mixtures.'* 5th ed., Canadian Portland Cement Association, Ottawa, Ontario.

Porter, H. F. (1910). "Preparation of concrete from selection of materials to final disposition." *Proceedings of the National Association of Cement Users.* American Concrete Institute, Detroit, MI, Vol 6, p 287.

Richart, F. E., Brandtzaeg, A., and Brown, R. L. (1928). "A study of failure of concrete under combined compressive stresses," University of Illinois Engineering Experiment Station, Bulletin No. 185, Urbana, IL.

U.S. Army Engineer Waterways Experiment Station. (1960). "Investigation of performance of concrete and concreting materials exposed to natural weathering," Volume 1, Active investigations, with annual supplements, Technical Report No. 6-553, Vicksburg, MS.

# Appendix A
# Photographs of Beams at Treat Island

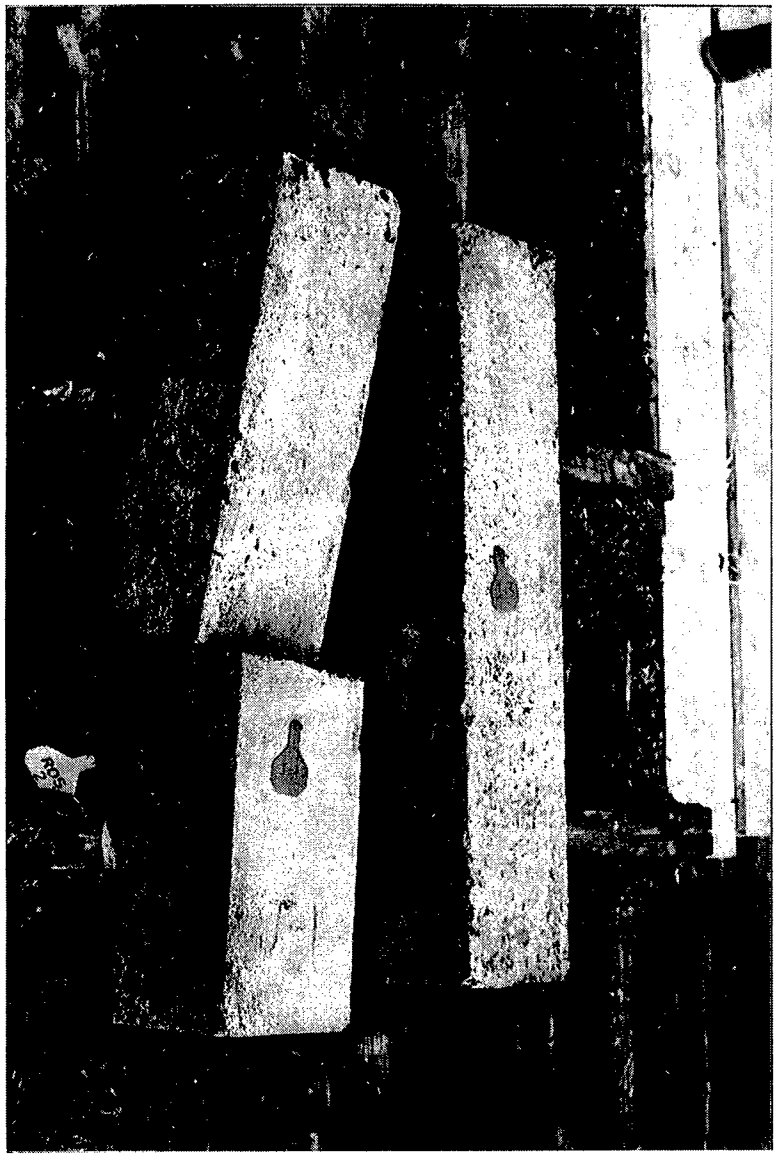

MIX J

MIX K

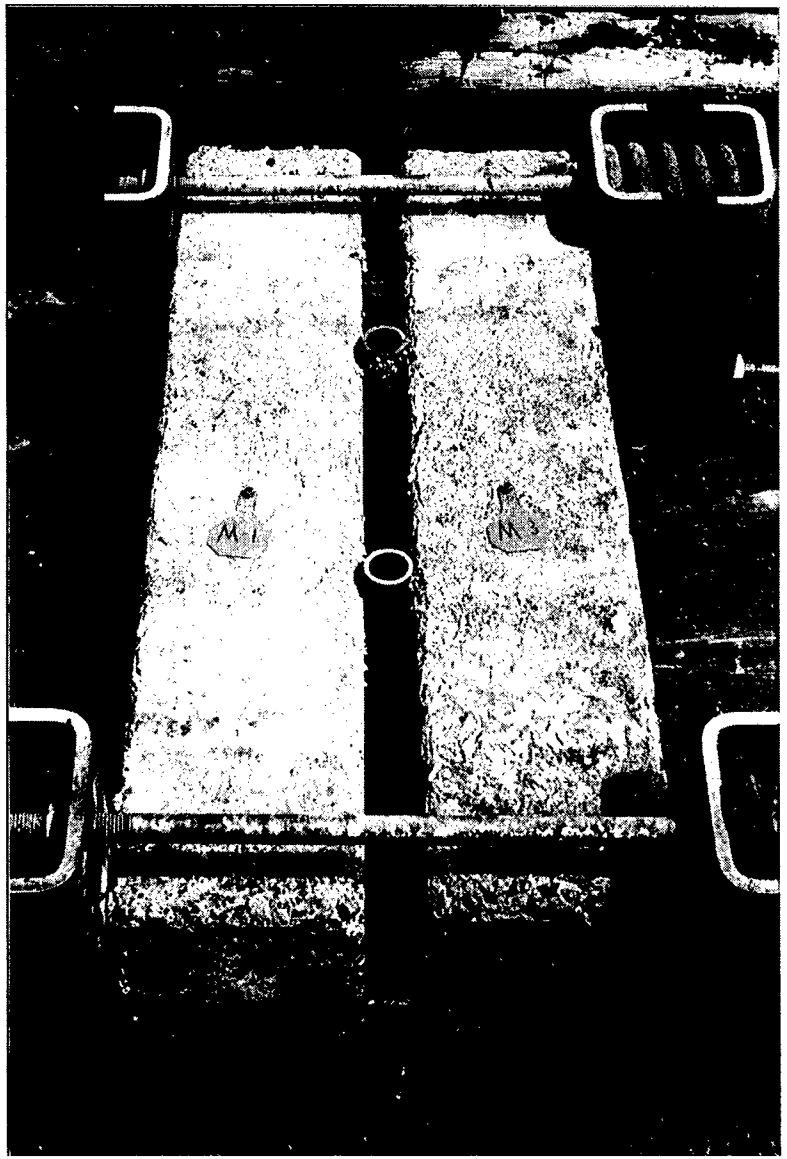


MIX M

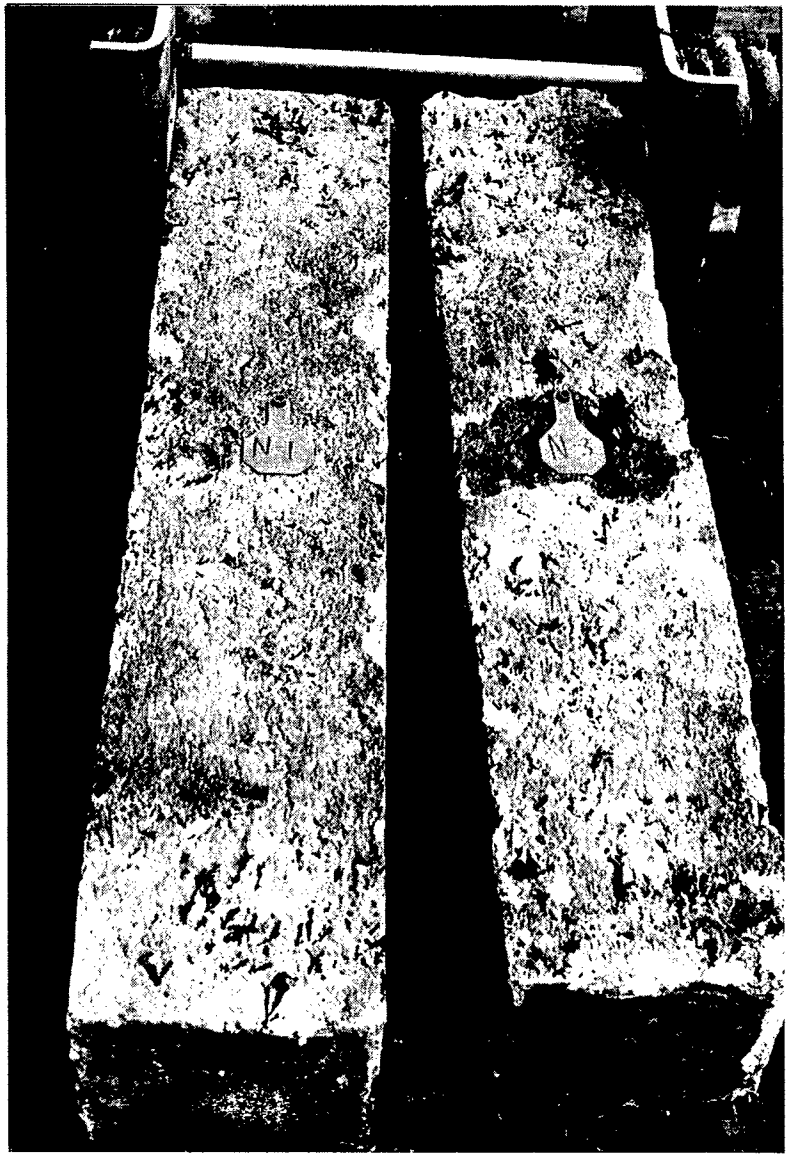


MIX N

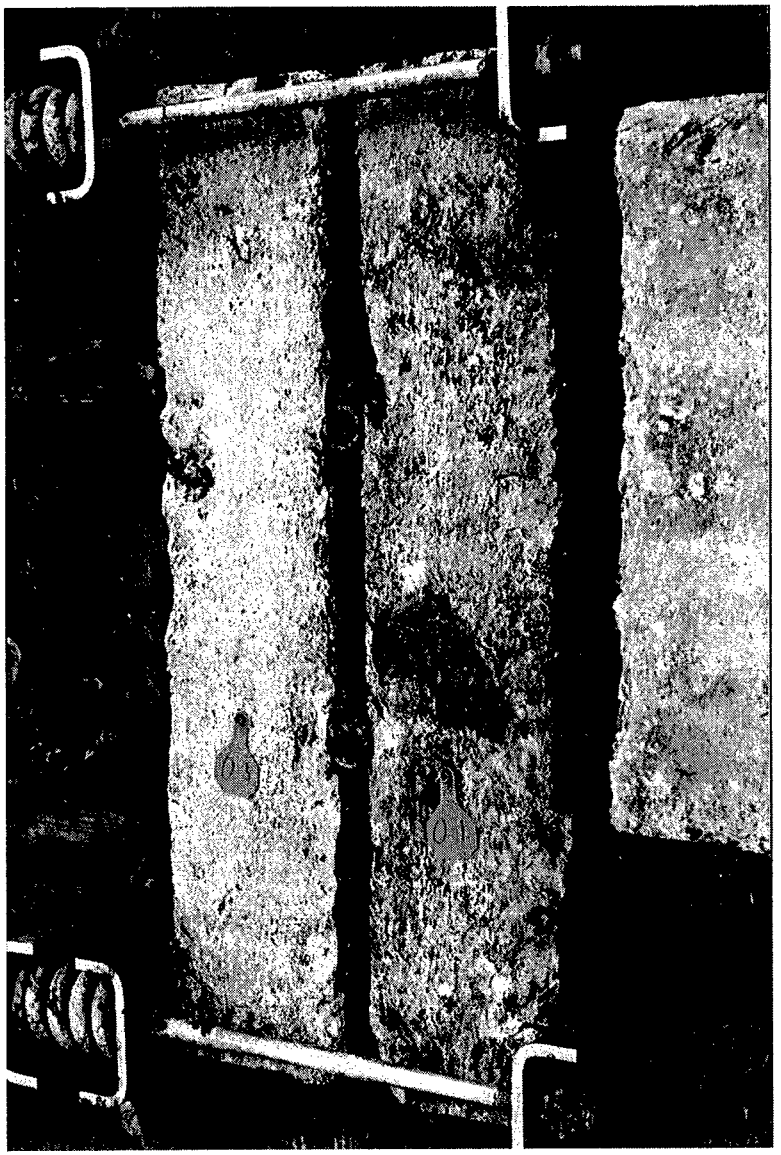

MIX O

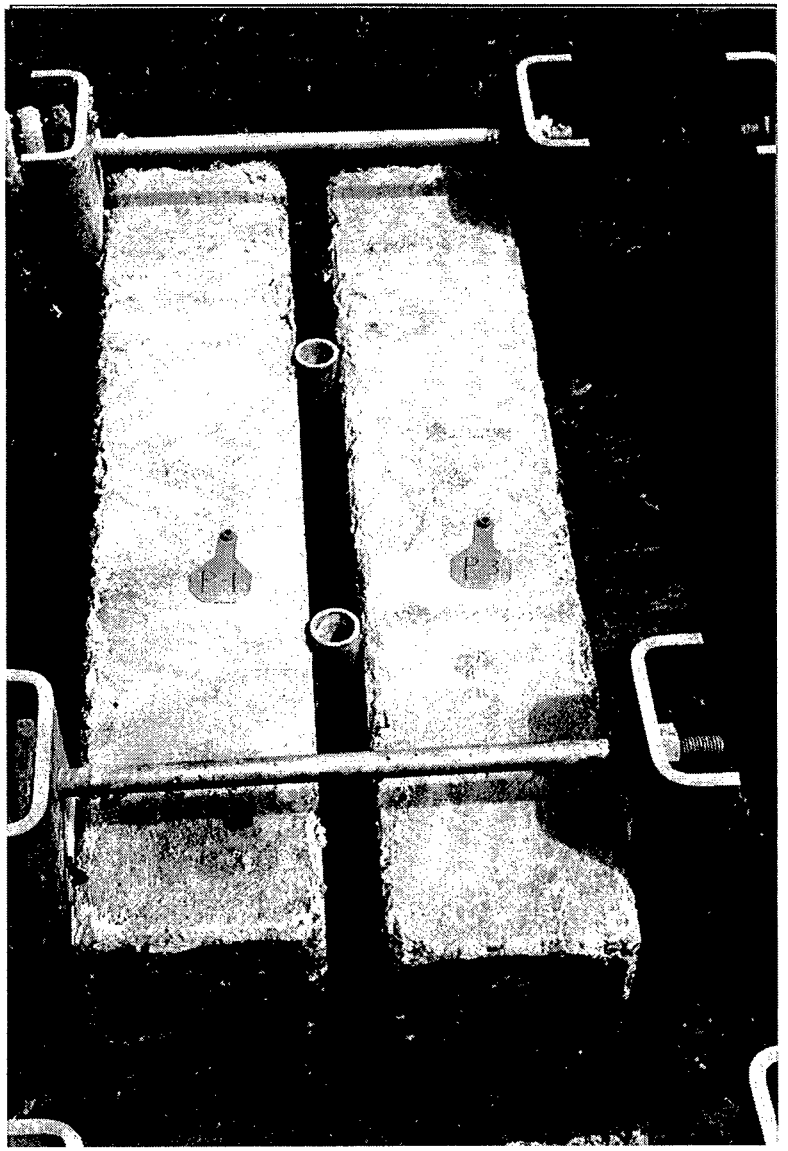

MIX P

# Appendix B
# Photographs of All Sides of Beams

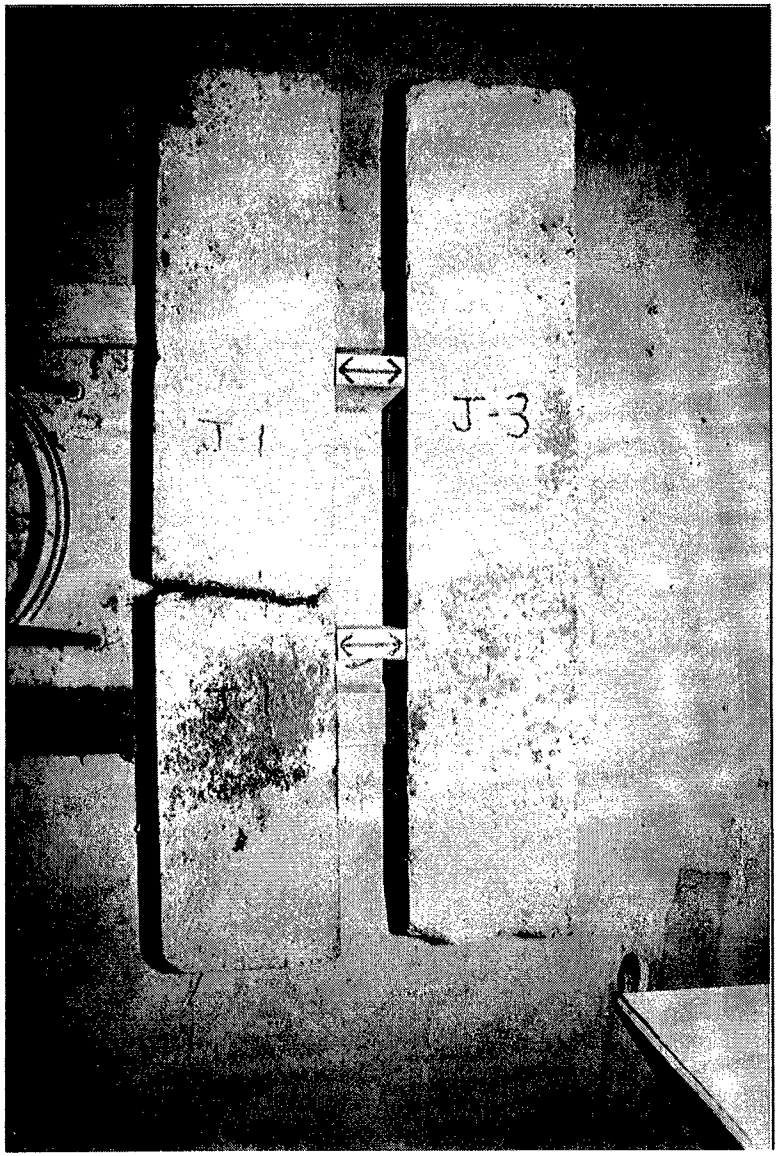


TOP

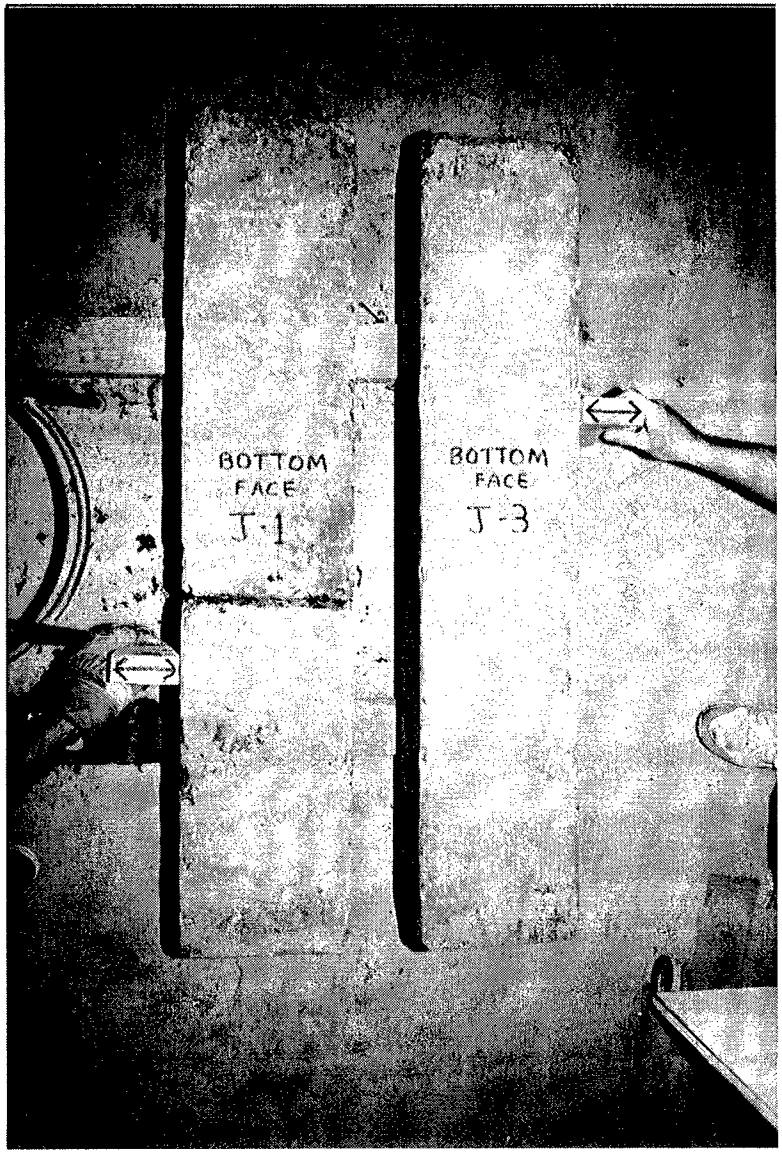


BOTTOM

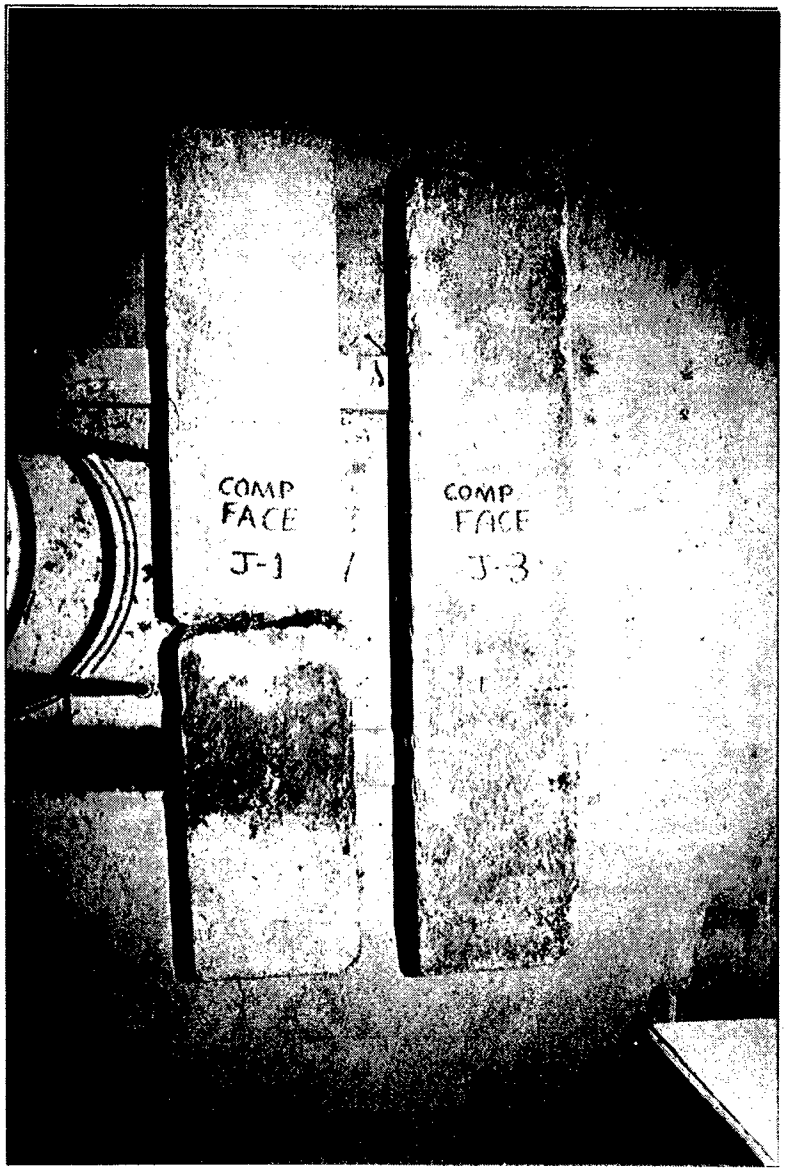


COMPRESSION


TENSION

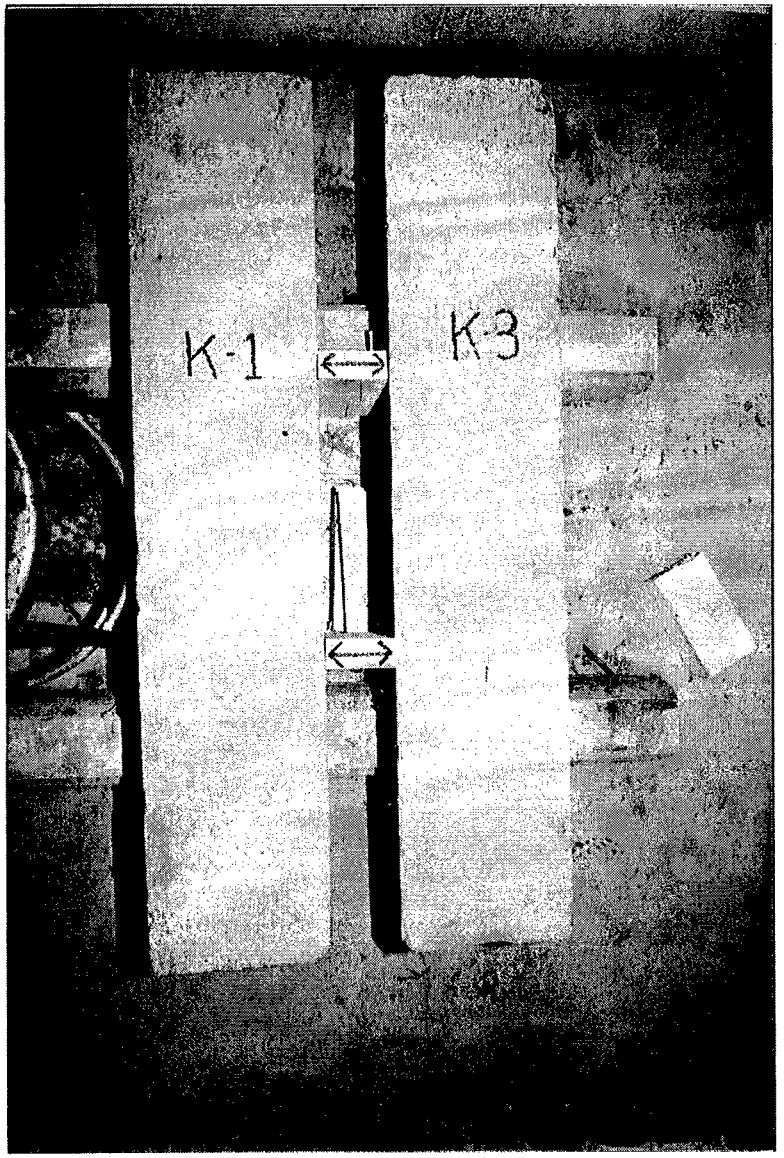


TOP

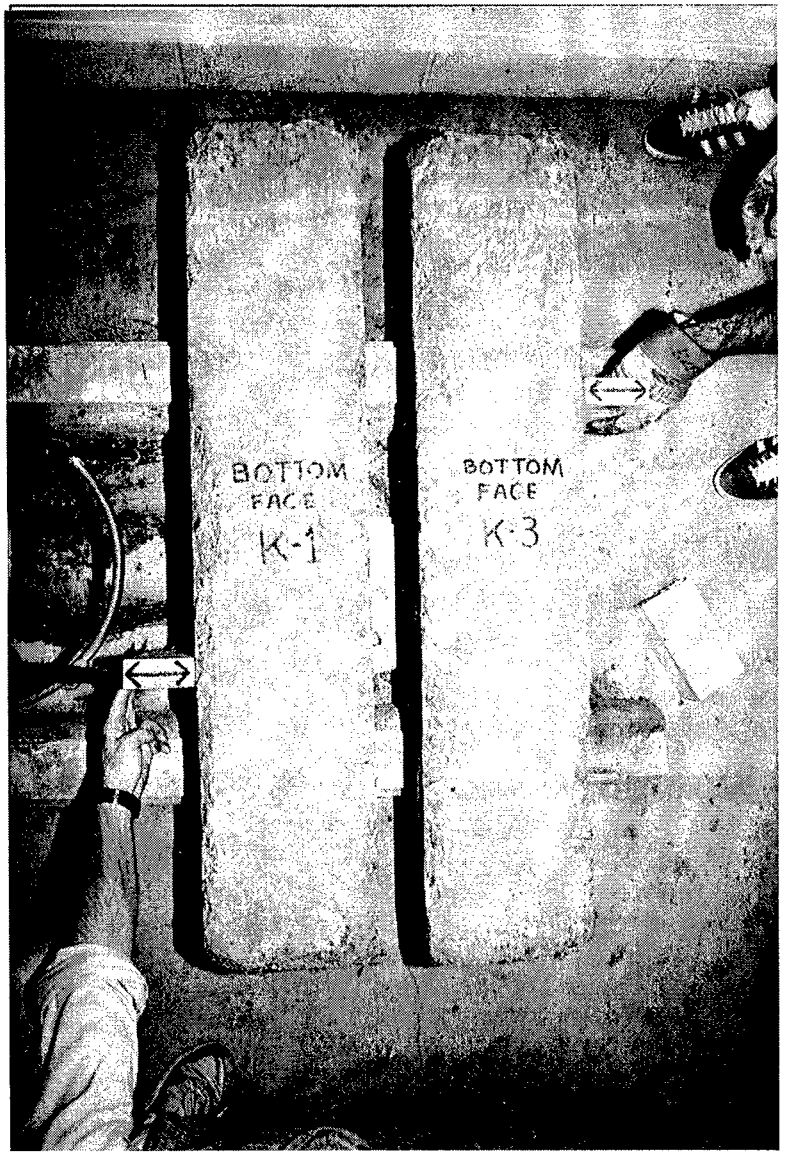


BOTTOM

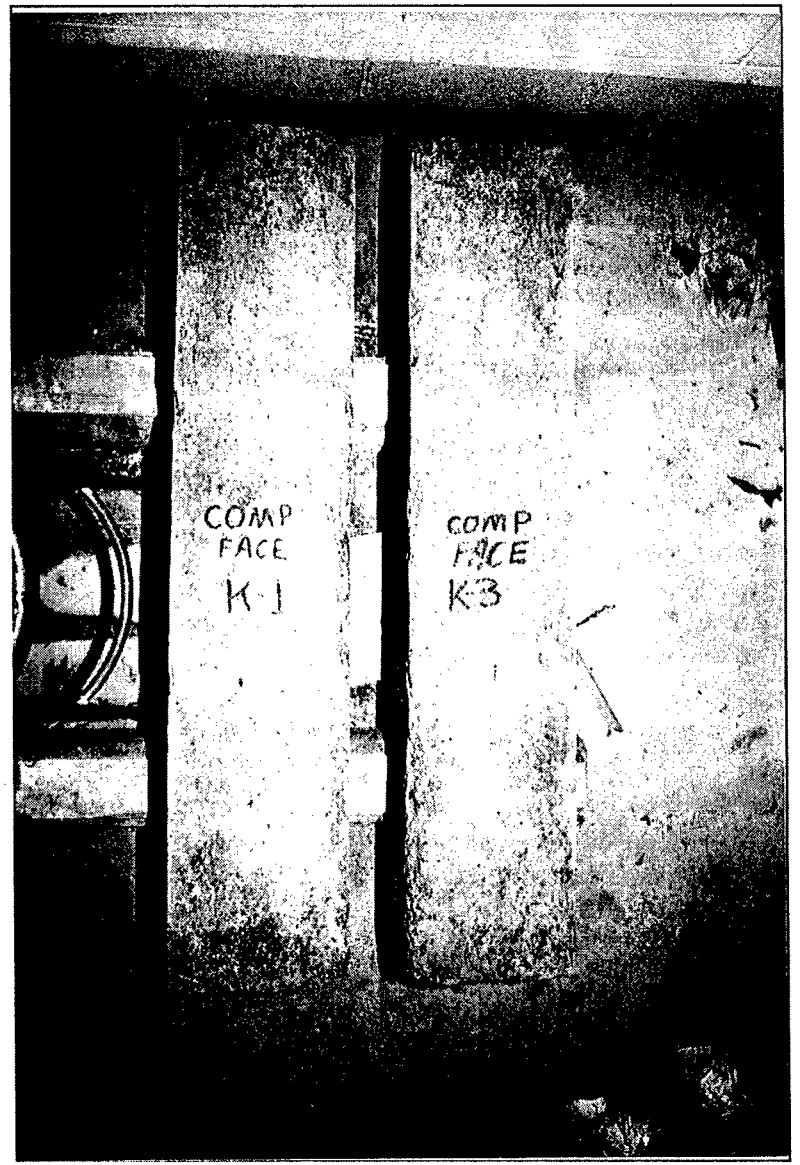


COMPRESSION


TENSION


TOP

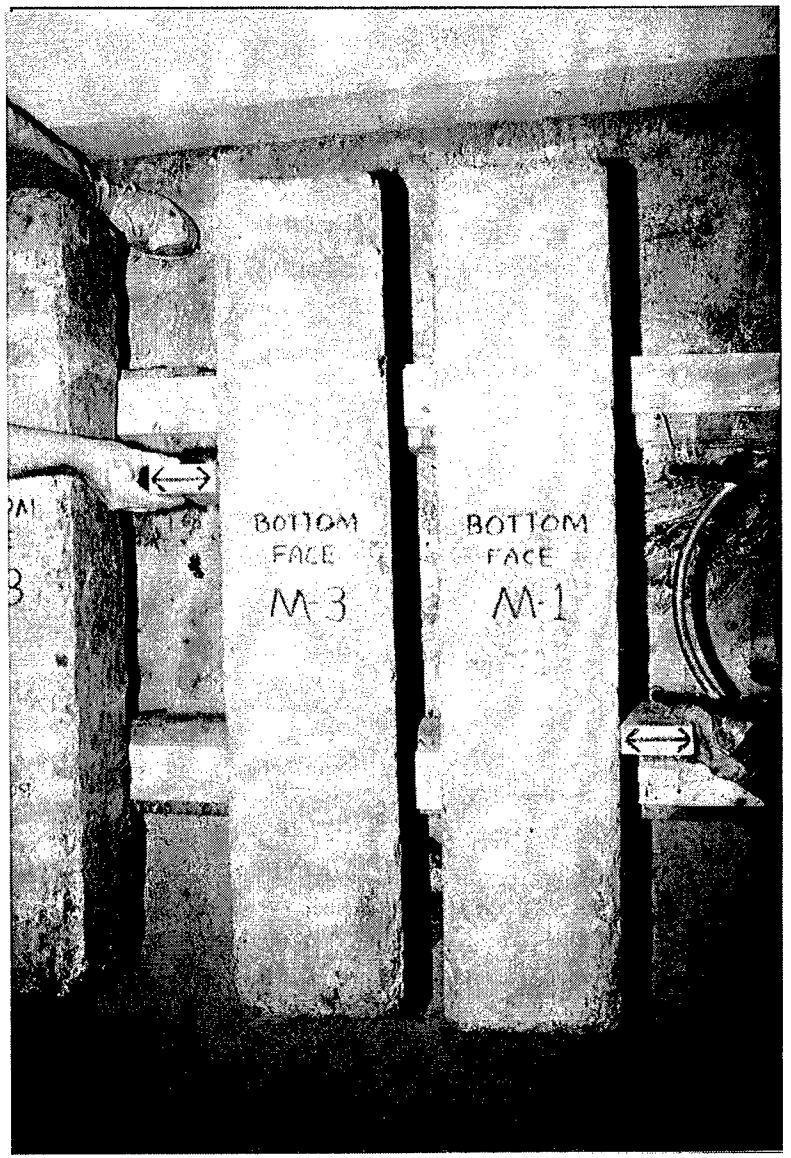


BOTTOM

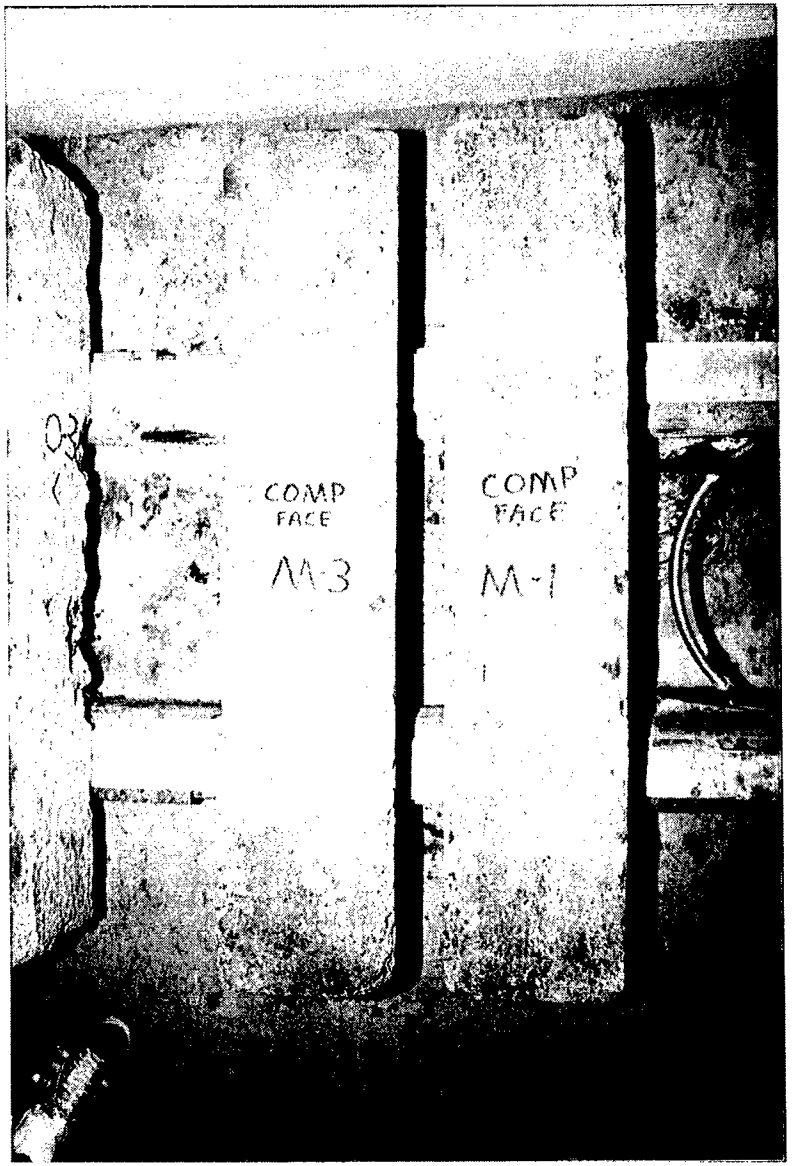


**COMPRESSION**

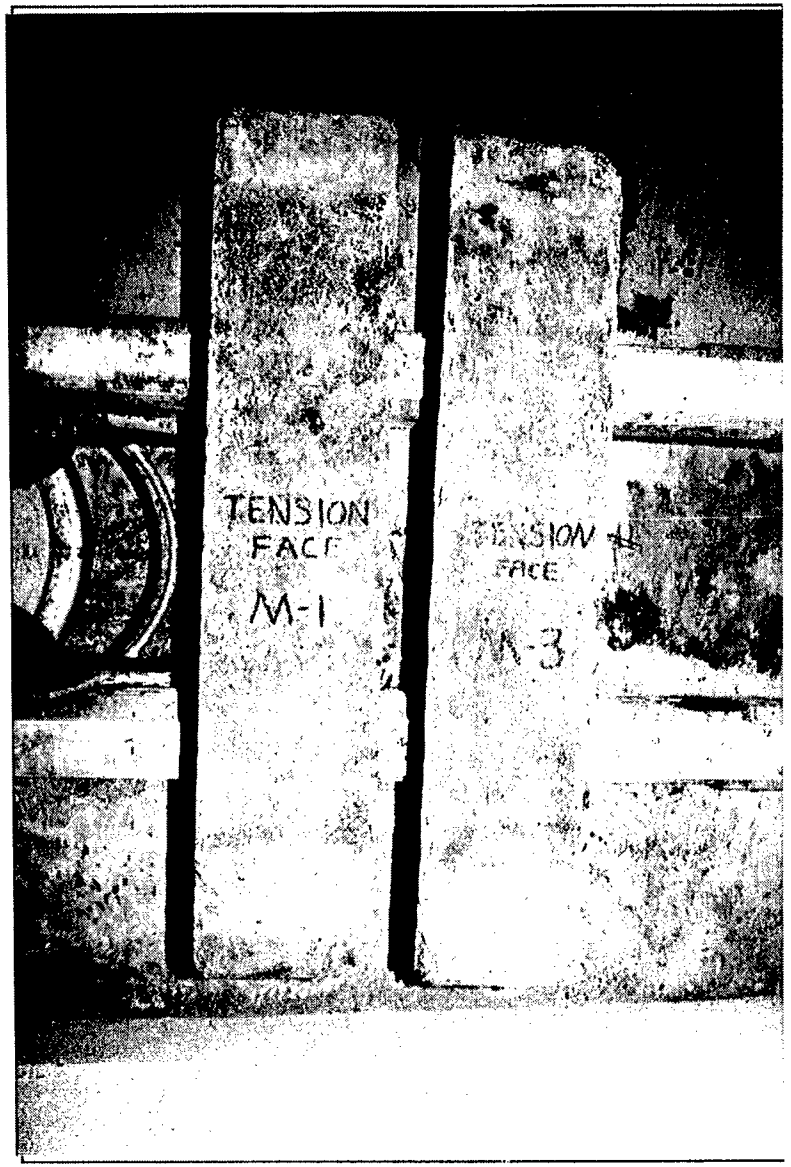


**TENSION**


TOP


BOTTOM


COMPRESSION


TENSION


TOP

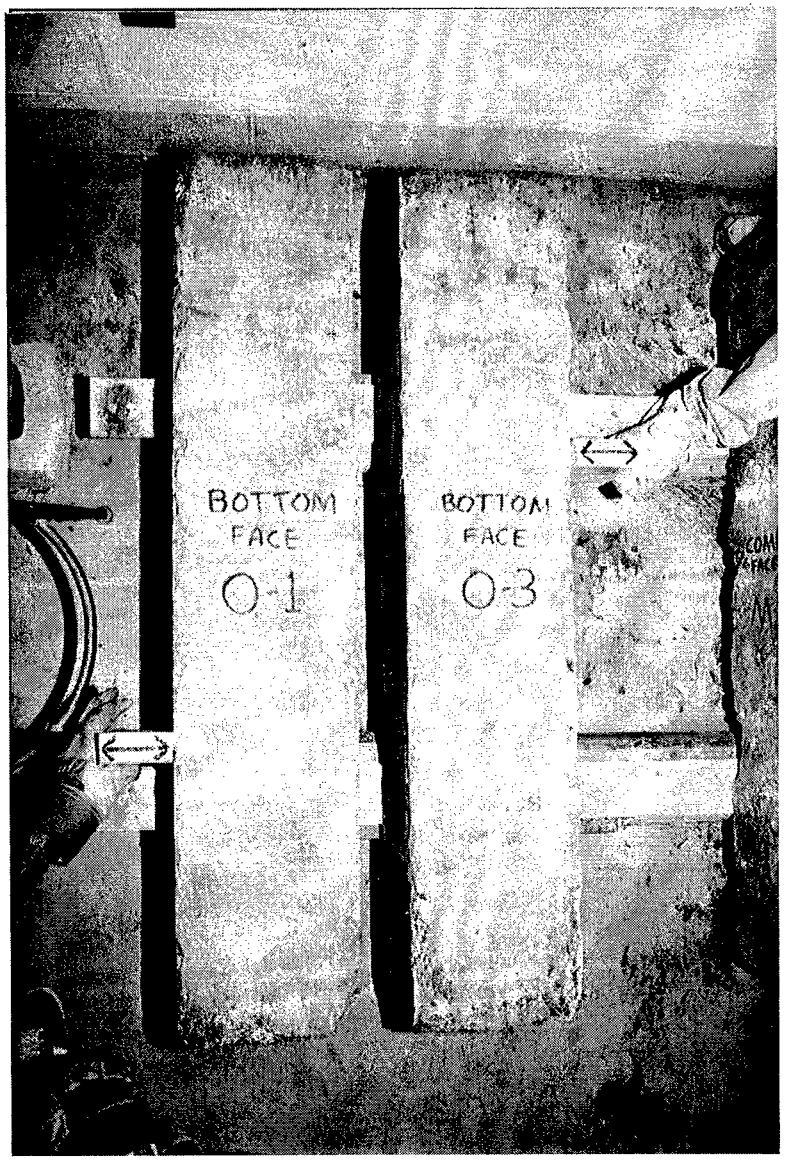


BOTTOM

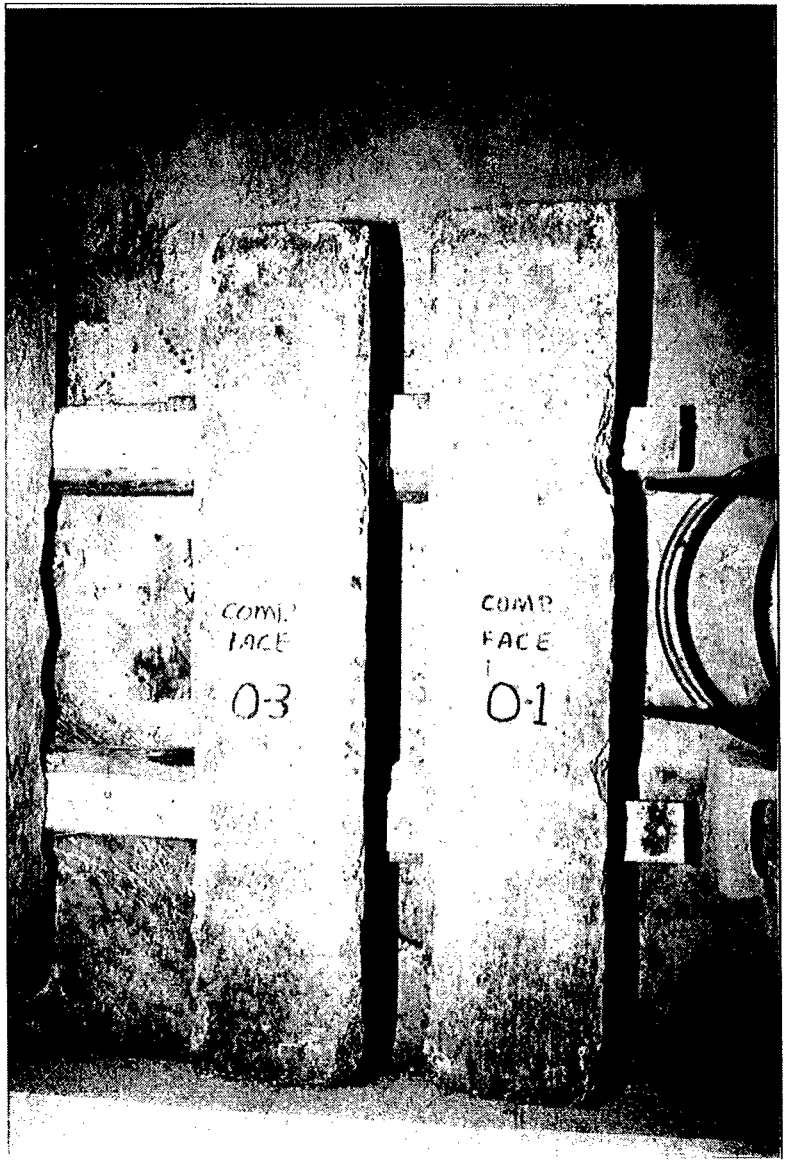


**COMPRESSION**


**TENSION**

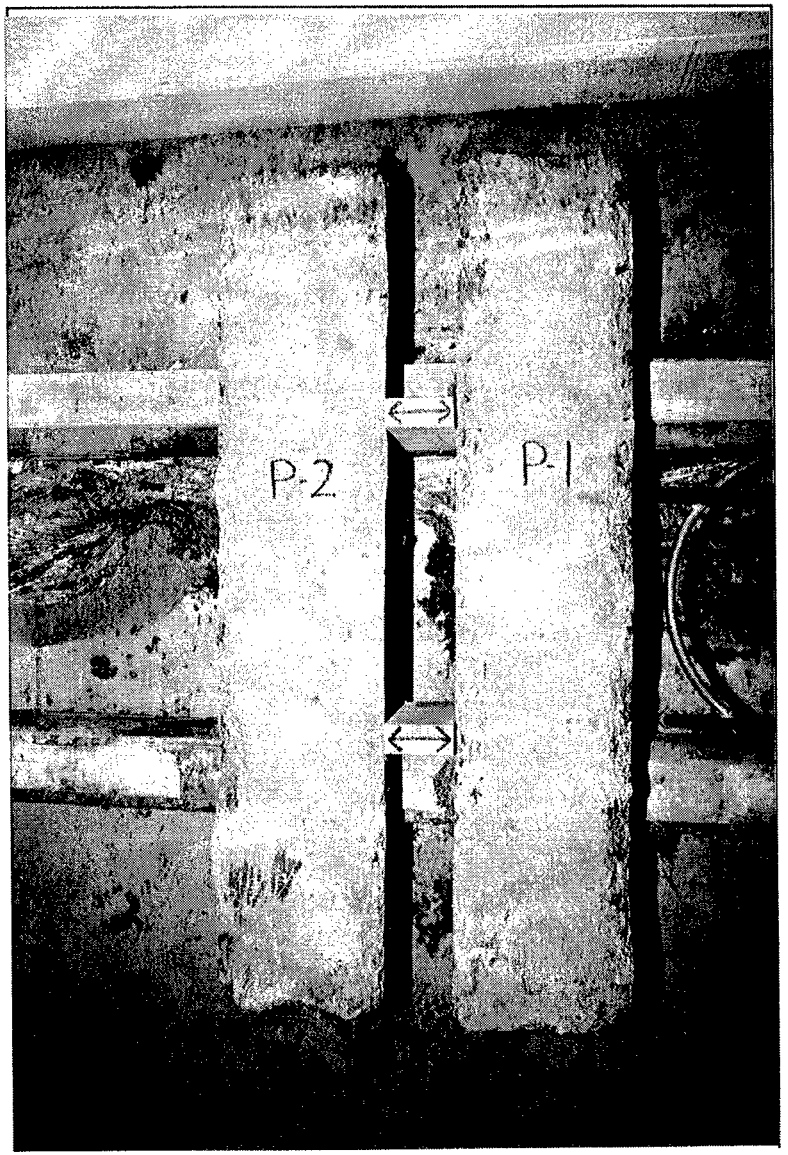


TOP


BOTTOM

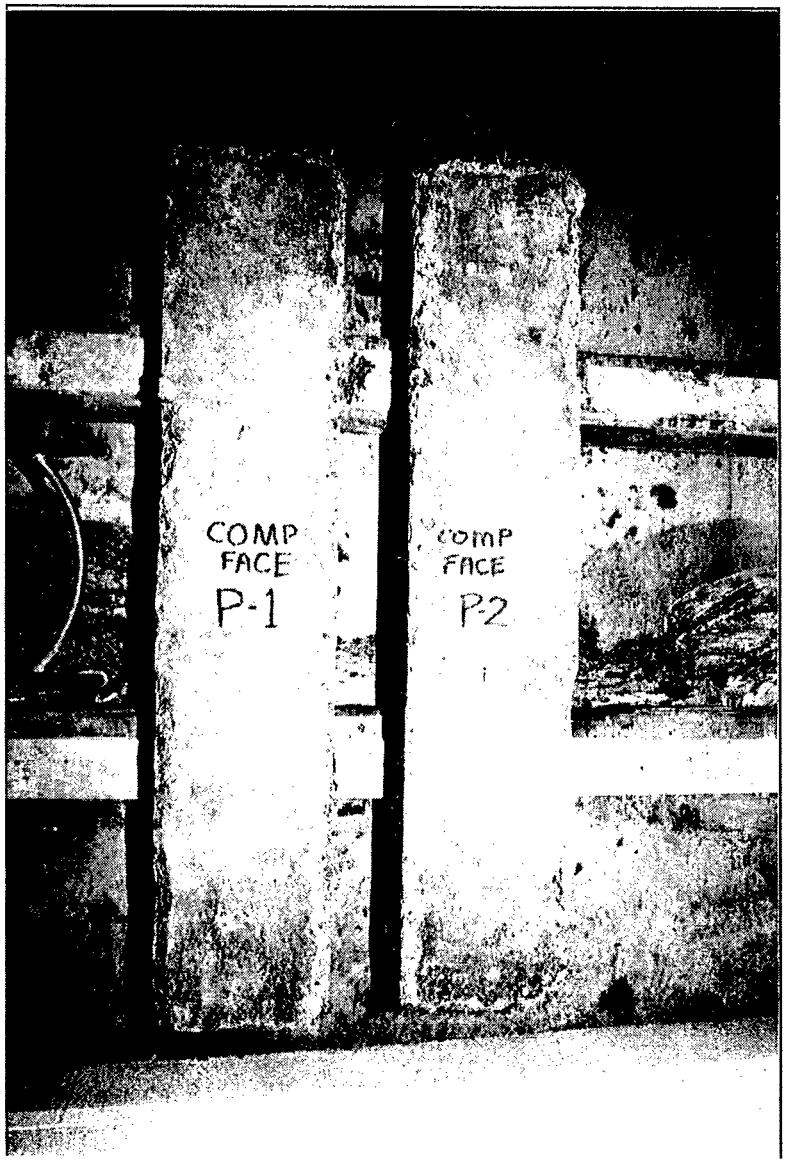


**COMPRESSION**

**TENSION**

# Appendix C
# Beam and Core Numbering Codes

# BEAM AND CORE CODES

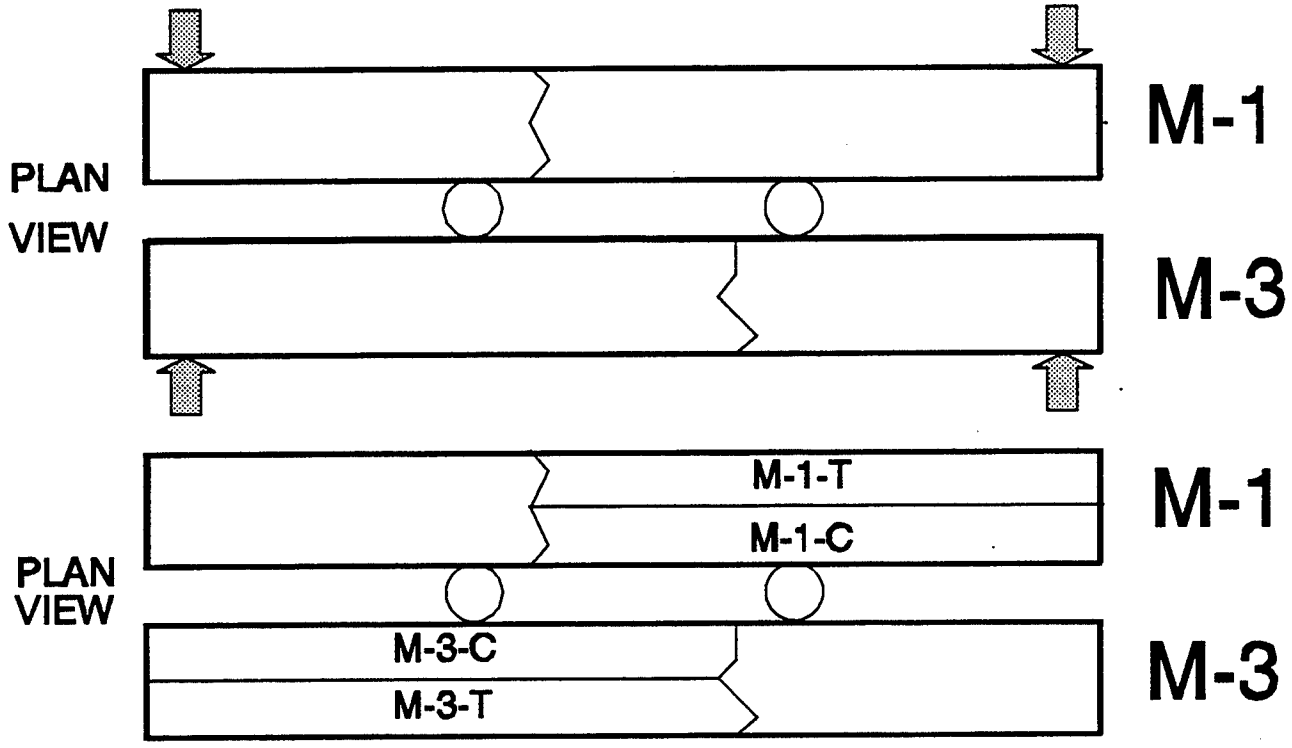


BEAM CODING

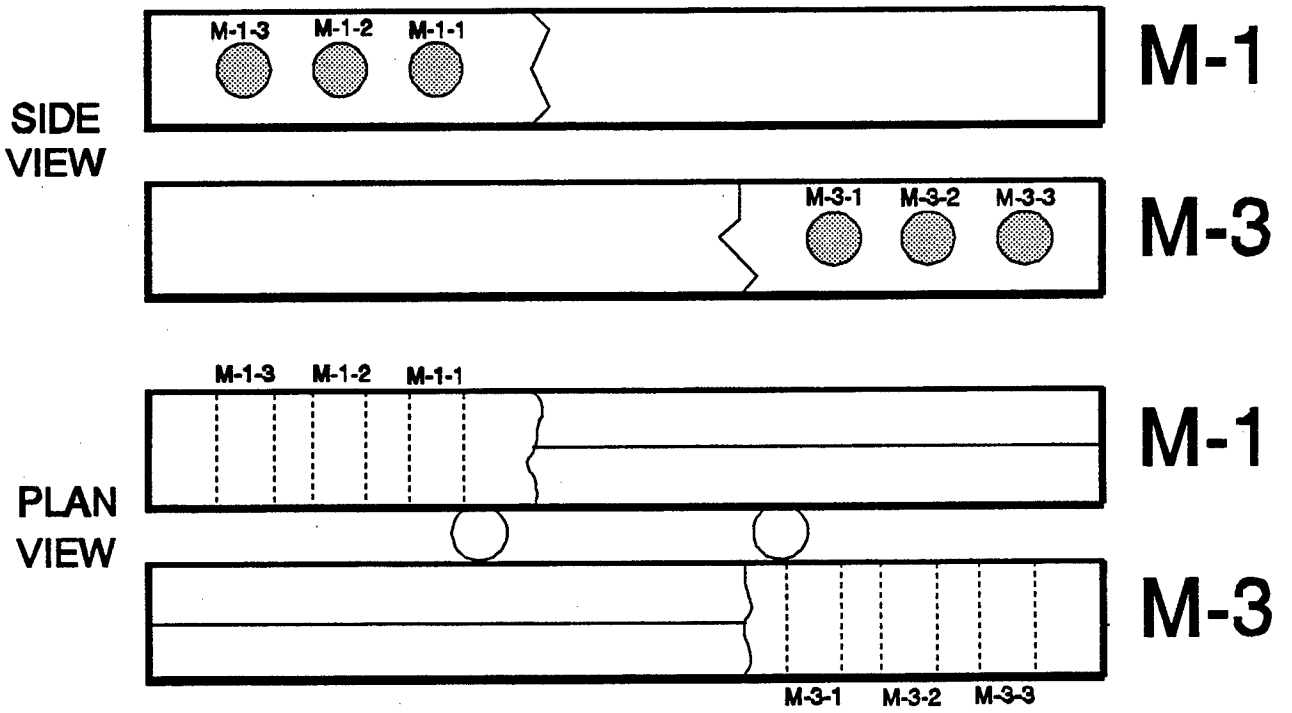


CORE CODING

# CORE NUMBERING CODES

SIDE VIEW

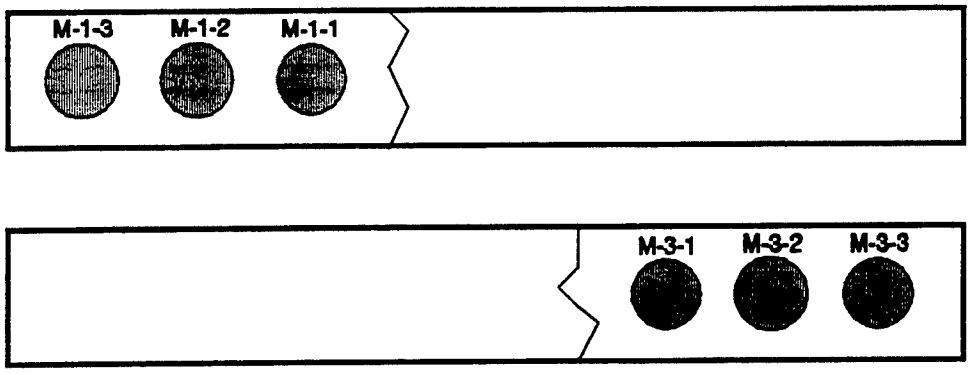


FROM THE 6 CORES, 3 WERE TESTED IN COMPRESSION AND 3 IN TENSION.

MIN. 1 OF EACH TEST PER BEAM

EG. M-1-2-T
TENSION TEST

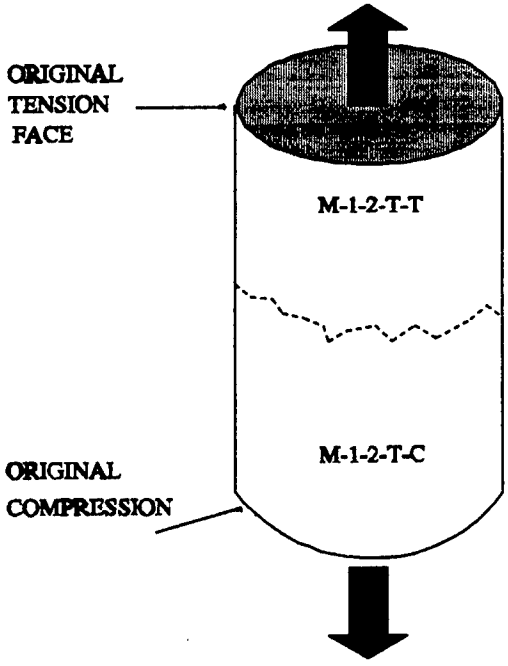


EG. M-1-3-C
COMPRESSION TEST

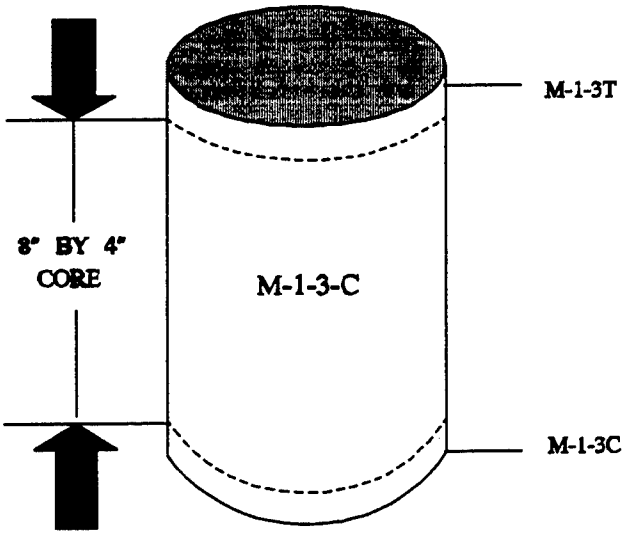

# Appendix D
# Pulse-Velocity Data

# PULSE VELOCITY DATA

| YEAR | 1975 | 1976 | 1977 | 1978 | 1979 | 1980 | 1981 | 1982 | 1983 | 1984 | 1985 | 1986 | 1987 | 1988 | 1989 | 1990 | 1991 | 1992 | 1993 |
|---|---|---|---|---|---|---|---|---|---|---|---|---|---|---|---|---|---|---|---|
| F/T CYCLE | 0 | 146 | 233 | 354 | 475 | 587 | 694 | 822 | 910 | 1020 | 1136 | 1280 | 1389 | 1499 | 1605 | 1740 | 1829 | 1904 | 2027 |
| BEAM | INITIAL (fps) | %V^2 | %V^2 | %V^2 | %V^2 | %V^2 | %V^2 | %V^2 | %V^2 | %V^2 | %V^2 | %V^2 | %V^2 | %V^2 | %V^2 | %V^2 | %V^2 | %V^2 | %V^2 |
| H-3 | 16095 | 103 | 102 | 101 | 106 | 107 | 105 | 95 | failed | - | - | - | - | - | - | - | - | - | - |
| I-1 | 15560 | 97 | 97 | 97 | 94 | 102 | 100 | 79 | NA | NA | 14 | 91 | 26 | 19 | NA | NA | NA | NA | 82 |
| I-3 | 16375 | 101 | 98 | 97 | 101 | 105 | 95 | crack | failed | - | - | - | - | - | - | - | - | - | 77 |
| J-1 | 14315 | 103 | 102 | 100 | 97 | 105 | 102 | 99 | failed | - | - | - | - | - | - | - | - | - | 96 |
| J-3 | 14590 | 106 | 105 | 101 | 102 | 108 | 106 | 103 | 86 | NA | 88 | 105 | 104 | 104 | 103 | 101 | 105 | 101 | 101 |
| K-1 | 14590 | 104 | 102 | 100 | 101 | 108 | 104 | 103 | 85 | NA | 110 | 111 | 111 | 109 | 107 | 107 | 91 | 92 | 94 |
| K-3 | 14260 | 103 | 100 | 100 | 99 | 107 | 103 | 108 | 84 | NA | 115 | 117 | 117 | 117 | 106 | 98 | 98 | 116 | 99 |
| L-1 | 16520 | 94 | 93 | 94 | 82 | 95 | failed | - | - | - | - | - | - | - | - | - | - | - | - |
| L-3 | 16305 | 99 | 101 | 98 | 95 | 103 | 92 | 86 | failed | - | - | - | - | - | - | - | - | - | - |
| M-1 | 14590 | 98 | 99 | 98 | 100 | 114 | 103 | 99 | 82 | NA | 105 | 106 | 109 | 107 | 106 | 104 | 101 | 107 | 82 |
| M-3 | 15060 | 101 | 100 | 99 | 103 | 109 | 105 | 102 | 85 | NA | 89 | 103 | 107 | 104 | 93 | 103 | 99 | 104 | 104 |
| N-1 | 14765 | 108 | 103 | 104 | 106 | 108 | 108 | 106 | 88 | NA | 96 | 90 | 107 | 106 | 103 | 102 | 82 | 104 | 89 |
| N-3 | 14705 | 103 | 103 | 102 | 109 | 107 | 107 | 105 | 88 | NA | 120 | 90 | 106 | 104 | 103 | 103 | 109 | 101 | 86 |
| O-1 | 14150 | 108 | 107 | 105 | 110 | 110 | 108 | 105 | 89 | NA | 90 | 105 | 110 | 105 | 108 | 107 | 115 | 108 | 90 |
| O-3 | 14370 | 104 | 105 | 102 | 105 | 108 | 106 | 104 | 88 | NA | 105 | 107 | 108 | 105 | 103 | 104 | 116 | 107 | 91 |
| P-1 | 14940 | 106 | 103 | 102 | 107 | 106 | 106 | 98 | 85 | NA | 103 | 102 | 106 | 103 | 90 | 89 | 105 | 107 | 90 |
| P-3 | 15245 | 109 | 105 | 105 | 111 | 109 | 110 | 99 | 88 | NA | 88 | 101 | 105 | 103 | 97 | 89 | 105 | 107 | 89 |

# Appendix E
# Flexural Test Results - Whole-Beam Series

Summary of flexural toughness testing results from U.S. Corps. WES fiberous concrete program at Treat Island exposure site.

| BEAM | FIBER TYPE | FCL (kN) | FCND (mm) | E (GPa) | FCS (MPa) | FCT (N*m) | I5 | I10 | I20 | R 5,10 | R 10,20 | REMARKS |
|---|---|---|---|---|---|---|---|---|---|---|---|---|
| J-1 | NONE | This beam failed while still at Treat Island exposure station. | | | | | | | | | | |
| J-3 | NONE | 54.7 | 0.200 | 25.8 | 4.54 | 5.54 | - | - | - | - | - | brittle failure |
| K-1 | STEEL 3/4" | 73.6 | 0.244 | 28.5 | 6.10 | 7.60 | 4.53 | 7.99 | 14.00 | 69 | 60 | |
| K-3 | STEEL 3/4" | 74.3 | 0.288 | 24.3 | 6.16 | 11.38 | 3.87 | 6.54 | 10.85 | 53 | 43 | |
| M-1 | STEEL 1" | 80.0 | 0.254 | 29.7 | 6.63 | 9.66 | 2.22 | 2.65 | 3.59 | 9 | 9 | |
| M-3 | STEEL 1" | 78.1 | 0.270 | 27.3 | 6.48 | 11.73 | 2.35 | 3.12 | 4.15 | 15 | 10 | |
| N-1 | GLASS 1" | 57.9 | 0.241 | 22.7 | 4.80 | 6.70 | - | - | - | - | - | brittle failure |
| N-3 | GLASS 1" | 26.6 | 0.174 | 14.4 | 2.21 | 4.81 | - | - | - | - | - | *severely corroded on one side |
| O-1 | GLASS 1" | 58.7 | 0.231 | 24.0 | 4.87 | 6.92 | - | - | - | - | - | brittle failure |
| O-3 | GLASS 1" | 58.5 | 0.224 | 24.6 | 4.85 | 6.57 | - | - | - | - | - | |
| P-1 | S-STEEL 1" | 61.7 | 0.231 | 25.2 | 5.12 | 7.32 | 4.07 | 7.21 | 13.01 | 63 | 58 | |
| P-2 | S-STEEL 1" | 40.0 | 0.136 | 27.7 | 3.32 | 2.94 | 4.96 | 10.07 | 20.35 | 102 | 103 | |

# US CORPS CONCRETE BEAM FLEXURAL TEST

## BEAM J-3 AUG/93 THIRD POINT LOADING

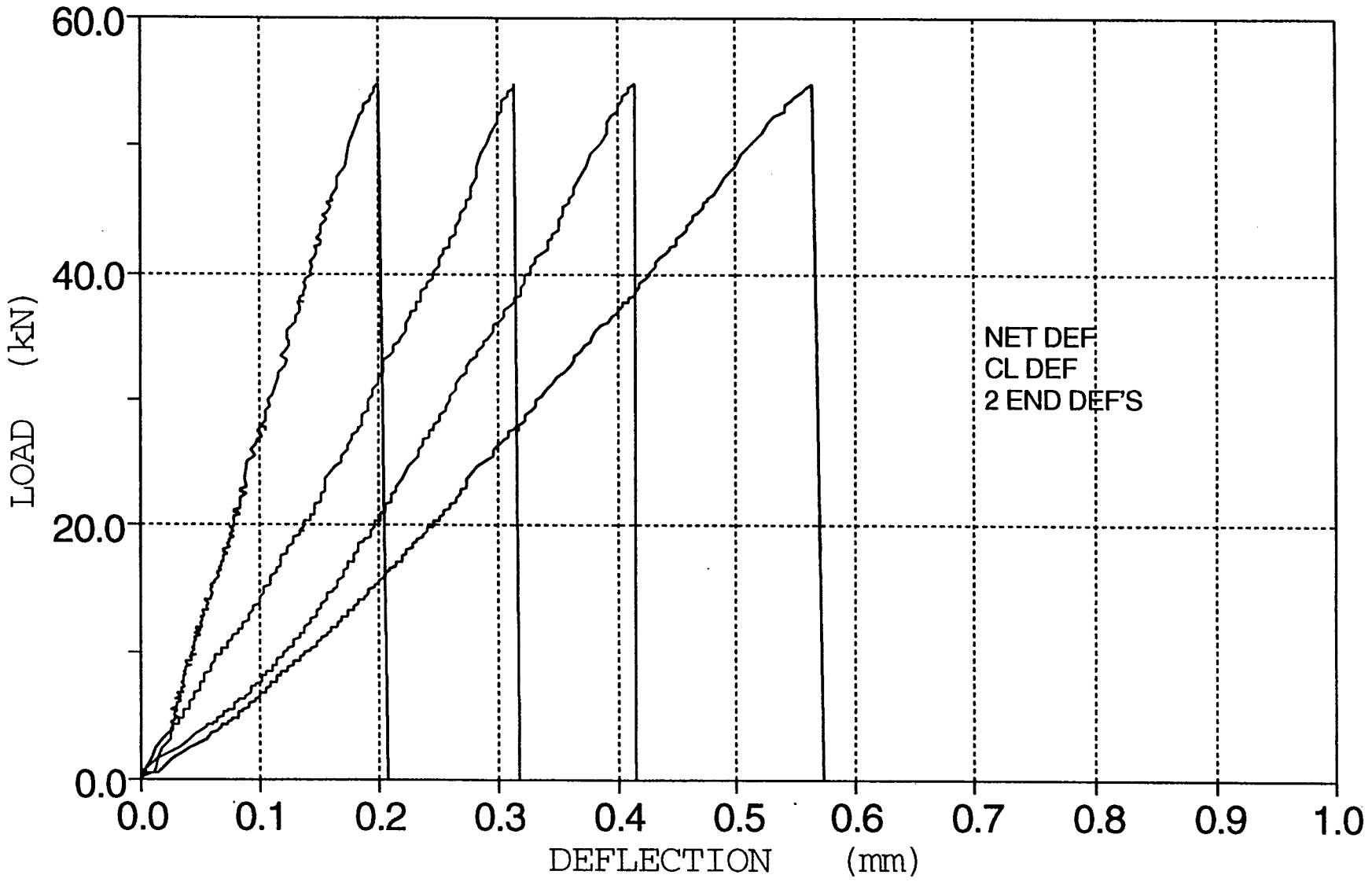

# US CORPS FIBER REINFORCED BEAM TEST

## BEAM K-1 AUG/93 THIRD POINT LOADING

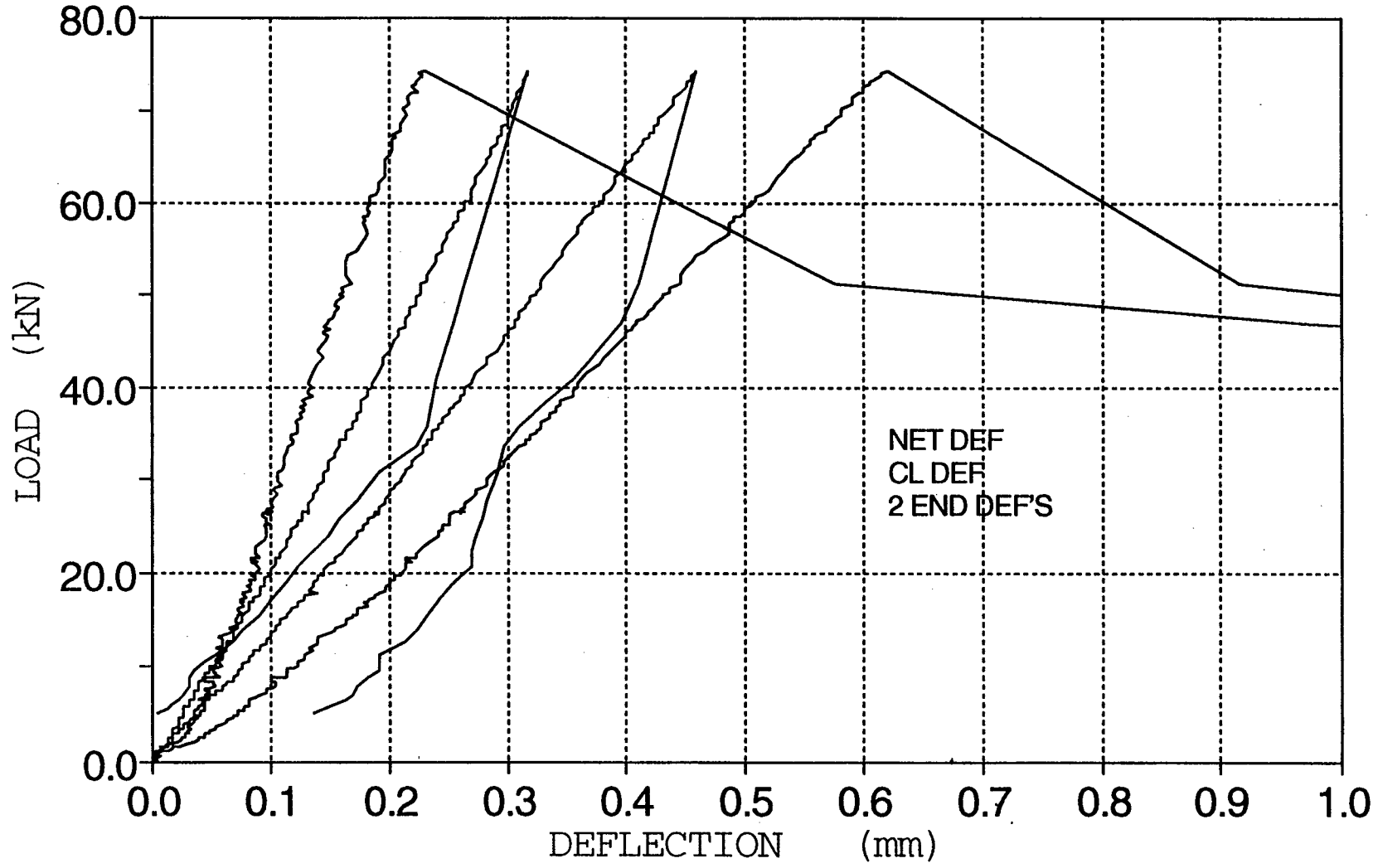

# US CORPS FIBER REINFORCED BEAM TEST

## BEAM K-1 AUG/93 THIRD POINT LOADING

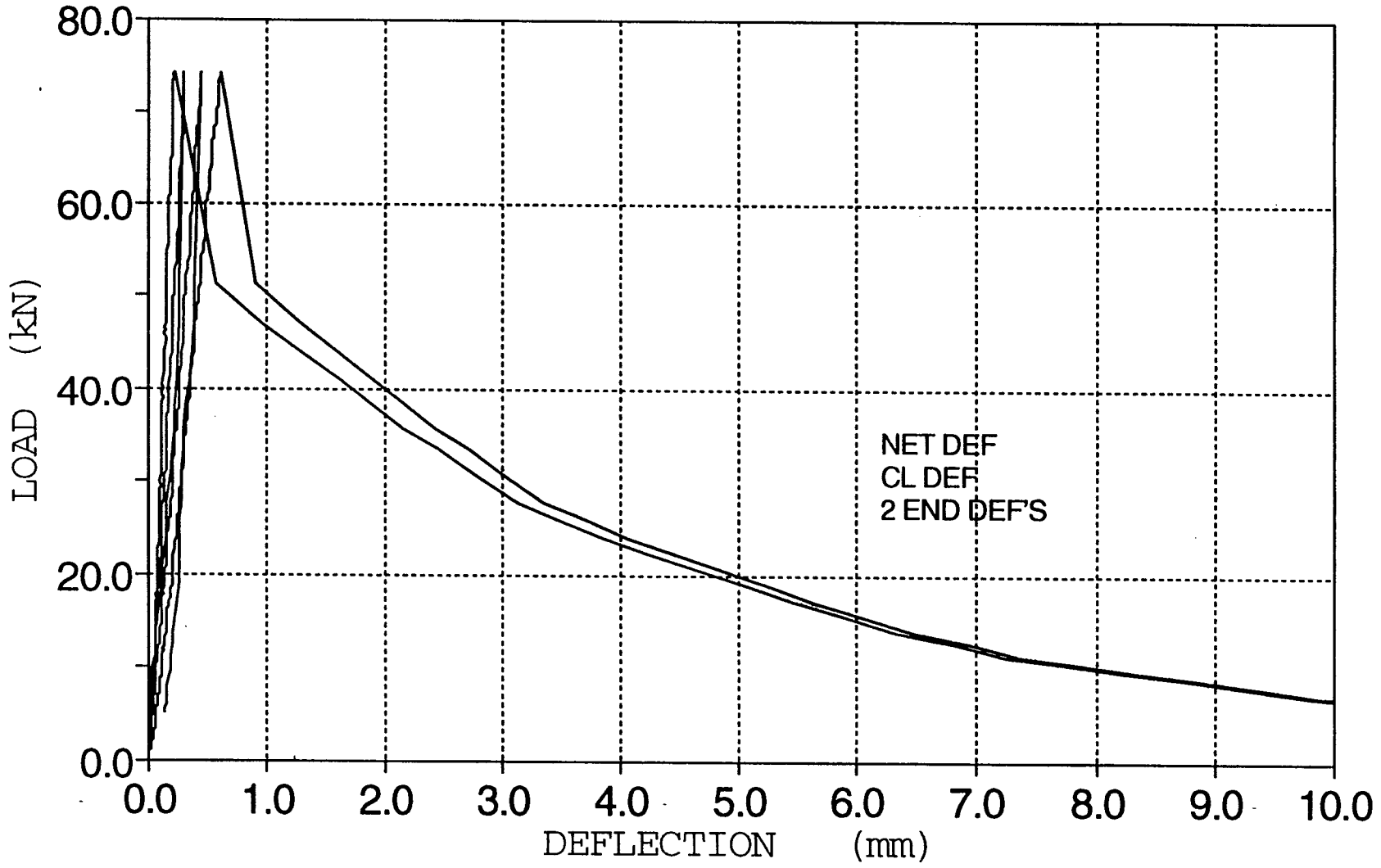

# US CORPS FIBER REINFORCED BEAM TEST

## BEAM K-3 AUG/93 THIRD POINT LOADING

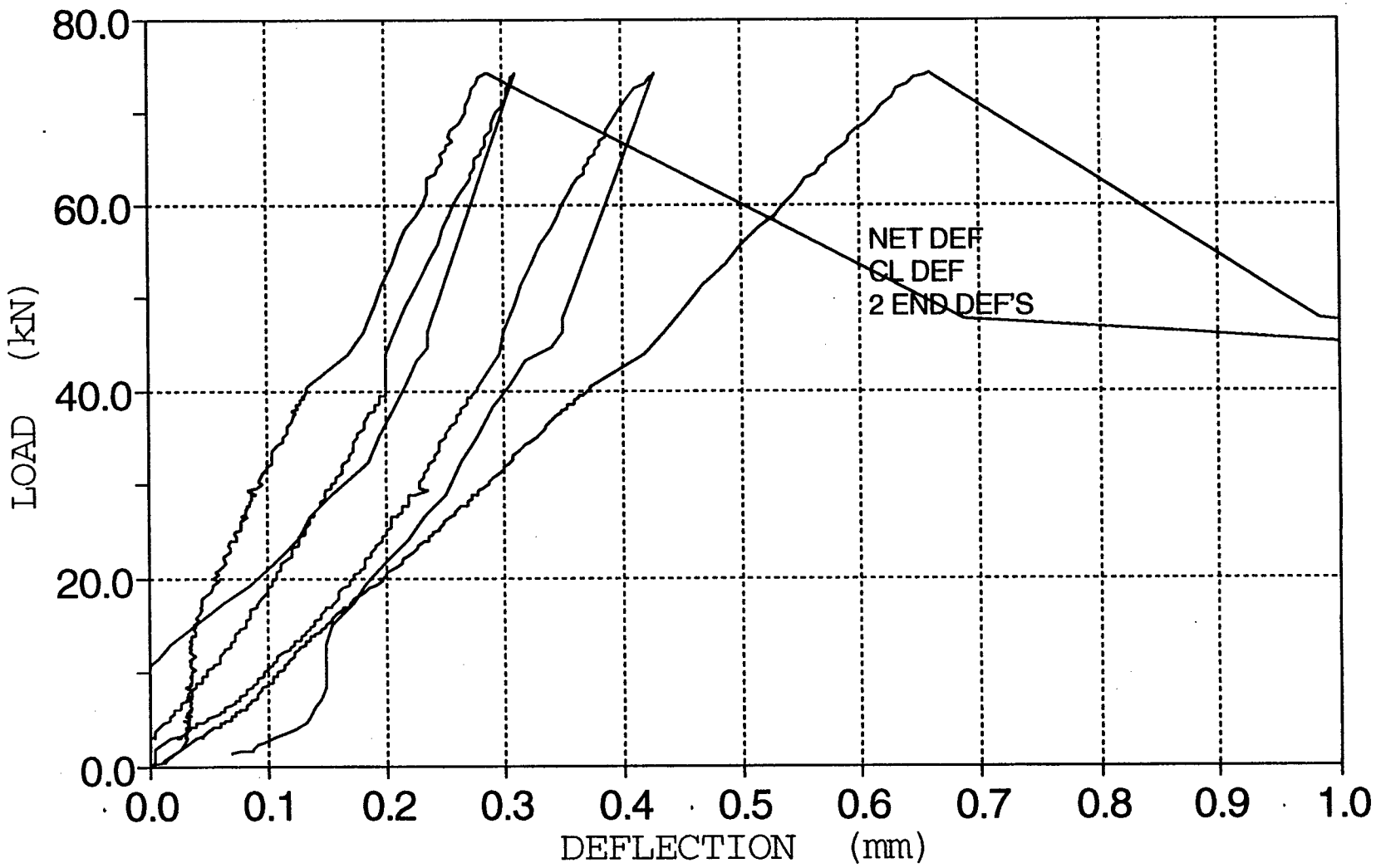

# US CORPS FIBER REINFORCED BEAM TEST

## BEAM K-3 AUG/93 THIRD POINT LOADING

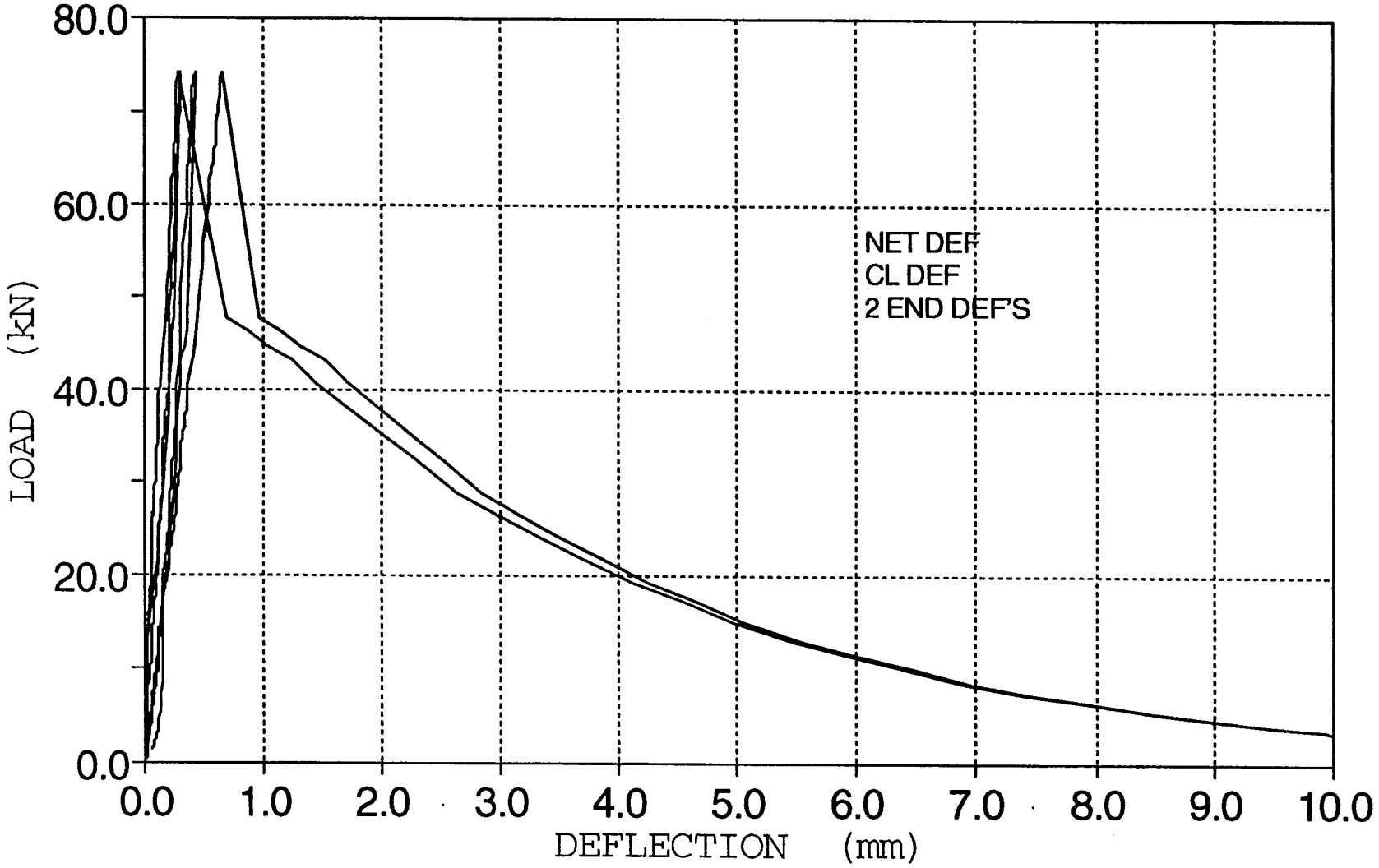

# US CORPS FIBER REINFORCED BEAM TEST

## BEAM M-1 AUG/93 THIRD POINT LOADING

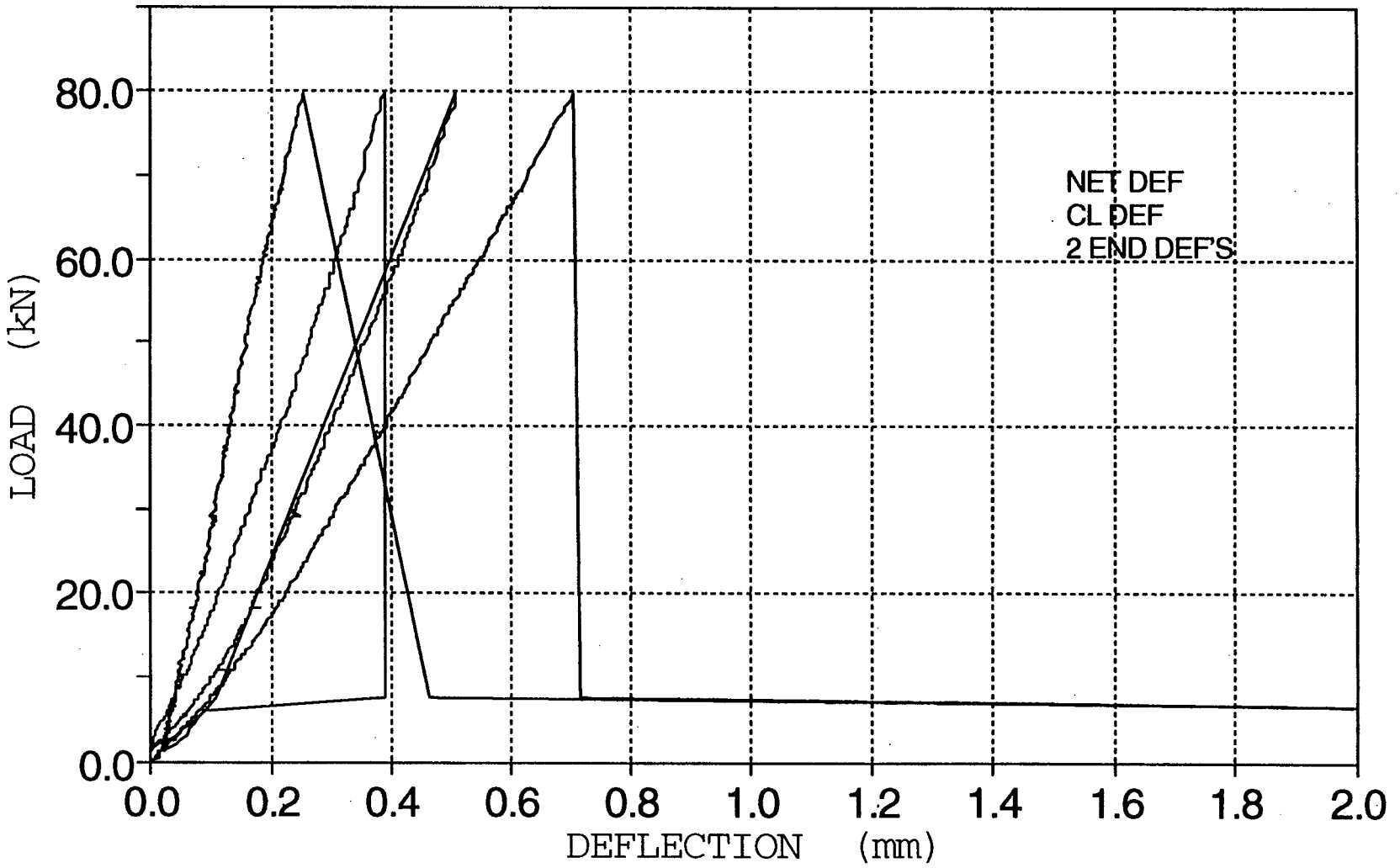

# US CORPS FIBER REINFORCED BEAM TEST

## BEAM M-3 AUG/93 THIRD POINT LOADING

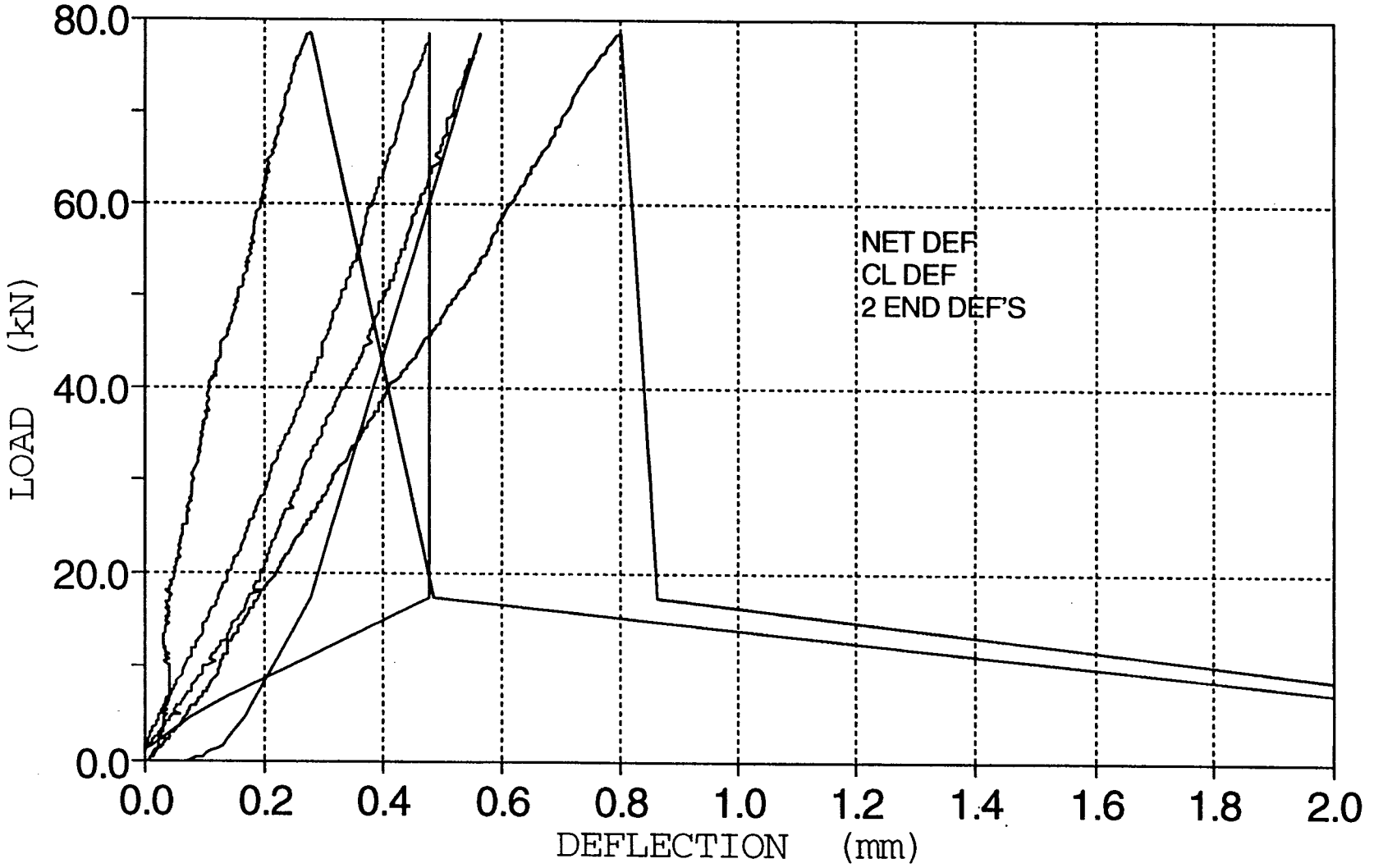

# US CORPS FIBER REINFORCED BEAM TEST

## BEAM N-1 AUG/93 THIRD POINT LOADING

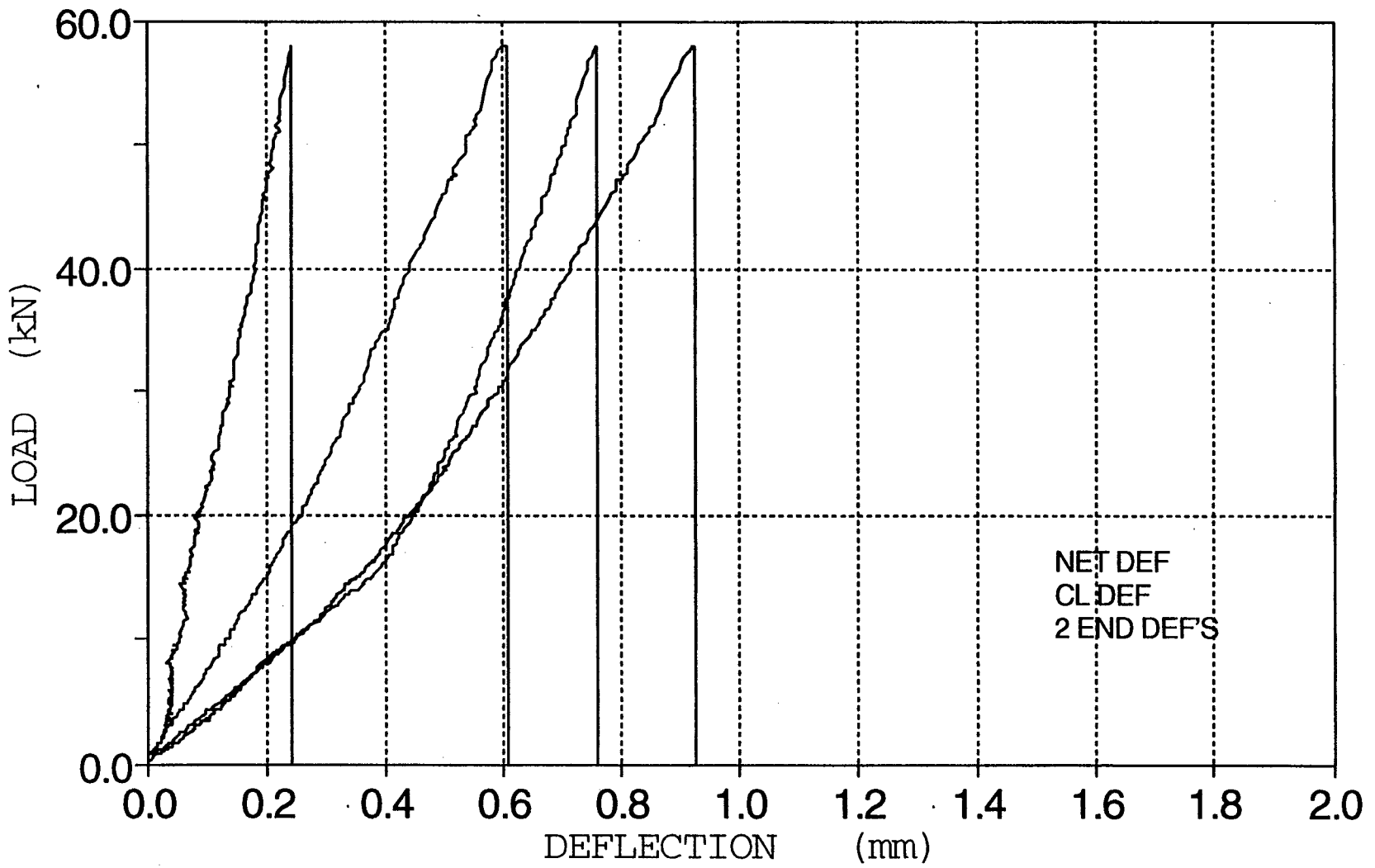

# US CORPS FIBER REINFORCED BEAM TEST

## BEAM N-3 AUG/93 THIRD POINT LOADING

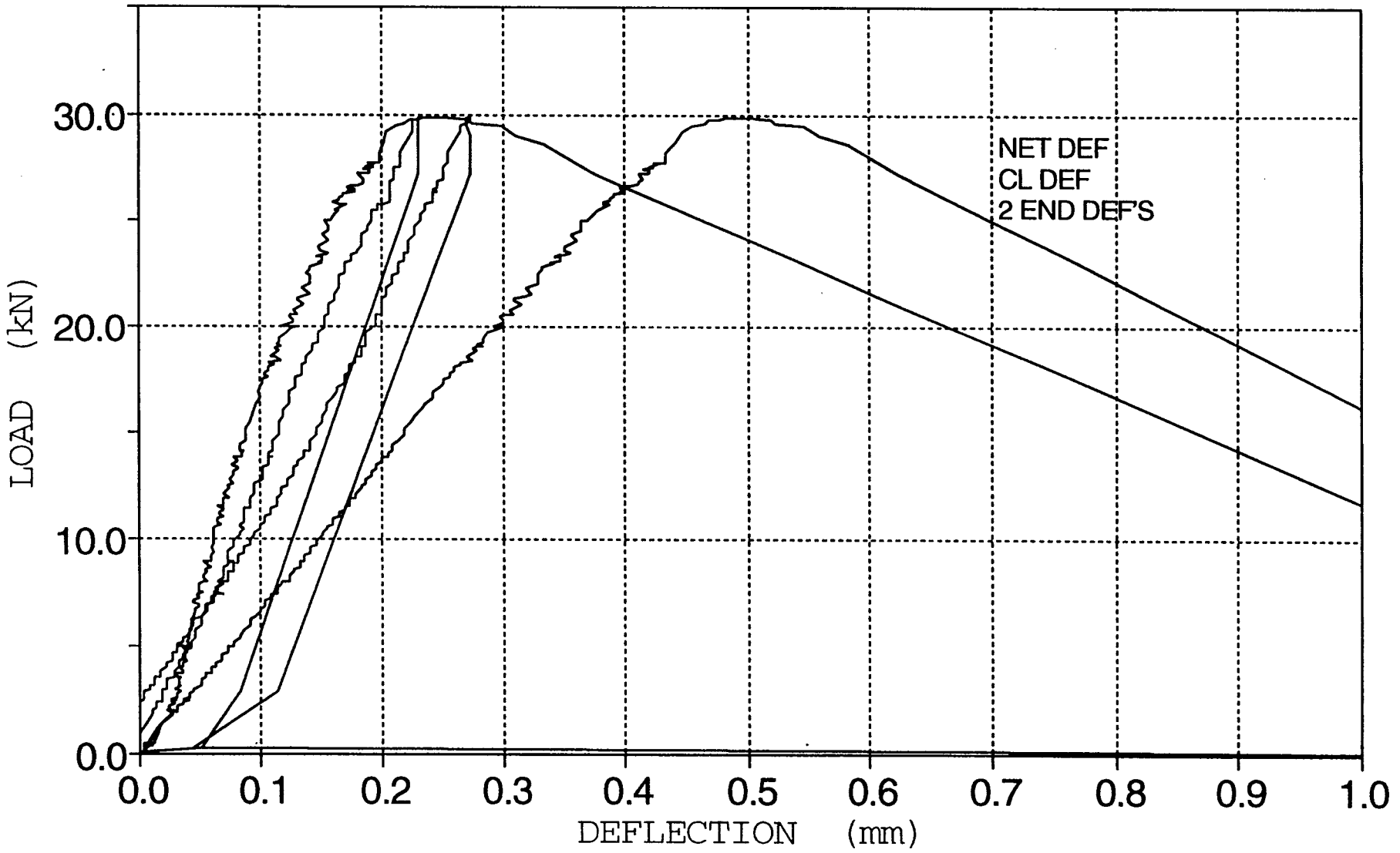

# US CORPS FIBER REINFORCED BEAM TEST

## BEAM N-3 AUG/93 THIRD POINT LOADING

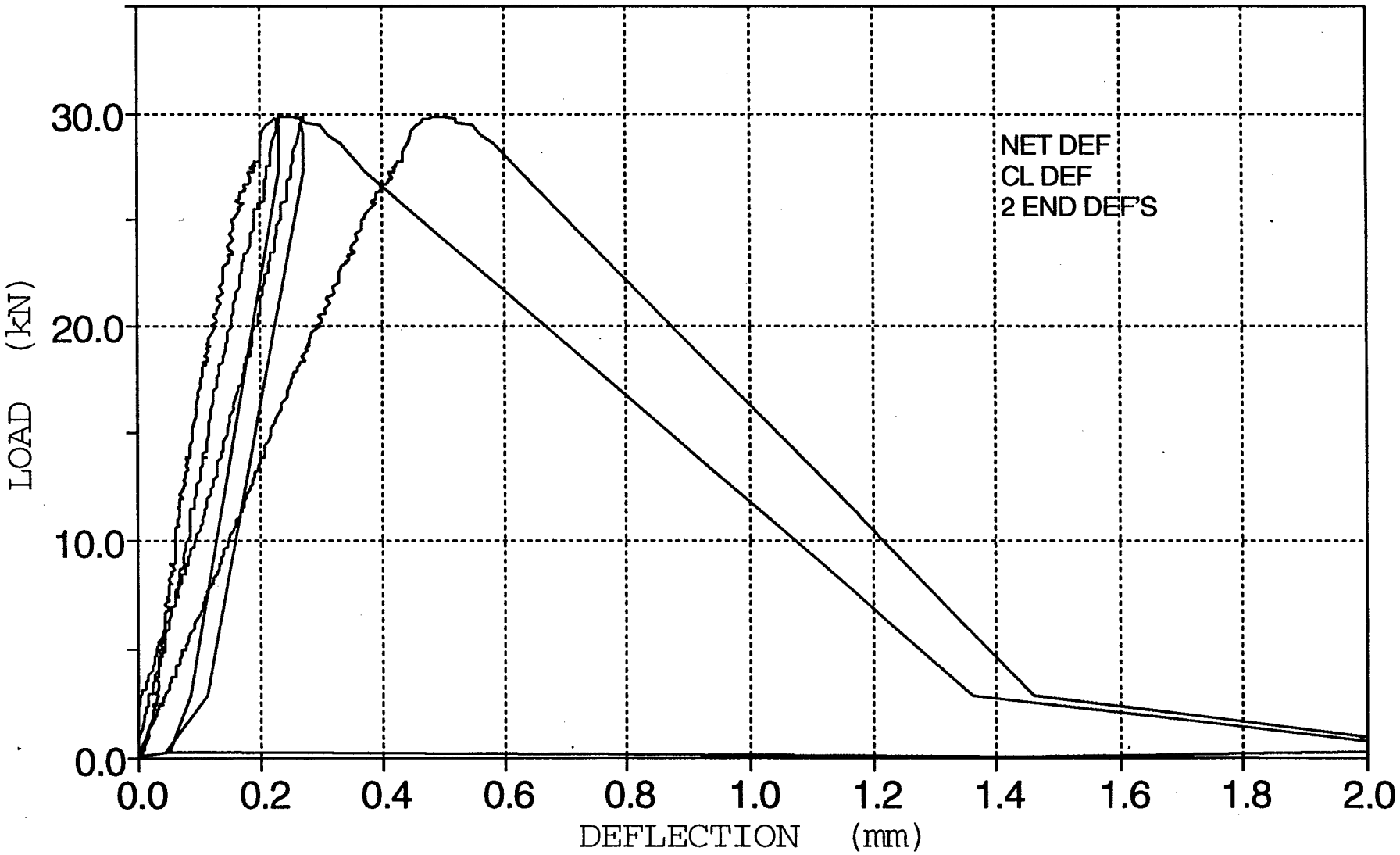

# US CORPS FIBER REINFORCED BEAM TEST

## BEAM O-1 AUG/93 THIRD POINT LOADING

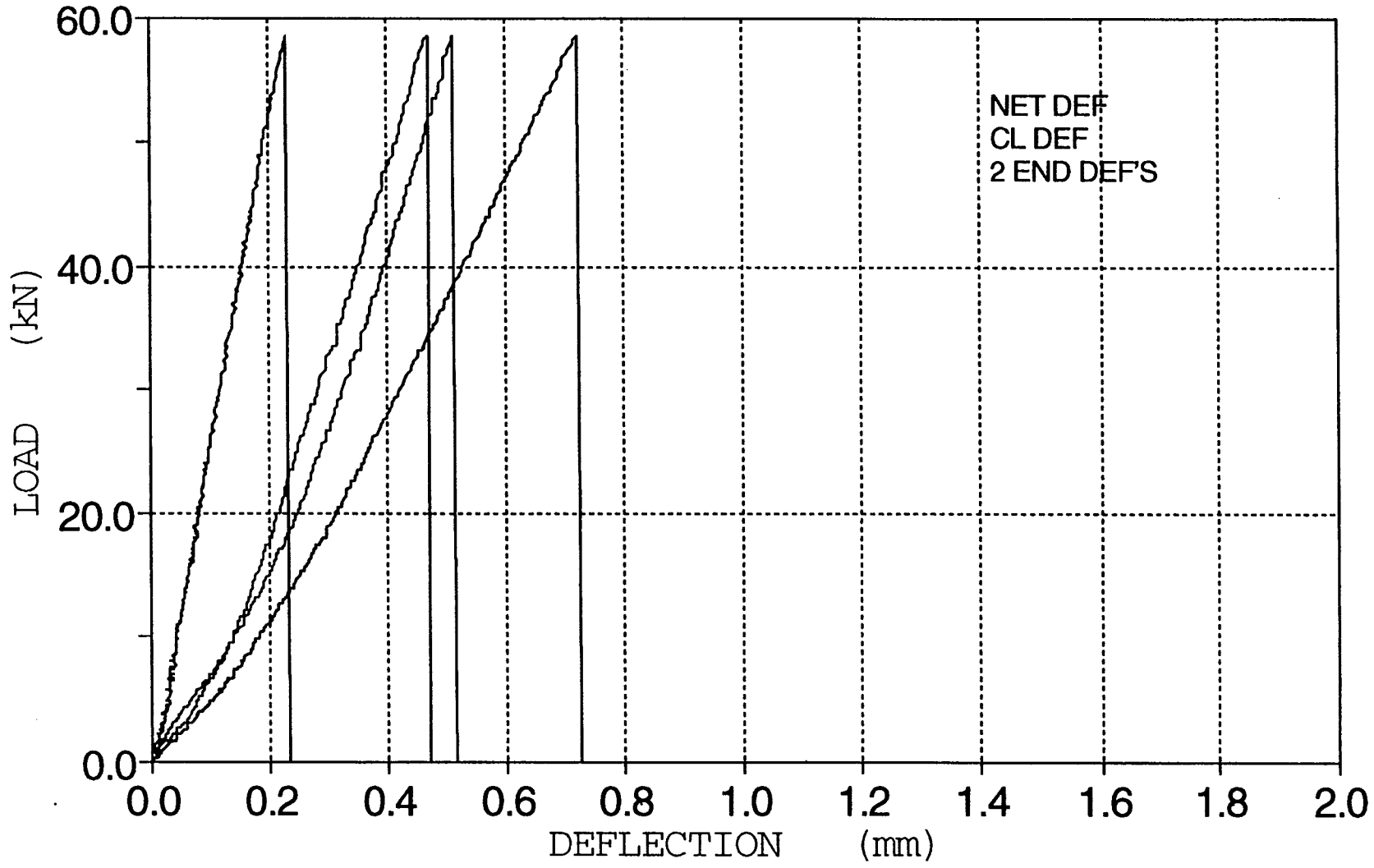

# US CORPS FIBER REINFORCED BEAM TEST

## BEAM O-3 AUG/93 THIRD POINT LOADING

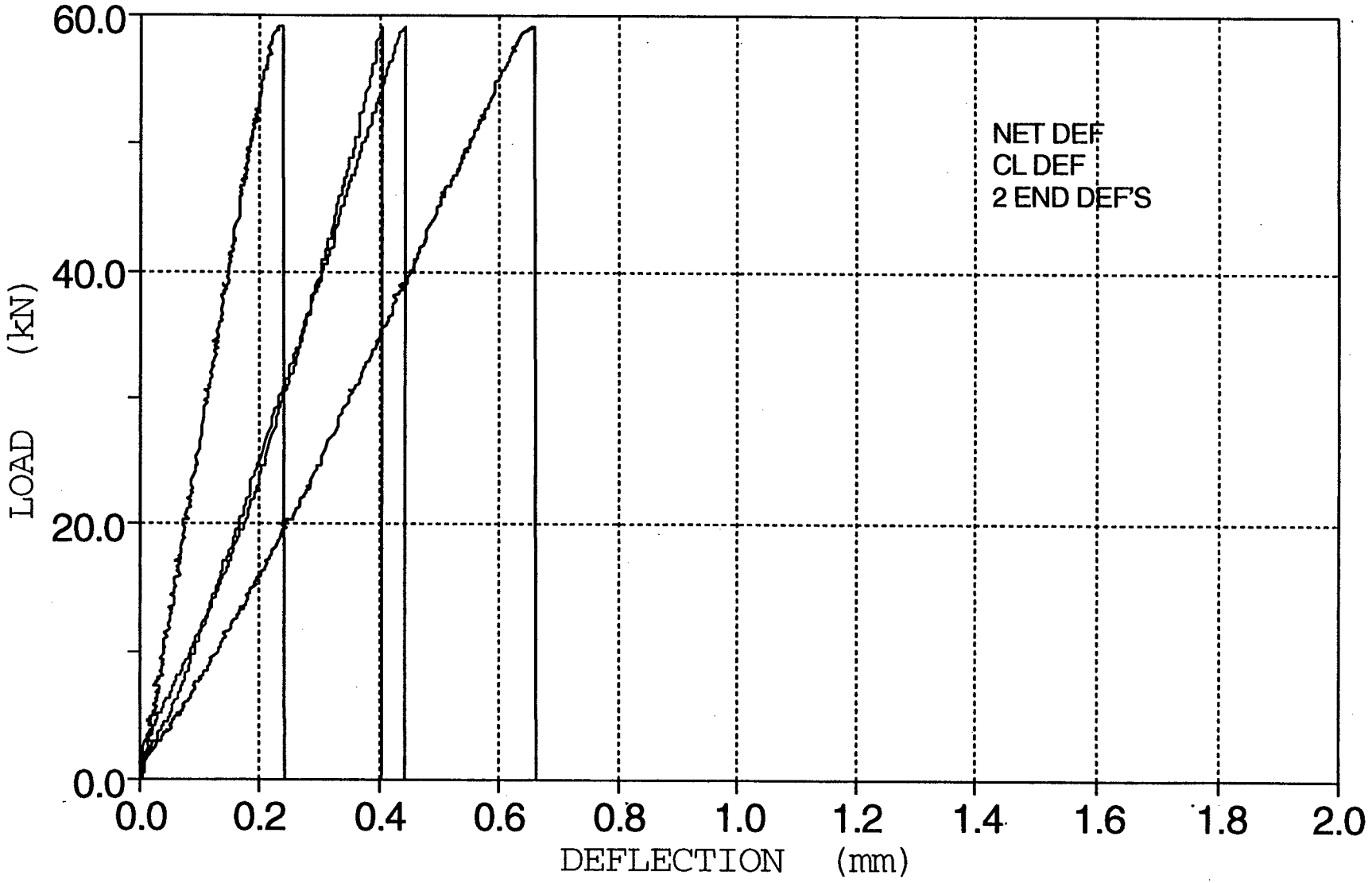

# US CORPS FIBER REINFORCED BEAM TEST

## BEAM P-1 AUG/93 THIRD POINT LOADING

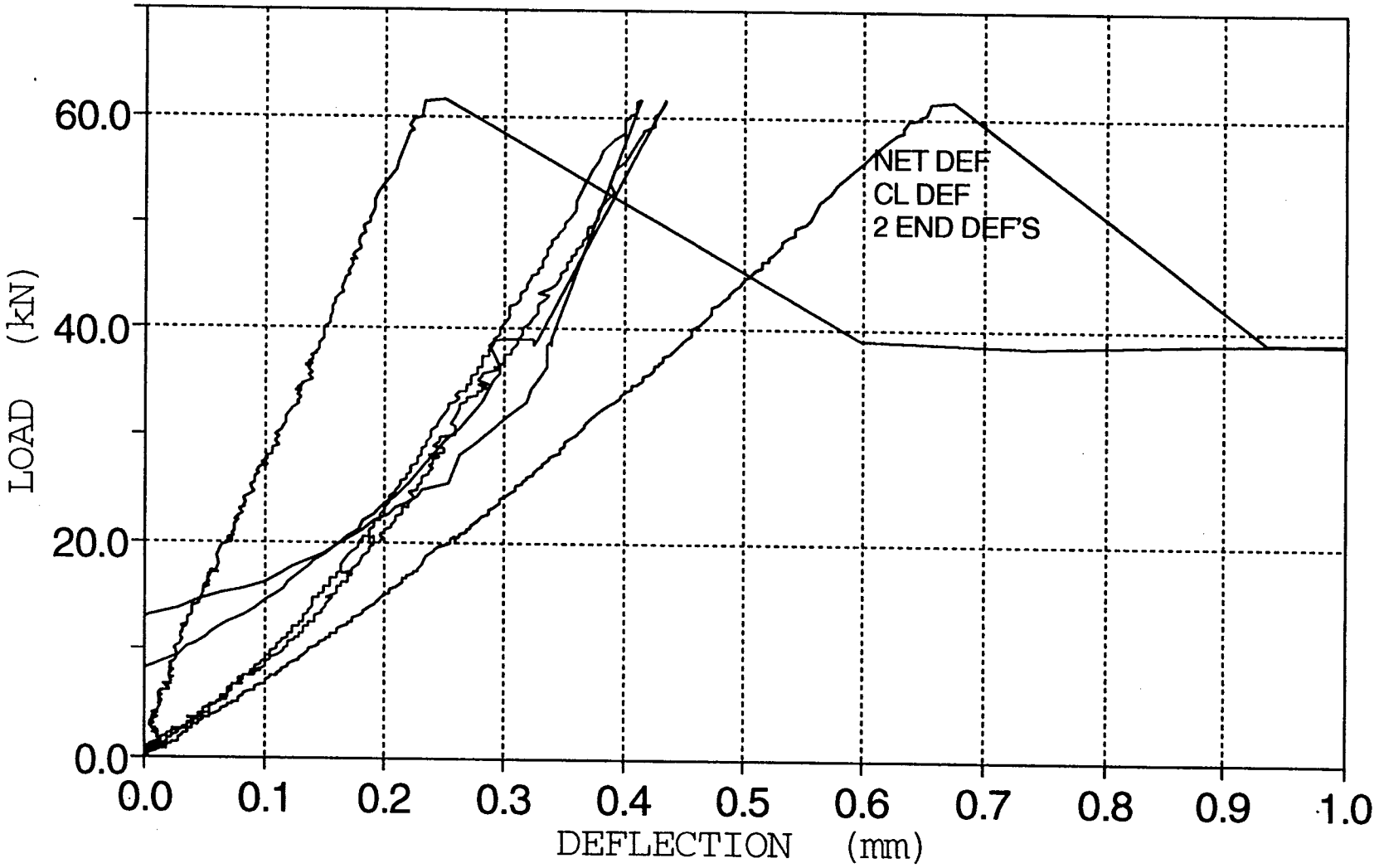

# US CORPS FIBER REINFORCED BEAM TEST

## BEAM P-1 AUG/93 THIRD POINT LOADING

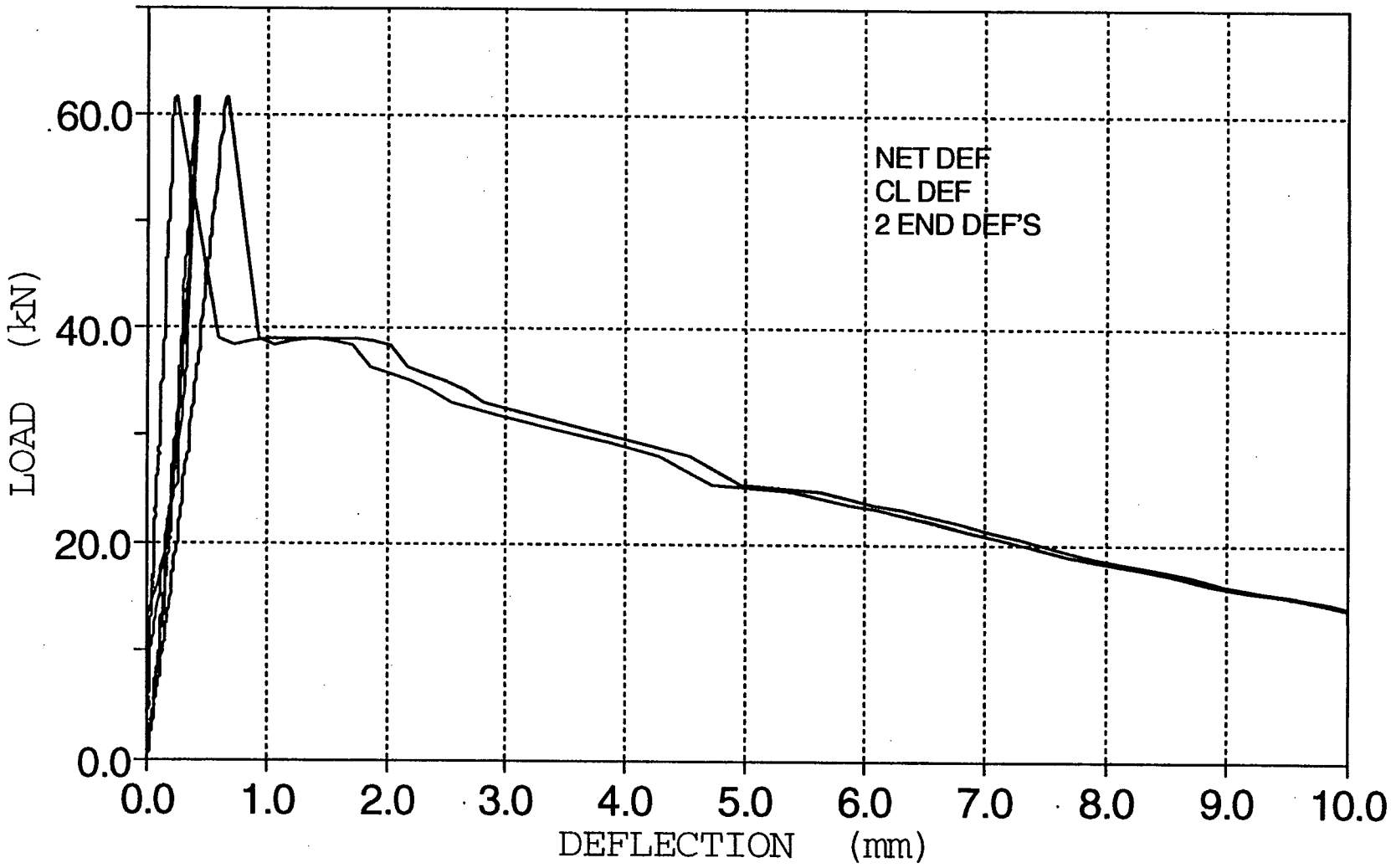

# US CORPS FIBER REINFORCED BEAM TEST

## BEAM P-2 AUG/93 THIRD POINT LOADING

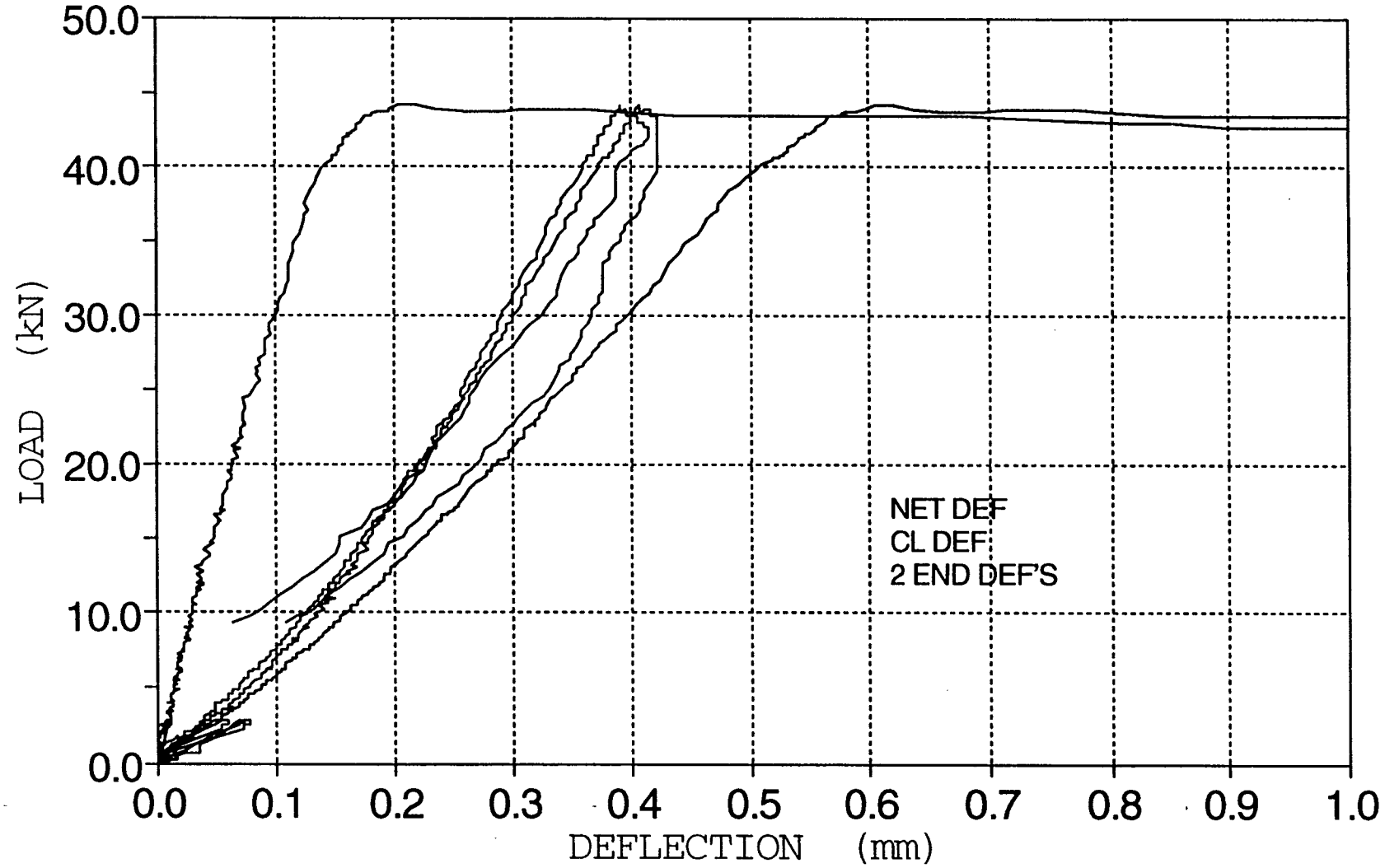

# US CORPS FIBER REINFORCED BEAM TEST

## BEAM P-2 AUG/93 THIRD POINT LOADING

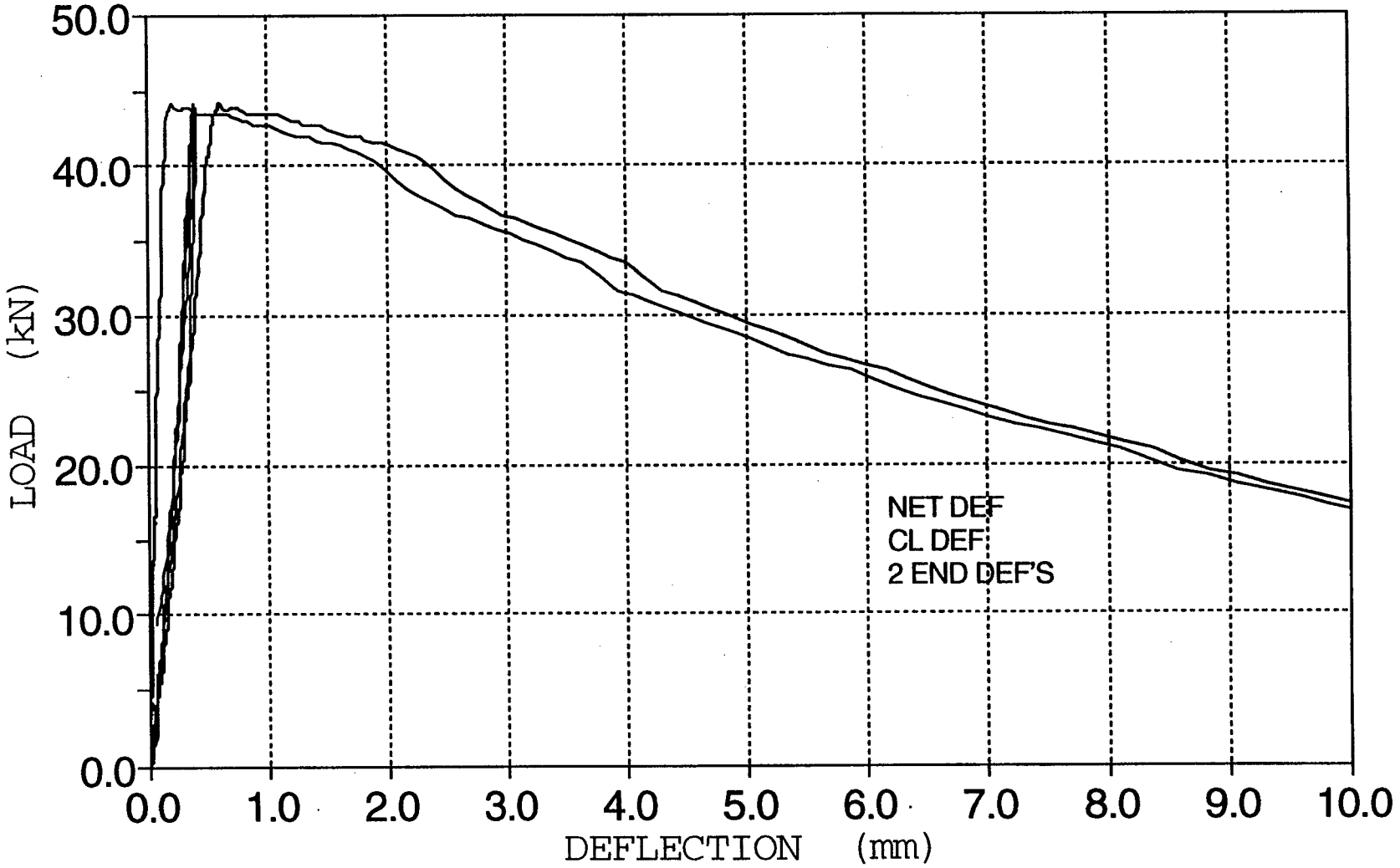

# Appendix F
# Flexural Test Results - Sawed-Beam Series

Results of second series of flexural toughness tests on U.S. Corps fiber reinforced beams.

| BEAM | FIBER TYPE | FCL (kN) | FCND (mm) | FCS (MPa) | FCT (N*m) | I5 | I10 | I20 | R 5,10 | R 10,20 | REMARKS |
|---|---|---|---|---|---|---|---|---|---|---|---|
| J1CT | NONE | 40.9 | 0.093 | 4.70 | 1.57 | - | - | - | - | - | brittle failure |
| J1TT | NONE | 25.3 | 0.100 | 2.92 | 1.23 | - | - | - | - | - | |
| J3CC | NONE | 42.6 | 0.047 | 4.89 | 2.11 | - | - | - | - | - | |
| J3TC | NONE | 34.6 | 0.099 | 3.97 | 1.78 | - | - | - | - | - | |
| K1CT | STEEL 3/4" | 67.1 | 0.178 | 7.70 | 5.22 | 5.81 | 11.29 | 25.55 | 110 | 143 | |
| K1TT | STEEL 3/4" | 62.3 | 0.134 | 7.15 | 4.02 | 5.58 | 11.14 | 19.66 | 111 | 85 | |
| K3CC | STEEL 3/4" | 53.0 | 0.123 | 6.09 | 3.26 | 5.24 | 10.72 | 19.10 | 110 | 84 | |
| K3TC | STEEL 3/4" | 52.4 | 0.135 | 6.02 | 3.26 | 5.85 | 12.17 | 22.45 | 126 | 103 | |
| M1CT | STEEL 1" | 58.6 | 0.161 | 6.73 | 4.62 | 4.85 | 8.33 | 11.06 | 70 | 27 | |
| M1TT | STEEL 1" | 61.9 | 0.151 | 7.01 | 4.32 | 5.25 | 9.33 | 13.14 | 82 | 38 | |
| M3CC | STEEL 1" | 47.8 | 0.137 | 5.49 | 3.83 | 4.26 | 7.03 | 8.88 | 55 | 19 | |
| M3TC | STEEL 1" | 40.8 | 0.077 | 4.68 | 1.73 | 4.44 | 7.67 | 11.54 | 65 | 39 | |
| N1CT | GLASS 1" | 54.6 | 0.101 | 6.27 | 2.95 | - | - | - | - | - | brittle failure |
| N1TT | GLASS 1" | 55.3 | 0.154 | 6.35 | 4.38 | - | - | - | - | - | |
| N3CC | GLASS 1" | 49.6 | 0.098 | 5.69 | 2.29 | - | - | - | - | - | |
| N3TC | GLASS 1" | 43.0 | 0.132 | 4.94 | 2.43 | - | - | - | - | - | |
| O1CT | GLASS 1" | 50.1 | 0.163 | 5.57 | 3.39 | - | - | - | - | - | brittle failure |
| O1TT | GLASS 1" | 45.3 | 0.067 | 5.20 | 3.21 | - | - | - | - | - | |
| 03CC | GLASS 1" | 40.9 | 0.141 | 4.70 | 2.39 | - | - | - | - | - | |
| O3TC | GLASS 1" | 45.6 | 0.135 | 5.24 | 2.75 | - | - | - | - | - | |
| P1CT | S-STEEL 1" | 44.0 | 0.107 | 5.05 | 2.77 | 4.97 | 9.82 | 18.89 | 97 | 91 | |
| P1TT | S-STEEL 1" | 45.9 | 0.107 | 5.27 | 2.15 | 5.63 | 11.05 | 22.74 | 108 | 117 | |
| P2CC | S-STEEL 1" | 50.7 | 0.119 | 5.82 | 2.98 | 5.53 | 11.65 | 23.53 | 122 | 119 | |
| P2TC | S-STEEL 1" | 106.1 | 0.120 | 12.18 | 5.81 | 5.36 | 8.74 | 14.26 | 68 | 55 | |

# FLEXURAL TEST RESULTS

## SECOND SERIES

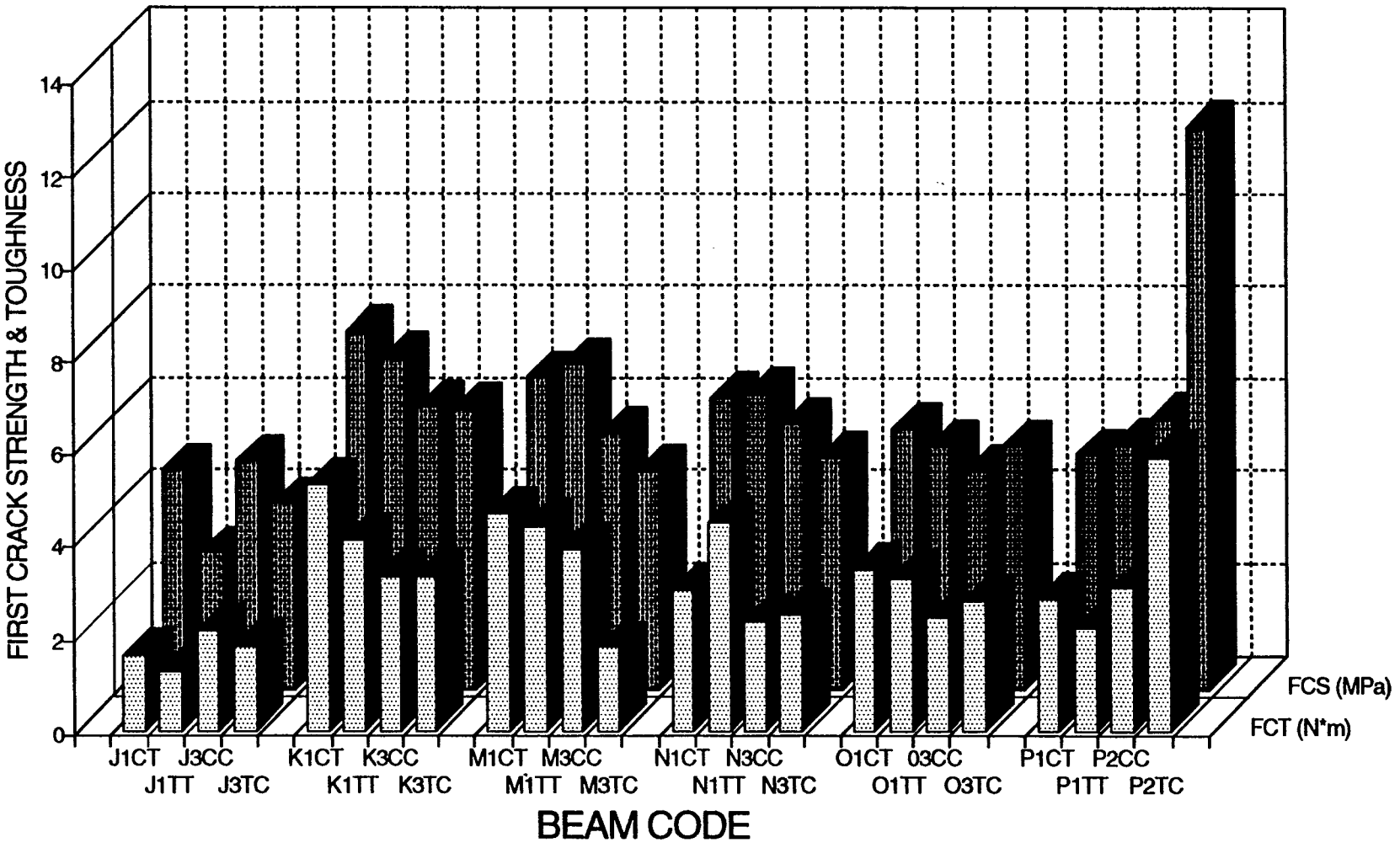

# TOUGHNESS INDICES
## SECOND SERIES

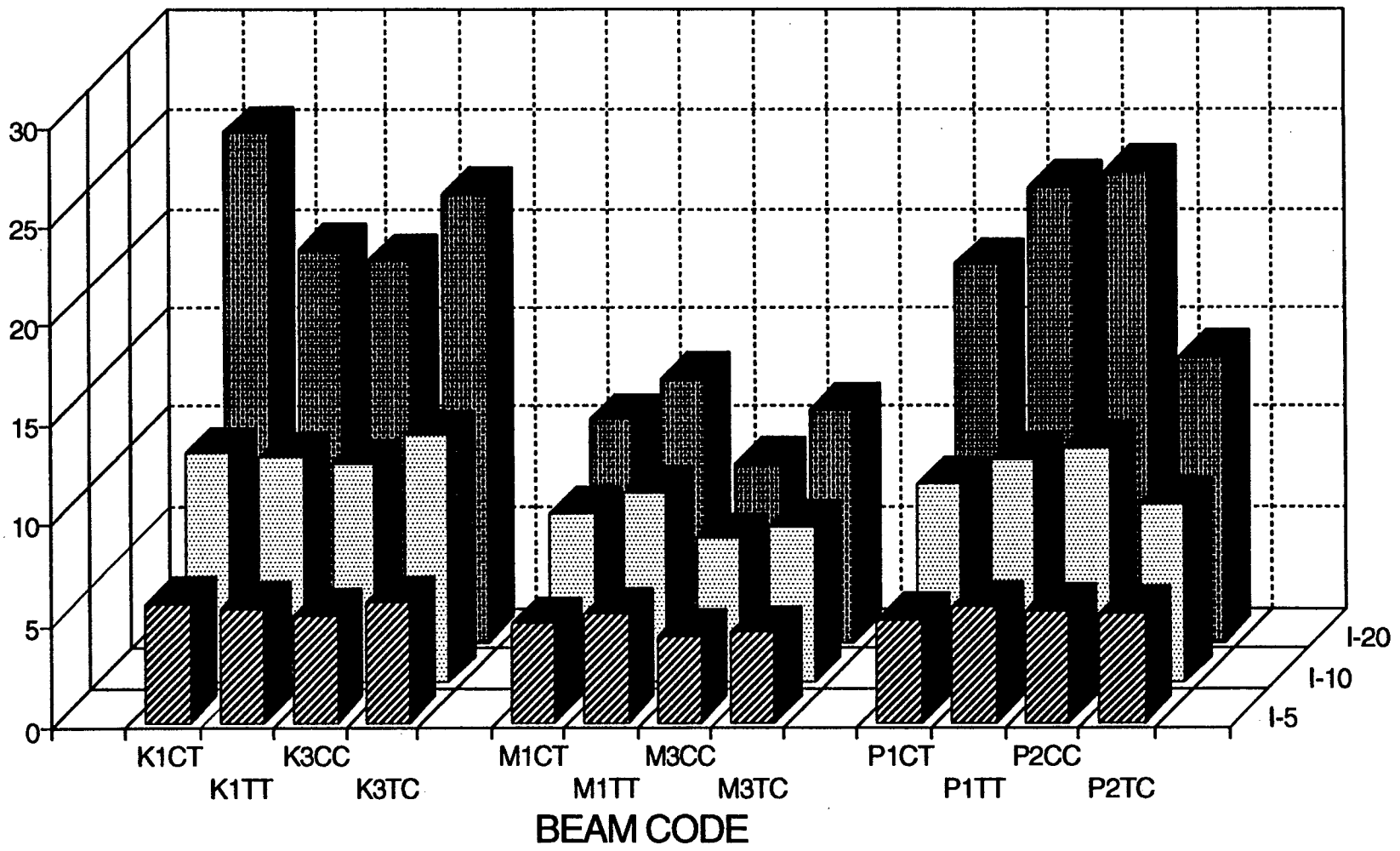

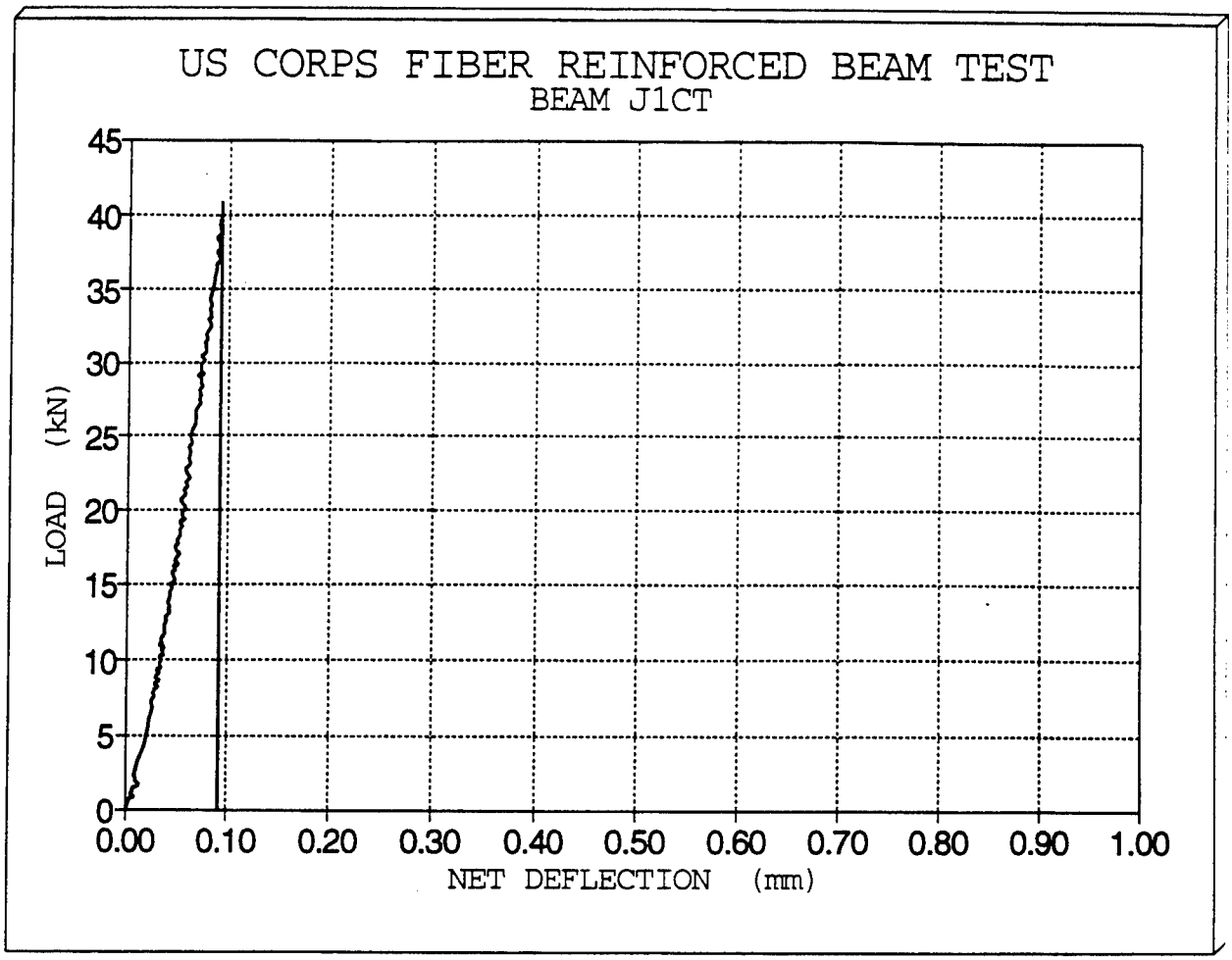
US CORPS FIBER REINFORCED BEAM TEST
BEAM J1CT
LOAD (kN)
0
5
10
15
20
25
30
35
40
45
0.00
0.10
0.20
0.30
0.40
0.50
0.60
0.70
0.80
0.90
1.00
NET DEFLECTION (mm)

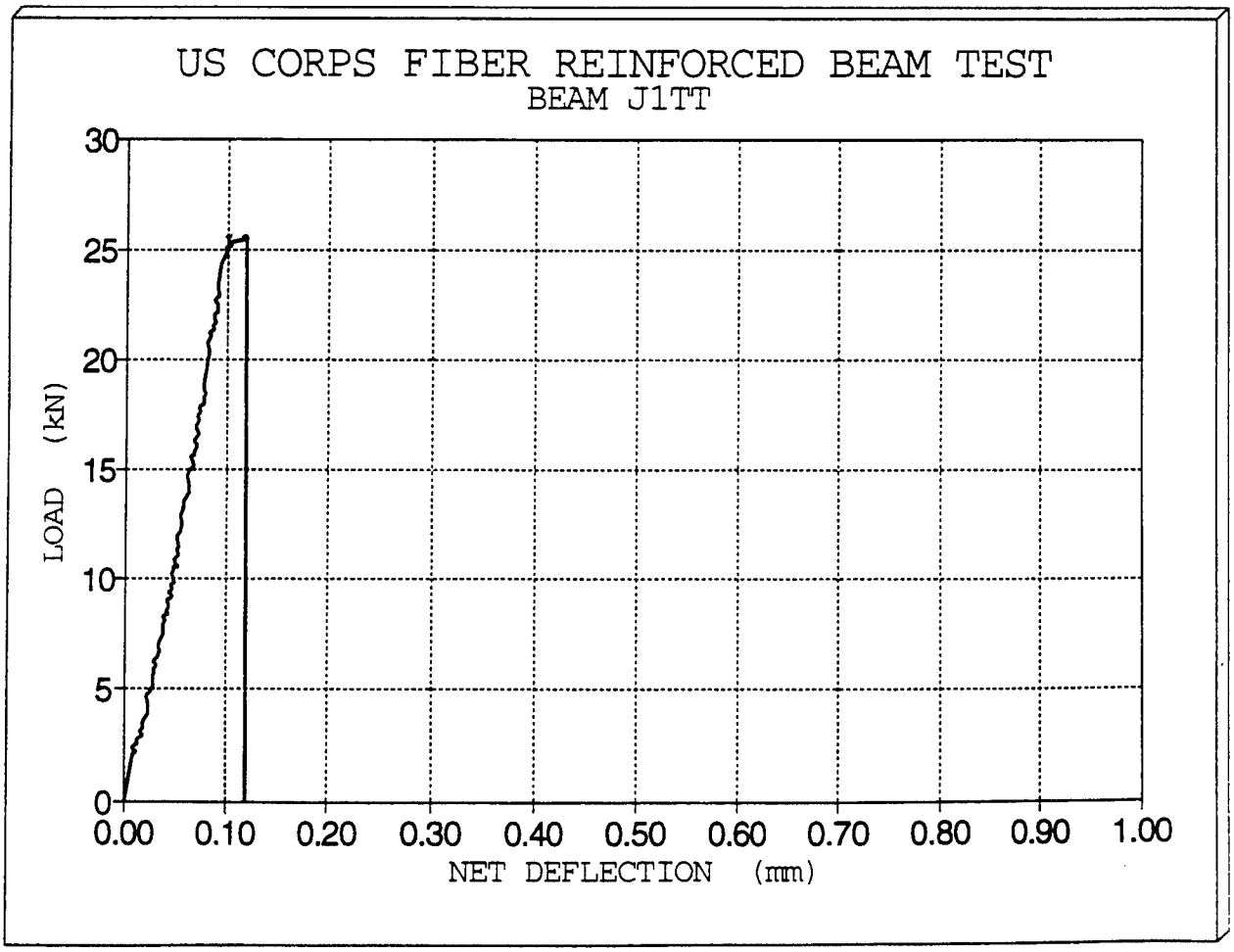
US CORPS FIBER REINFORCED BEAM TEST
BEAM J1TT
LOAD (kN)
0
5
10
15
20
25
30
0.00
0.10
0.20
0.30
0.40
0.50
0.60
0.70
0.80
0.90
1.00
NET DEFLECTION (mm)

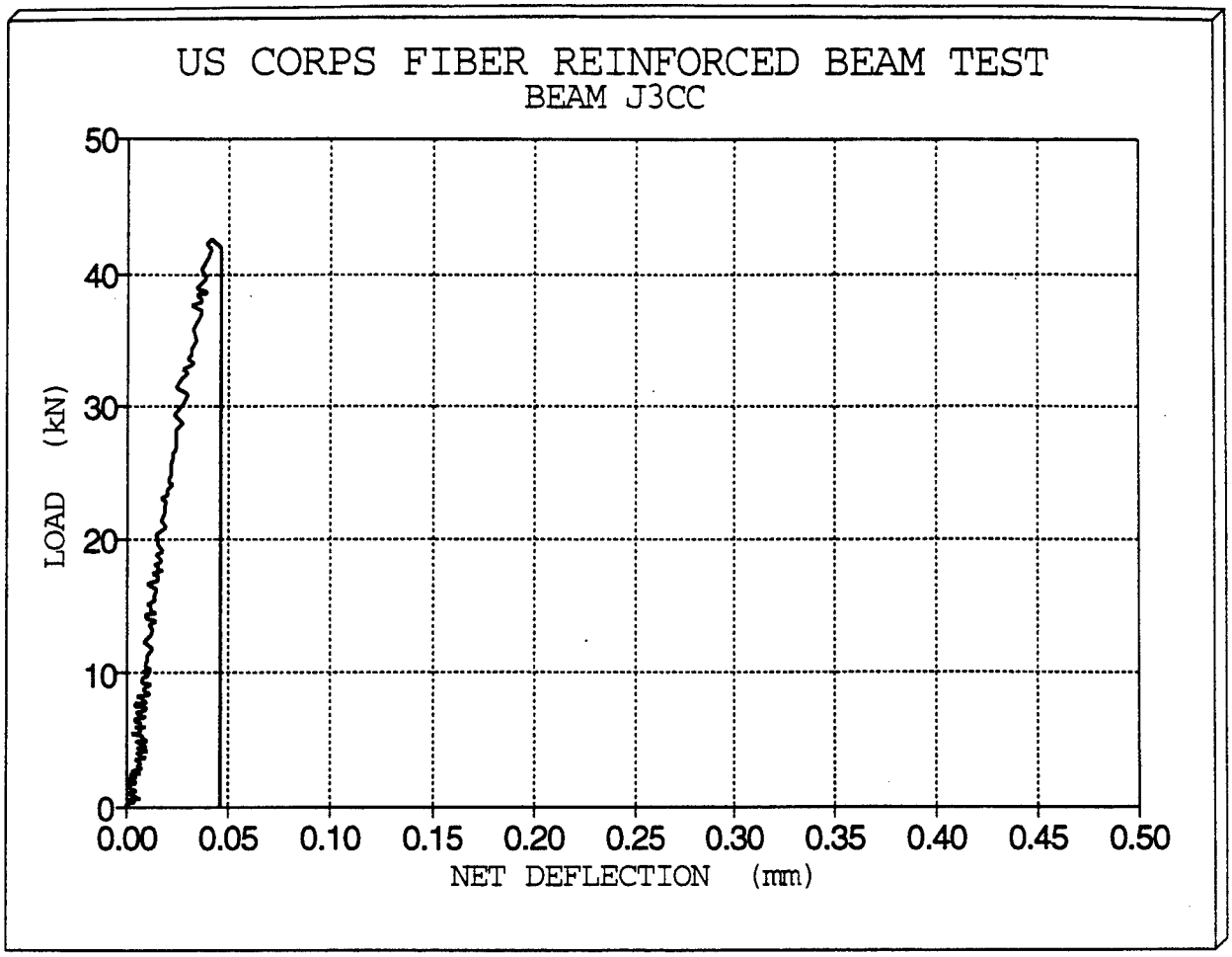
US CORPS FIBER REINFORCED BEAM TEST
BEAM J3CC
LOAD (kN)
0
10
20
30
40
50
0.00
0.05
0.10
0.15
0.20
0.25
0.30
0.35
0.40
0.45
0.50
NET DEFLECTION (mm)

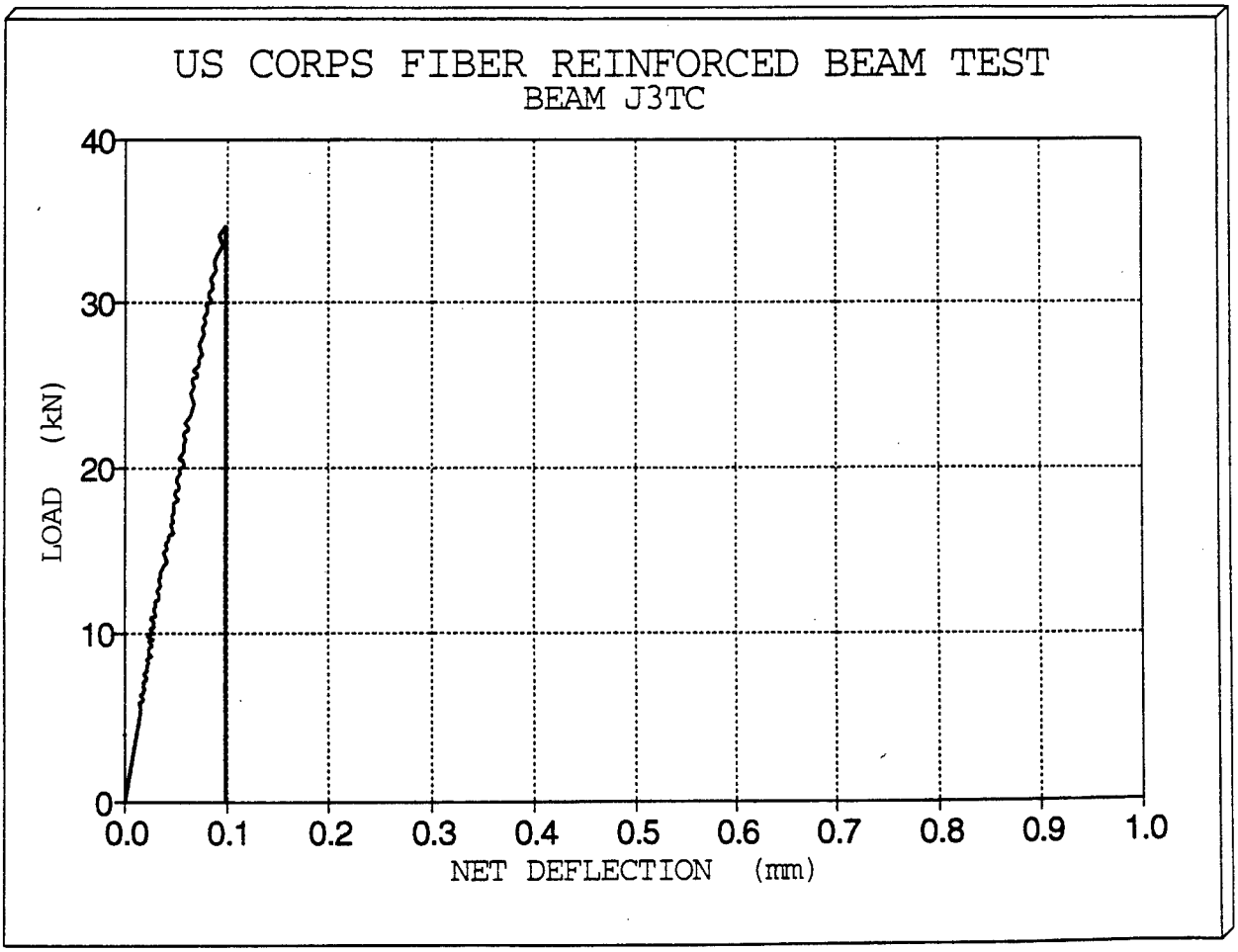
US CORPS FIBER REINFORCED BEAM TEST
BEAM J3TC
LOAD (kN)
0
10
20
30
40
0.0
0.1
0.2
0.3
0.4
0.5
0.6
0.7
0.8
0.9
1.0
NET DEFLECTION (mm)

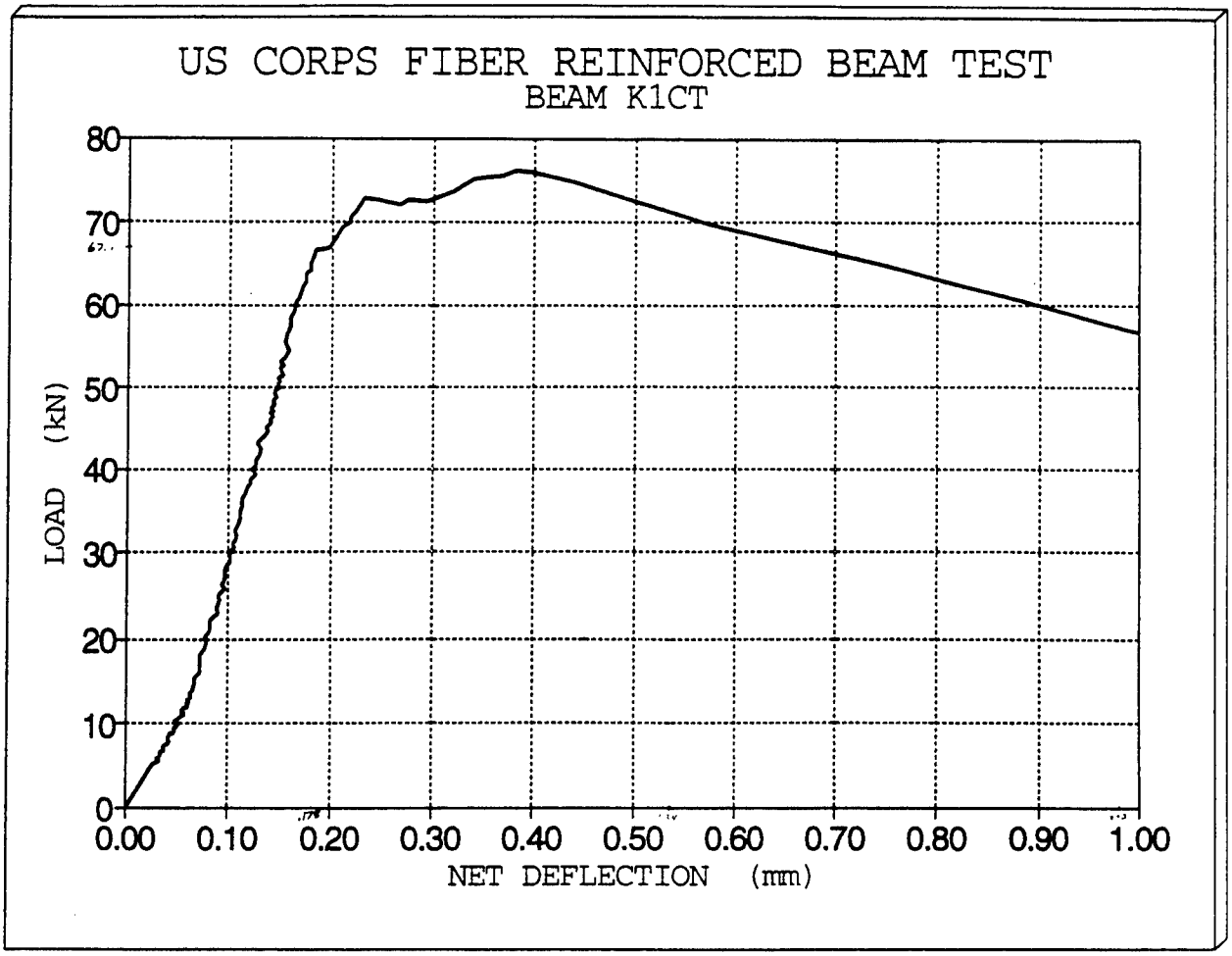
US CORPS FIBER REINFORCED BEAM TEST
BEAM K1CT
LOAD (kN)
0
10
20
30
40
50
60
70
80
0.00
0.10
0.20
0.30
0.40
0.50
0.60
0.70
0.80
0.90
1.00
NET DEFLECTION (mm)

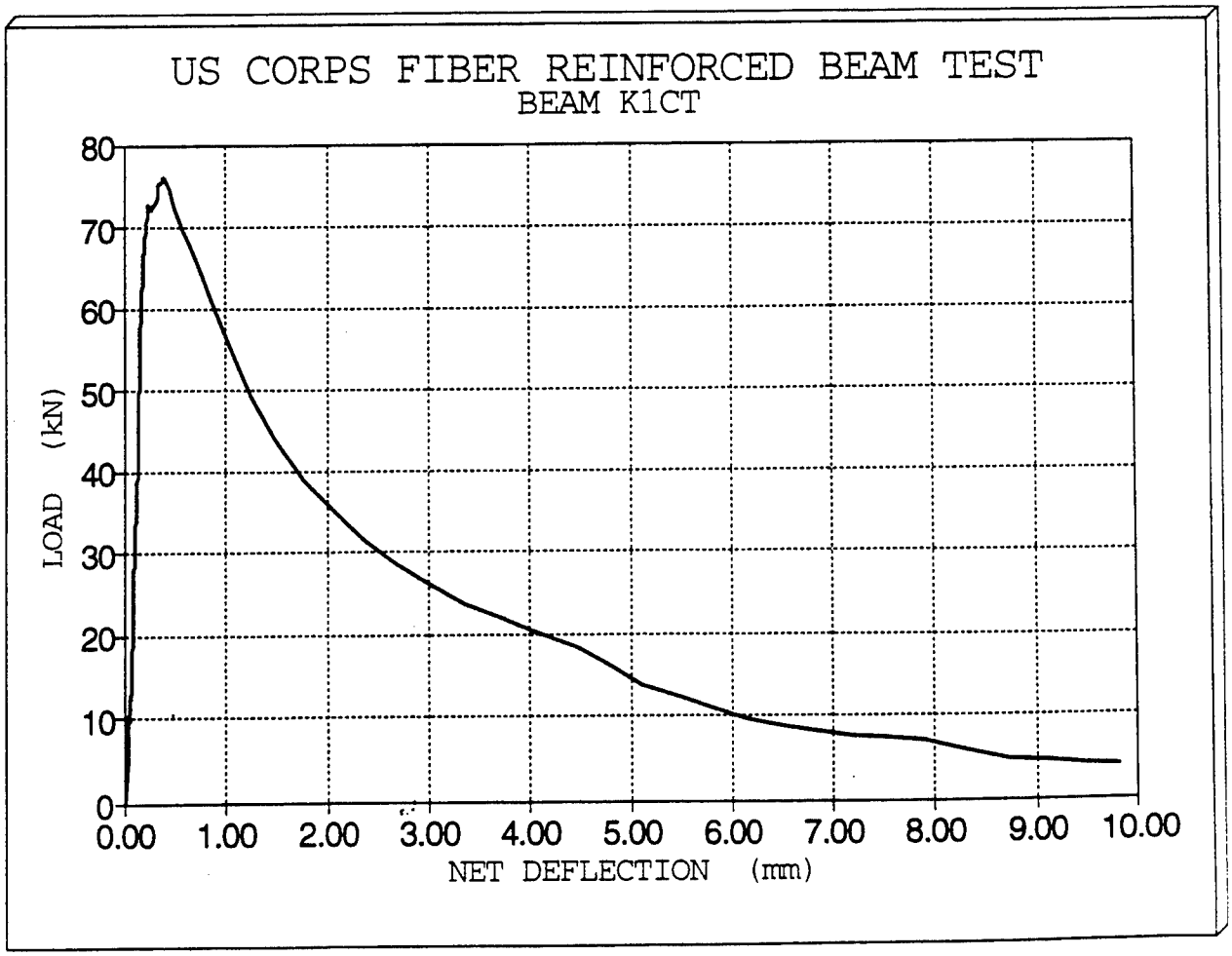
US CORPS FIBER REINFORCED BEAM TEST
BEAM K1CT
LOAD (kN)
0
10
20
30
40
50
60
70
80
0.00
1.00
2.00
3.00
4.00
5.00
6.00
7.00
8.00
9.00
10.00
NET DEFLECTION (mm)

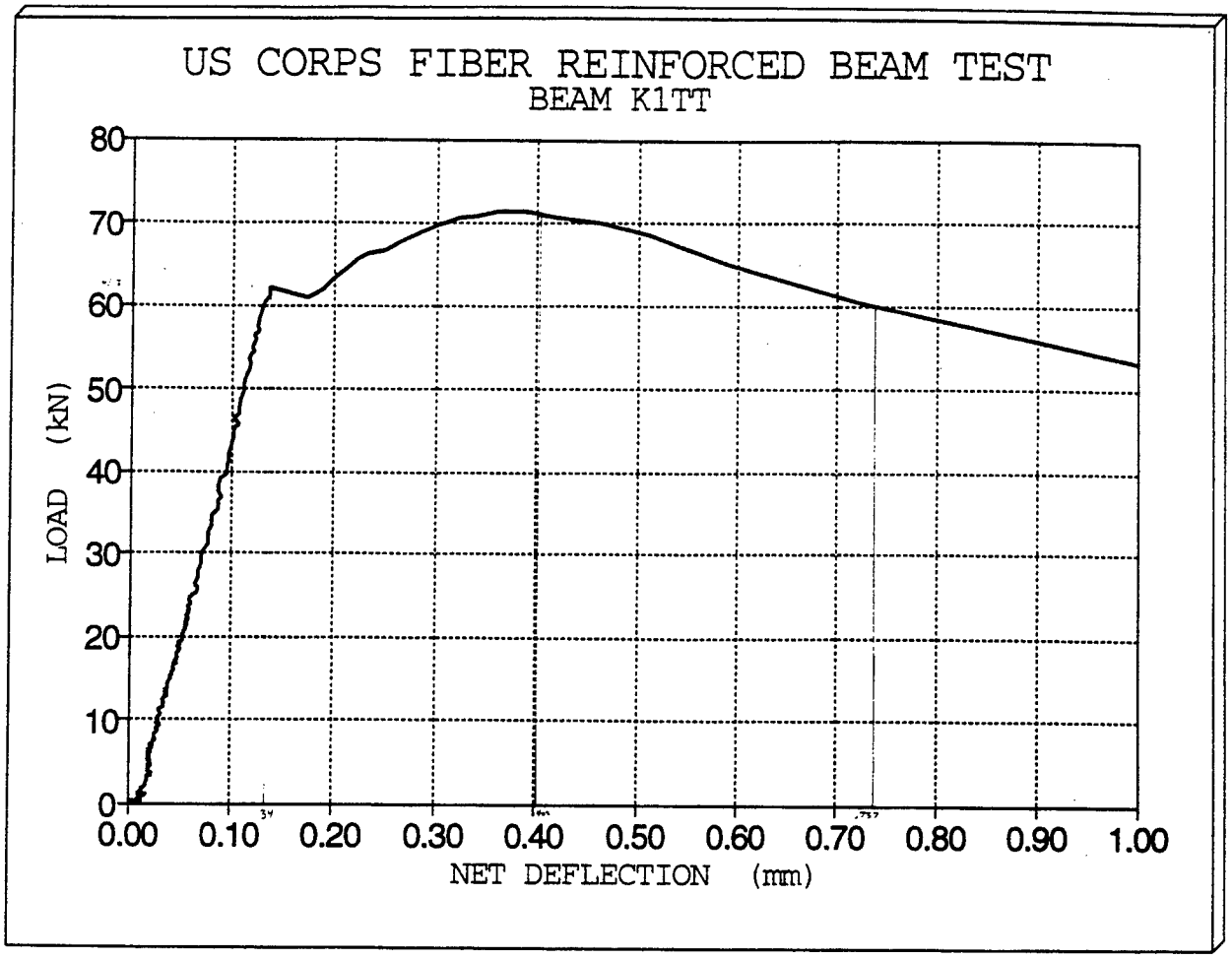
US CORPS FIBER REINFORCED BEAM TEST
BEAM K1TT
LOAD (kN)
80
70
60
50
40
30
20
10
0
0.00
0.10
0.20
0.30
0.40
0.50
0.60
0.70
0.80
0.90
1.00
NET DEFLECTION (mm)

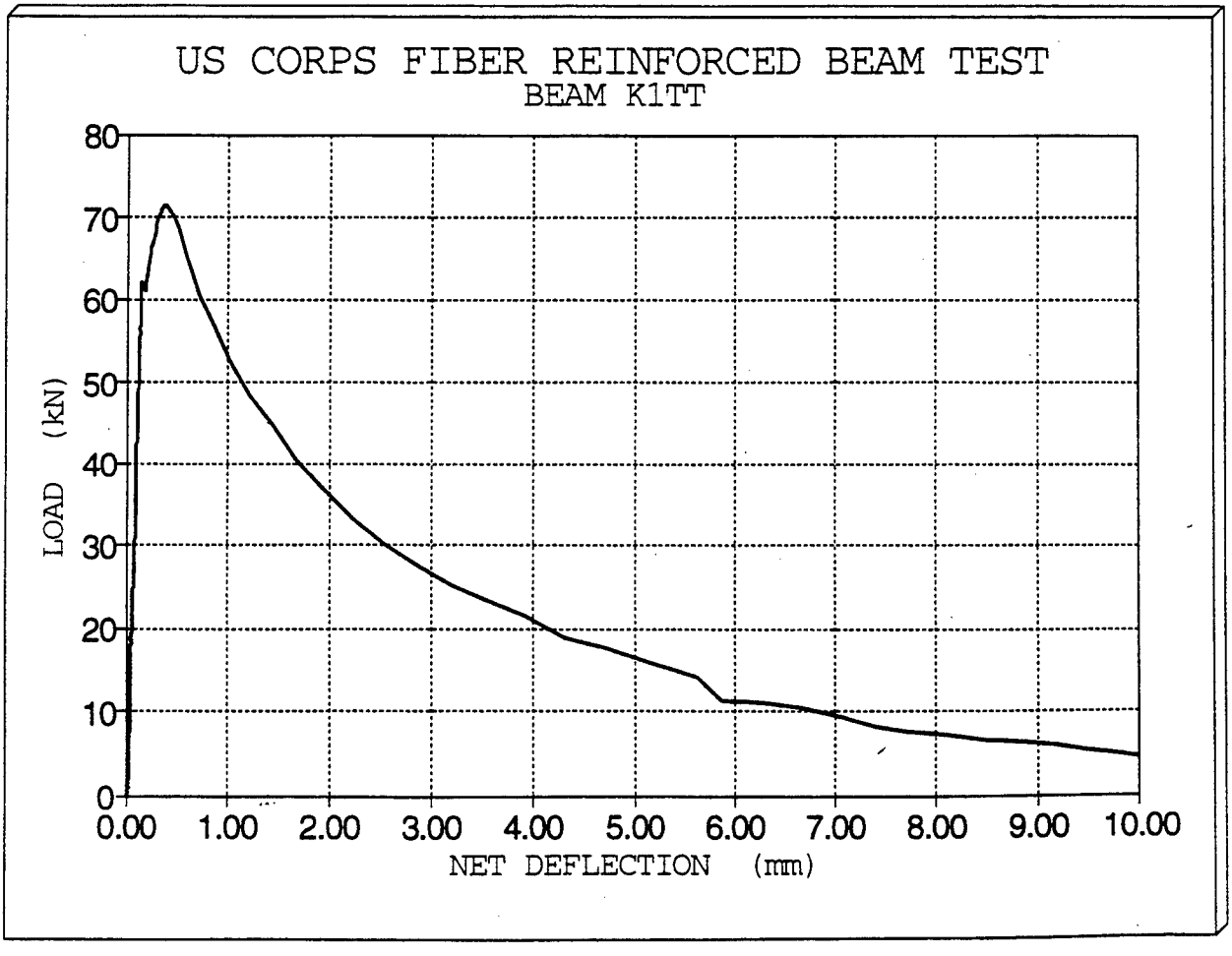
US CORPS FIBER REINFORCED BEAM TEST
BEAM K1TT
LOAD (kN)
80
70
60
50
40
30
20
10
0
0.00
1.00
2.00
3.00
4.00
5.00
6.00
7.00
8.00
9.00
10.00
NET DEFLECTION (mm)

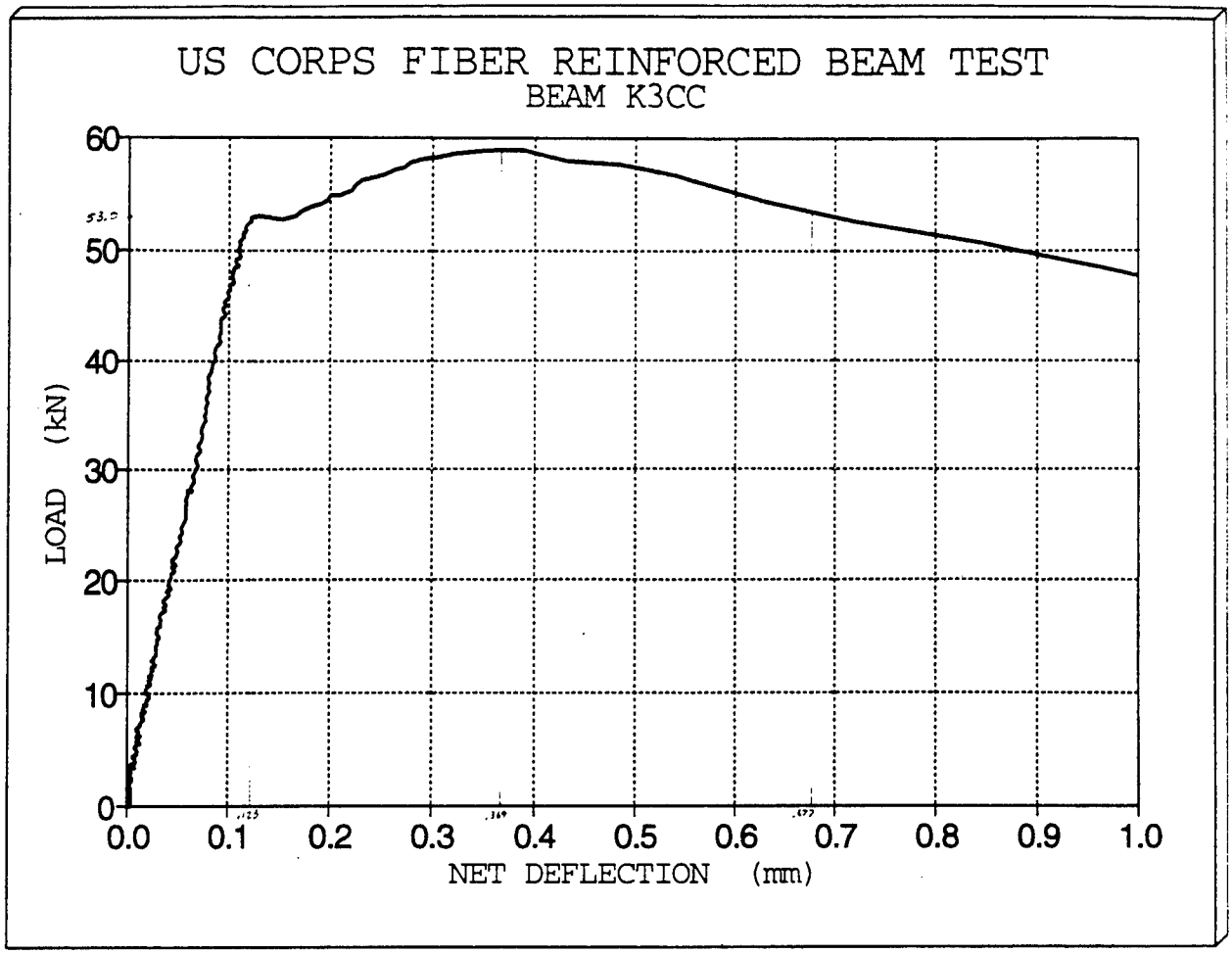
US CORPS FIBER REINFORCED BEAM TEST
BEAM K3CC
LOAD (kN)
0
10
20
30
40
50
60
0.0
0.1
0.2
0.3
0.4
0.5
0.6
0.7
0.8
0.9
1.0
NET DEFLECTION (mm)

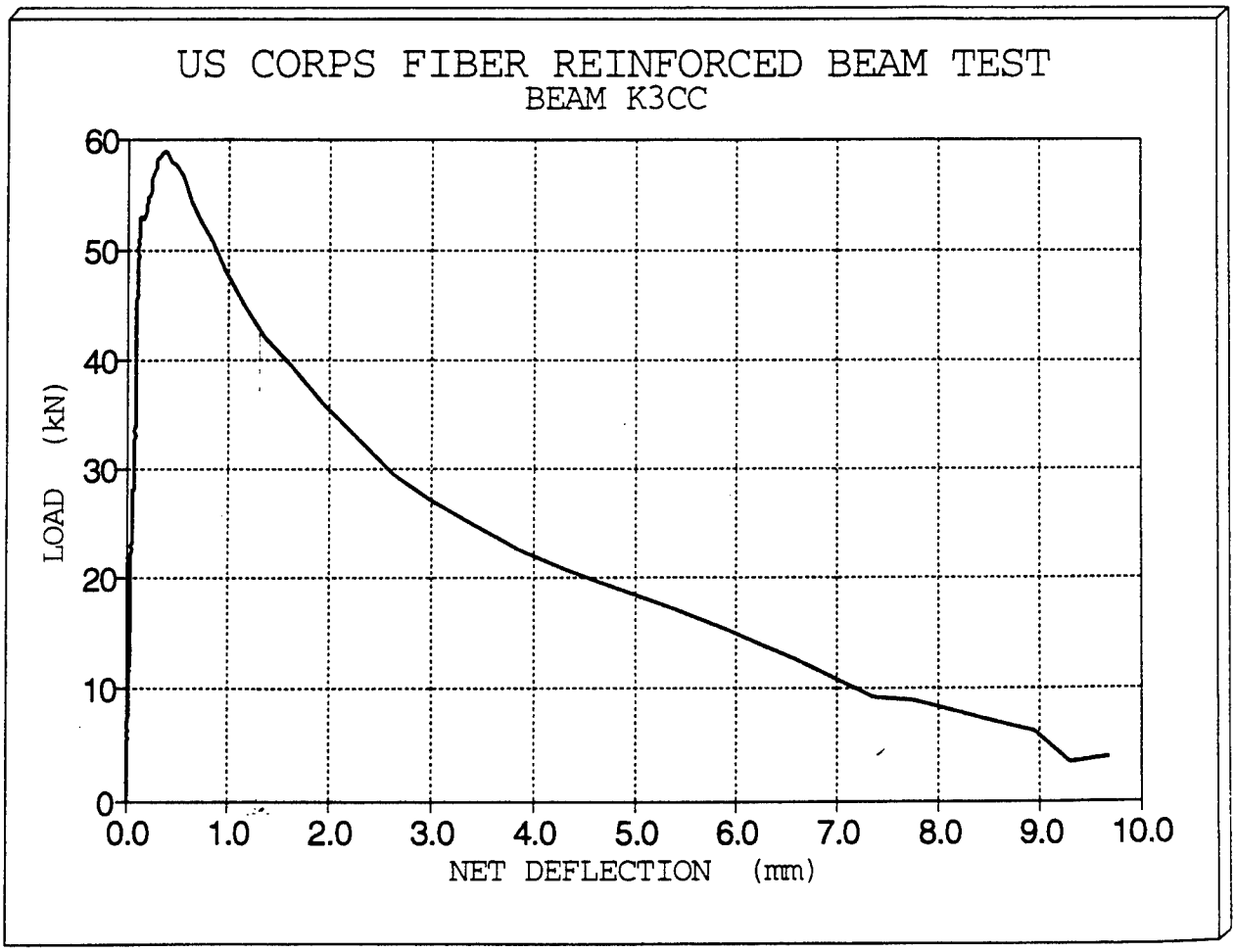
US CORPS FIBER REINFORCED BEAM TEST
BEAM K3CC
LOAD (kN)
0
10
20
30
40
50
60
0.0
1.0
2.0
3.0
4.0
5.0
6.0
7.0
8.0
9.0
10.0
NET DEFLECTION (mm)

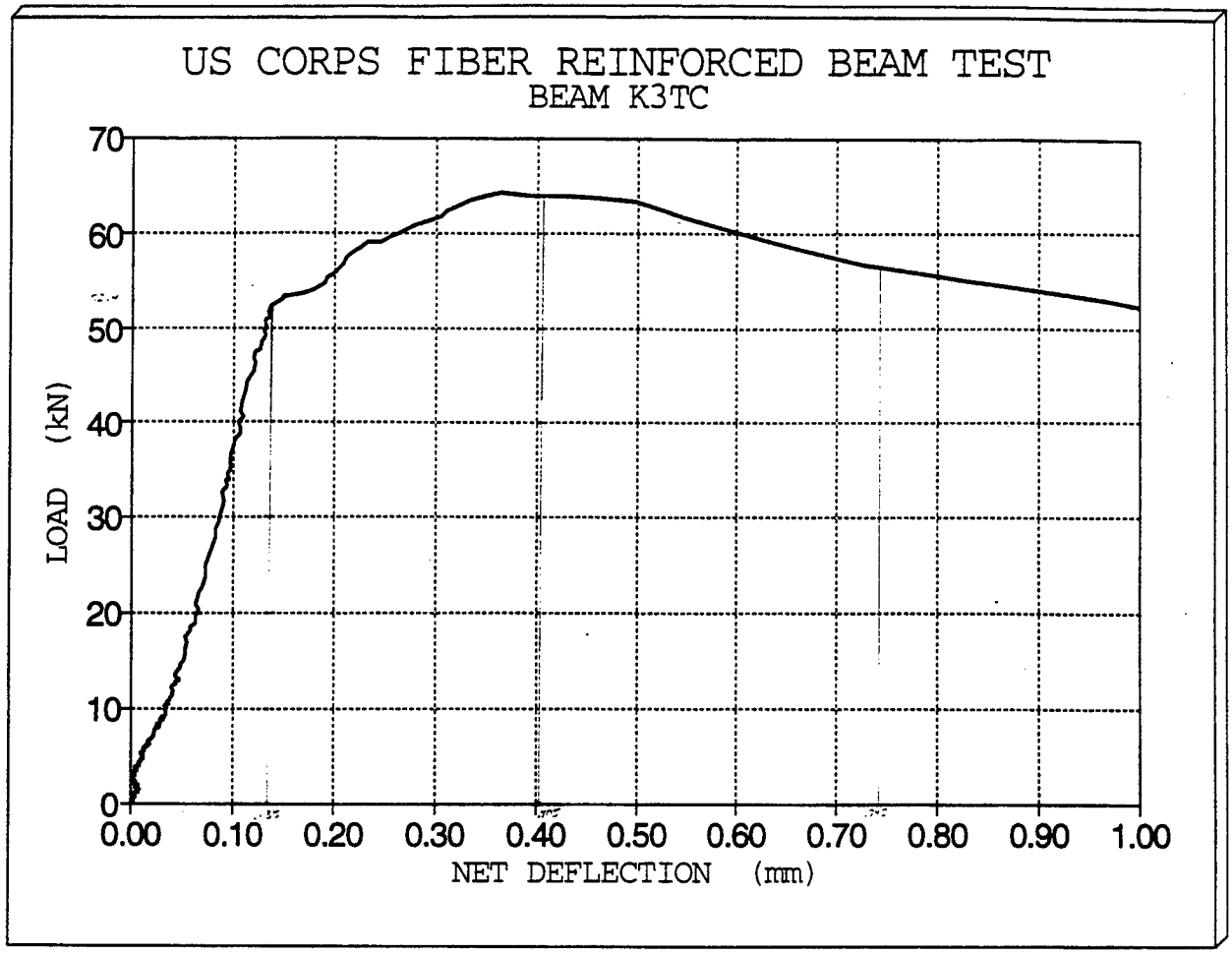
US CORPS FIBER REINFORCED BEAM TEST
BEAM K3TC
LOAD (kN)
70
60
50
40
30
20
10
0
0.00
0.10
0.20
0.30
0.40
0.50
0.60
0.70
0.80
0.90
1.00
NET DEFLECTION (mm)

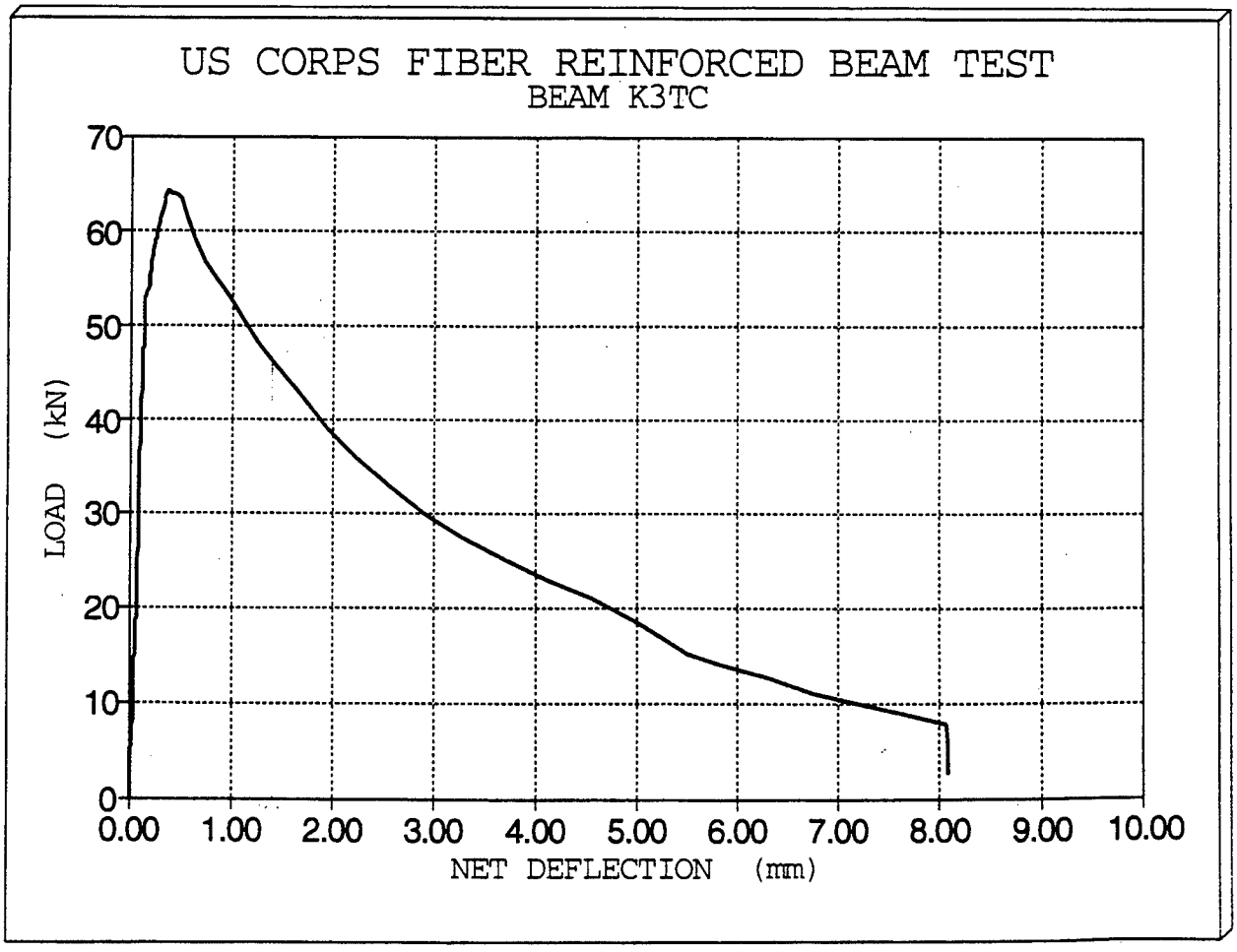
US CORPS FIBER REINFORCED BEAM TEST
BEAM K3TC
LOAD (kN)
70
60
50
40
30
20
10
0
0.00
1.00
2.00
3.00
4.00
5.00
6.00
7.00
8.00
9.00
10.00
NET DEFLECTION (mm)

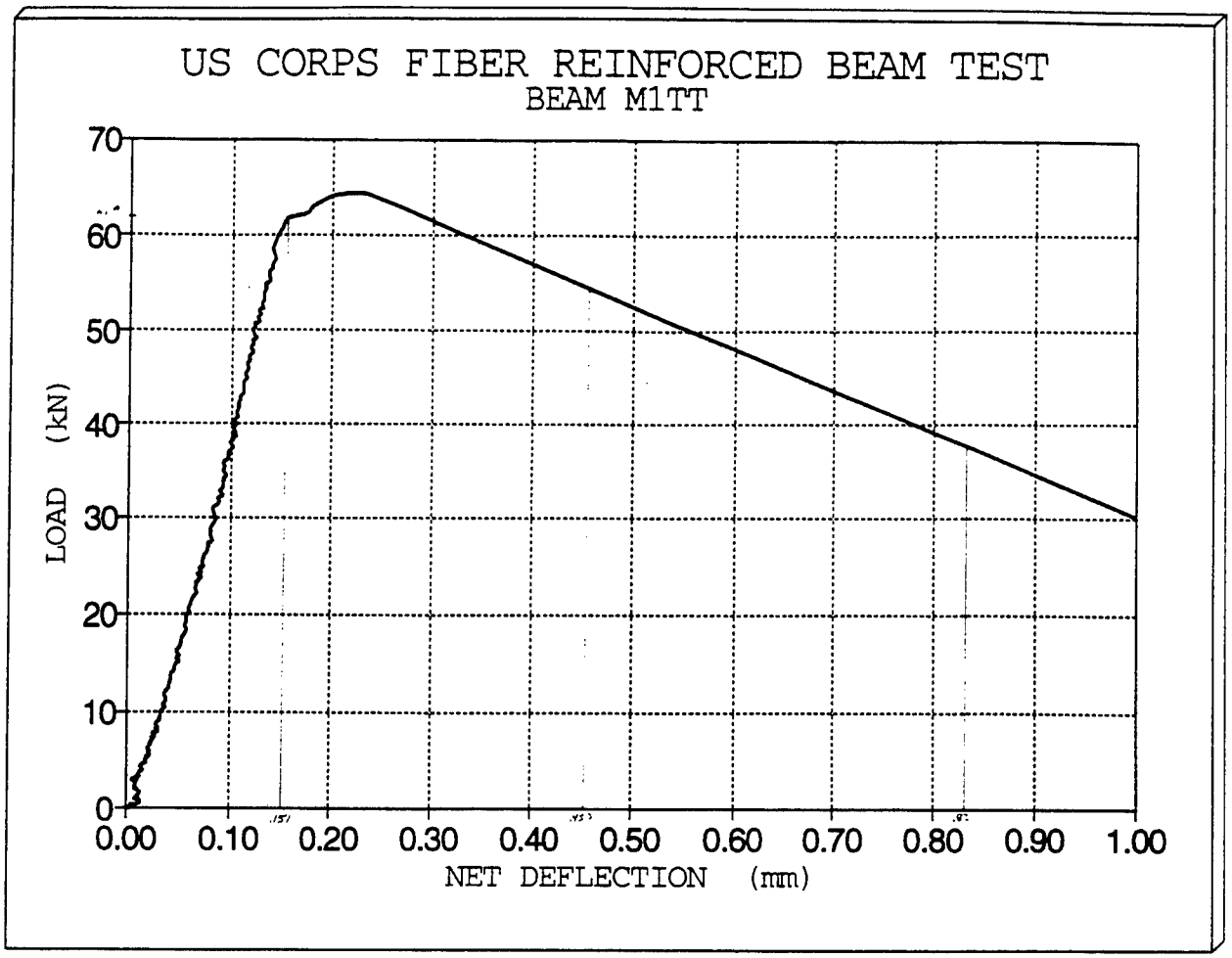
US CORPS FIBER REINFORCED BEAM TEST
BEAM M1TT
LOAD (kN)
70
60
50
40
30
20
10
0
0.00
0.10
0.20
0.30
0.40
0.50
0.60
0.70
0.80
0.90
1.00
NET DEFLECTION (mm)

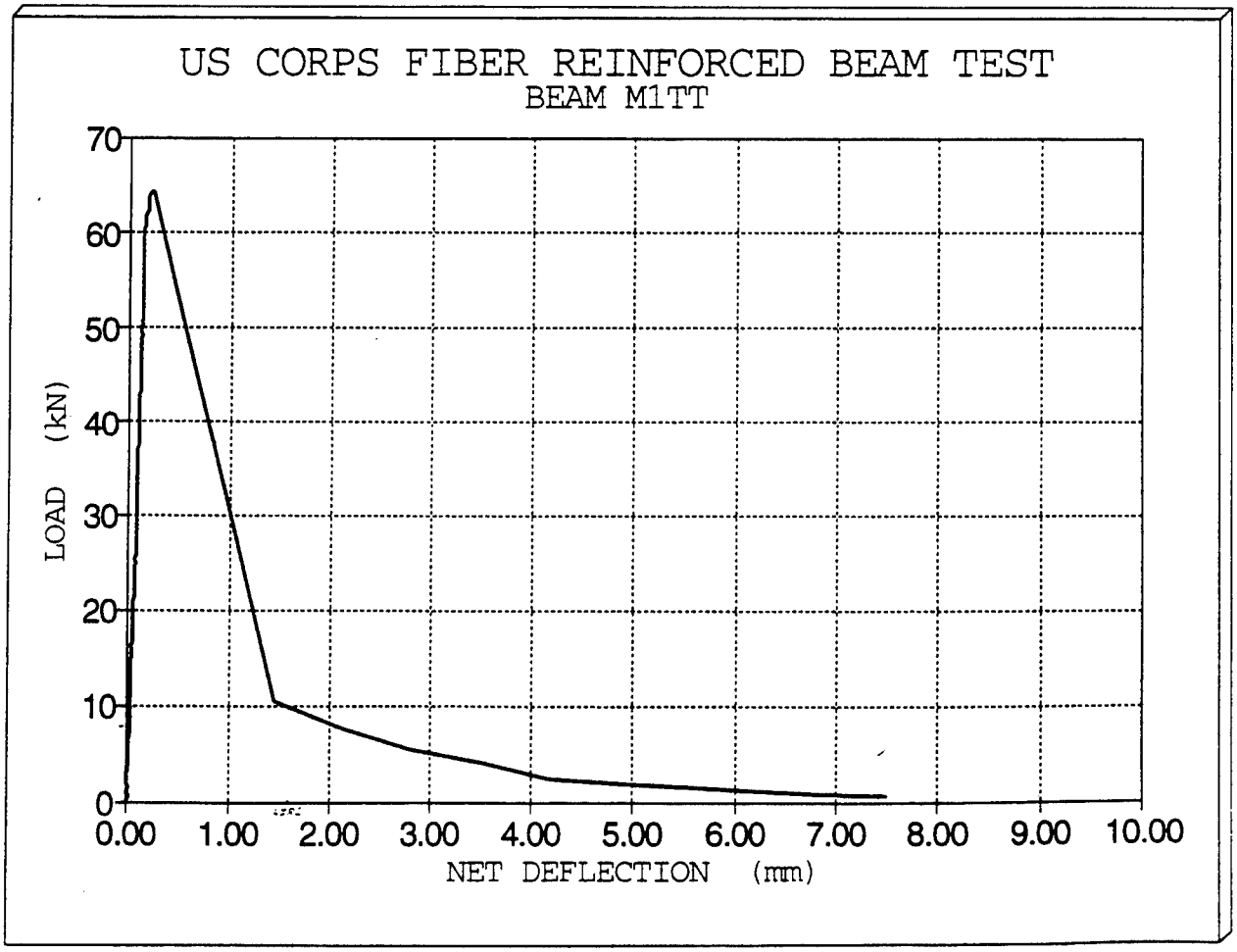
US CORPS FIBER REINFORCED BEAM TEST
BEAM M1TT
LOAD (kN)
70
60
50
40
30
20
10
0
0.00
1.00
2.00
3.00
4.00
5.00
6.00
7.00
8.00
9.00
10.00
NET DEFLECTION (mm)

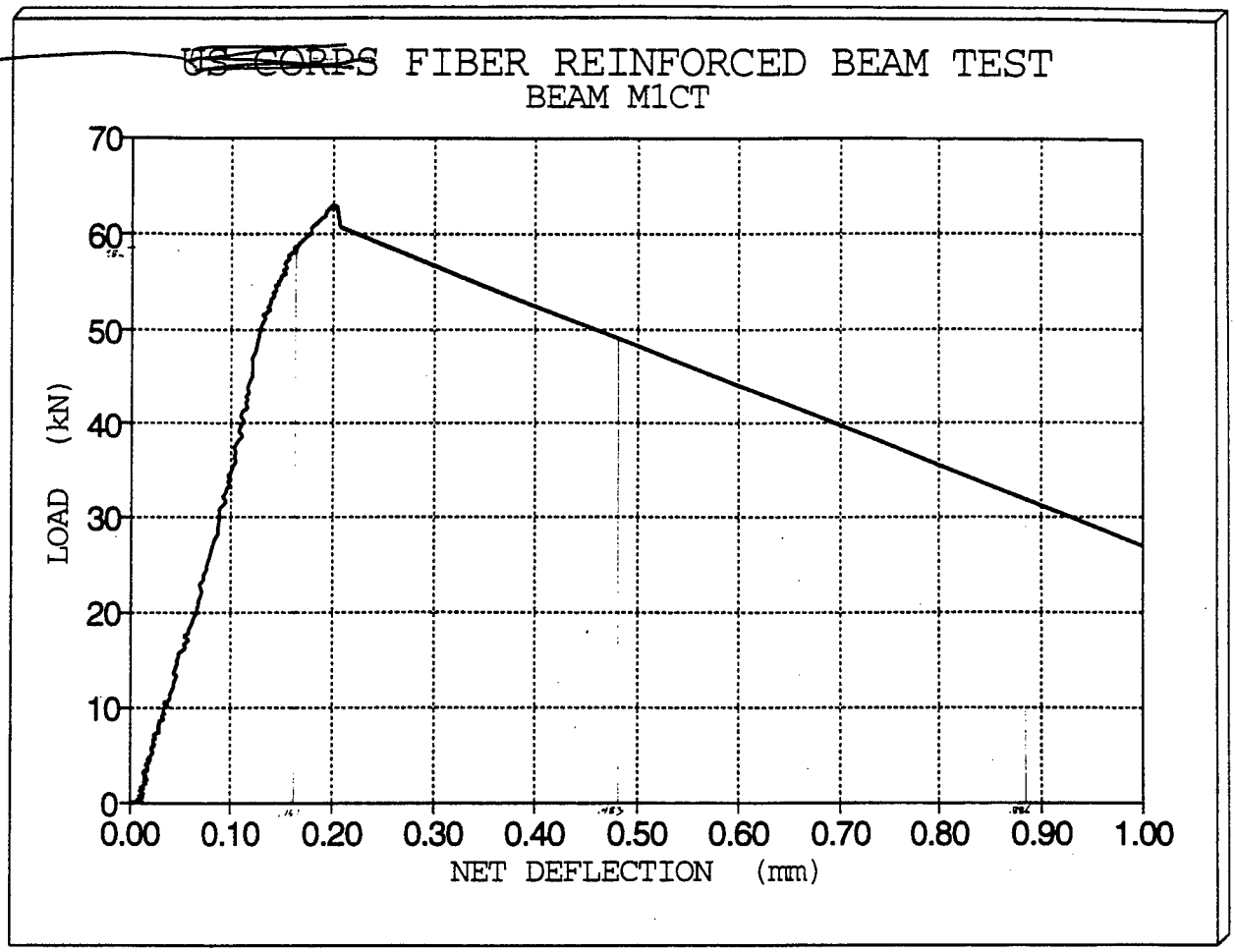
~~US CORPS~~ FIBER REINFORCED BEAM TEST
BEAM M1CT
LOAD (kN)
70
60
50
40
30
20
10
0
0.00
0.10
0.20
0.30
0.40
0.50
0.60
0.70
0.80
0.90
1.00
NET DEFLECTION (mm)

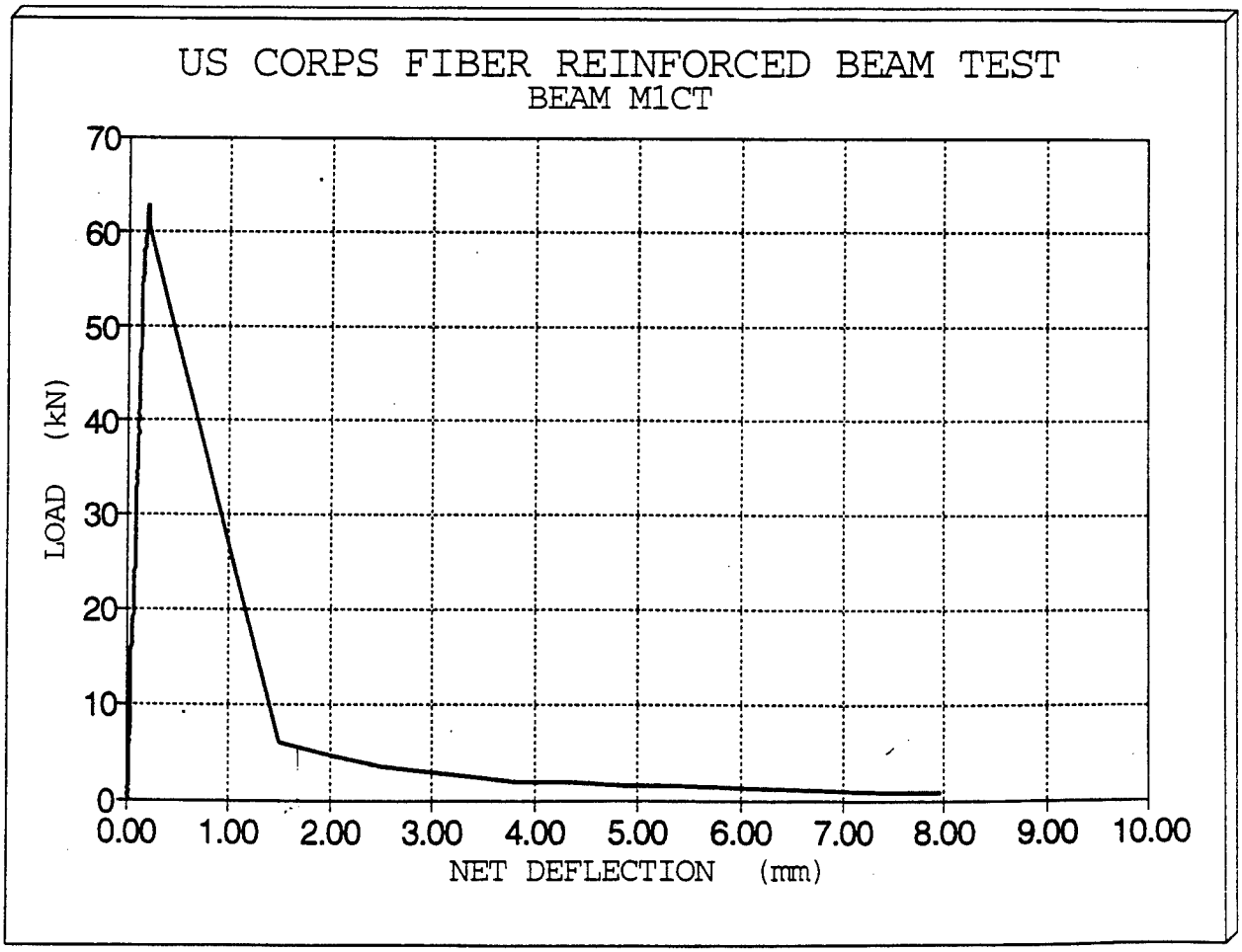
US CORPS FIBER REINFORCED BEAM TEST
BEAM M1CT
LOAD (kN)
70
60
50
40
30
20
10
0
0.00
1.00
2.00
3.00
4.00
5.00
6.00
7.00
8.00
9.00
10.00
NET DEFLECTION (mm)

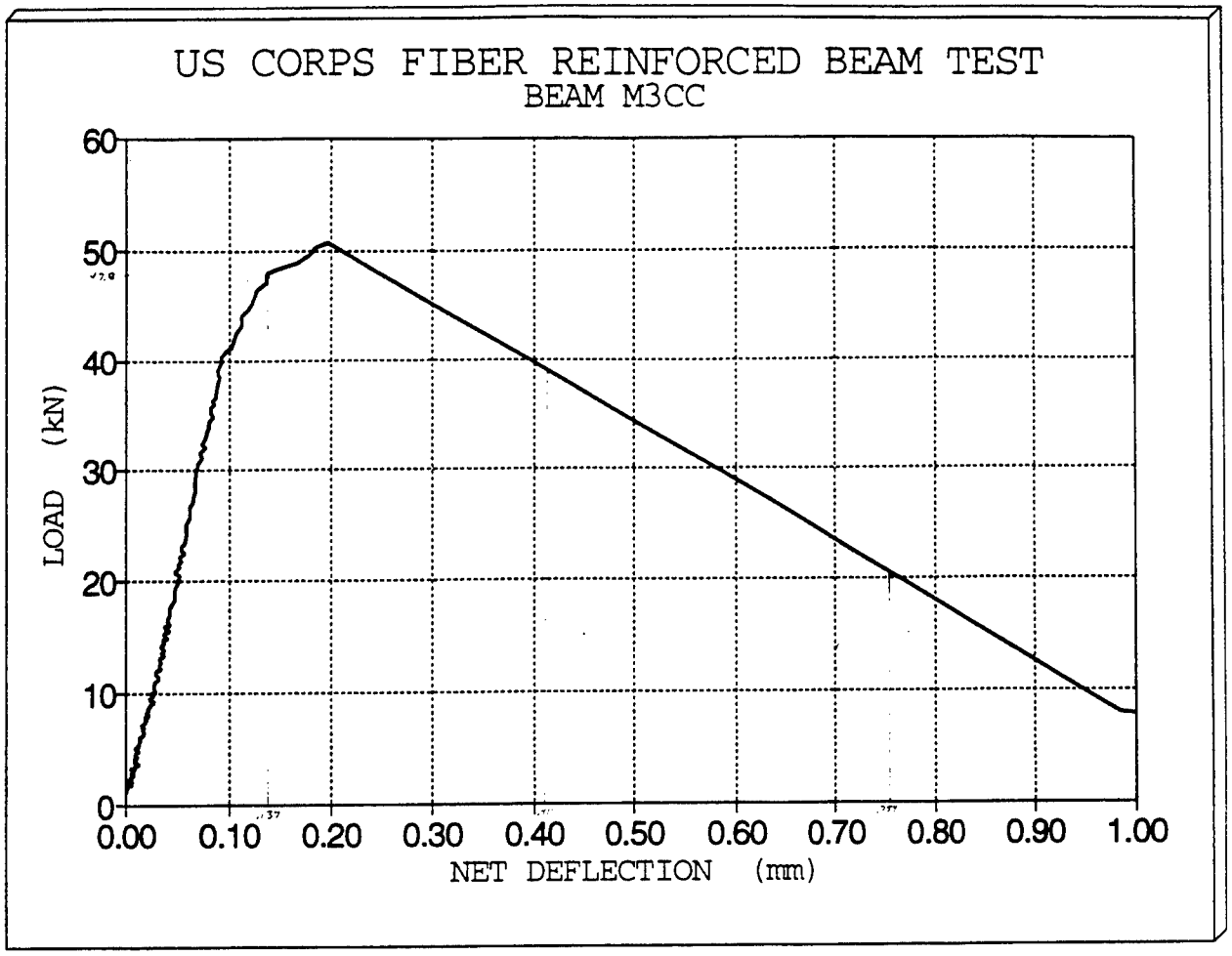
US CORPS FIBER REINFORCED BEAM TEST
BEAM M3CC
LOAD (kN)
60
50
40
30
20
10
0
0.00
0.10
0.20
0.30
0.40
0.50
0.60
0.70
0.80
0.90
1.00
NET DEFLECTION (mm)

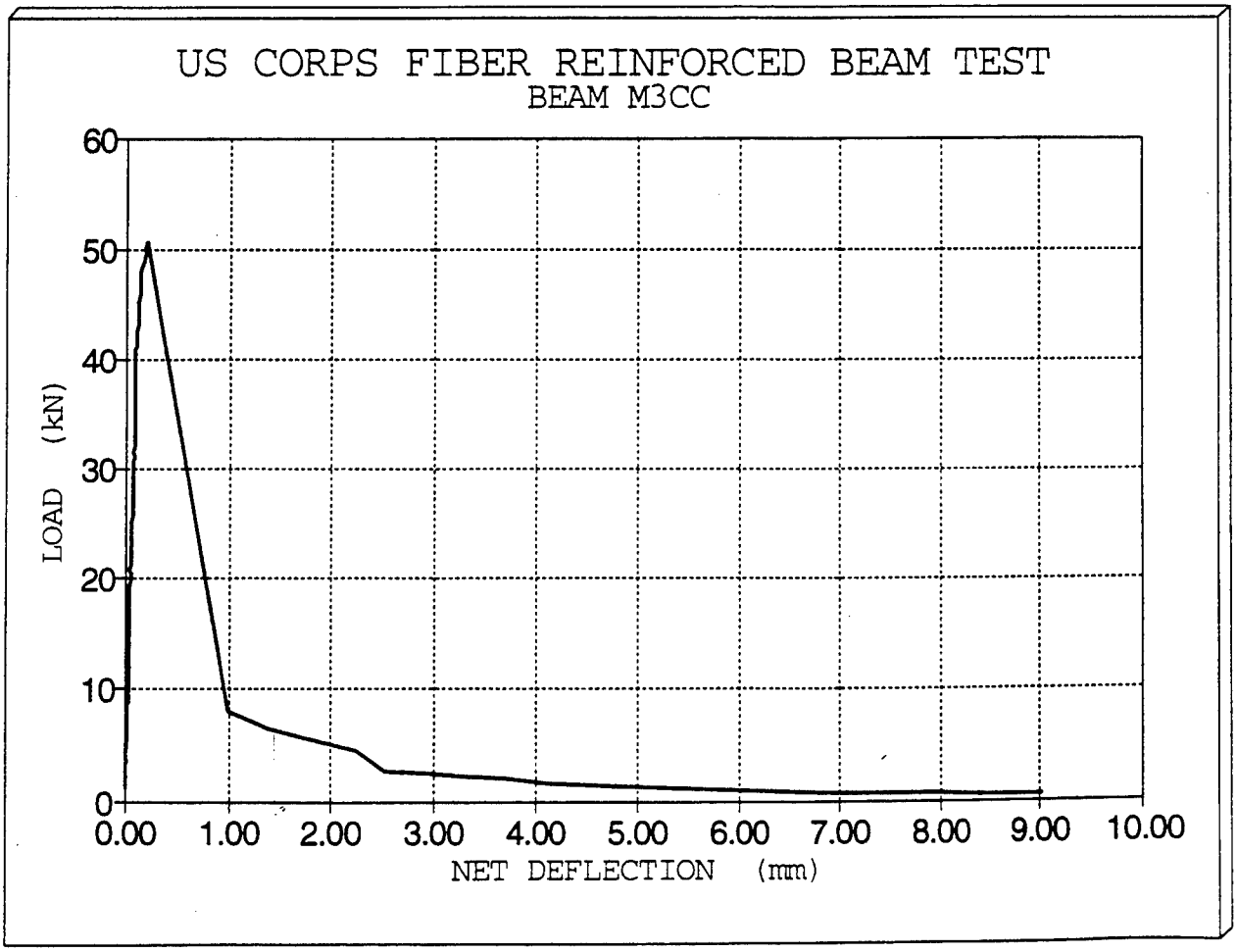
US CORPS FIBER REINFORCED BEAM TEST
BEAM M3CC
LOAD (kN)
60
50
40
30
20
10
0
0.00
1.00
2.00
3.00
4.00
5.00
6.00
7.00
8.00
9.00
10.00
NET DEFLECTION (mm)

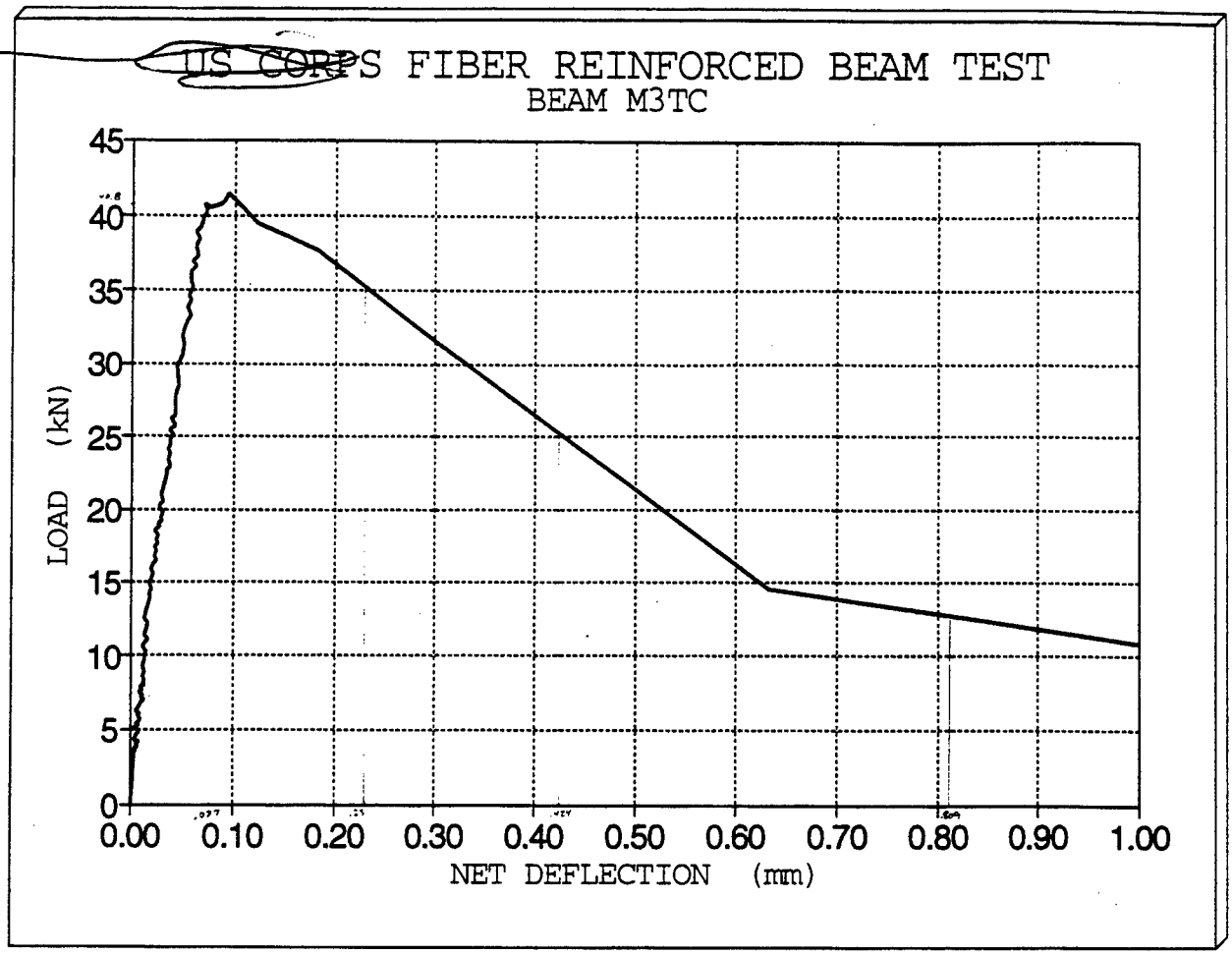
US CORPS FIBER REINFORCED BEAM TEST
BEAM M3TC
LOAD (kN)
0
5
10
15
20
25
30
35
40
45
0.00
0.10
0.20
0.30
0.40
0.50
0.60
0.70
0.80
0.90
1.00
NET DEFLECTION (mm)

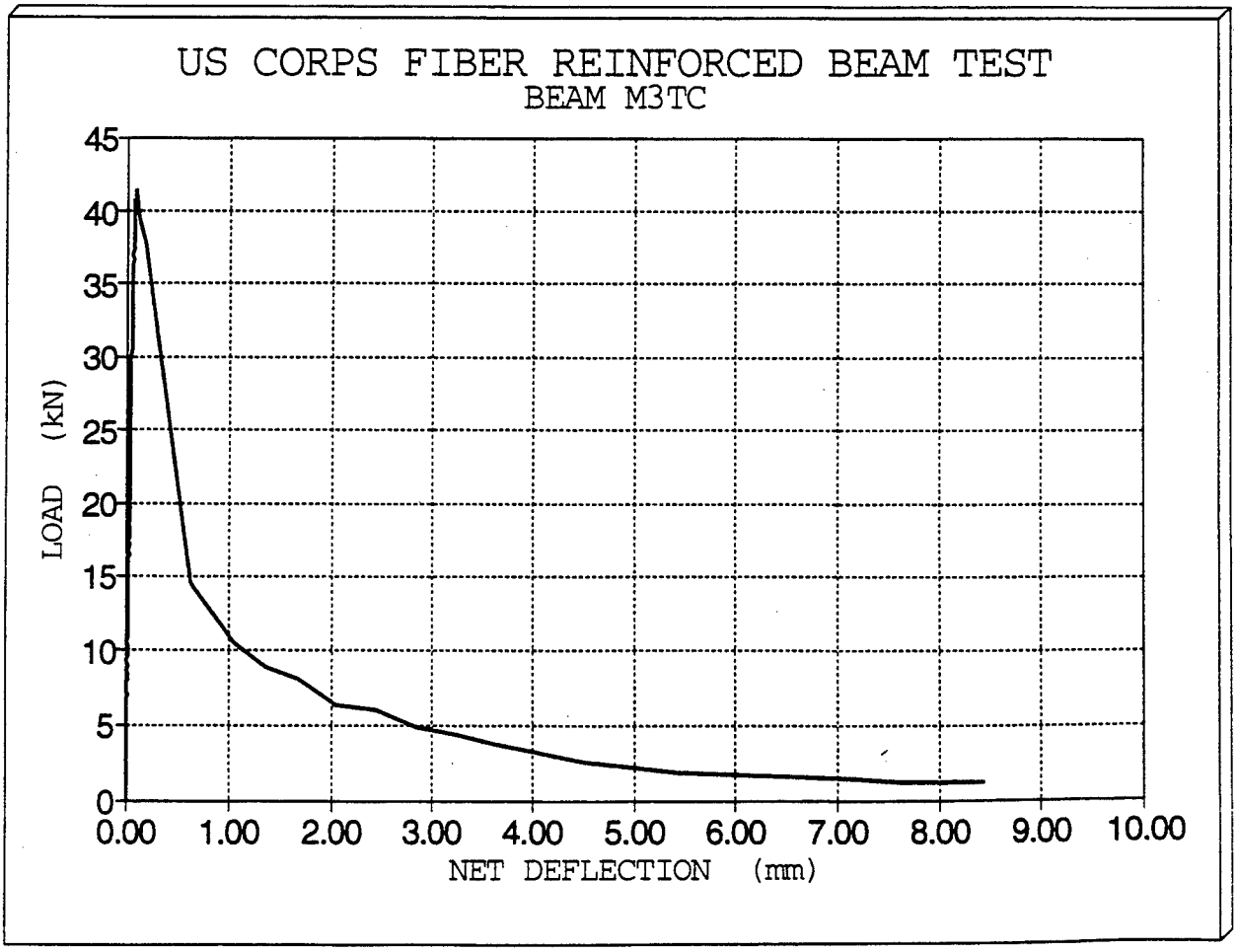
US CORPS FIBER REINFORCED BEAM TEST
BEAM M3TC
LOAD (kN)
0
5
10
15
20
25
30
35
40
45
0.00
1.00
2.00
3.00
4.00
5.00
6.00
7.00
8.00
9.00
10.00
NET DEFLECTION (mm)

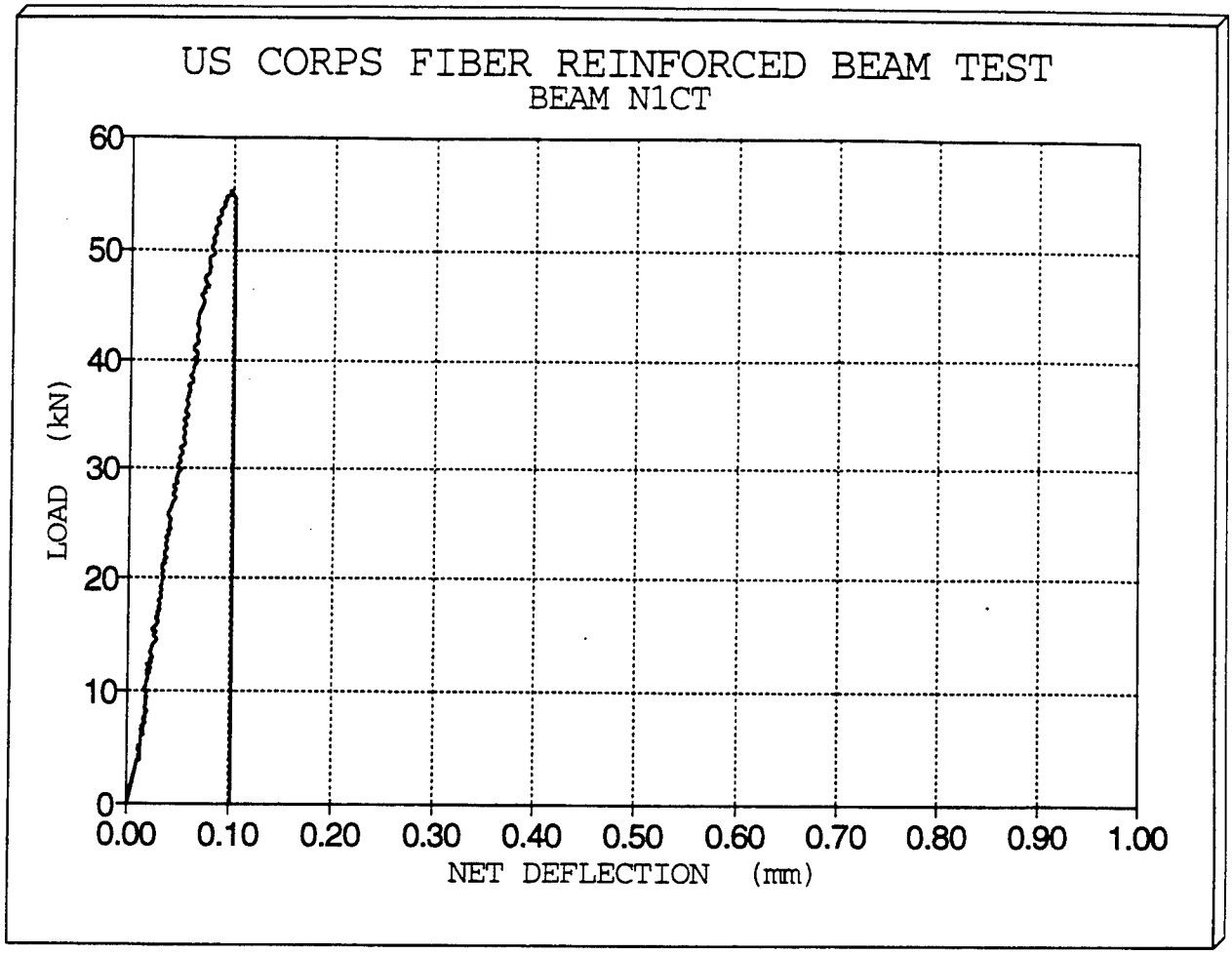
US CORPS FIBER REINFORCED BEAM TEST
BEAM N1CT
LOAD (kN)
60
50
40
30
20
10
0
0.00
0.10
0.20
0.30
0.40
0.50
0.60
0.70
0.80
0.90
1.00
NET DEFLECTION (mm)

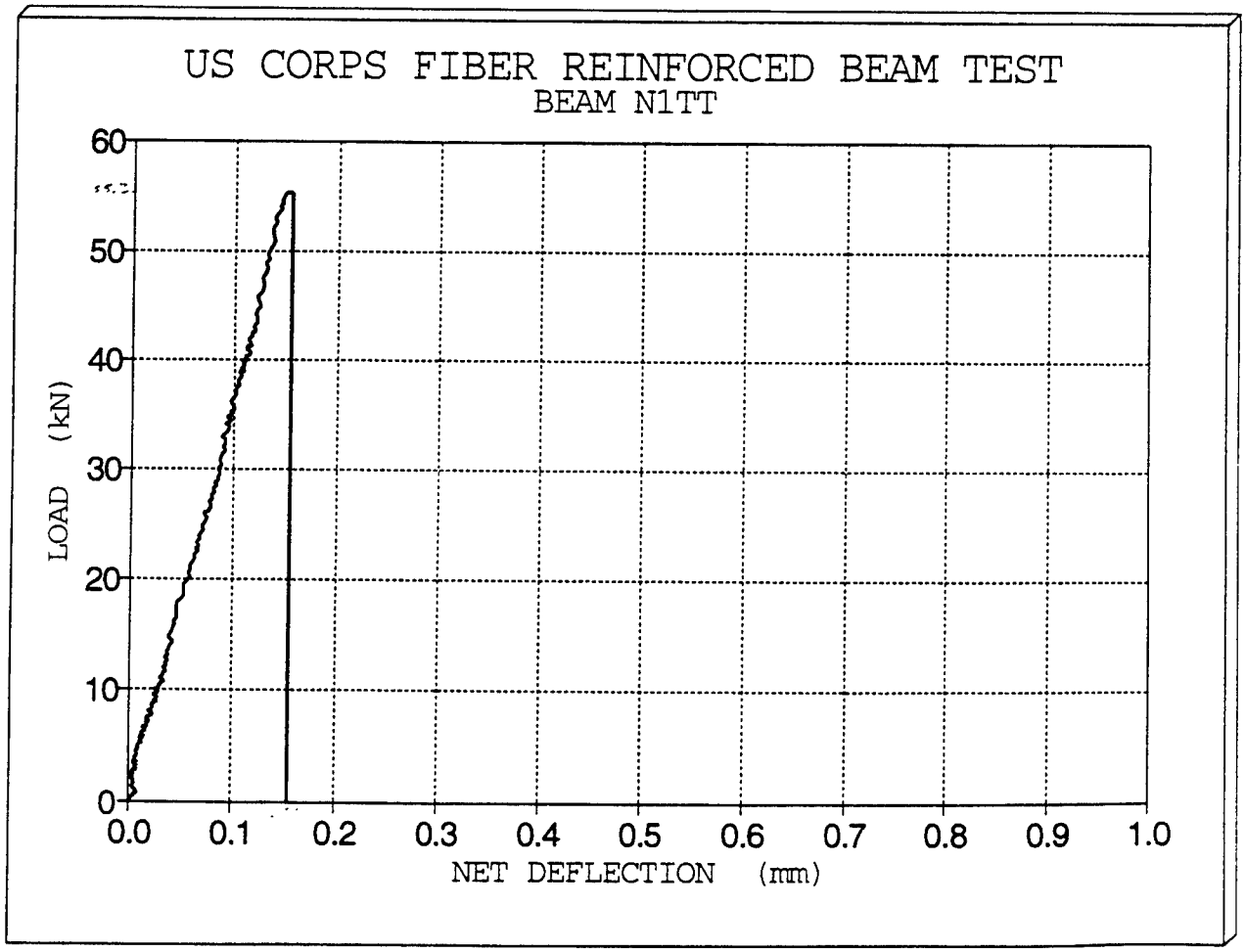
US CORPS FIBER REINFORCED BEAM TEST
BEAM N1TT
LOAD (kN)
60
50
40
30
20
10
0
0.0
0.1
0.2
0.3
0.4
0.5
0.6
0.7
0.8
0.9
1.0
NET DEFLECTION (mm)

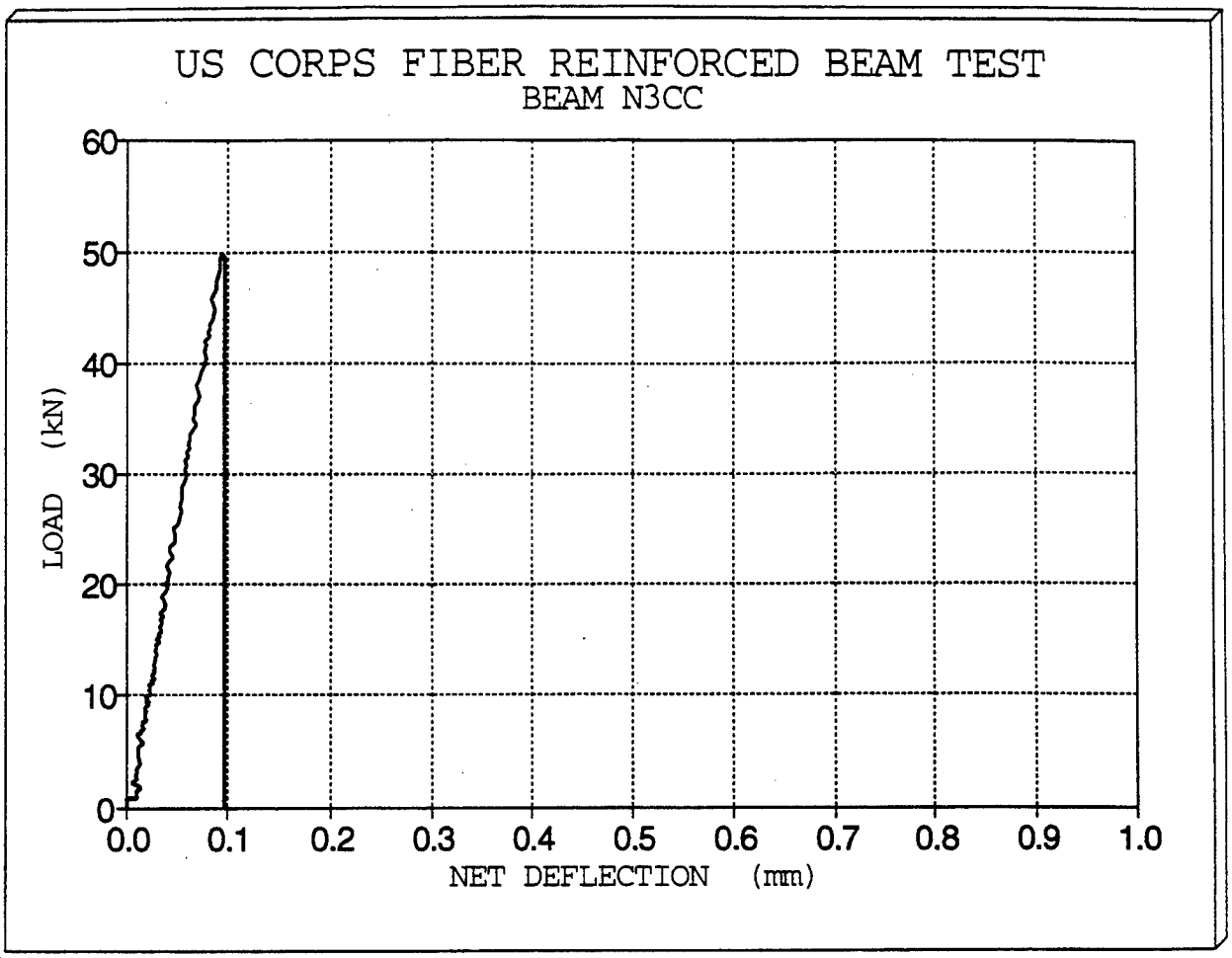
US CORPS FIBER REINFORCED BEAM TEST
BEAM N3CC
LOAD (kN)
60
50
40
30
20
10
0
0.0
0.1
0.2
0.3
0.4
0.5
0.6
0.7
0.8
0.9
1.0
NET DEFLECTION (mm)

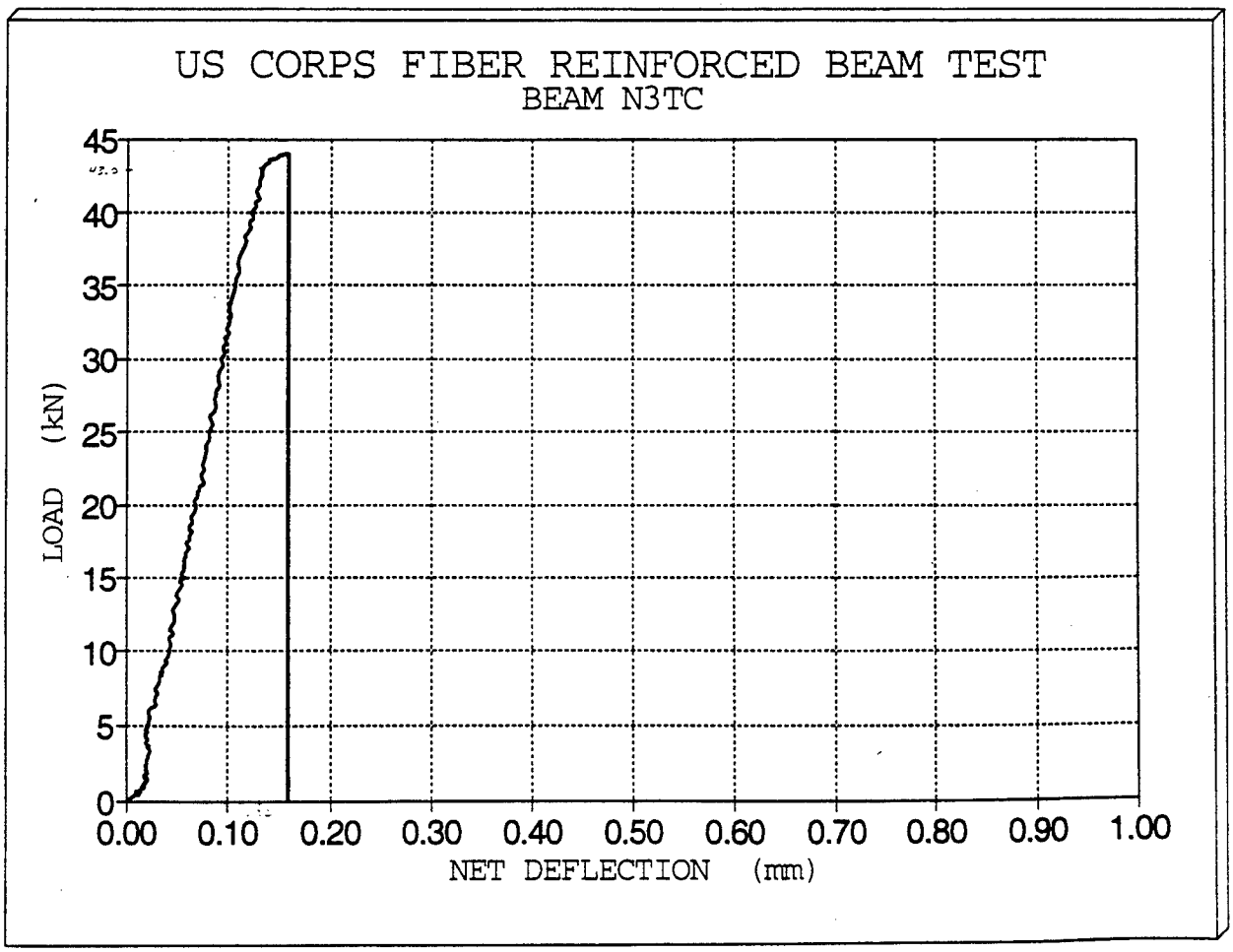
US CORPS FIBER REINFORCED BEAM TEST
BEAM N3TC
LOAD (kN)
45
40
35
30
25
20
15
10
5
0
0.00
0.10
0.20
0.30
0.40
0.50
0.60
0.70
0.80
0.90
1.00
NET DEFLECTION (mm)

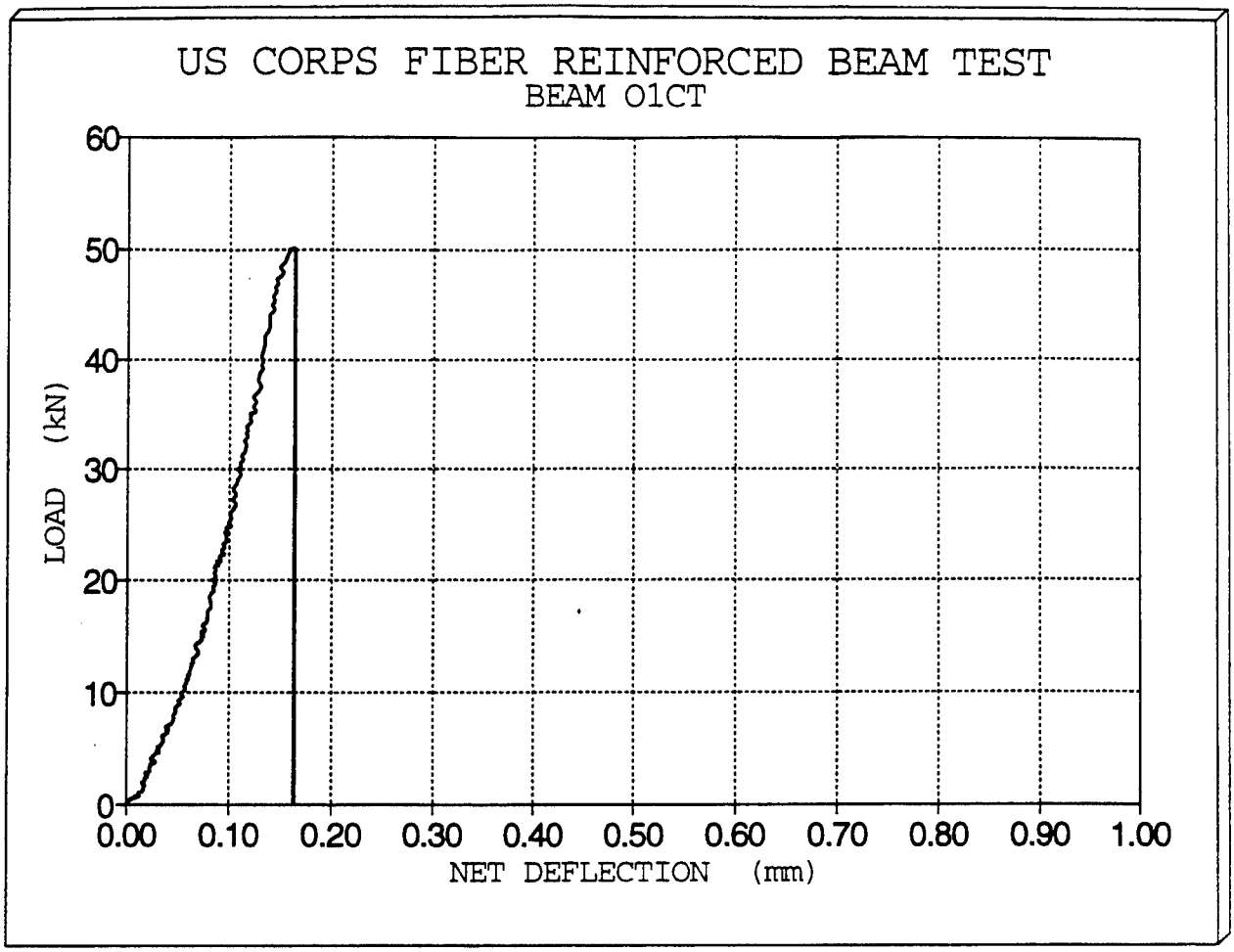
US CORPS FIBER REINFORCED BEAM TEST
BEAM O1CT
LOAD (kN)
60
50
40
30
20
10
0
0.00
0.10
0.20
0.30
0.40
0.50
0.60
0.70
0.80
0.90
1.00
NET DEFLECTION (mm)

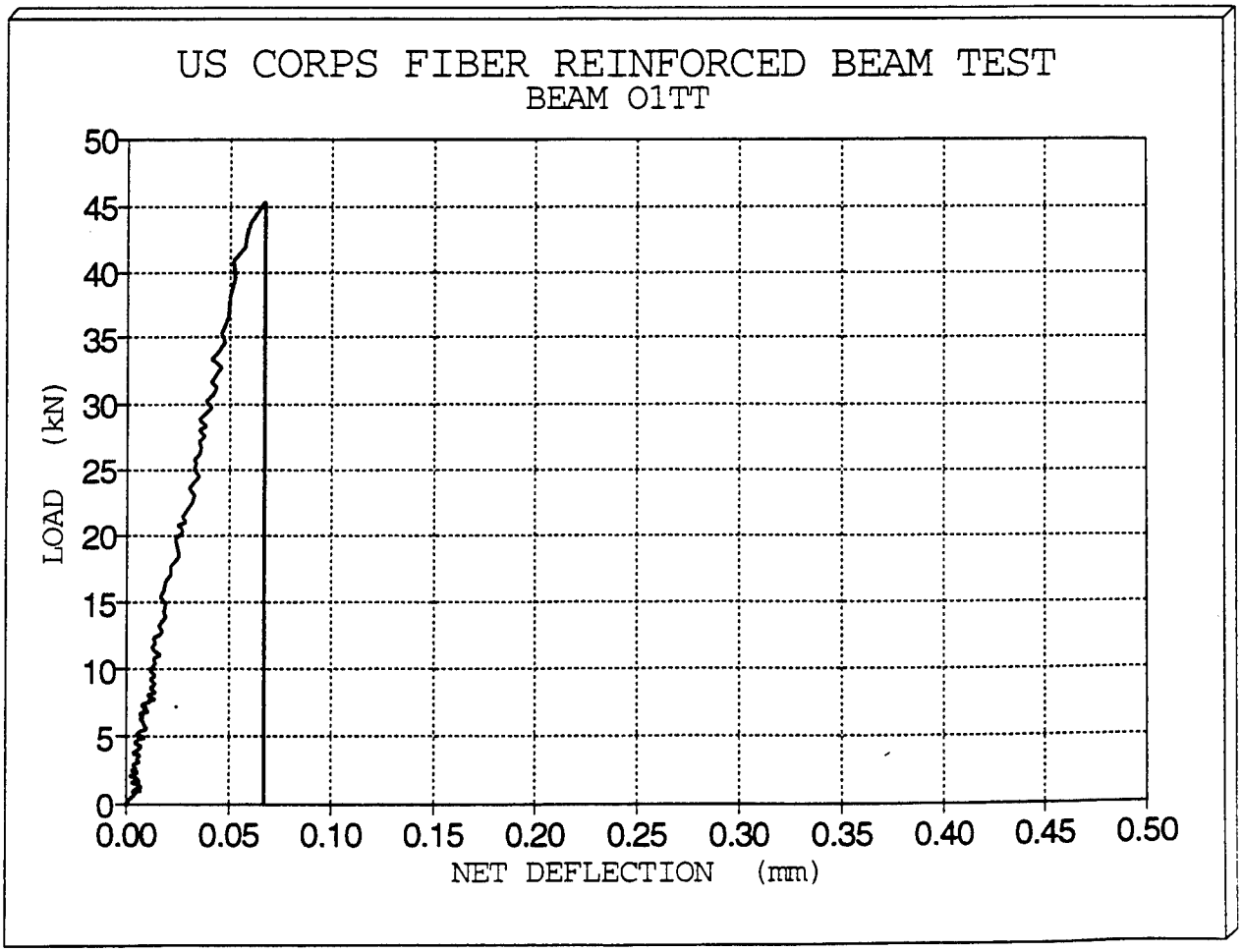
US CORPS FIBER REINFORCED BEAM TEST
BEAM O1TT
LOAD (kN)
50
45
40
35
30
25
20
15
10
5
0
0.00
0.05
0.10
0.15
0.20
0.25
0.30
0.35
0.40
0.45
0.50
NET DEFLECTION (mm)

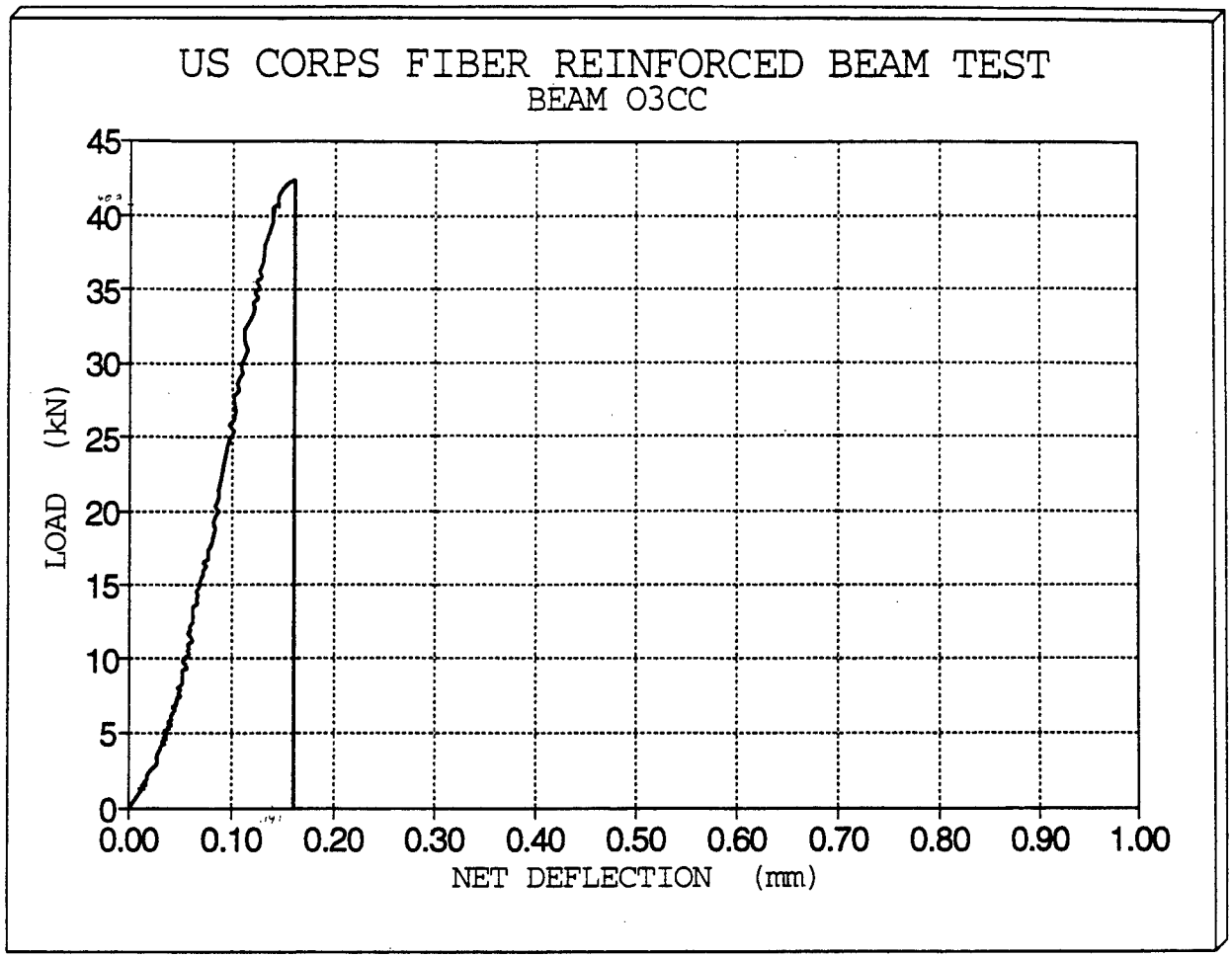
US CORPS FIBER REINFORCED BEAM TEST
BEAM O3CC
LOAD (kN)
0
5
10
15
20
25
30
35
40
45
0.00
0.10
0.20
0.30
0.40
0.50
0.60
0.70
0.80
0.90
1.00
NET DEFLECTION (mm)

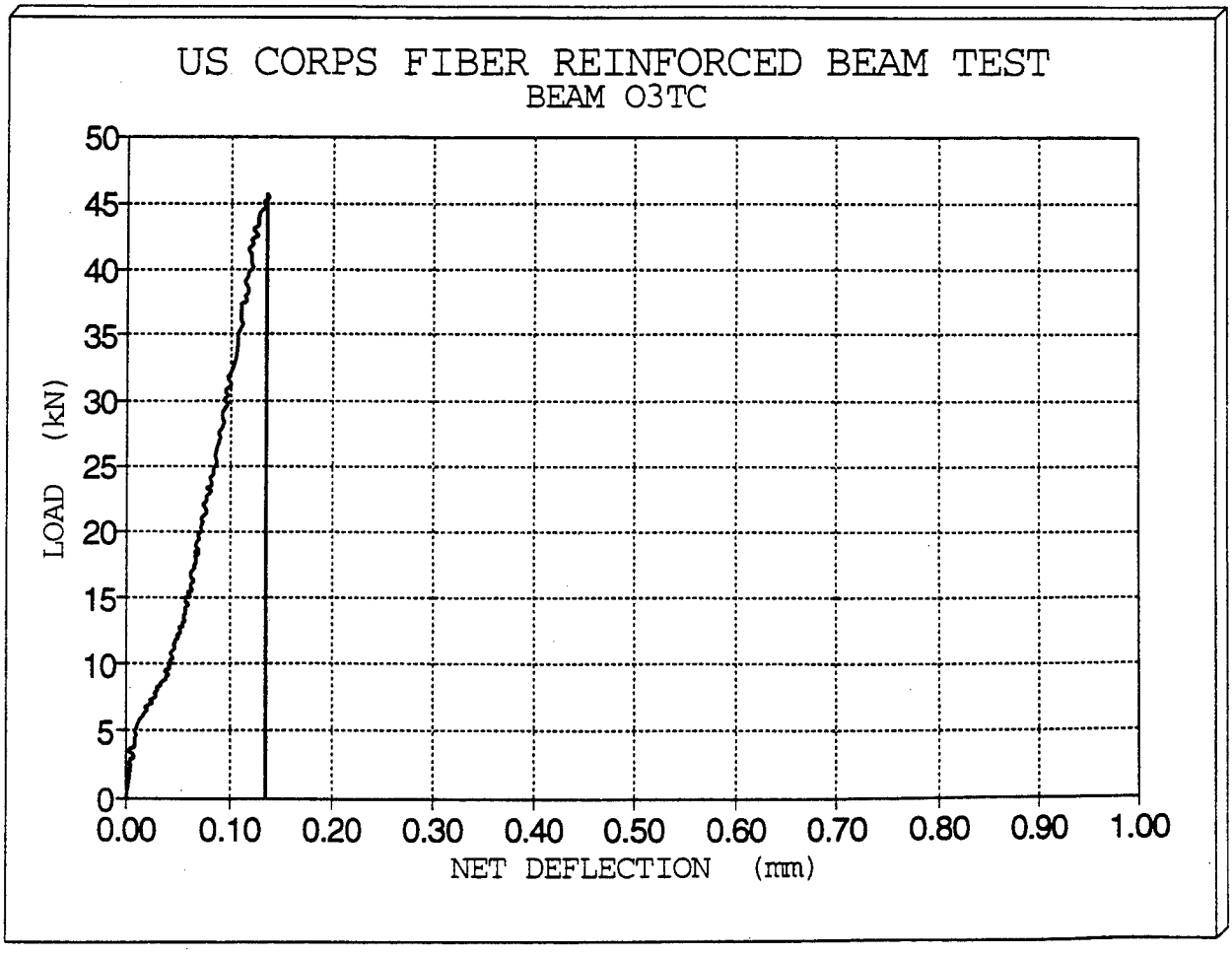
US CORPS FIBER REINFORCED BEAM TEST
BEAM O3TC
LOAD (kN)
0
5
10
15
20
25
30
35
40
45
50
0.00
0.10
0.20
0.30
0.40
0.50
0.60
0.70
0.80
0.90
1.00
NET DEFLECTION (mm)

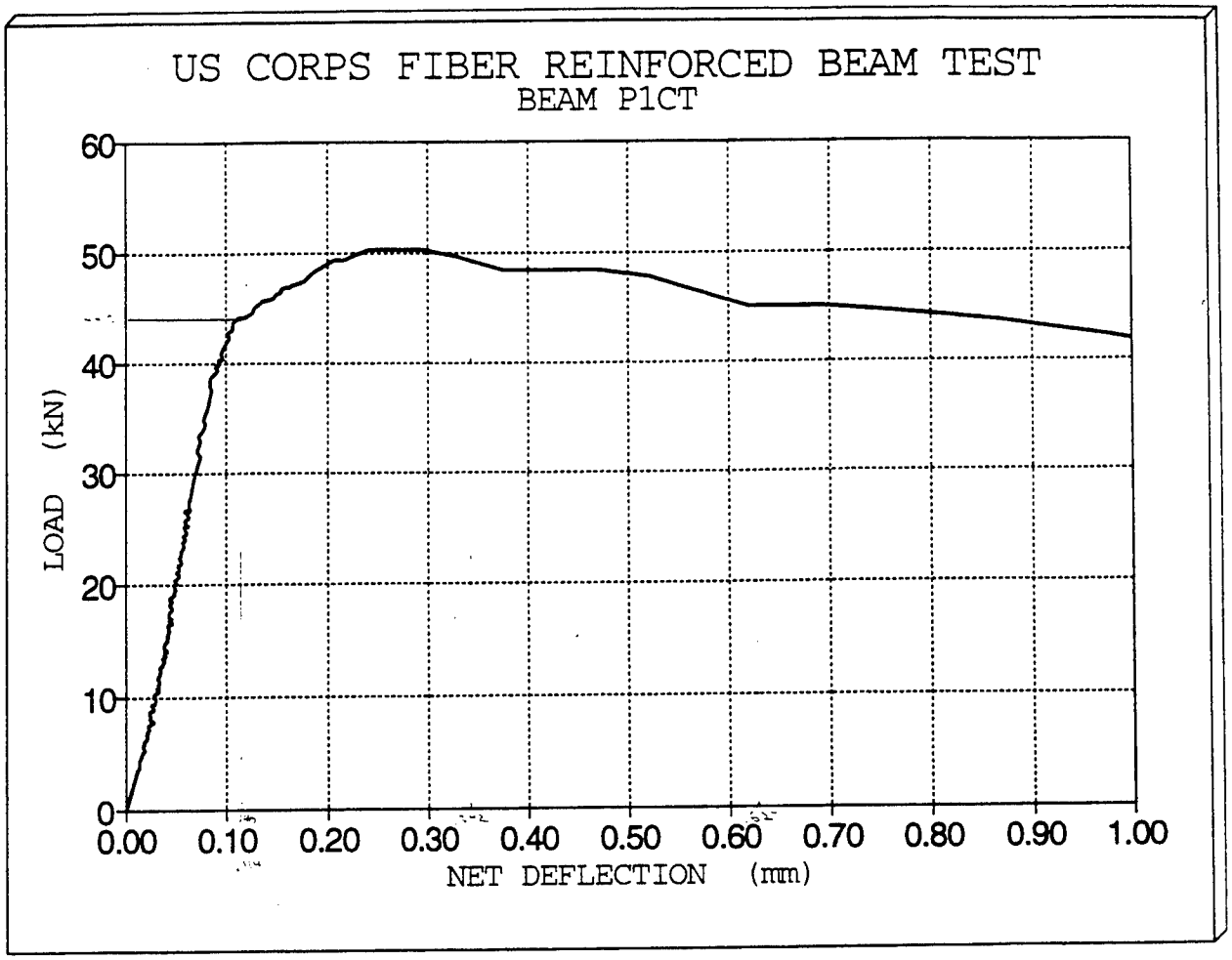
US CORPS FIBER REINFORCED BEAM TEST
BEAM P1CT
LOAD (kN)
60
50
40
30
20
10
0
0.00
0.10
0.20
0.30
0.40
0.50
0.60
0.70
0.80
0.90
1.00
NET DEFLECTION (mm)

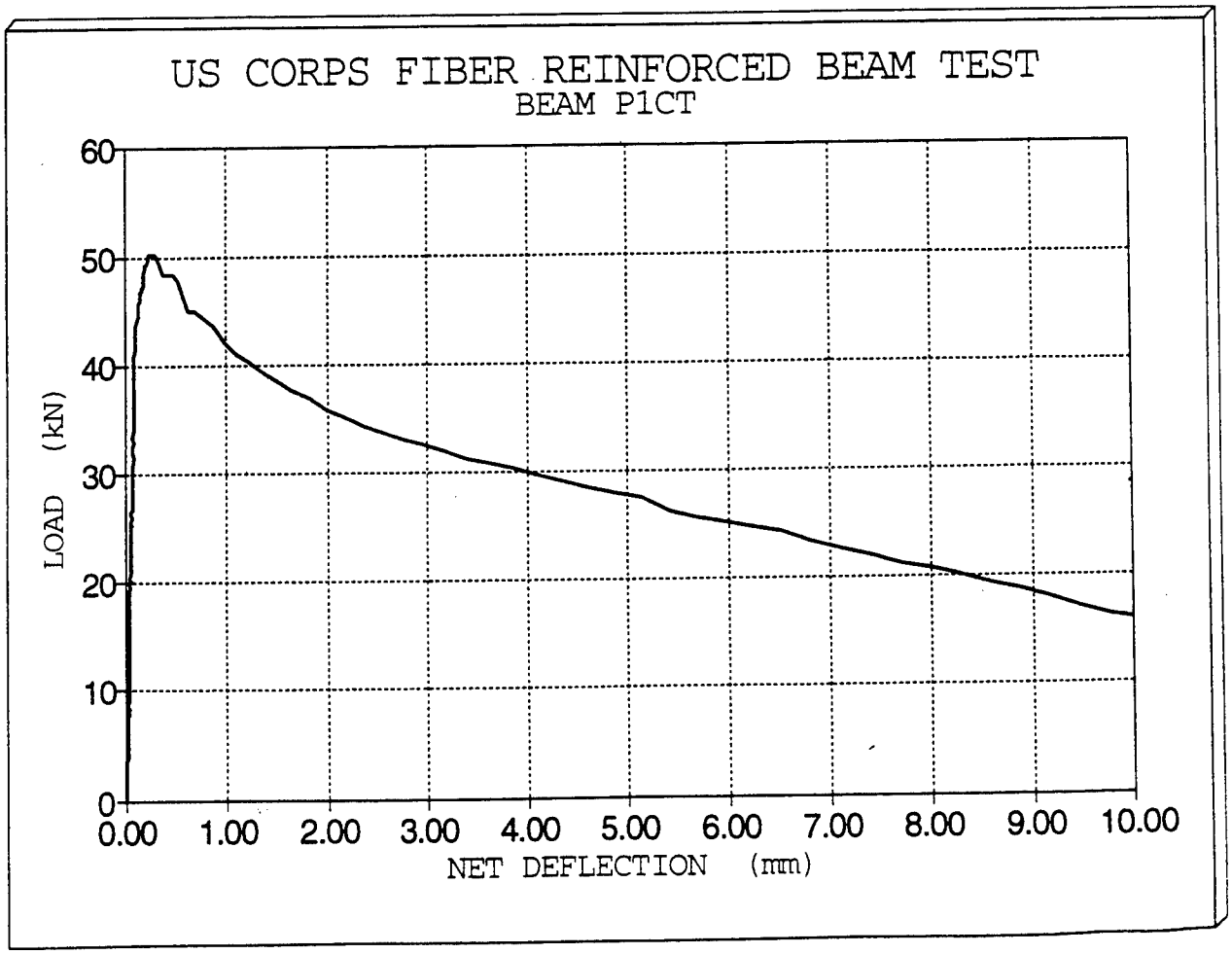
US CORPS FIBER REINFORCED BEAM TEST
BEAM P1CT
LOAD (kN)
60
50
40
30
20
10
0
0.00
1.00
2.00
3.00
4.00
5.00
6.00
7.00
8.00
9.00
10.00
NET DEFLECTION (mm)

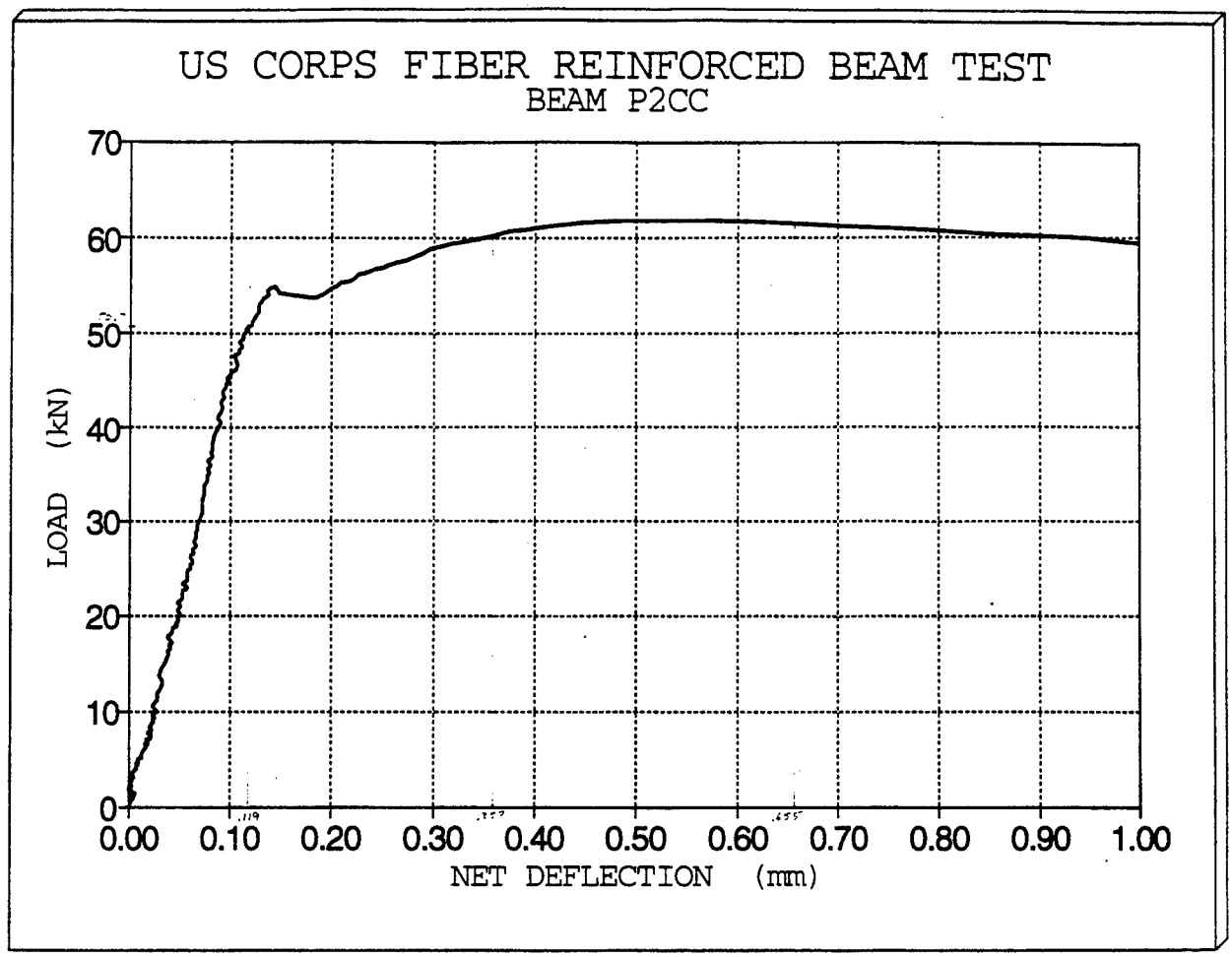
US CORPS FIBER REINFORCED BEAM TEST
BEAM P2CC
LOAD (kN)
70
60
50
40
30
20
10
0
0.00
0.10
0.20
0.30
0.40
0.50
0.60
0.70
0.80
0.90
1.00
NET DEFLECTION (mm)

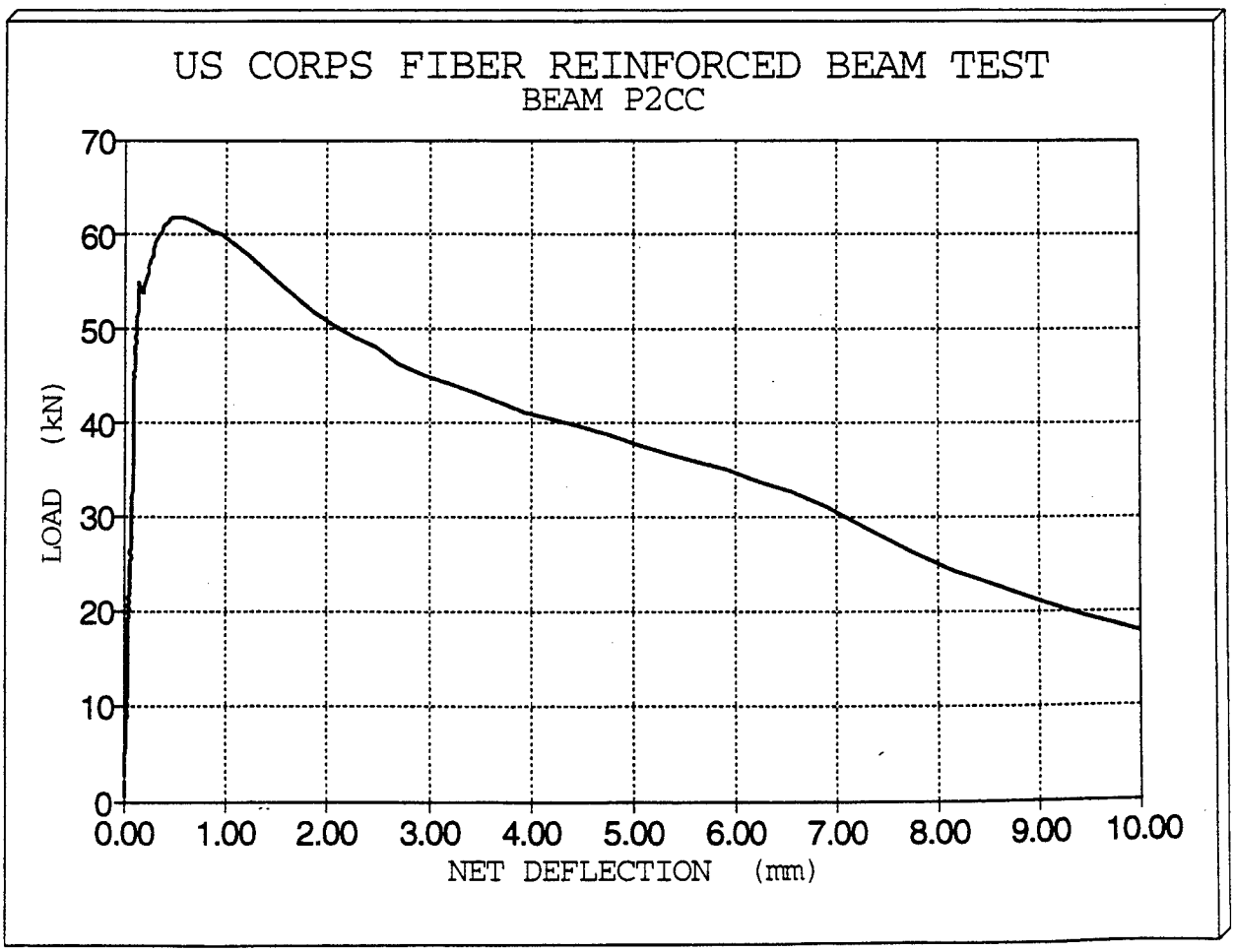
US CORPS FIBER REINFORCED BEAM TEST
BEAM P2CC
LOAD (kN)
70
60
50
40
30
20
10
0
0.00
1.00
2.00
3.00
4.00
5.00
6.00
7.00
8.00
9.00
10.00
NET DEFLECTION (mm)

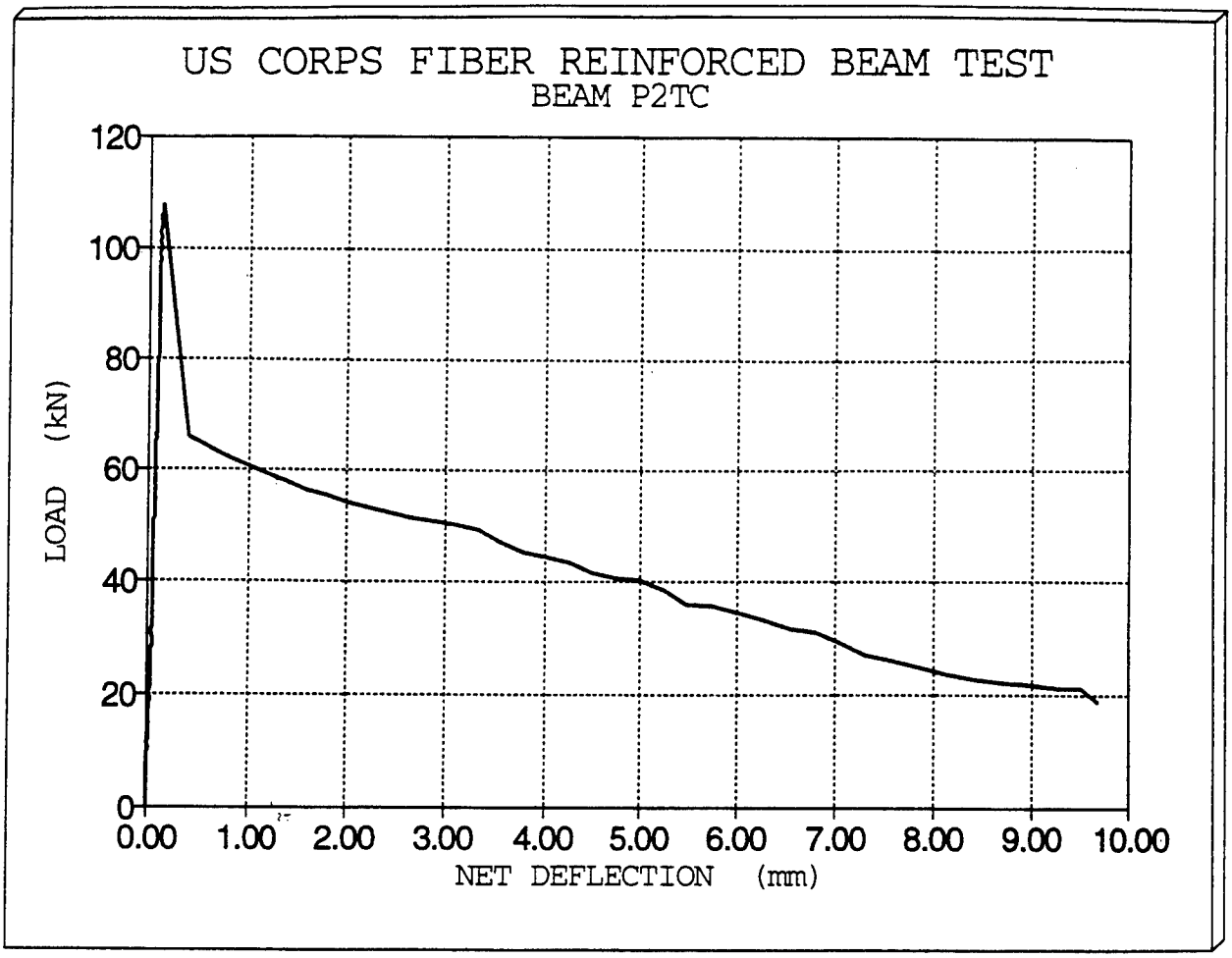
US CORPS FIBER REINFORCED BEAM TEST
BEAM P2TC
LOAD (kN)
120
100
80
60
40
20
0
0.00
1.00
2.00
3.00
4.00
5.00
6.00
7.00
8.00
9.00
10.00
NET DEFLECTION (mm)

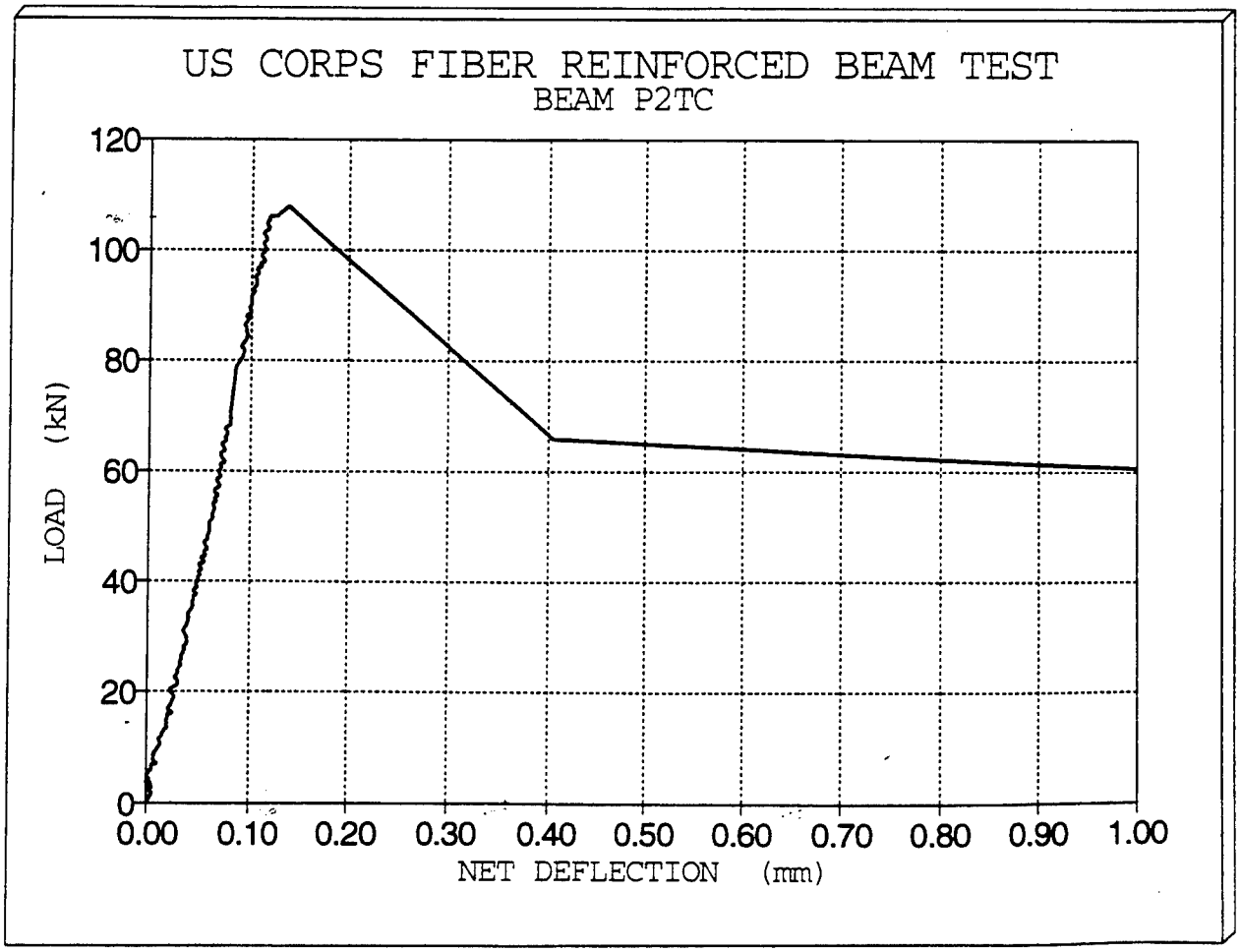
US CORPS FIBER REINFORCED BEAM TEST
BEAM P2TC
LOAD (kN)
120
100
80
60
40
20
0
0.00
0.10
0.20
0.30
0.40
0.50
0.60
0.70
0.80
0.90
1.00
NET DEFLECTION (mm)

# Appendix G
# Indirect Tension Test Results

# INDIRECT TENSION TEST RESULTS

| MIX | CORE CODE | FAILURE STRESS (PSI) | FAILURE STRESS (MPa) | AVG.FAILURE STRESS (PSI) | (MPa) | COEFFICIENT VARIATION |
|---|---|---|---|---|---|---|
| | J-1-1-T | 757 | 5.22 | | | |
| J | J-1-2-T | 624 | 4.30 | 803 | 5.54 | 25.7 |
| | J-3-3-T | 1028 | 7.09 | | | |
| | K-1-2-T | 837 | 5.77 | | | |
| K | K-3-1-T | 975 | 6.72 | 850 | 5.86 | 14.0 |
| | K-3-3-T | 738 | 5.09 | | | |
| | M-1-2-T | 1038 | 7.16 | | | |
| M | M-1-3-T | 960 | 6.62 | 996 | 6.87 | 4.0 |
| | M-3-3-T | 989 | 6.82 | | | |
| | N-1-1-T | 545 | 3.76 | | | |
| N | N-3-1-T | 512 | 3.53 | 459 | 3.16 | 26.4 |
| | N-3-3-T | 320 | 2.21 | | | |
| | O-1-3-T | 522 | 3.60 | | | |
| O | O-3-1-T | 933 | 6.43 | 729 | 5.03 | 28.1 |
| | O-3-2-T | 733 | 5.05 | | | |
| | P-1-1-T | 949 | 6.54 | | | |
| P | P-2-2-T | 858 | 5.92 | 806 | 5.56 | 21.7 |
| | P-2-3-T | 610 | 4.21 | | | |

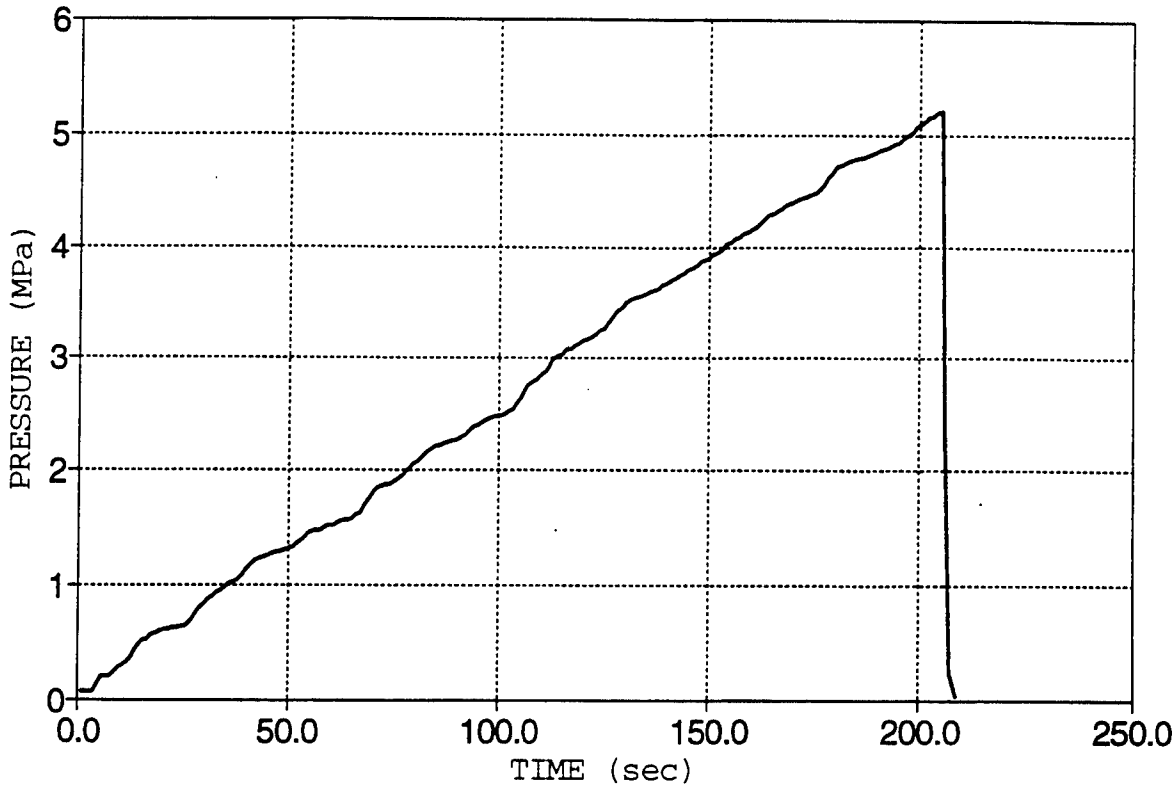
INDIRECT TENSION TEST
CORE J-1-1T
PRESSURE (MPa)
0
1
2
3
4
5
6
0.0
50.0
100.0
150.0
200.0
250.0
TIME (sec)

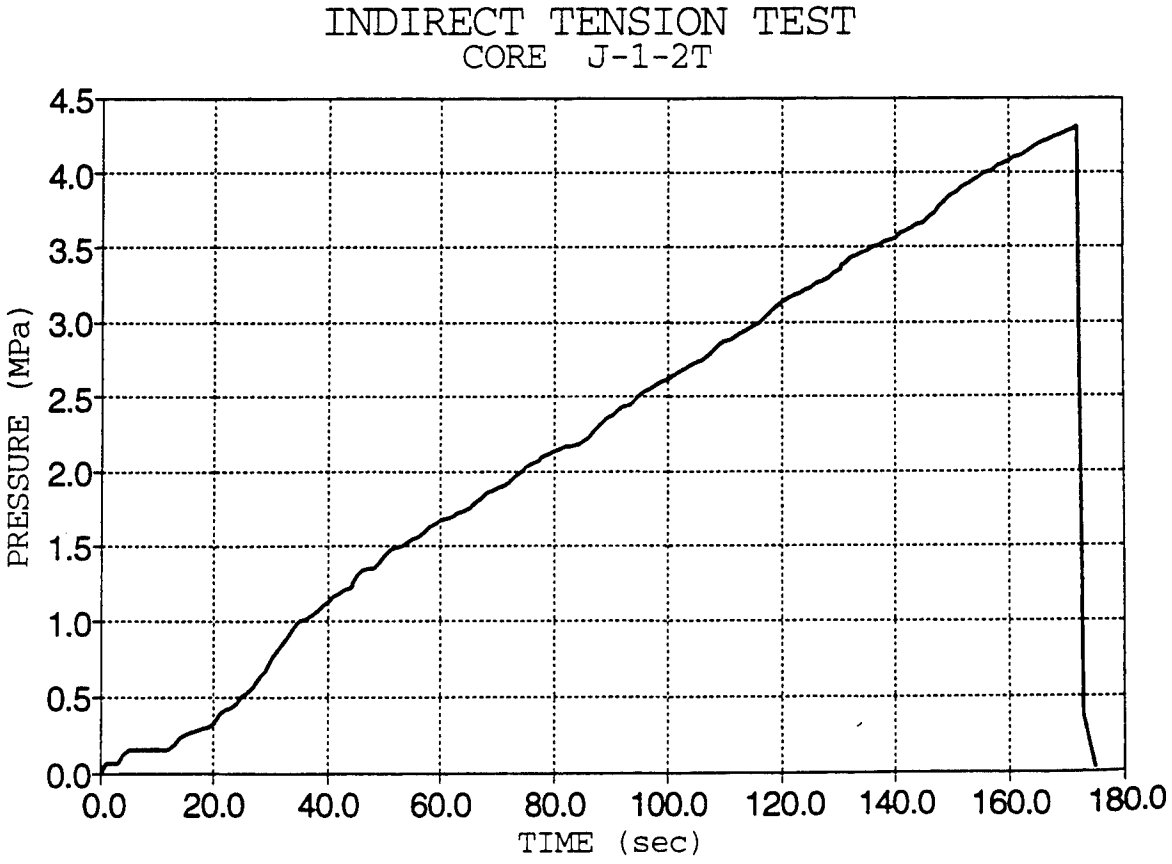
INDIRECT TENSION TEST
CORE J-1-2T
PRESSURE (MPa)
0.0
0.5
1.0
1.5
2.0
2.5
3.0
3.5
4.0
4.5
0.0
20.0
40.0
60.0
80.0
100.0
120.0
140.0
160.0
180.0
TIME (sec)

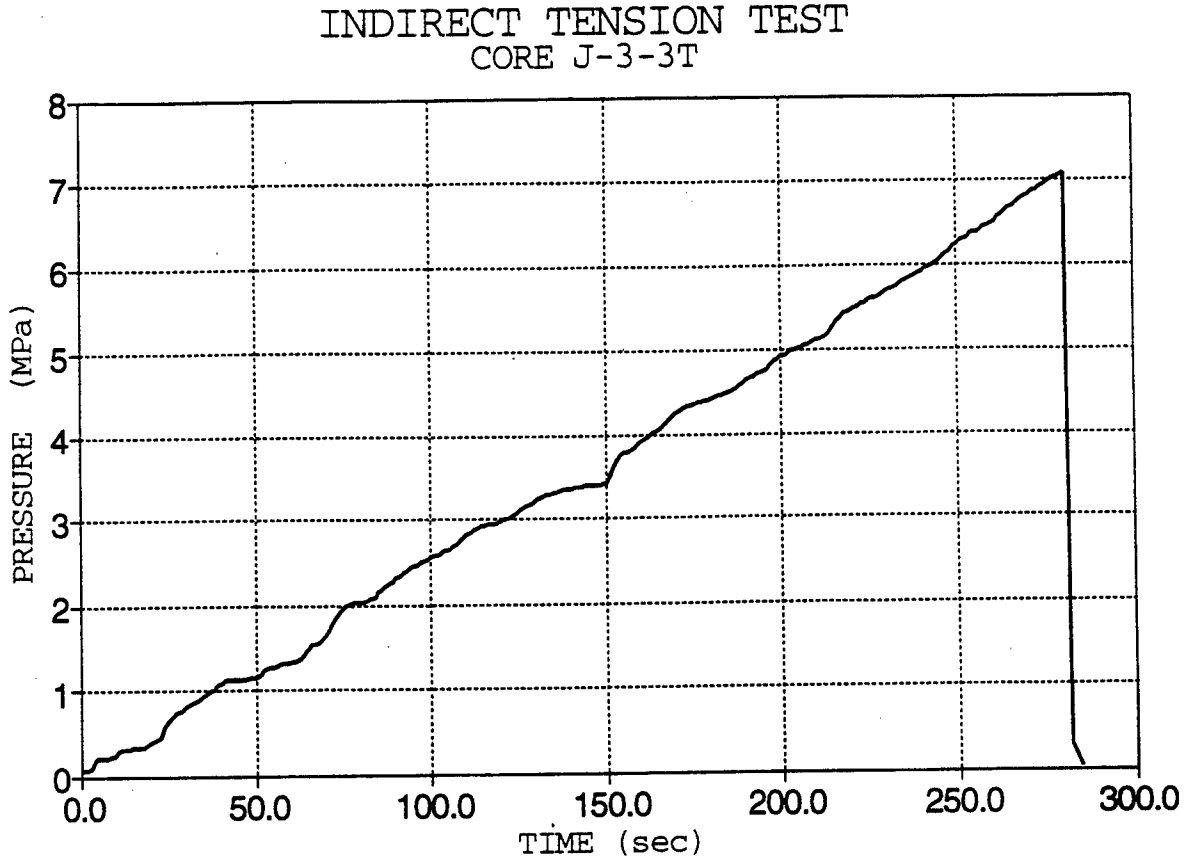
INDIRECT TENSION TEST
CORE J-3-3T
PRESSURE (MPa)
0
1
2
3
4
5
6
7
8
0.0
50.0
100.0
150.0
200.0
250.0
300.0
TIME (sec)

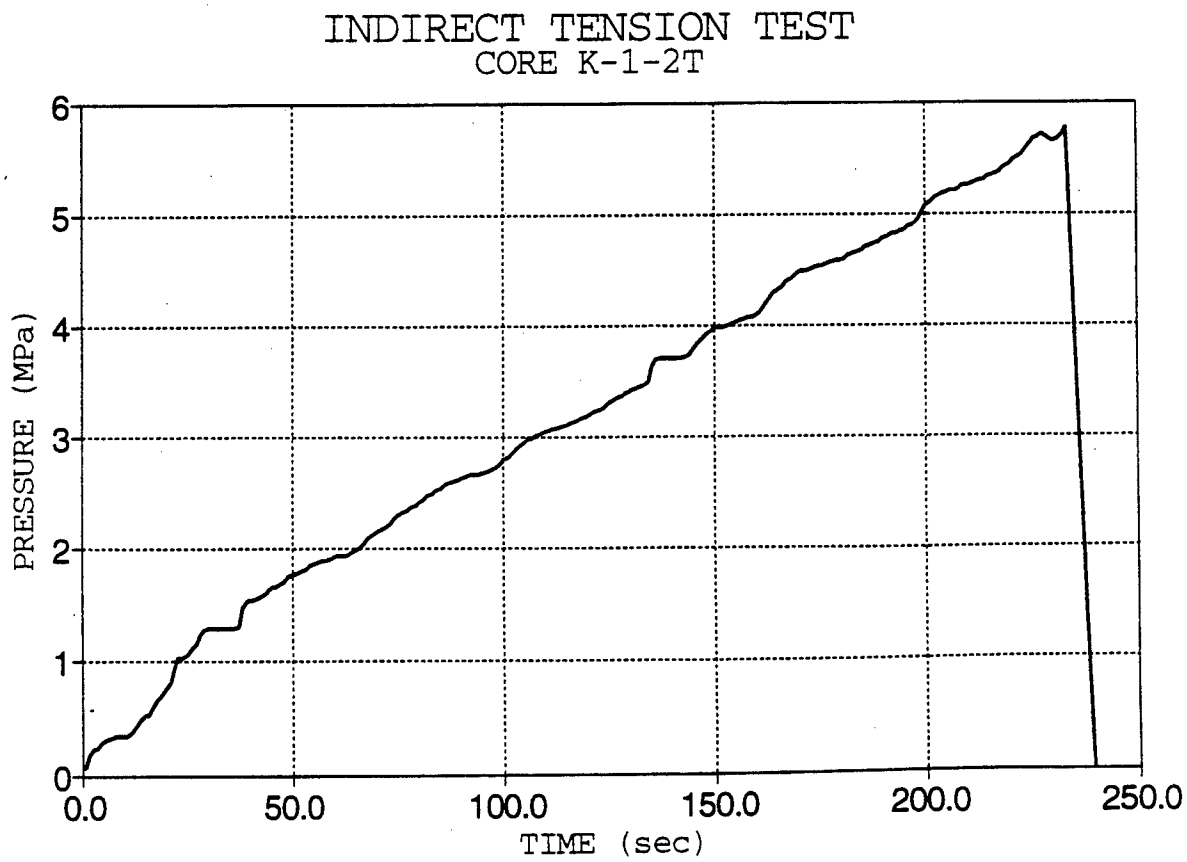
INDIRECT TENSION TEST
CORE K-1-2T
PRESSURE (MPa)
0
1
2
3
4
5
6
0.0
50.0
100.0
150.0
200.0
250.0
TIME (sec)

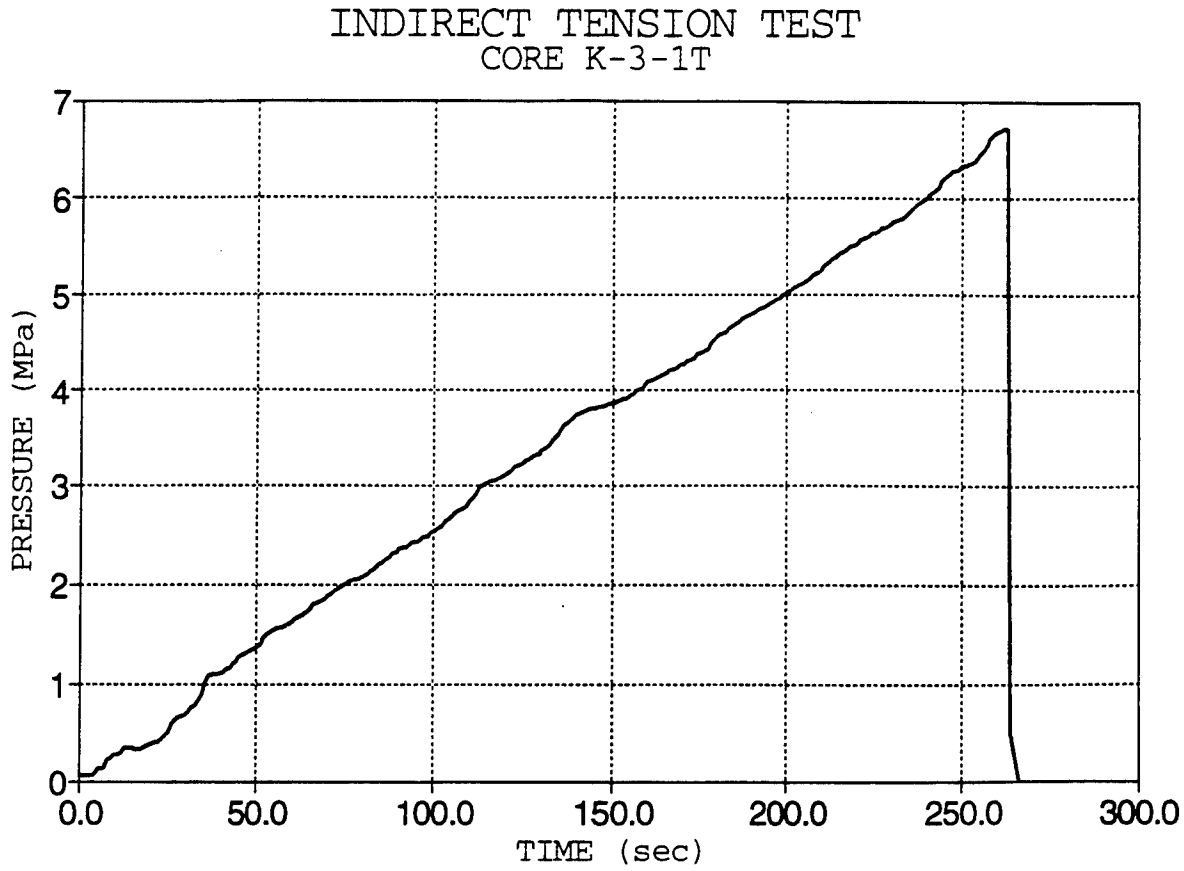
INDIRECT TENSION TEST
CORE K-3-1T
PRESSURE (MPa)
0
1
2
3
4
5
6
7
0.0
50.0
100.0
150.0
200.0
250.0
300.0
TIME (sec)

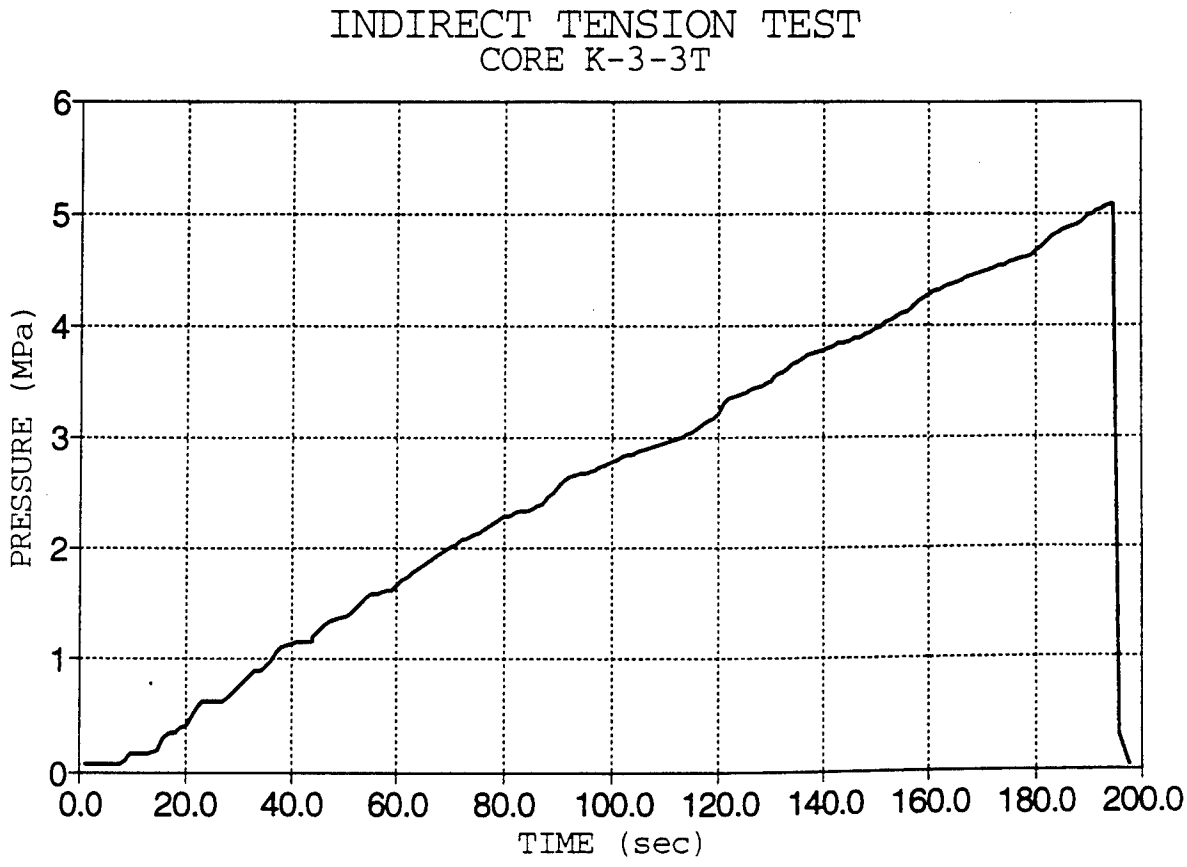
INDIRECT TENSION TEST
CORE K-3-3T
PRESSURE (MPa)
0
1
2
3
4
5
6
0.0
20.0
40.0
60.0
80.0
100.0
120.0
140.0
160.0
180.0
200.0
TIME (sec)

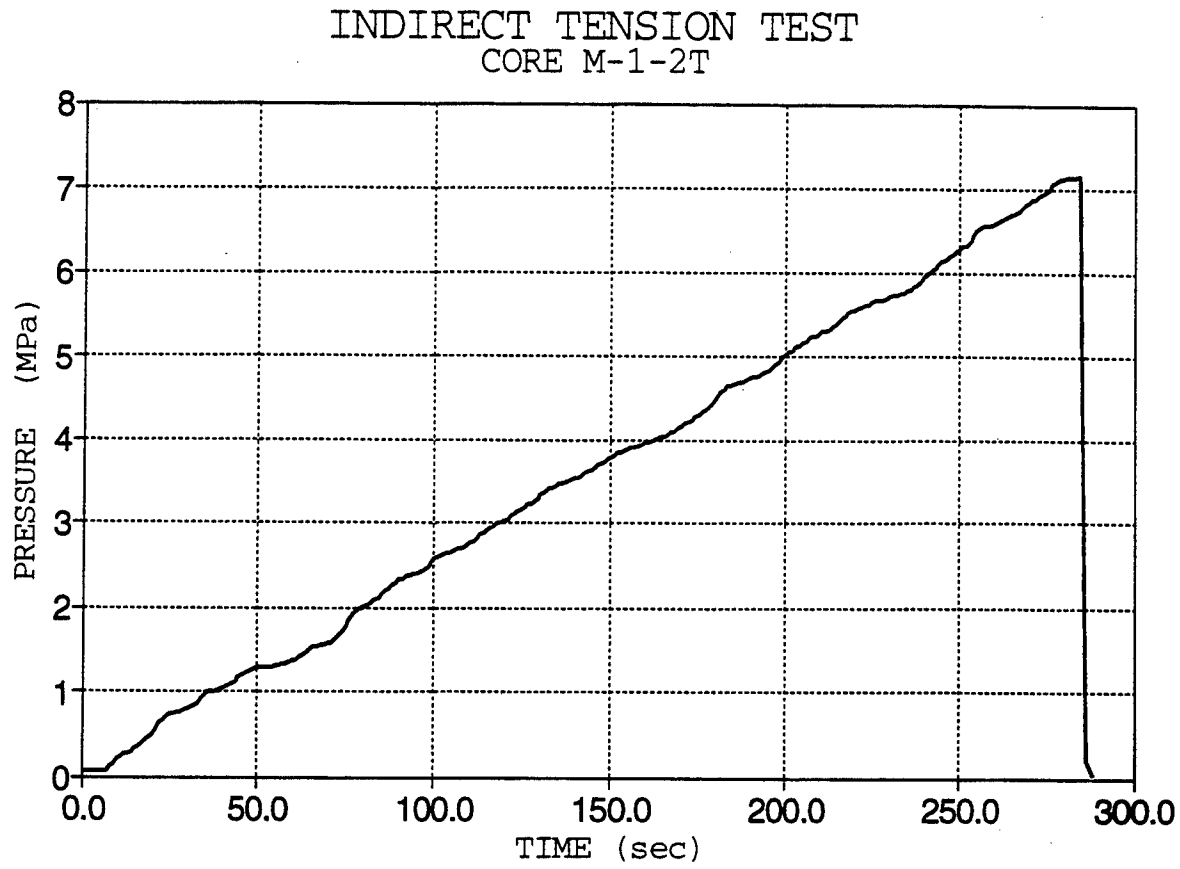
INDIRECT TENSION TEST
CORE M-1-2T
PRESSURE (MPa)
0
1
2
3
4
5
6
7
8
0.0
50.0
100.0
150.0
200.0
250.0
300.0
TIME (sec)

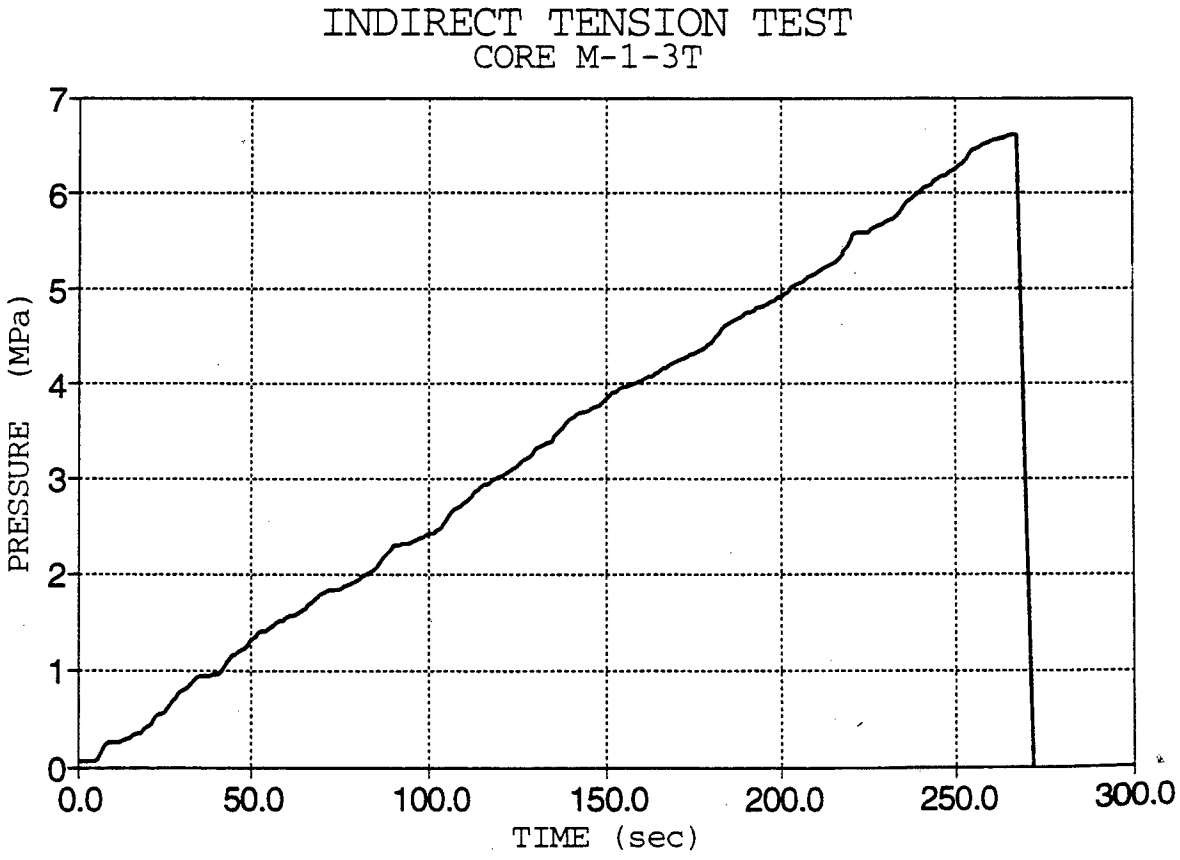
INDIRECT TENSION TEST
CORE M-1-3T
PRESSURE (MPa)
0
1
2
3
4
5
6
7
0.0
50.0
100.0
150.0
200.0
250.0
300.0
TIME (sec)

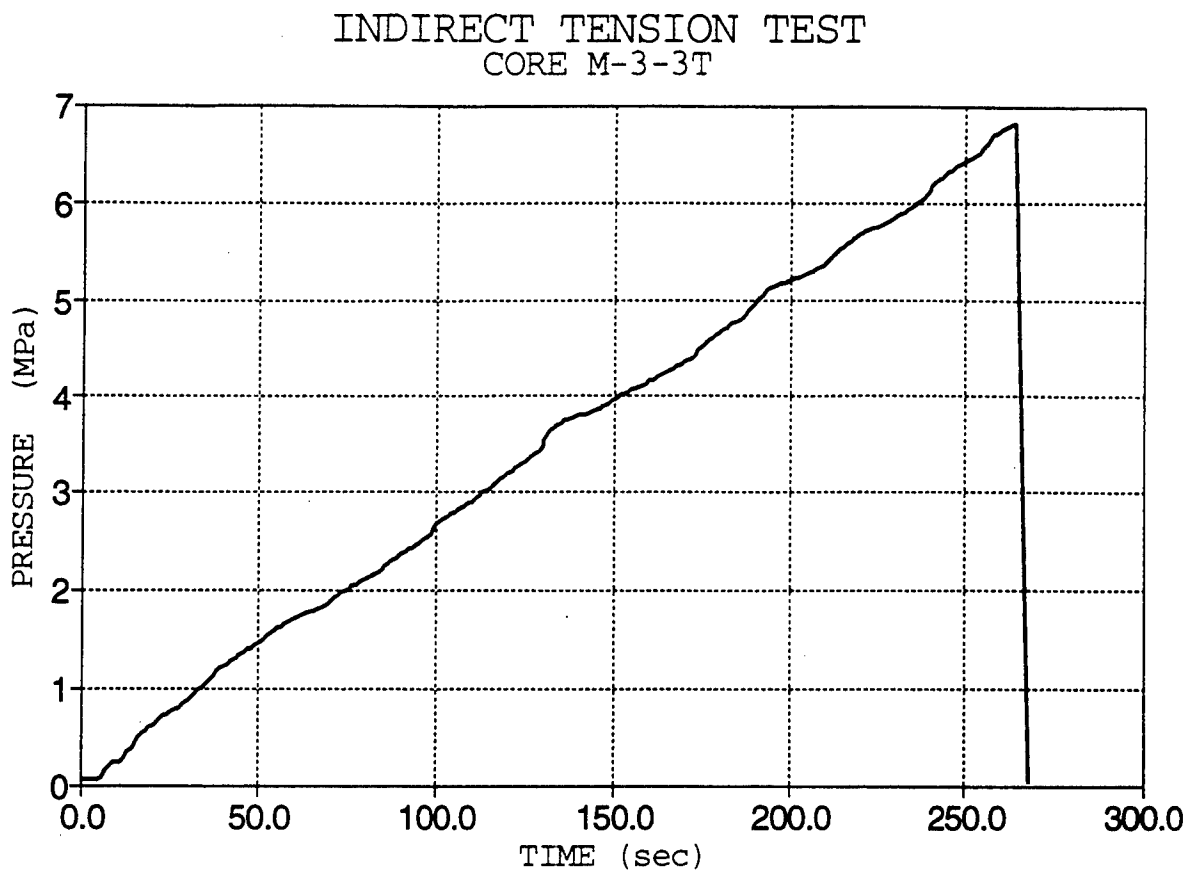
INDIRECT TENSION TEST
CORE M-3-3T
PRESSURE (MPa)
0
1
2
3
4
5
6
7
0.0
50.0
100.0
150.0
200.0
250.0
300.0
TIME (sec)

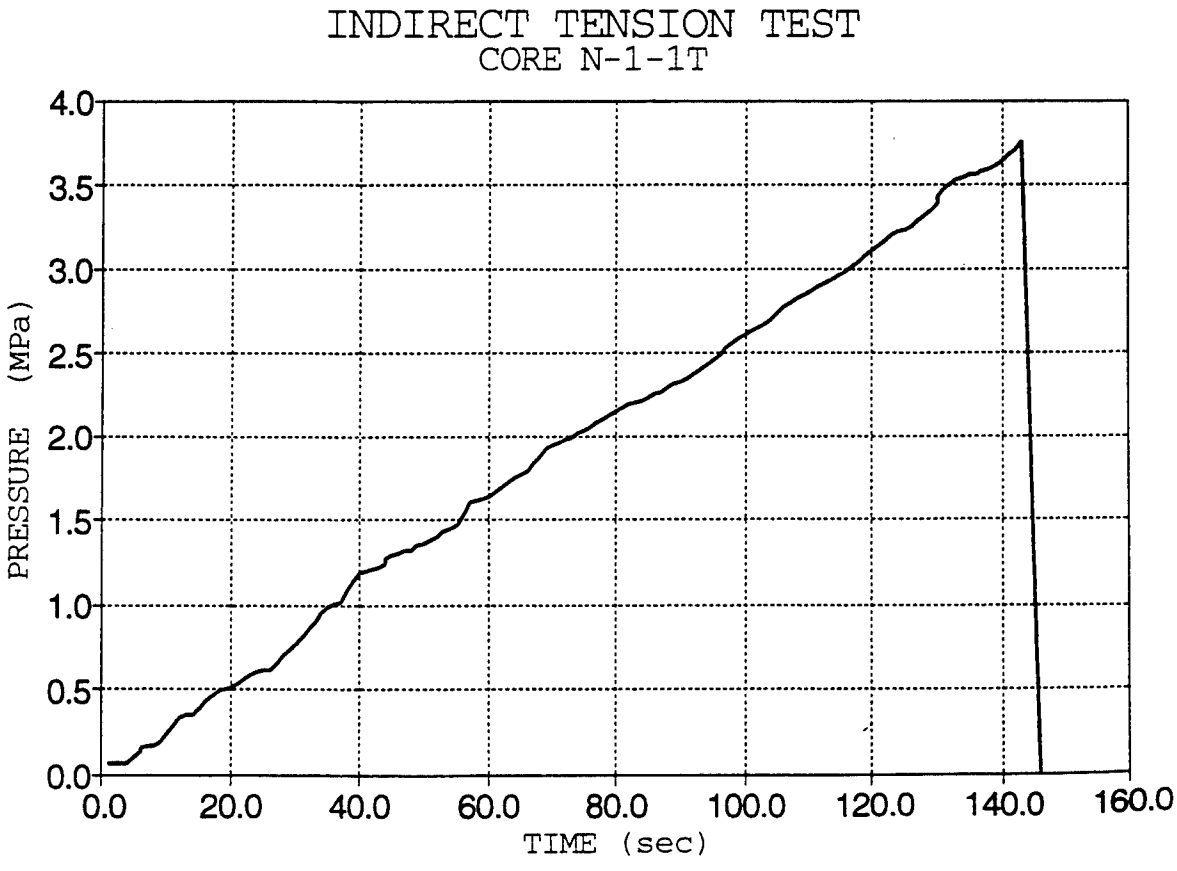
INDIRECT TENSION TEST
CORE N-1-1T
PRESSURE (MPa)
0.0
0.5
1.0
1.5
2.0
2.5
3.0
3.5
4.0
0.0
20.0
40.0
60.0
80.0
100.0
120.0
140.0
160.0
TIME (sec)

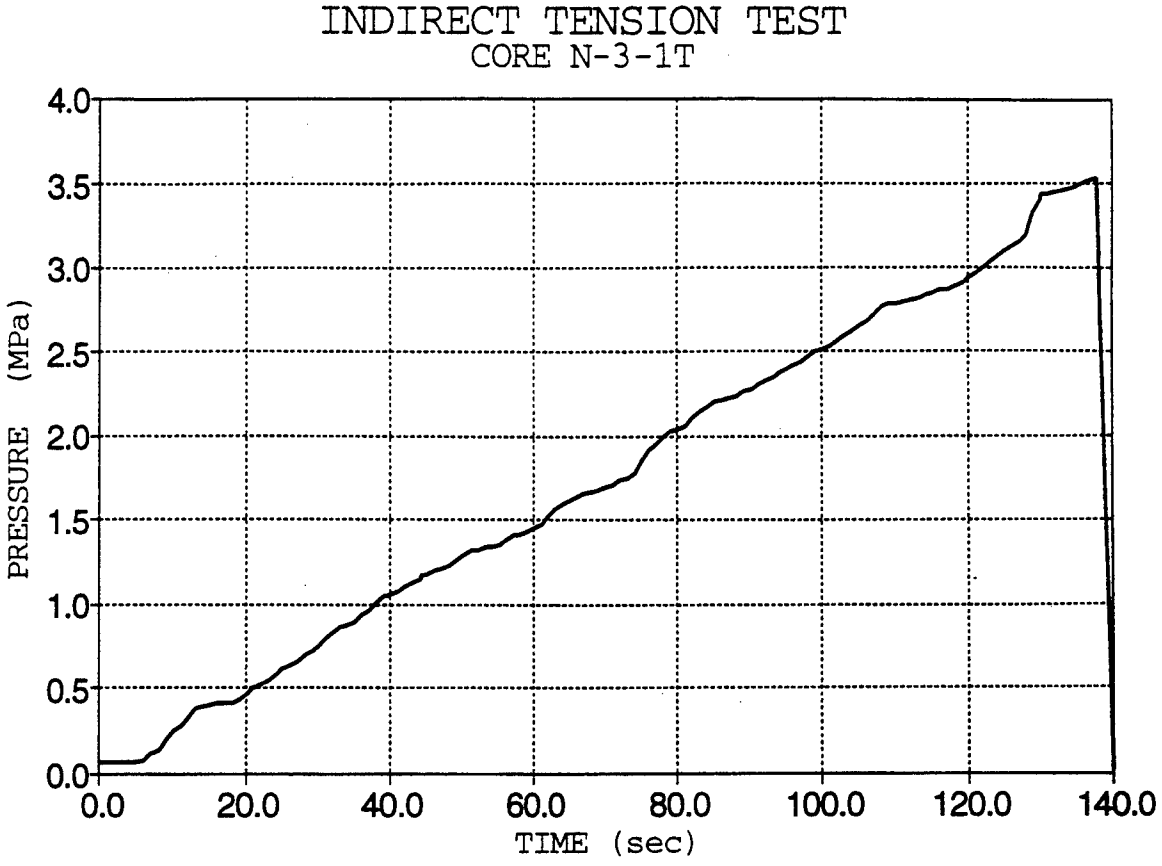
INDIRECT TENSION TEST
CORE N-3-1T
PRESSURE (MPa)
4.0
3.5
3.0
2.5
2.0
1.5
1.0
0.5
0.0
0.0
20.0
40.0
60.0
80.0
100.0
120.0
140.0
TIME (sec)

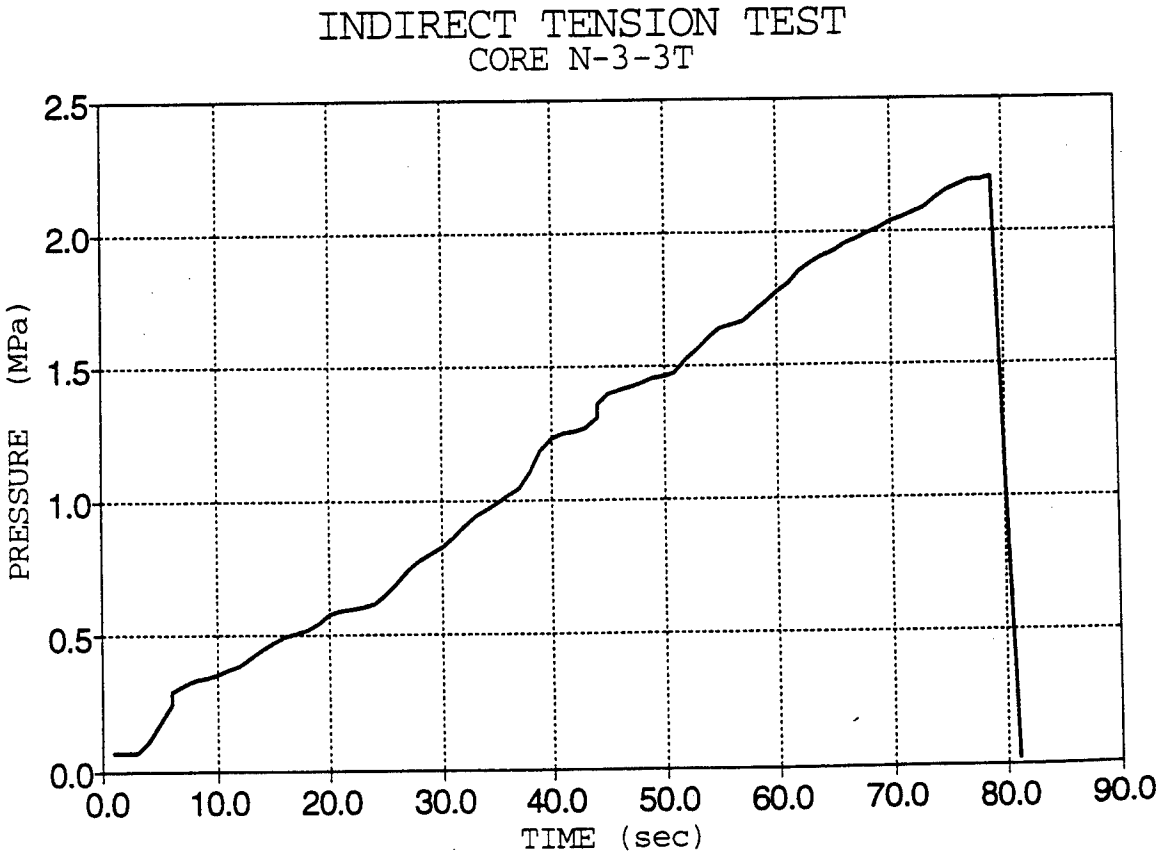
INDIRECT TENSION TEST
CORE N-3-3T
PRESSURE (MPa)
2.5
2.0
1.5
1.0
0.5
0.0
0.0
10.0
20.0
30.0
40.0
50.0
60.0
70.0
80.0
90.0
TIME (sec)

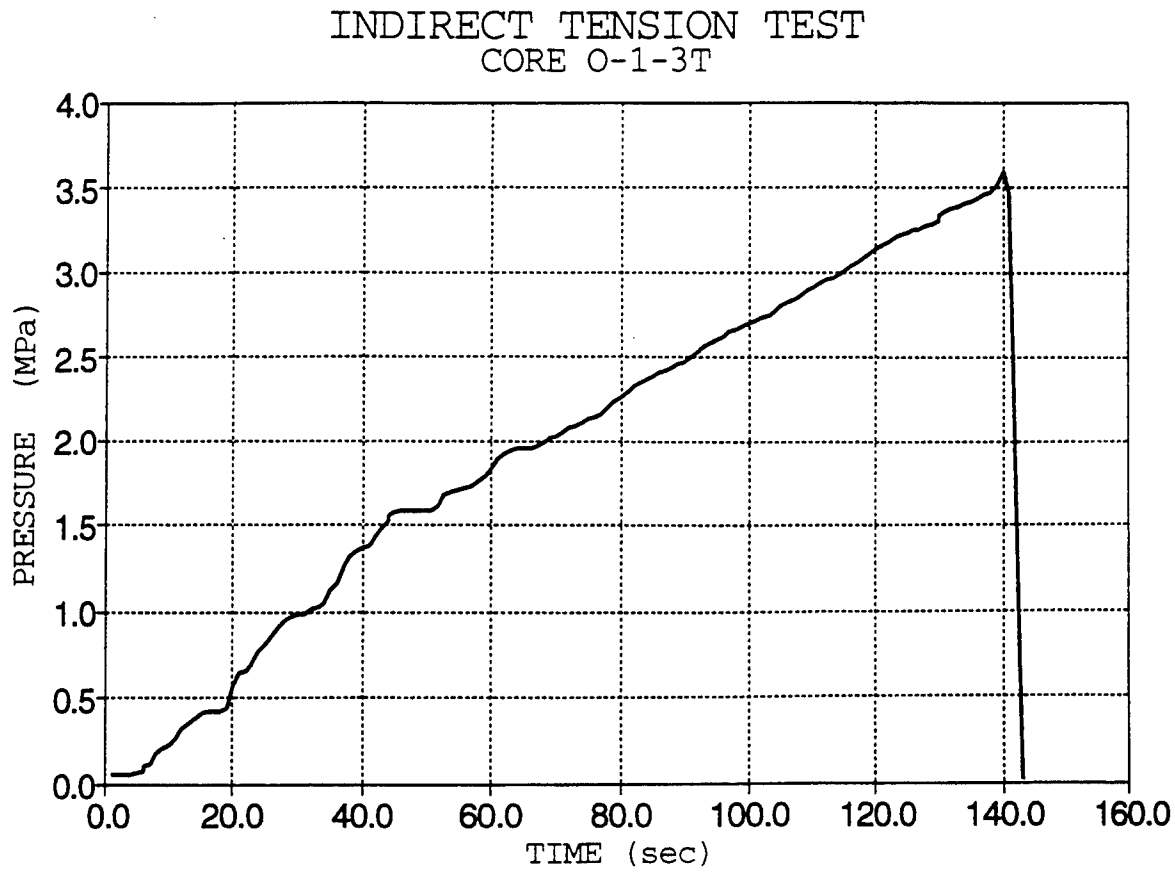
INDIRECT TENSION TEST
CORE O-1-3T
PRESSURE (MPa)
4.0
3.5
3.0
2.5
2.0
1.5
1.0
0.5
0.0
0.0
20.0
40.0
60.0
80.0
100.0
120.0
140.0
160.0
TIME (sec)

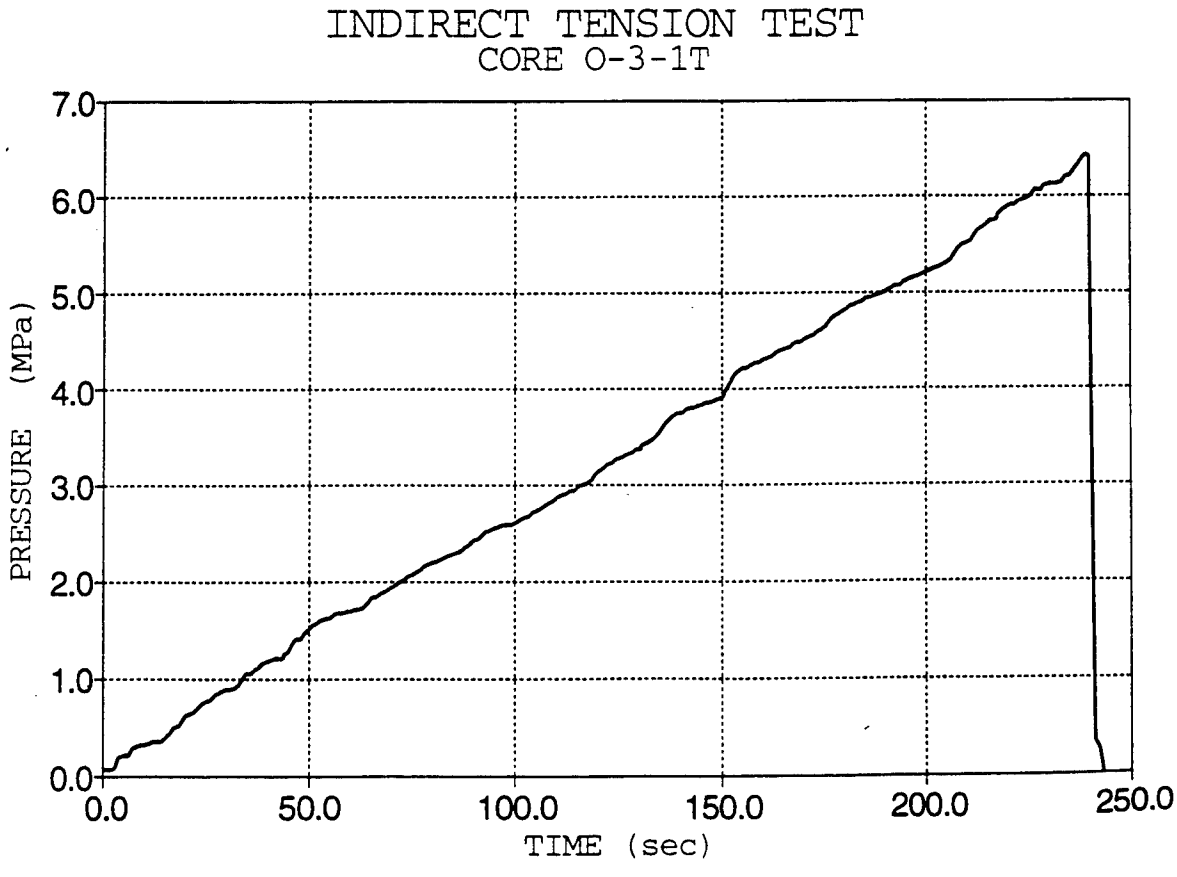
INDIRECT TENSION TEST
CORE O-3-1T
PRESSURE (MPa)
7.0
6.0
5.0
4.0
3.0
2.0
1.0
0.0
0.0
50.0
100.0
150.0
200.0
250.0
TIME (sec)

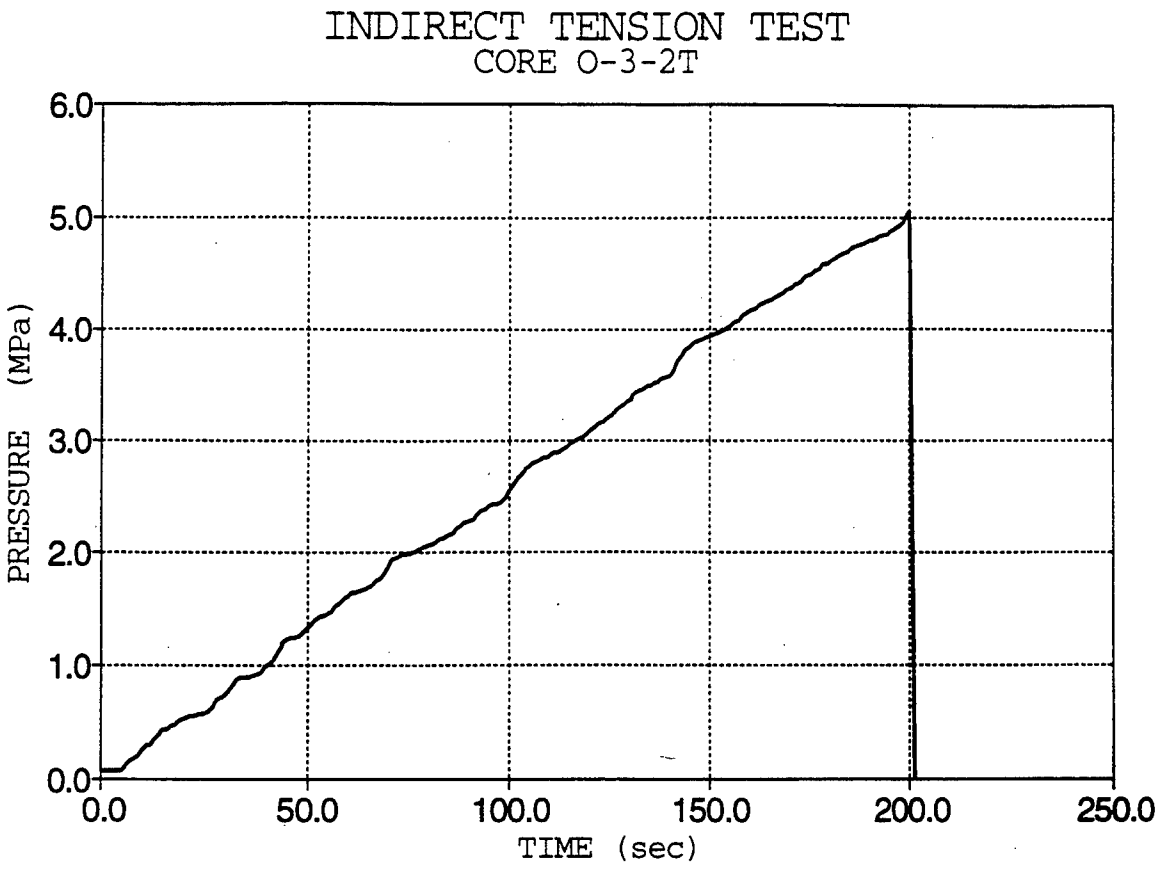
INDIRECT TENSION TEST
CORE O-3-2T
PRESSURE (MPa)
6.0
5.0
4.0
3.0
2.0
1.0
0.0
0.0
50.0
100.0
150.0
200.0
250.0
TIME (sec)

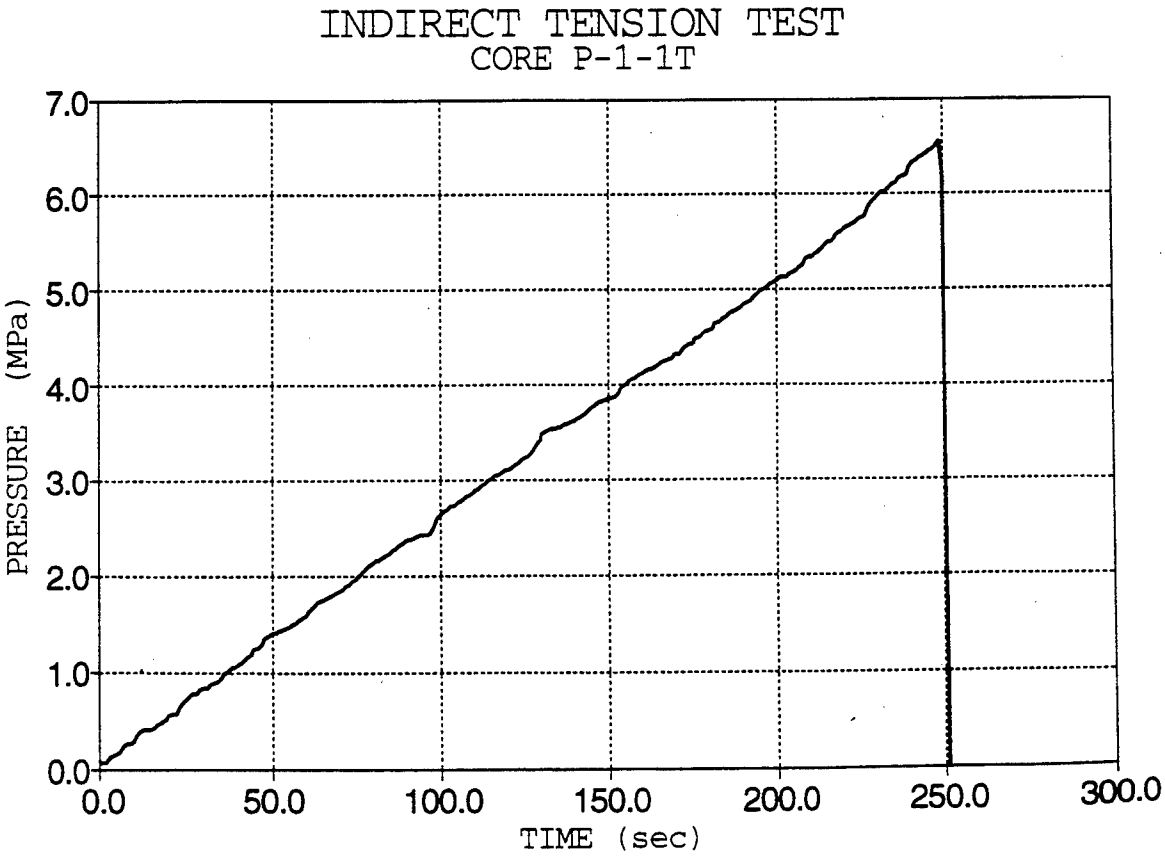
INDIRECT TENSION TEST
CORE P-1-1T
PRESSURE (MPa)
7.0
6.0
5.0
4.0
3.0
2.0
1.0
0.0
0.0
50.0
100.0
150.0
200.0
250.0
300.0
TIME (sec)

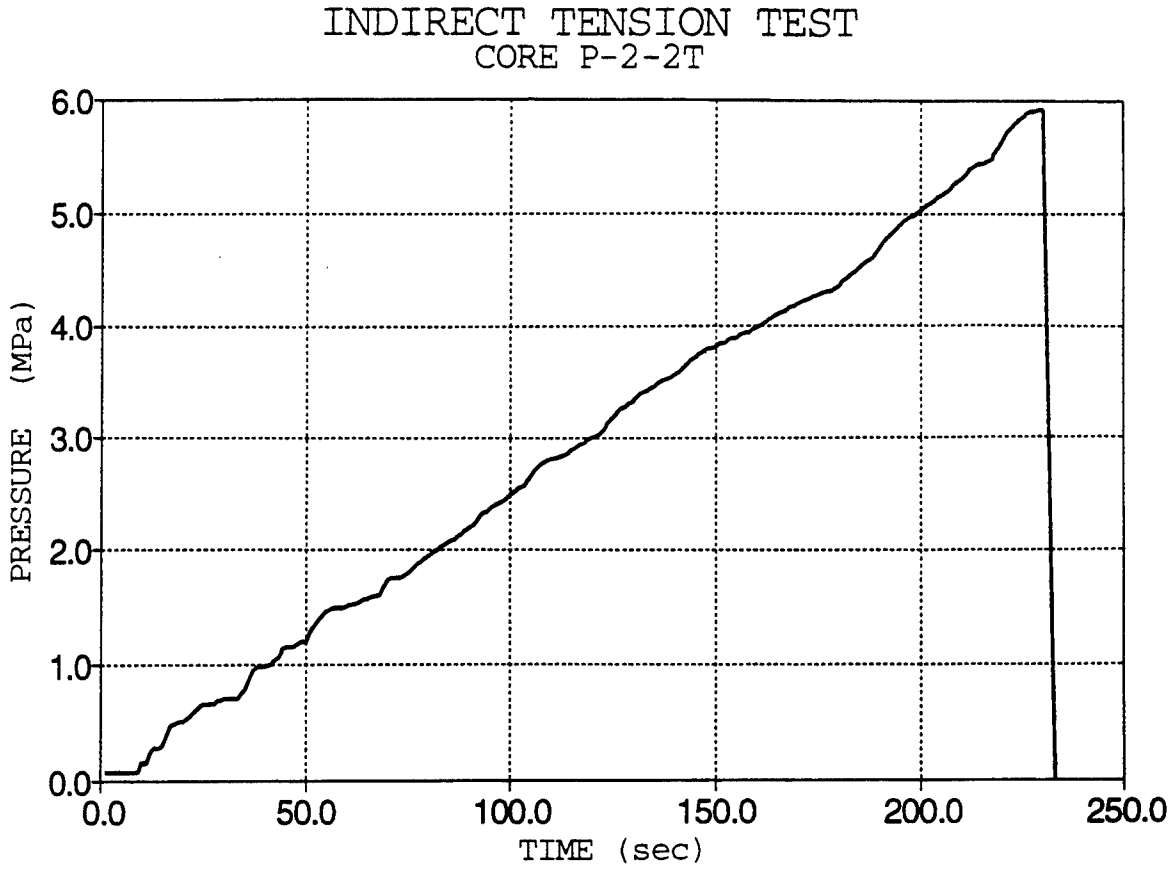
INDIRECT TENSION TEST
CORE P-2-2T
PRESSURE (MPa)
6.0
5.0
4.0
3.0
2.0
1.0
0.0
0.0
50.0
100.0
150.0
200.0
250.0
TIME (sec)

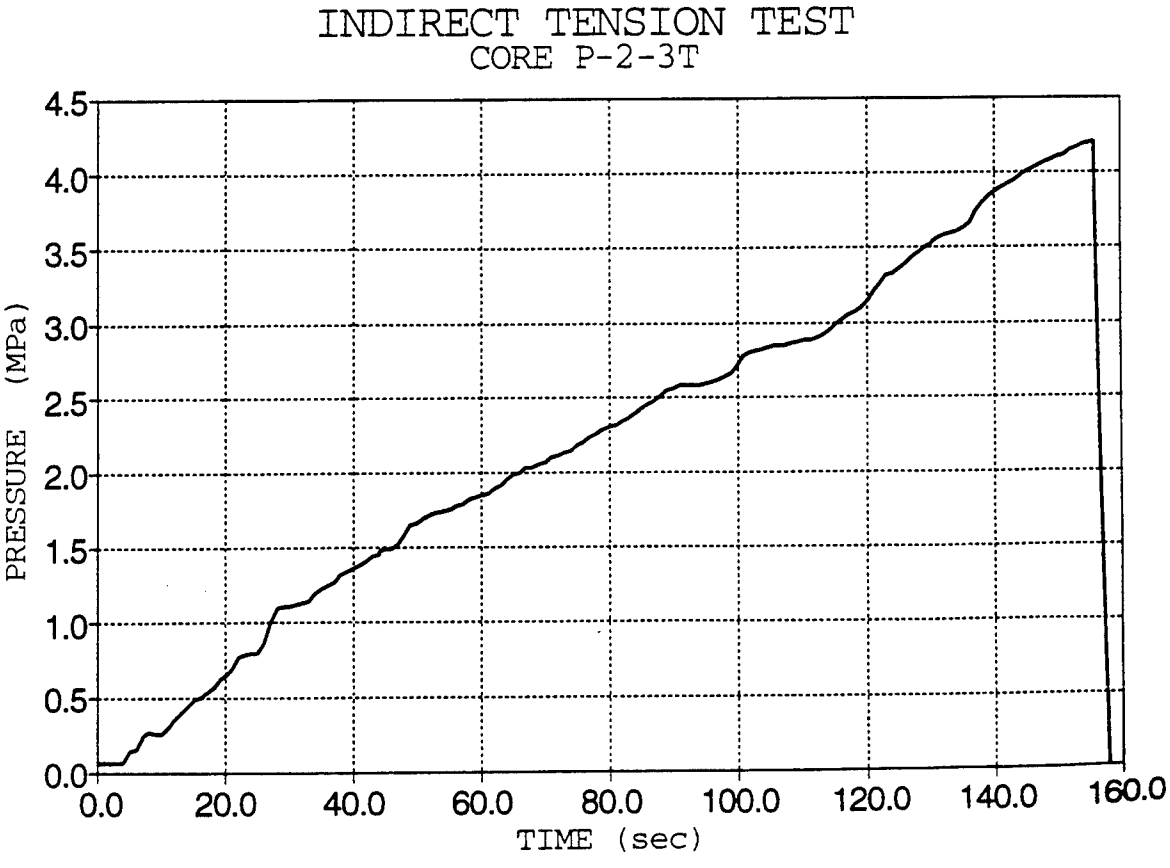
INDIRECT TENSION TEST
CORE P-2-3T
PRESSURE (MPa)
4.5
4.0
3.5
3.0
2.5
2.0
1.5
1.0
0.5
0.0
0.0
20.0
40.0
60.0
80.0
100.0
120.0
140.0
160.0
TIME (sec)

# Appendix H
# Resonant Frequency - Whole-Beam Series

## BEAM J1 SMALL

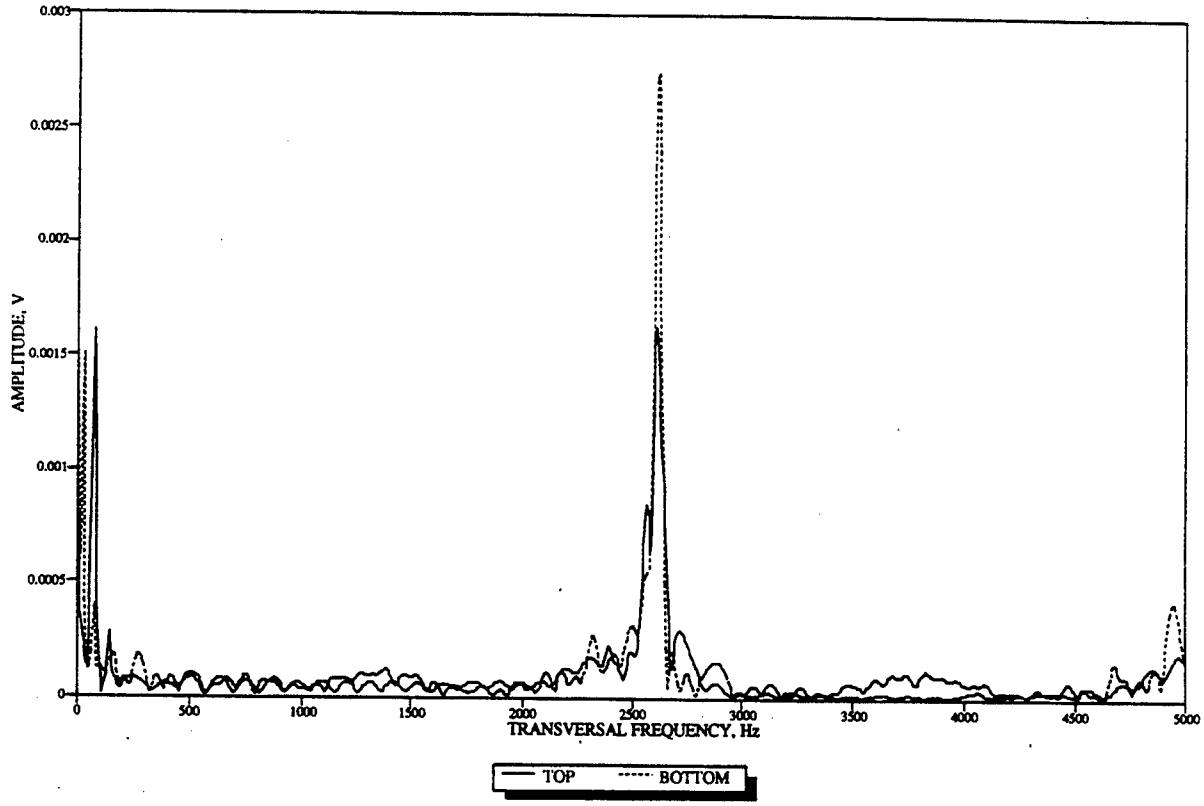


## BEAM J1 SMALL

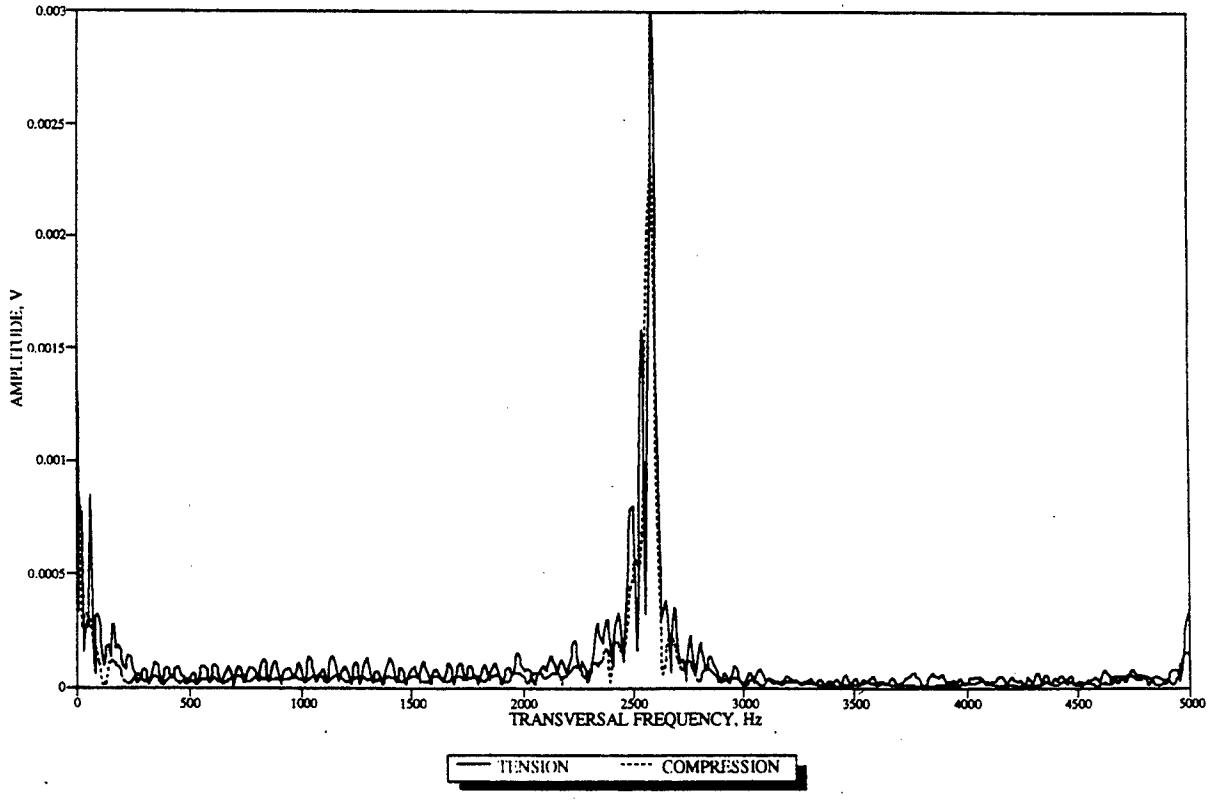

## BEAM J1 SMALL

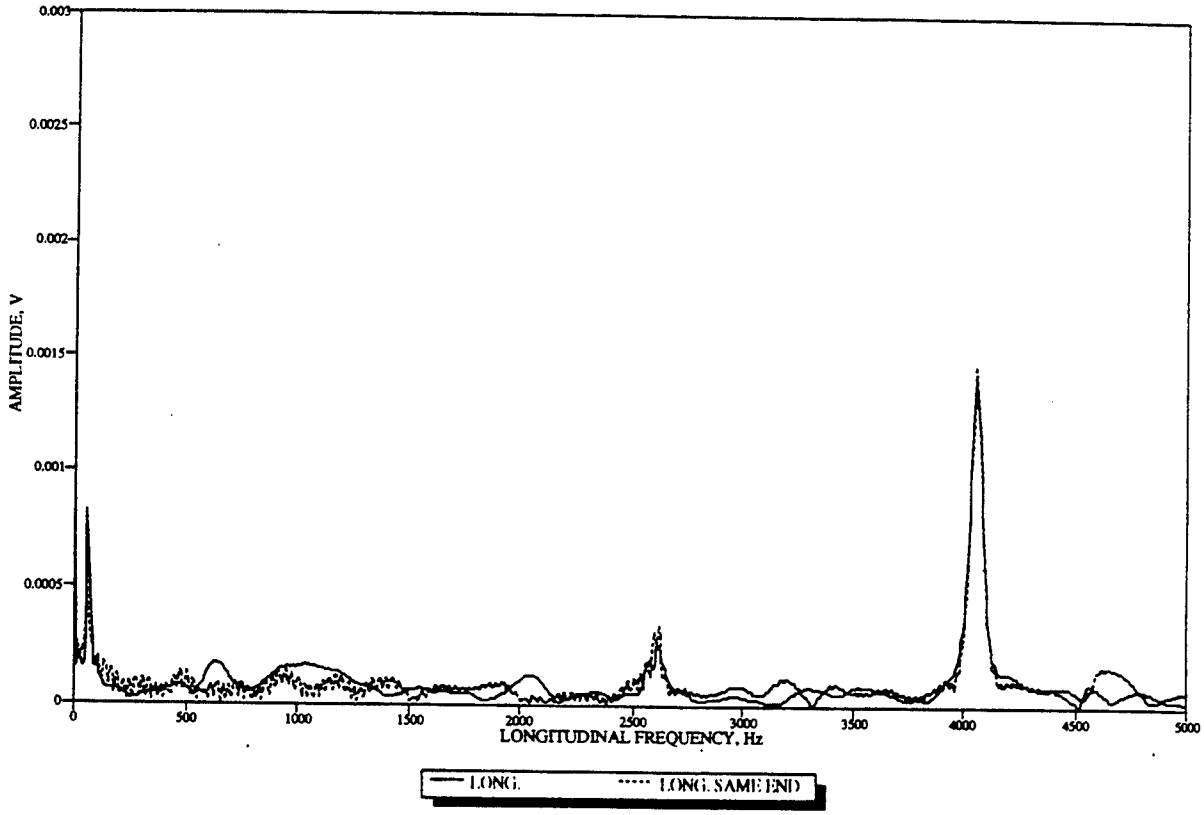


## BEAM J1 SMALL

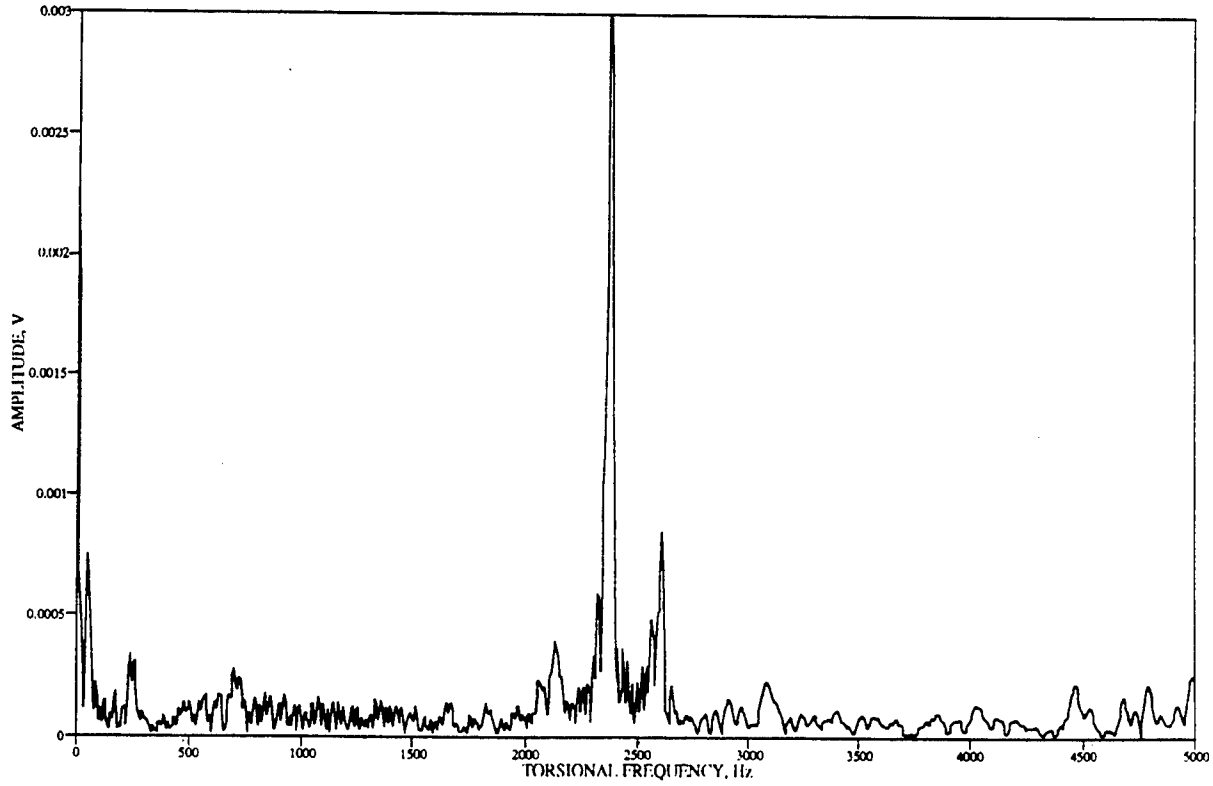

## BEAM J1 BIG

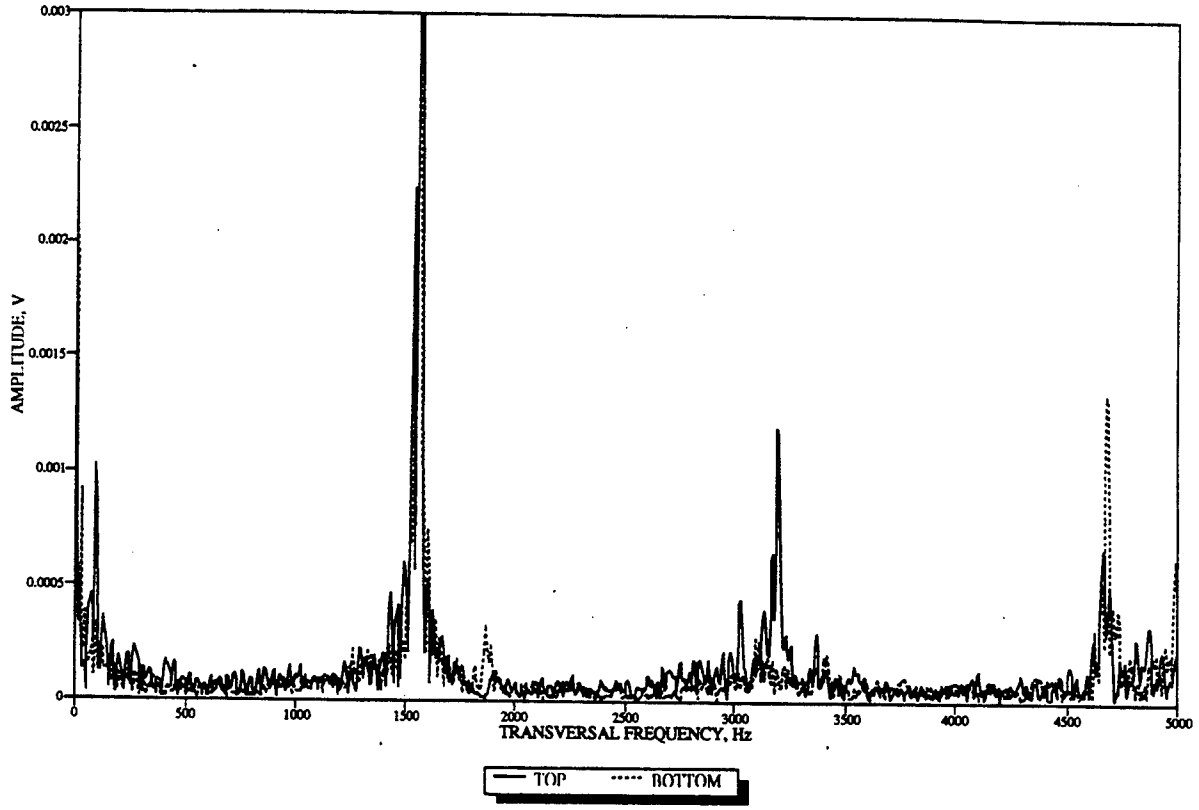


---

## BEAM J1 BIG

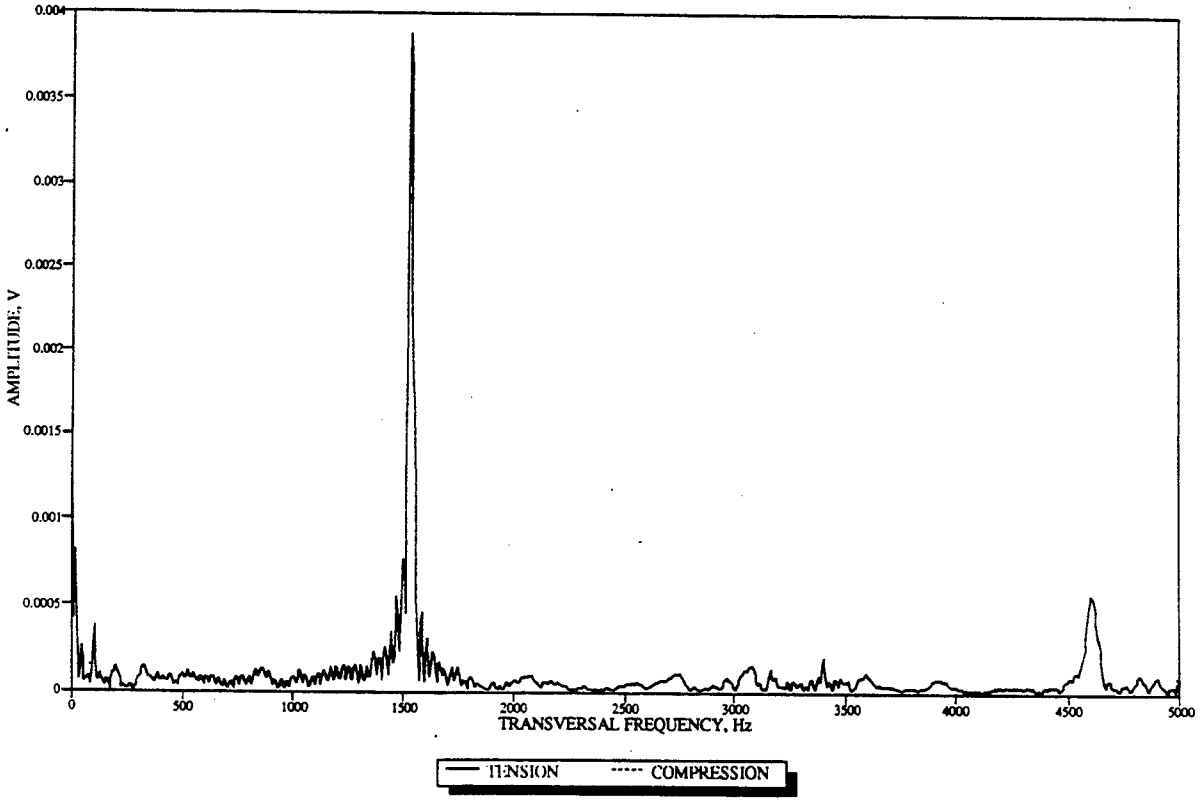

BEAM J1 BIG

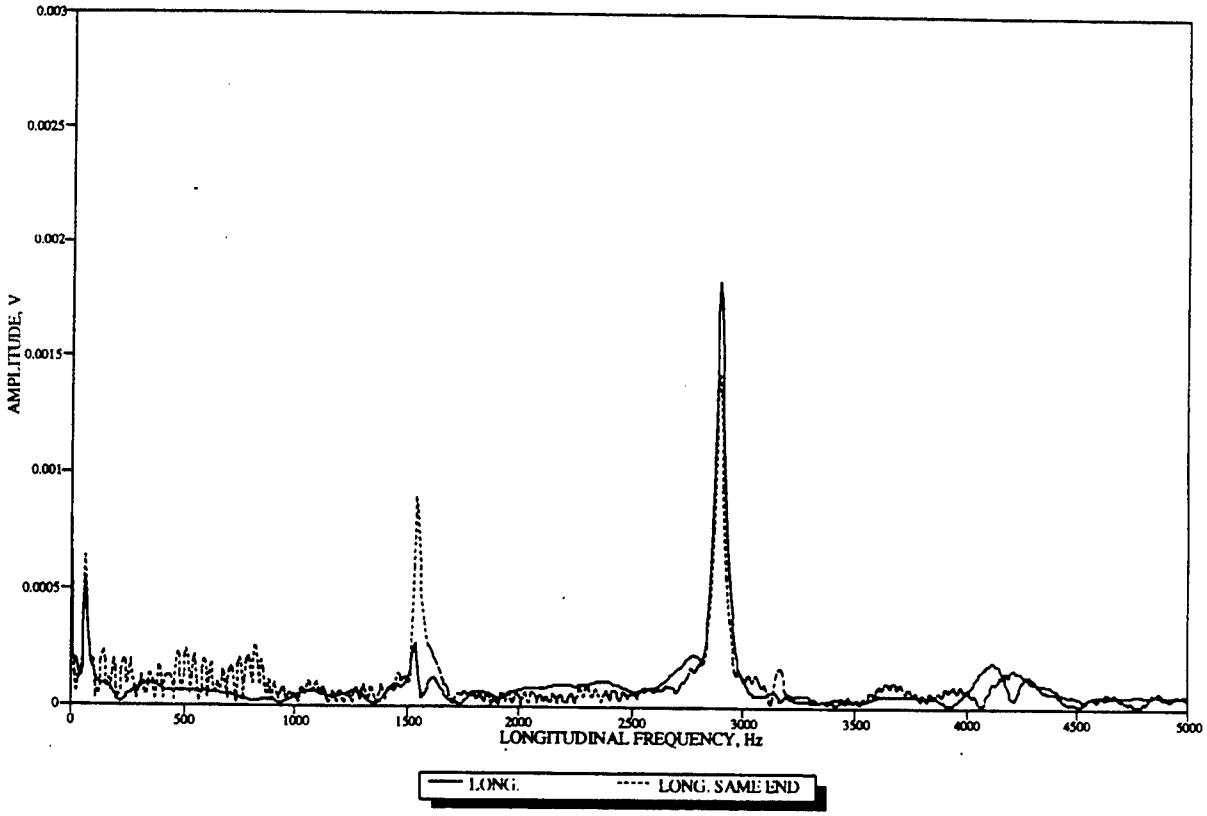


BEAM J1 BIG

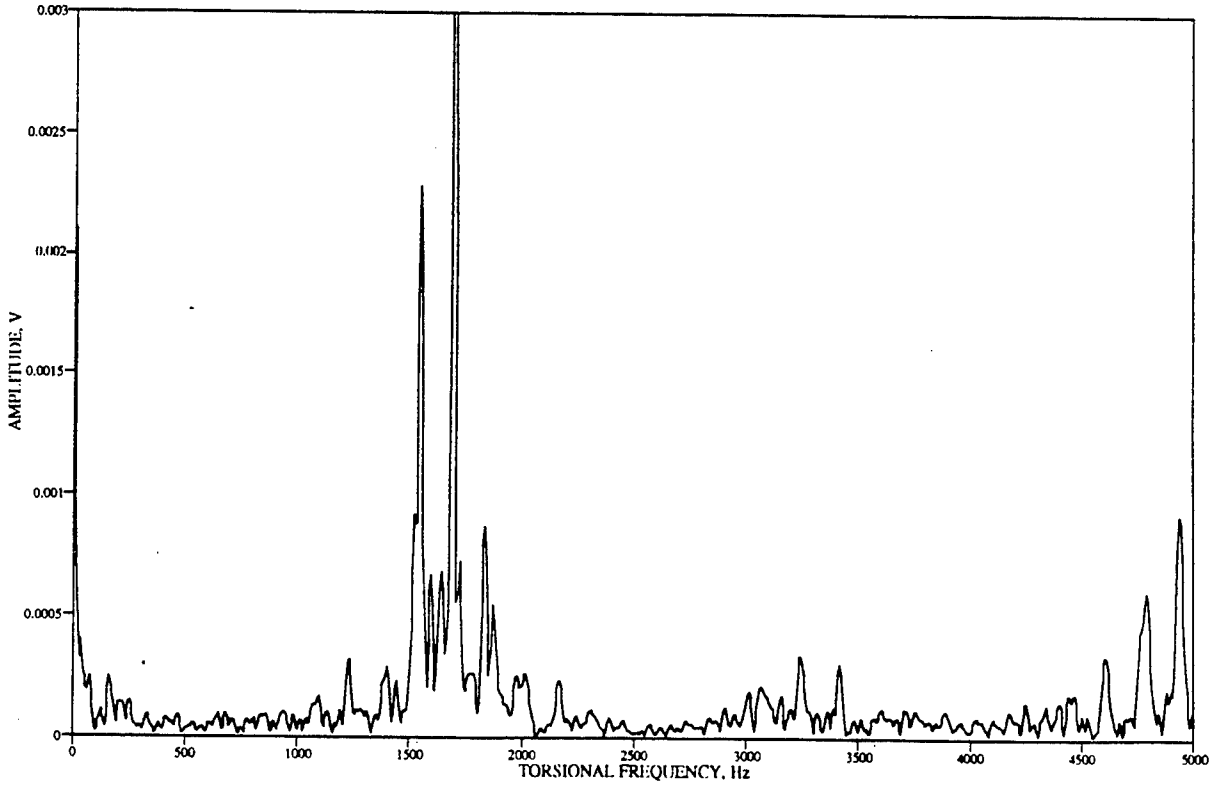

BEAM J3

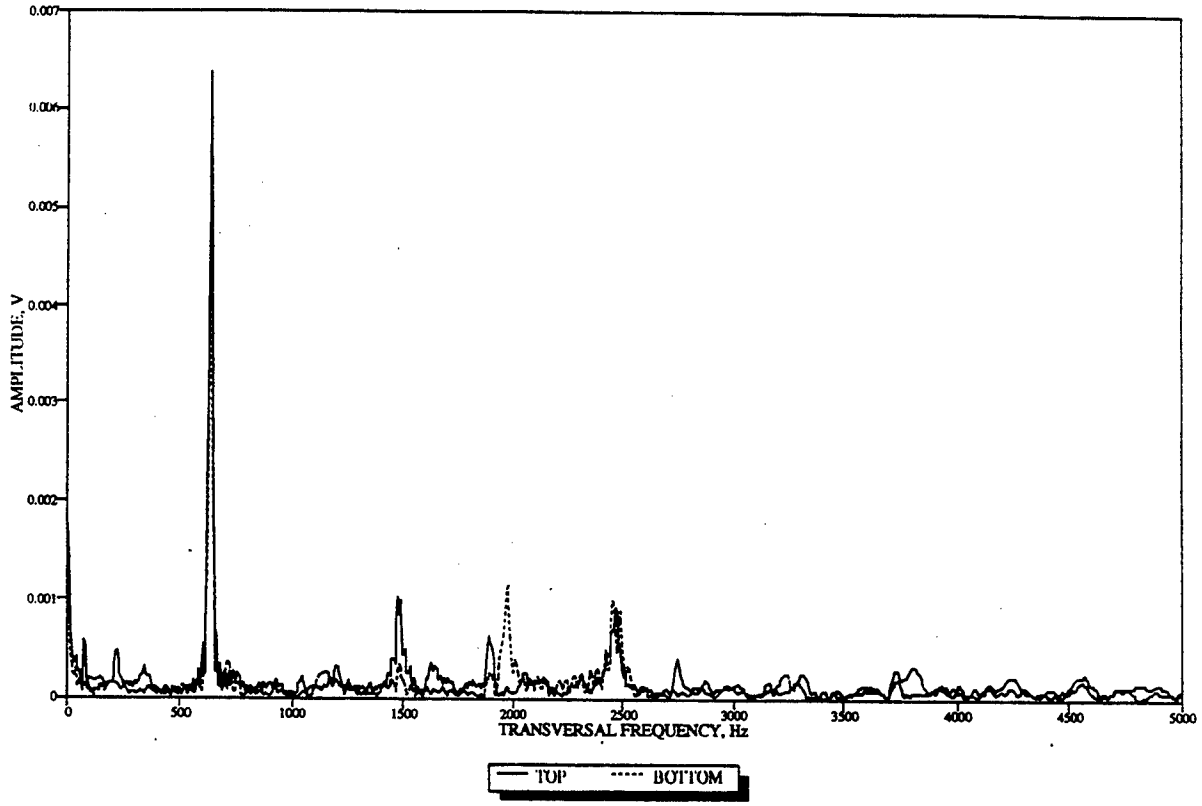


BEAM J3

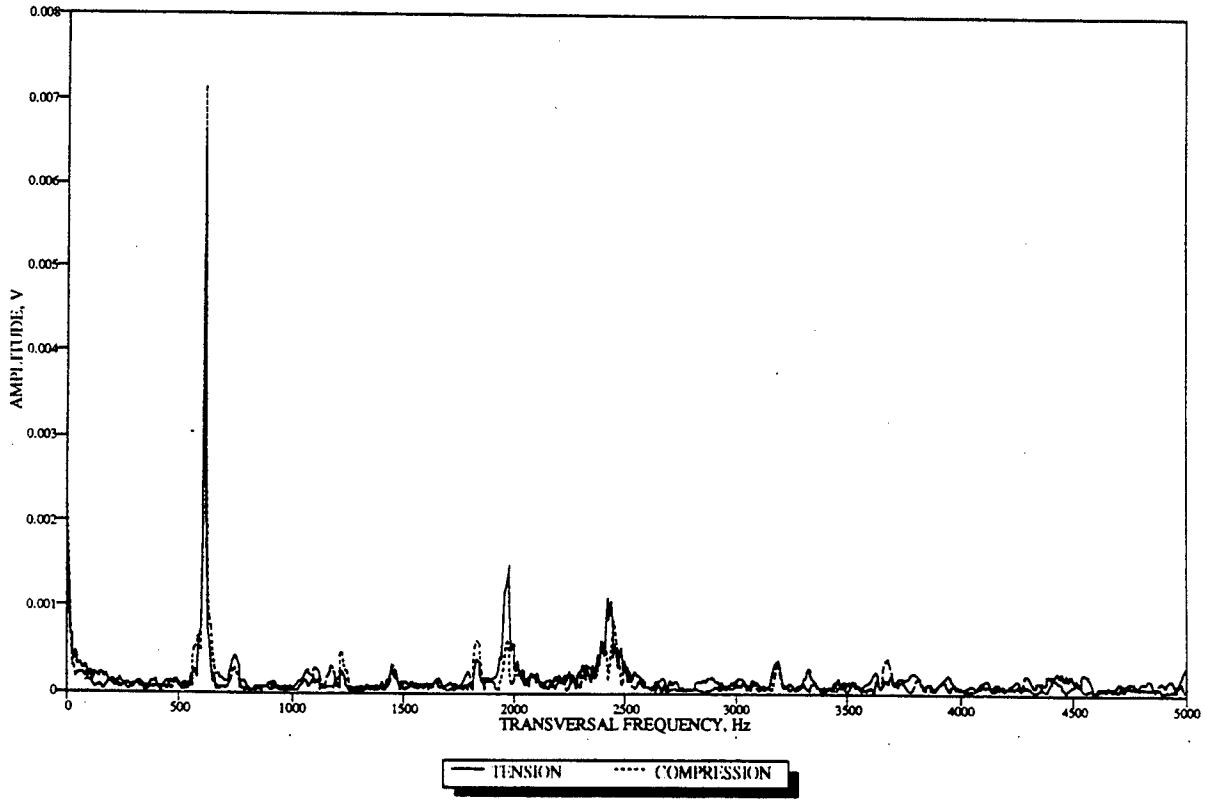

## BEAM J3

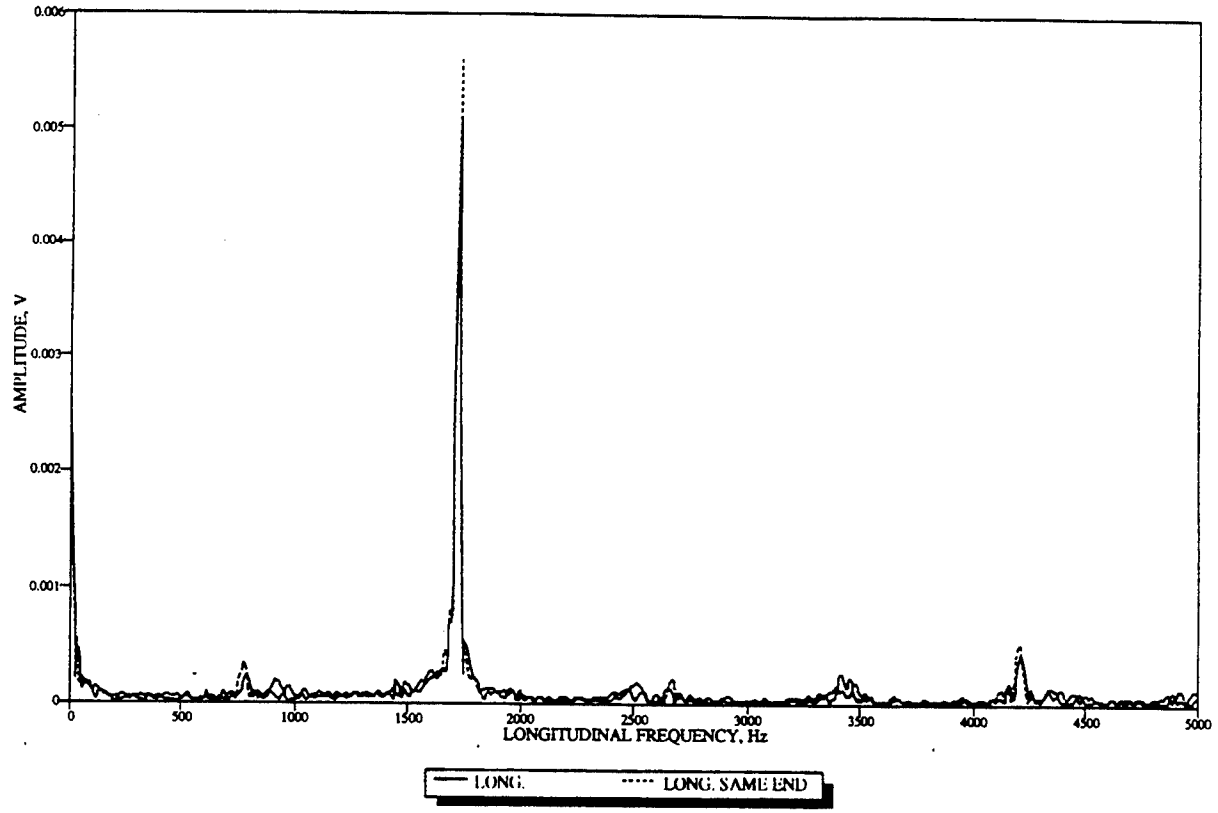


## BEAM J3

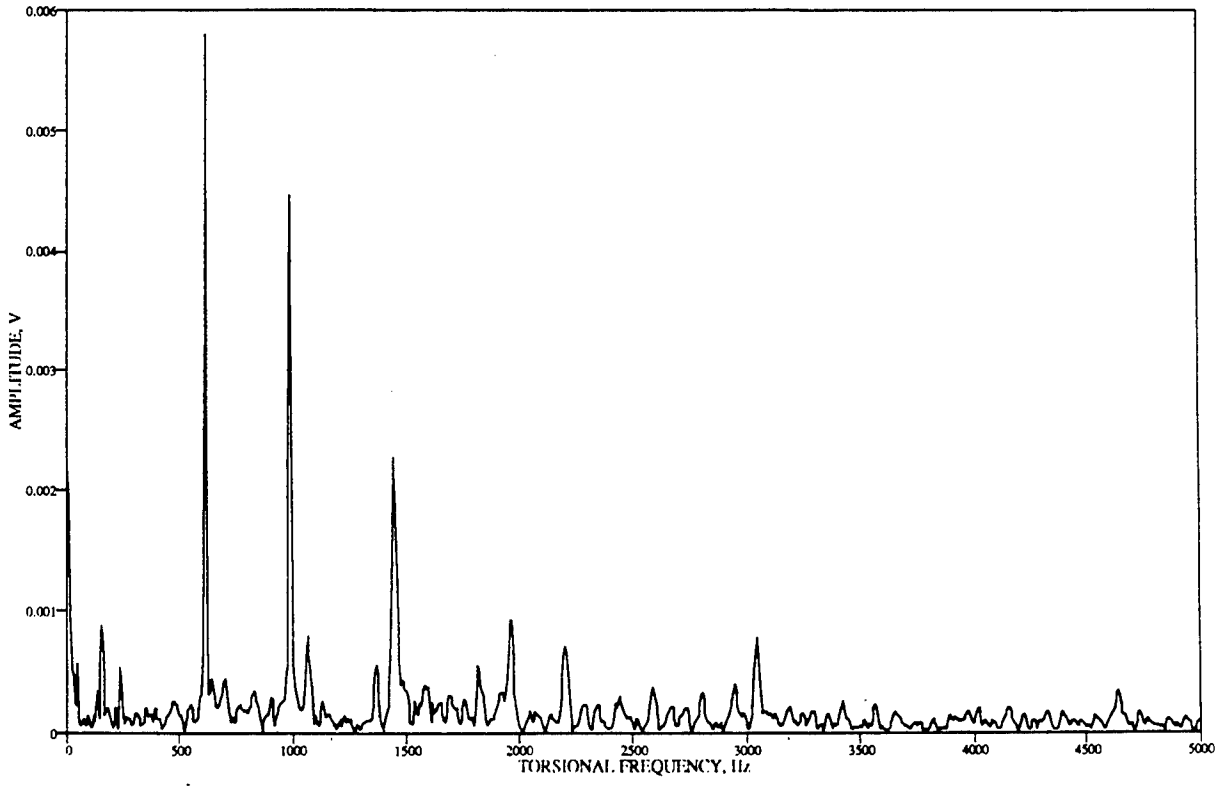

## BEAM K1

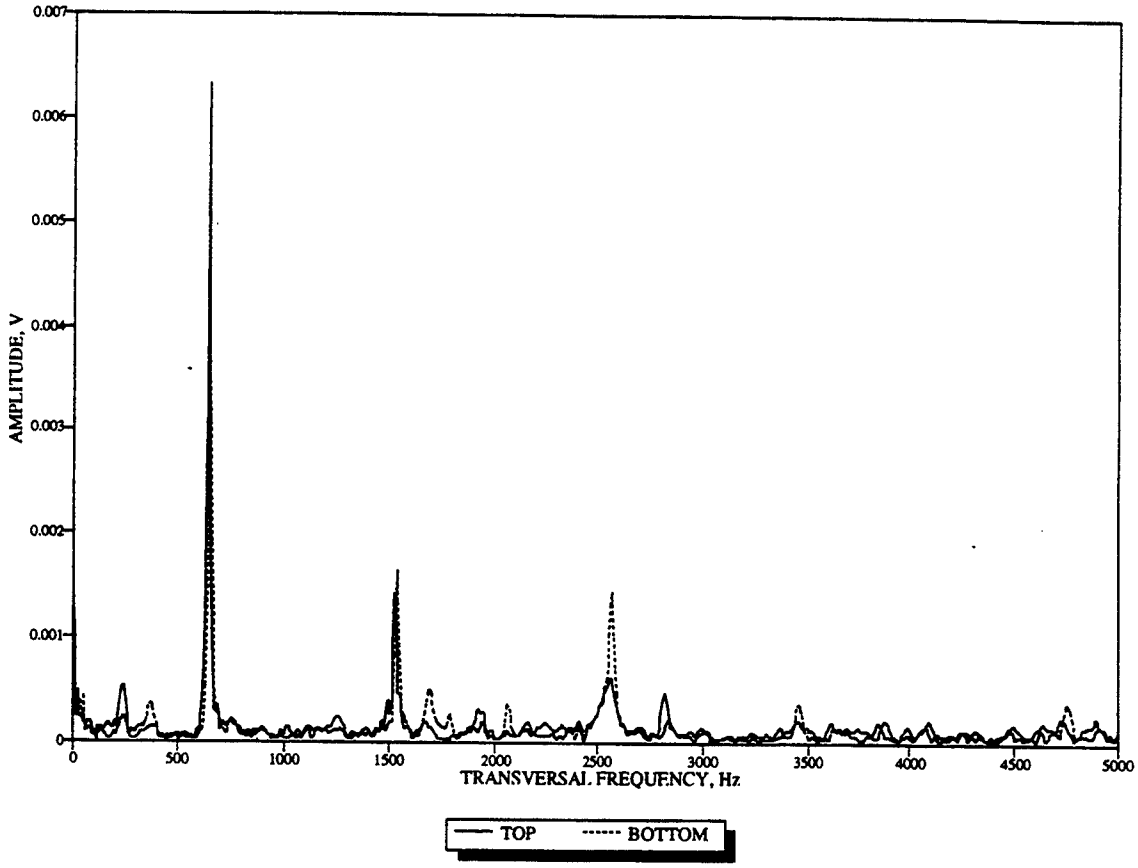


## BEAM K1

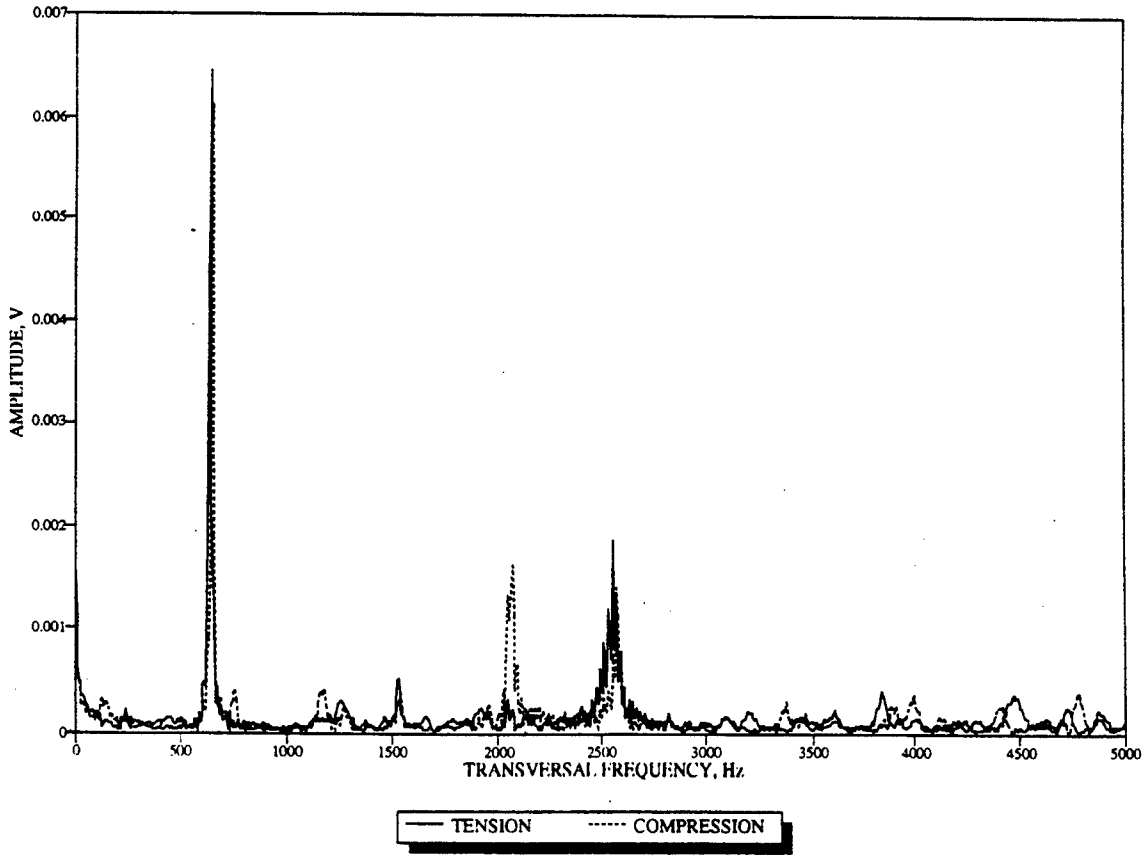

## BEAM K1

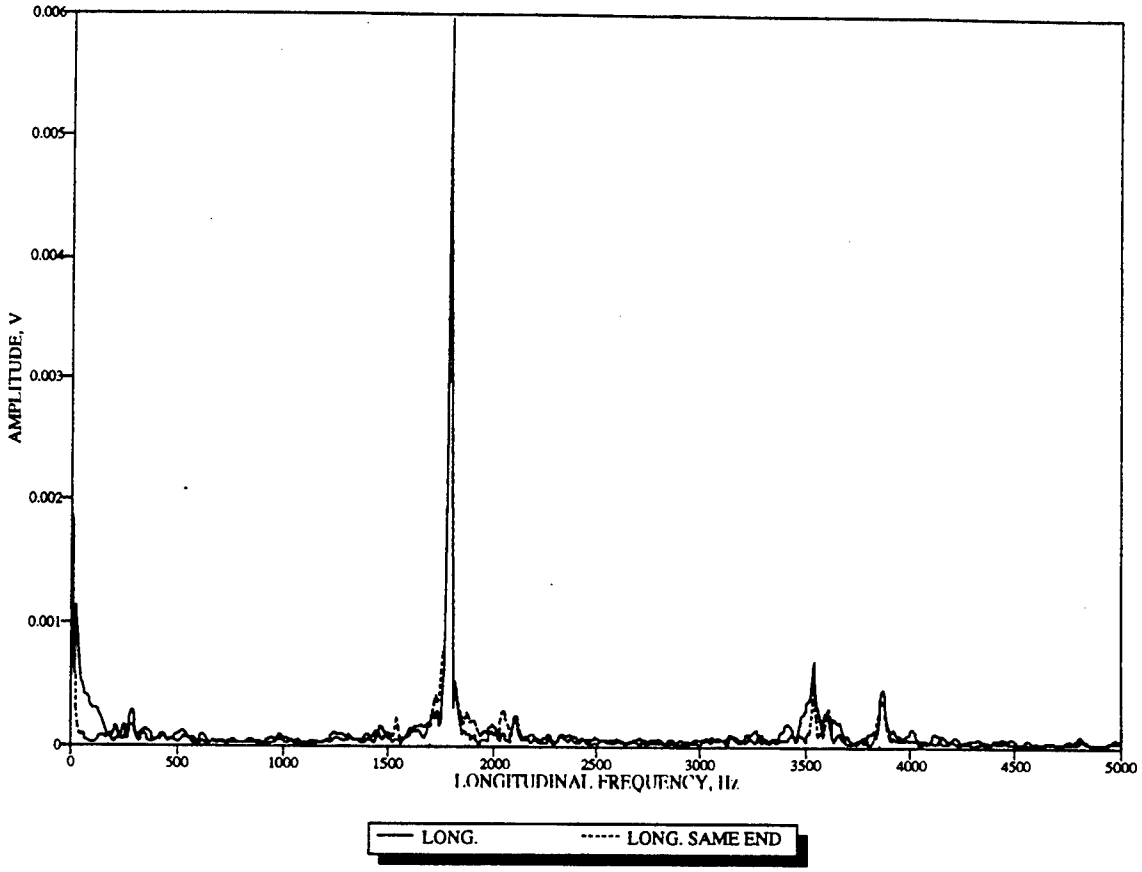


## BEAM K1

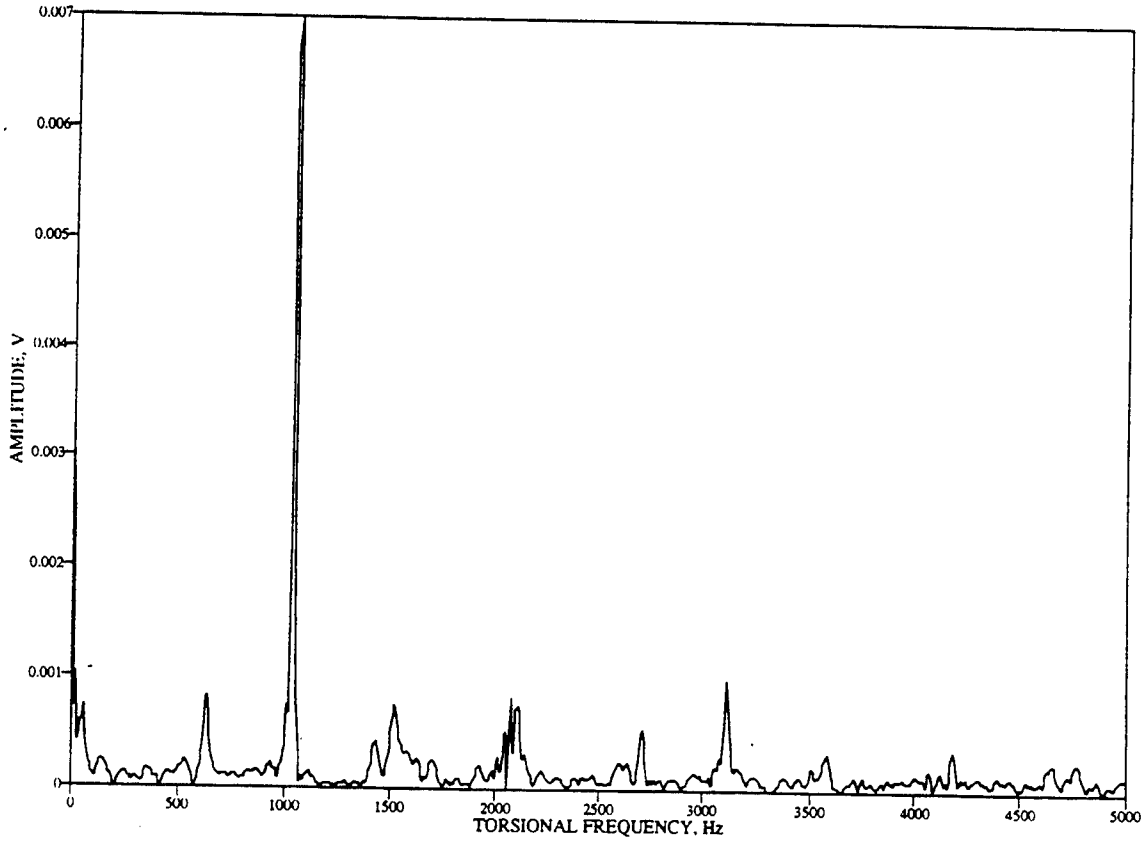

# BEAM K3

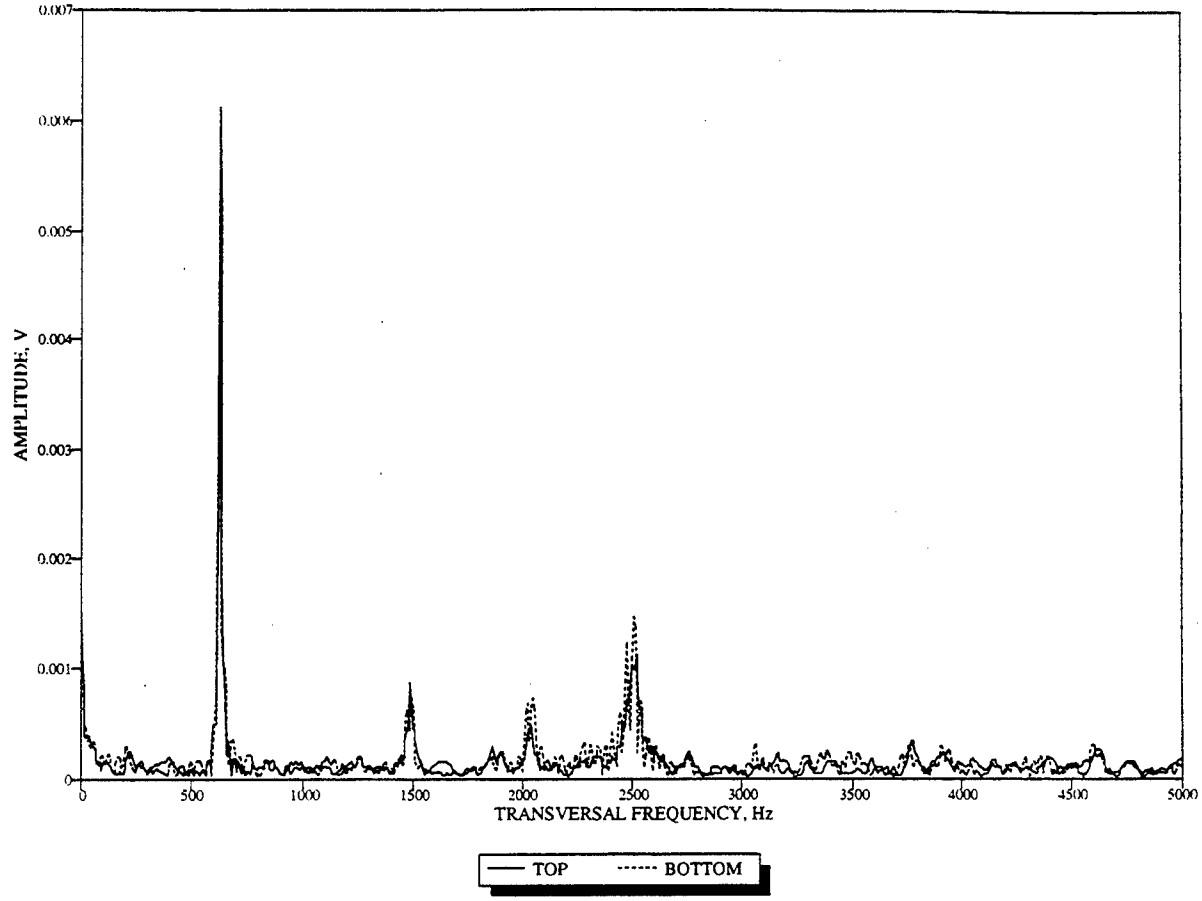


# BEAM K3

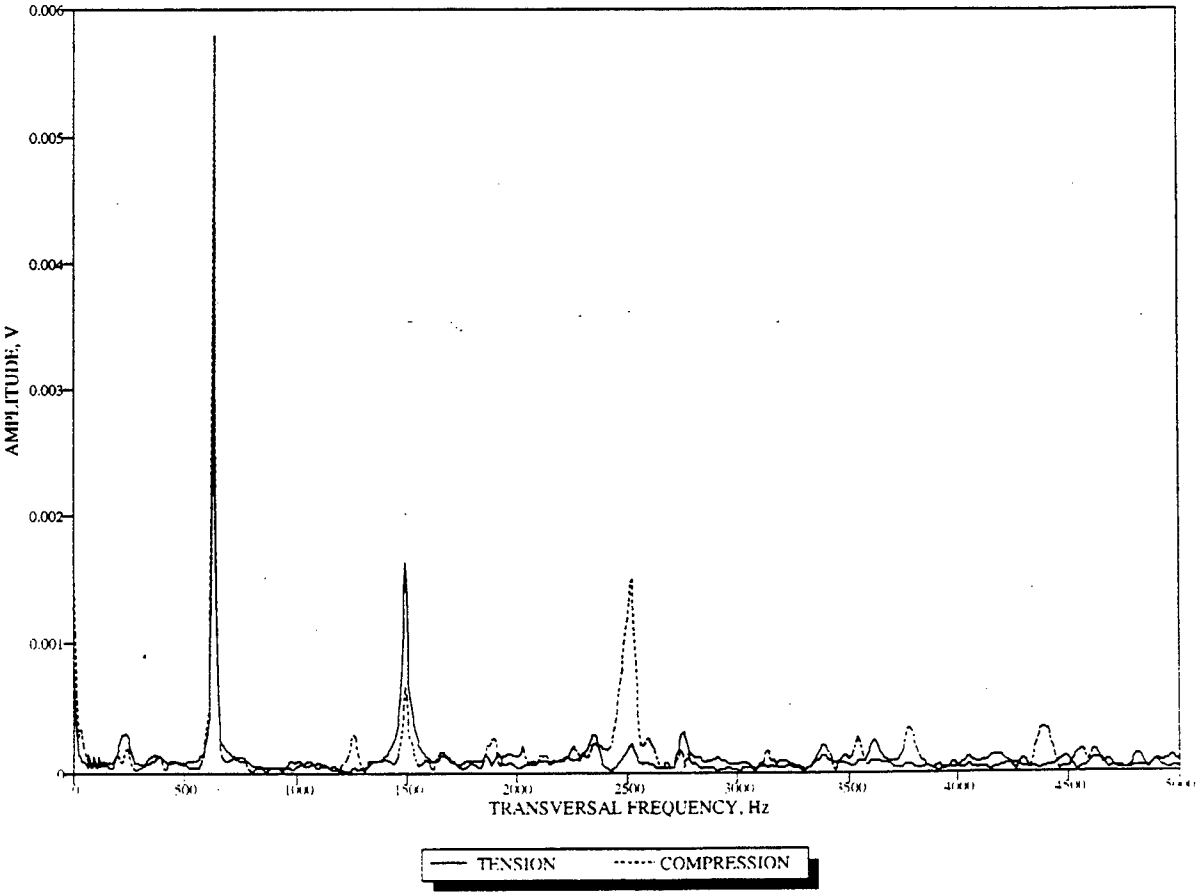

## BEAM K3

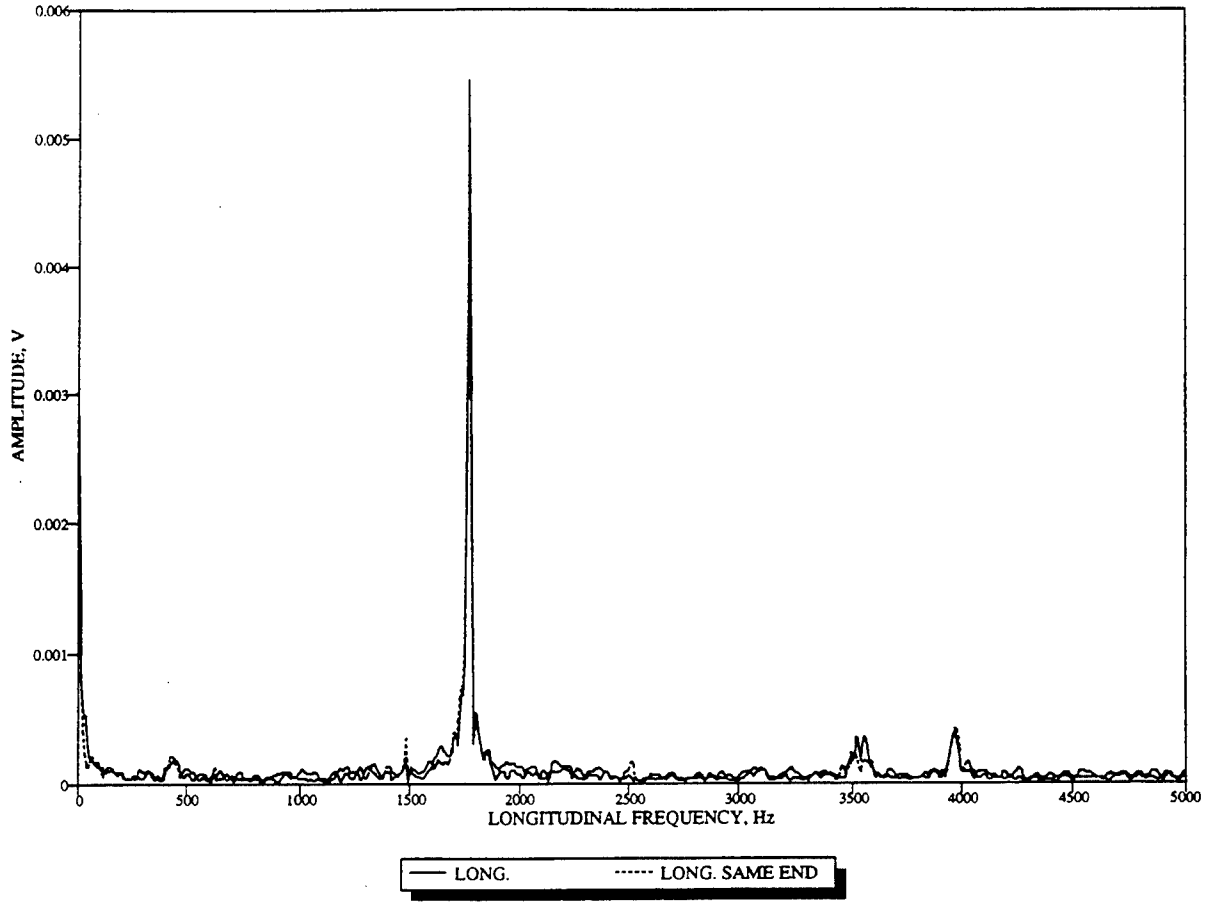


## BEAM K3

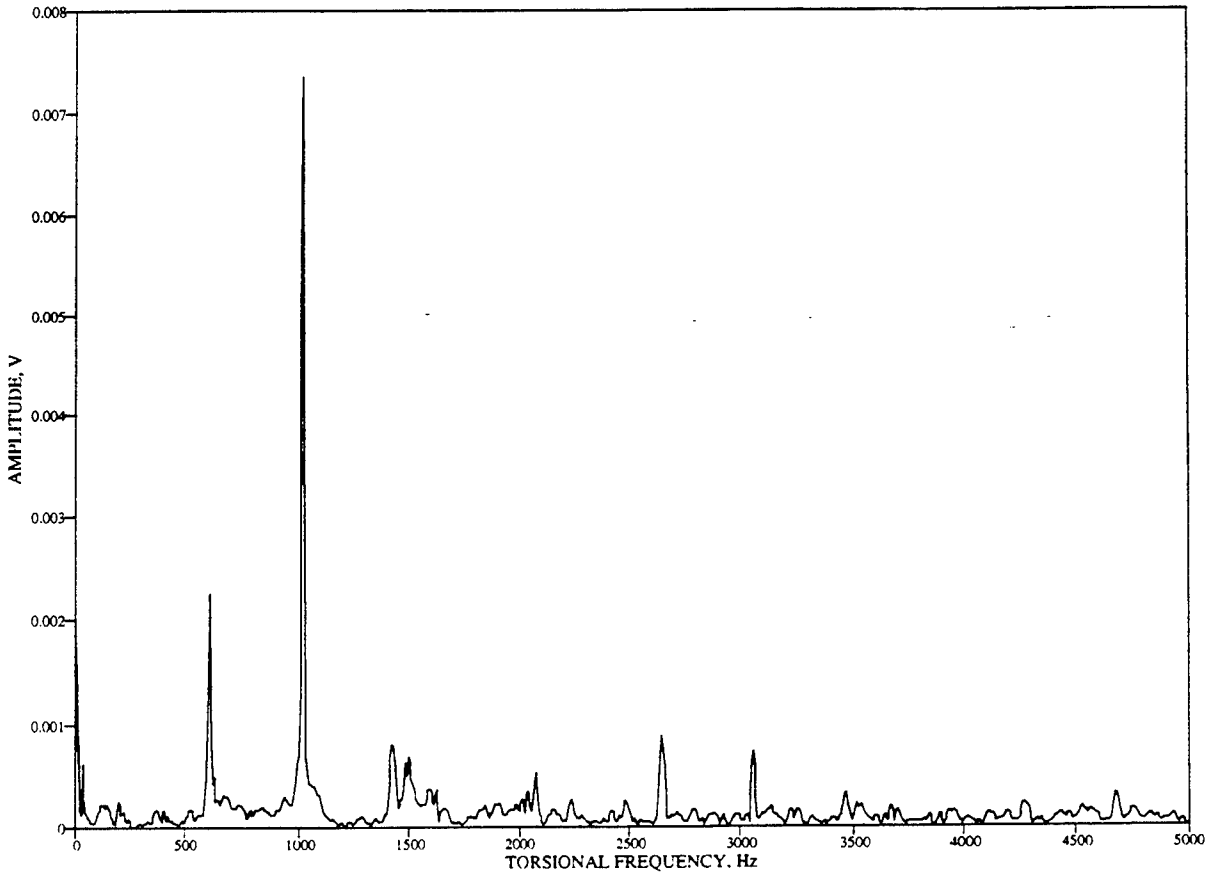

## BEAM M1

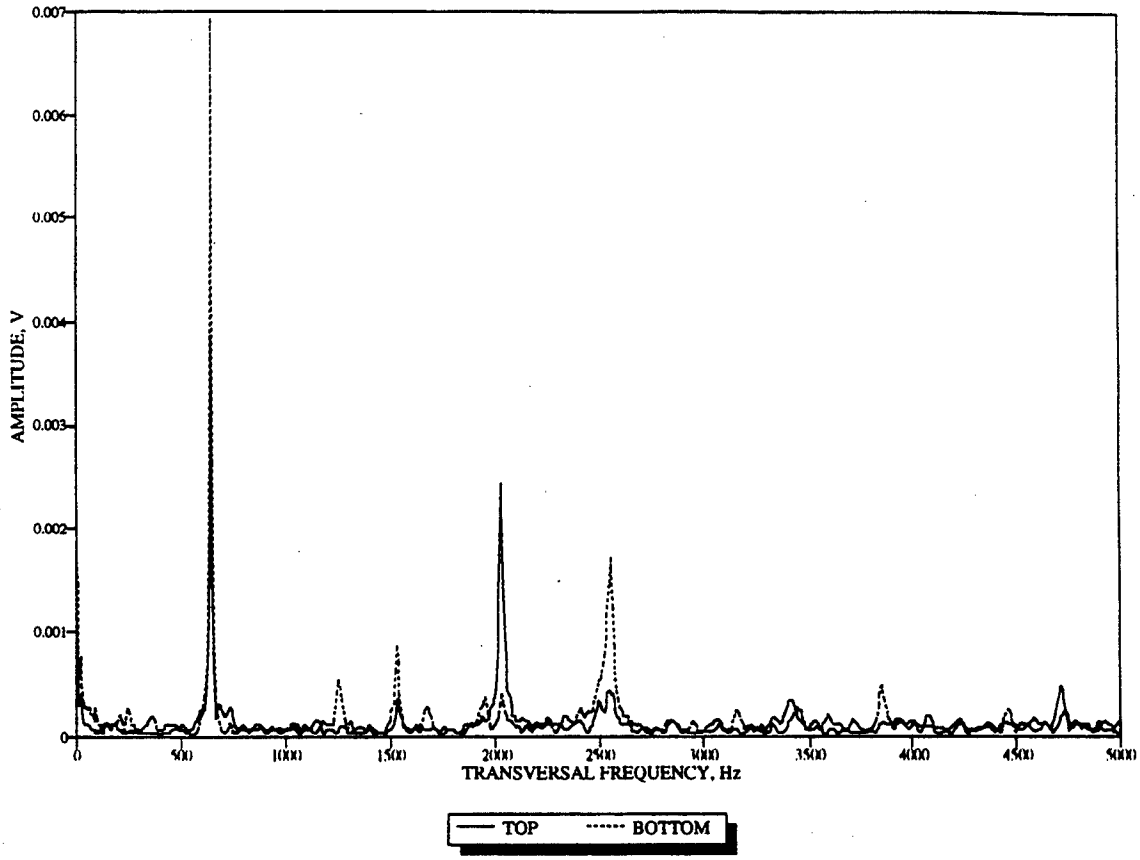


## BEAM M1

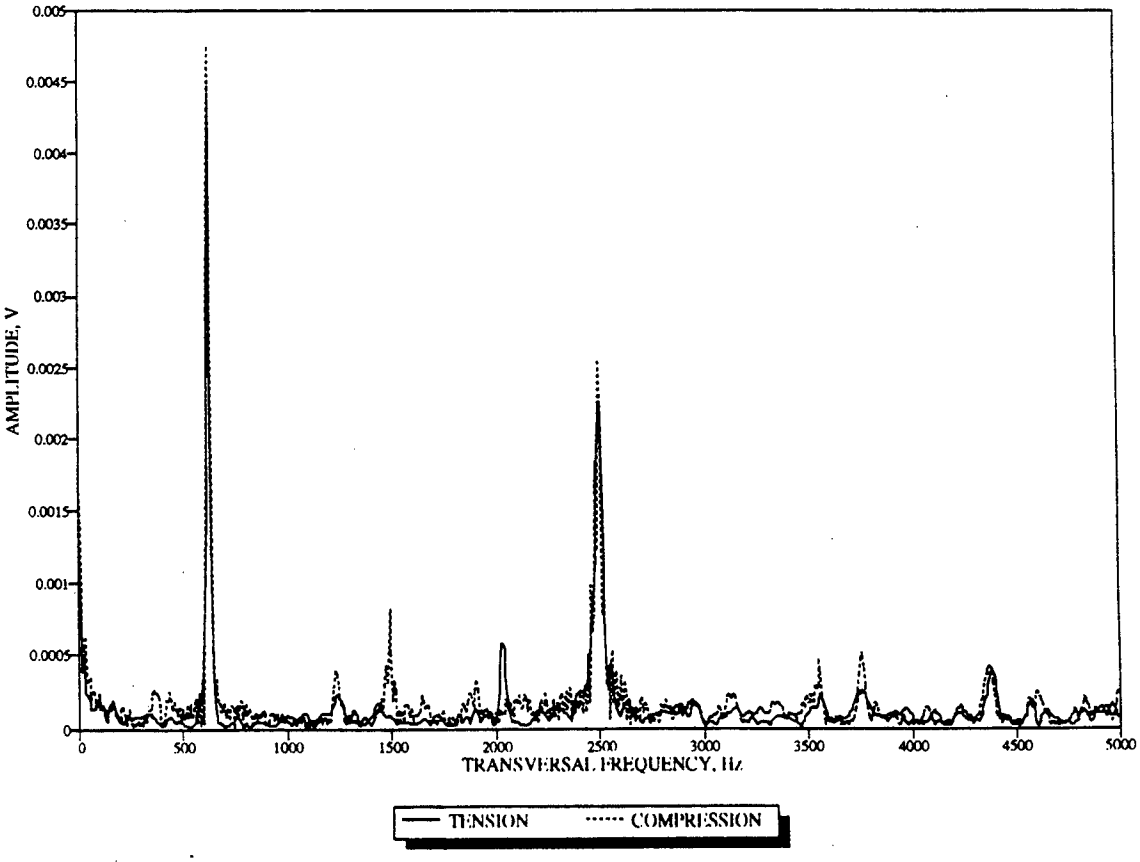

BEAM M1

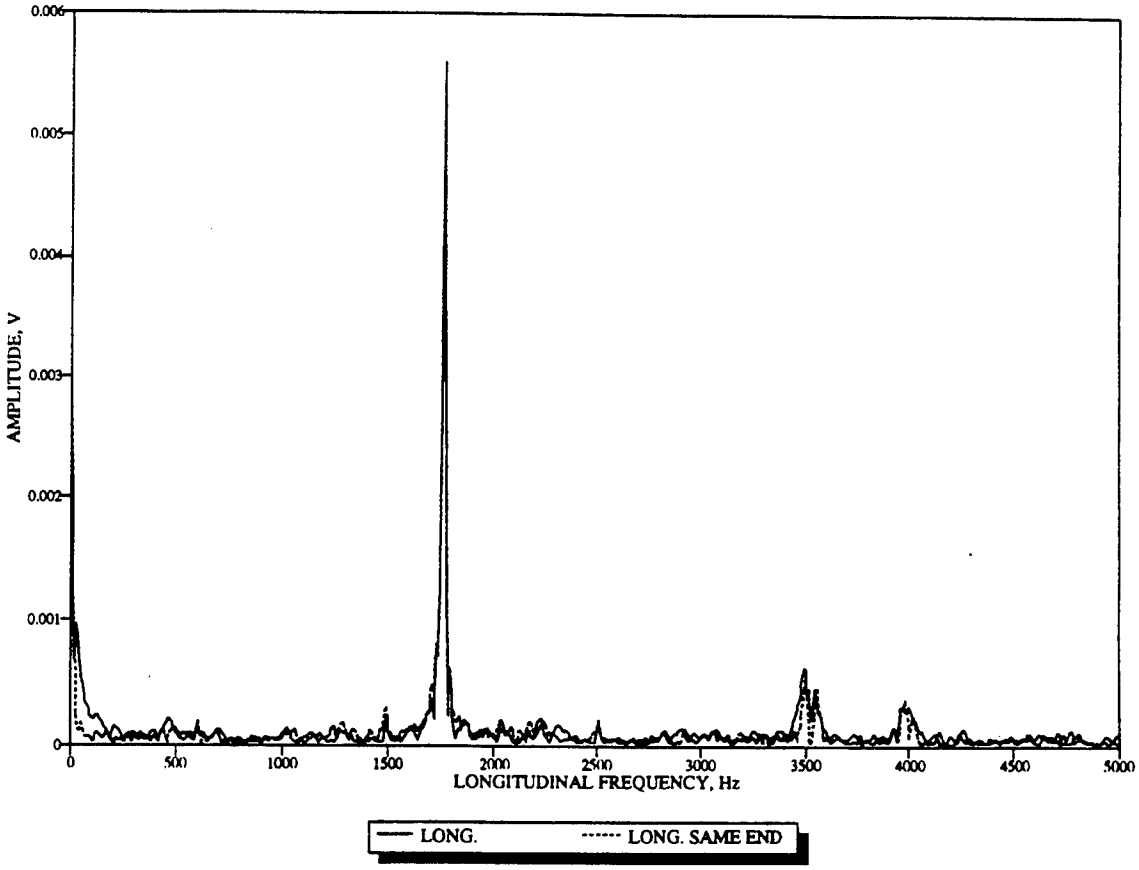


BEAM M1

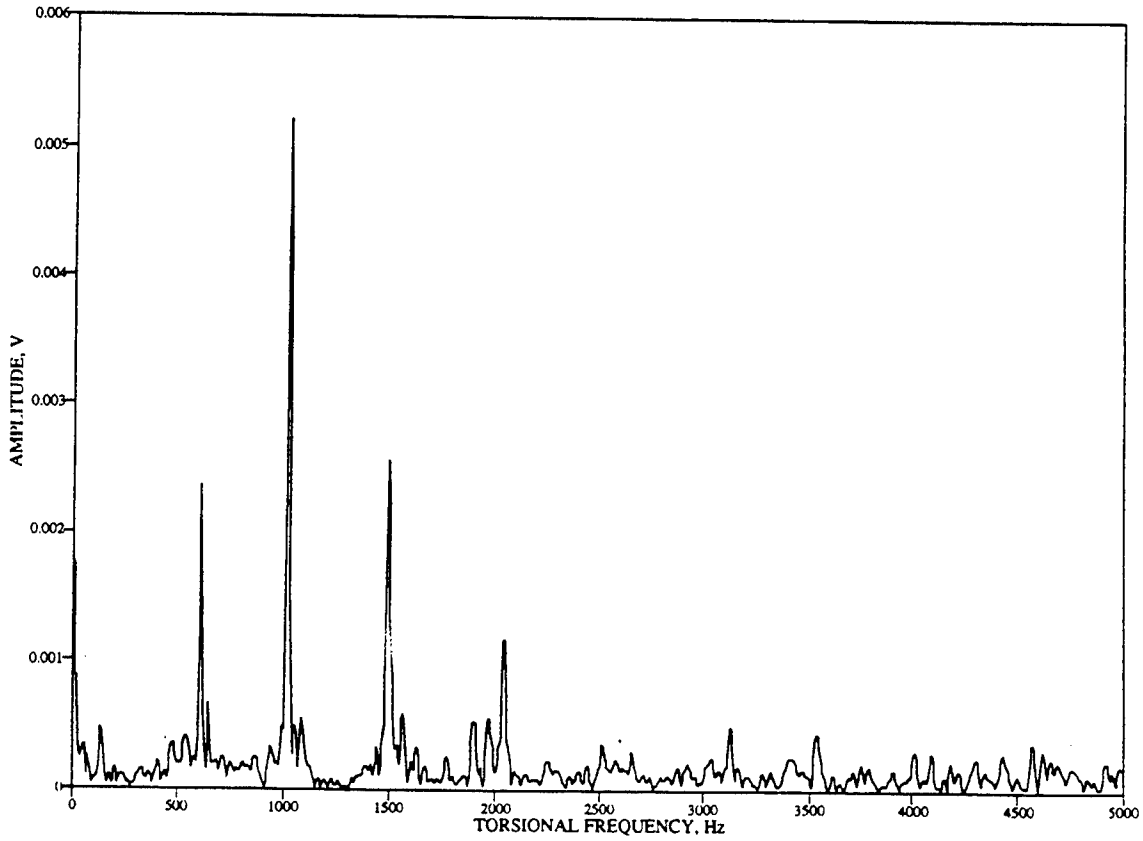

## BEAM M3

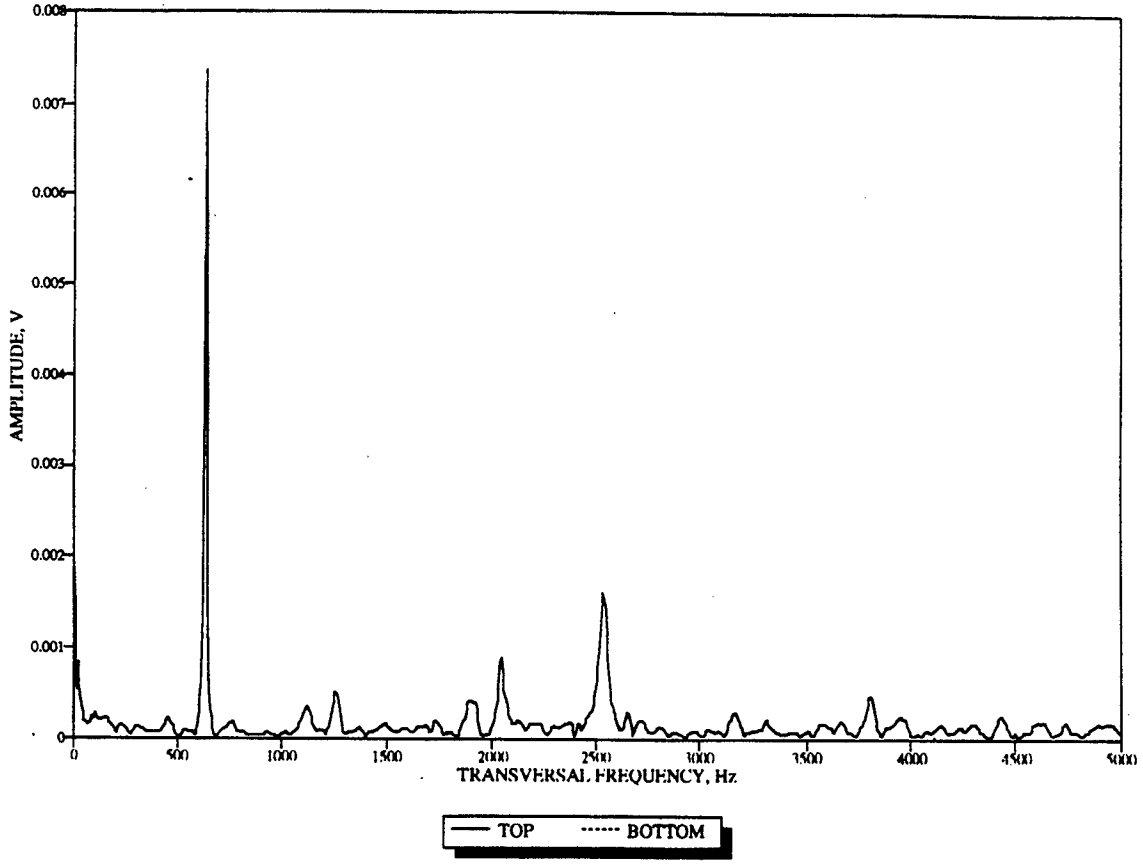


---

## BEAM M3

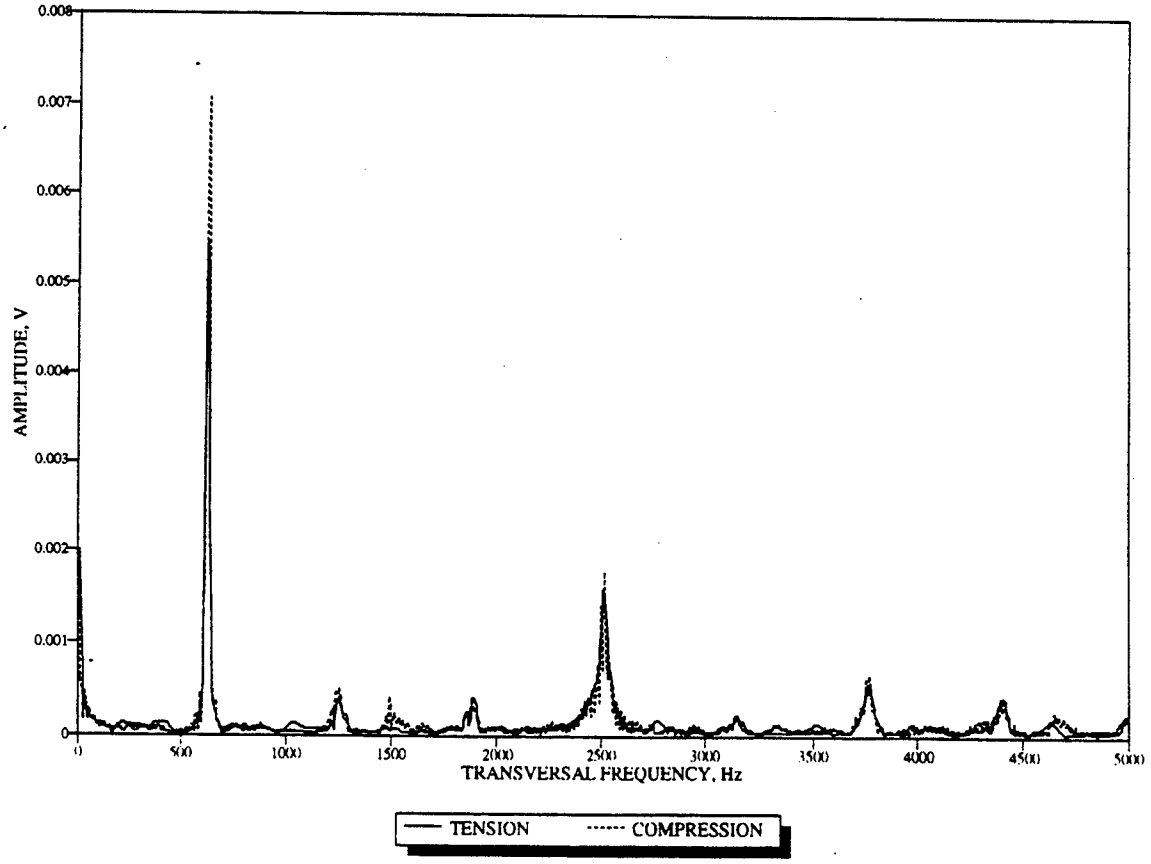

## BEAM M3

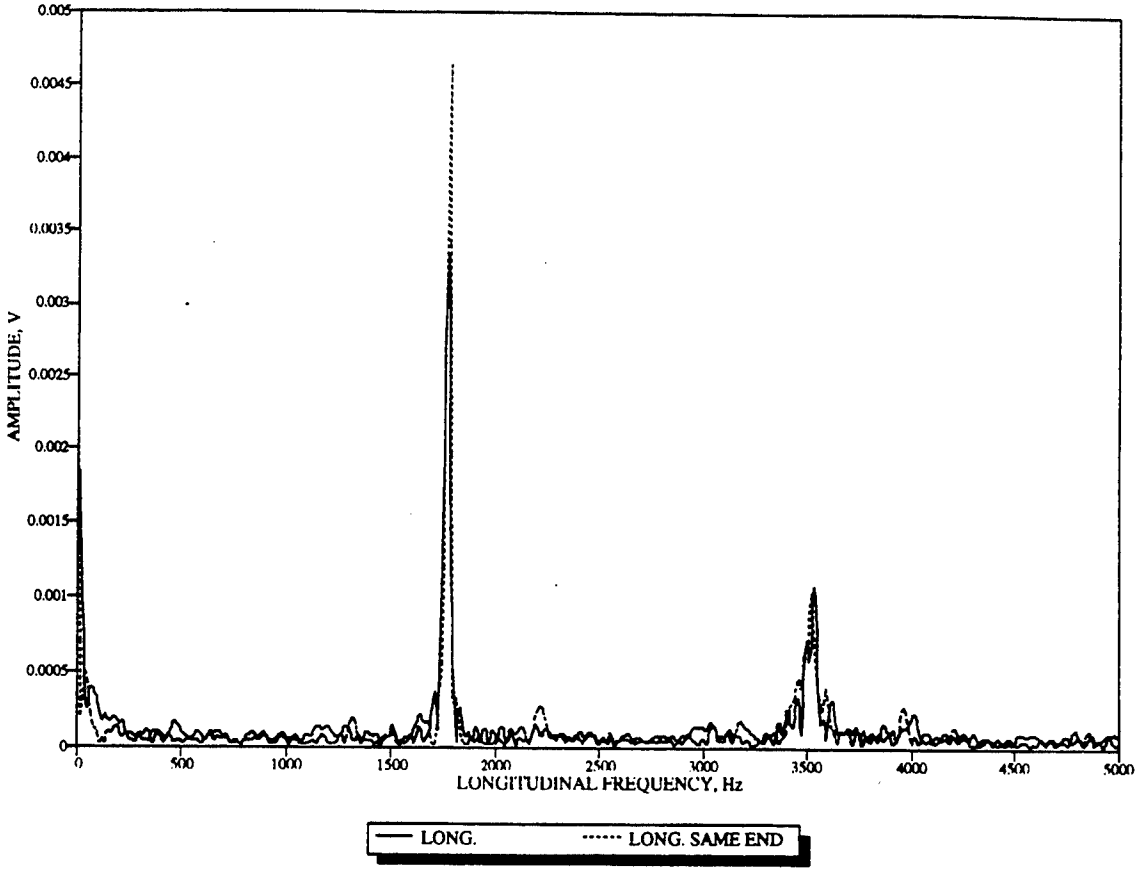


## BEAM M3

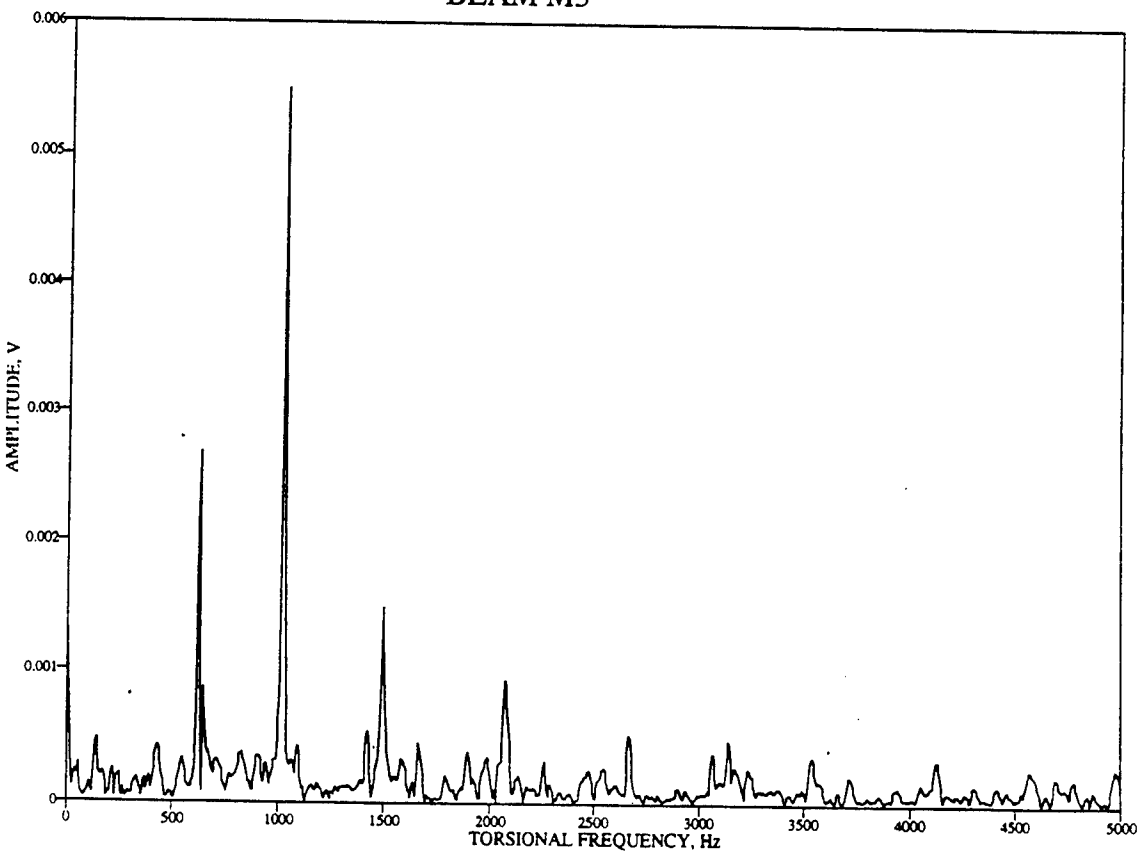

## BEAM N1

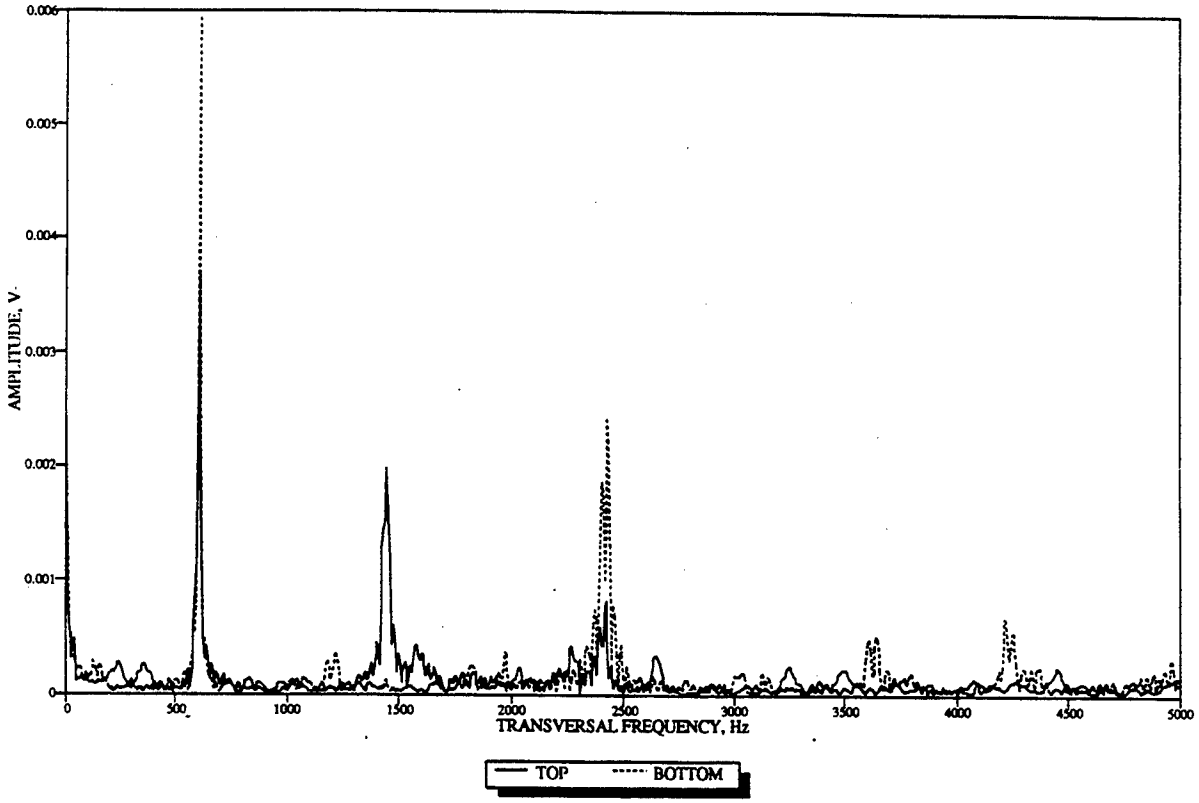


## BEAM N1

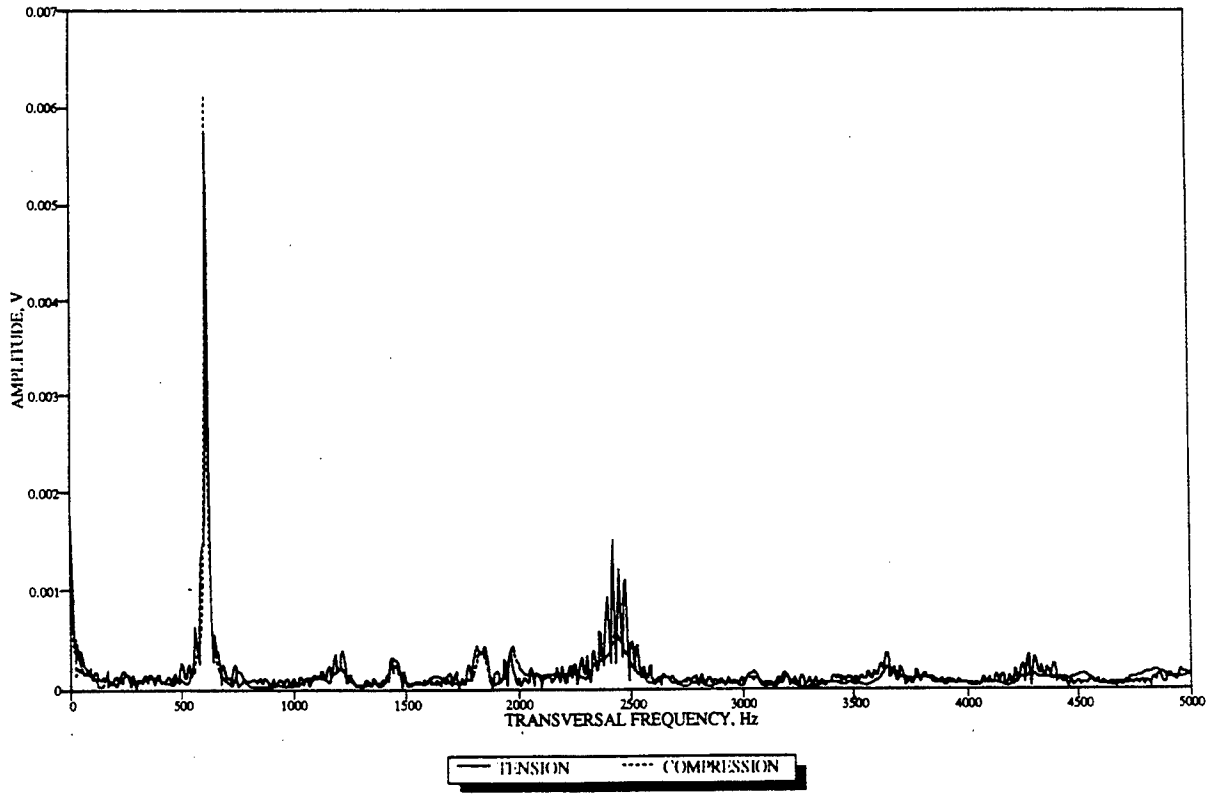

BEAM N1

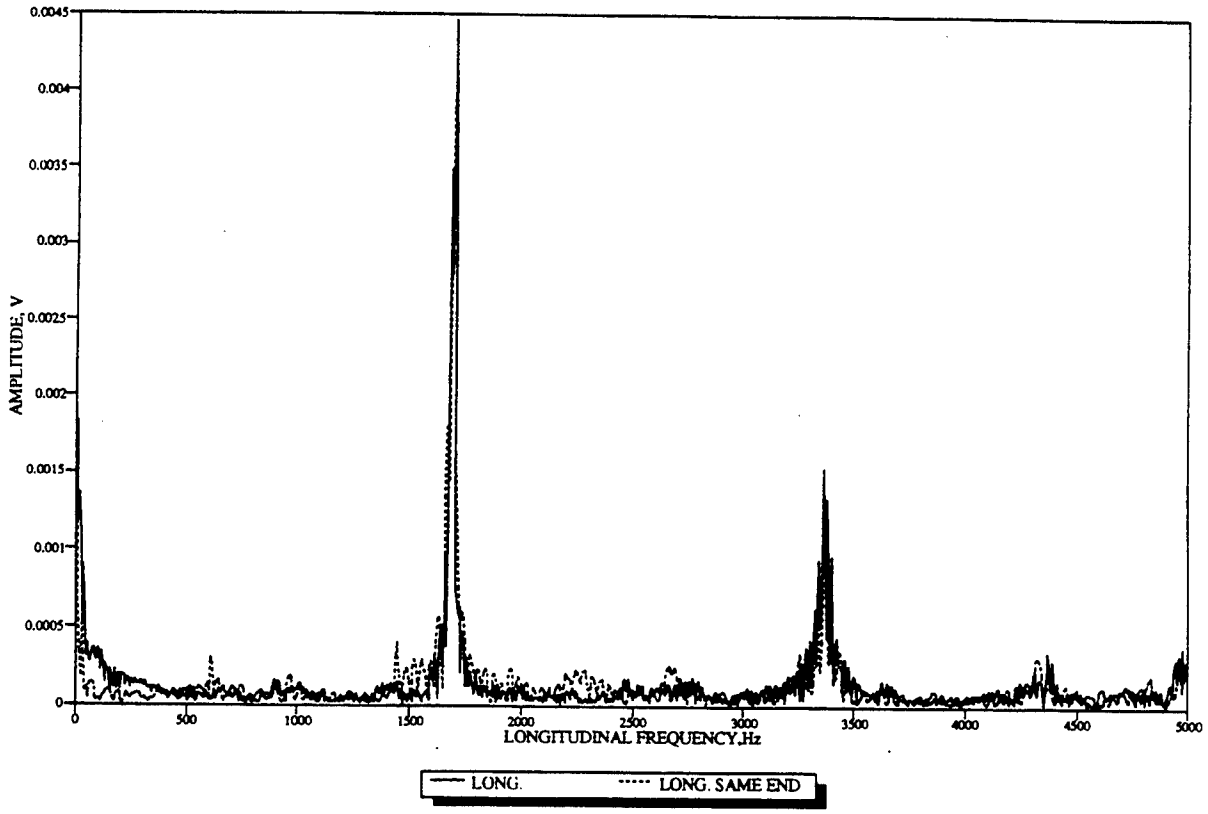


BEAM N1

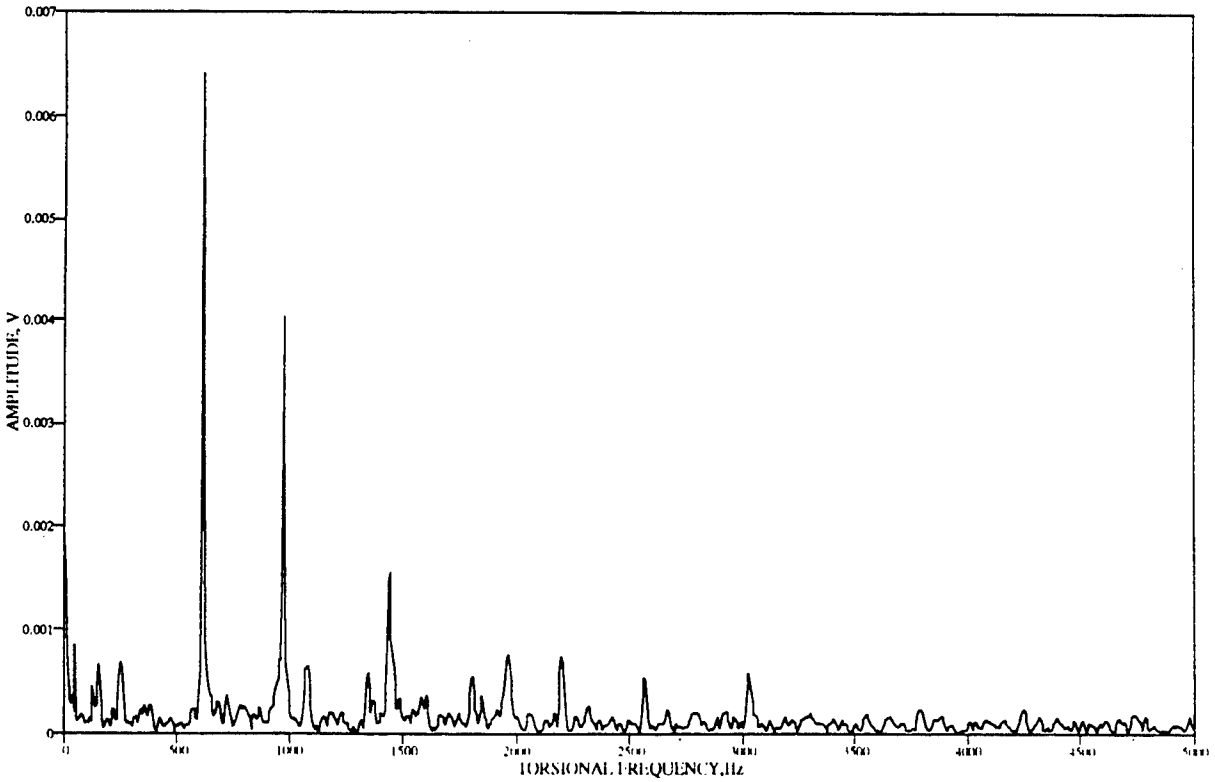

BEAM N3

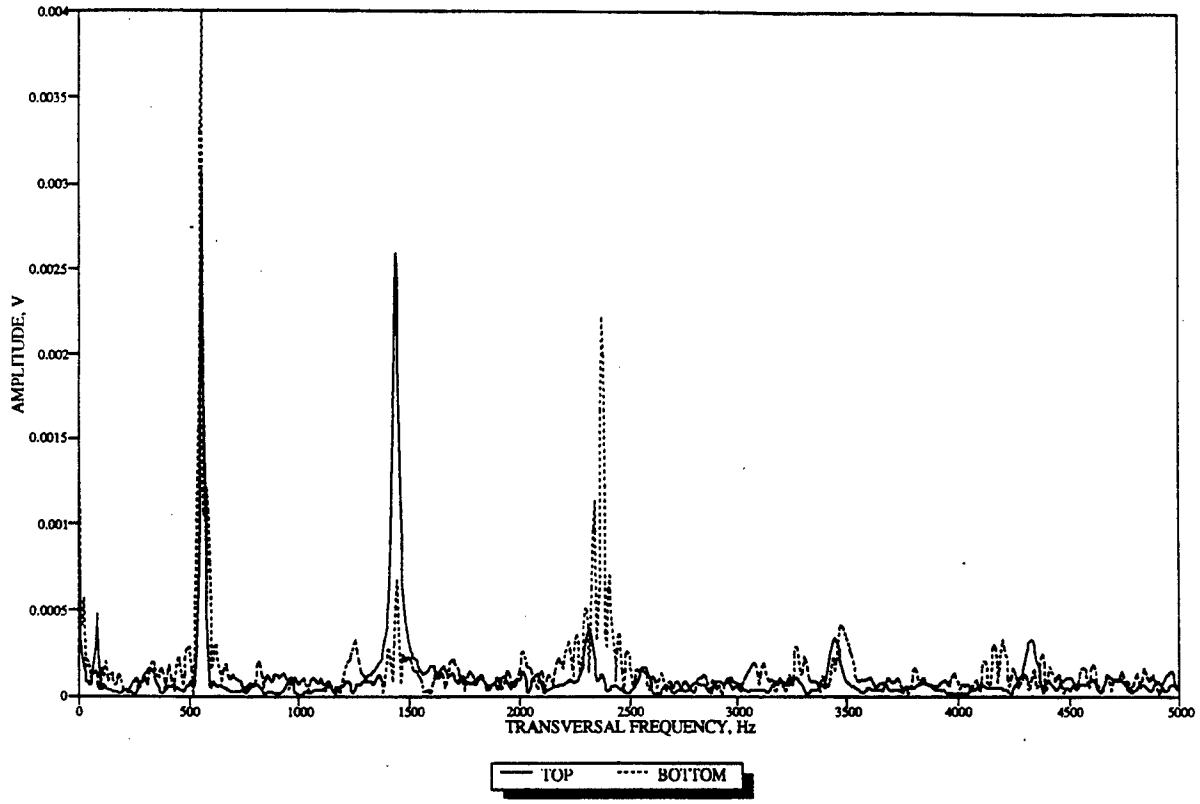


BEAM N3

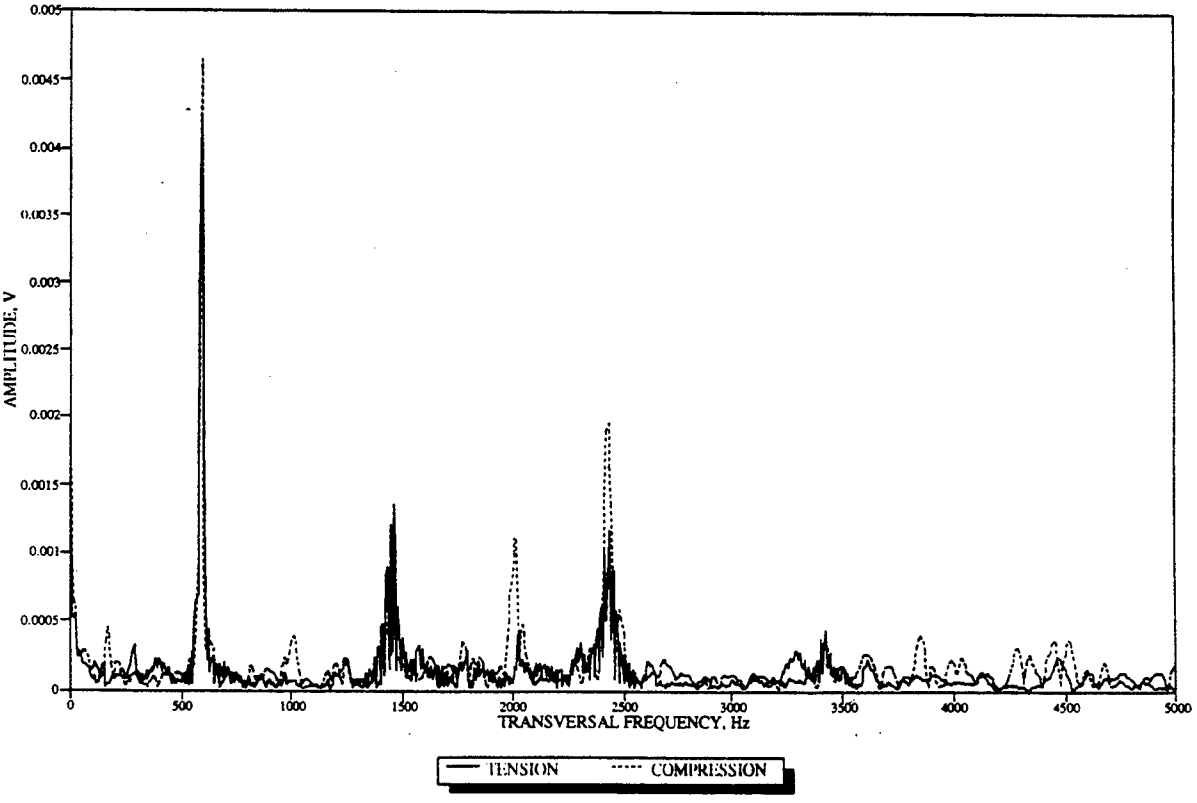

BEAM N3

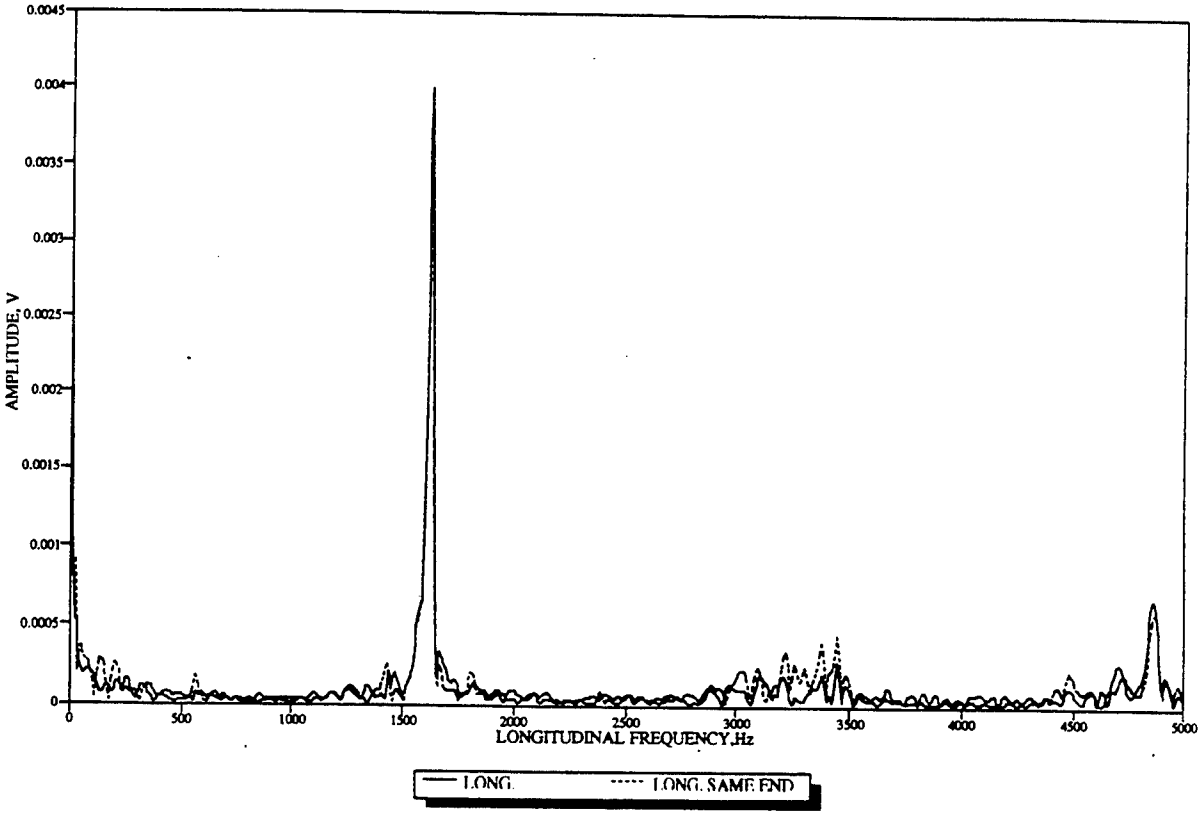


BEAM N3

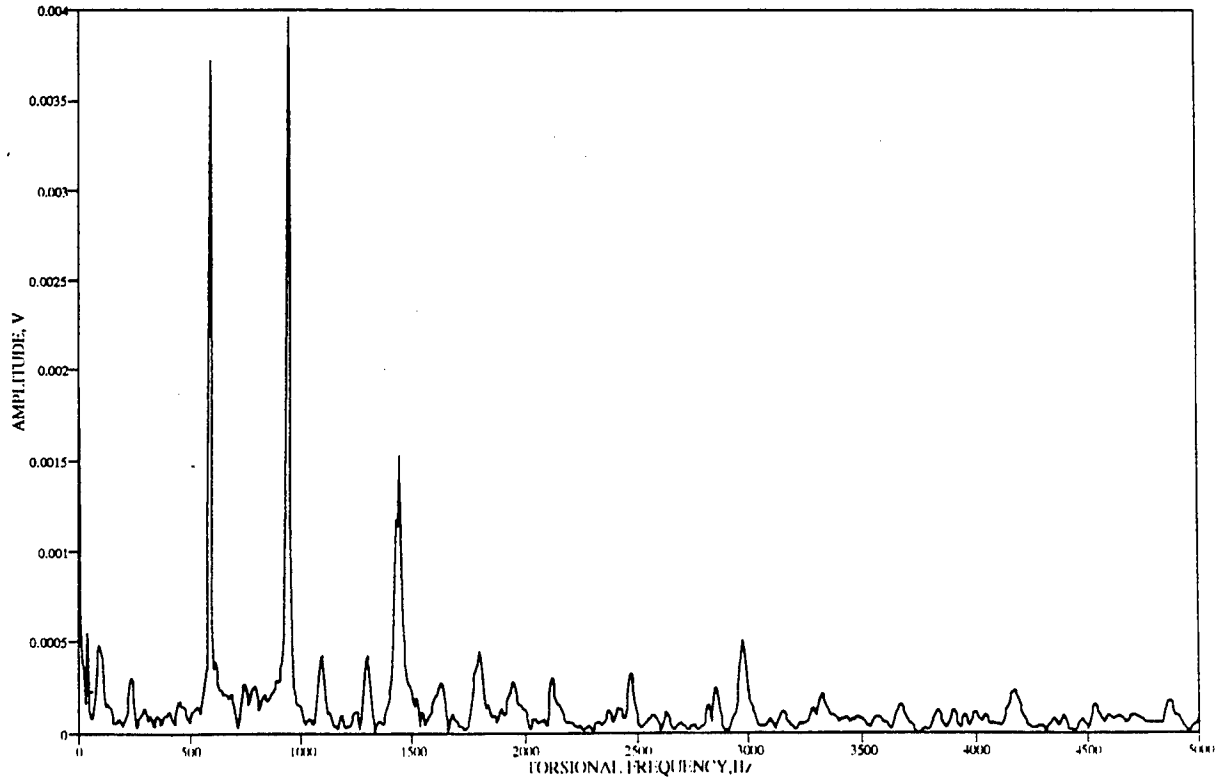

## BEAM O1

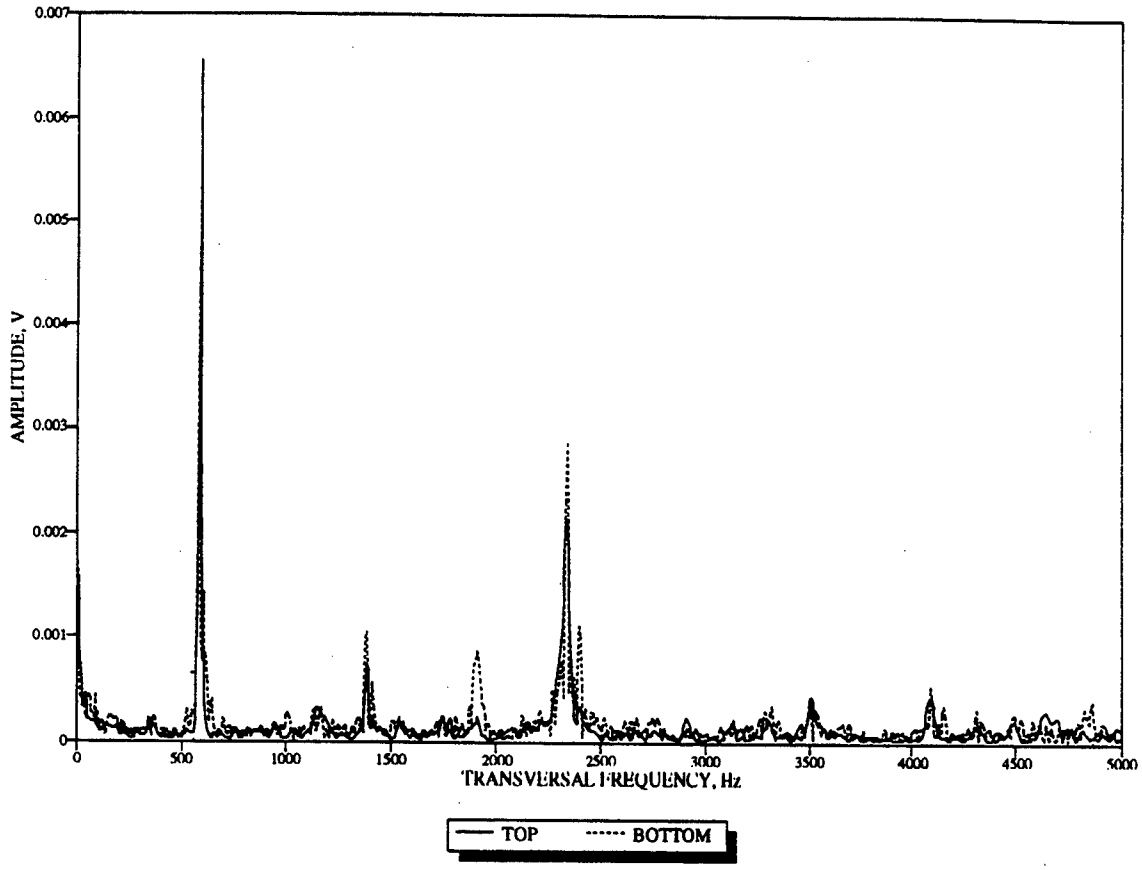


## BEAM O1

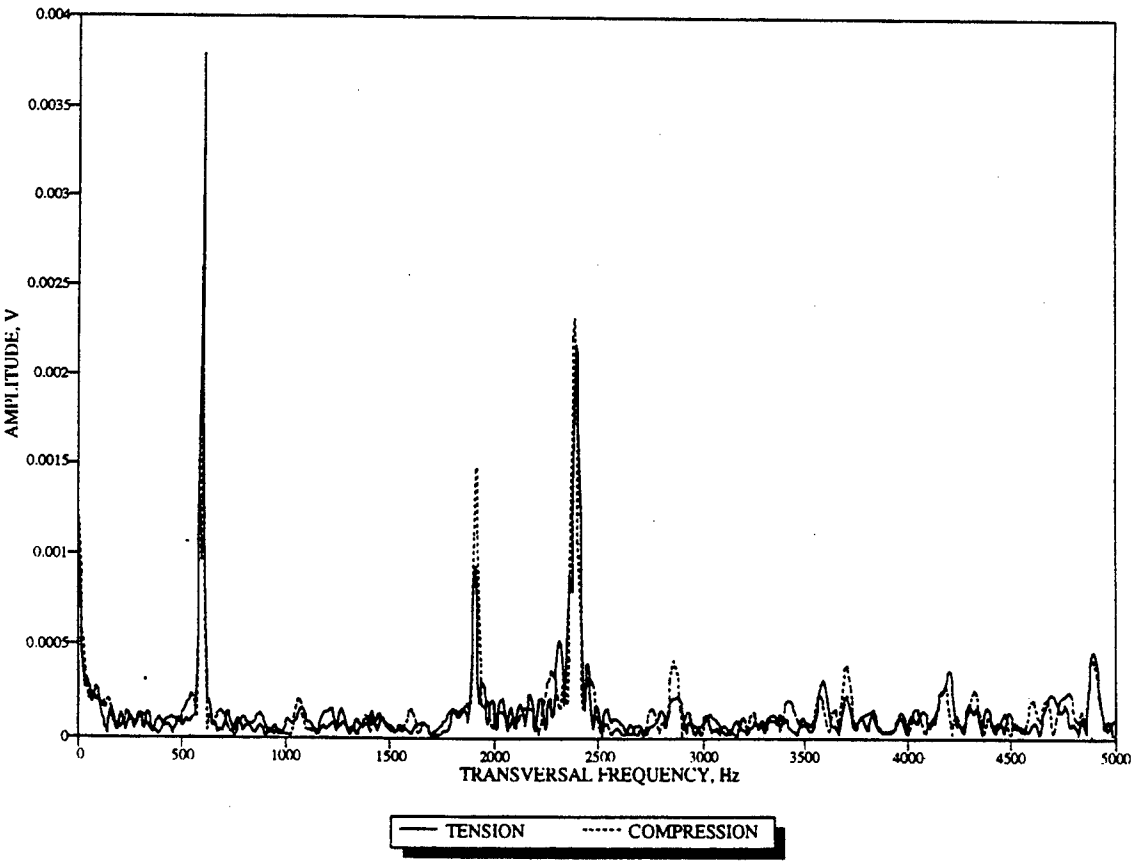

BEAM O1

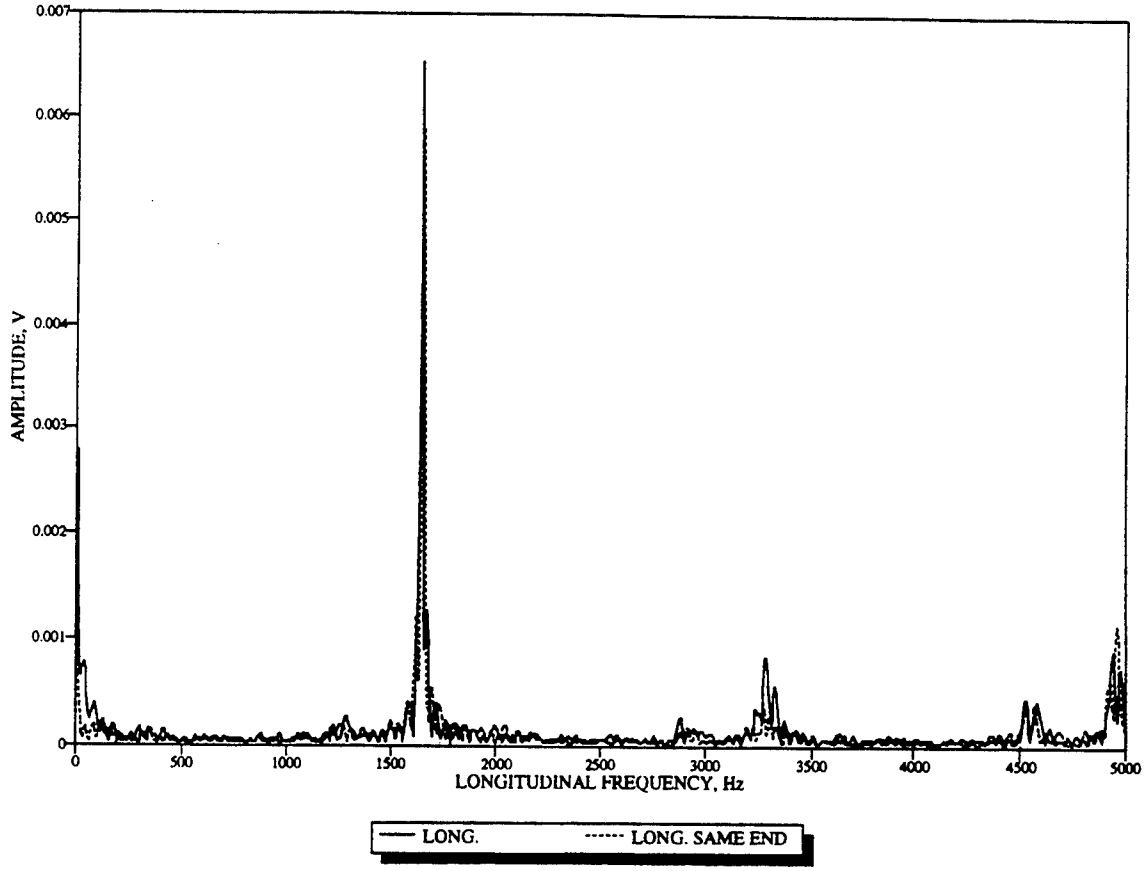


BEAM O1

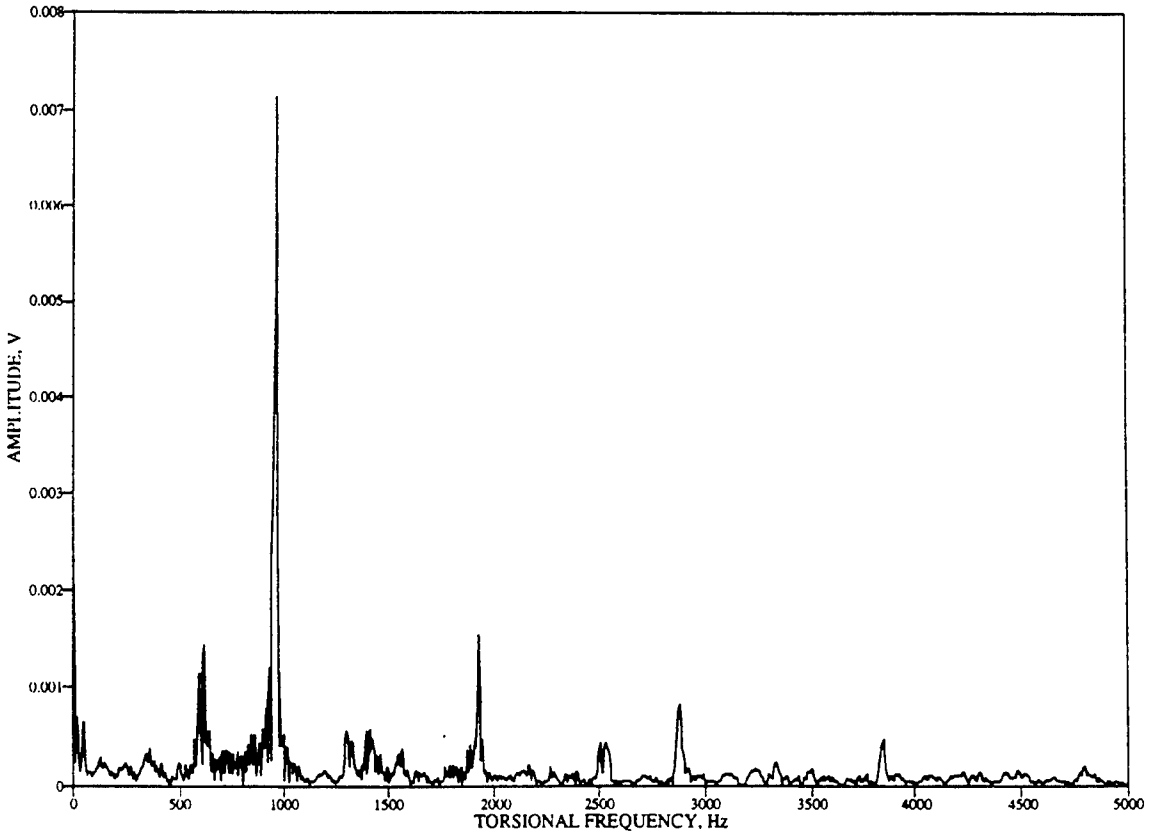

## BEAM O3

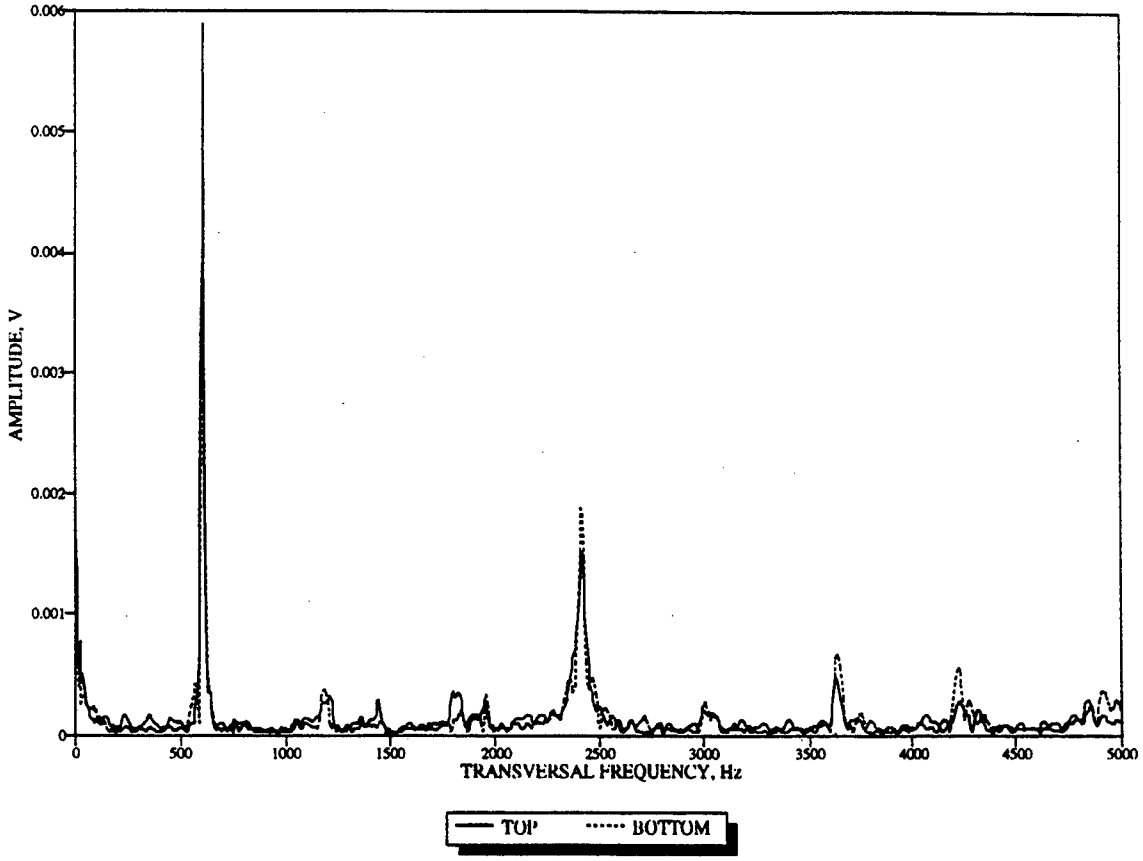


## BEAM O3

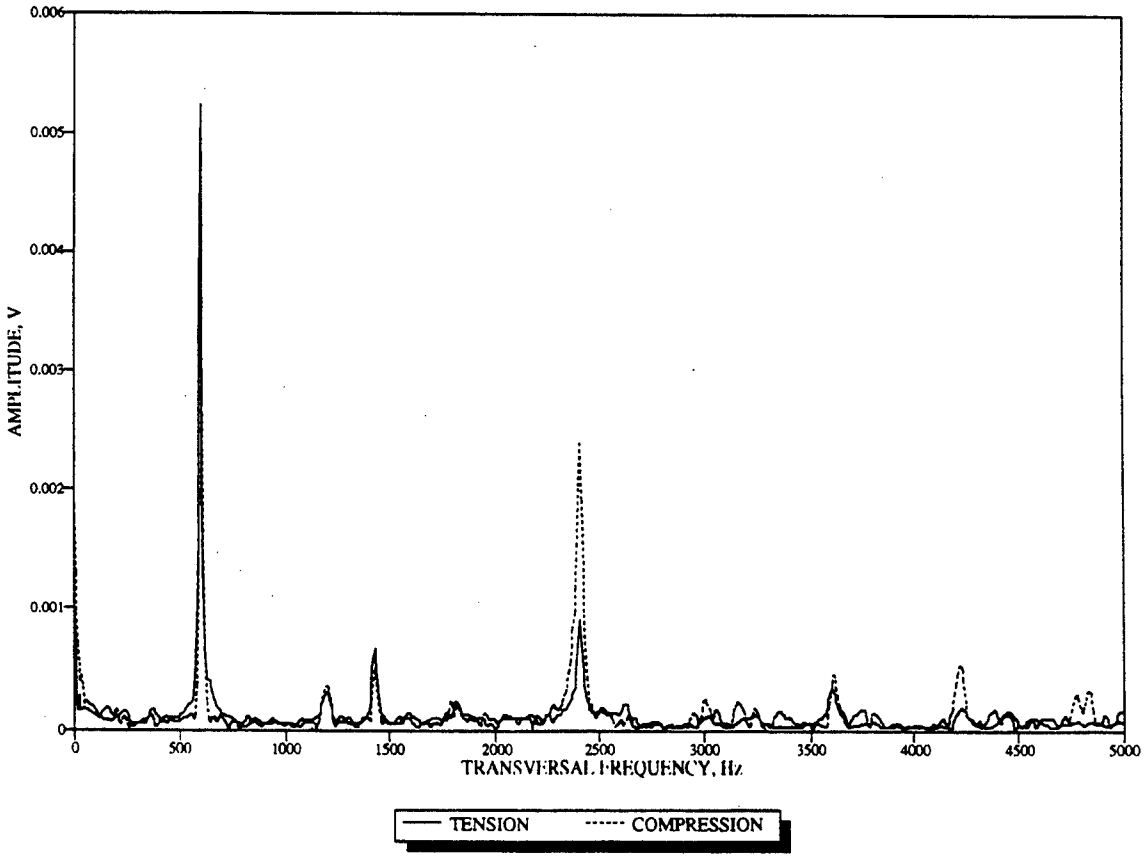

## BEAM O3

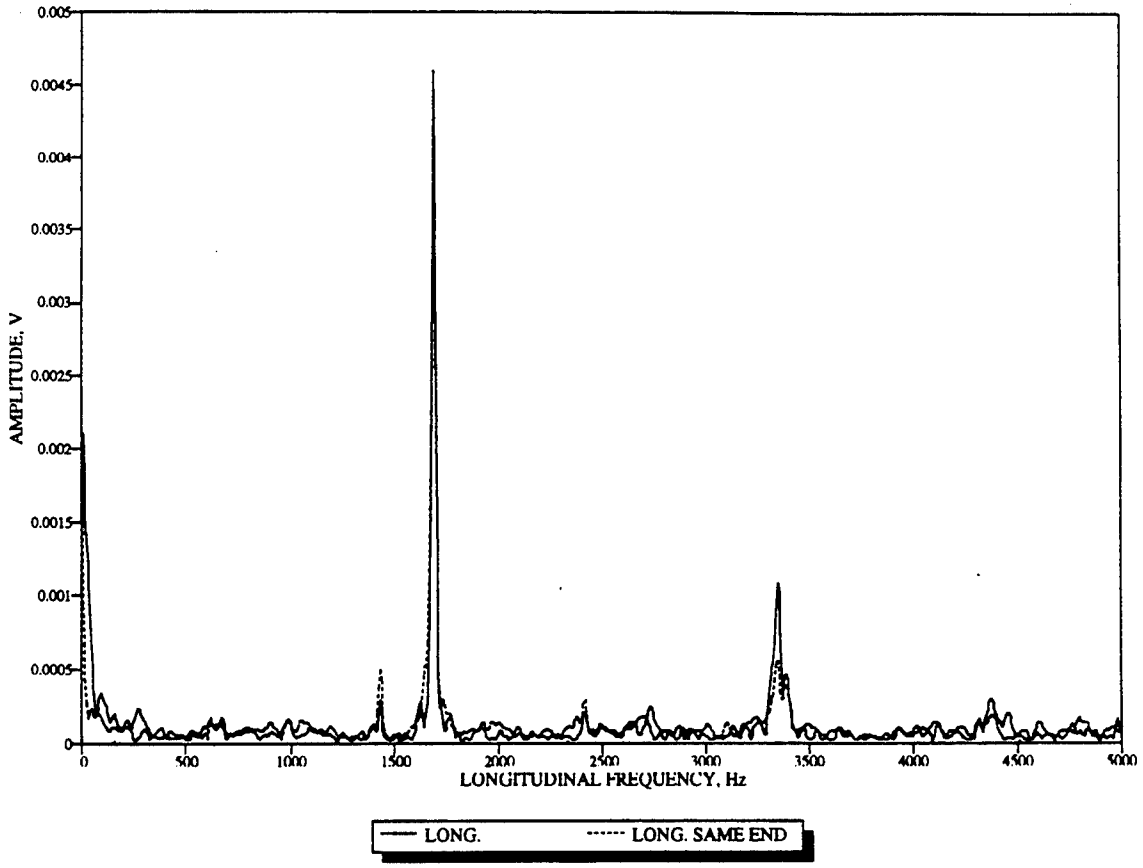


## BEAM O3

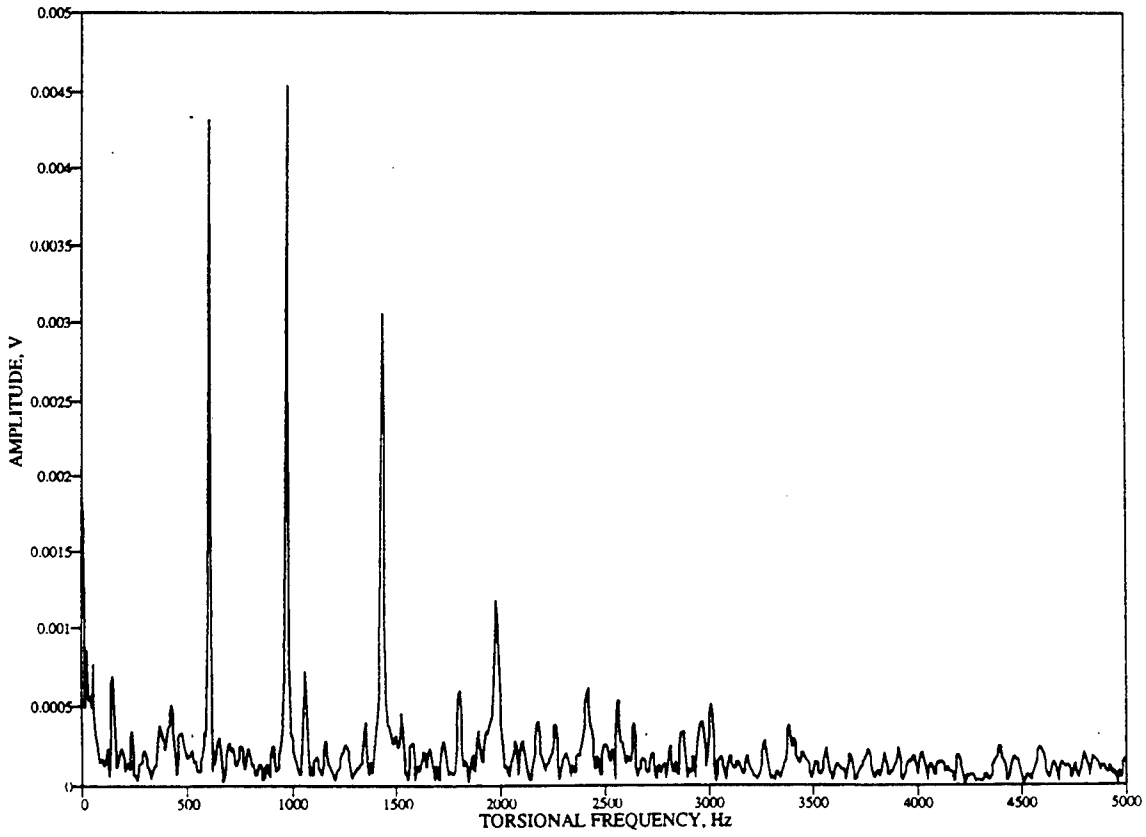

## BEAM P1

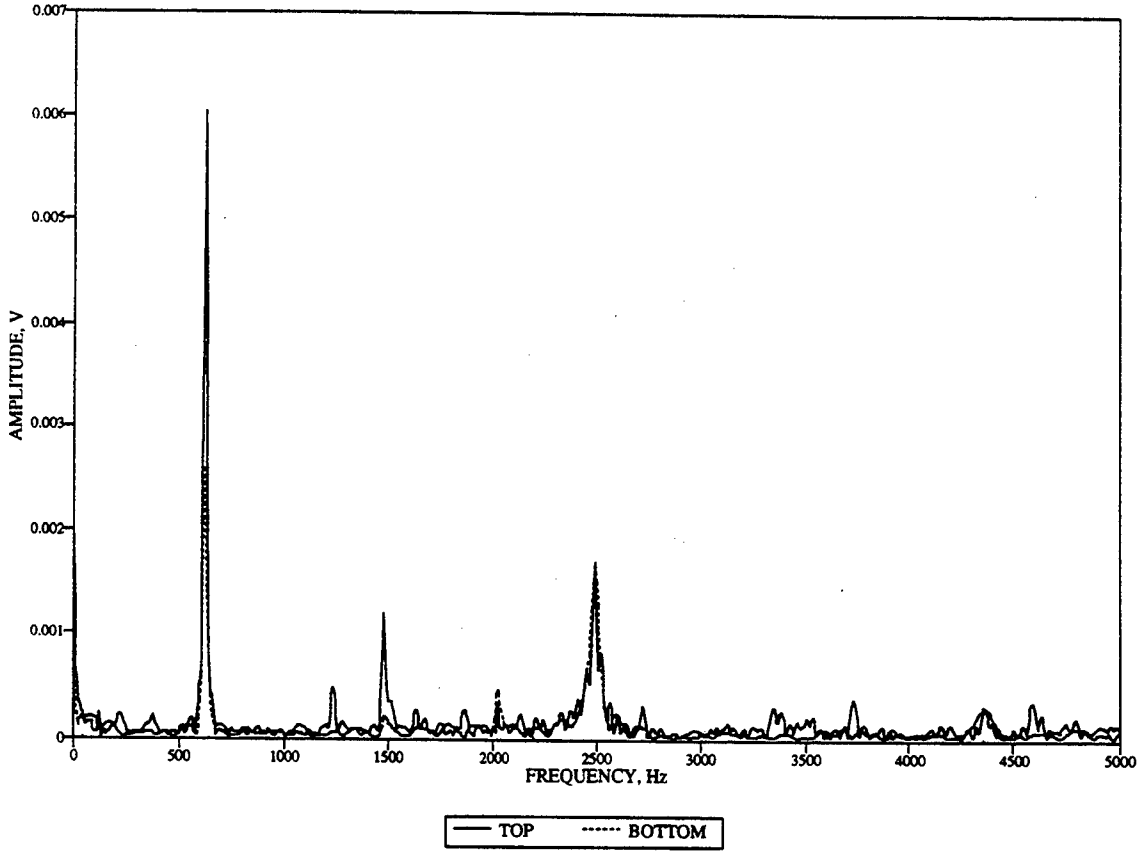


---

## BEAM P1

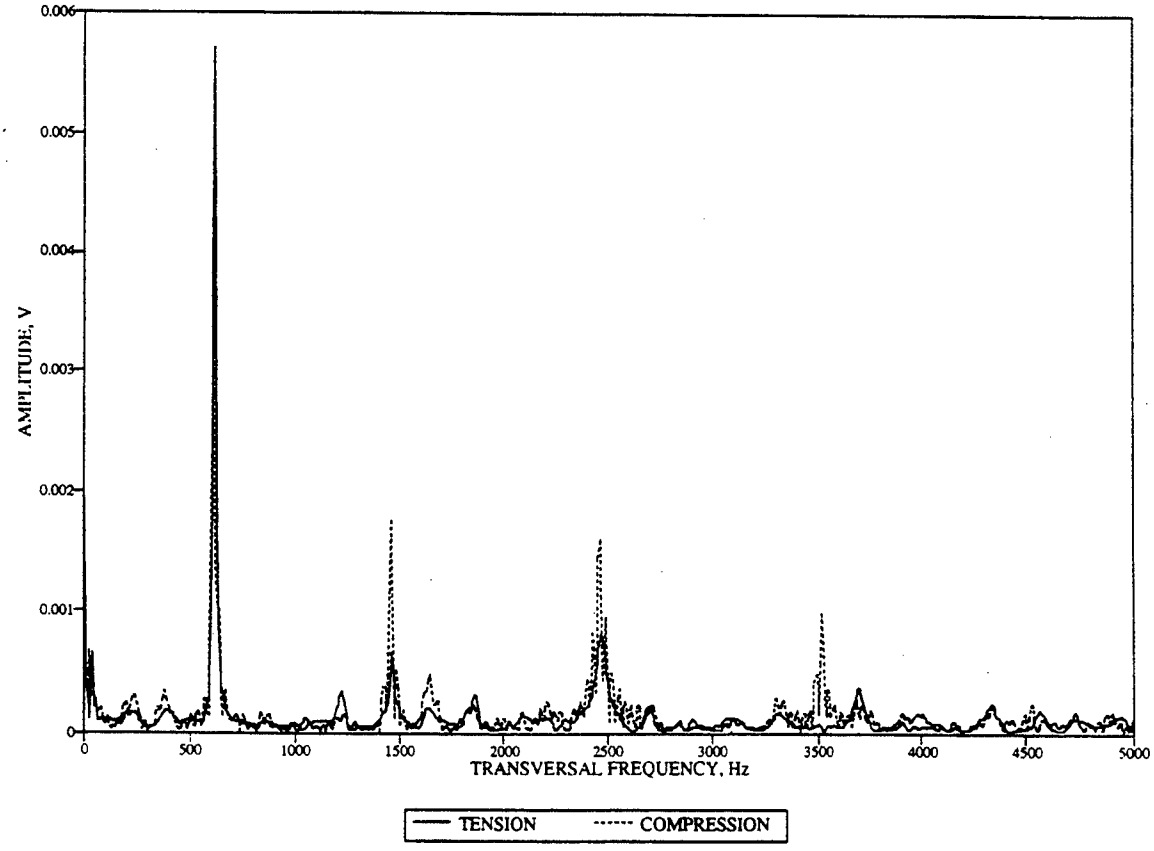

BEAM P1

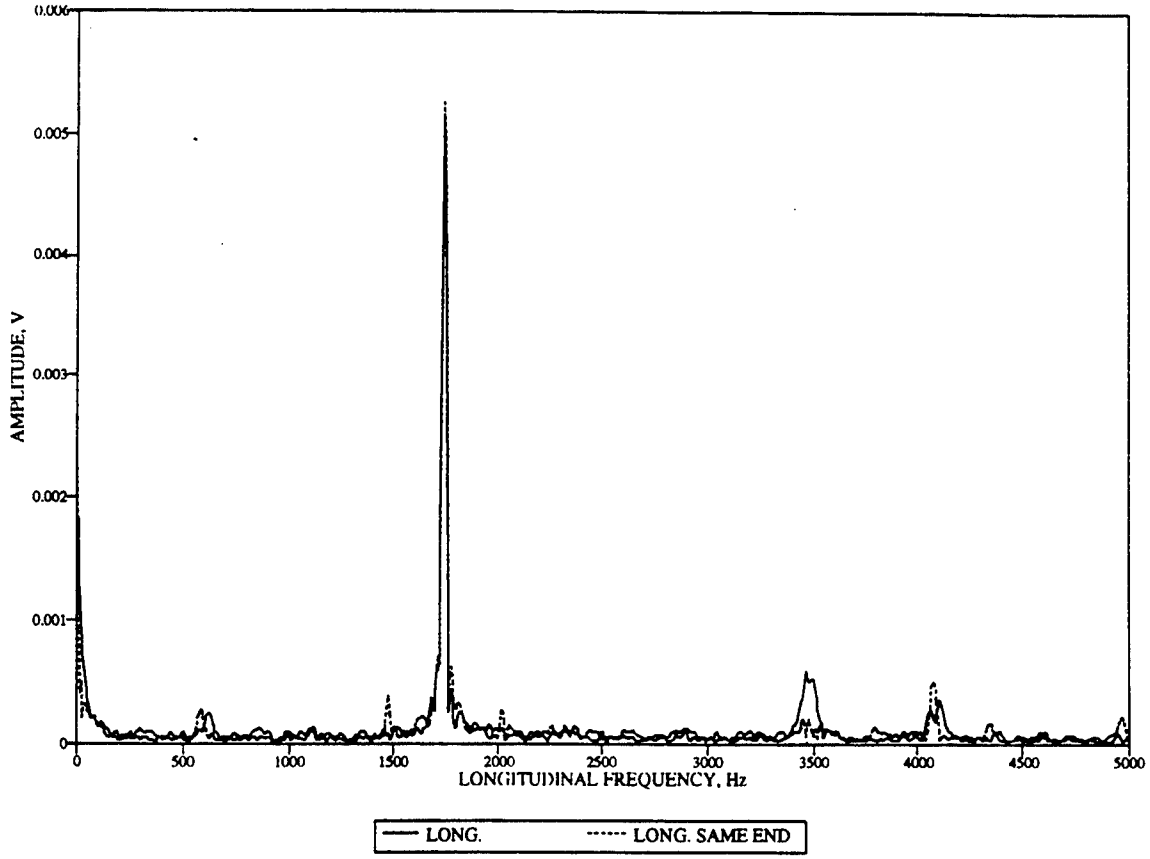


BEAM P1

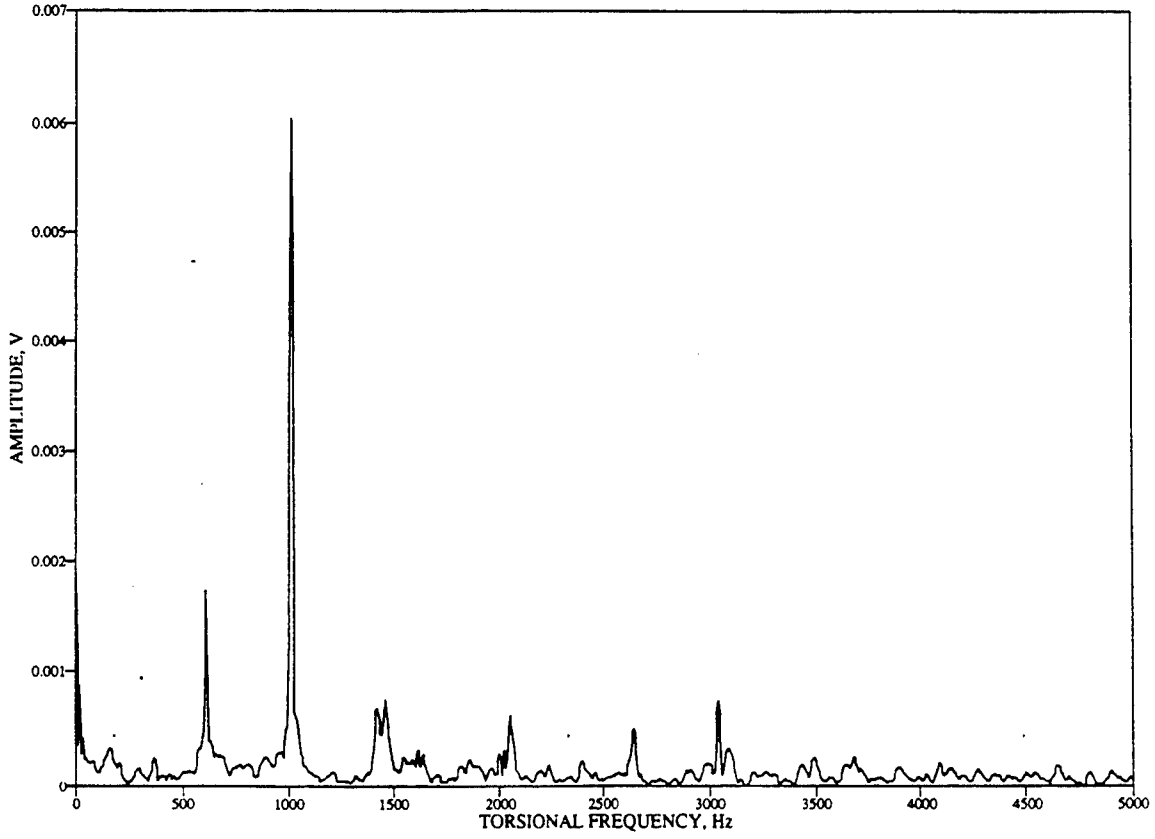

## BEAM P2

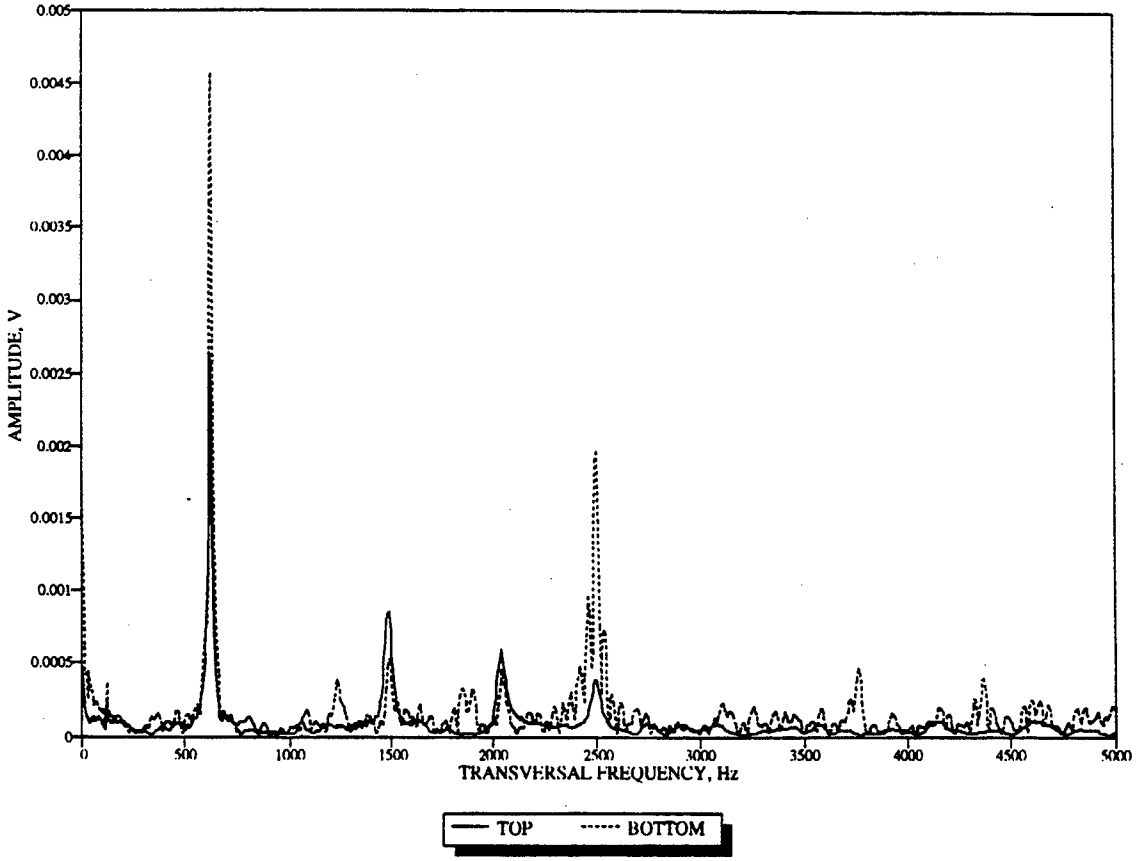


## BEAM P2

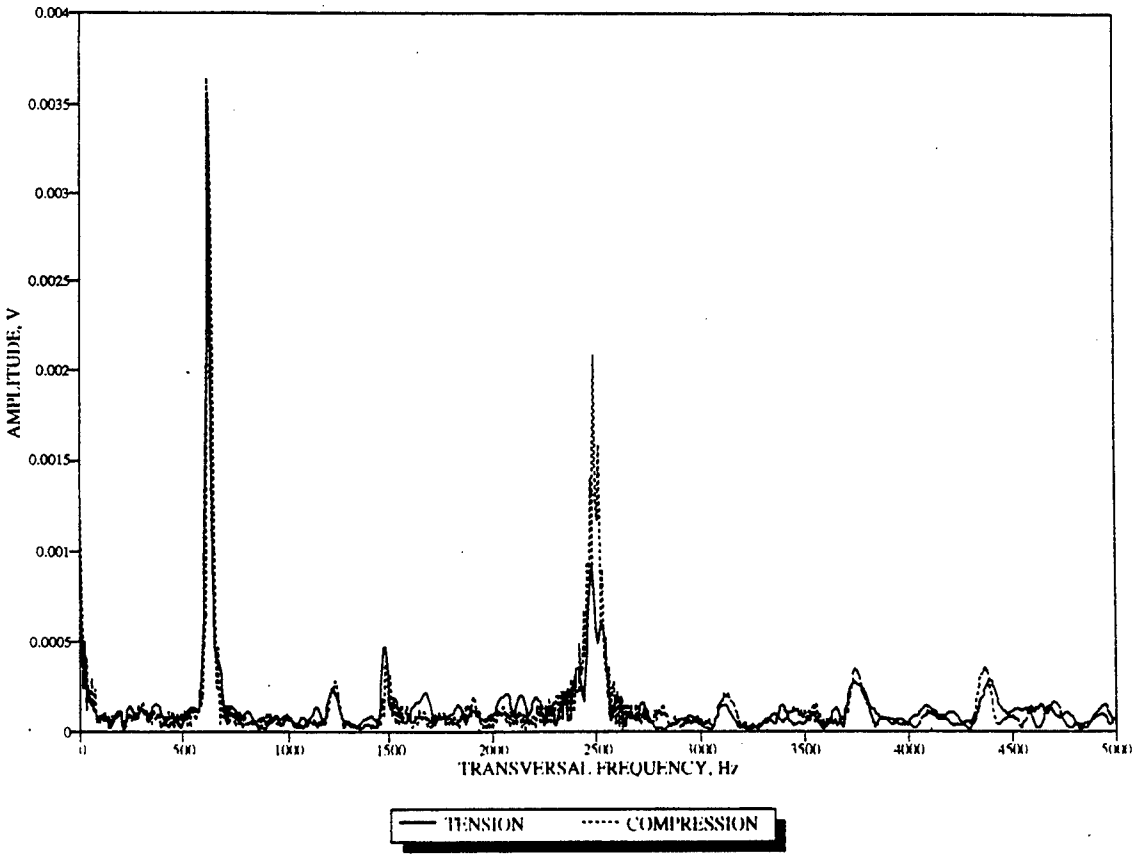

## BEAM P2

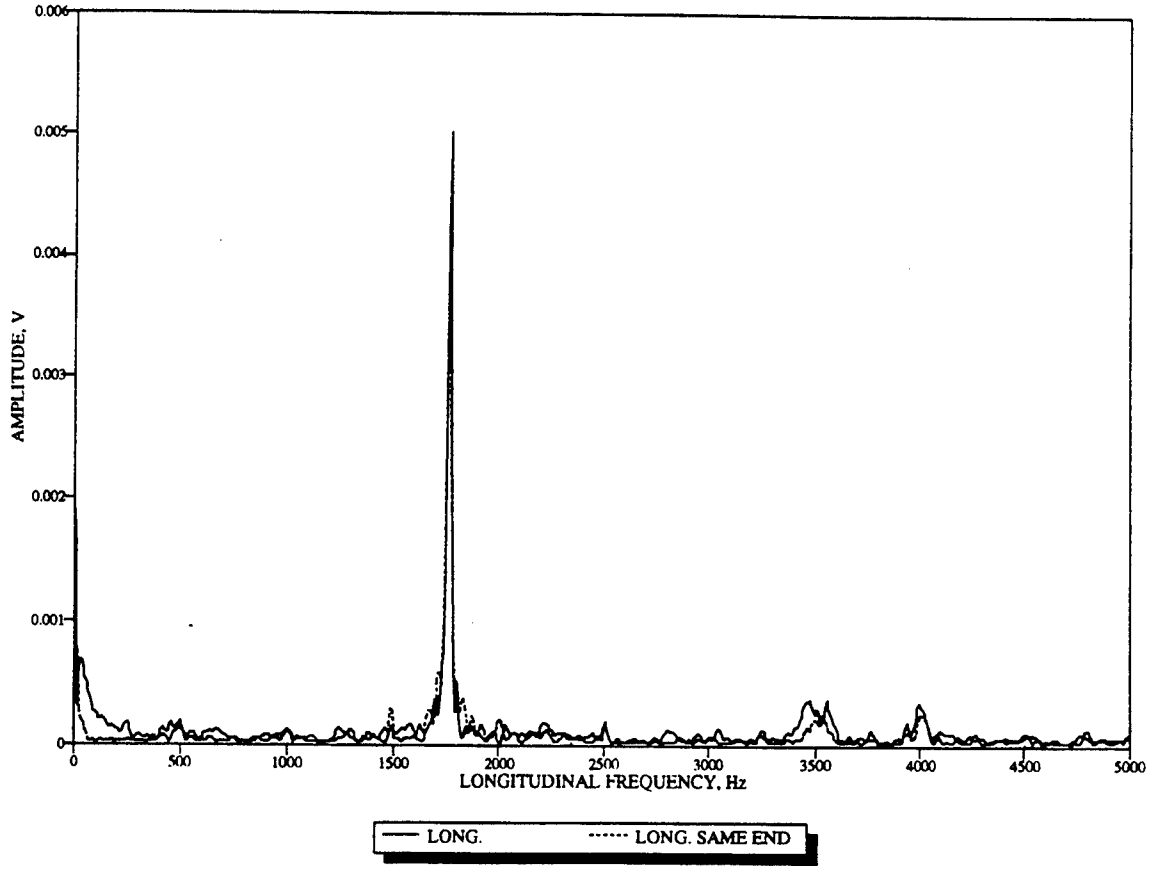


## BEAM P2

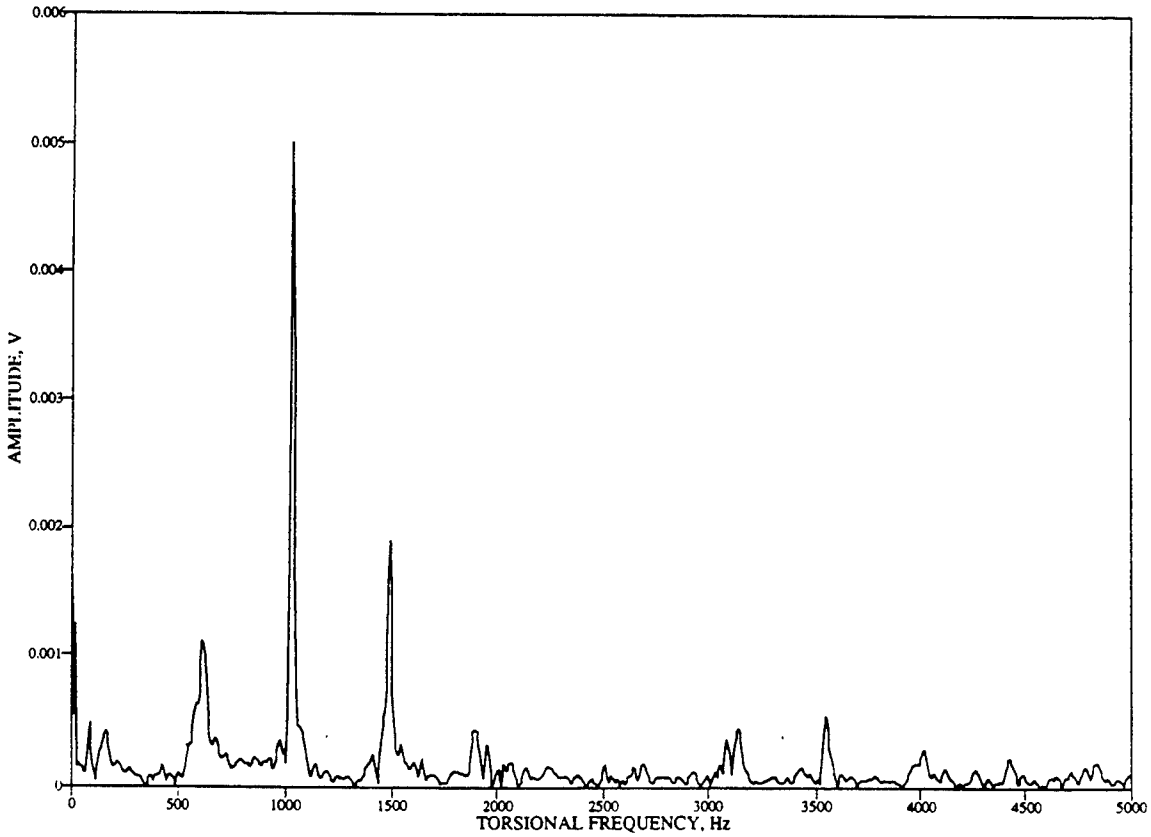

# Appendix I
# Resonant Frequency - Sawed-Beam Series

## BEAM J1H (COMPRESSION)

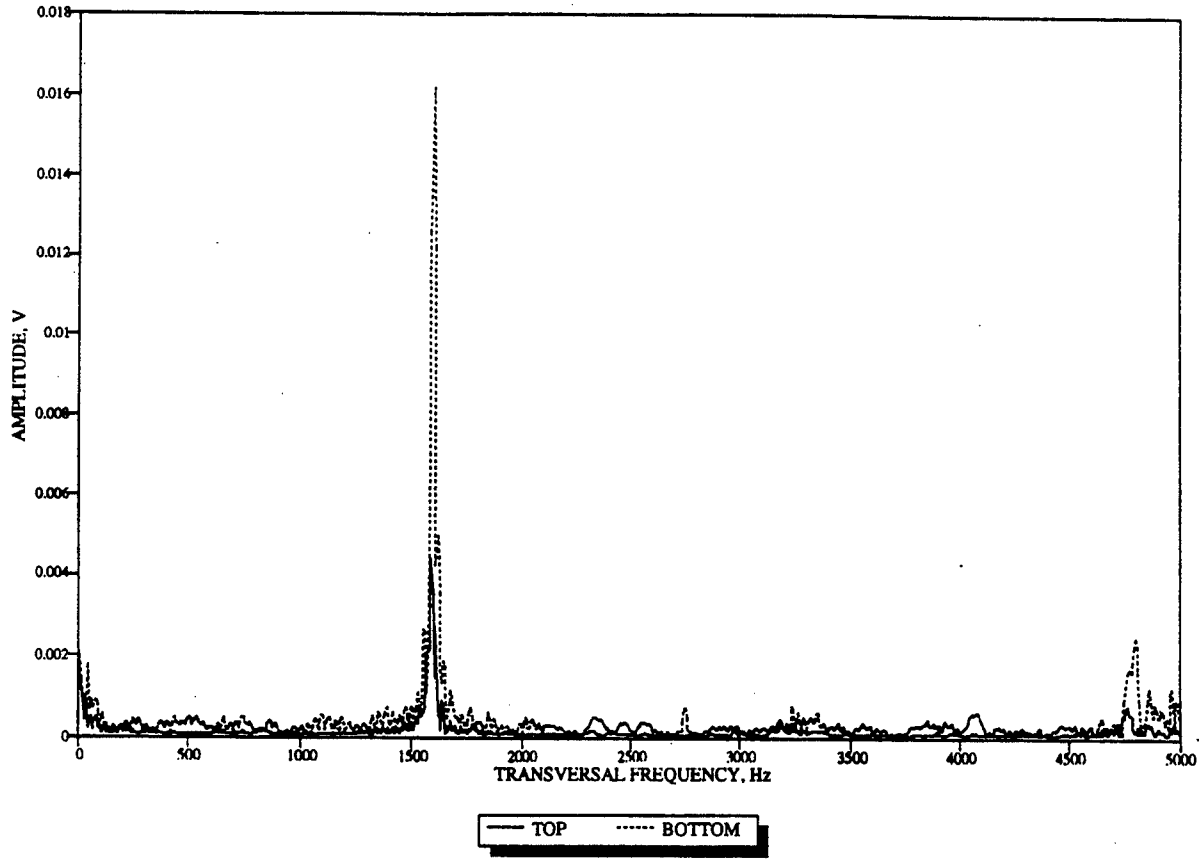


## BEAM J1H (COMPRESSION)

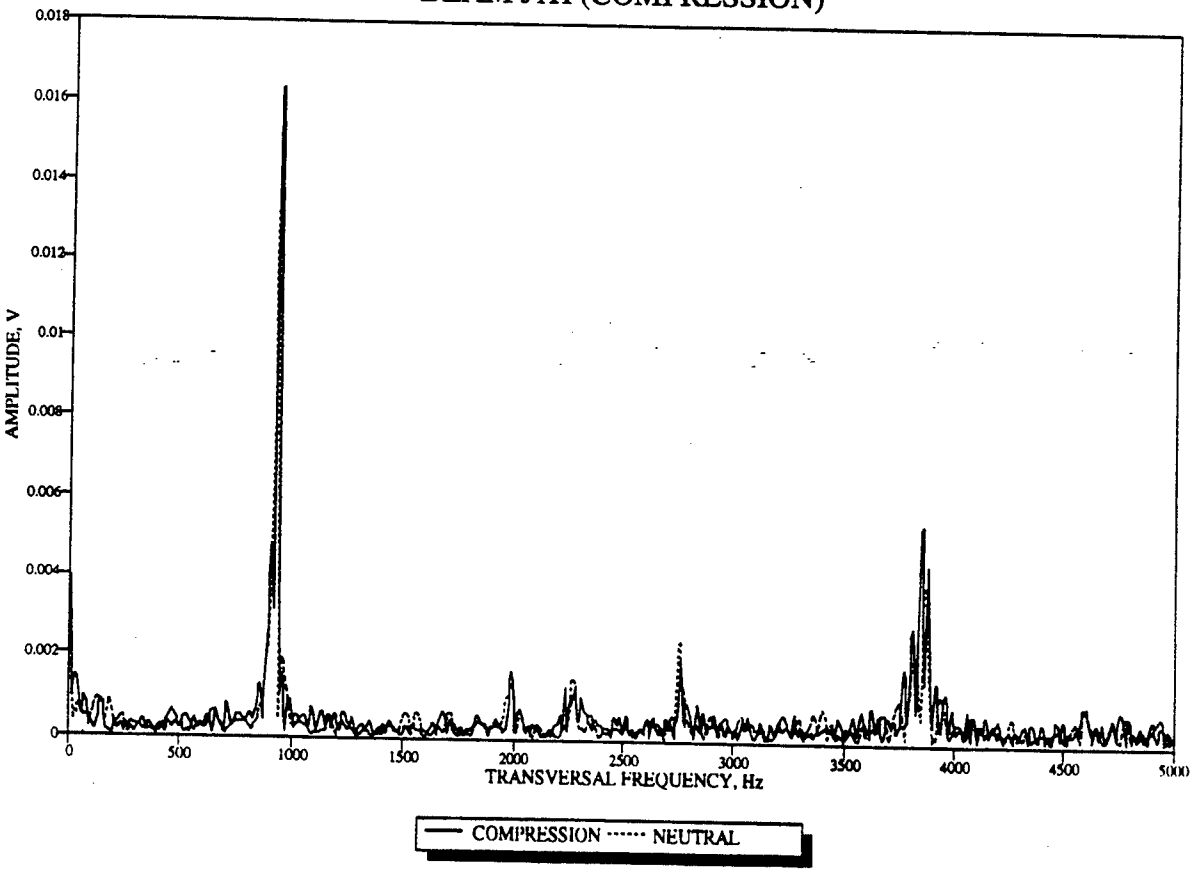

## BEAM J1H (COMPRESSION)

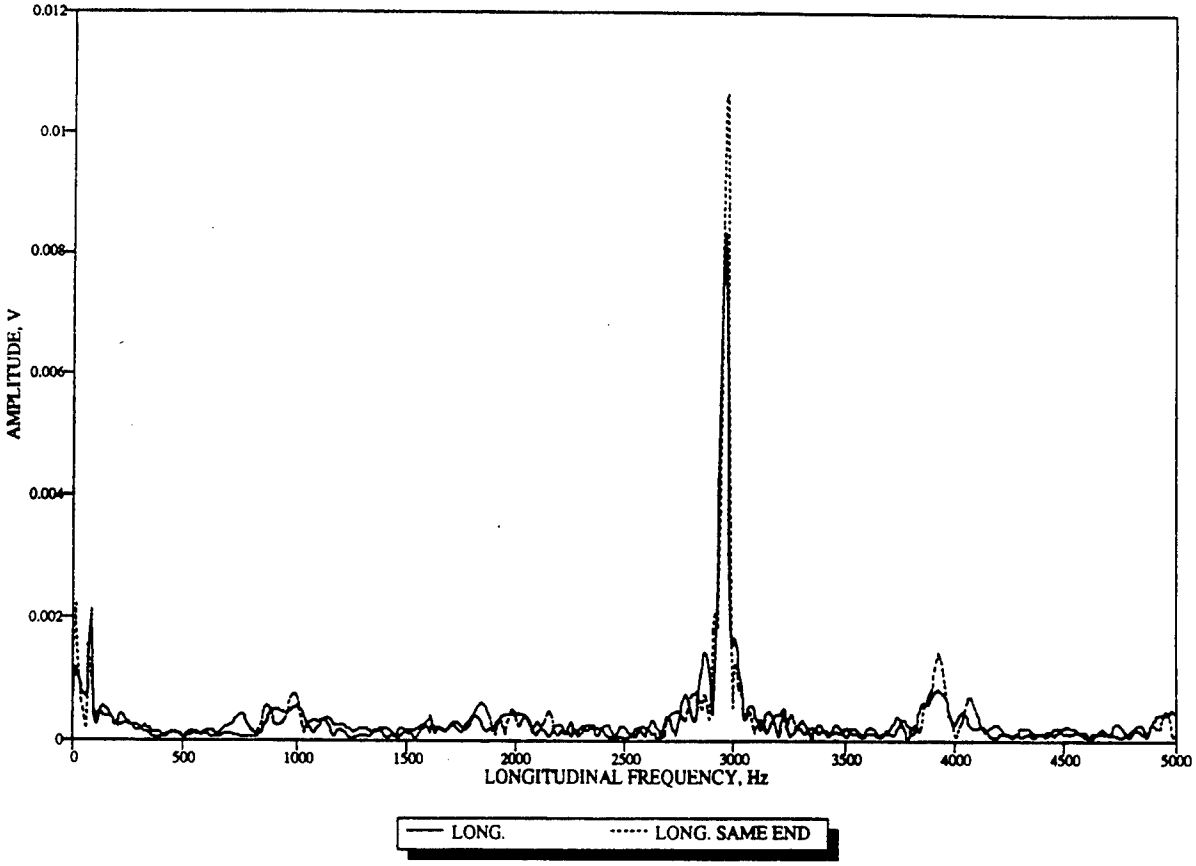


## BEAM J1H (COMPRESSION)

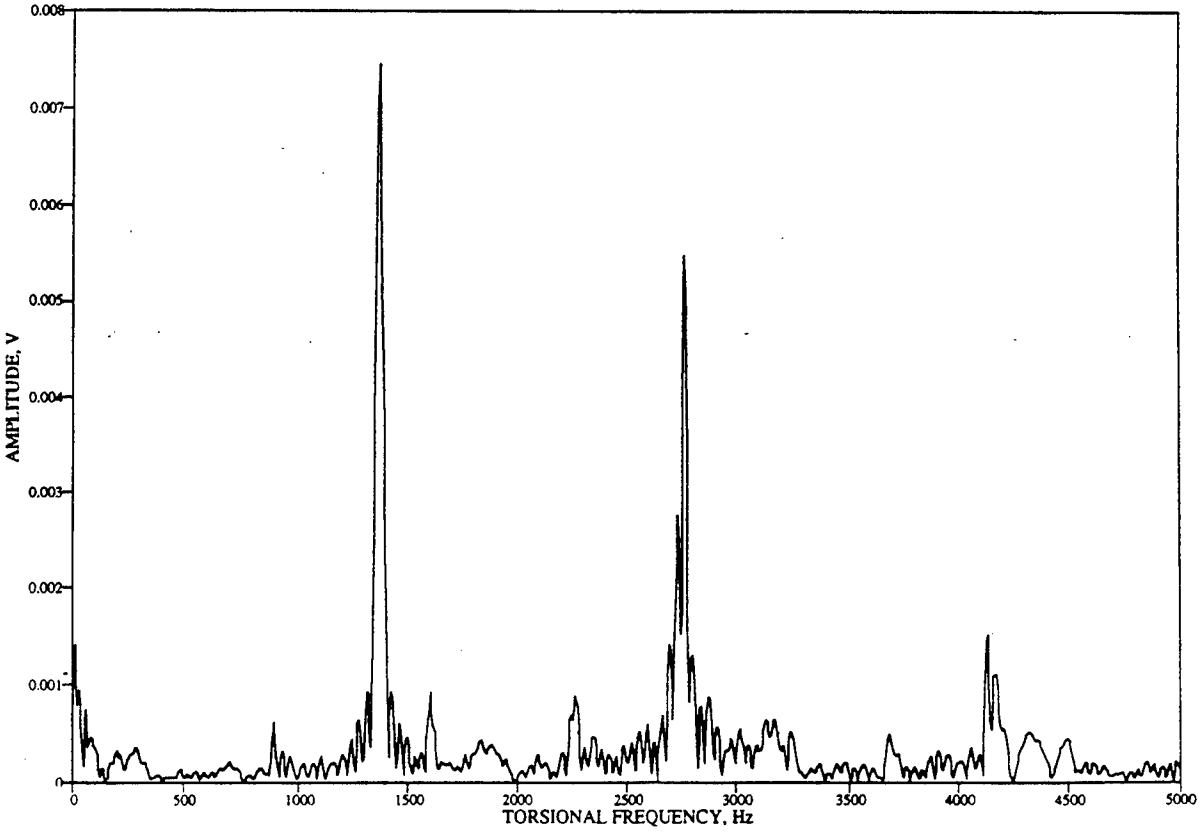

## BEAM J1H (TENSION)

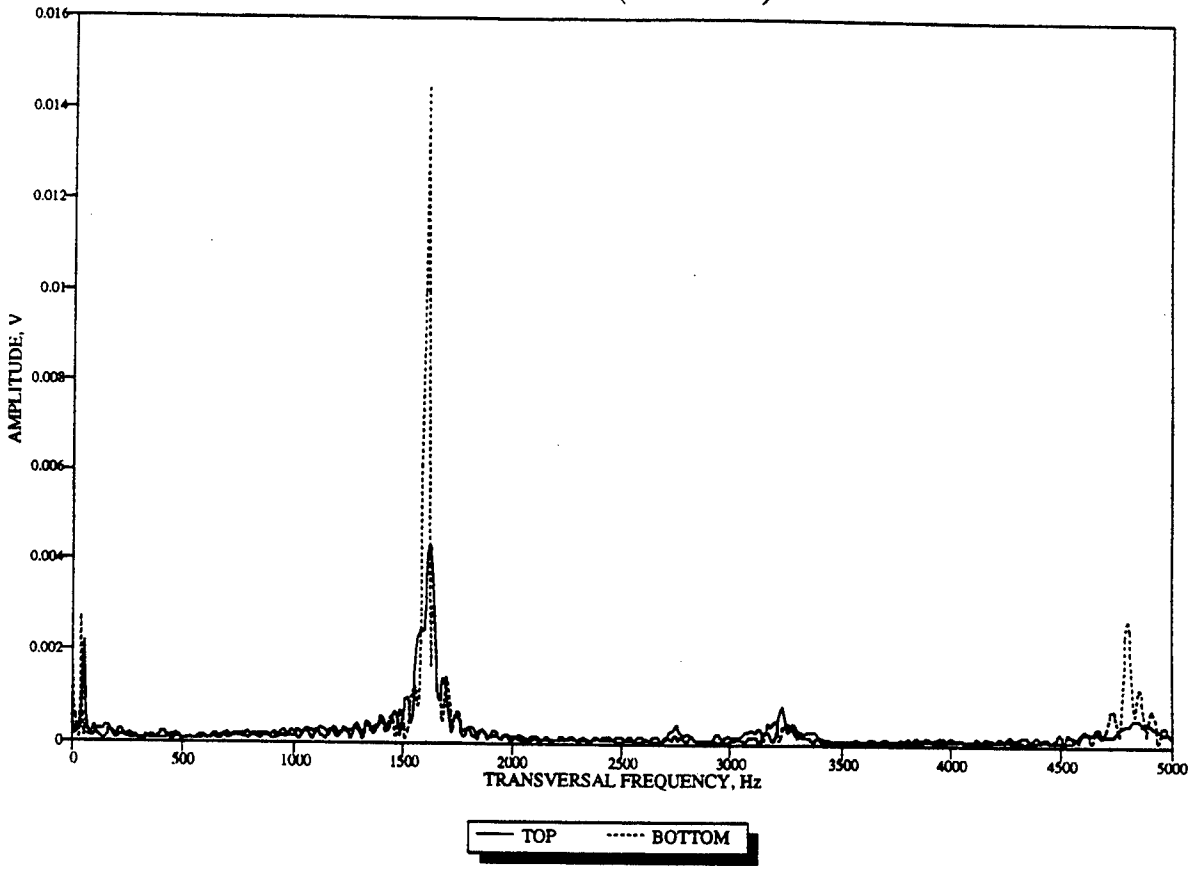


## BEAM J1H (TENSION)

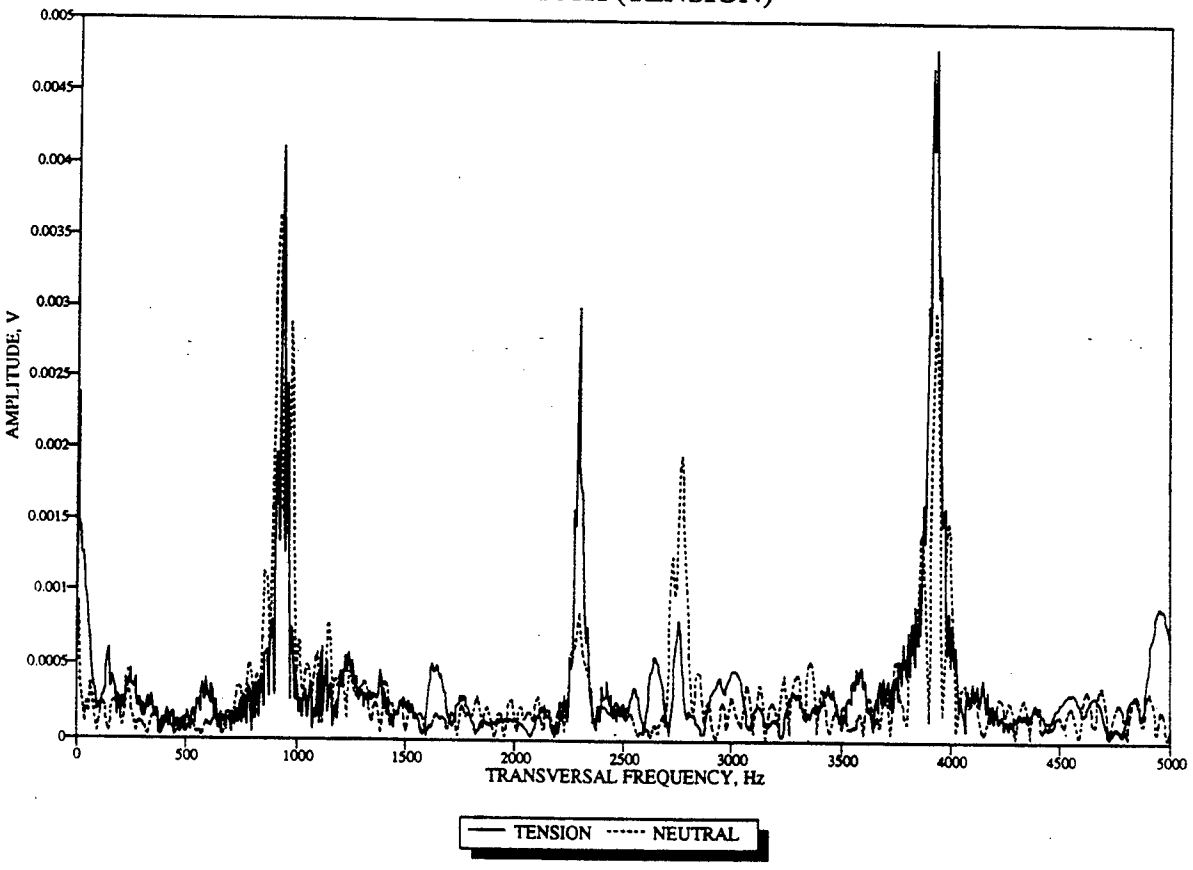

## BEAM J1H (TENSION)

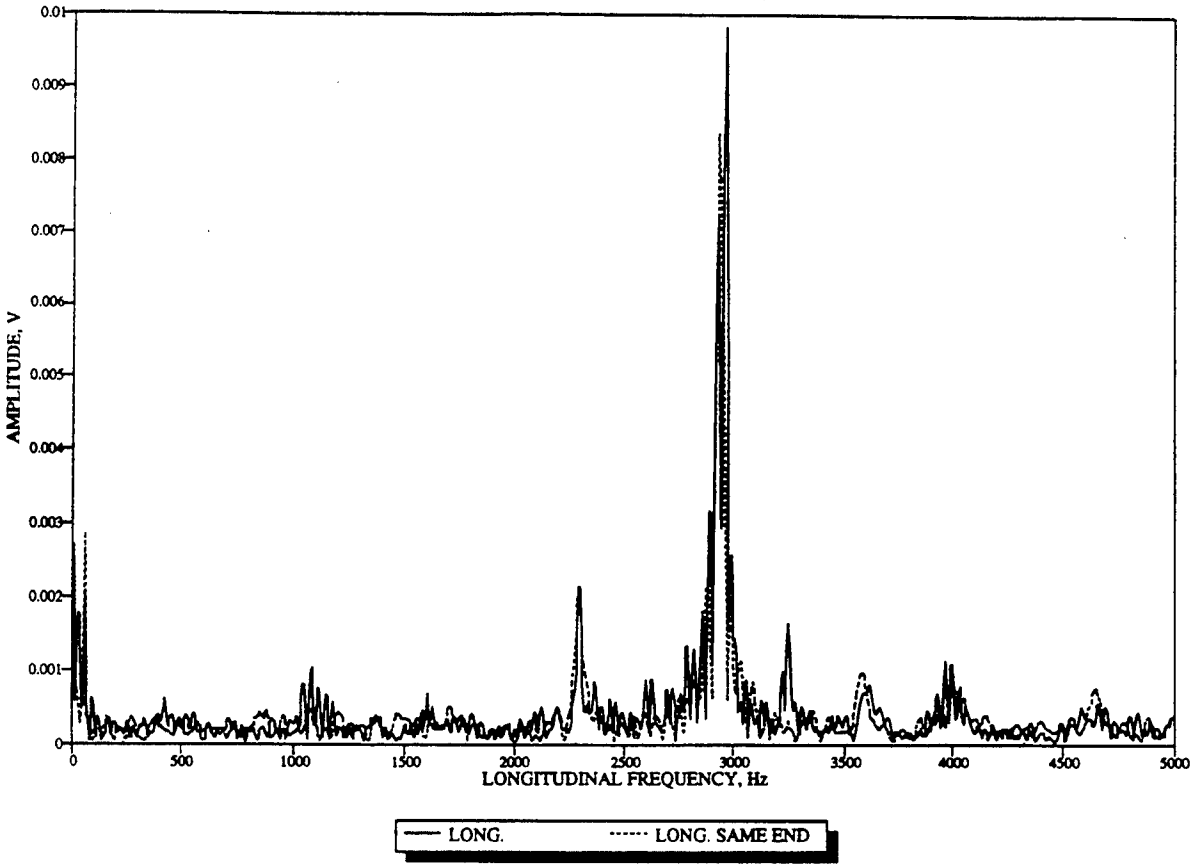


## BEAM J1H (TENSION)

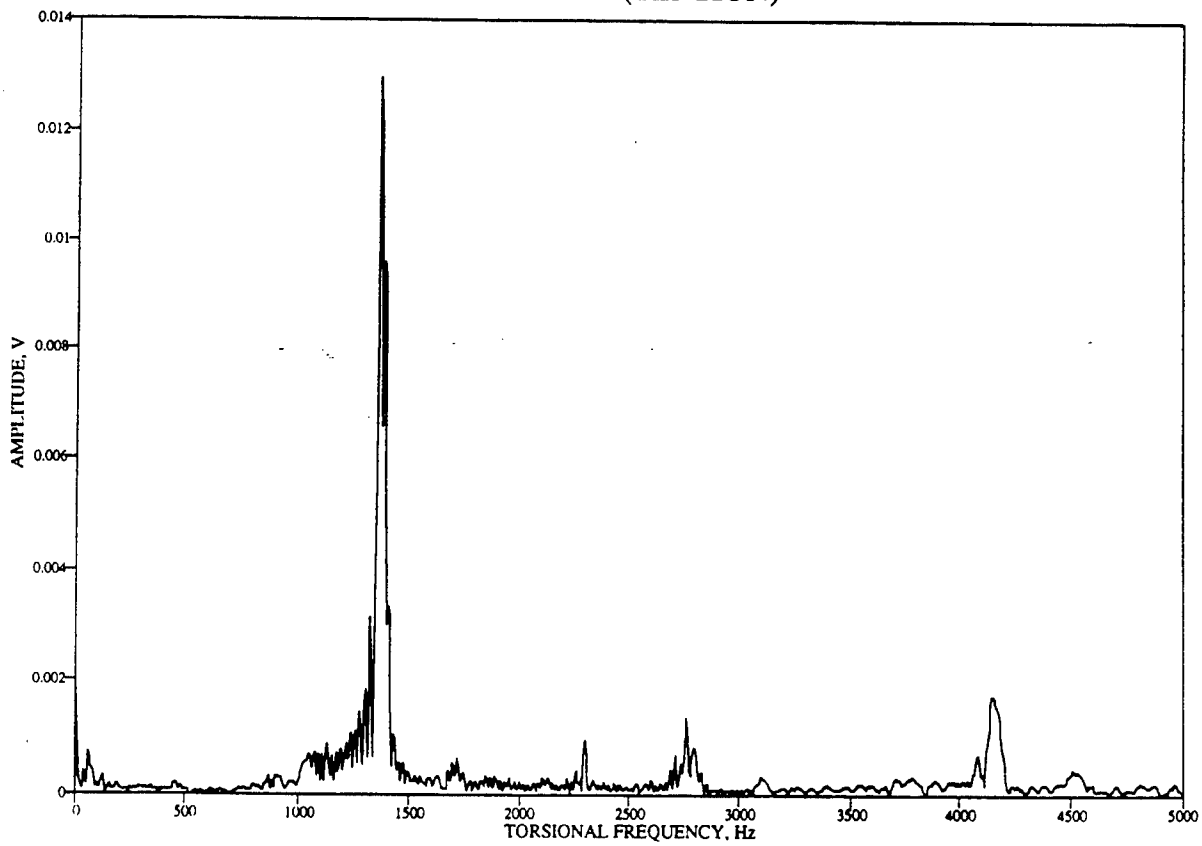

## BEAM J3H (COMPRESSION)

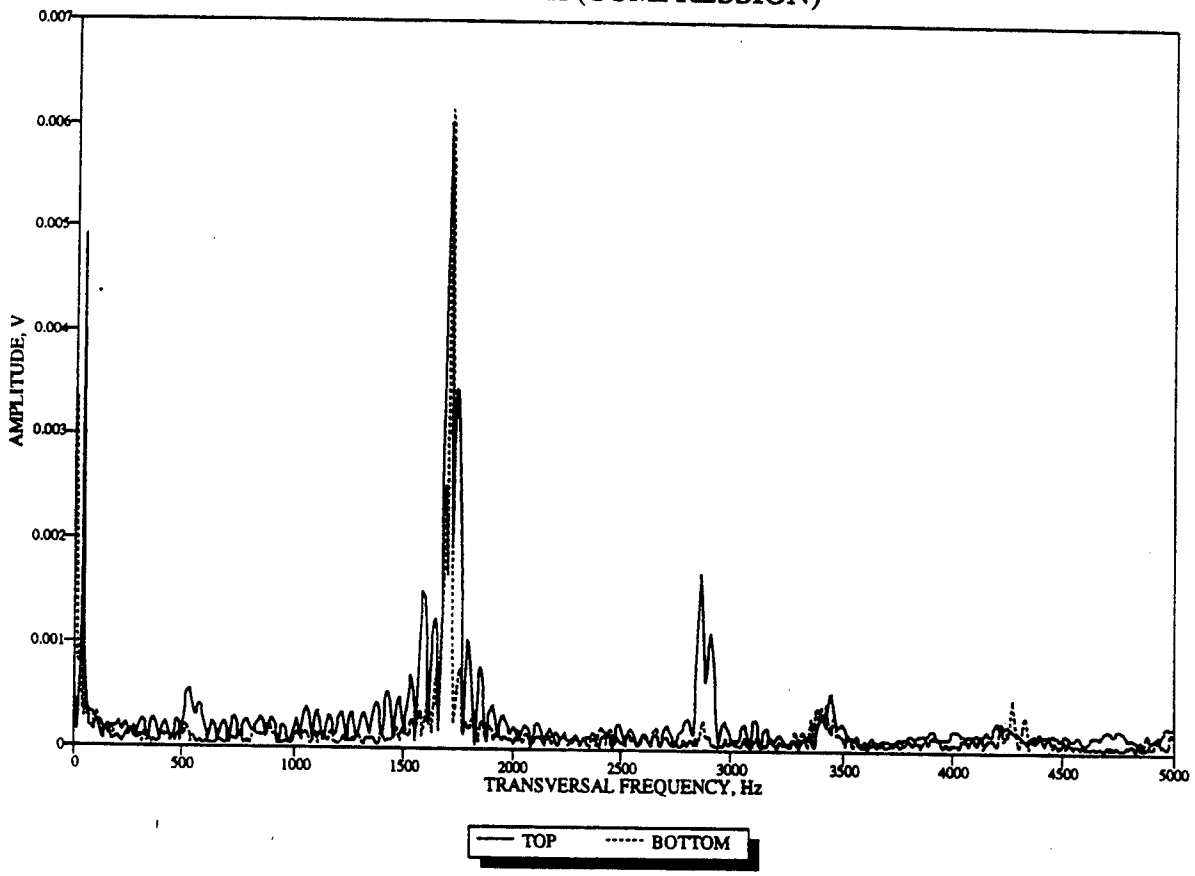


## BEAMJ3H (COMPRESSION)

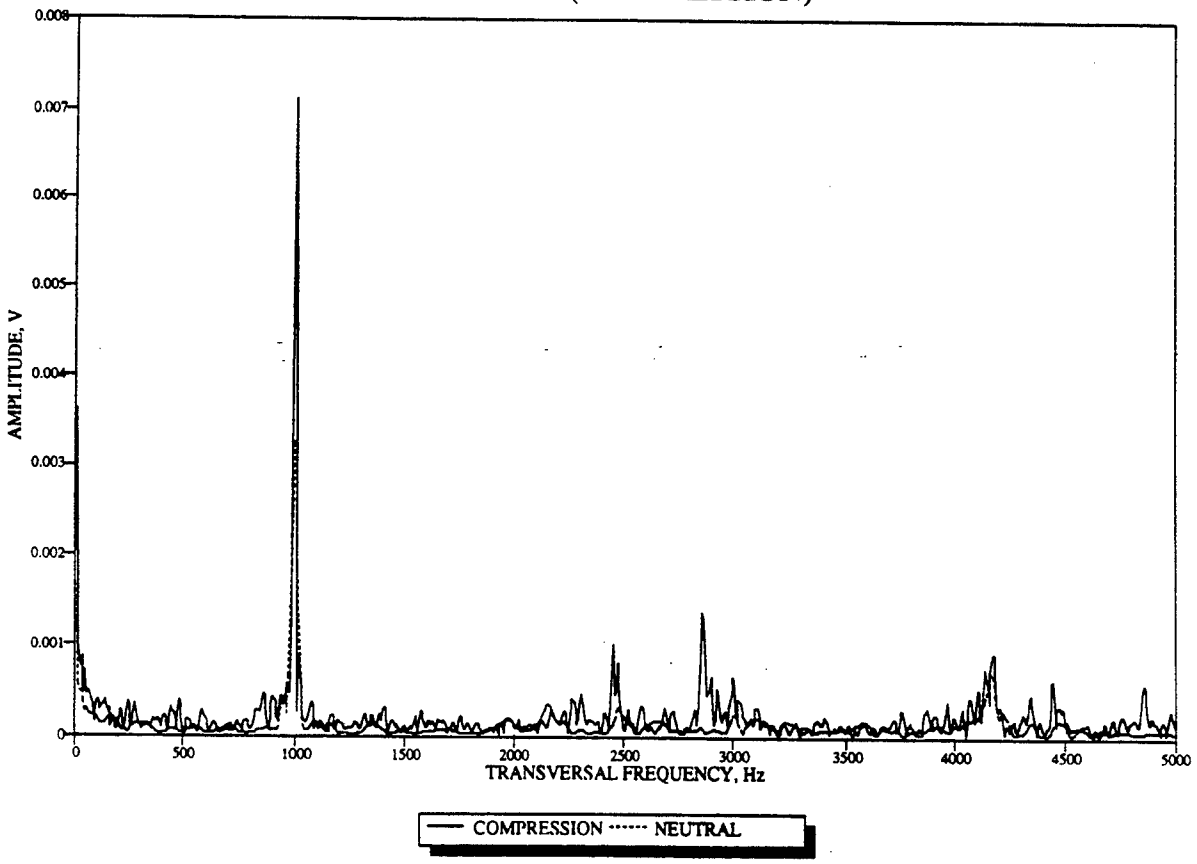

## BEAMJ3H (COMPRESSION)

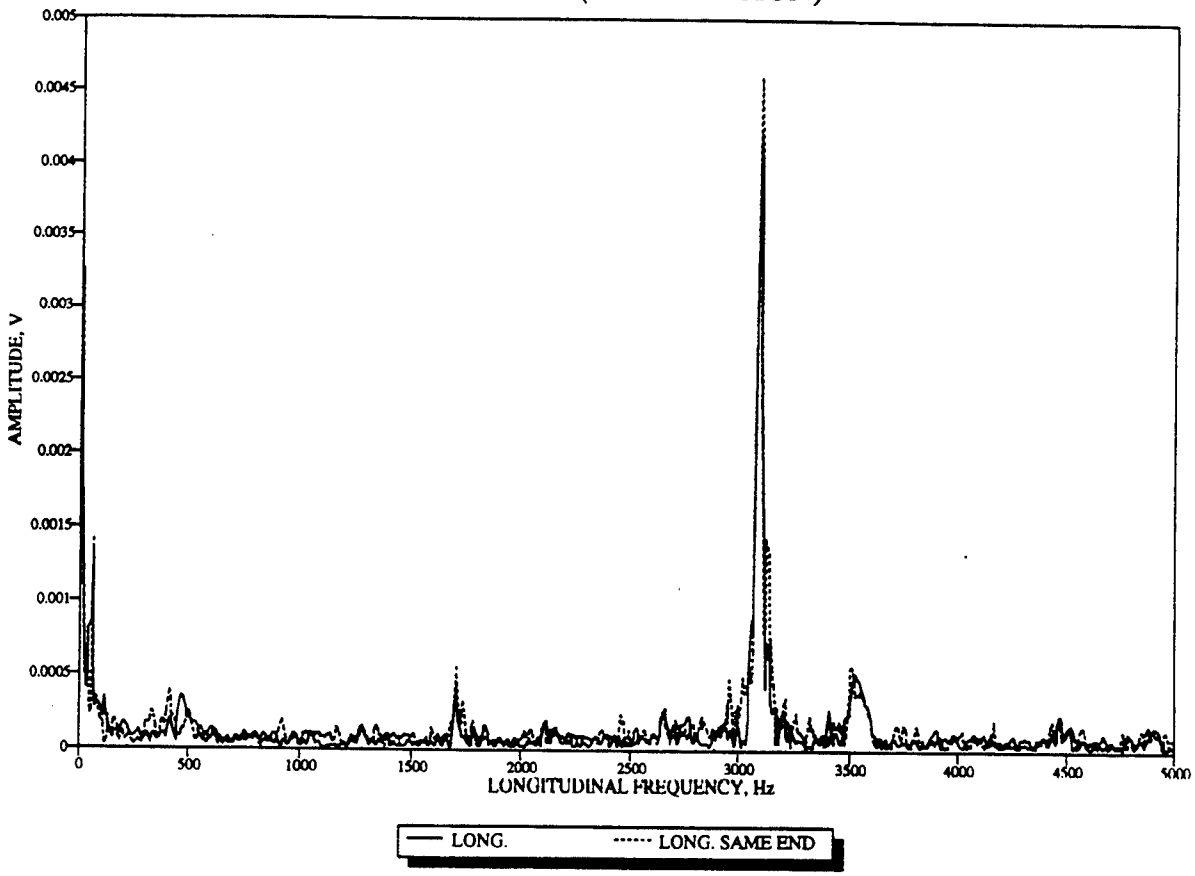


## BEAMJ3H (COMPRESSION)

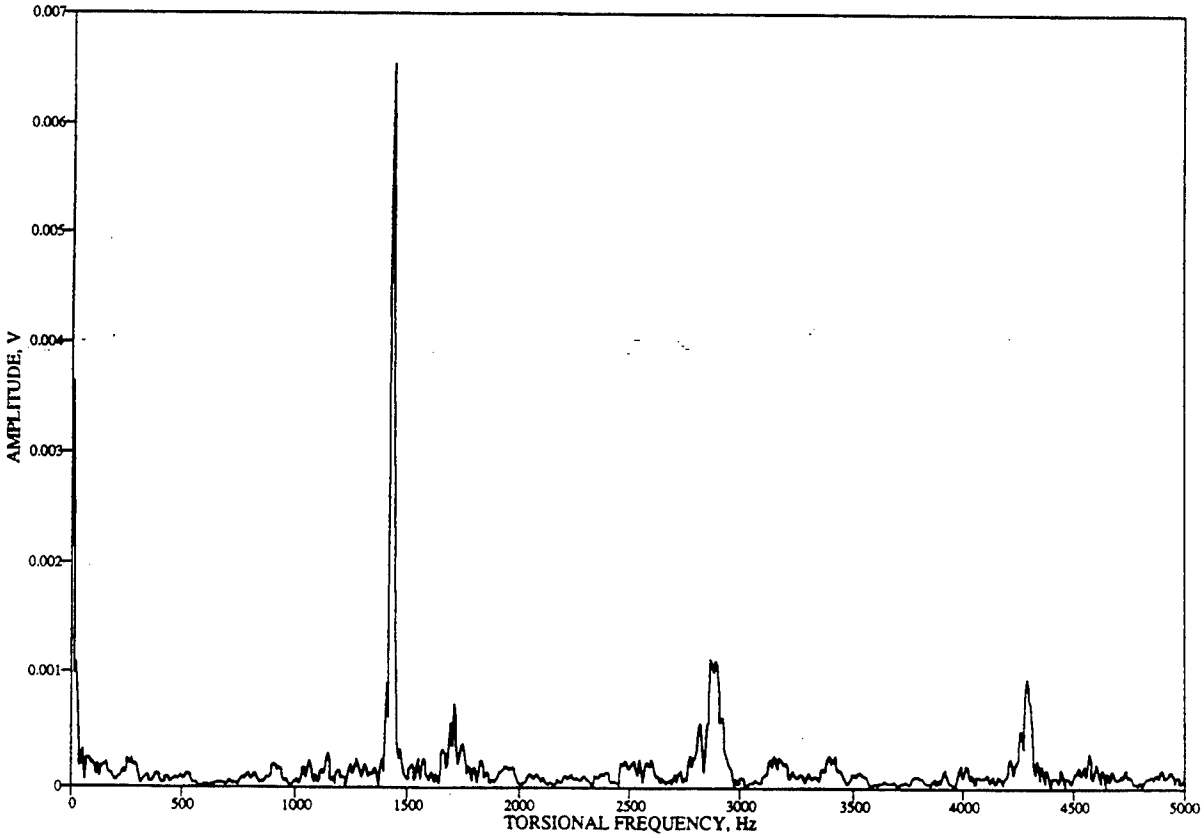

## BEAM J3H (TENSION)

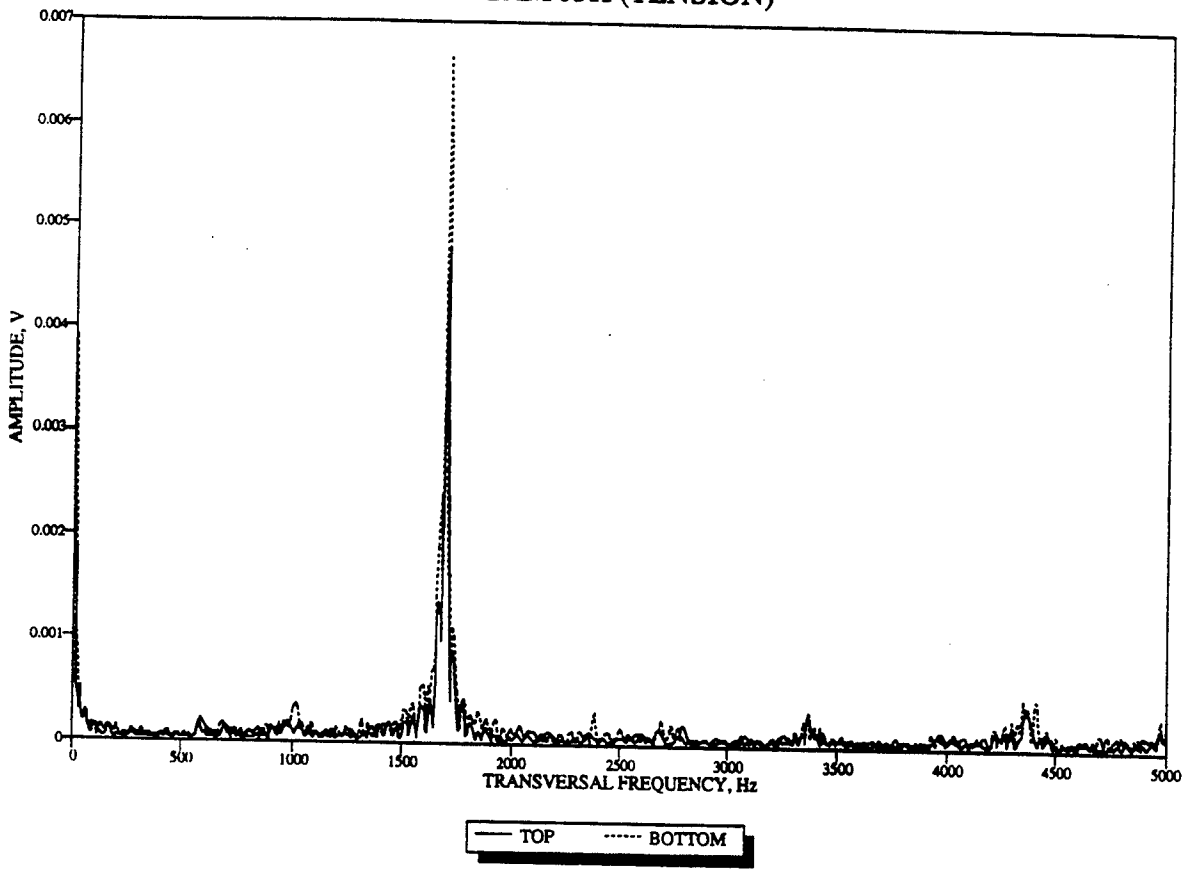


## BEAM J3H (TENSION)

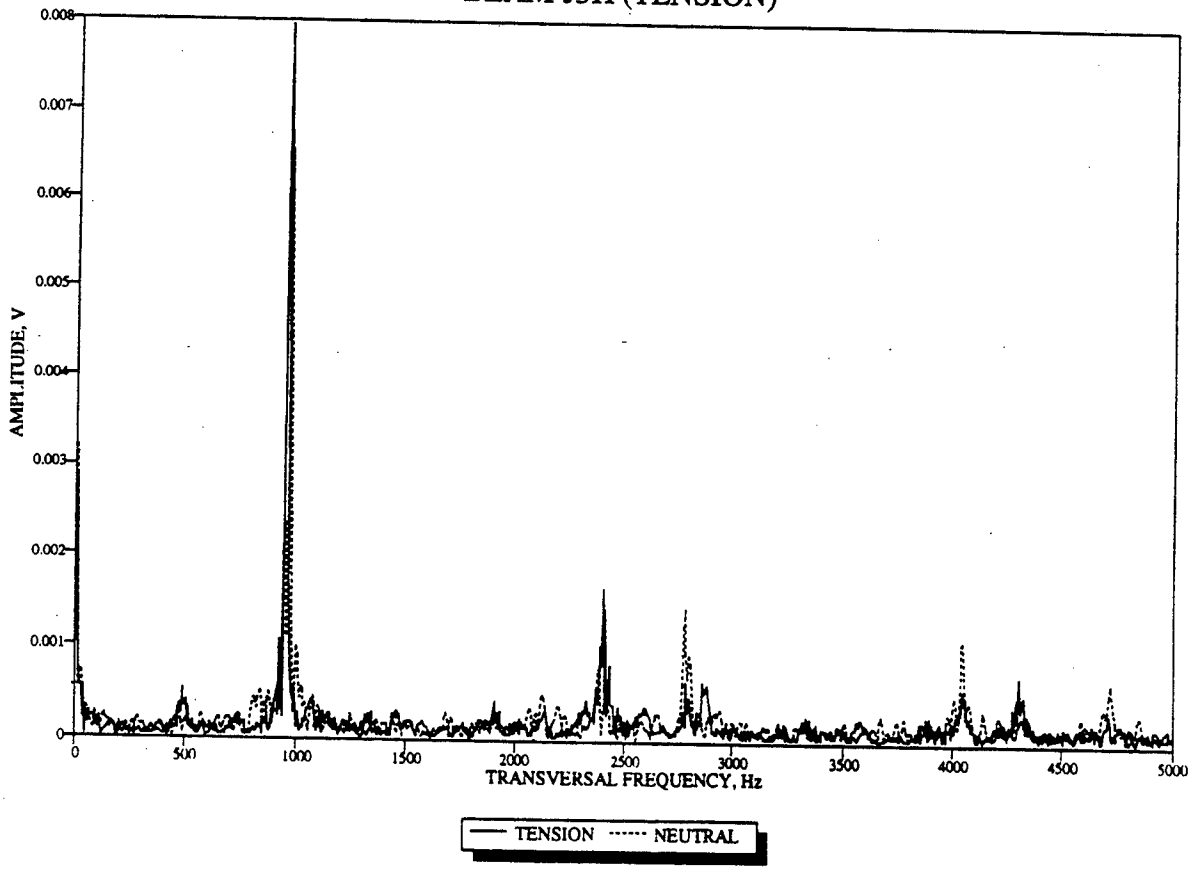

## BEAM J3H (TENSION)

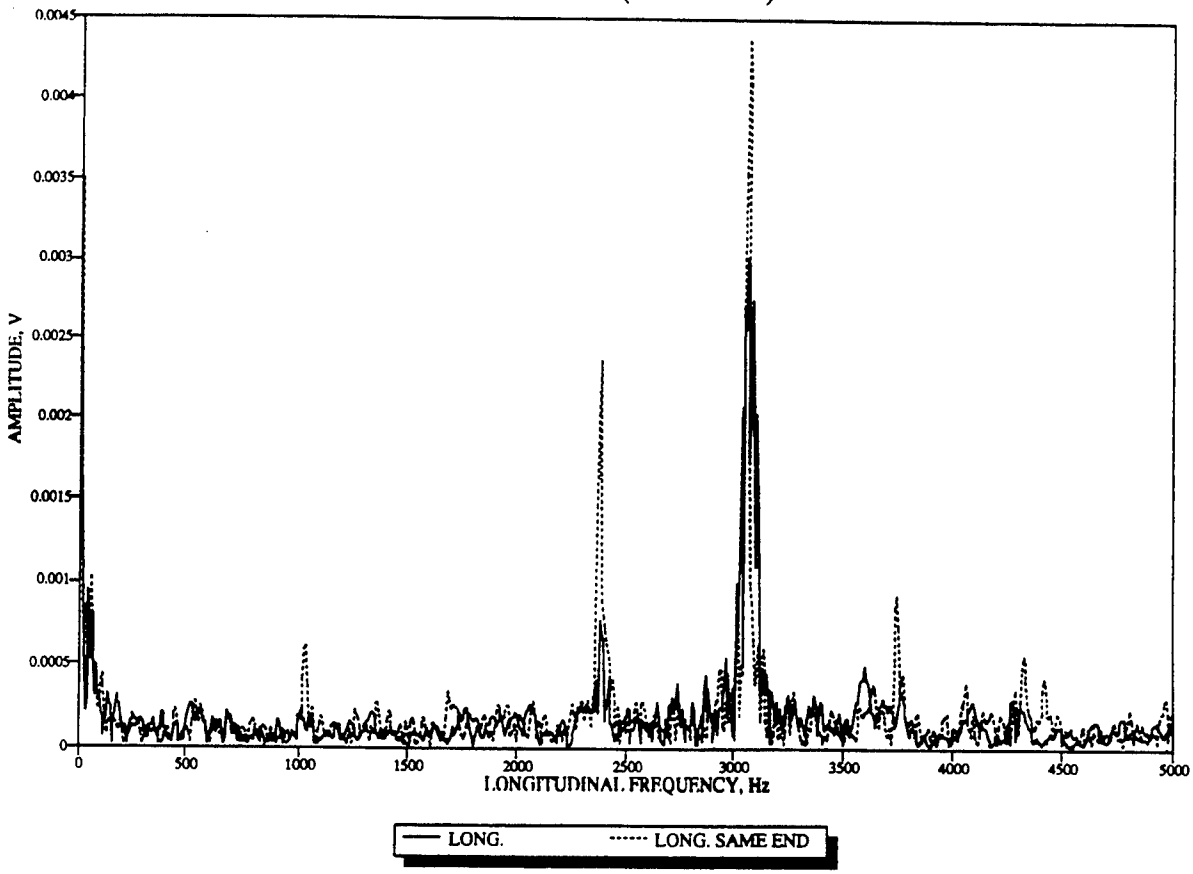


## BEAM J3H (TENSION)

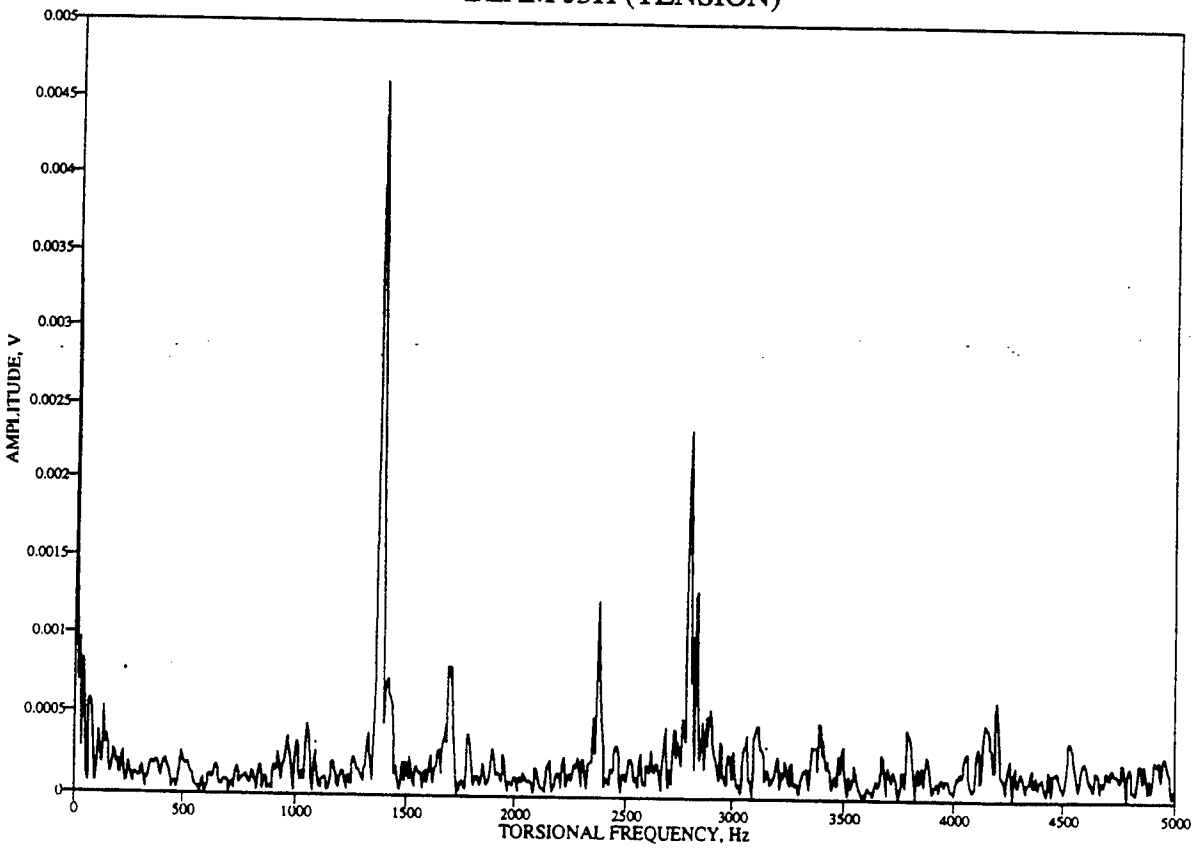

## BEAM K1H (COMPRESSION)

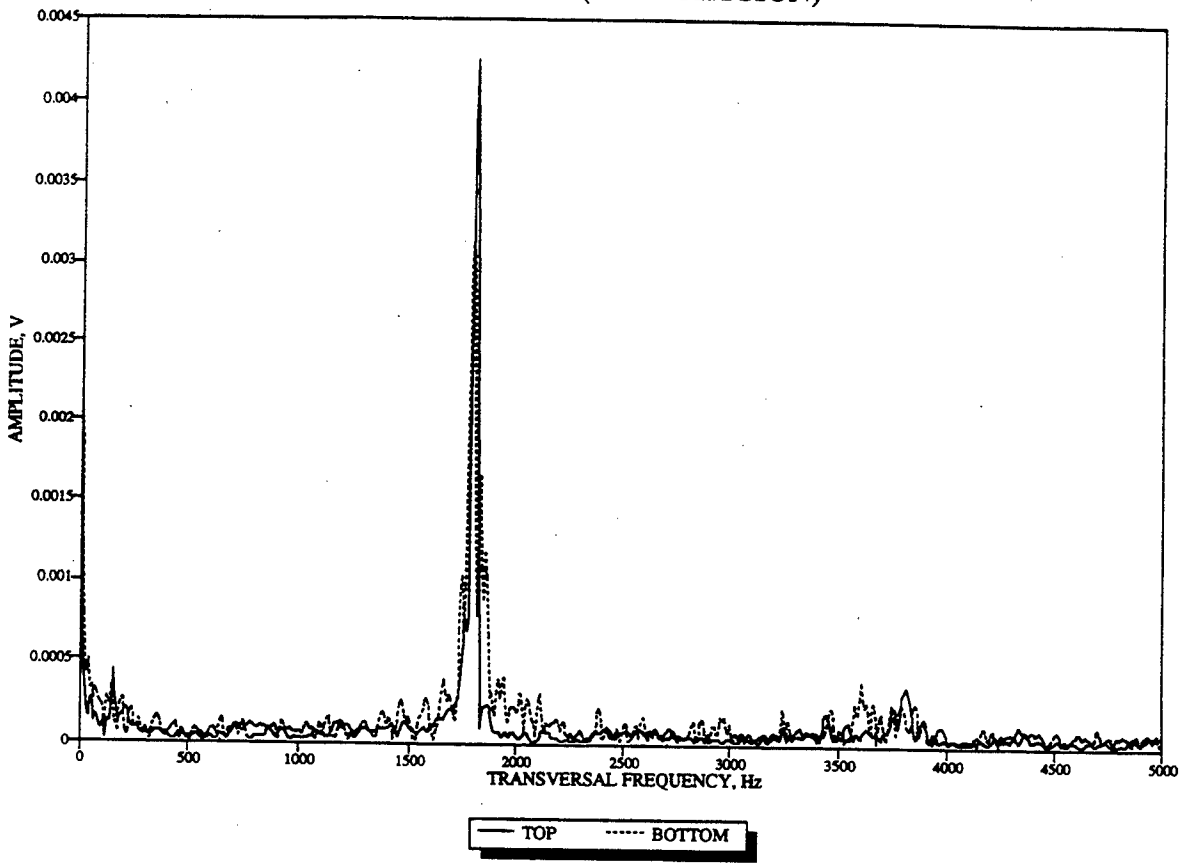


## BEAM K1H (COMPRESSION)

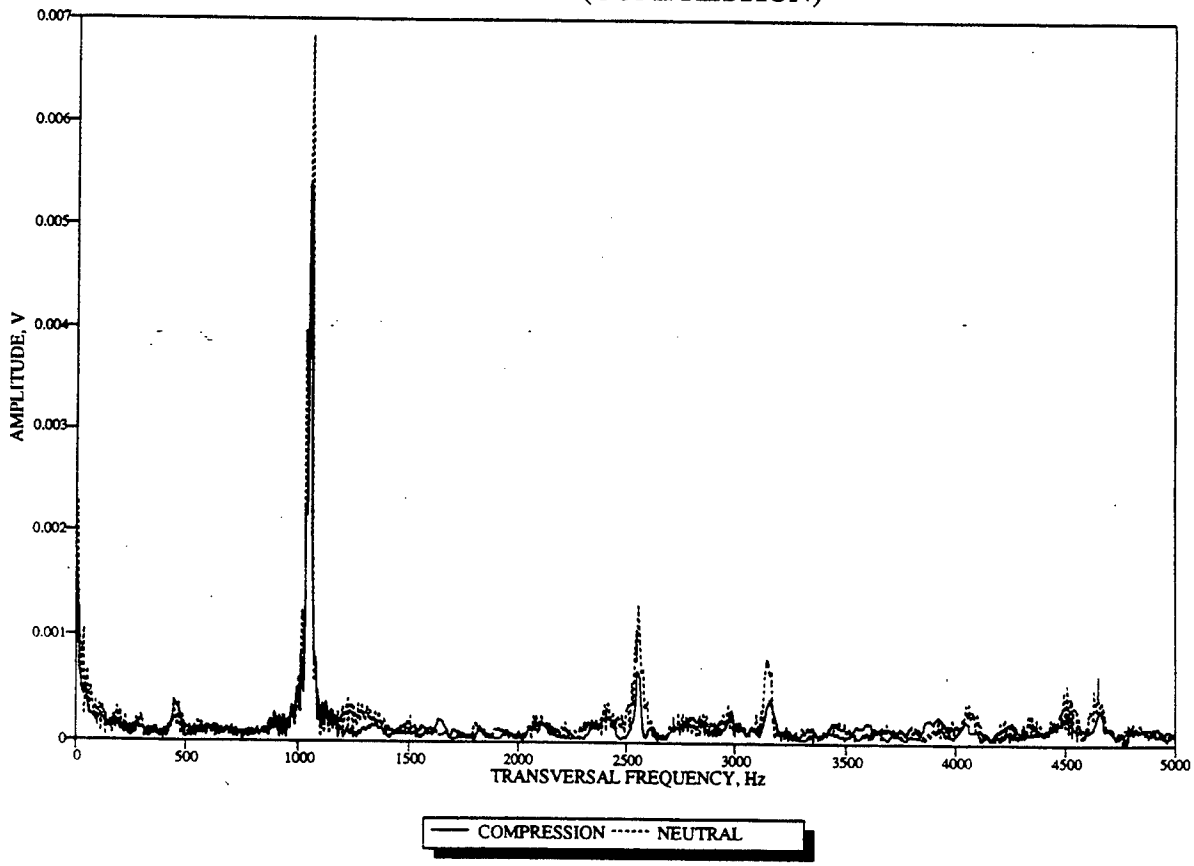

## BEAM K1H (COMPRESSION)

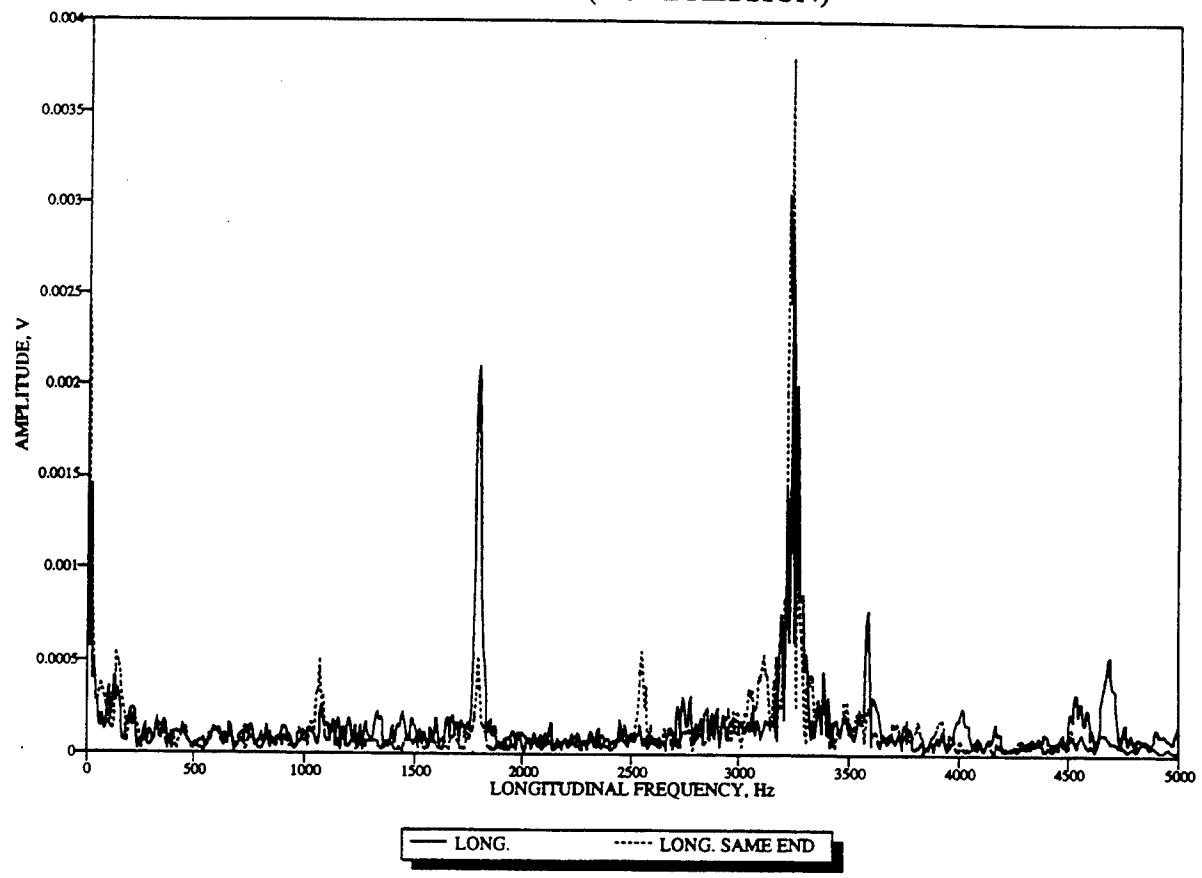


## BEAM K1H (COMPRESSION)

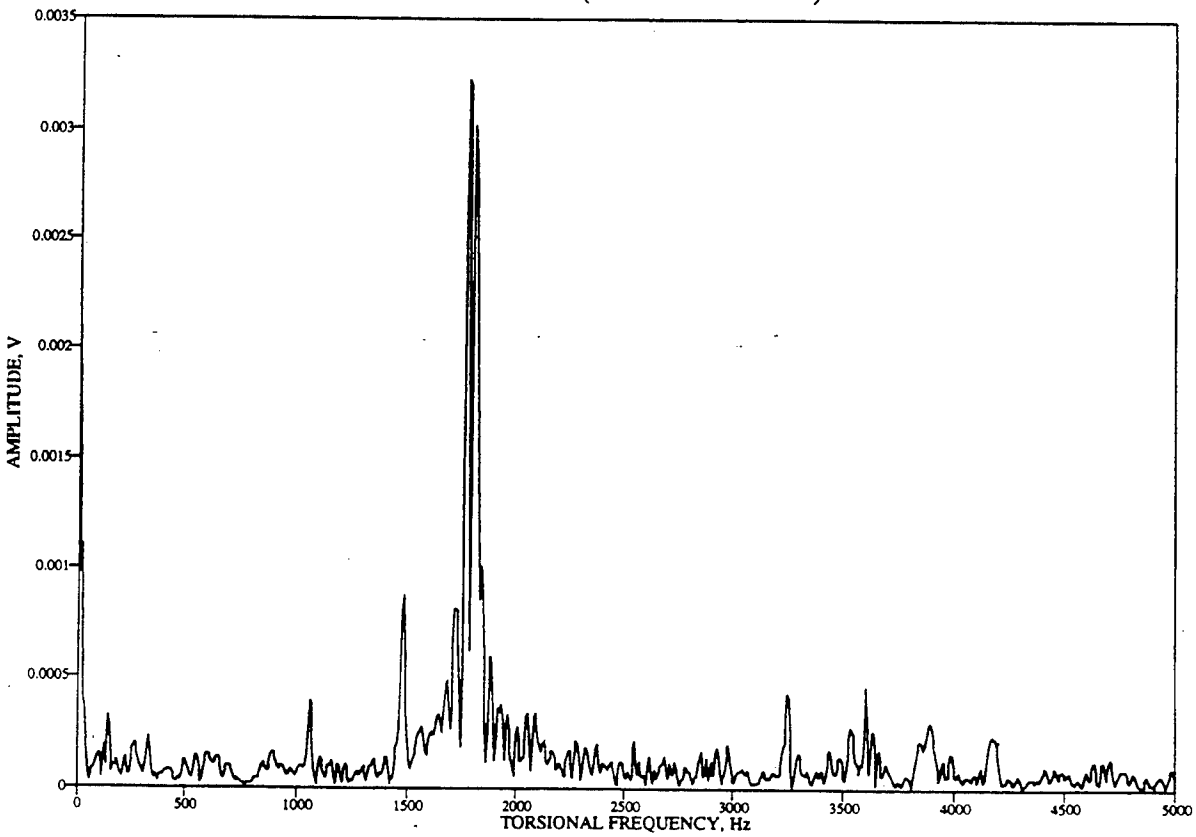

## BEAM K1H (TENSION)

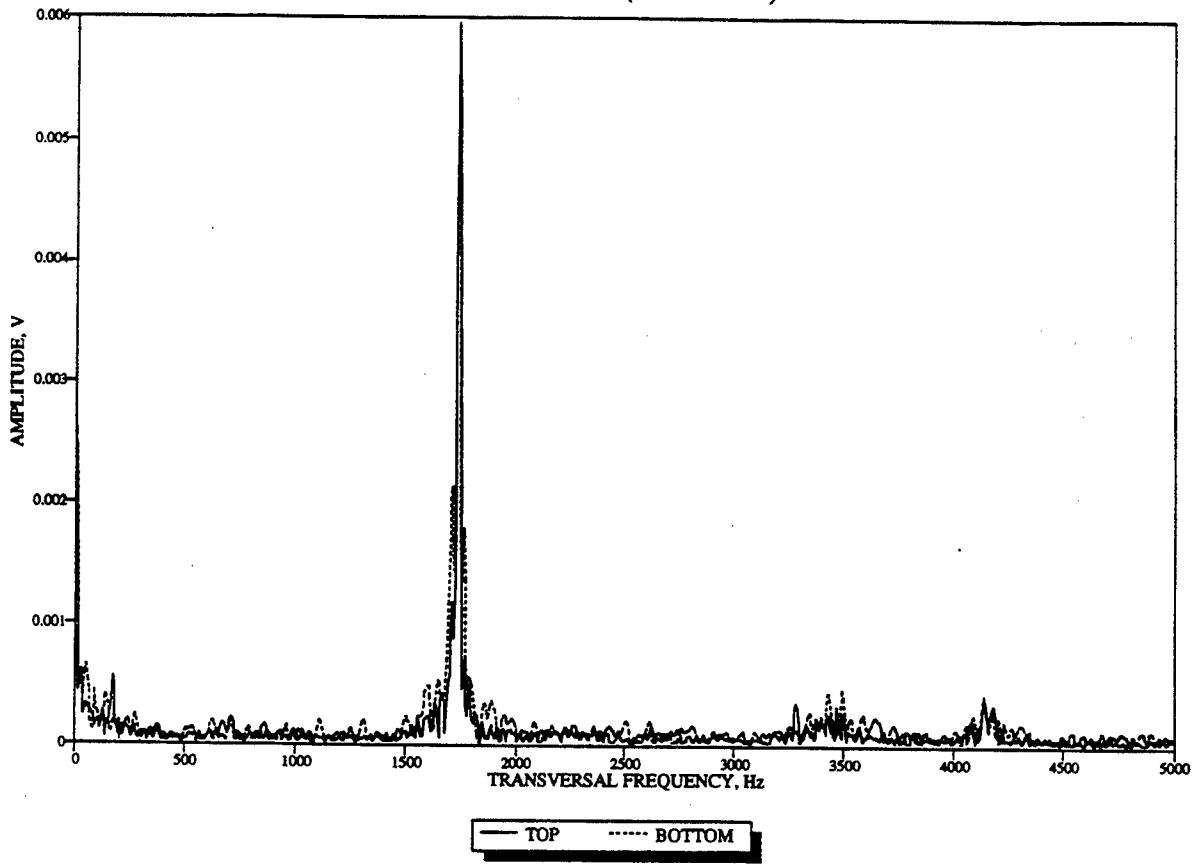


---

## BEAM K1H (TENSION)

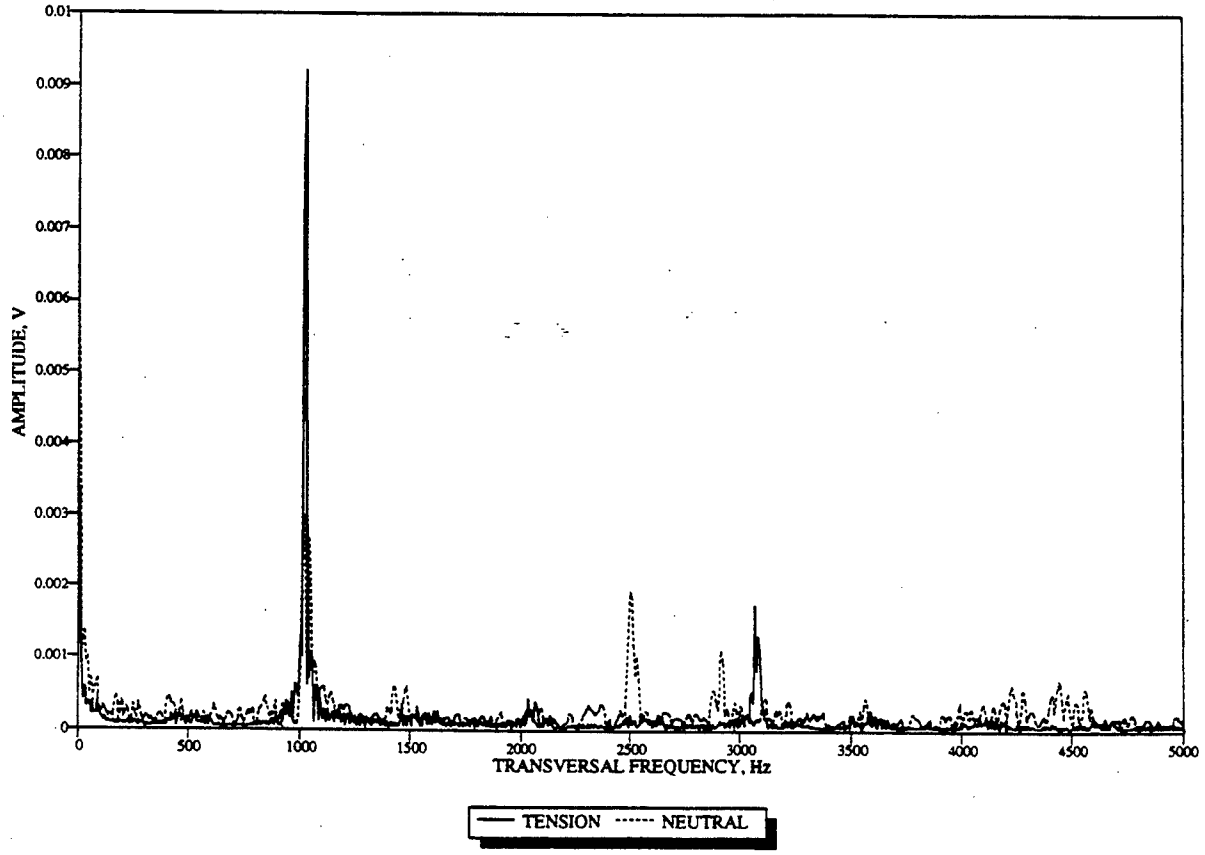

## BEAM K1H (TENSION)

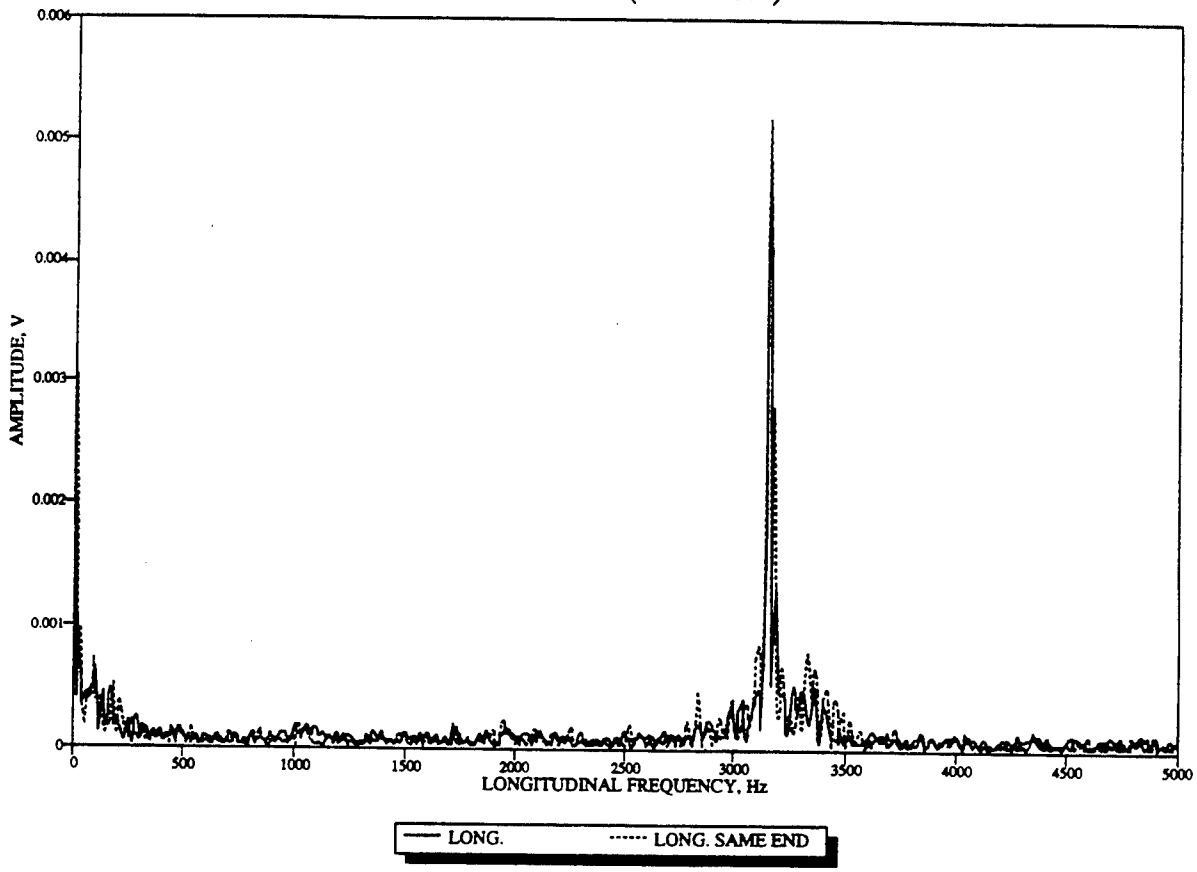


## BEAM K1H (TENSION)

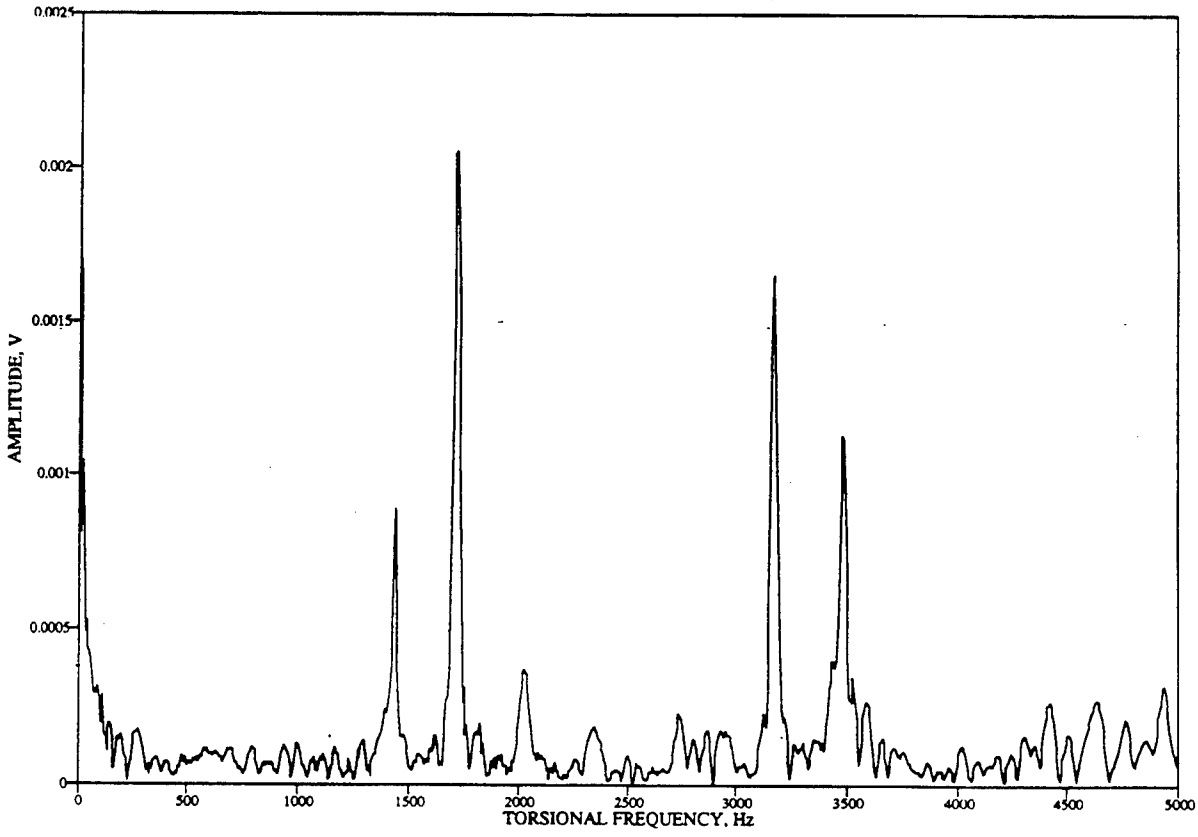

## BEAM K3H (COMPRESSION)

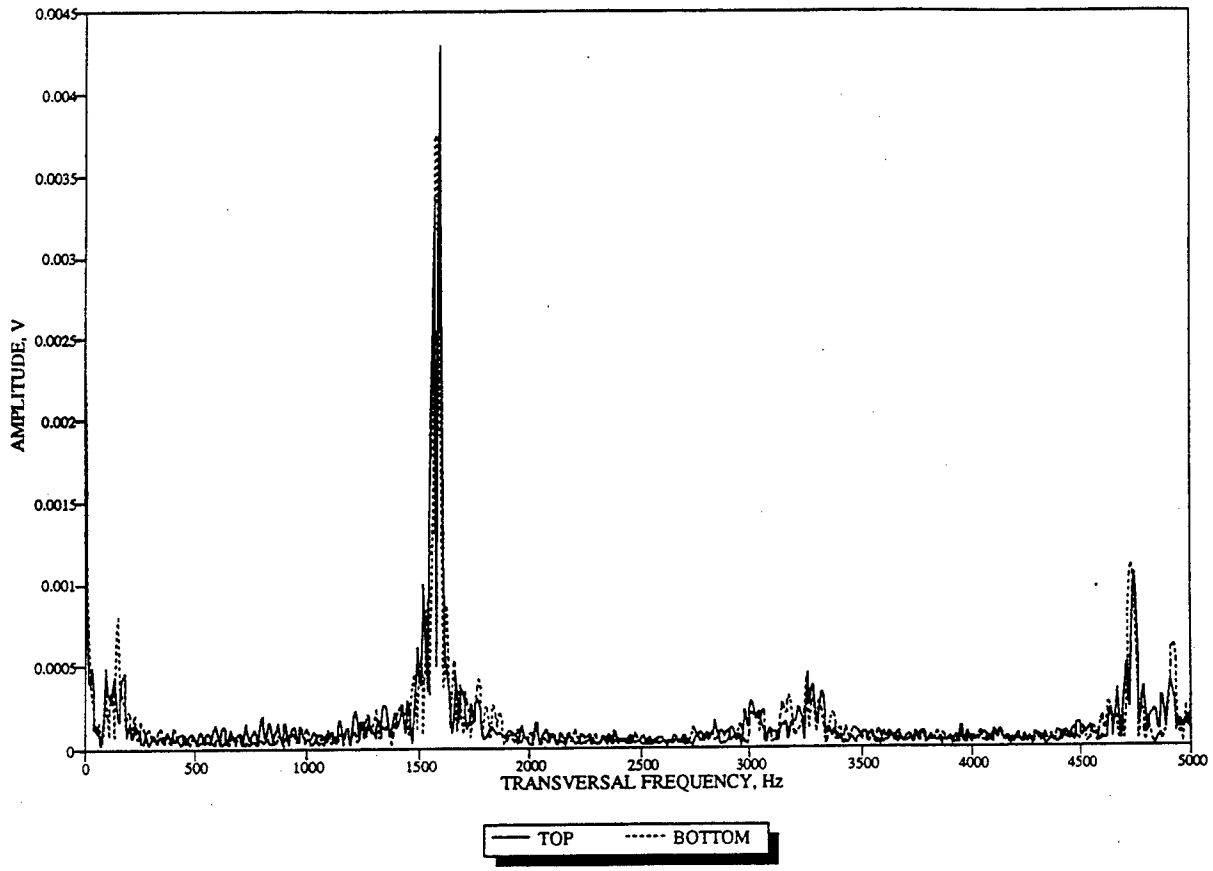


## BEAM K3H (COMPRESSION)

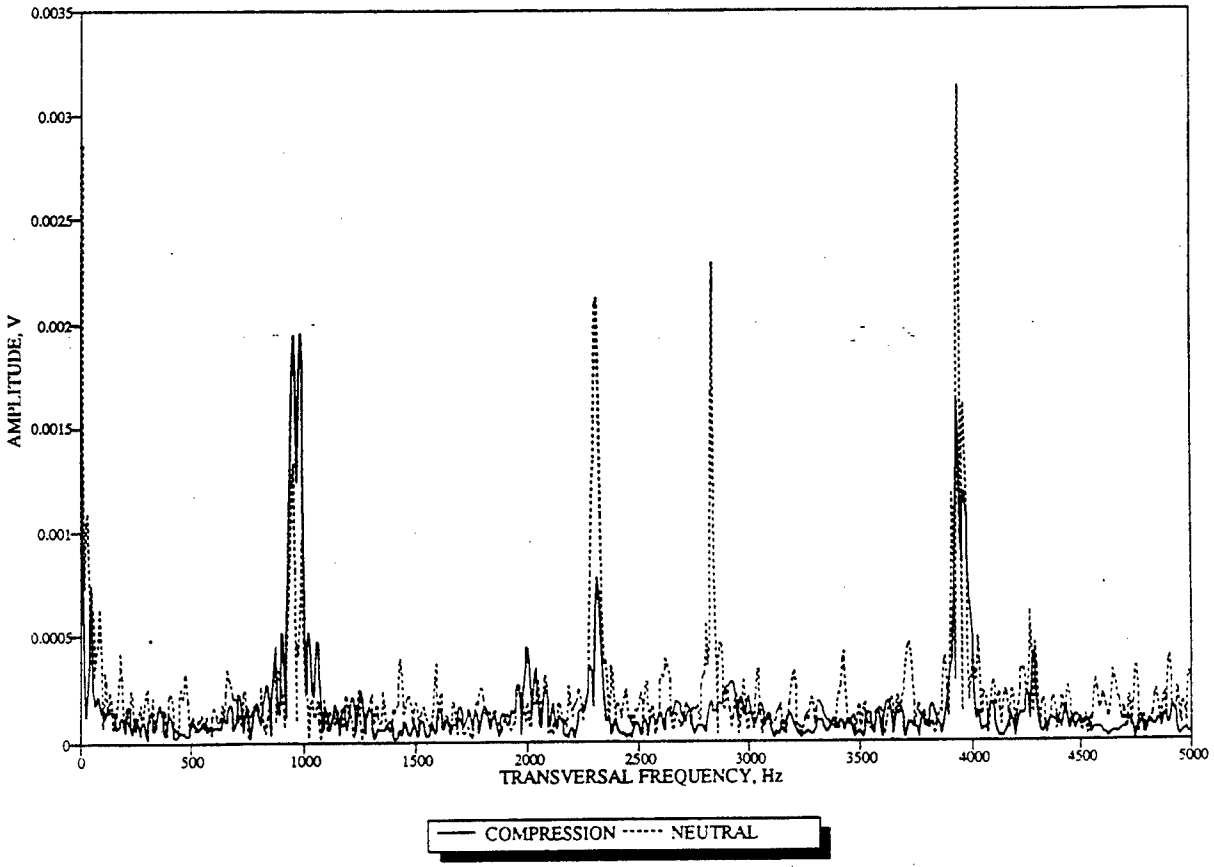

## BEAM K3H (COMPRESSION)

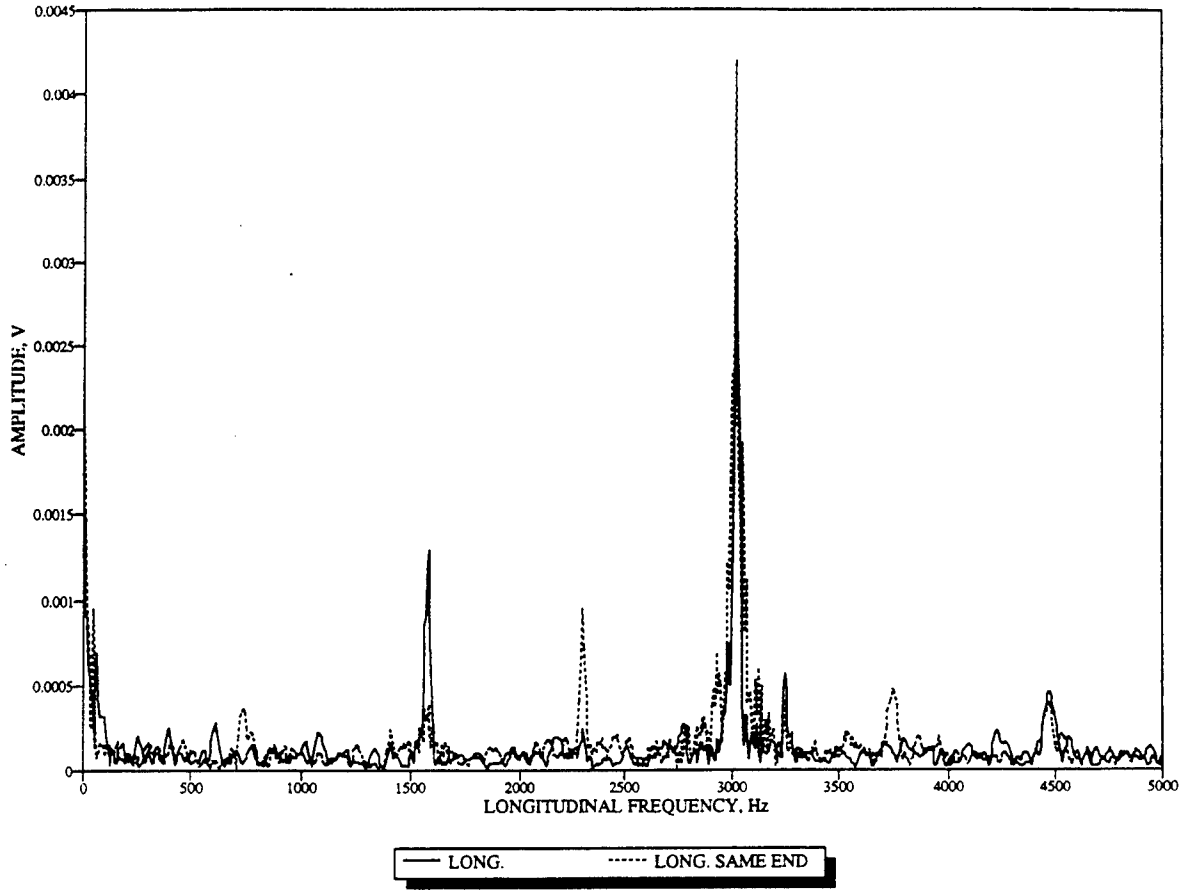


## BEAM K3H (COMPRESSION)

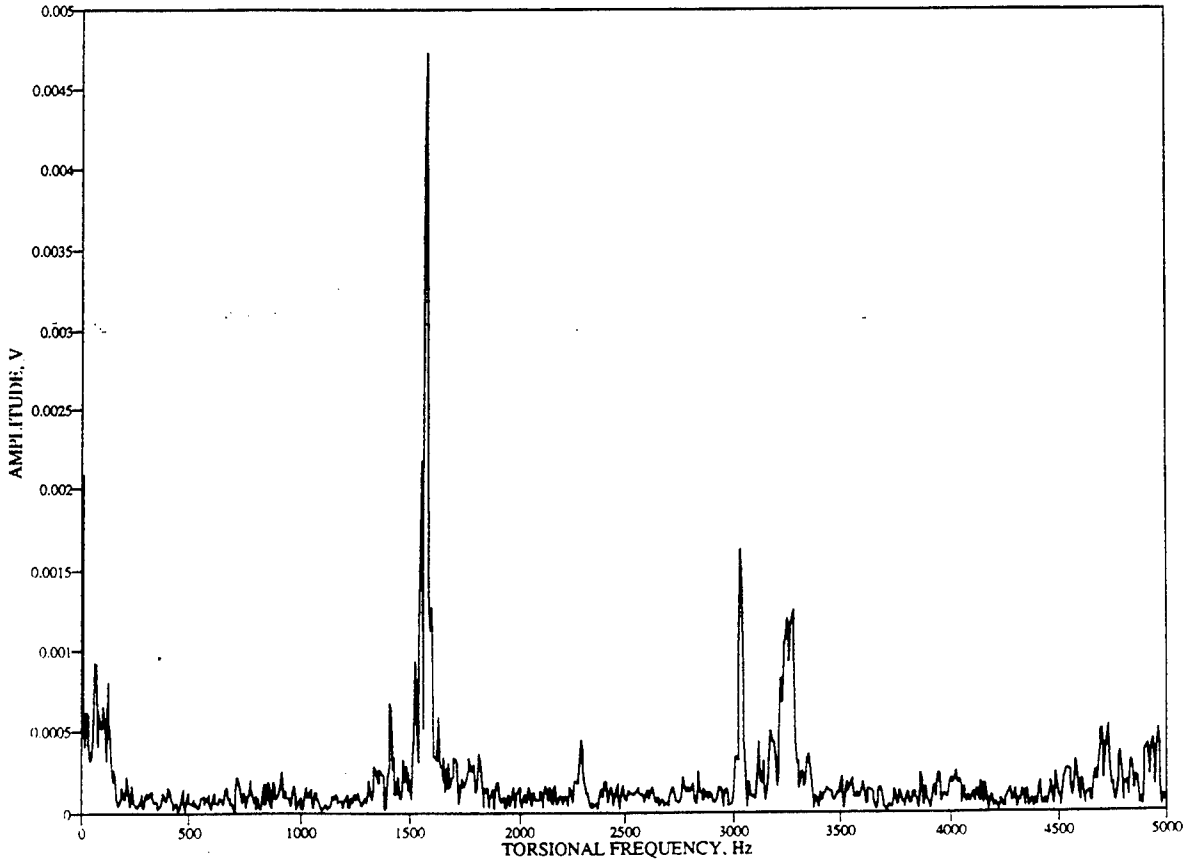

## BEAM K3H (TENSION)

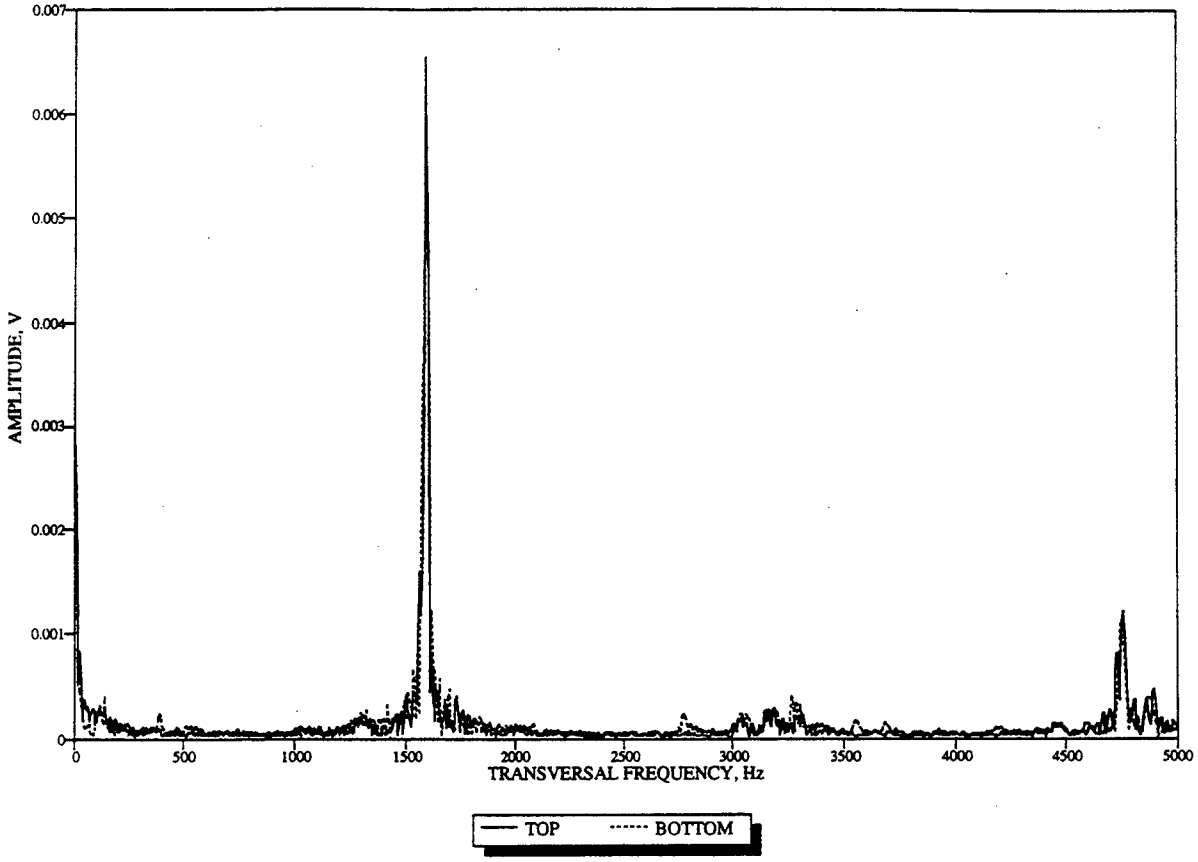


## BEAM K3H (TENSION)

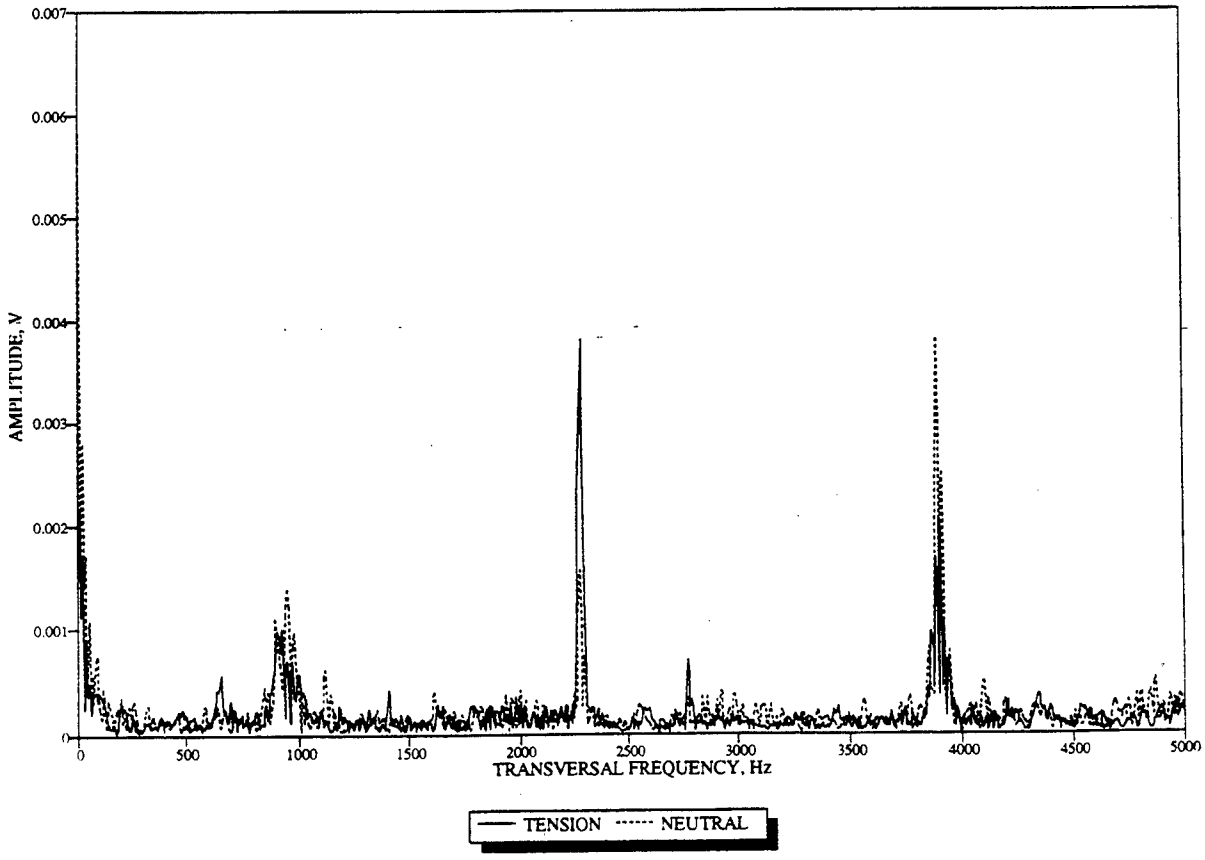

## BEAM K3H (TENSION)

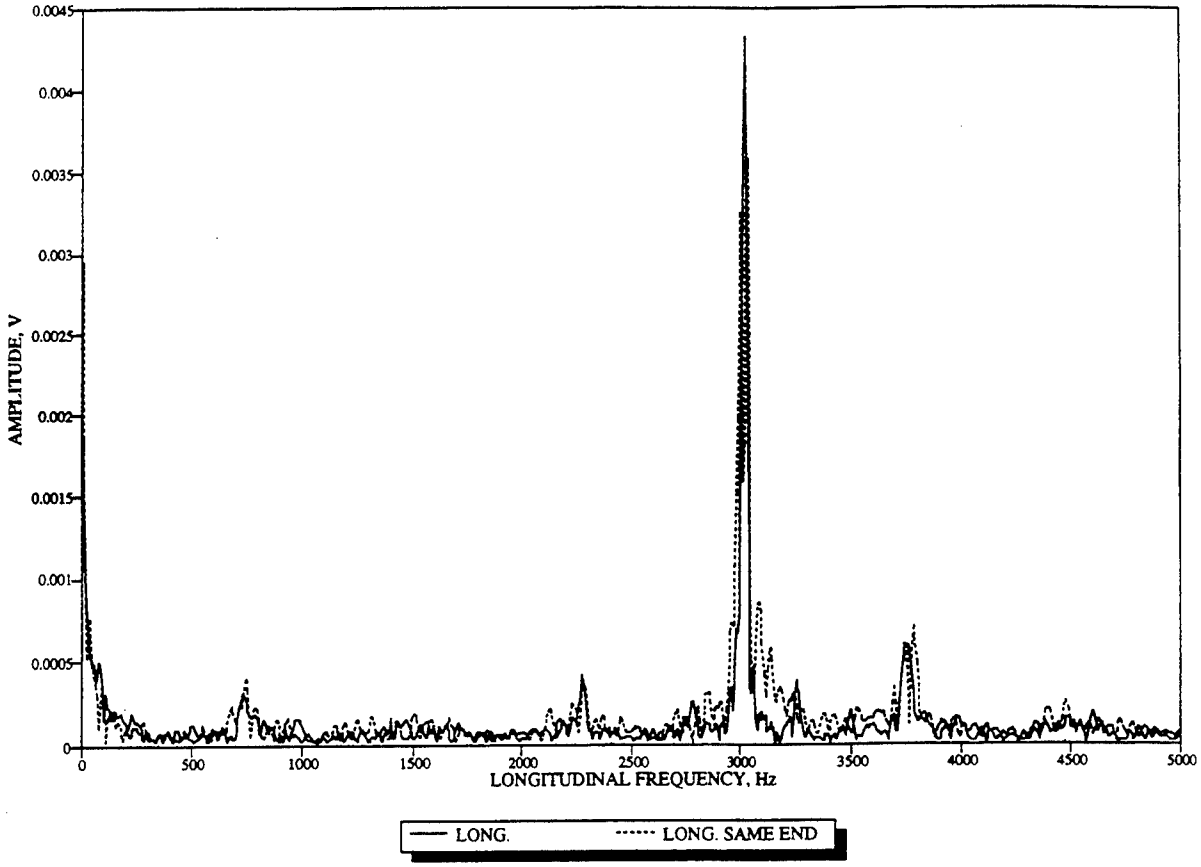


## BEAM K3H (TENSION)

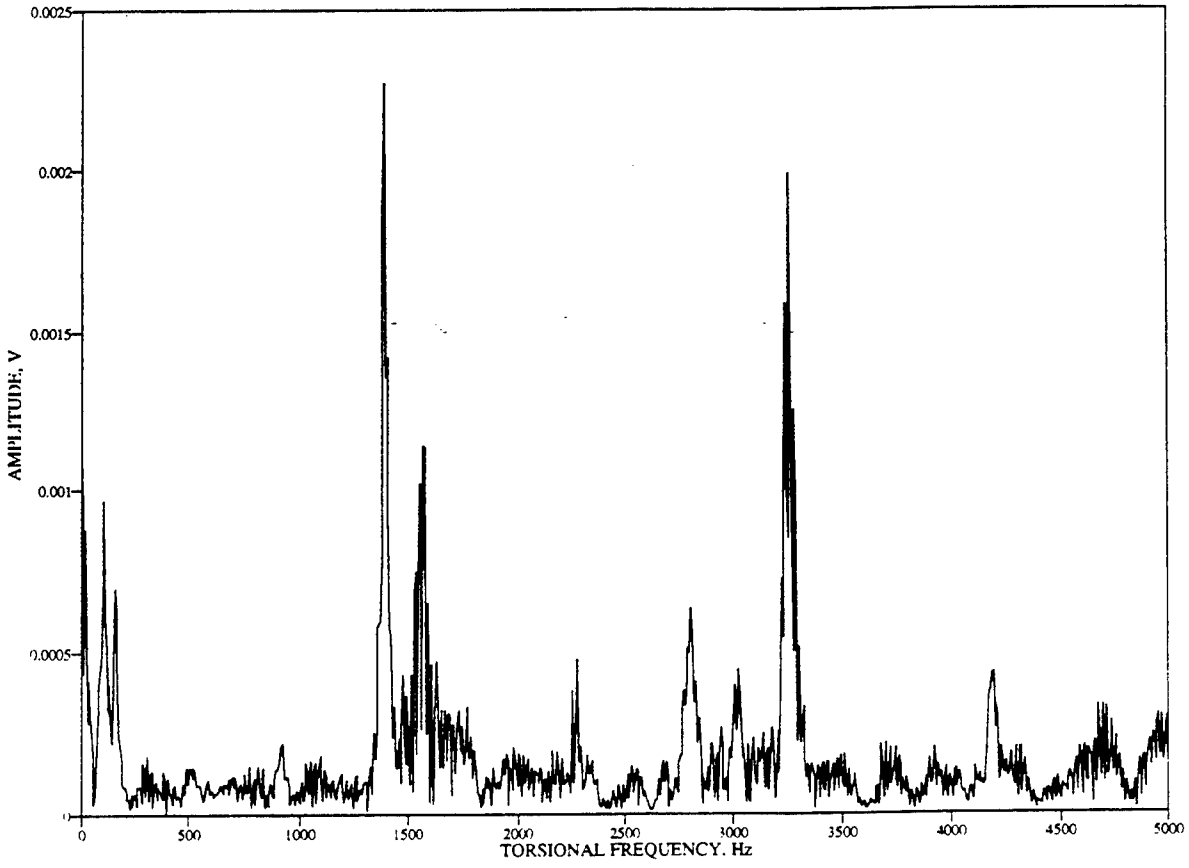

## BEAM M1H (COMPRESSION)

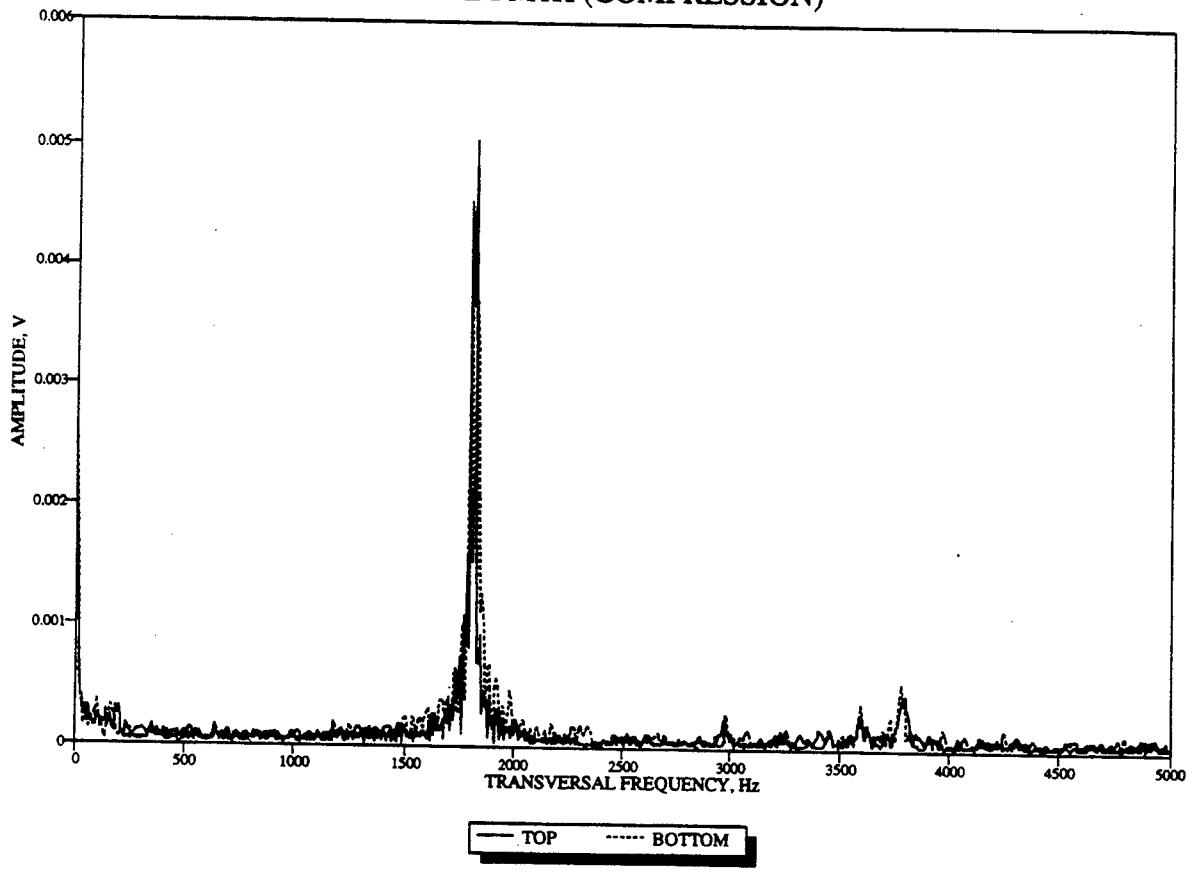


## BEAM M1H (COMPRESSION)

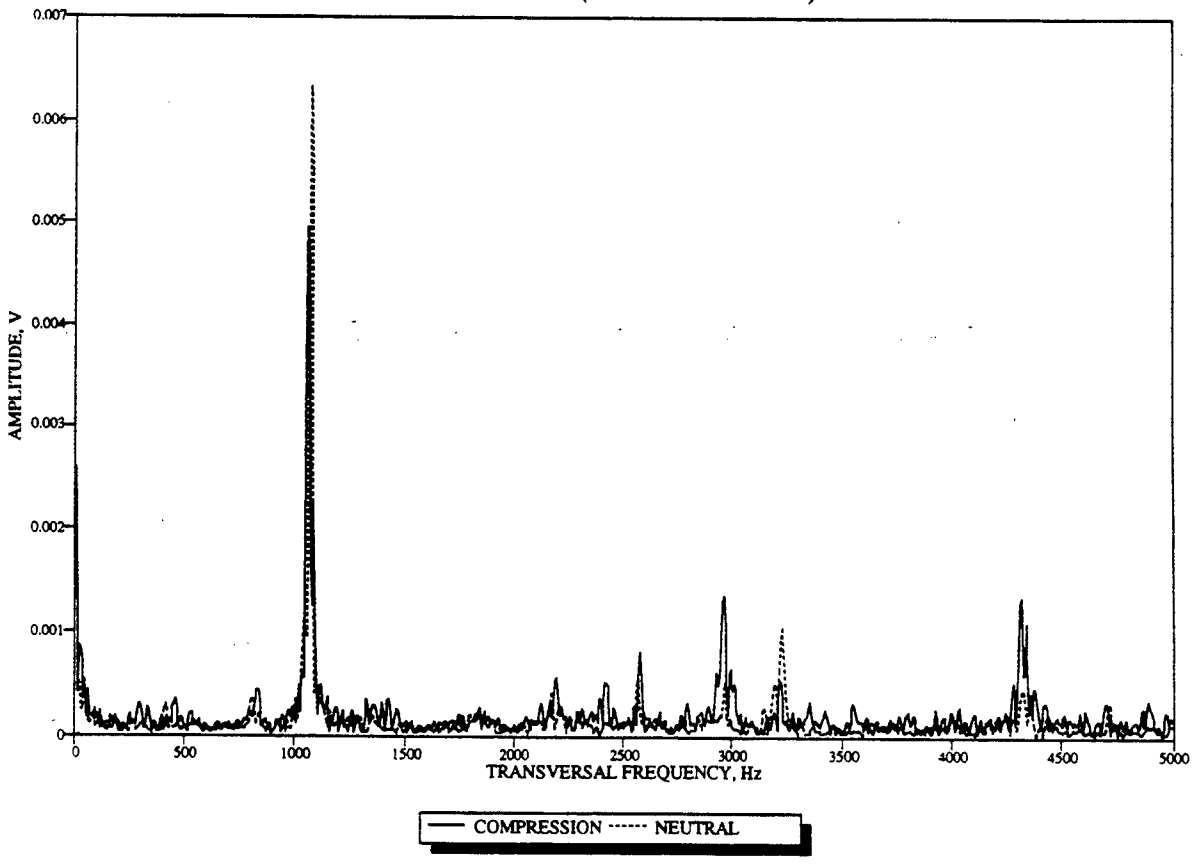

## BEAM M1H (COMPRESSION)

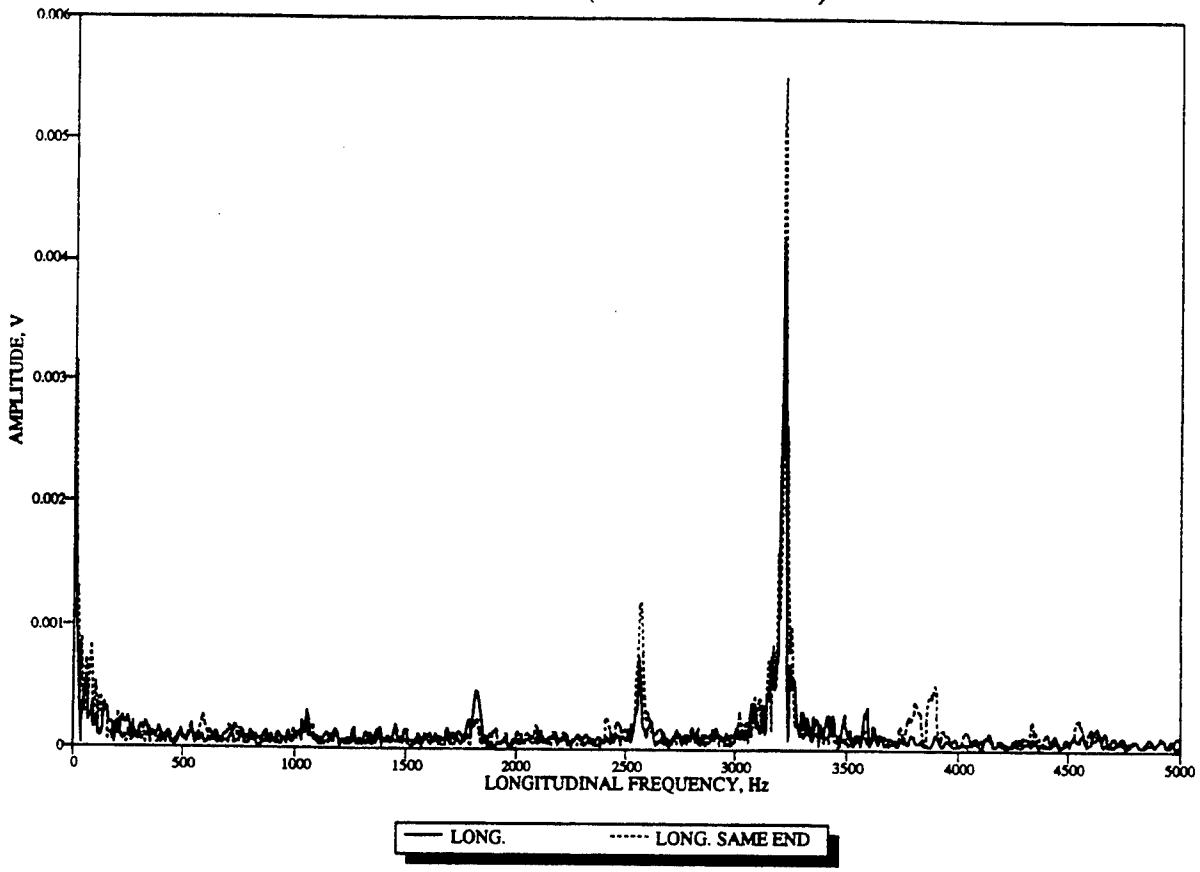


## BEAM M1H (COMPRESSION)

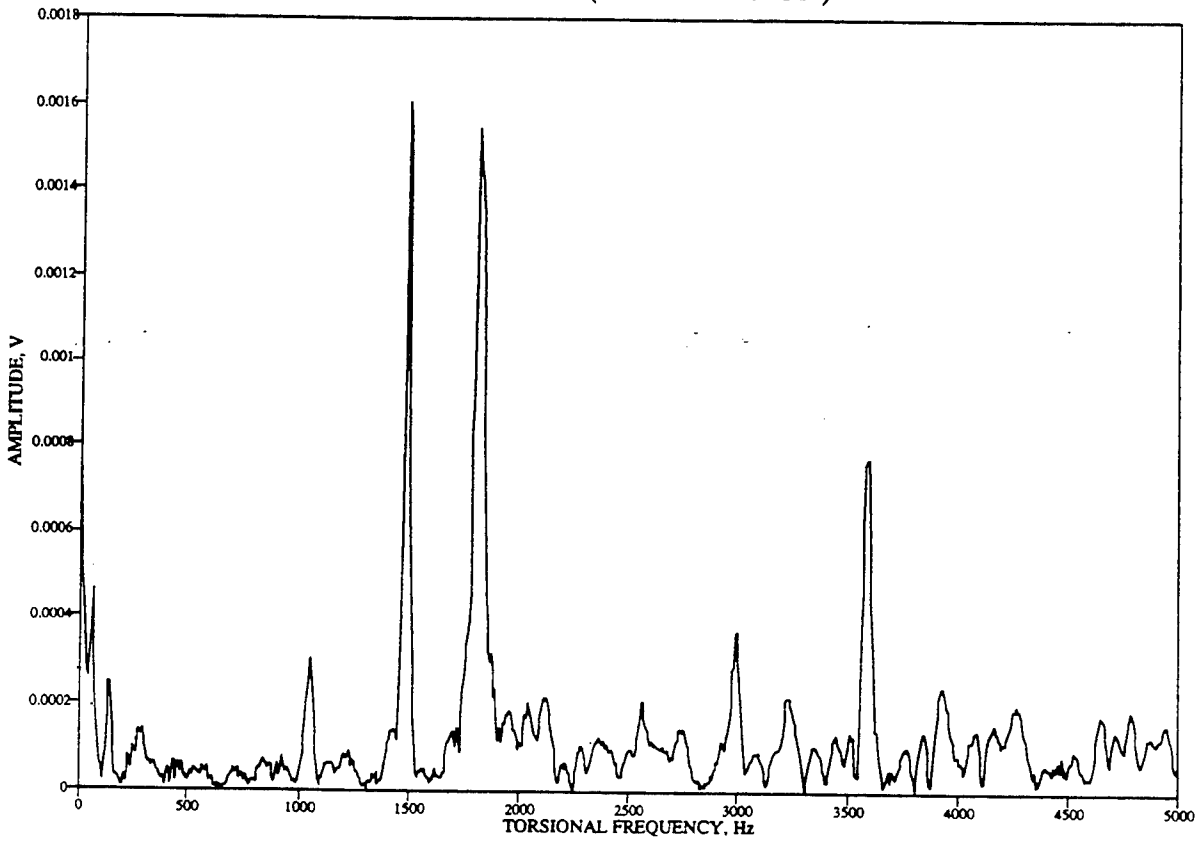

## BEAM M1H (TENSION)

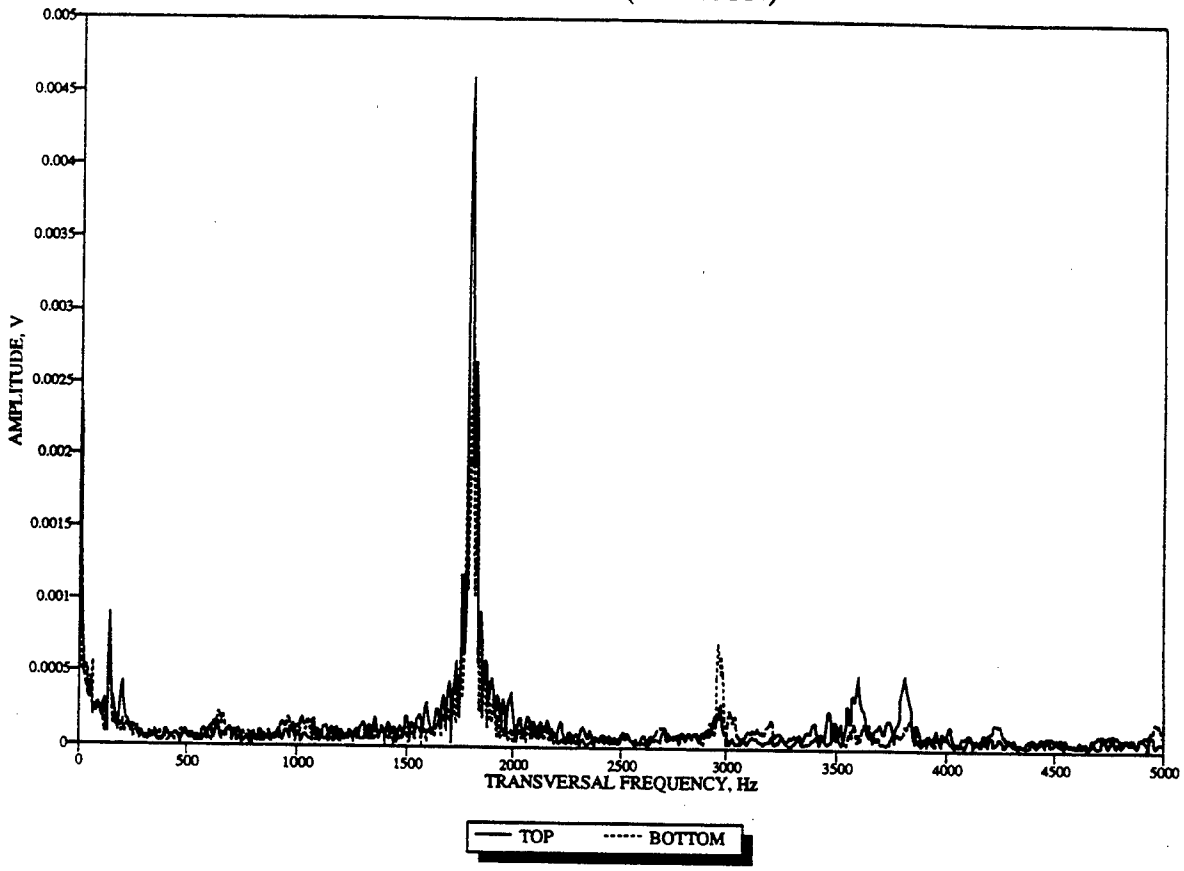


## BEAM M1H (TENSION)

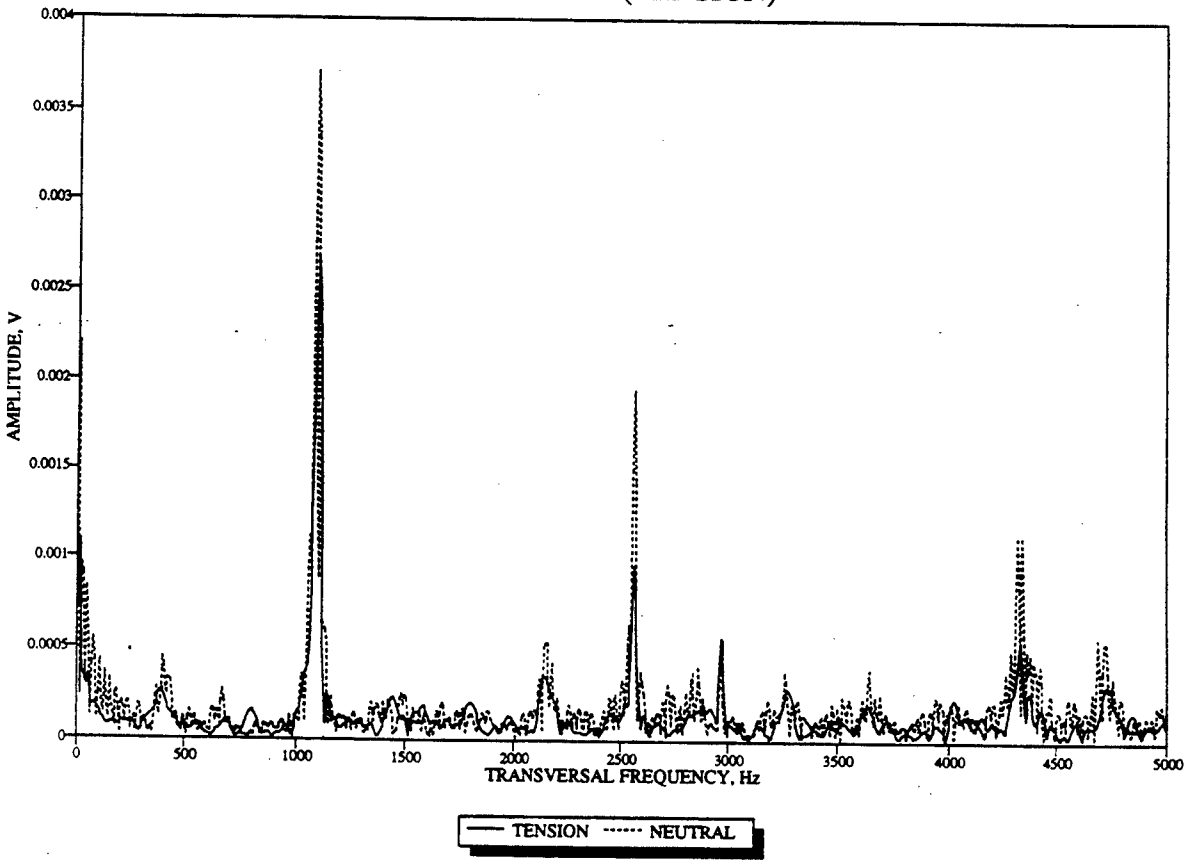

## BEAM M1H (TENSION)

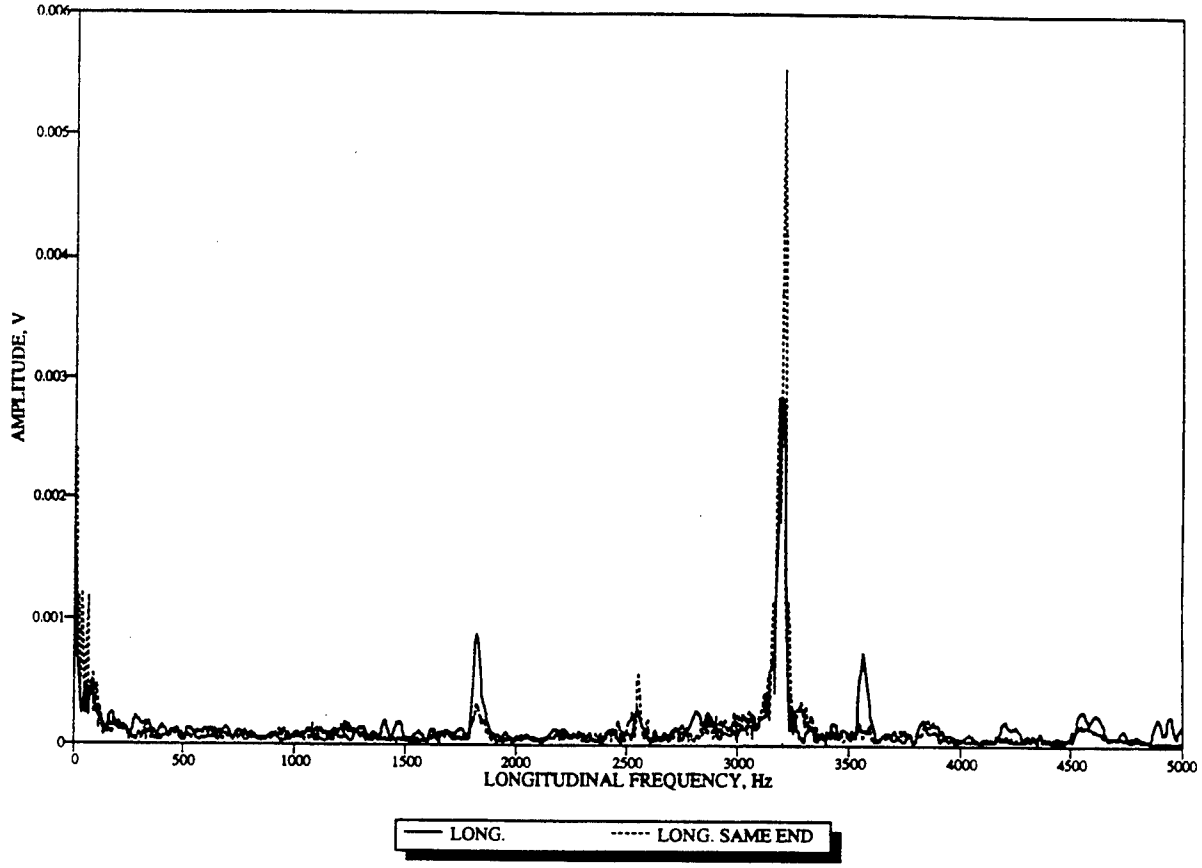


## BEAM M1H (TENSION)

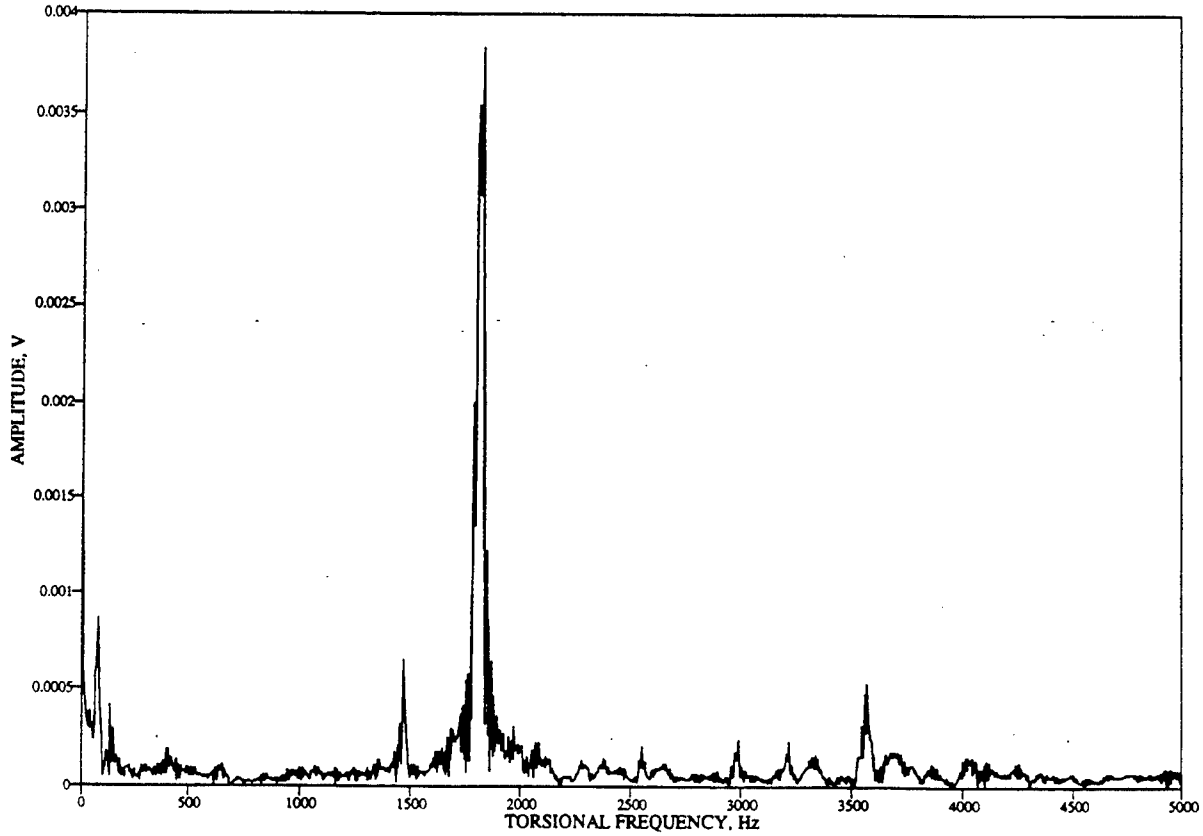

## BEAM M3H(COMPRESSION)

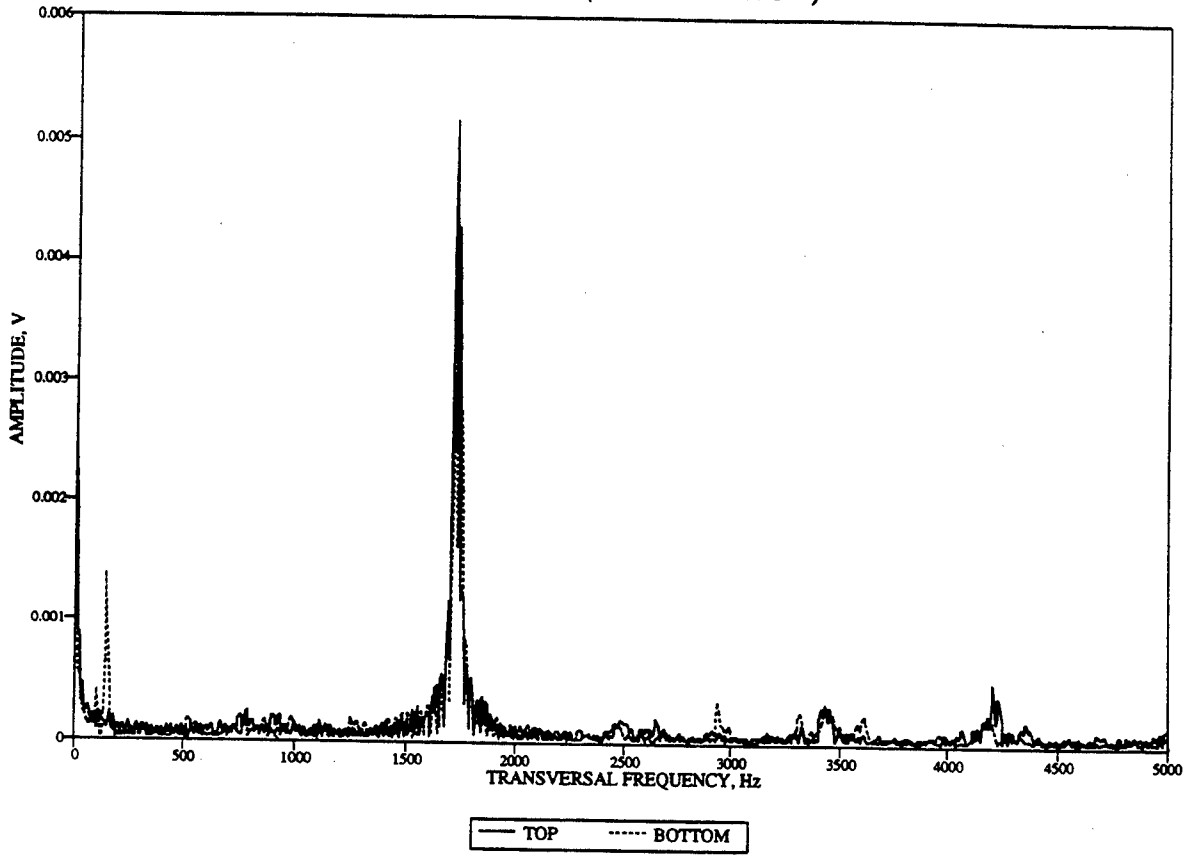


## BEAM M3H(COMPRESSION)

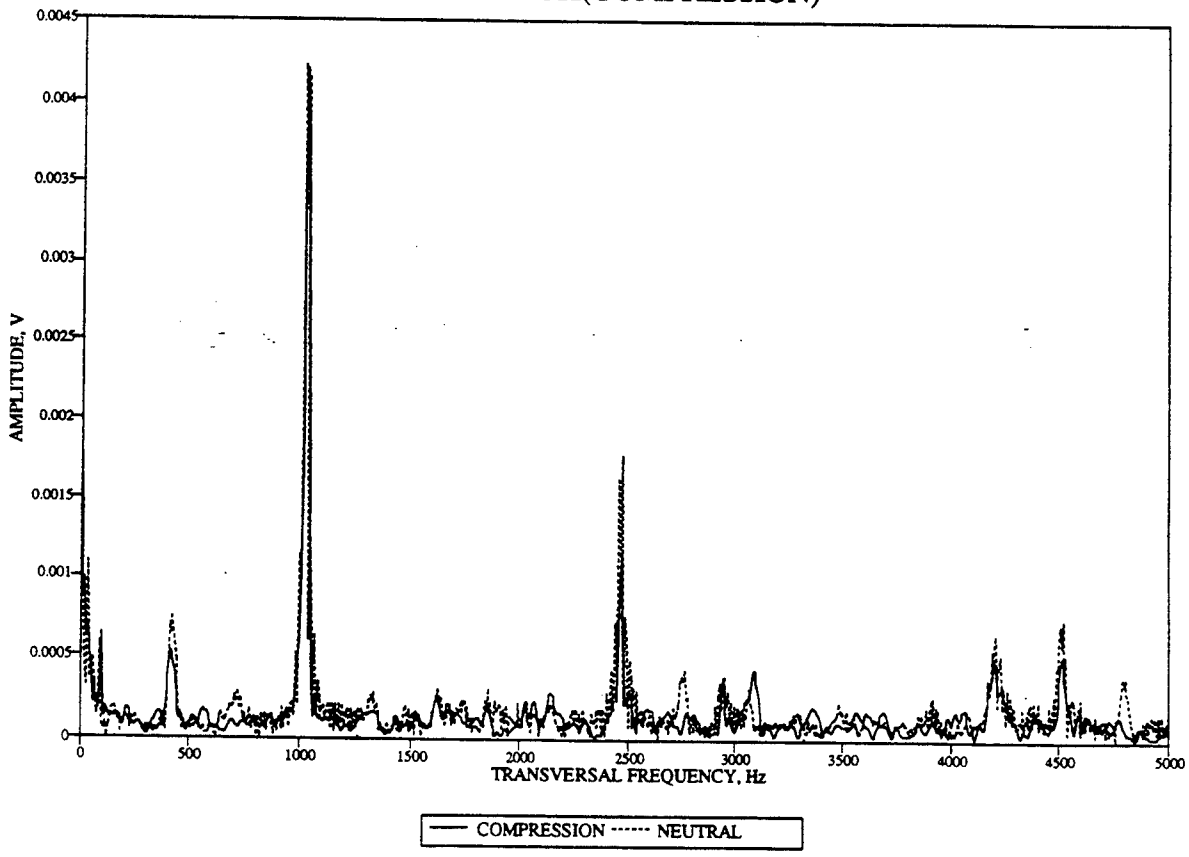

## BEAM M3H(COMPRESSION)

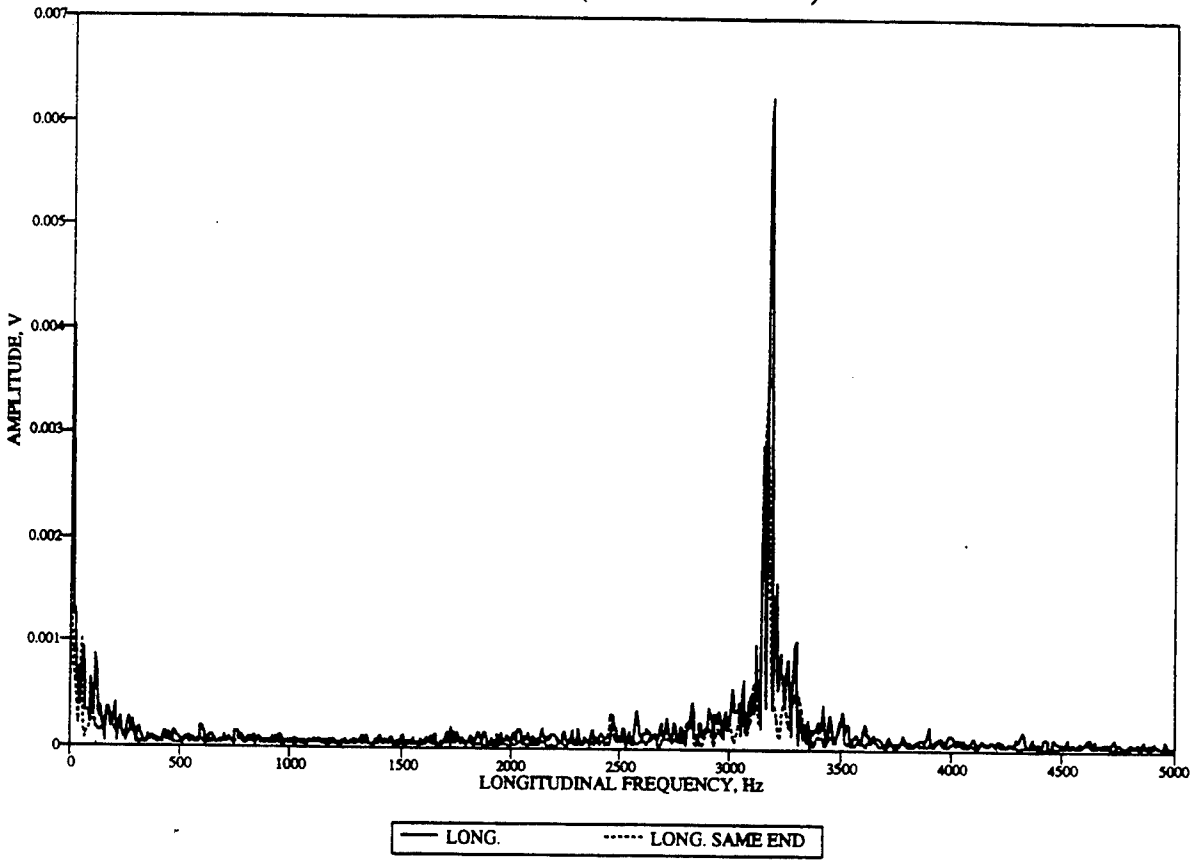


## BEAM M3H(COMPRESSION)

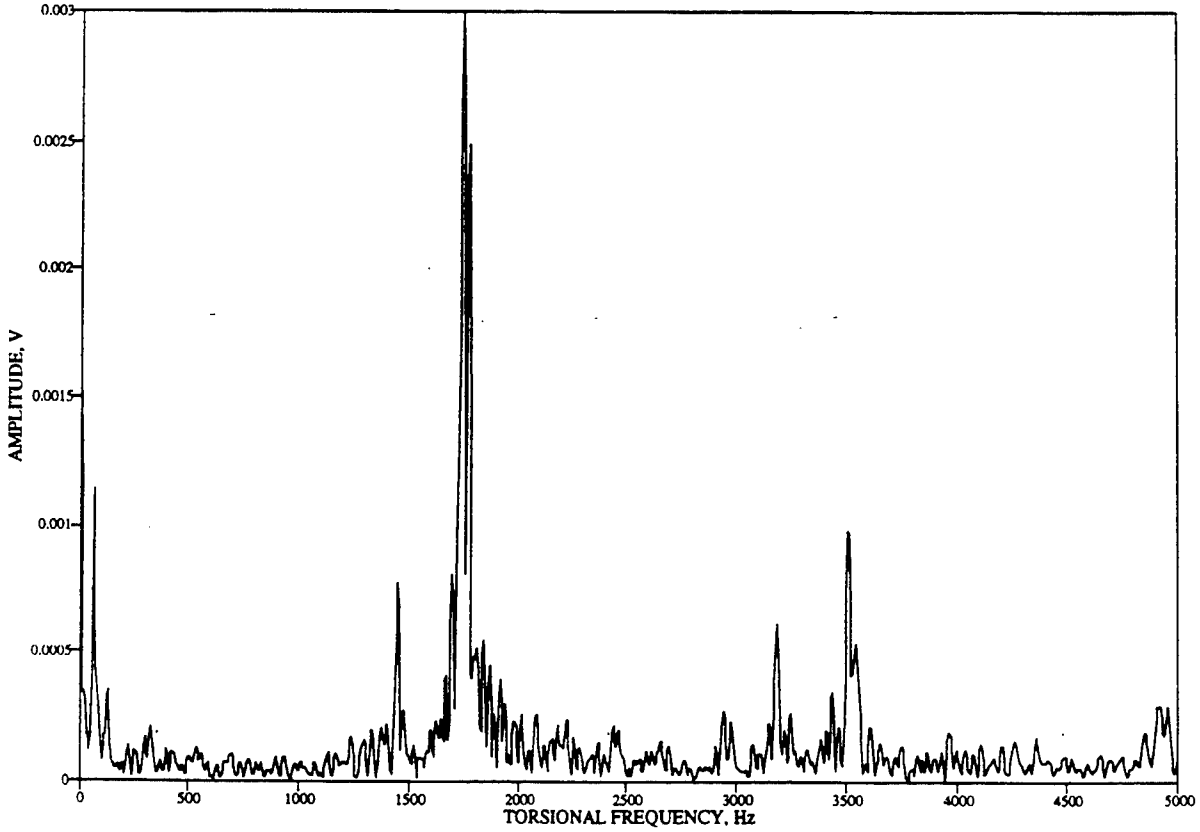

## BEAM M3H(TENSION)

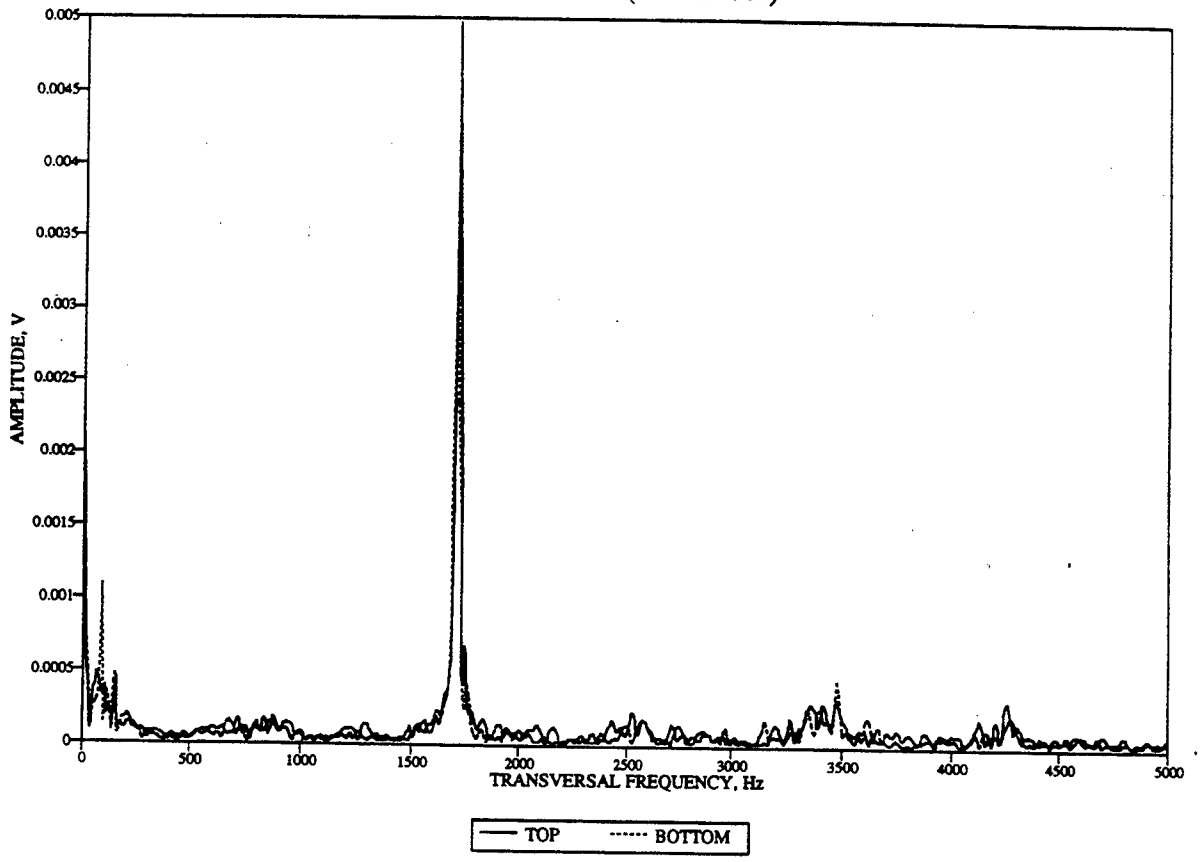


## BEAM M3H(TENSION)

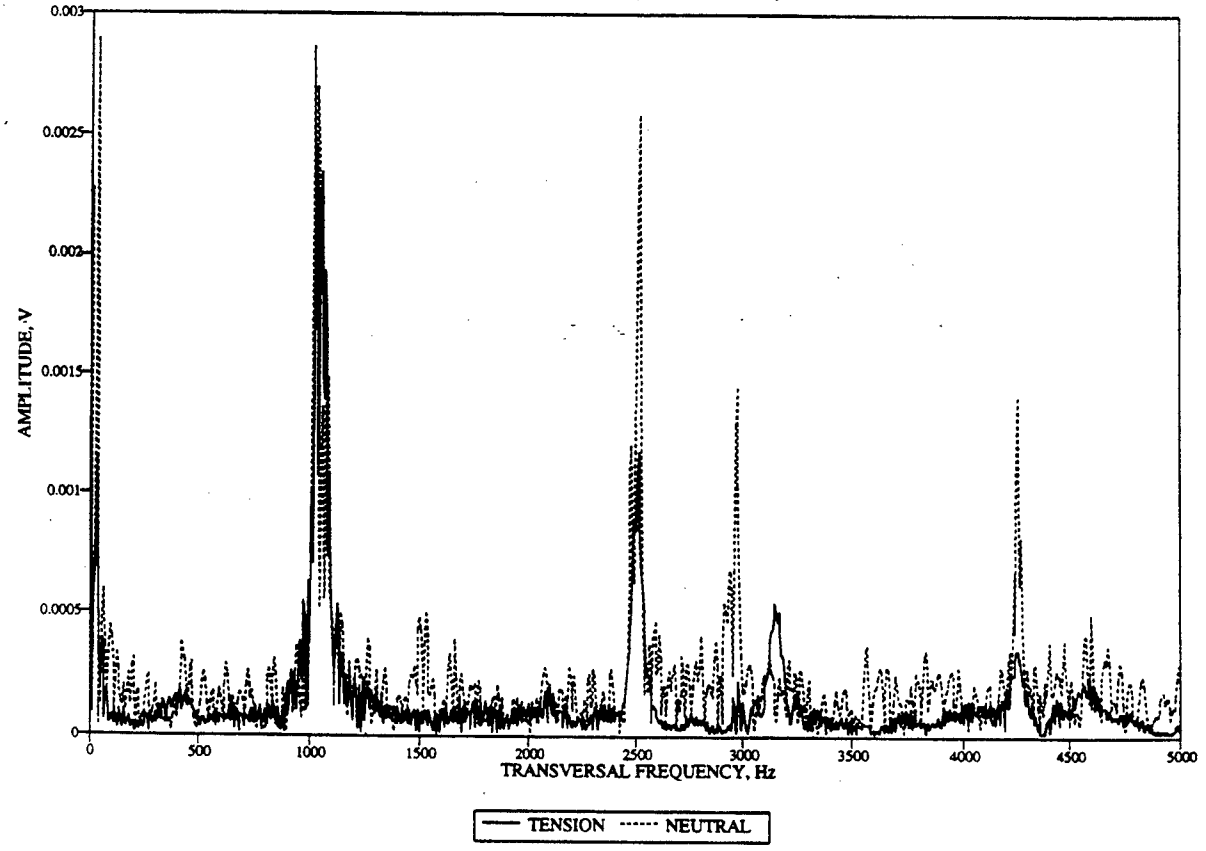

## BEAM M3H(TENSION)

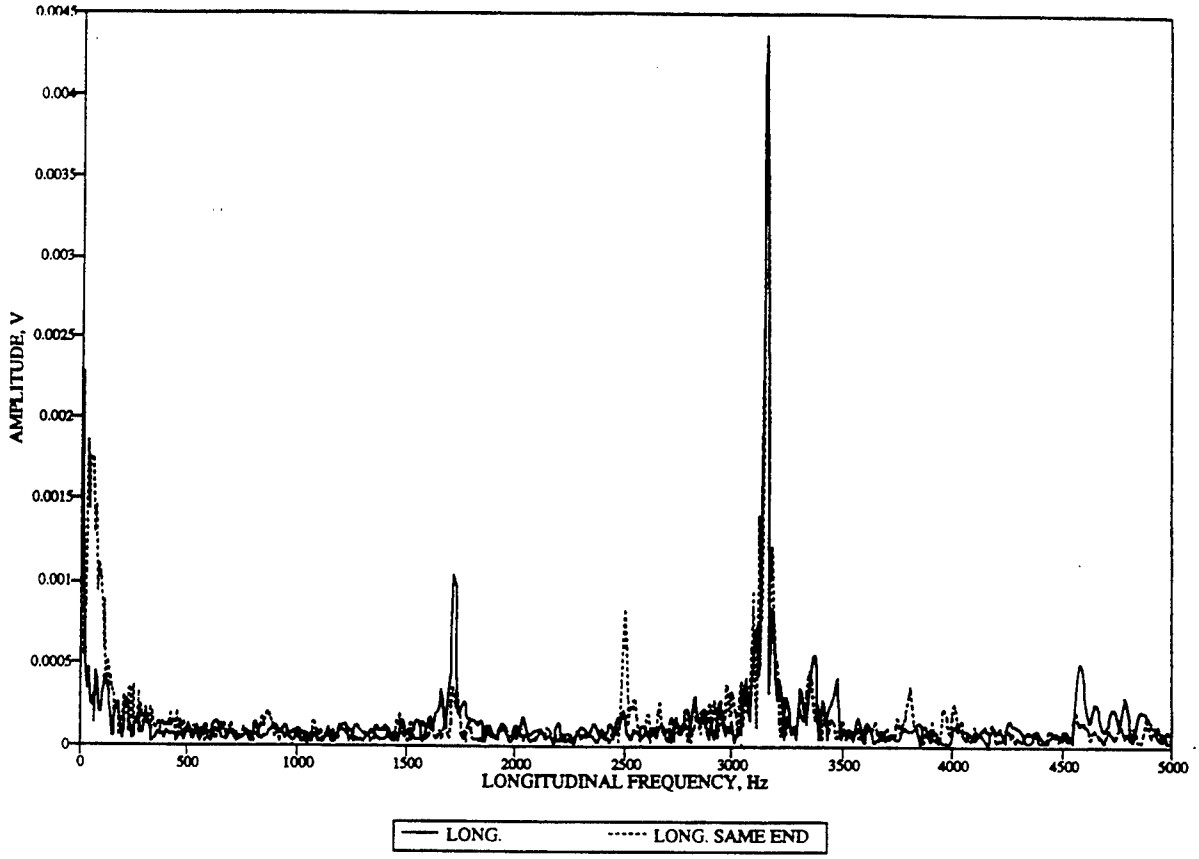


## BEAM M3H(TENSION)

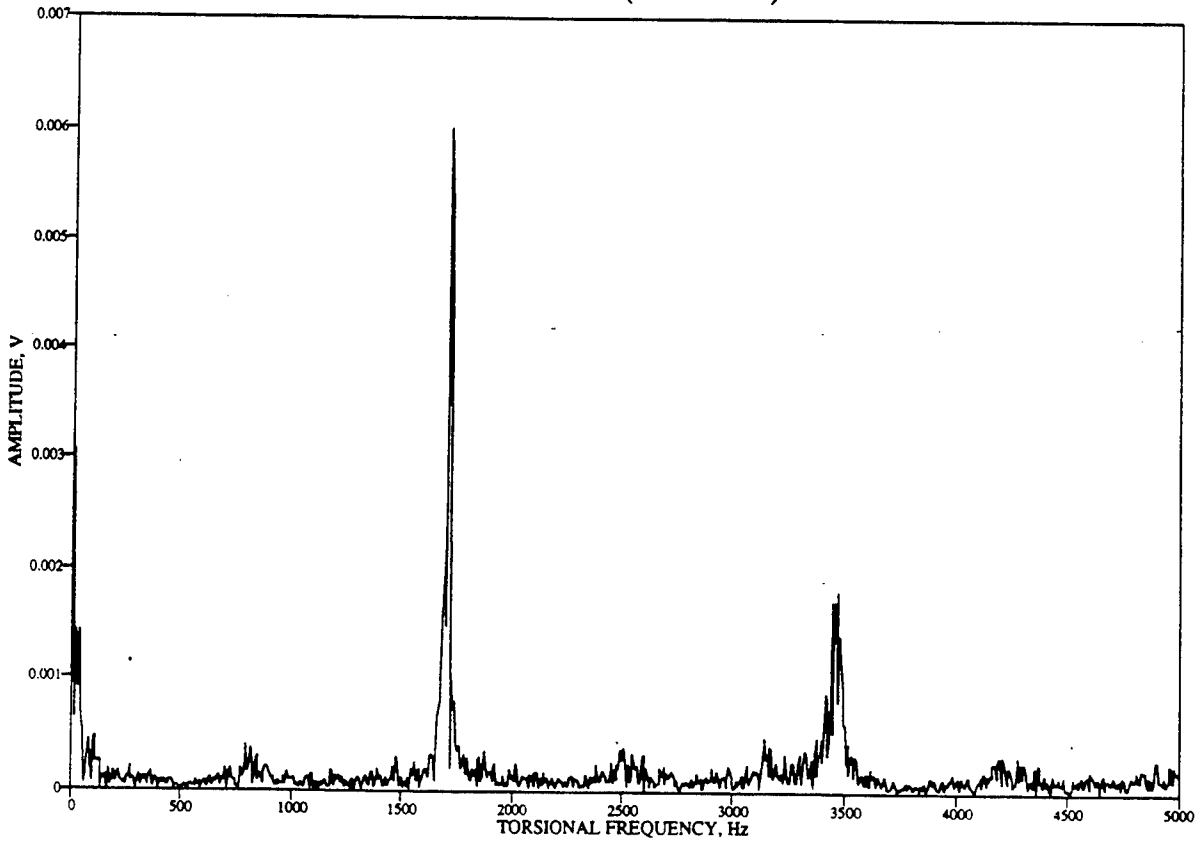

## BEAM N1H (COMPRESSION)

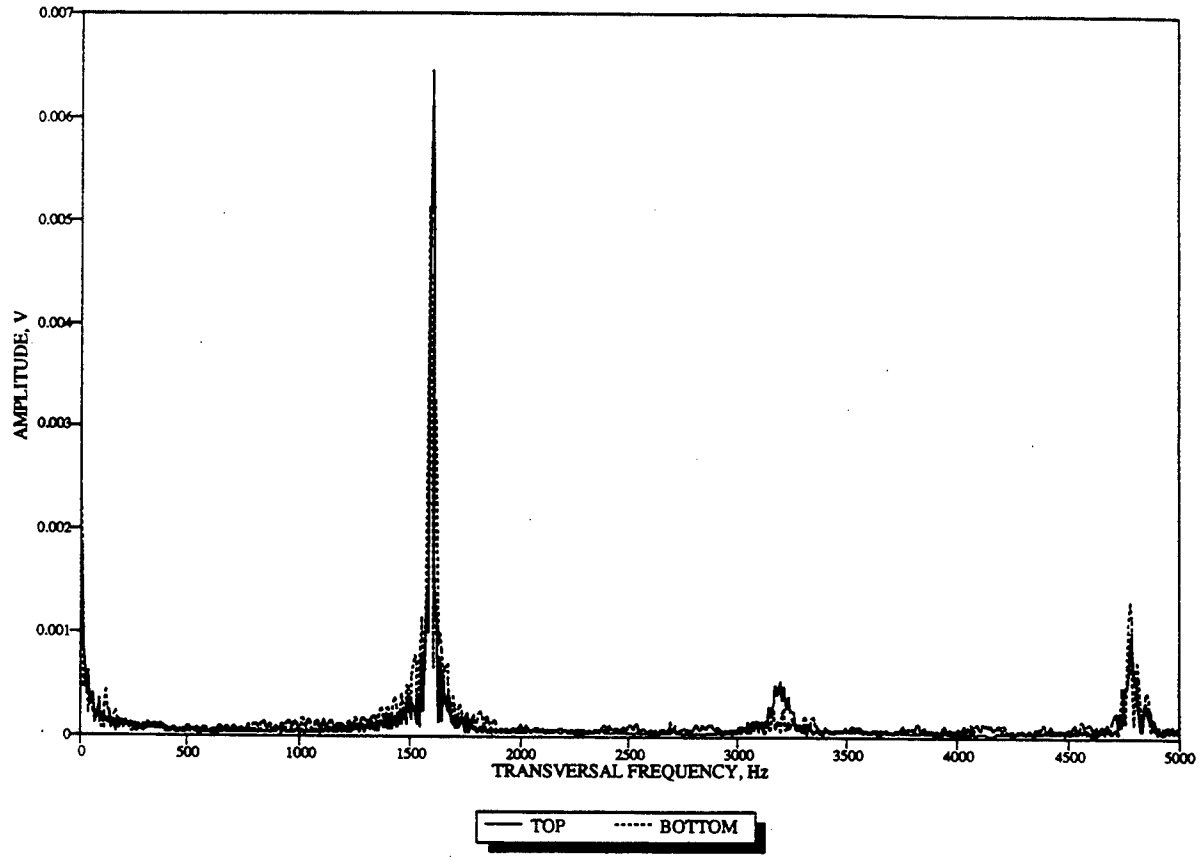


## BEAM N1H (COMPRESSION)

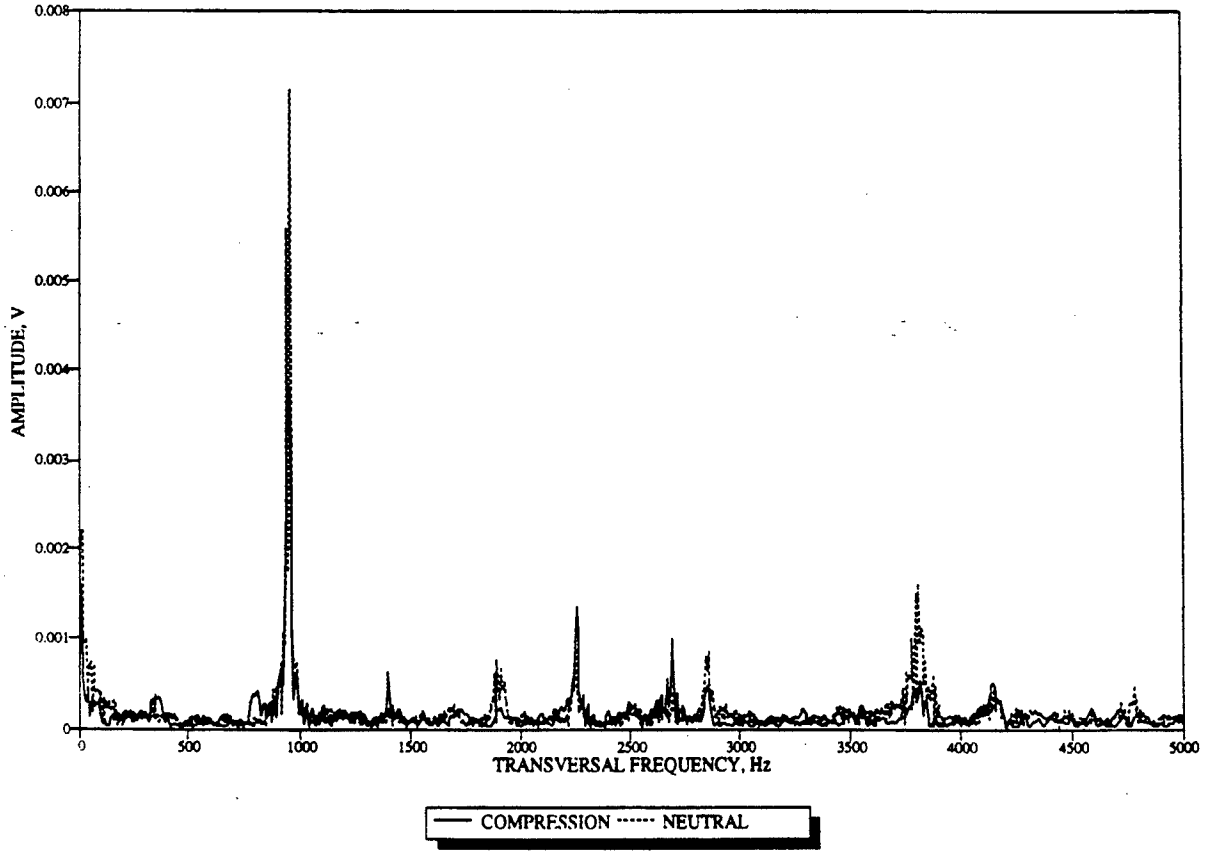

## BEAM N1H (COMPRESSION)

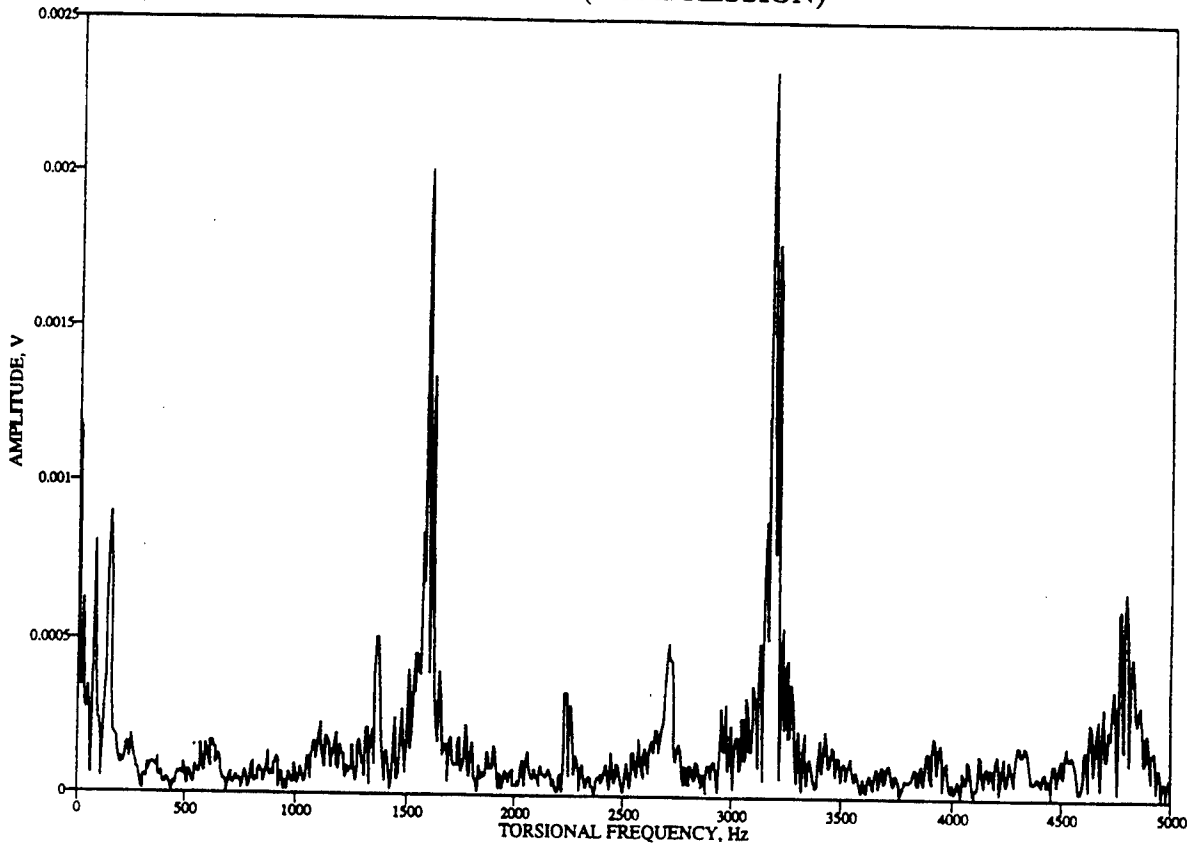


## BEAM N1H (COMPRESSION)

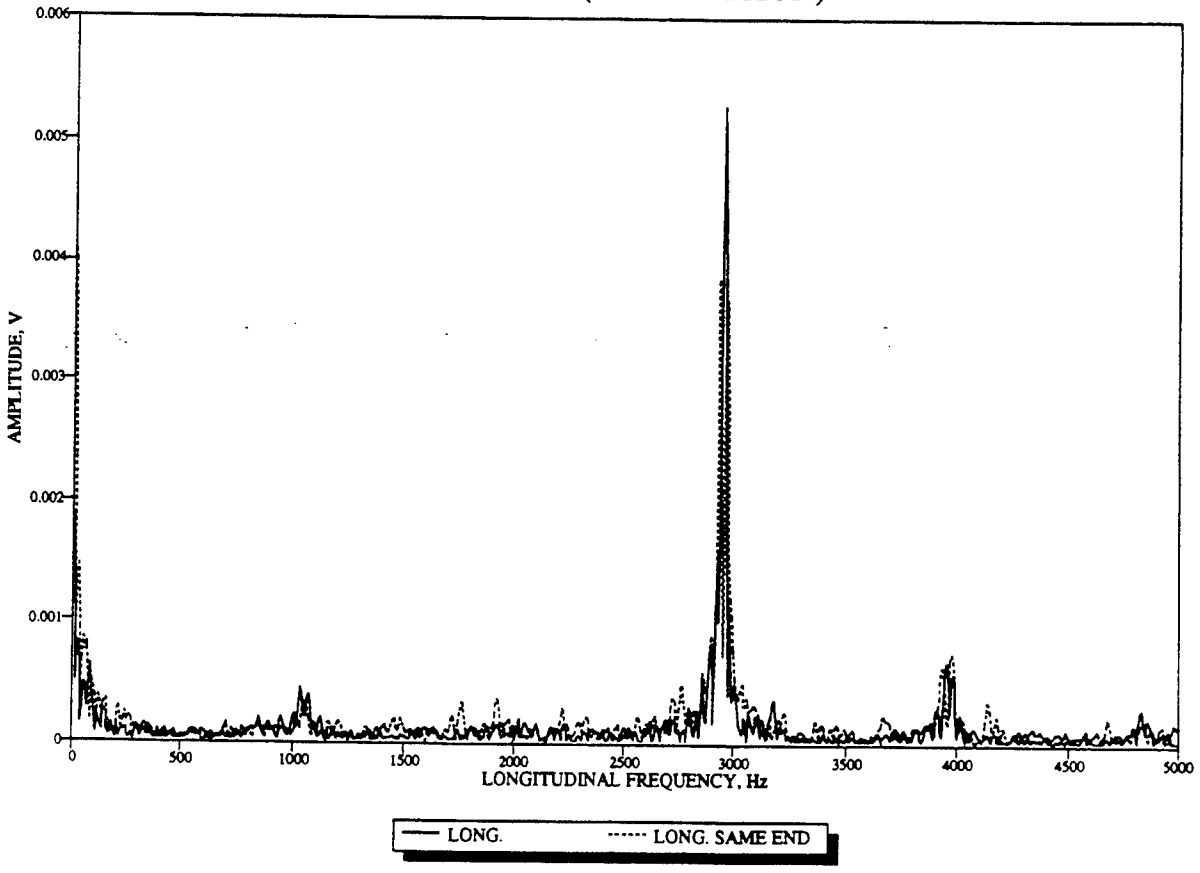

## BEAM N1H (TENSION)

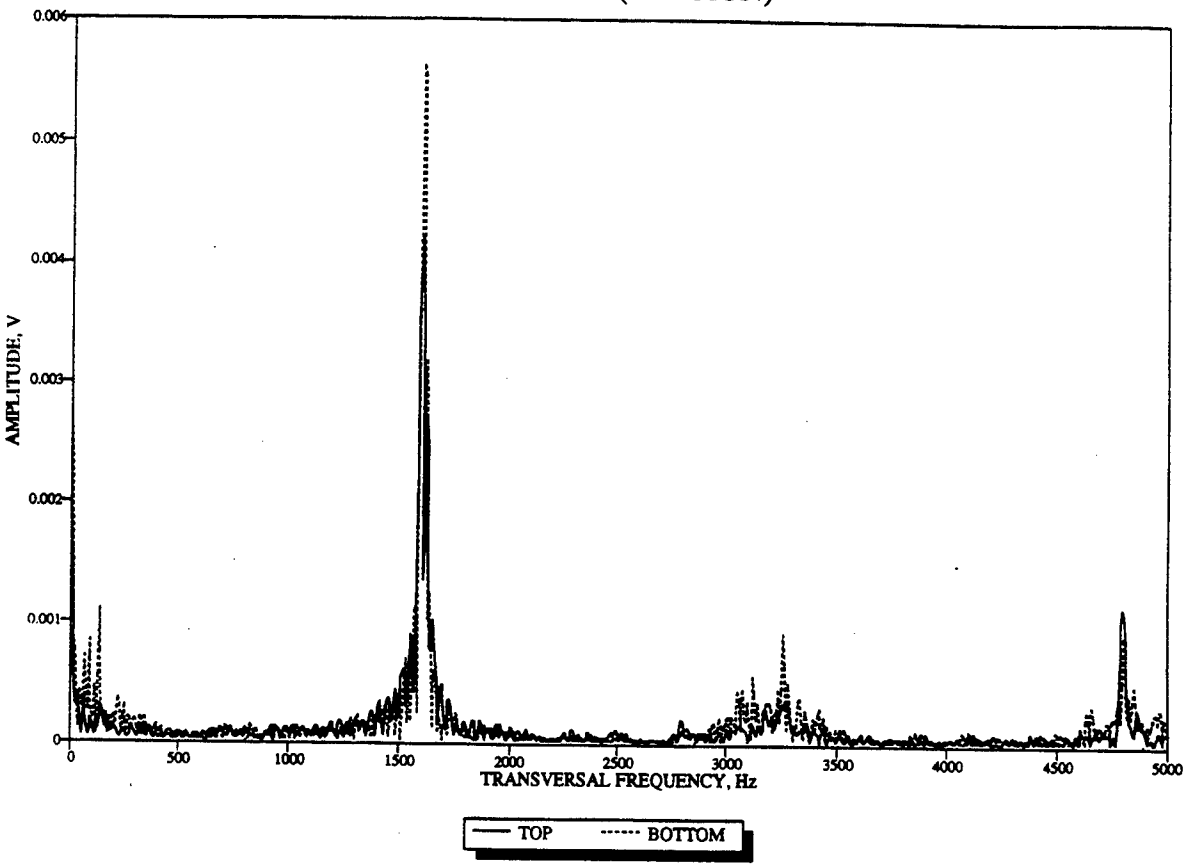


## BEAM N1H (TENSION)

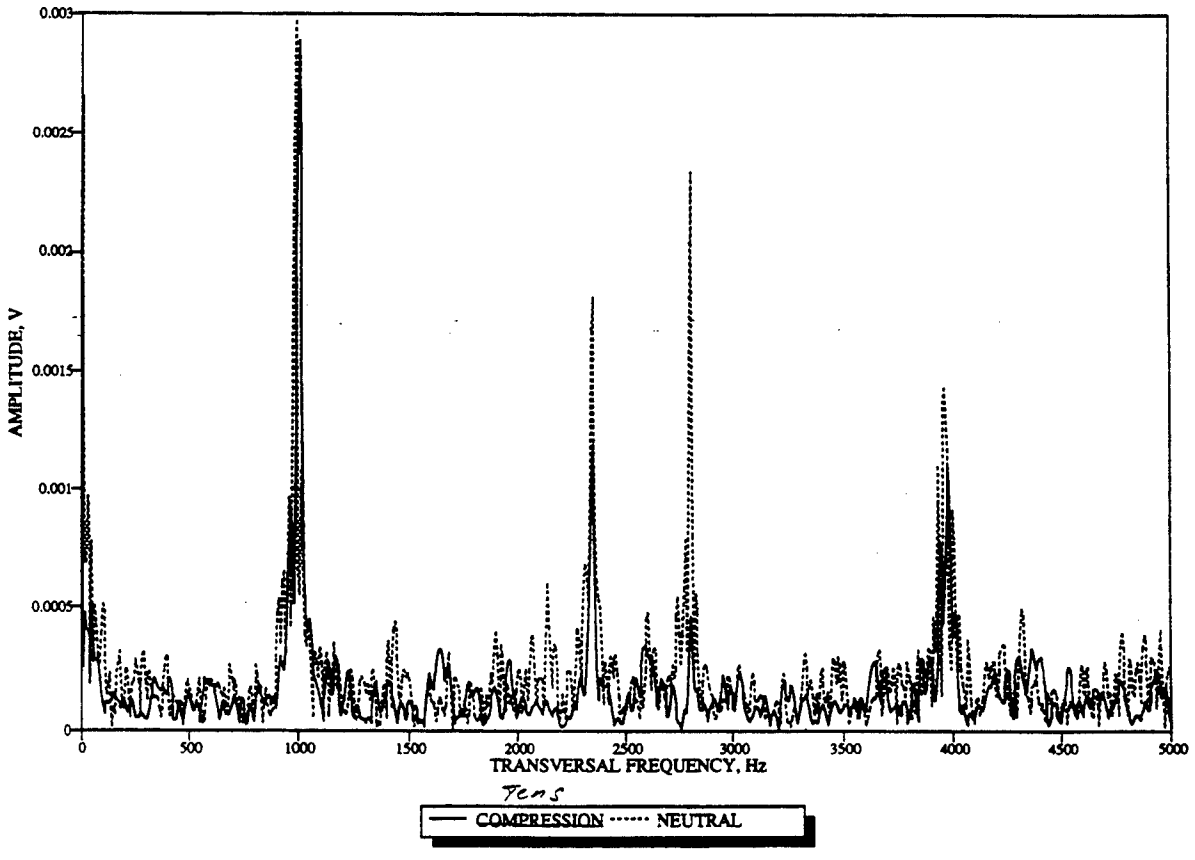

## BEAM N1H (TENSION)

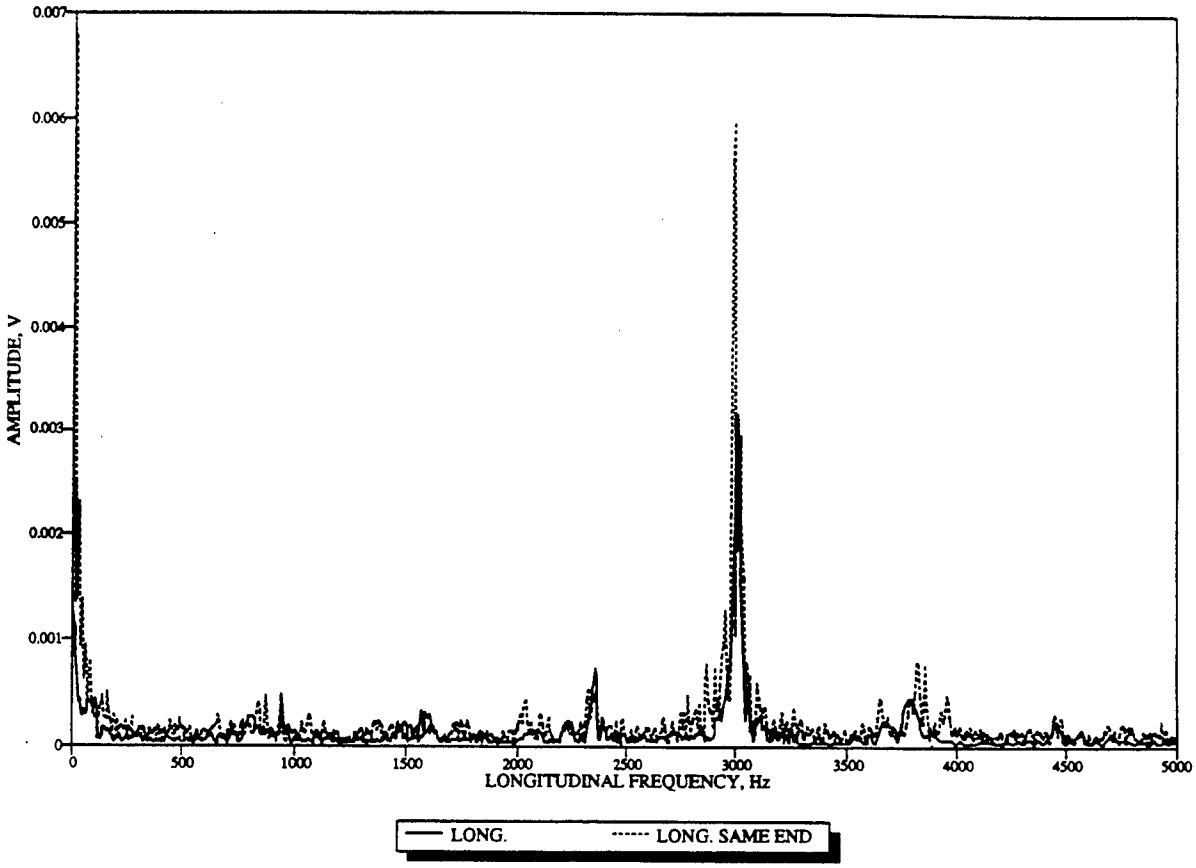


## BEAM N1H (TENSION)

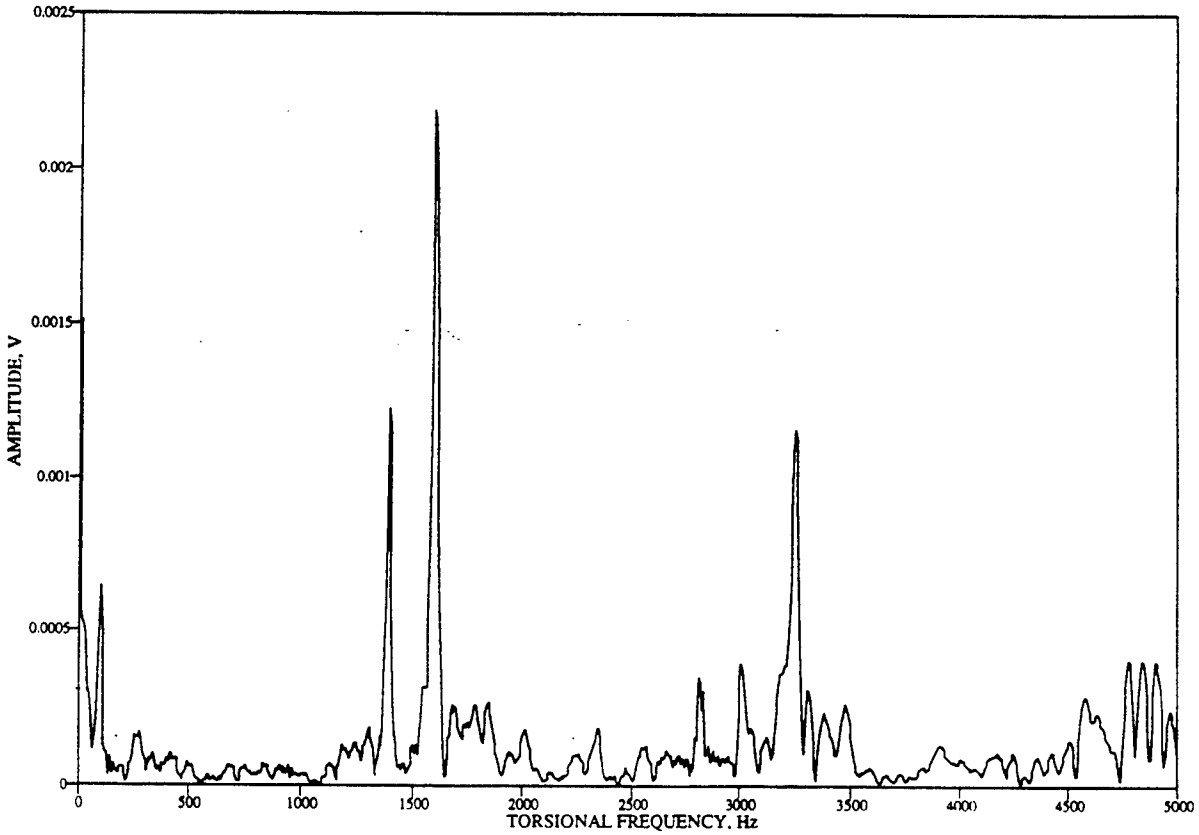

## BEAM N3H (COMPRESSION)

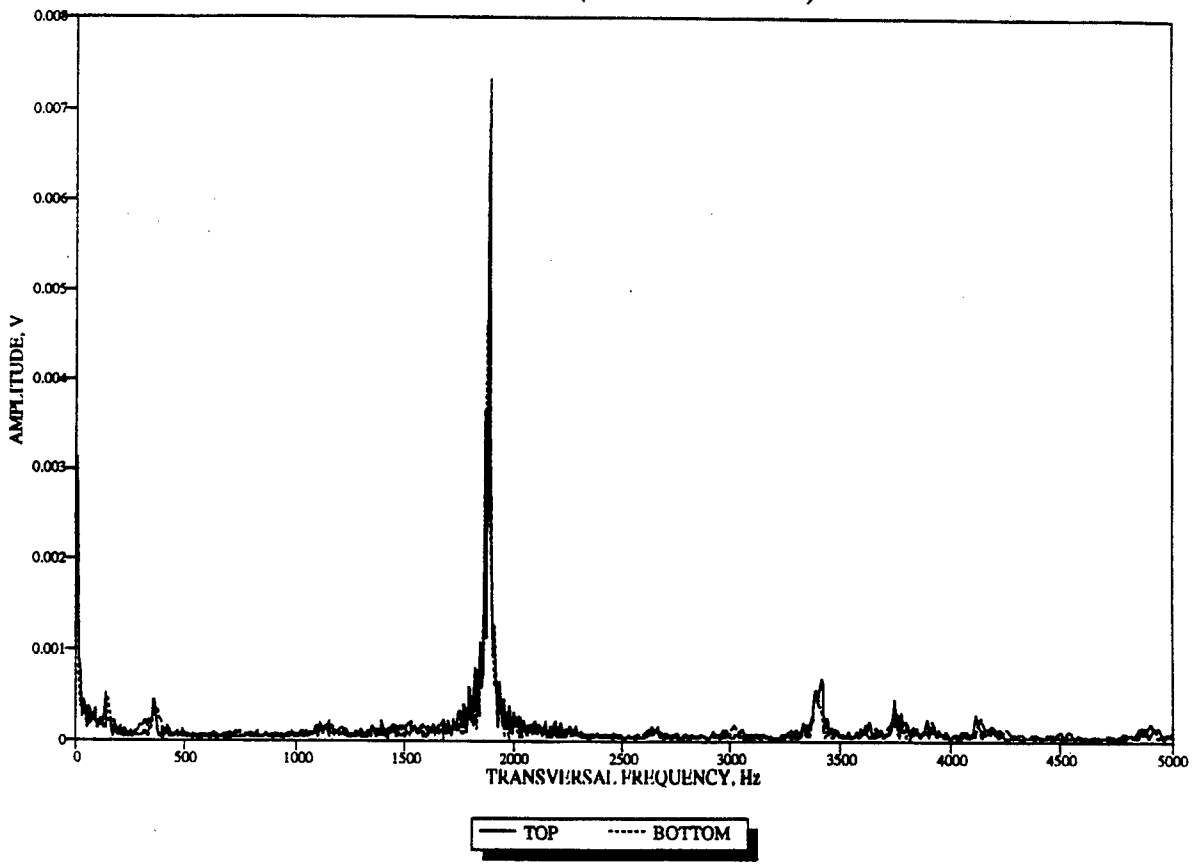


## BEAM N3H (COMPRESSION)

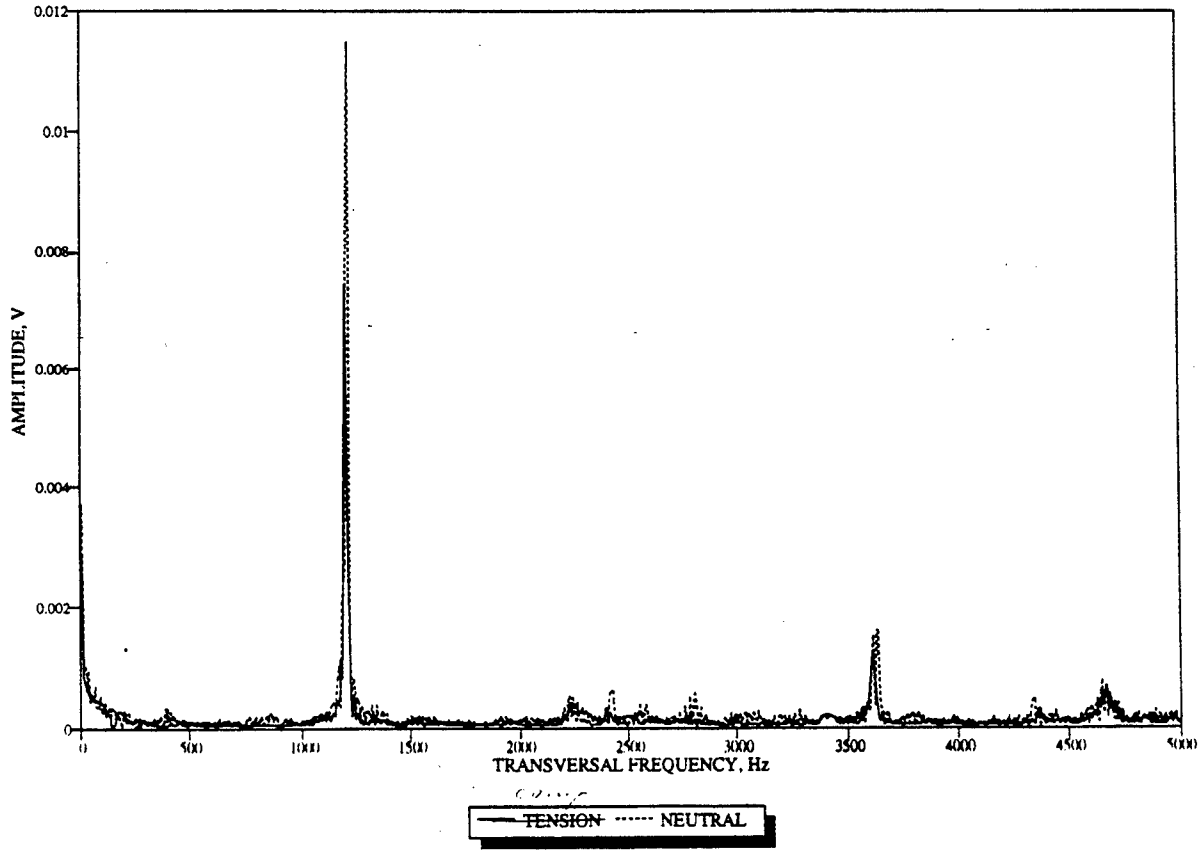

## BEAM N3H (COMPRESSION)

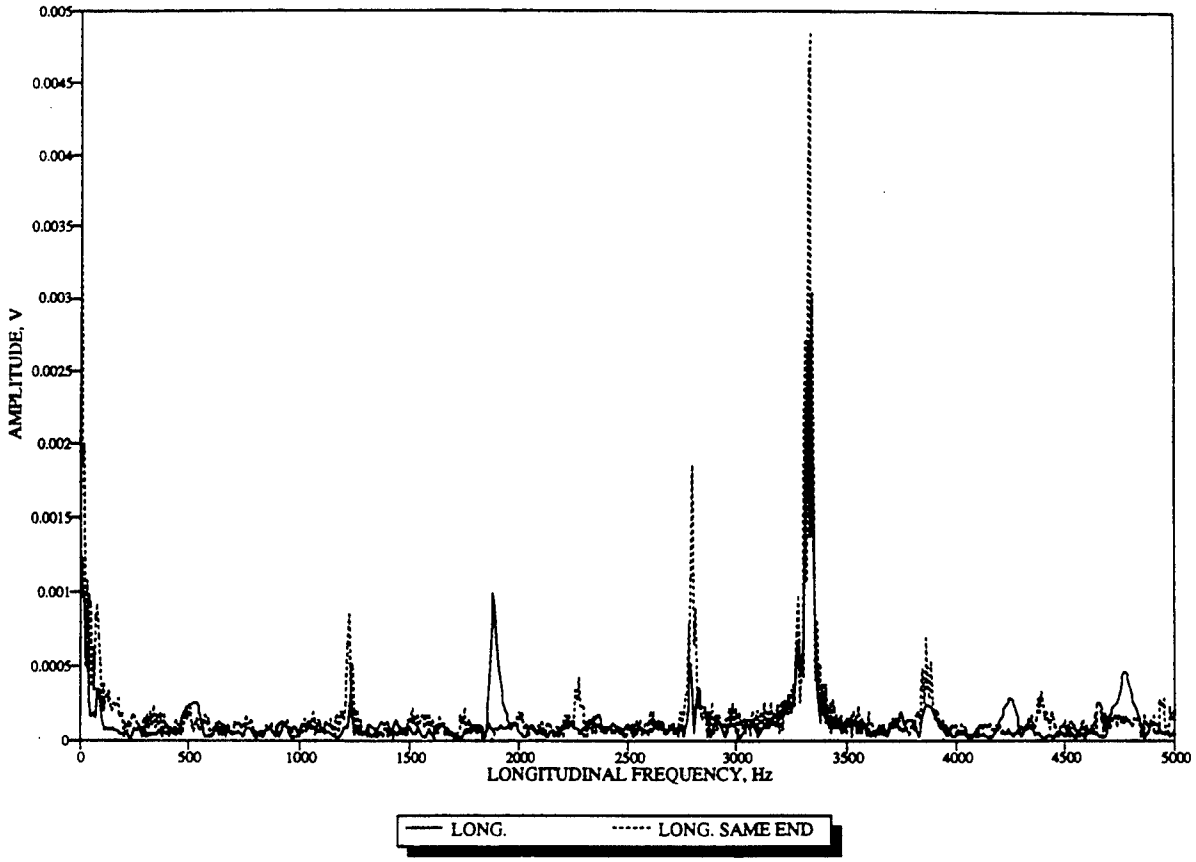


## BEAM N3H (COMPRESSION)

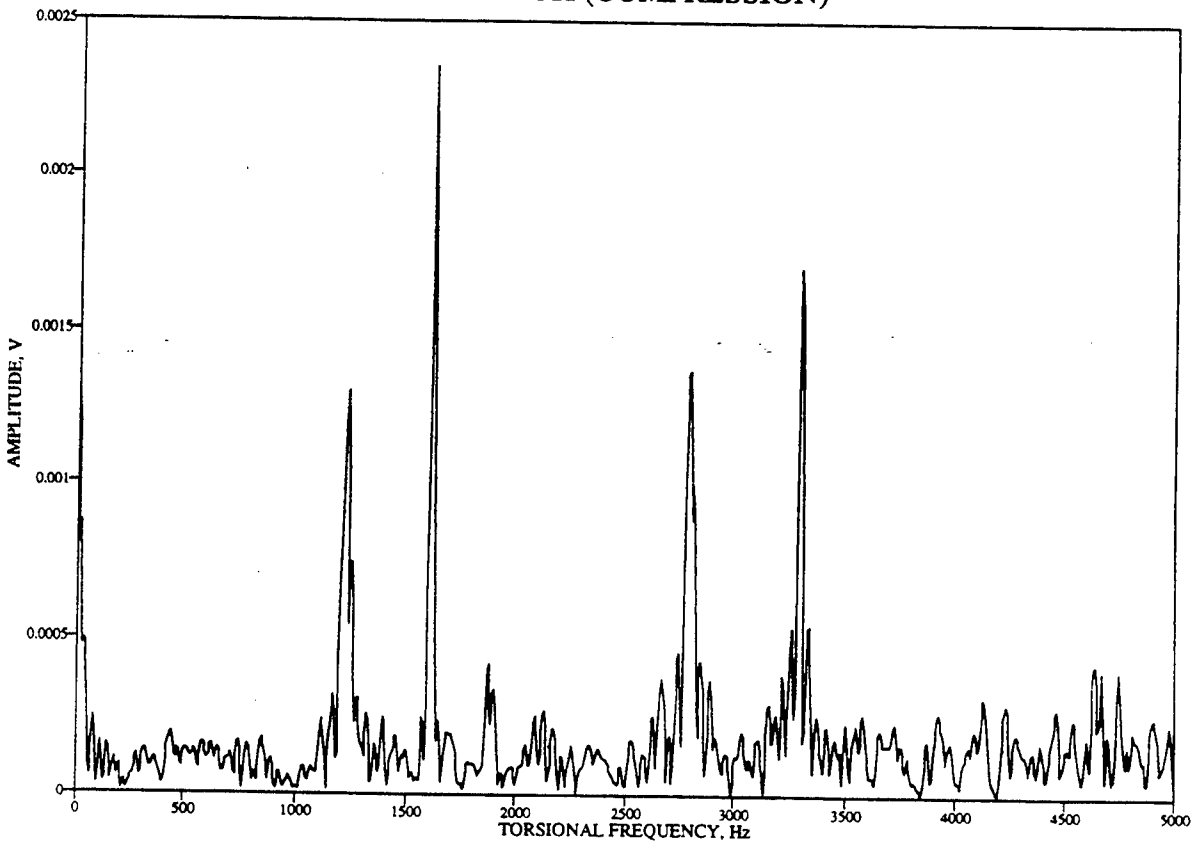

## BEAM N3H (TENSION)

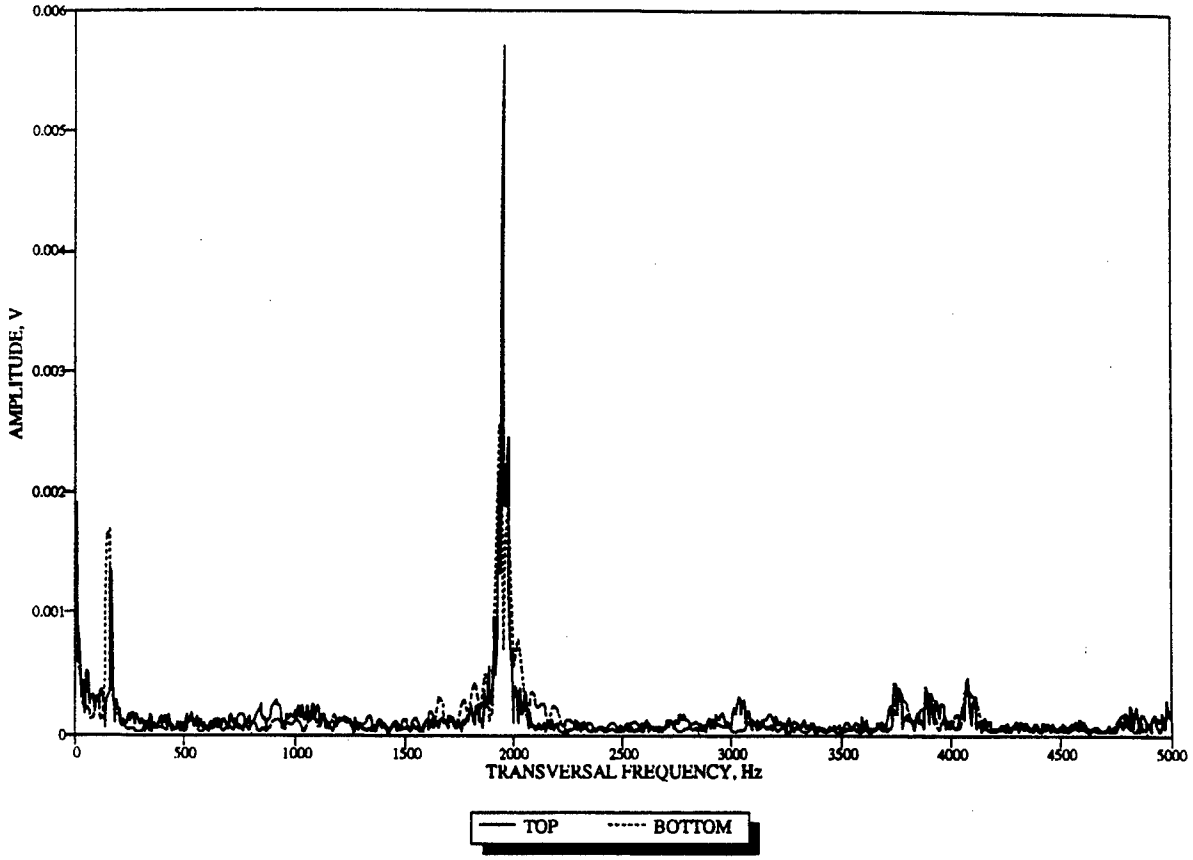


## BEAM N3H (TENSION)

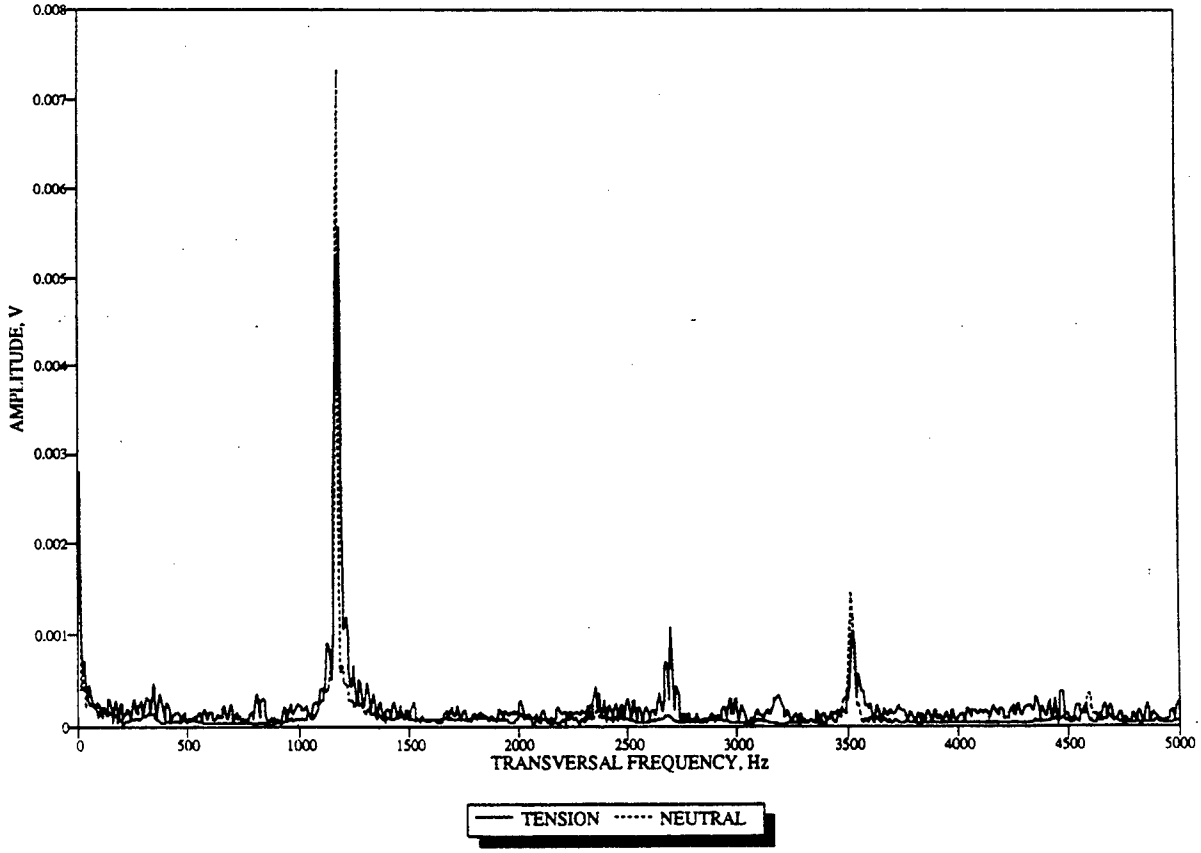

## BEAM N3H (TENSION)

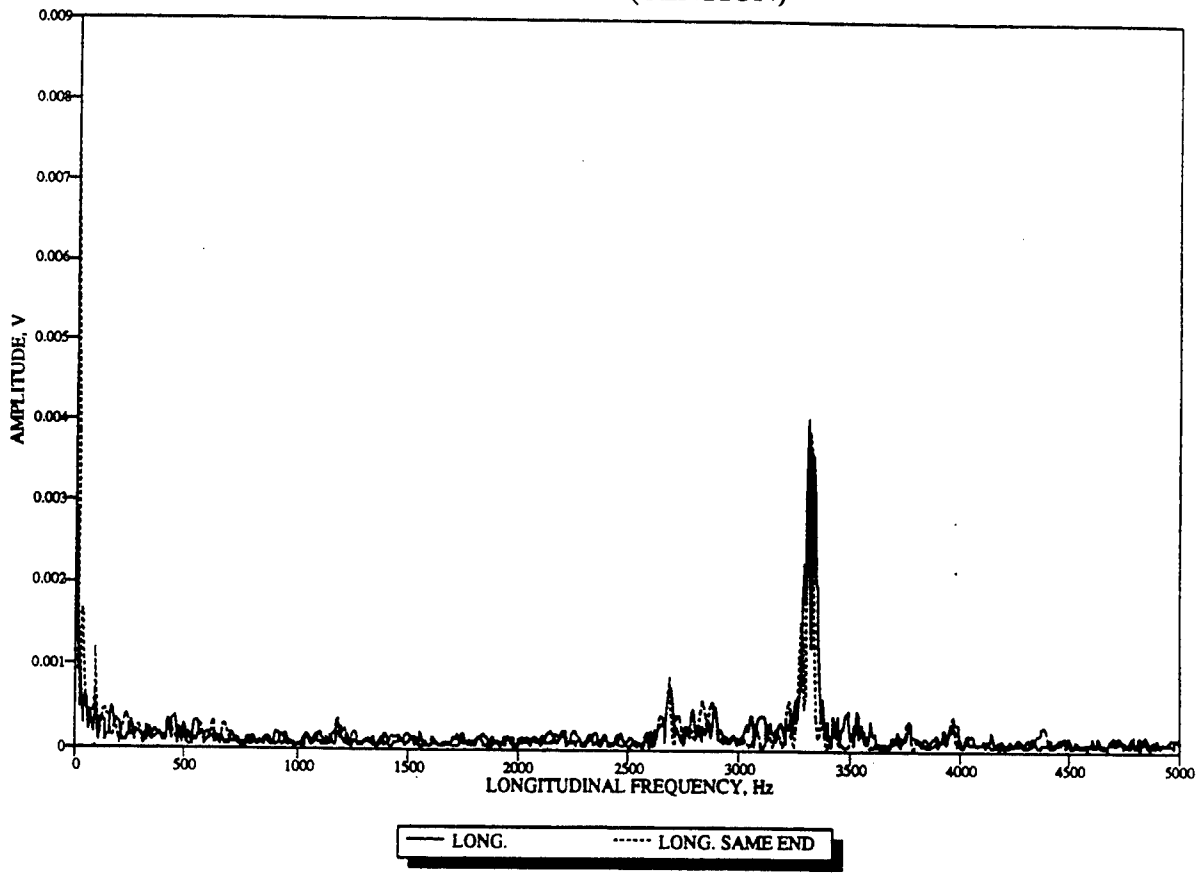


## BEAM N3H (TENSION)

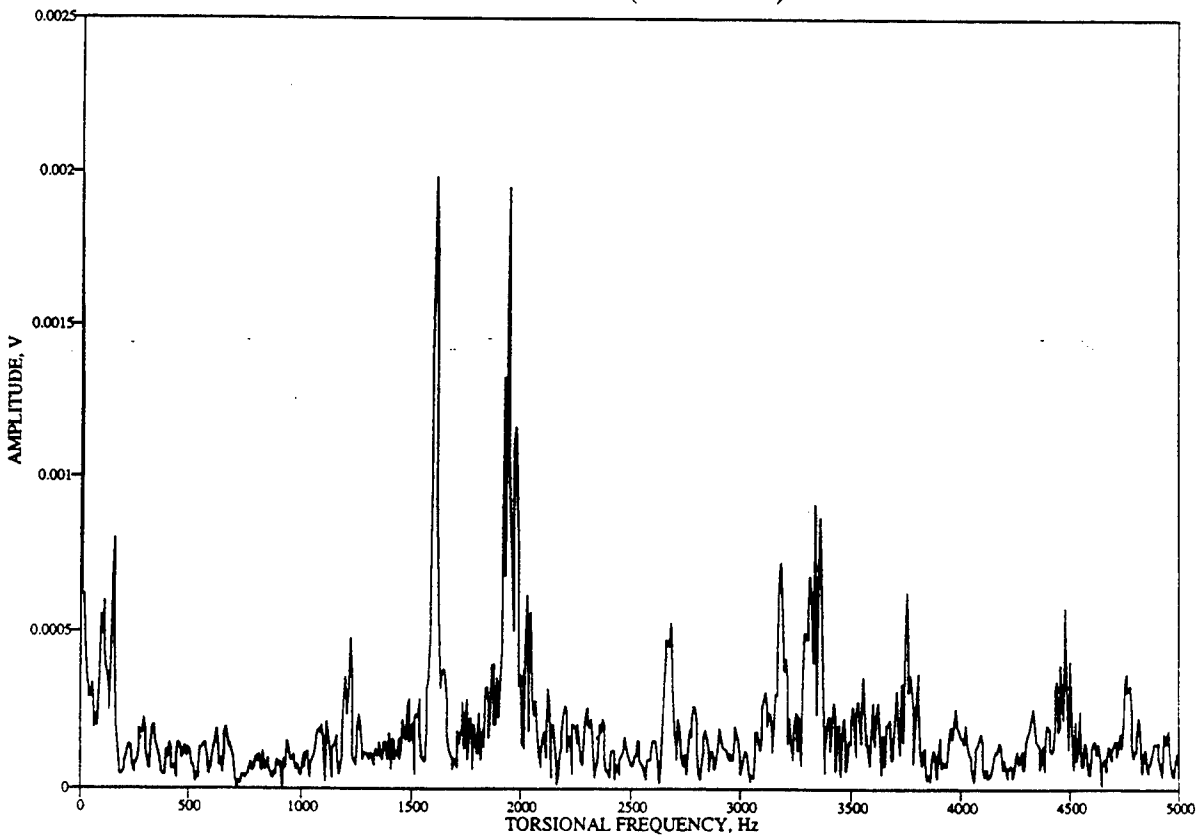

## BEAM O1 (COMPRESSION)

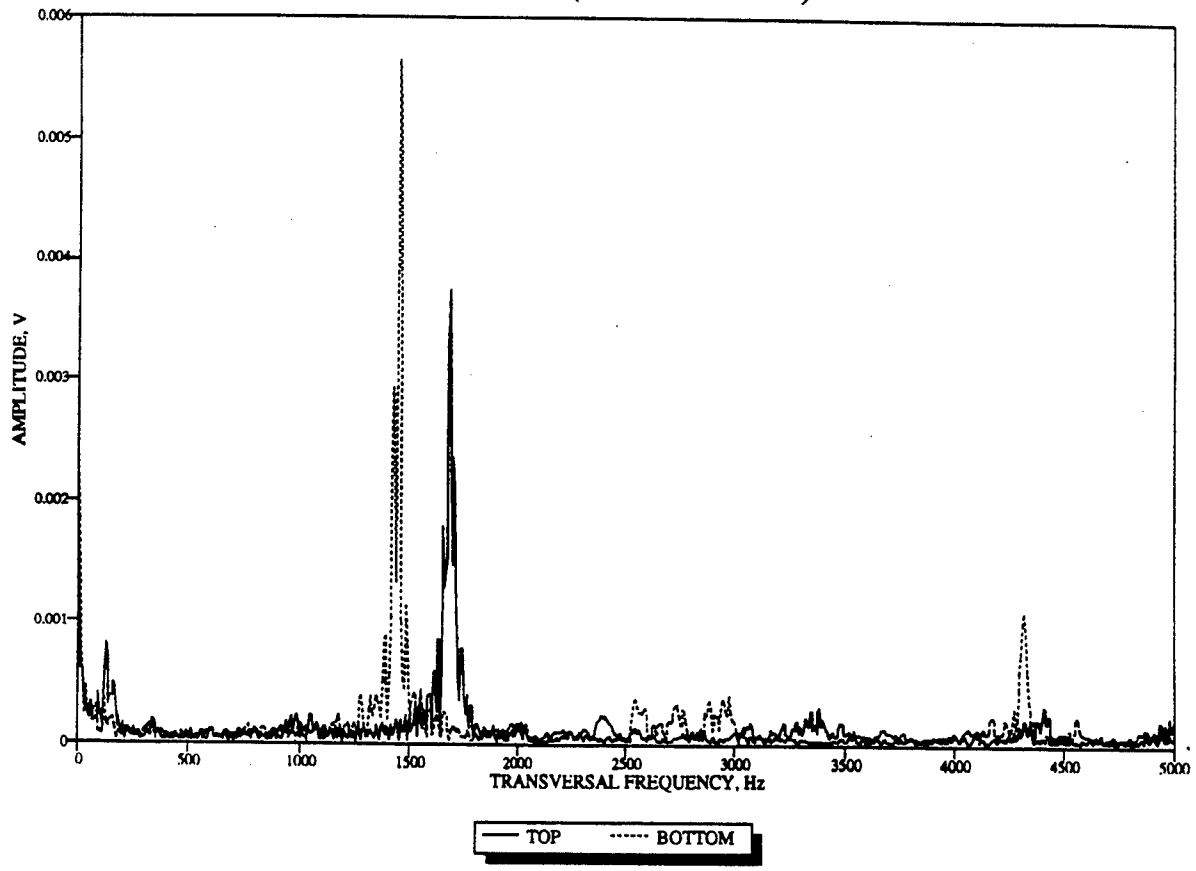


## BEAM O1 (COMPRESSION)

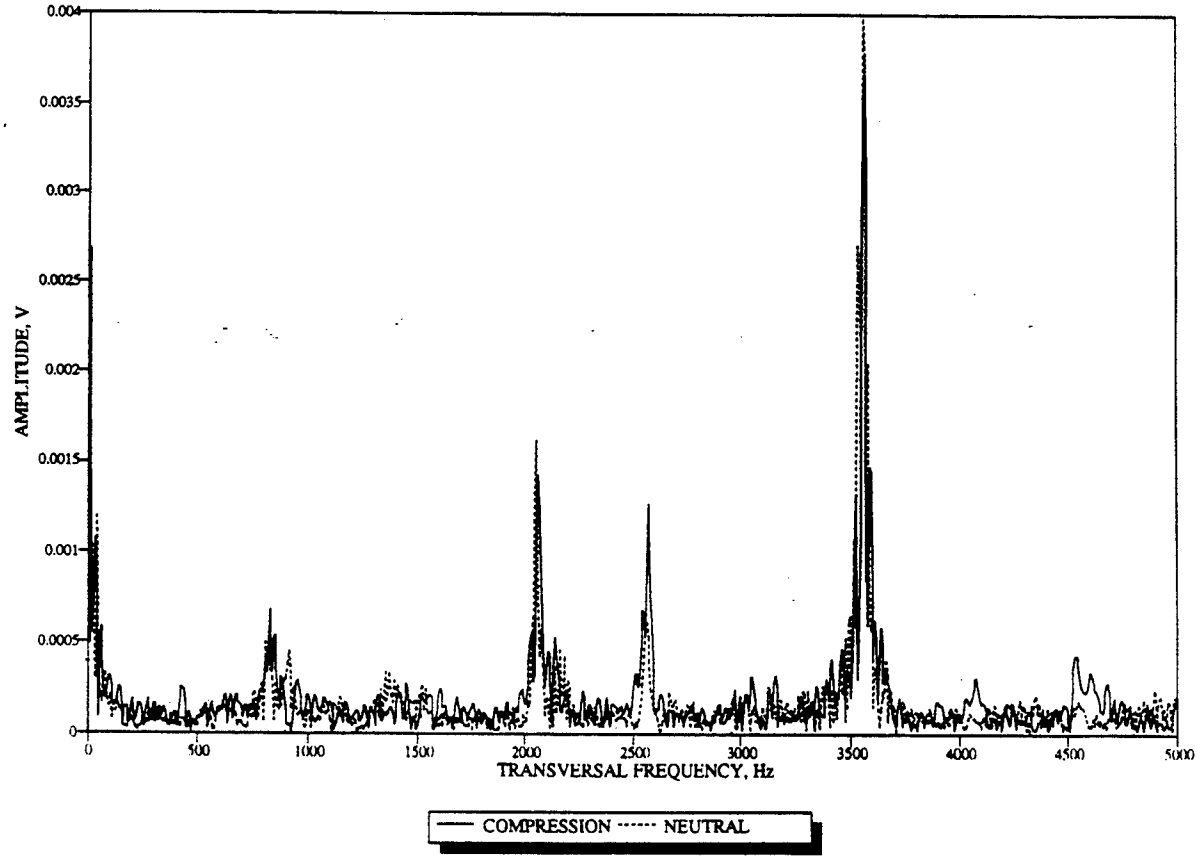

## BEAM O1 (COMPRESSION)

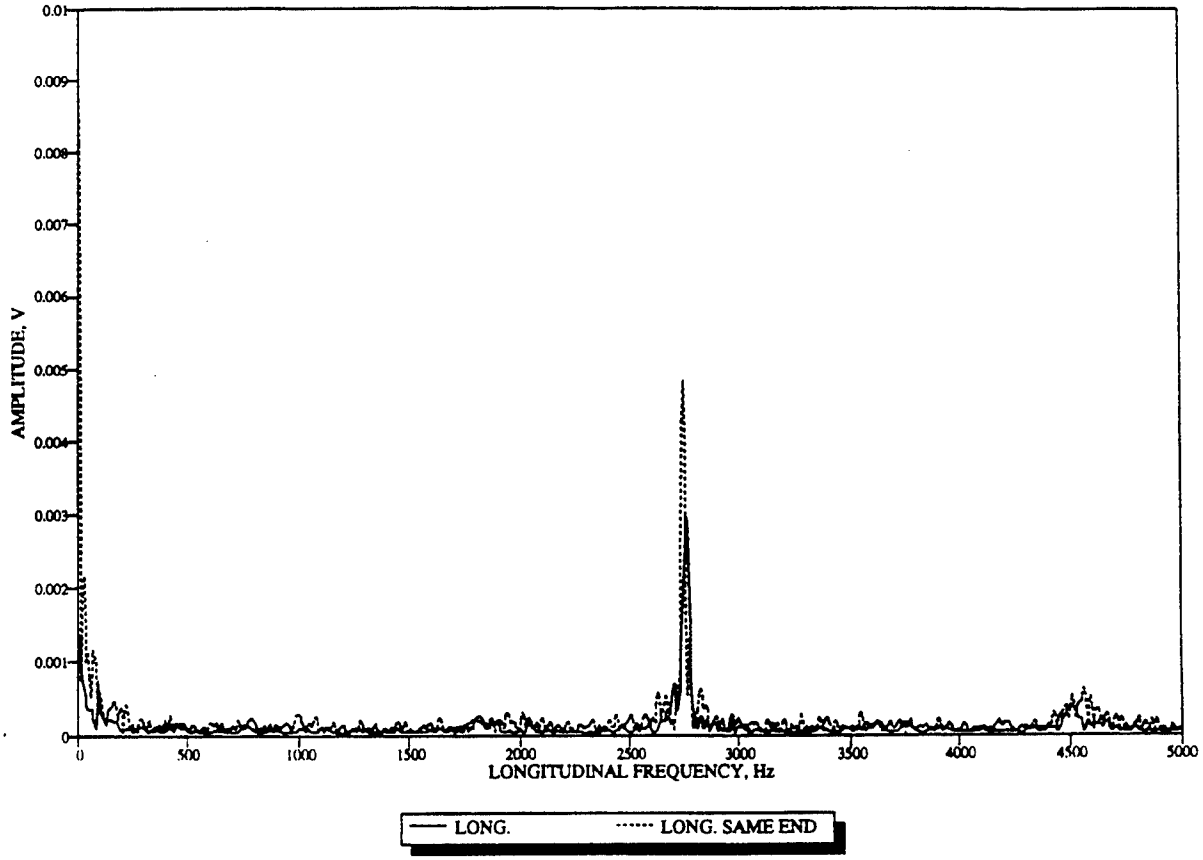


## BEAM O1 (COMPRESSION)

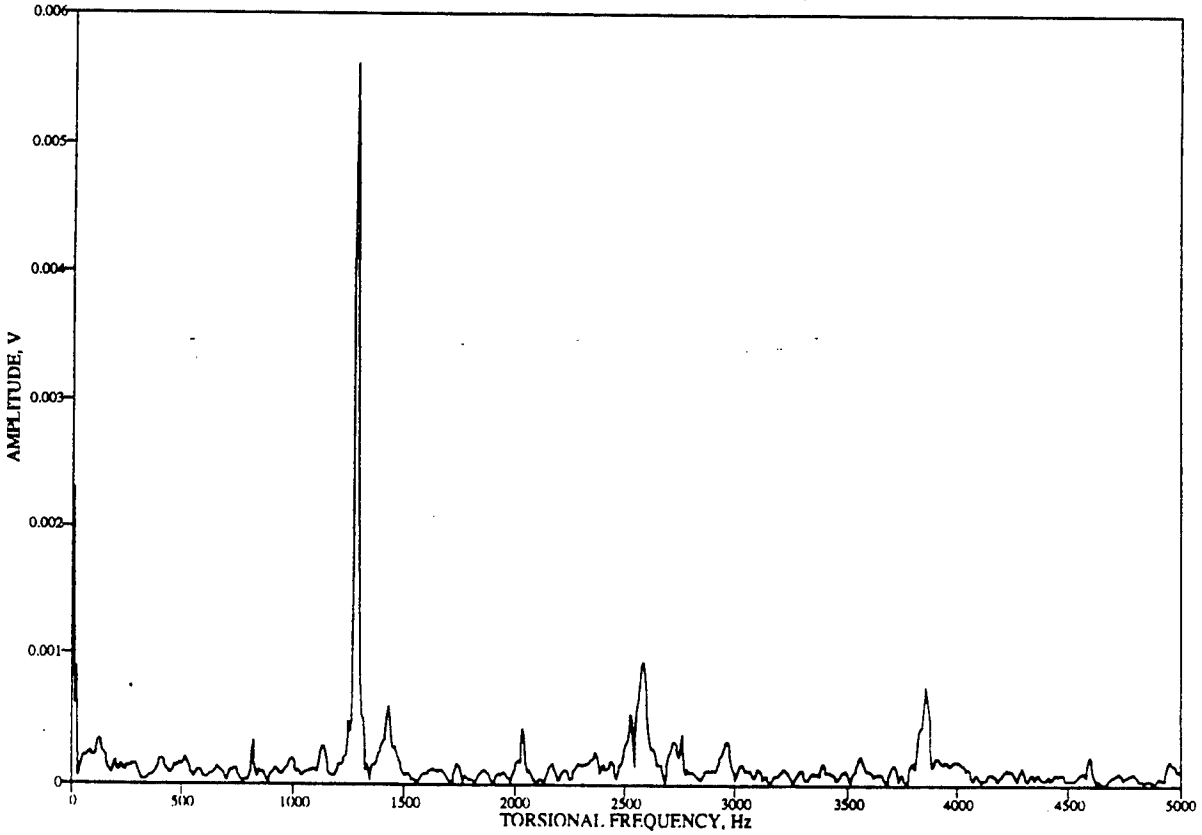

## BEAM O1 (TENSION)

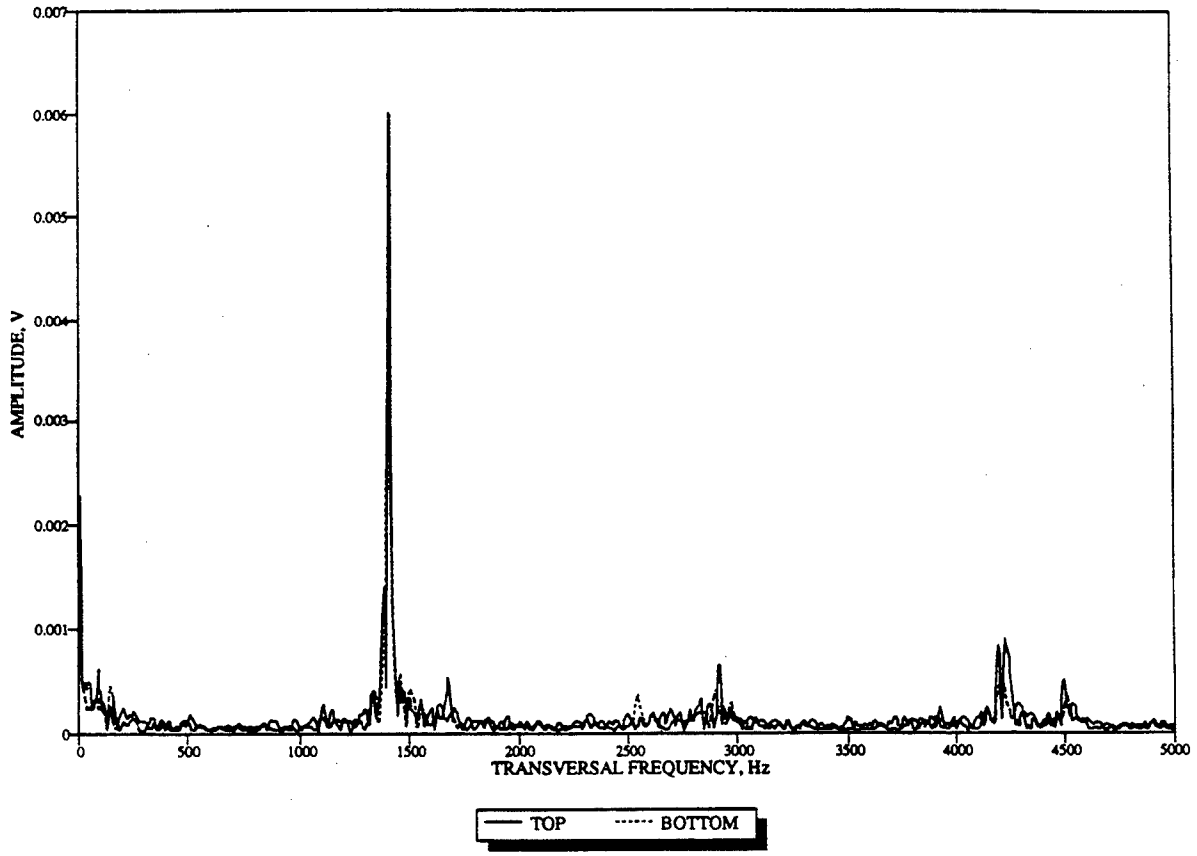


## BEAM O1 (TENSION)

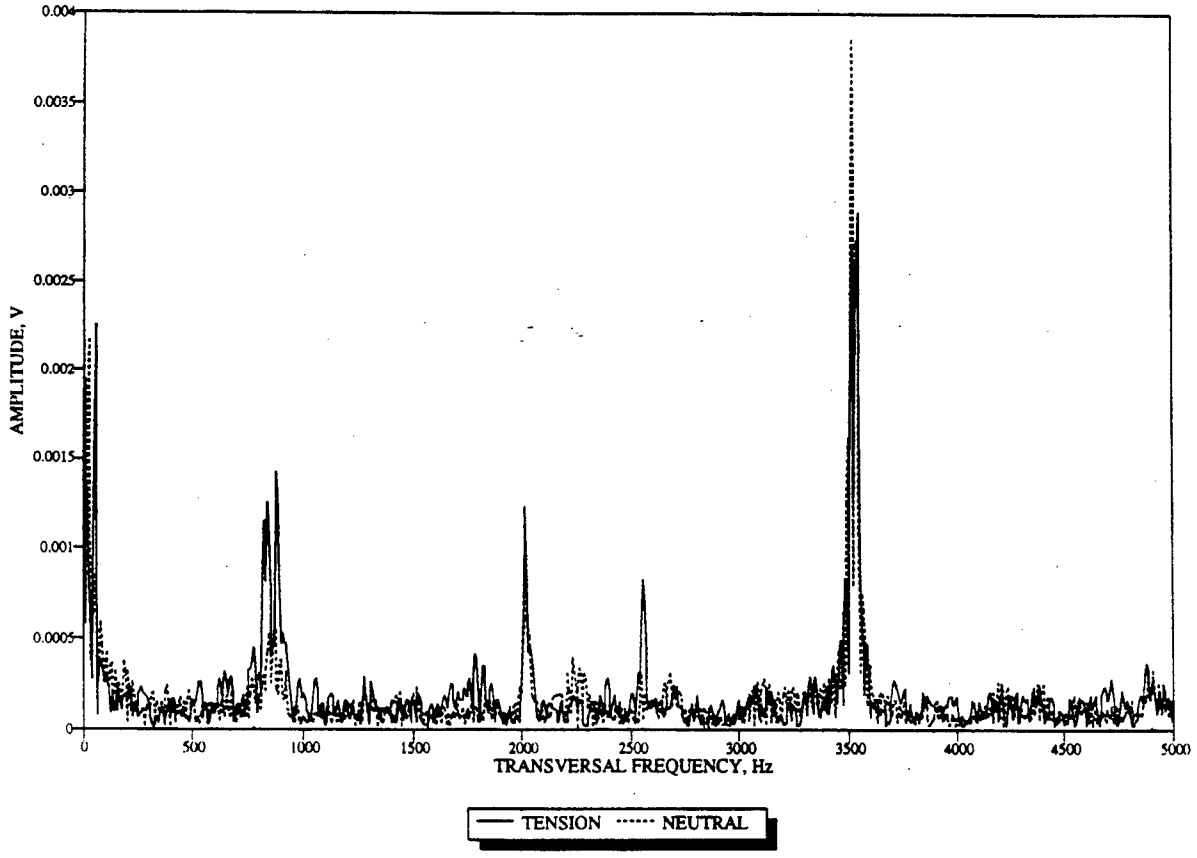

## BEAM O1 (TENSION)

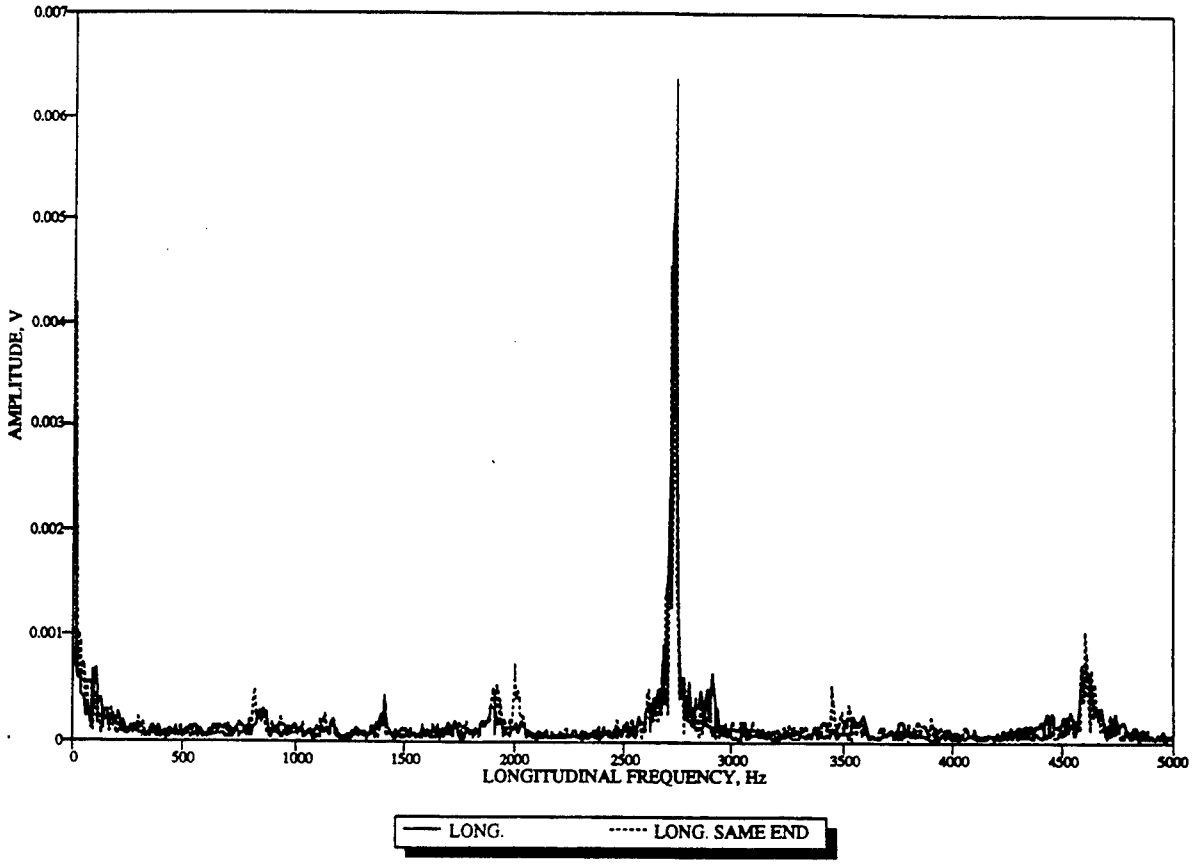


## BEAM O1 (TENSION)

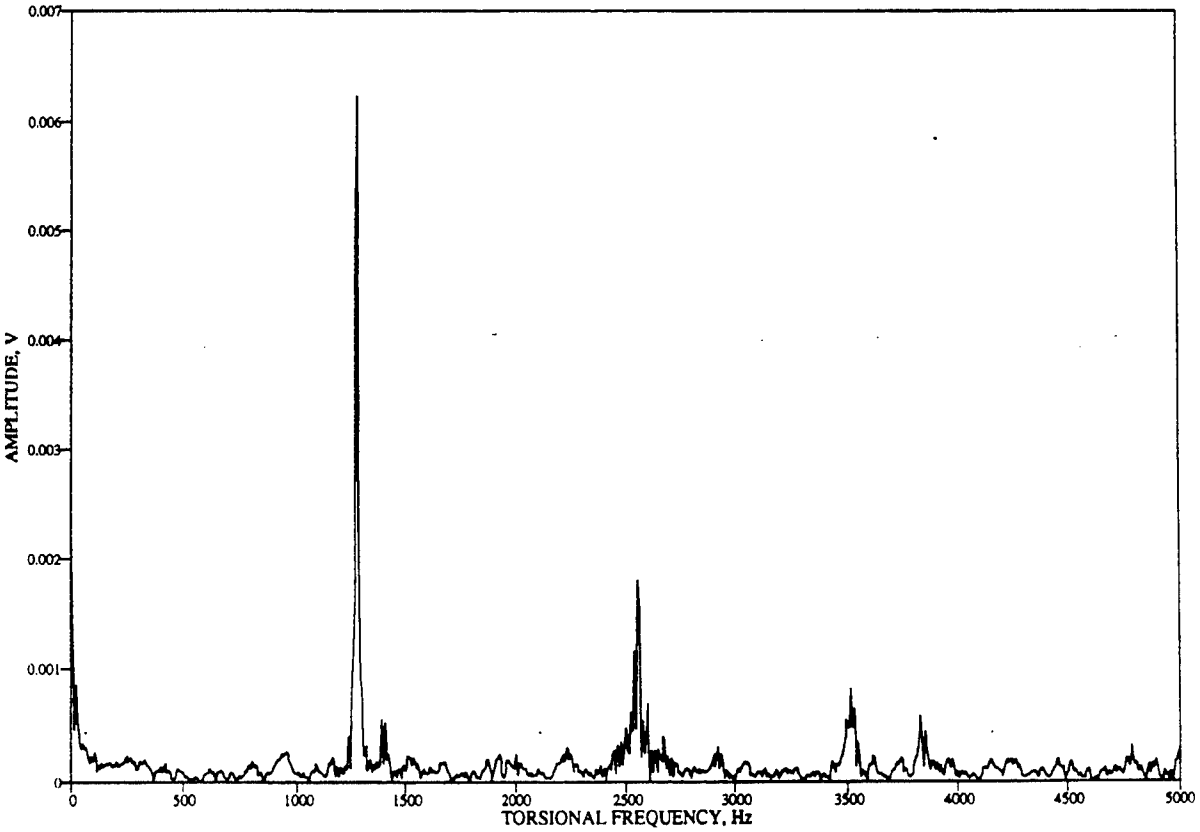

## BEAM O3H (COMPRESSION)

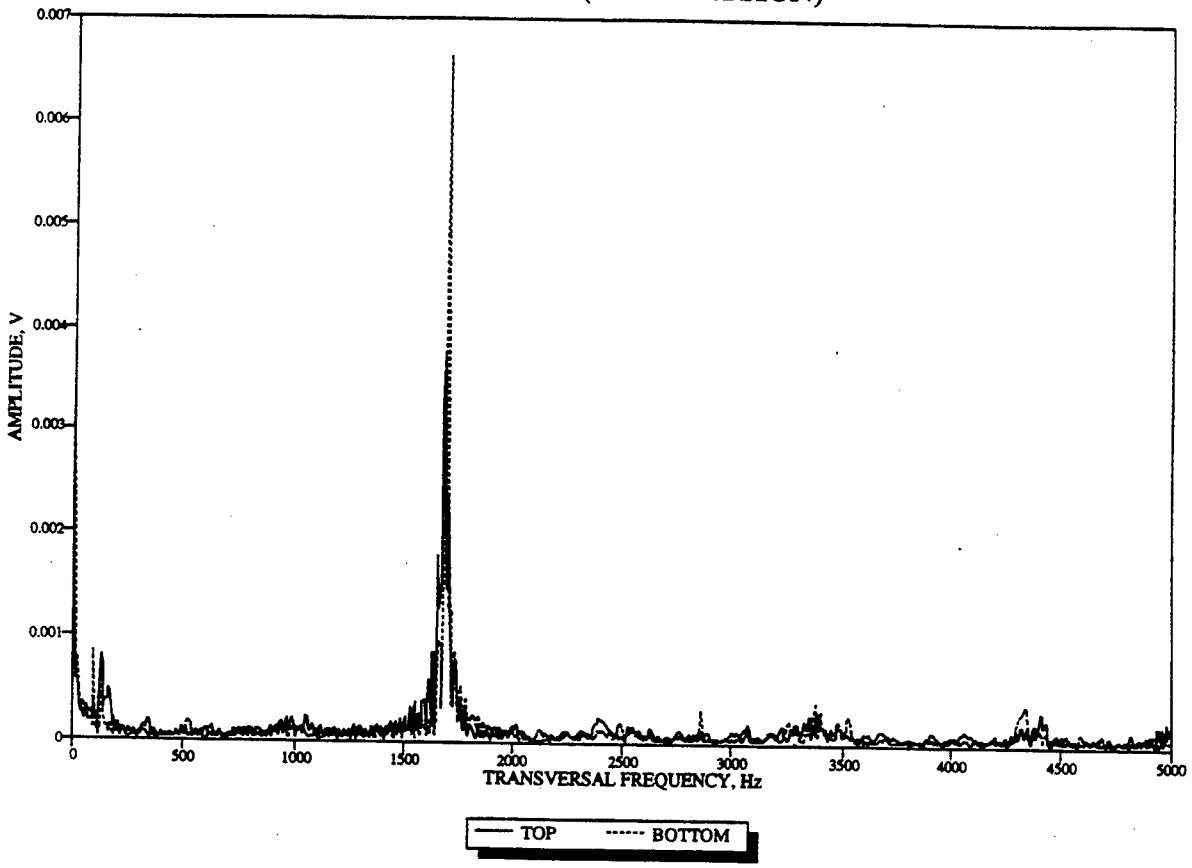


## BEAM O3H (COMPRESSION)

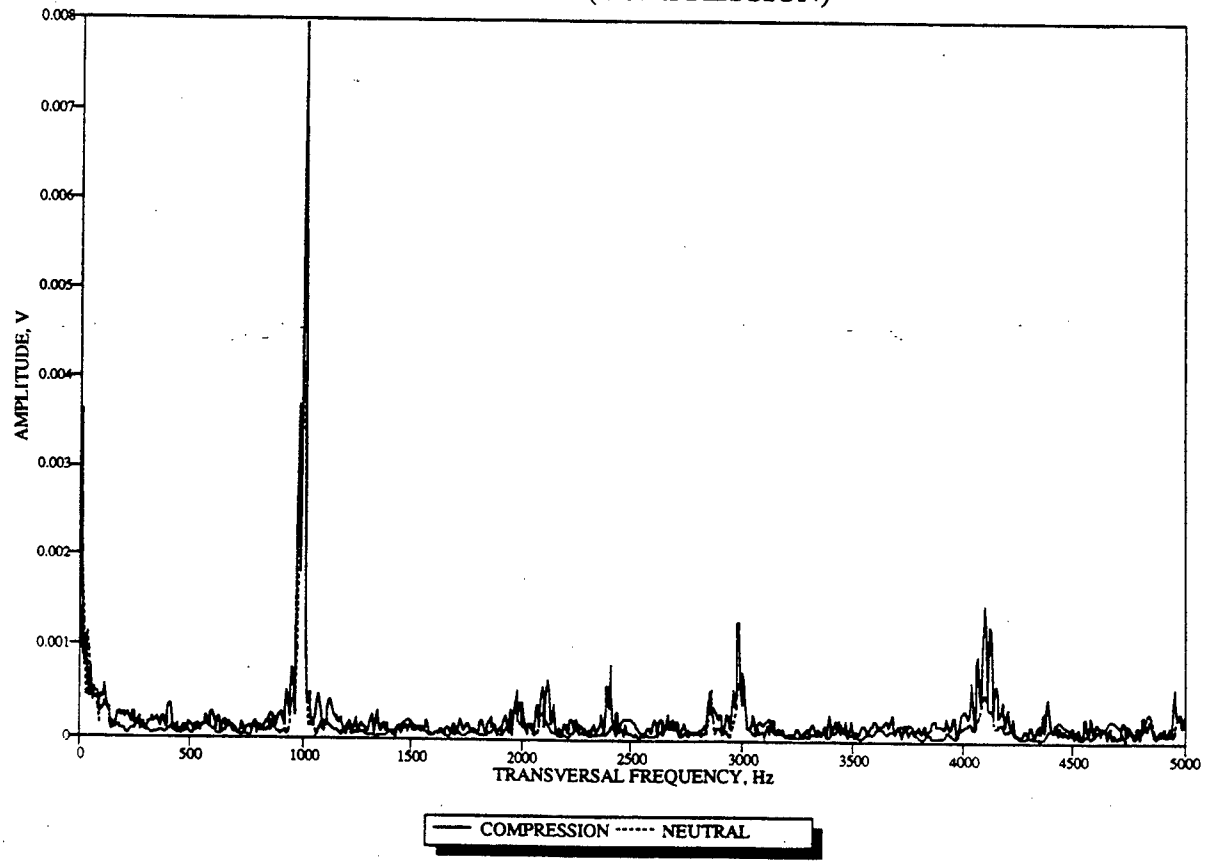

## BEAM O3H (COMPRESSION)

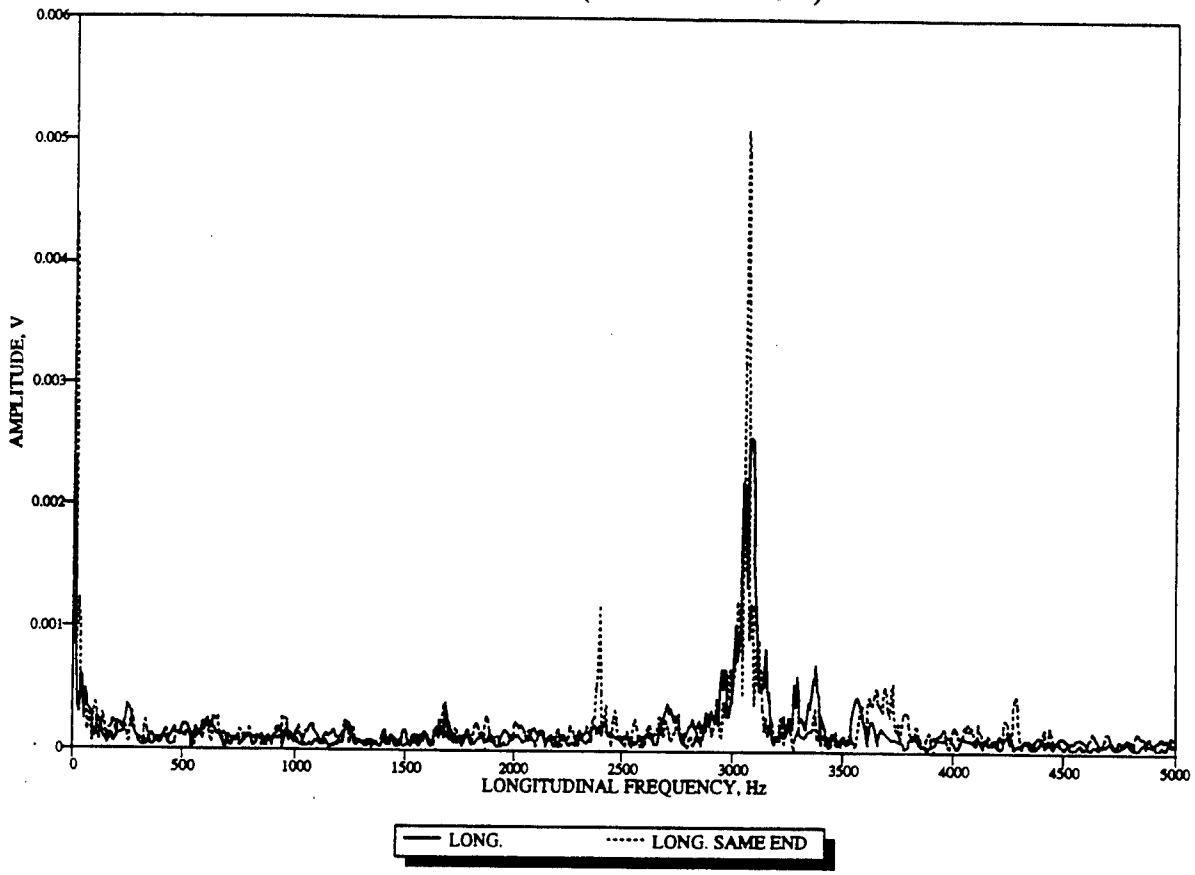


## BEAM O3H (COMPRESSION)

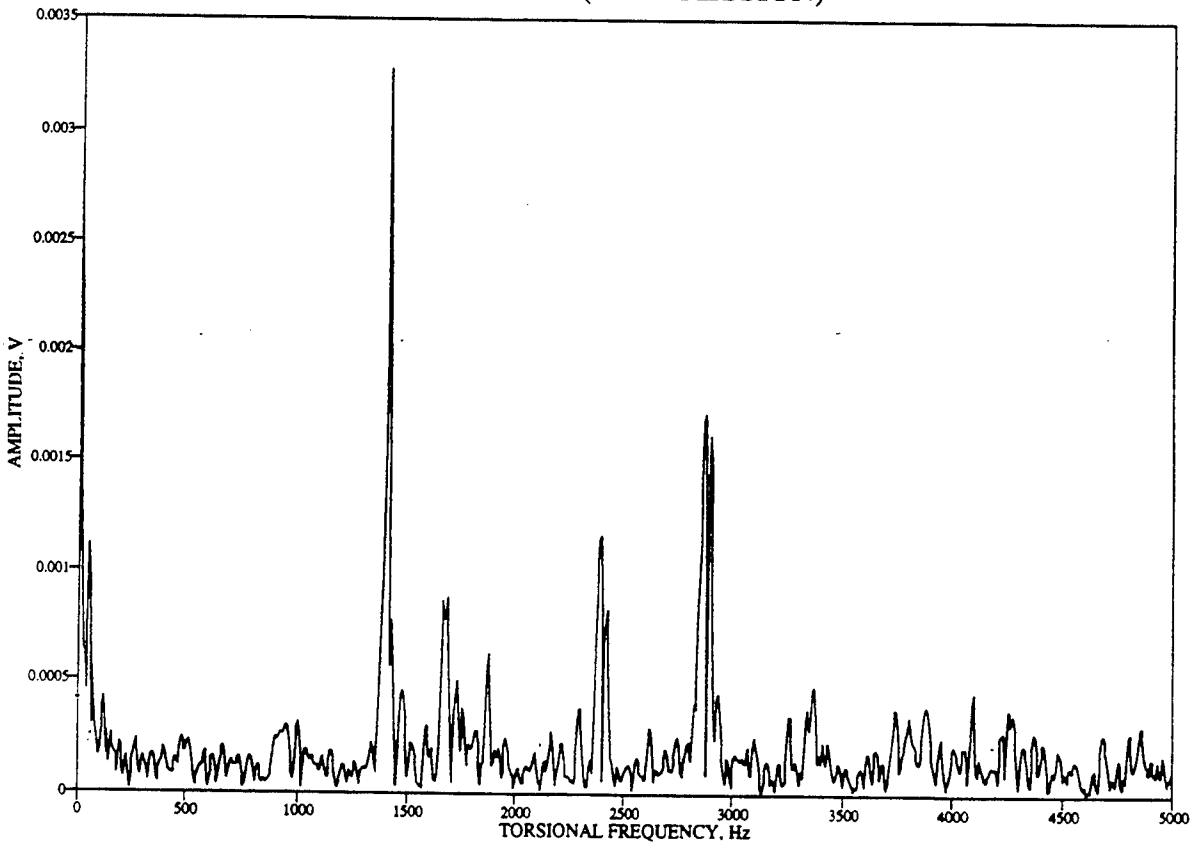

## BEAM O3H (TENSION)

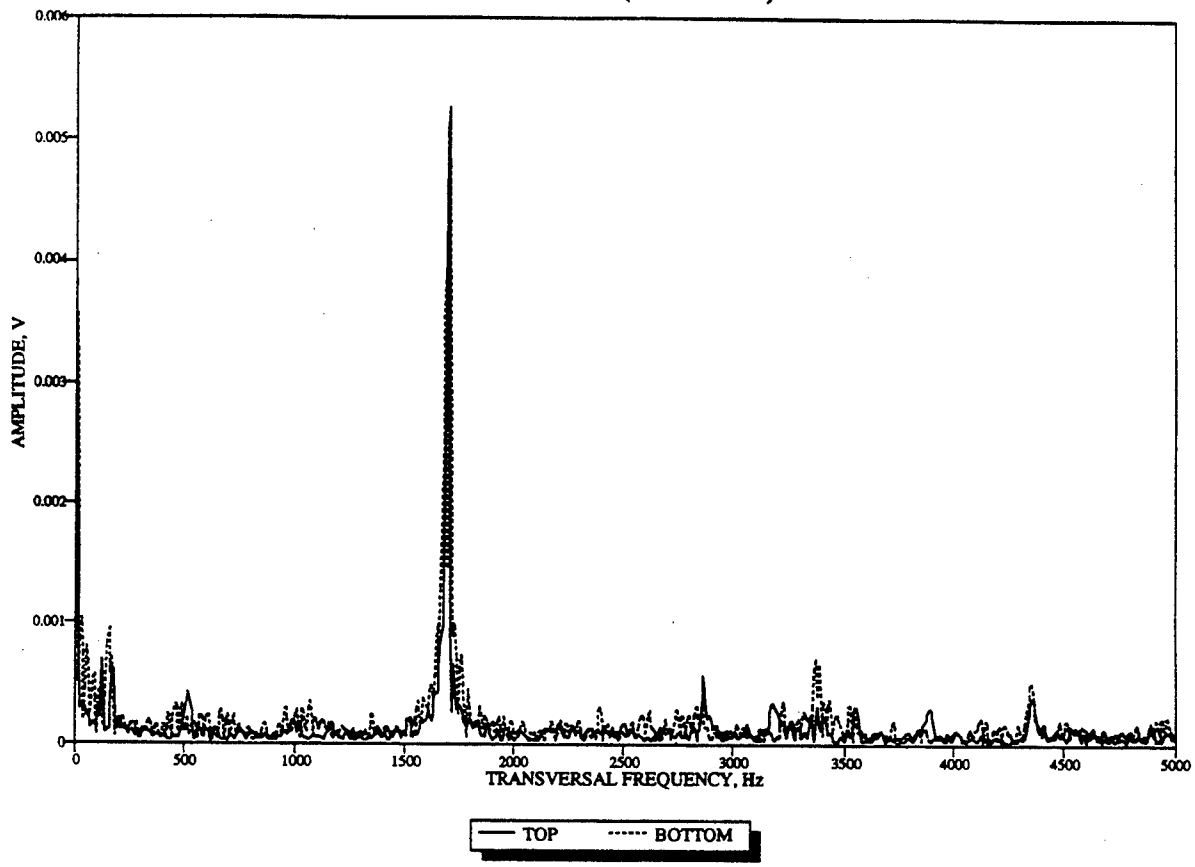


## BEAM O3H (TENSION)

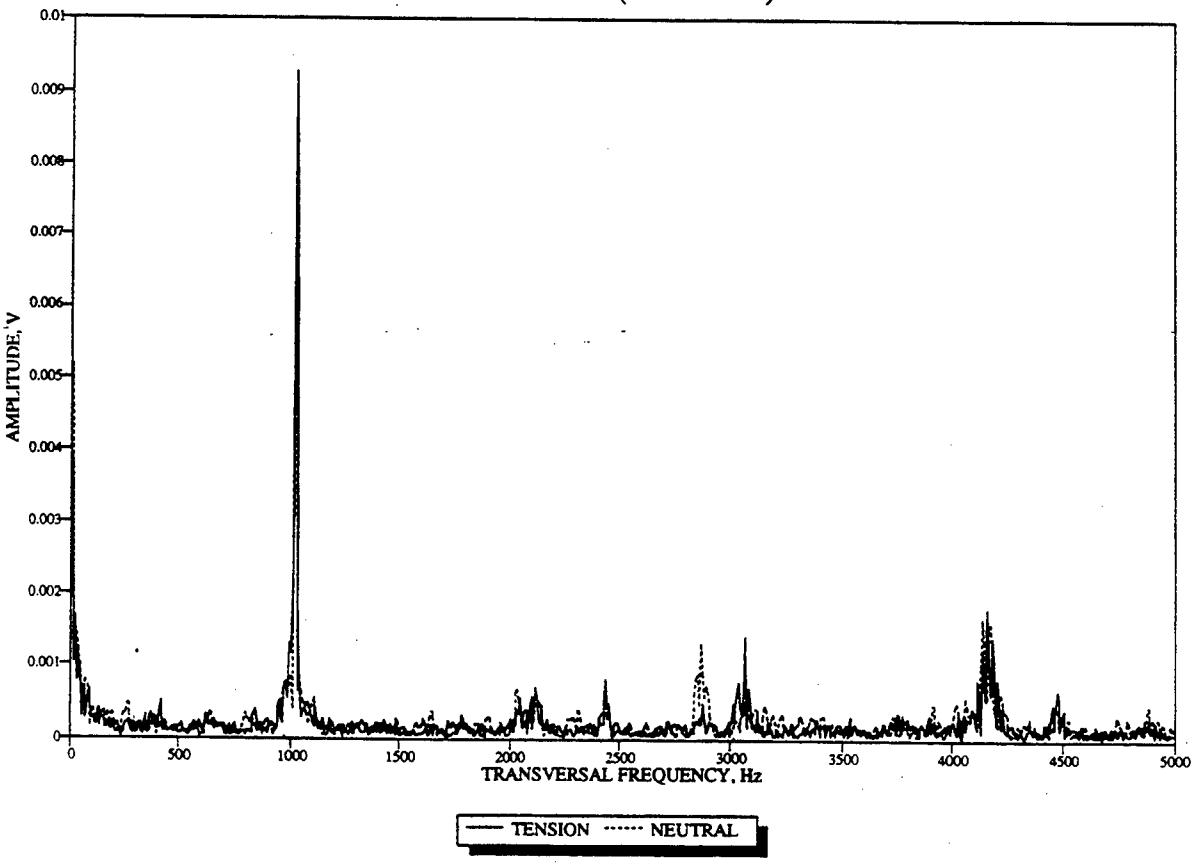

## BEAM O3H (TENSION)

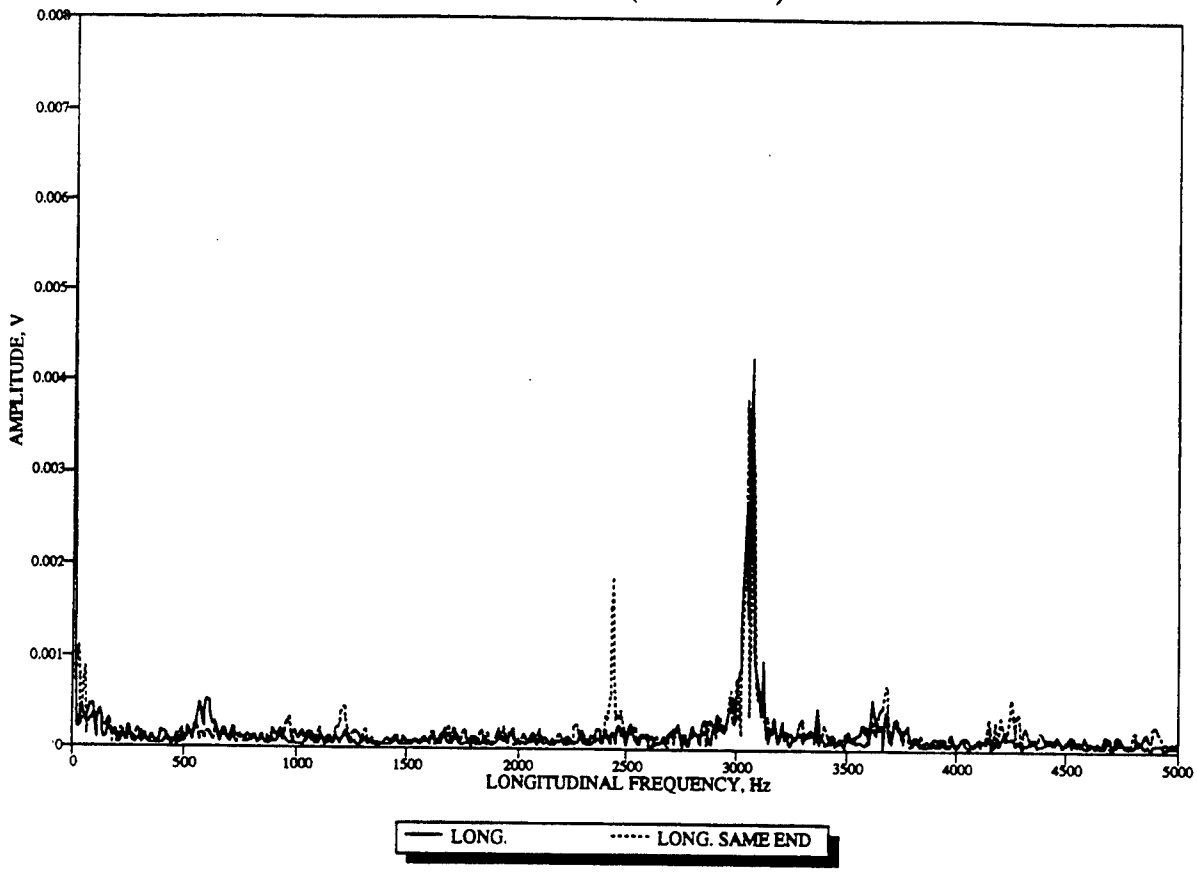


## BEAM O3H (TENSION)

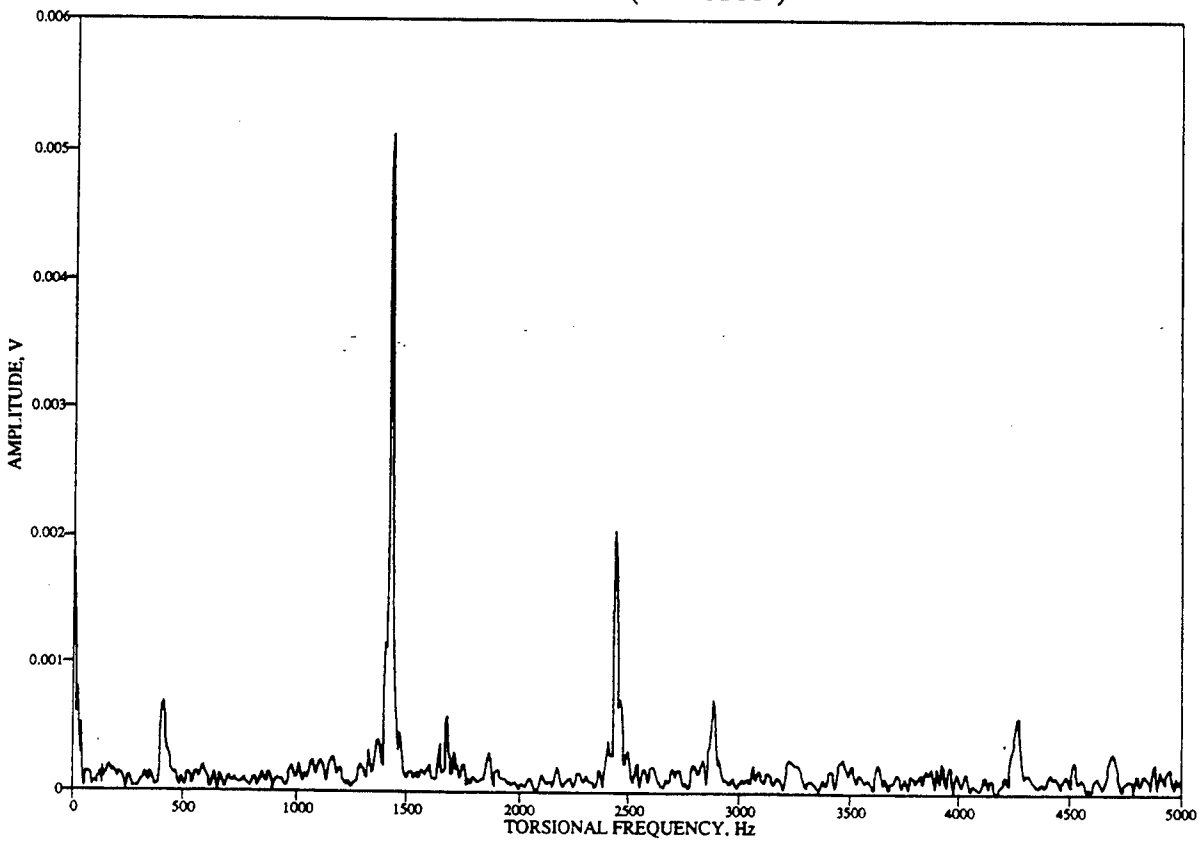

## BEAM P1H (COMPRESSION)

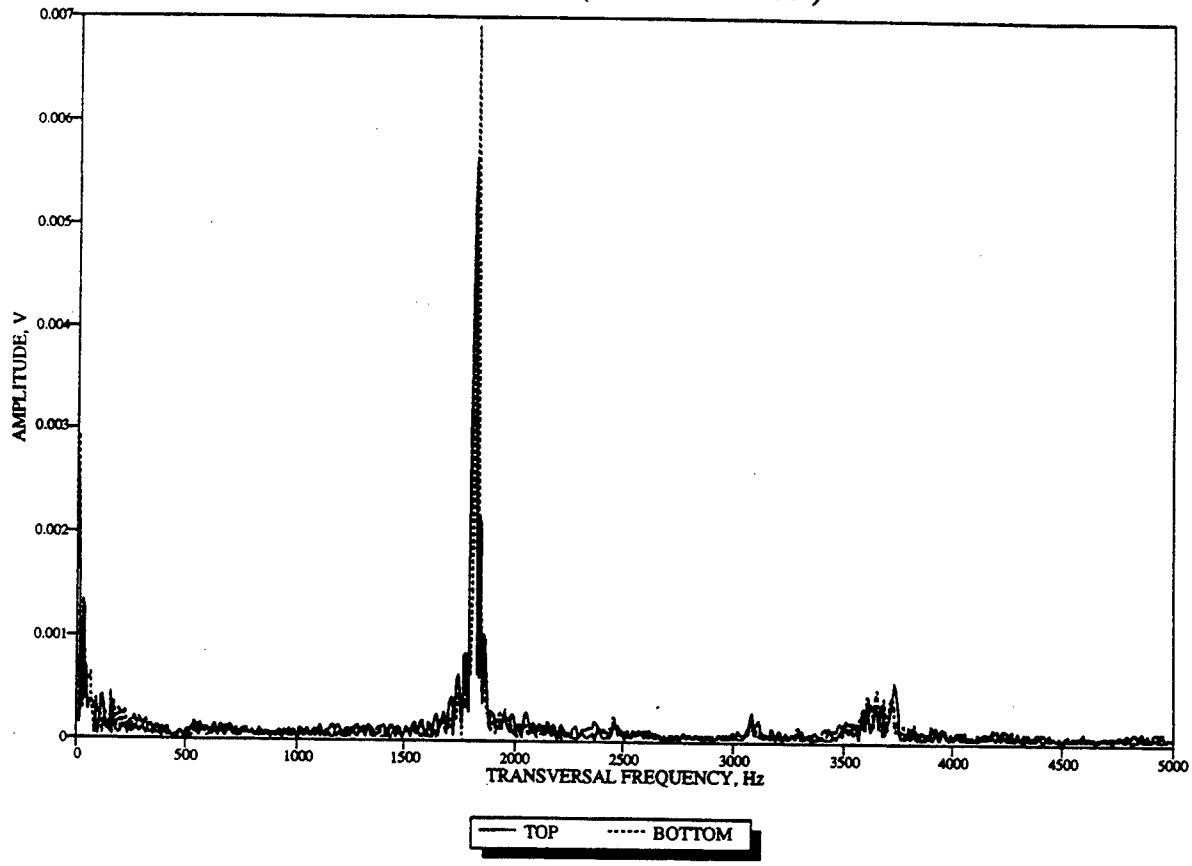


## BEAM P1H (COMPRESSION)

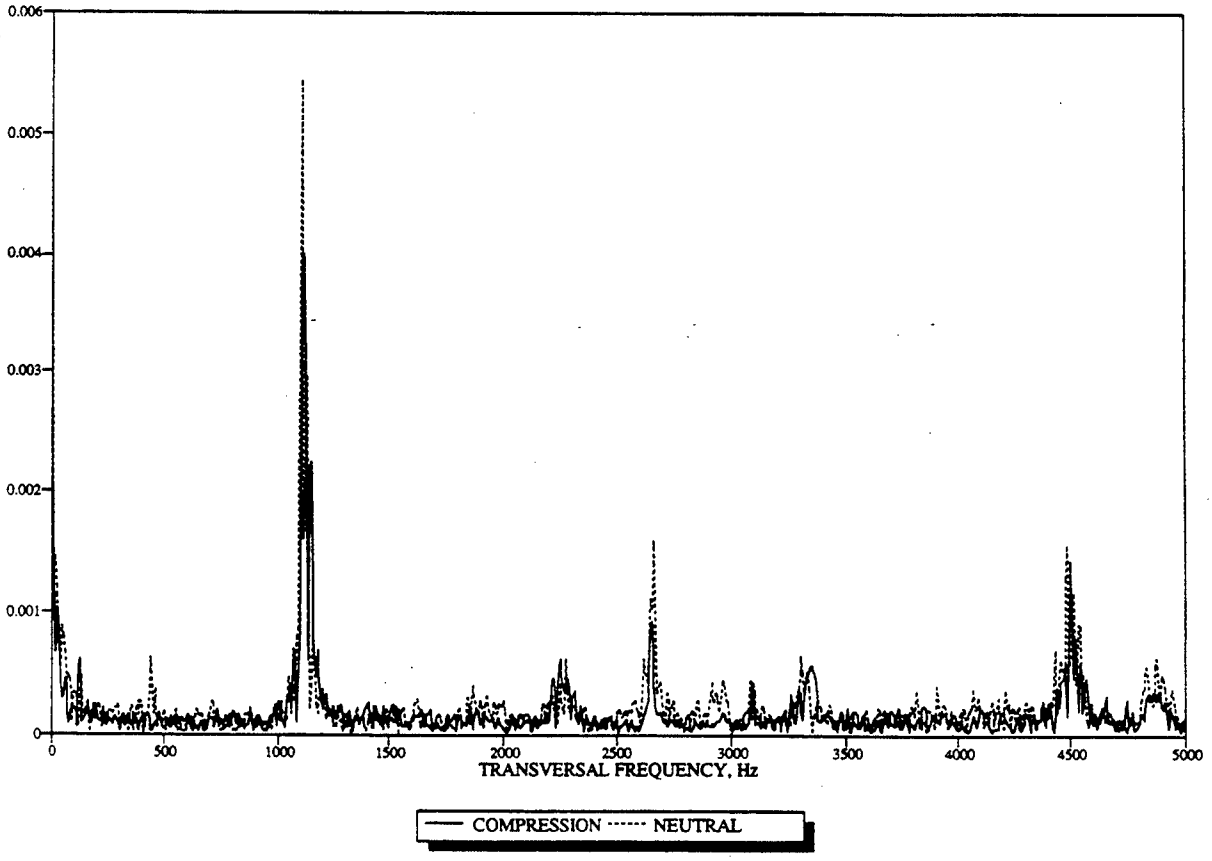

## BEAM P1H (COMPRESSION)

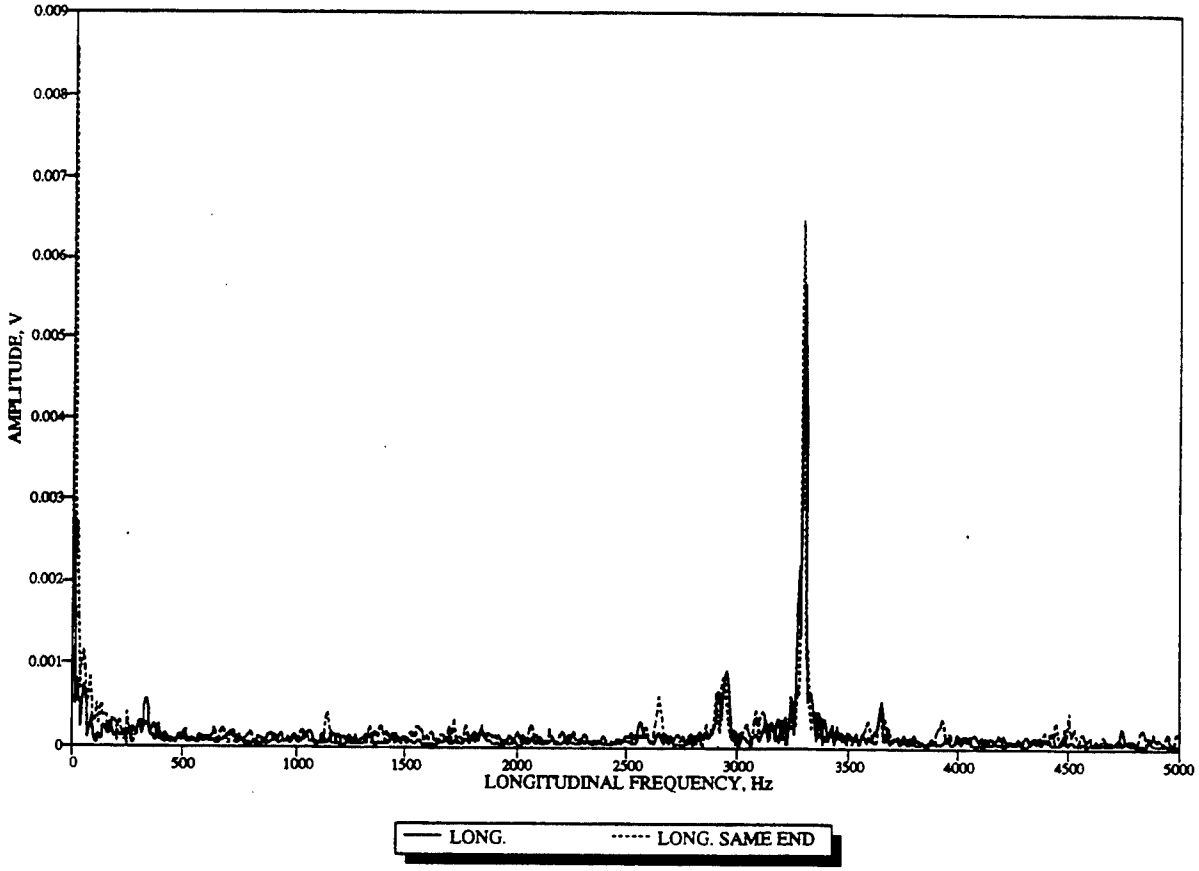


## BEAM P1H (COMPRESSION)

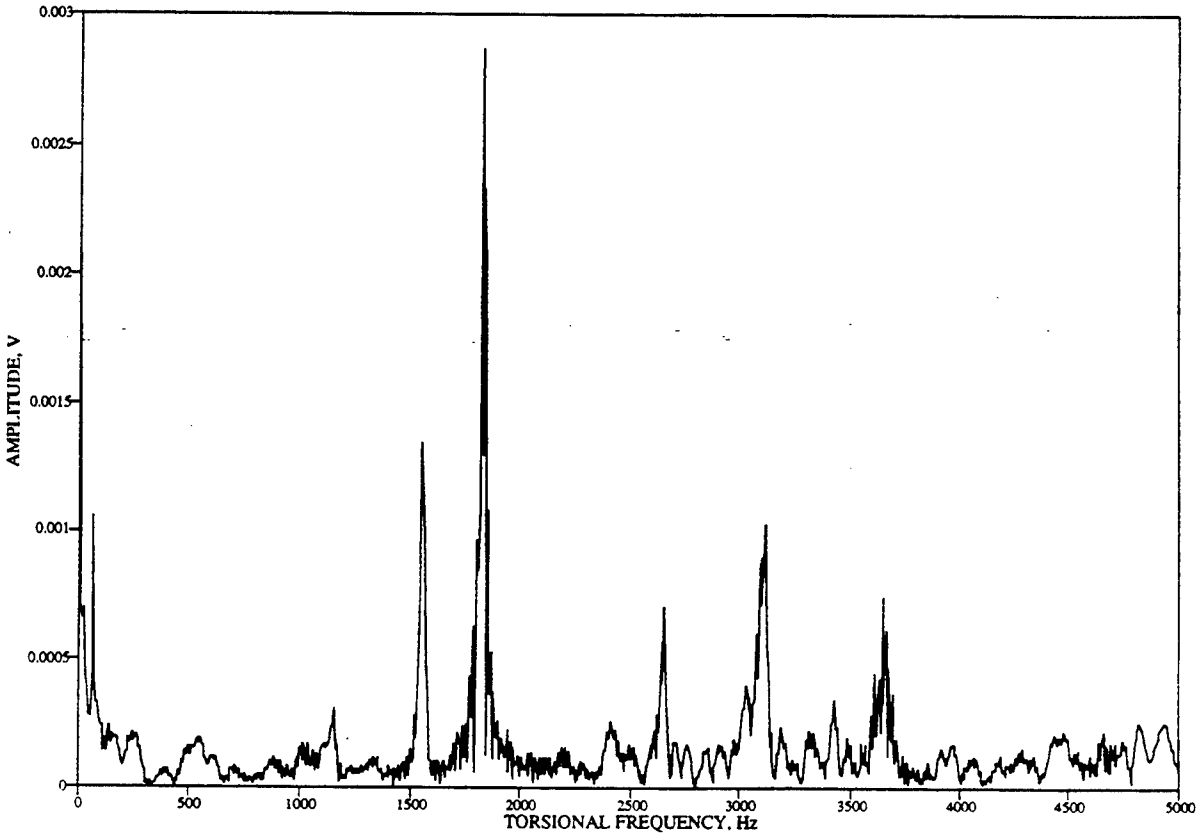

## BEAM P1H (TENSION)

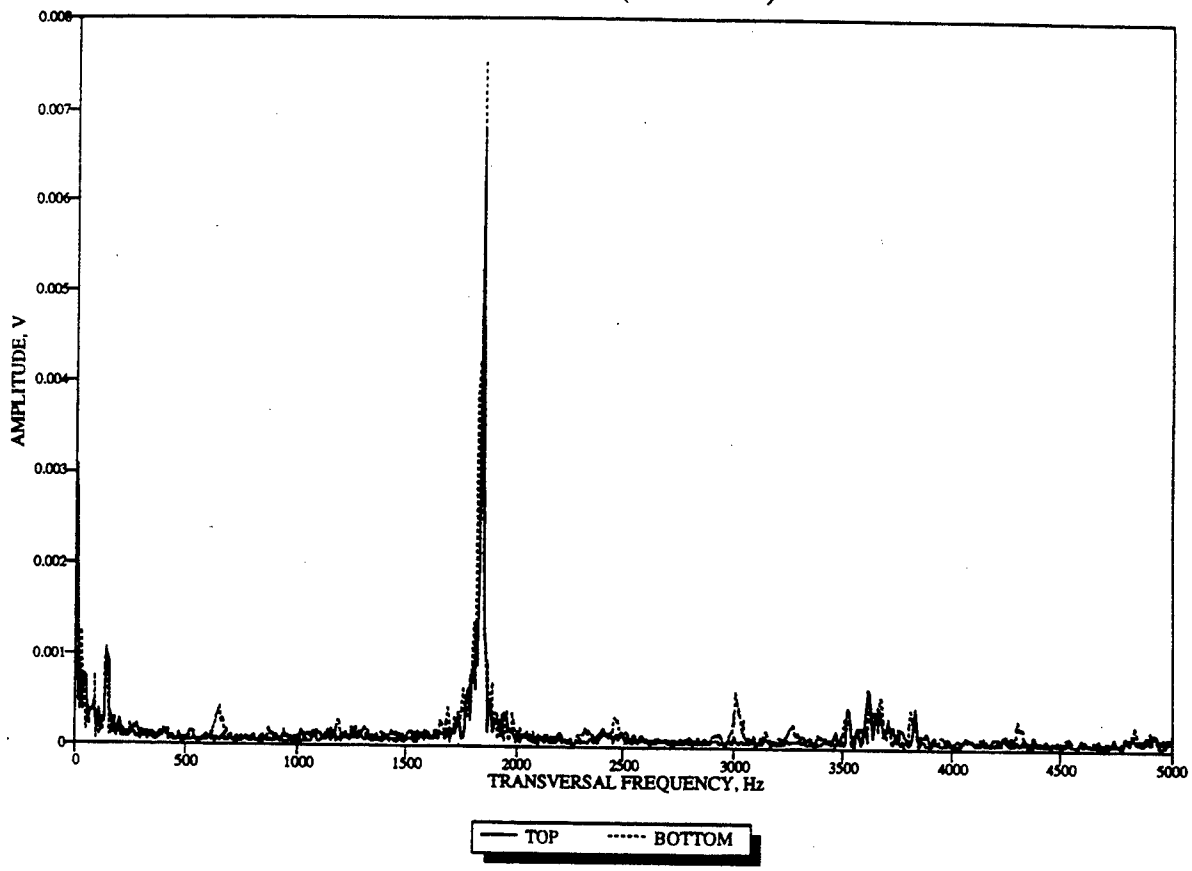


## BEAM P1H (TENSION)

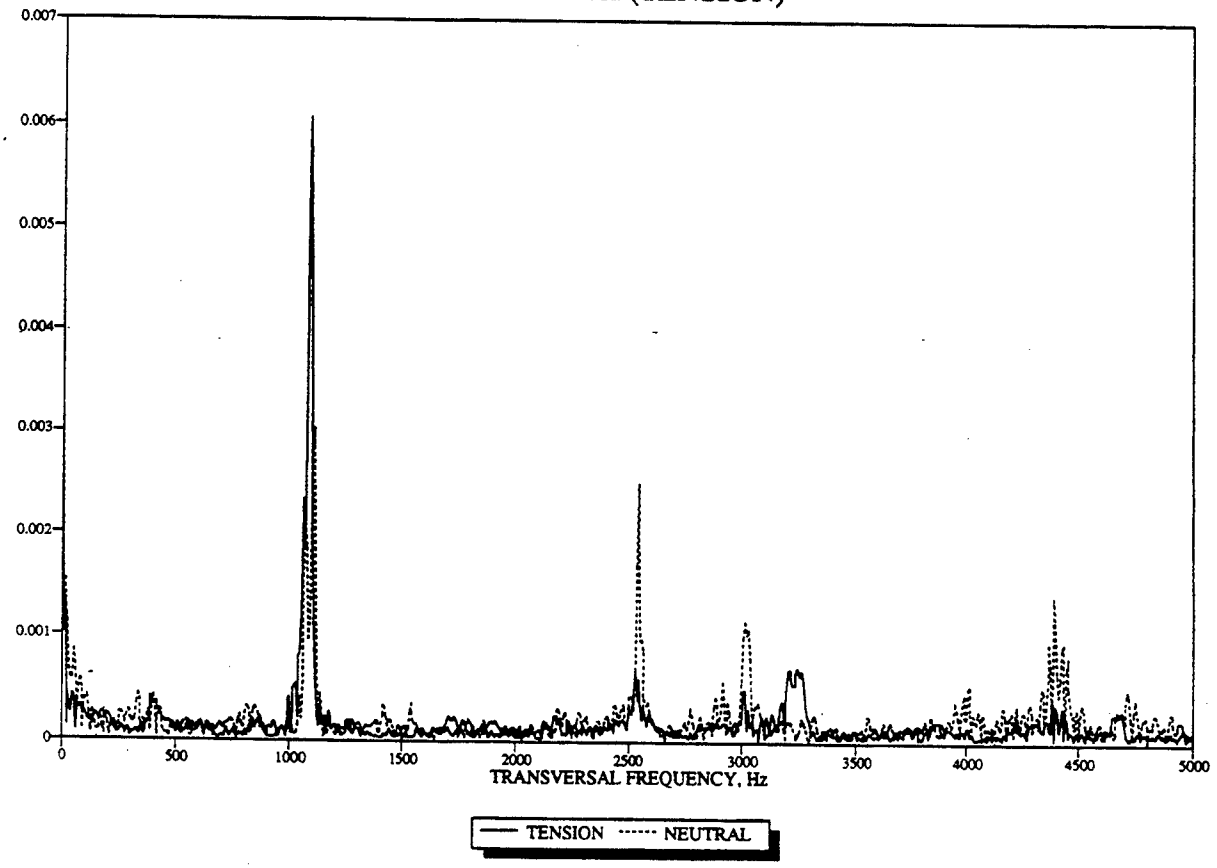

## BEAM P1H (TENSION)

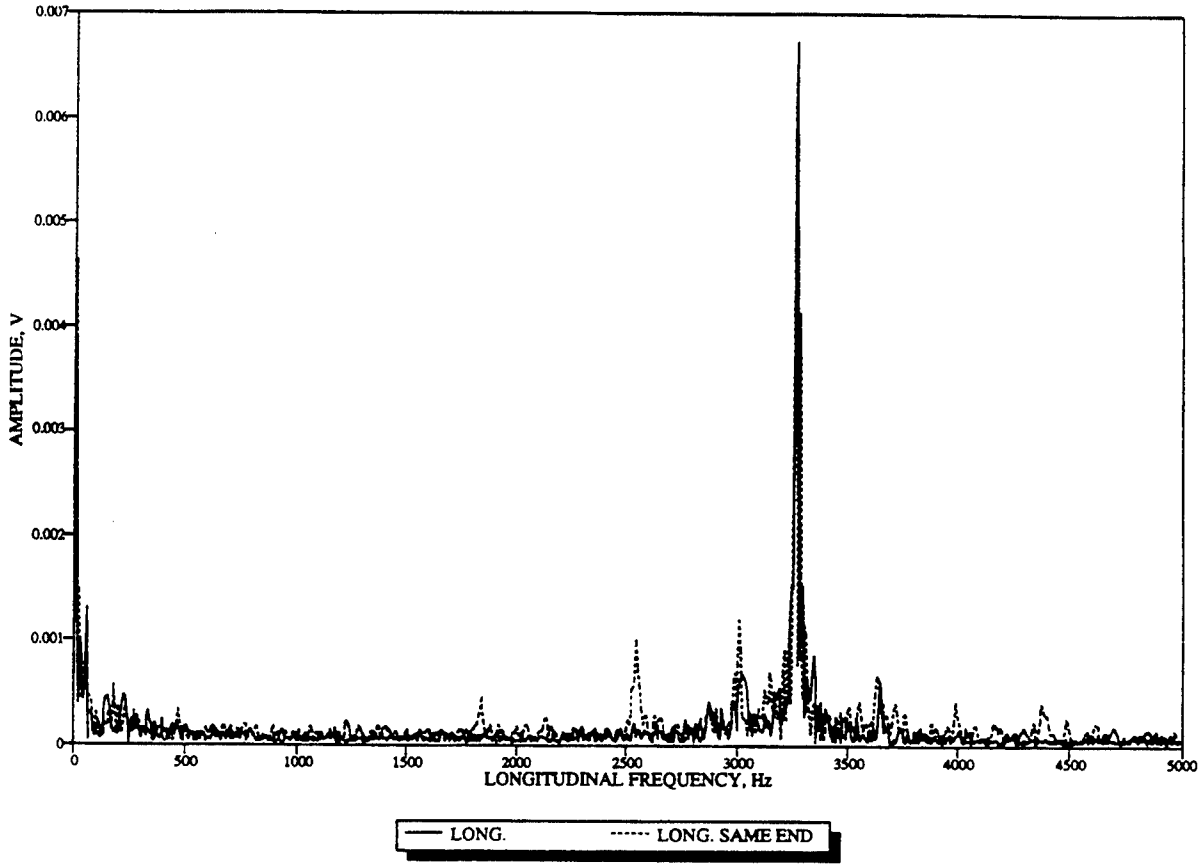


## BEAM P1H (TENSION)

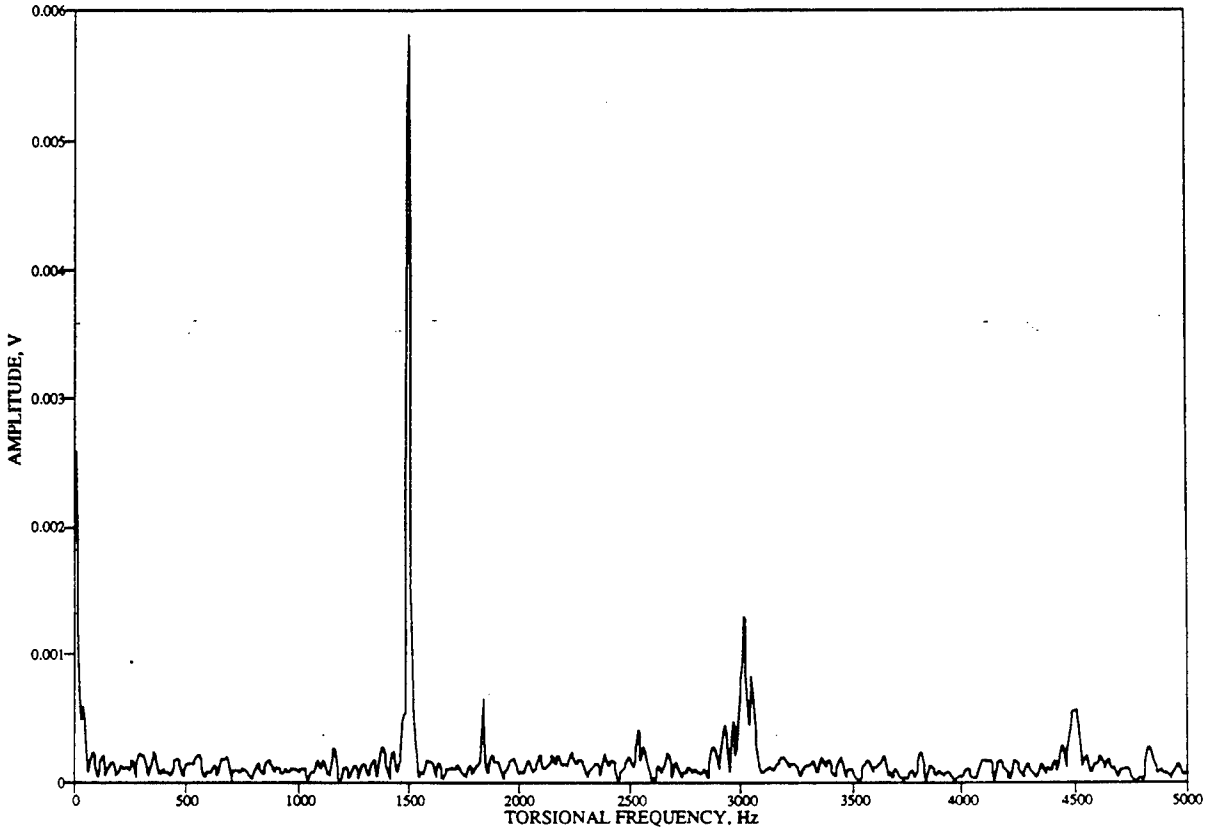

## BEAM P2H (COMPRESSION)

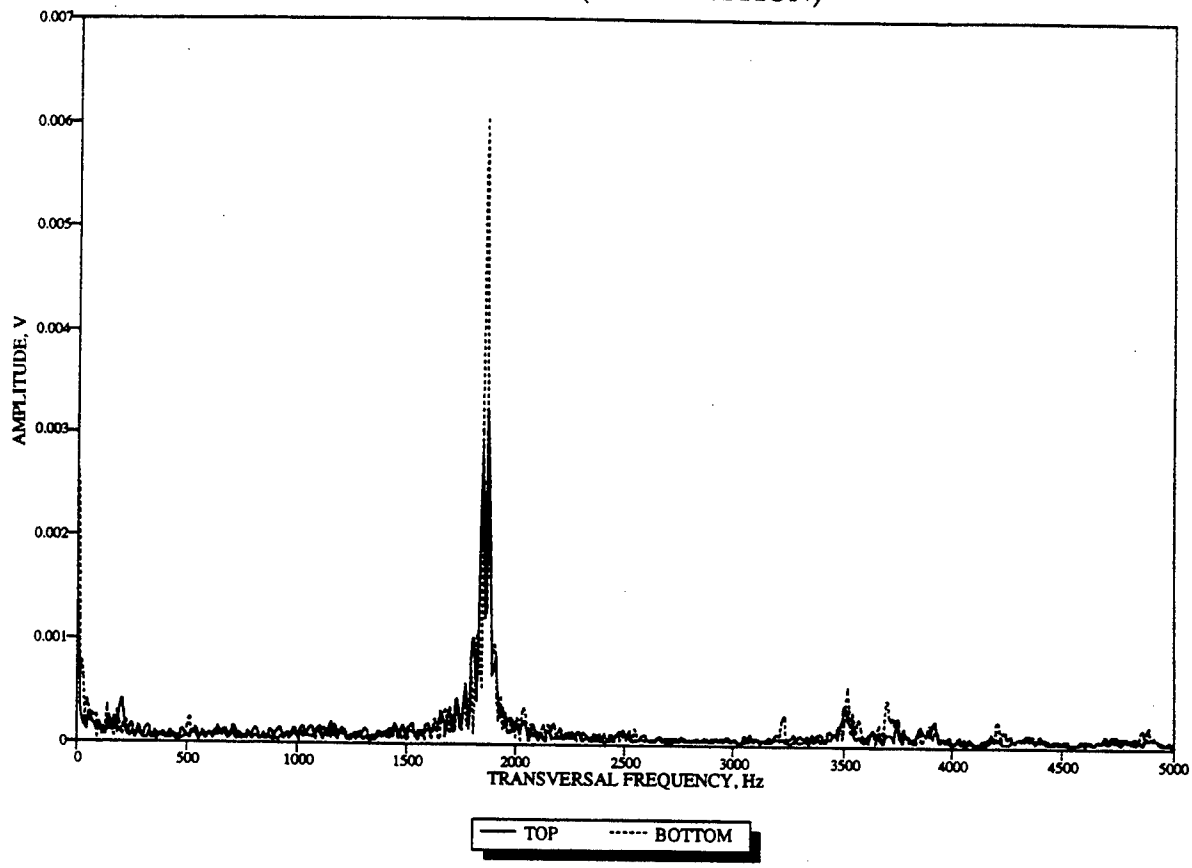


---

## BEAM P2H (COMPRESSION)

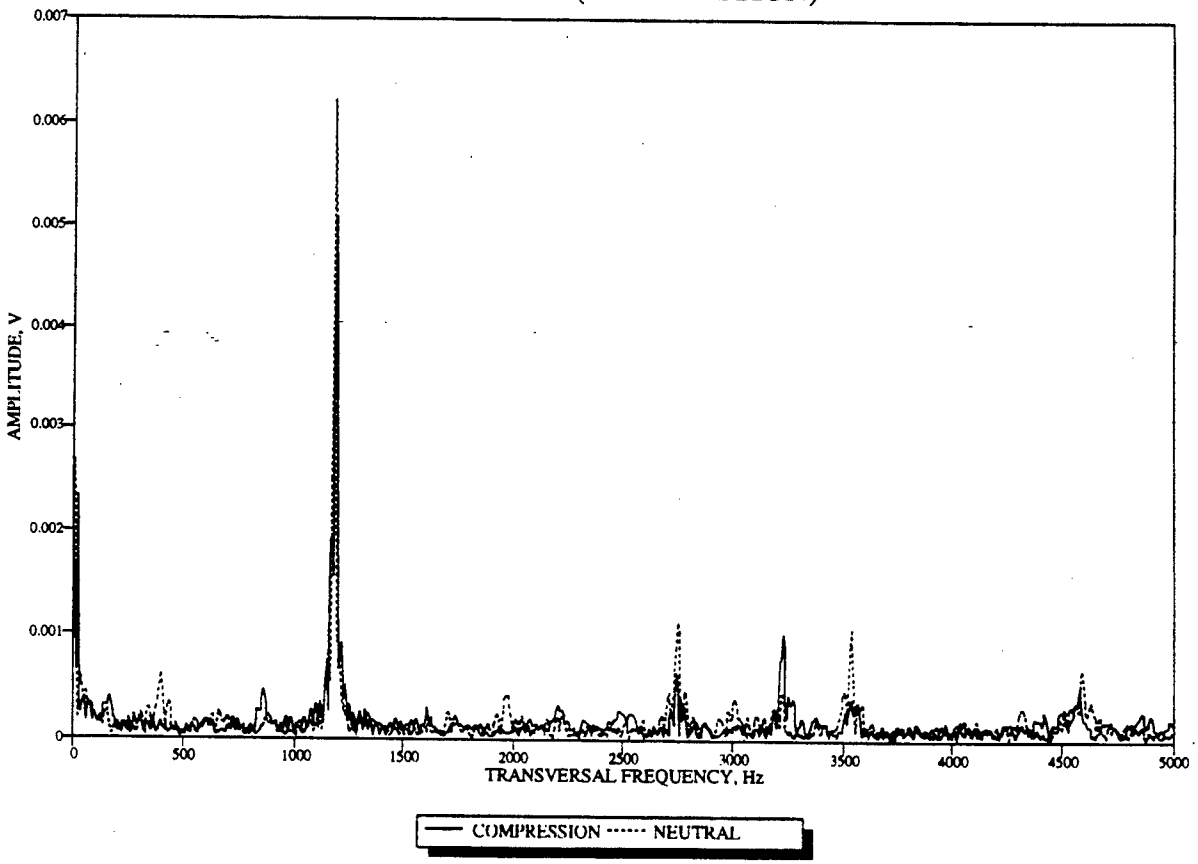

## BEAM P2H (COMPRESSION)

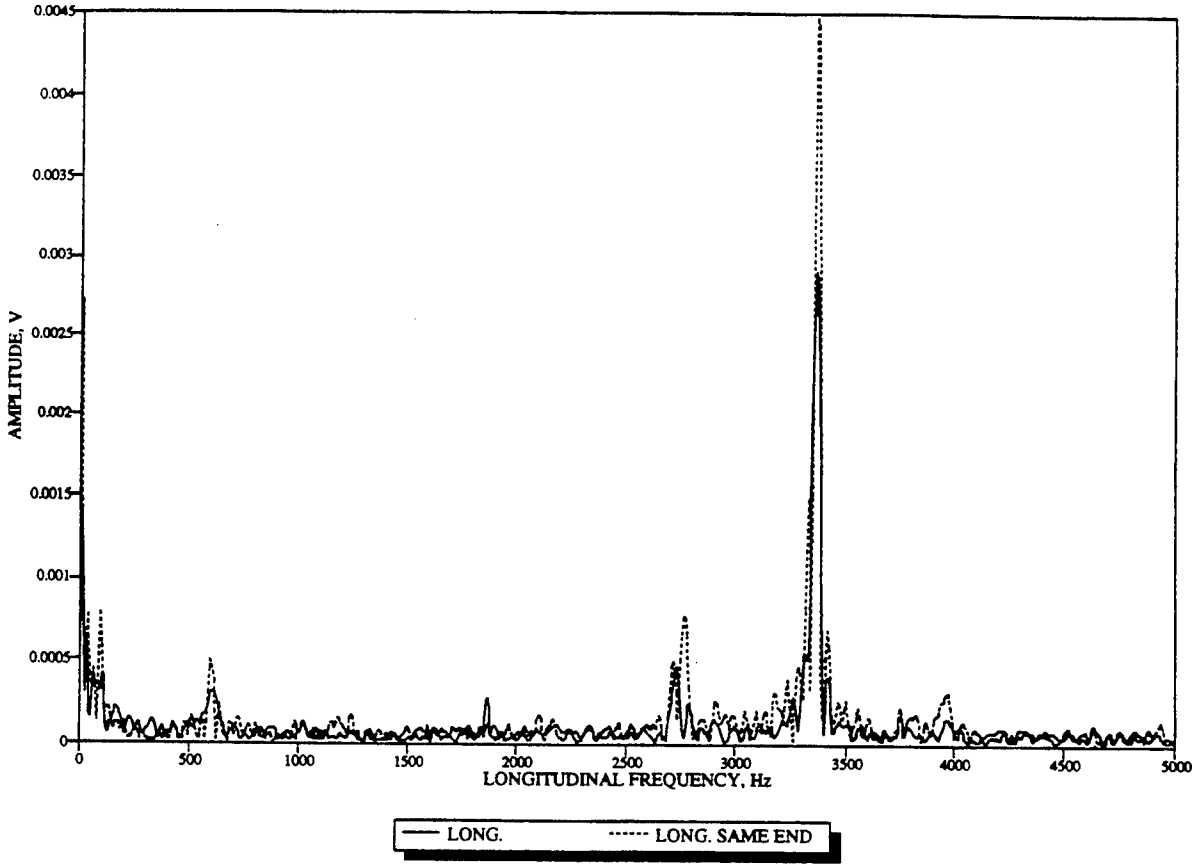


## BEAM P2H (COMPRESSION)

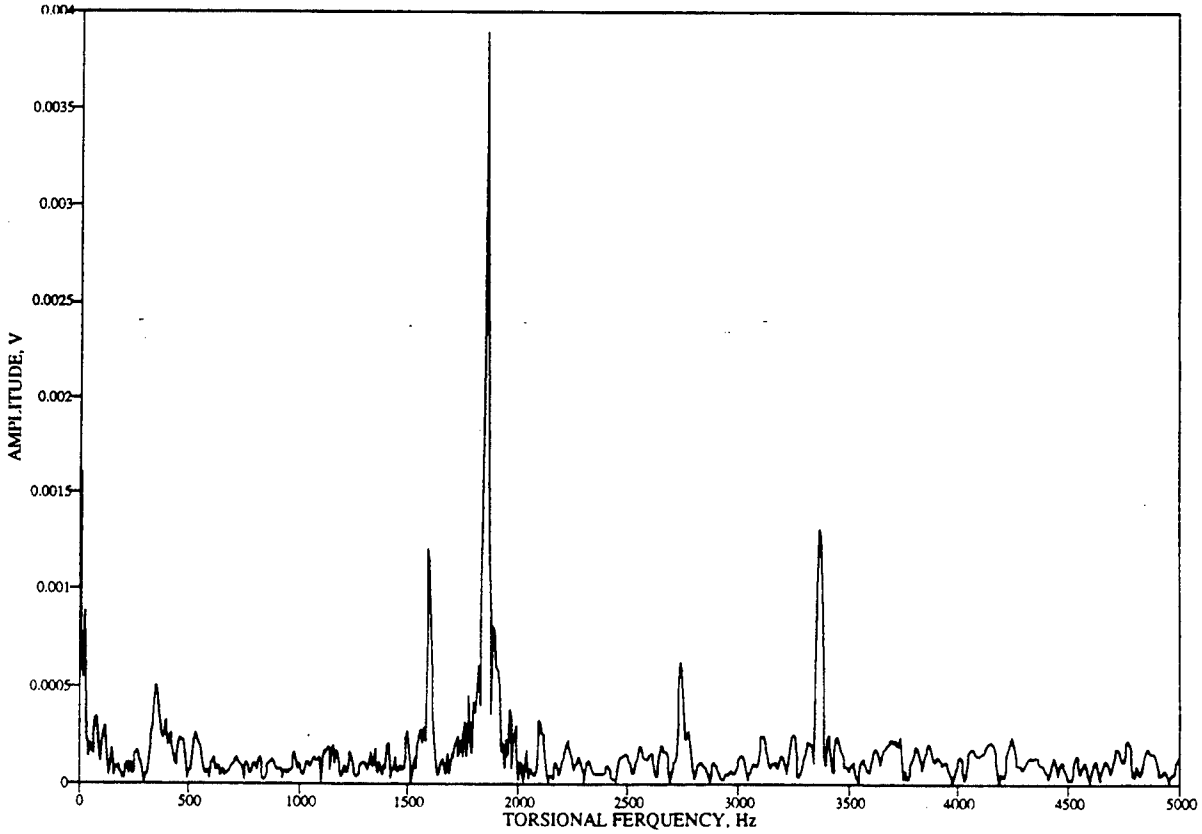

## BEAM P2H (TENSION)

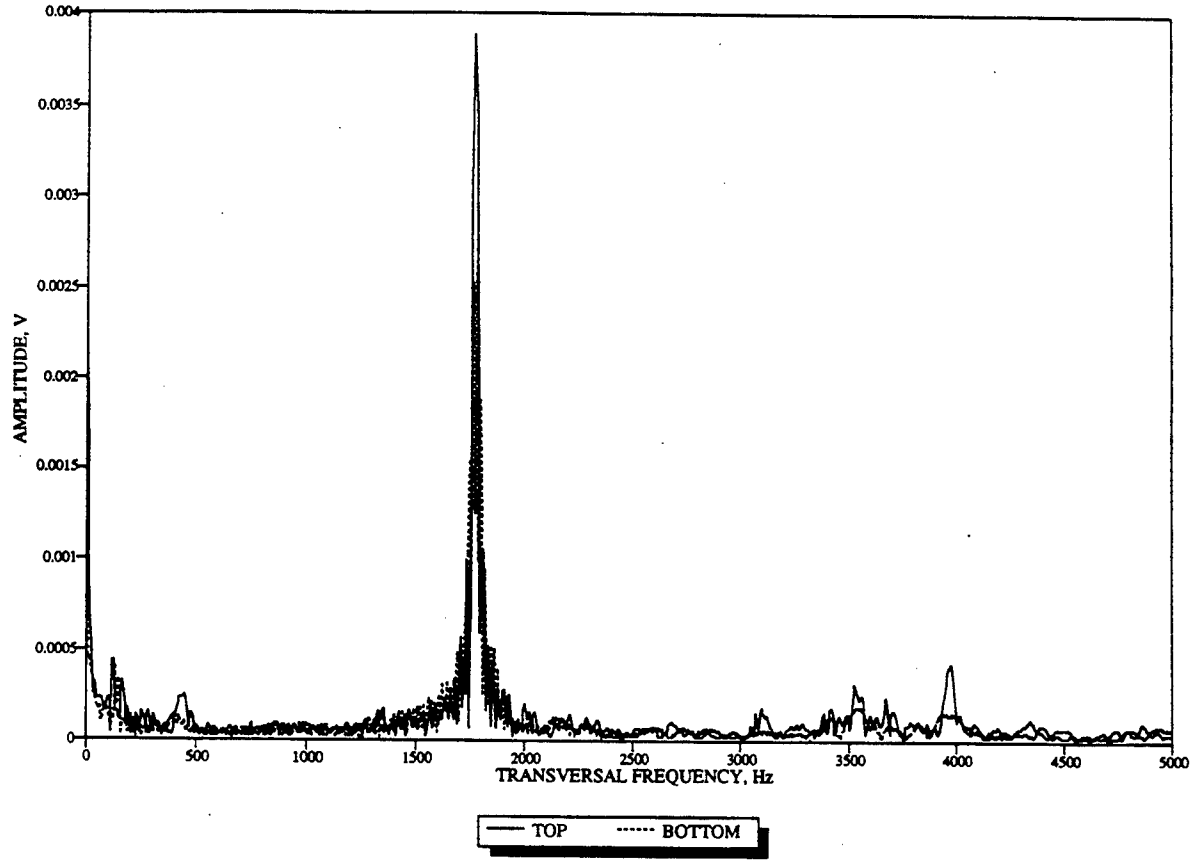


## BEAM P2H (TENSION)

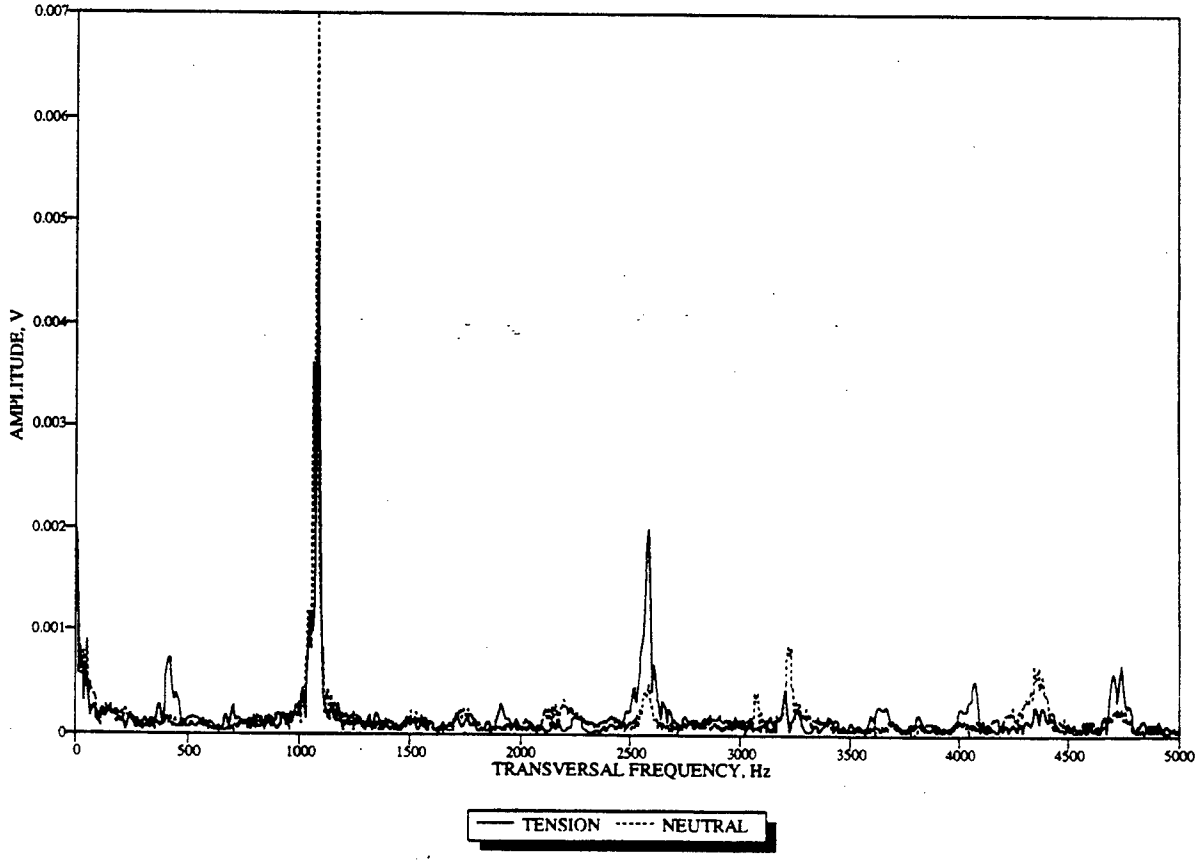

## BEAM P2H (TENSION)

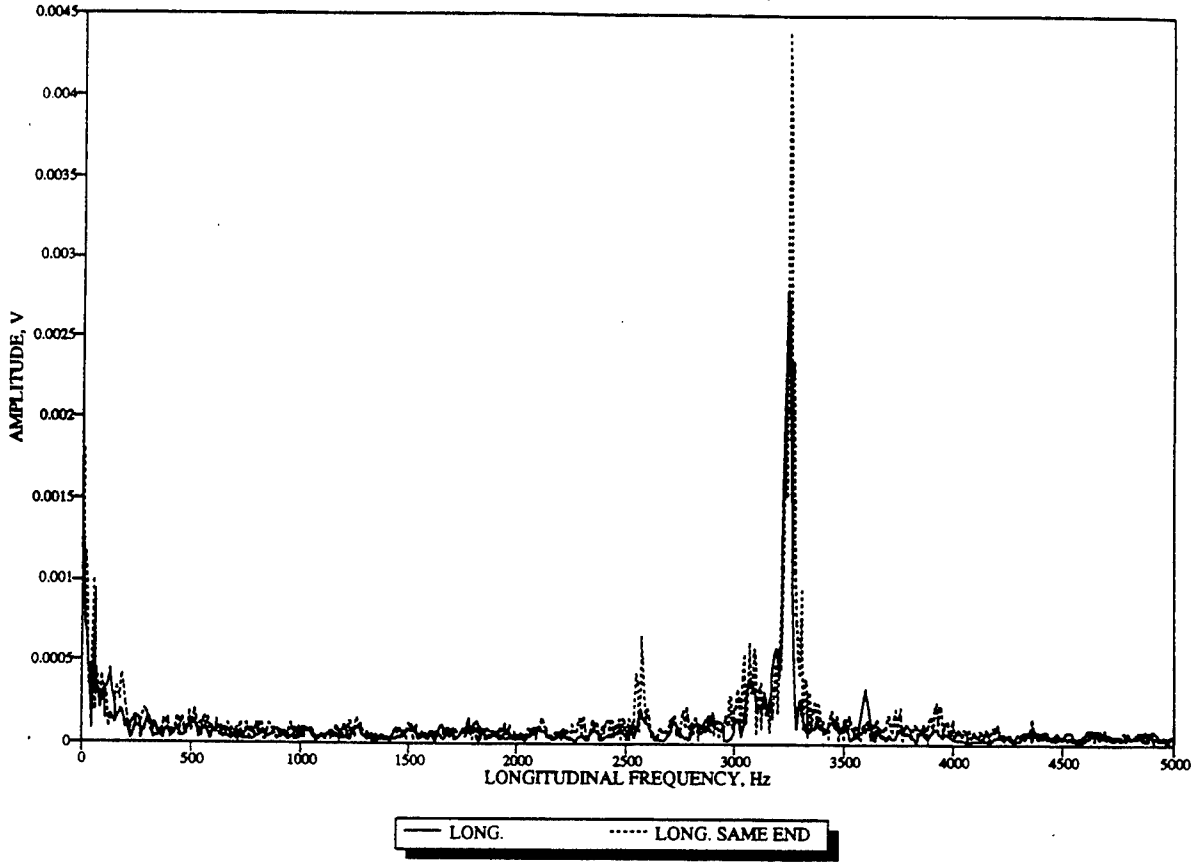


## BEAM P2H (TENSION)

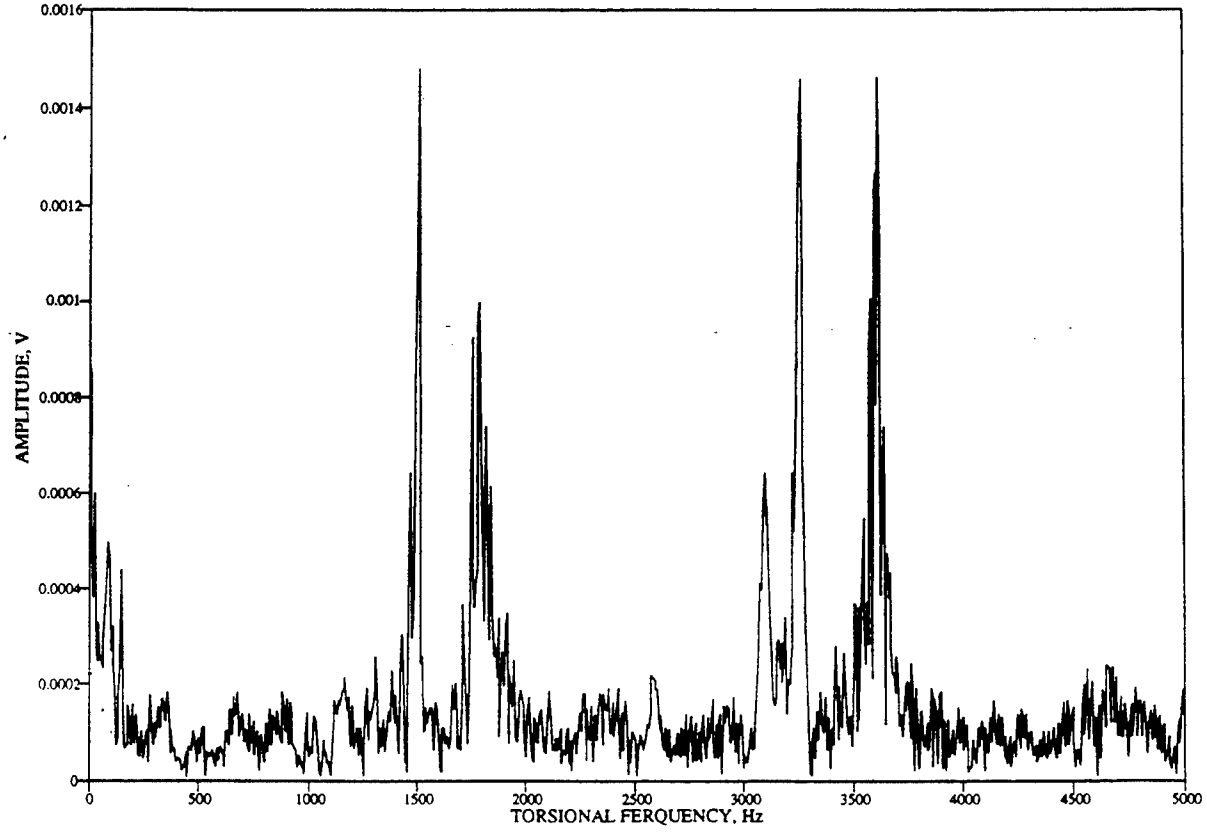

# Appendix J
# Scanning Electron Microscope Results

# E.M. SCAN BEAM J-1
## NO FIBERS

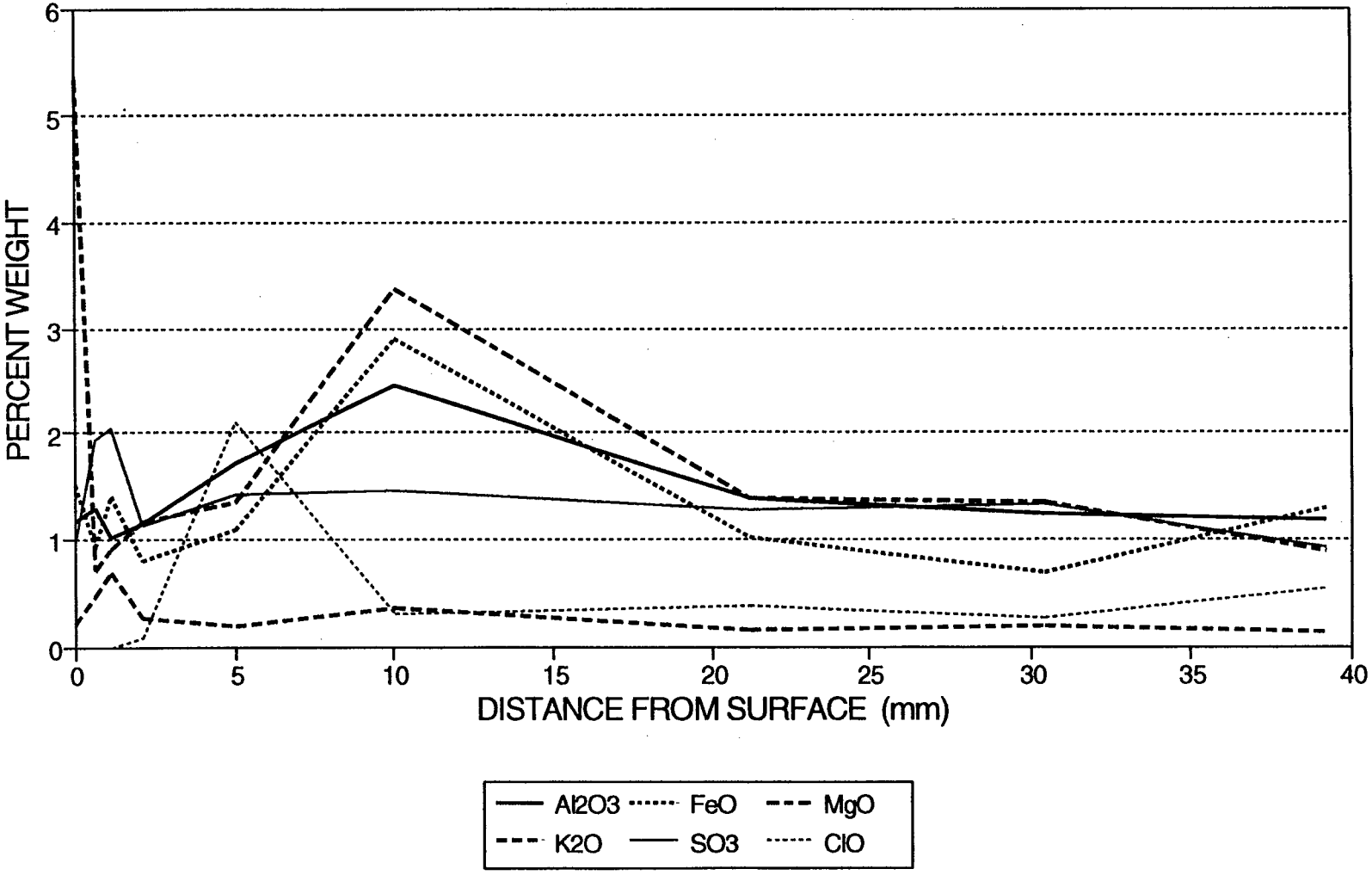

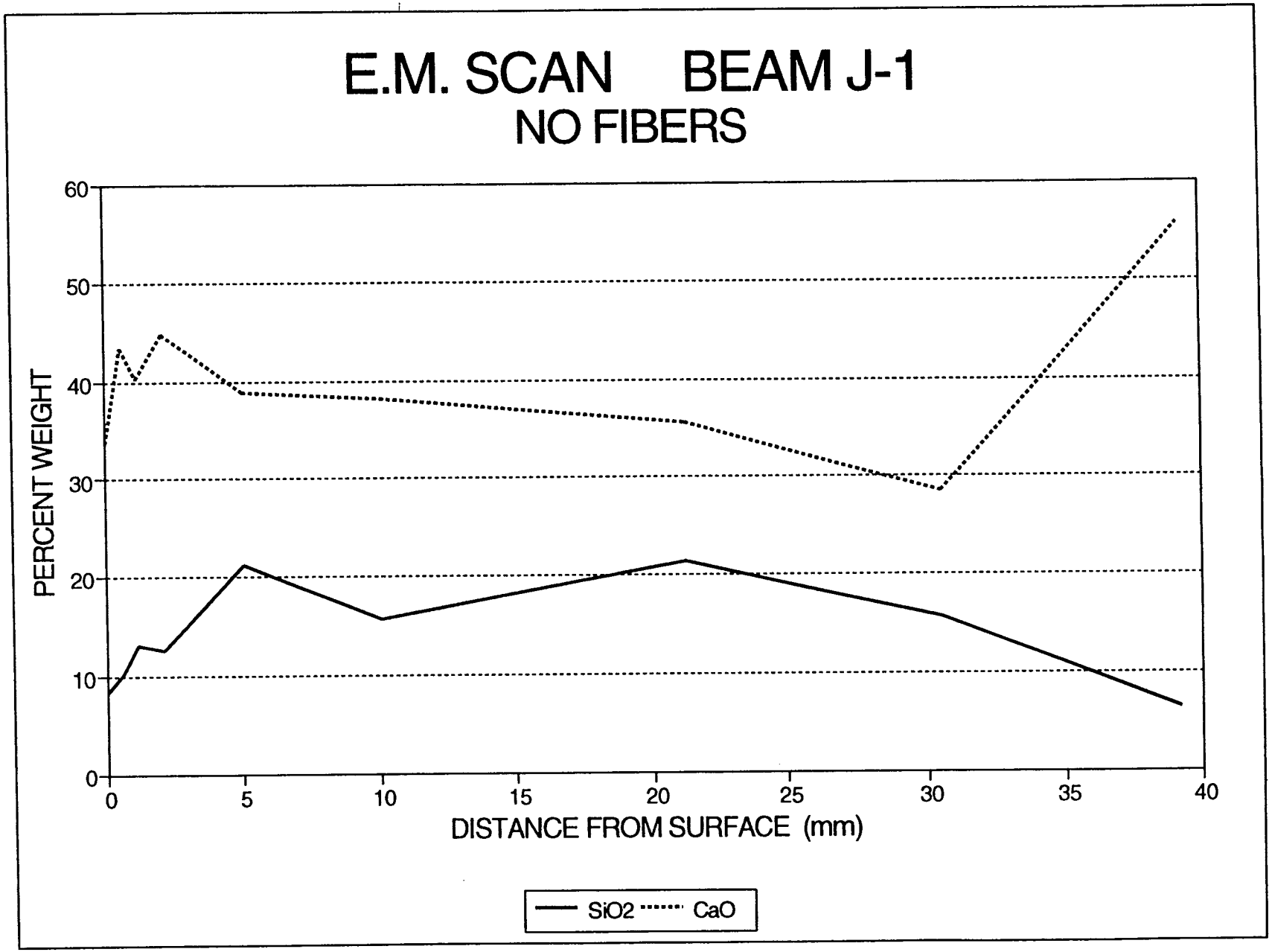
E.M. SCAN BEAM J-1
NO FIBERS
PERCENT WEIGHT
60
50
40
30
20
10
0
0
5
10
15
20
25
30
35
40
DISTANCE FROM SURFACE (mm)
SiO2
CaO

# E.M. SCAN BEAM K-1
## BRASS COATED STEEL FIBERS

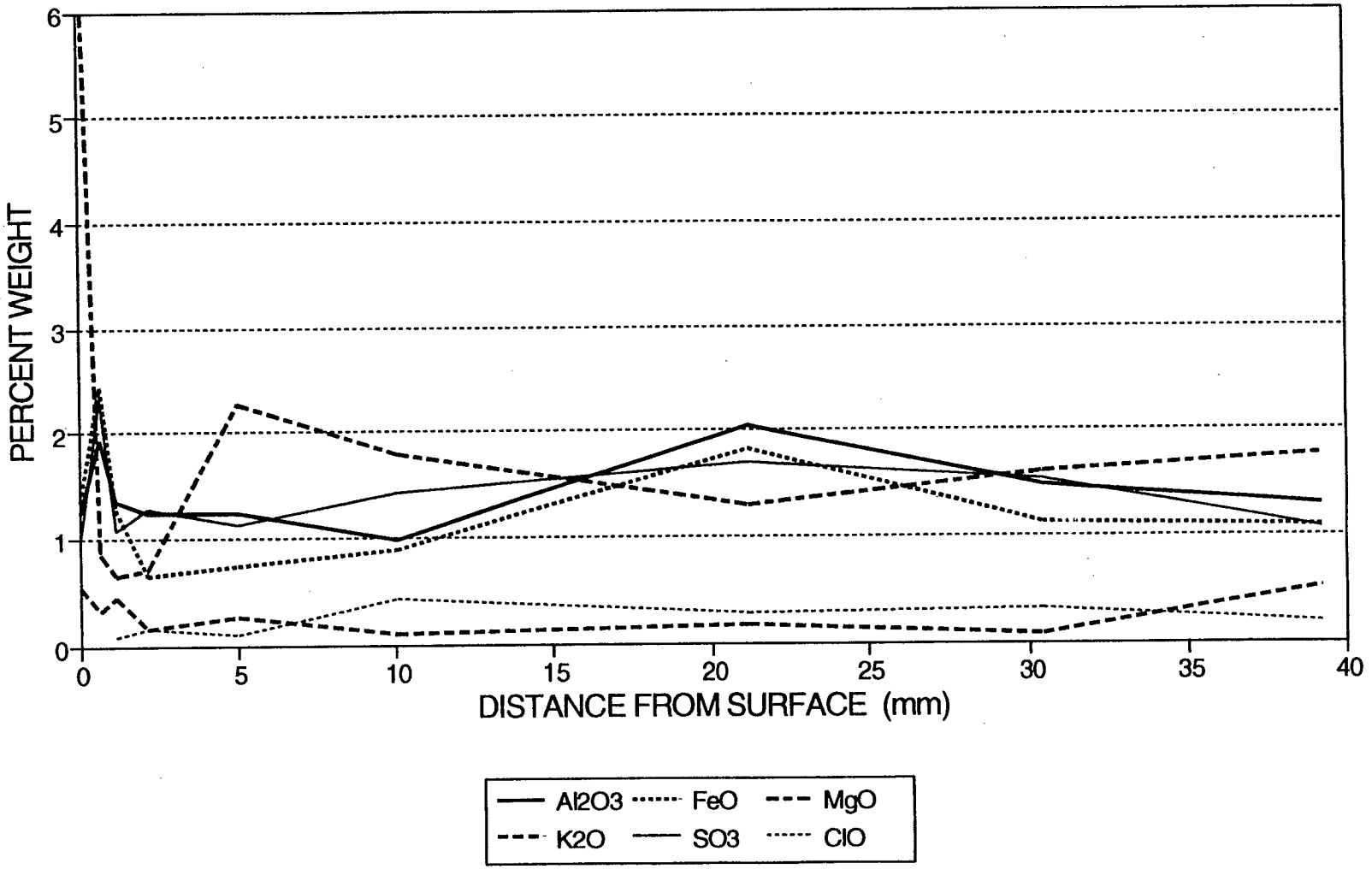

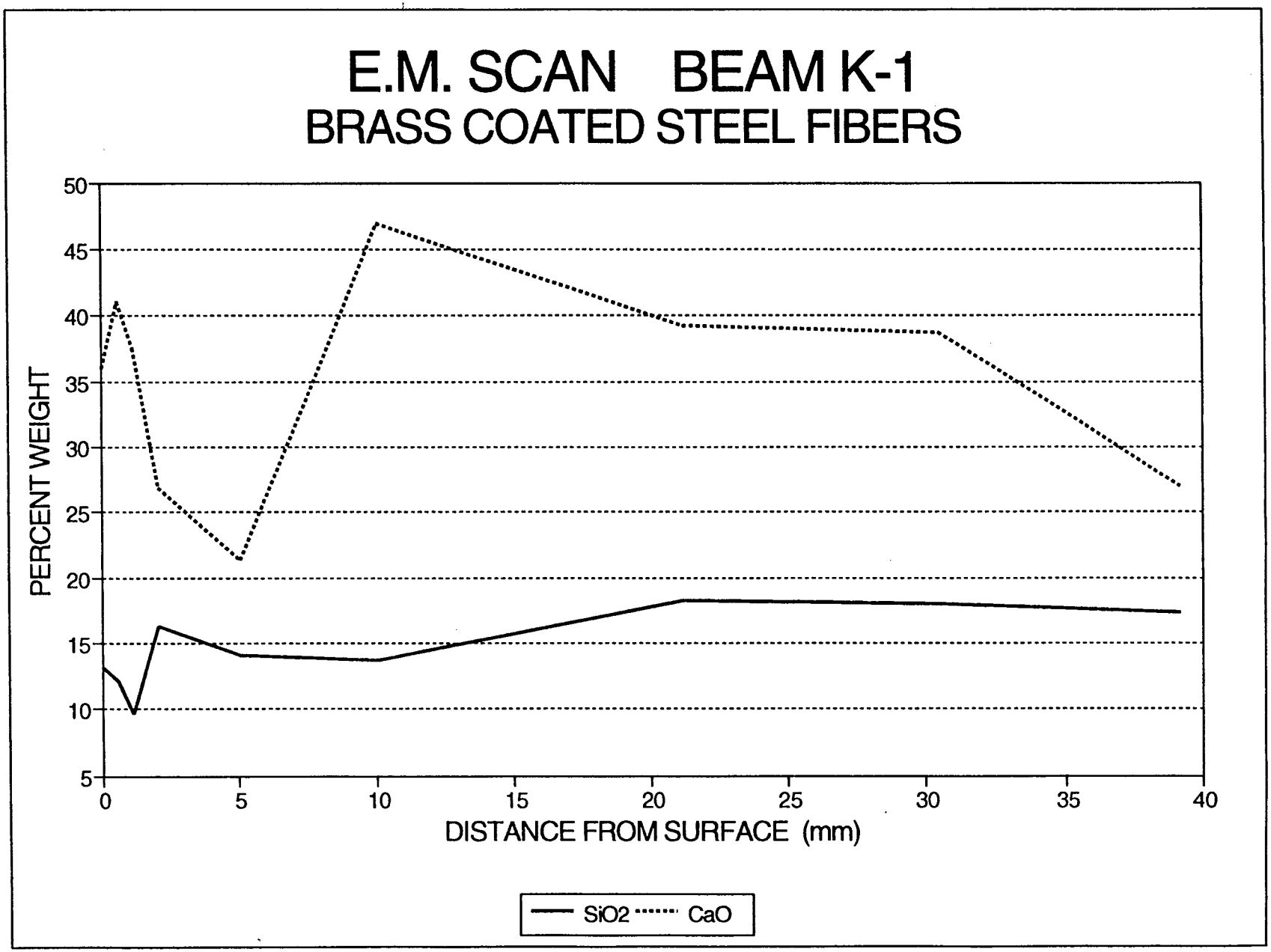
E.M. SCAN BEAM K-1
BRASS COATED STEEL FIBERS
PERCENT WEIGHT
50
45
40
35
30
25
20
15
10
5
0
5
10
15
20
25
30
35
40
DISTANCE FROM SURFACE (mm)
SiO2
CaO

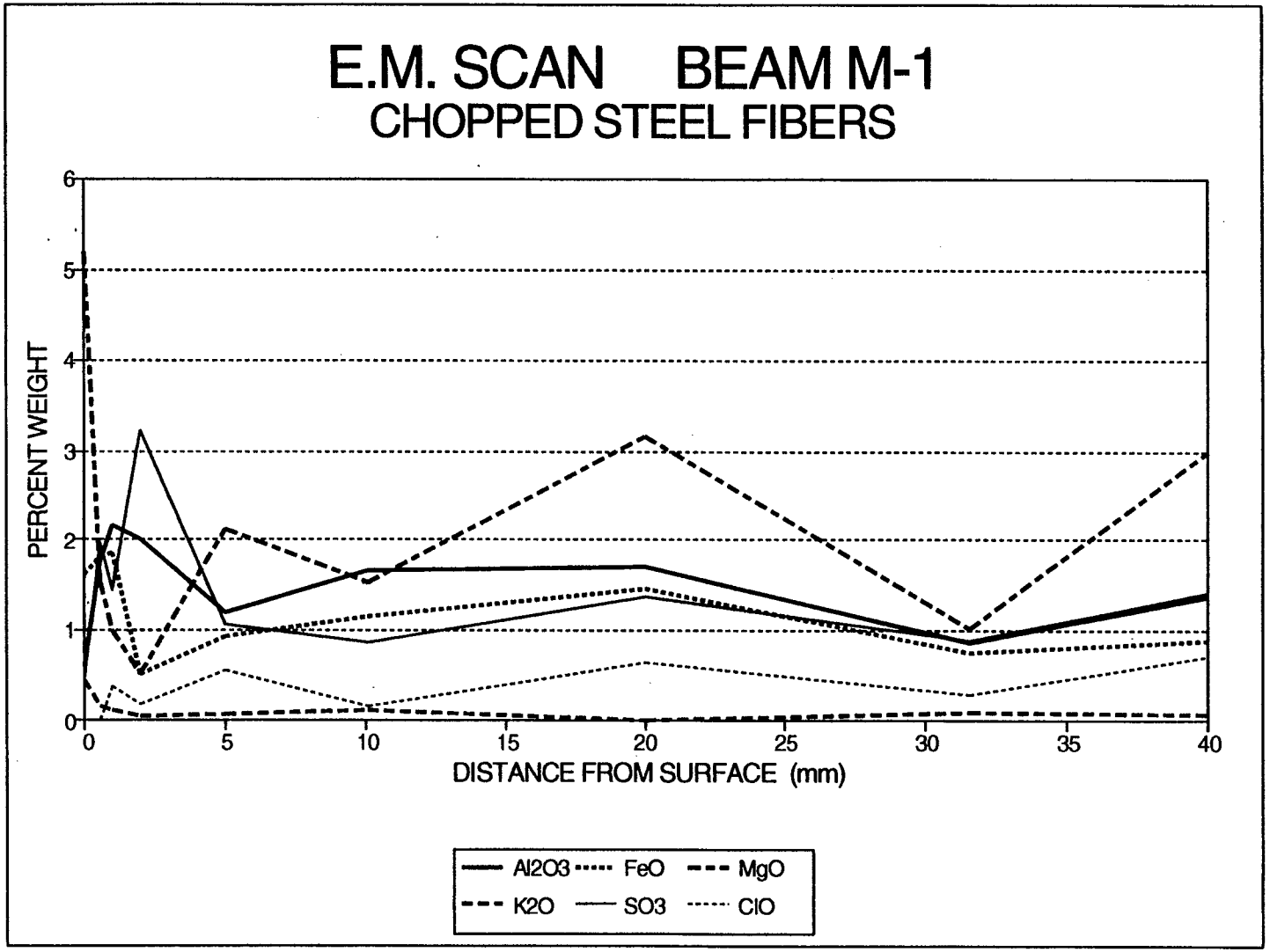
E.M. SCAN BEAM M-1
CHOPPED STEEL FIBERS
PERCENT WEIGHT
0
1
2
3
4
5
6
0
5
10
15
20
25
30
35
40
DISTANCE FROM SURFACE (mm)
Al2O3
FeO
MgO
K2O
SO3
ClO

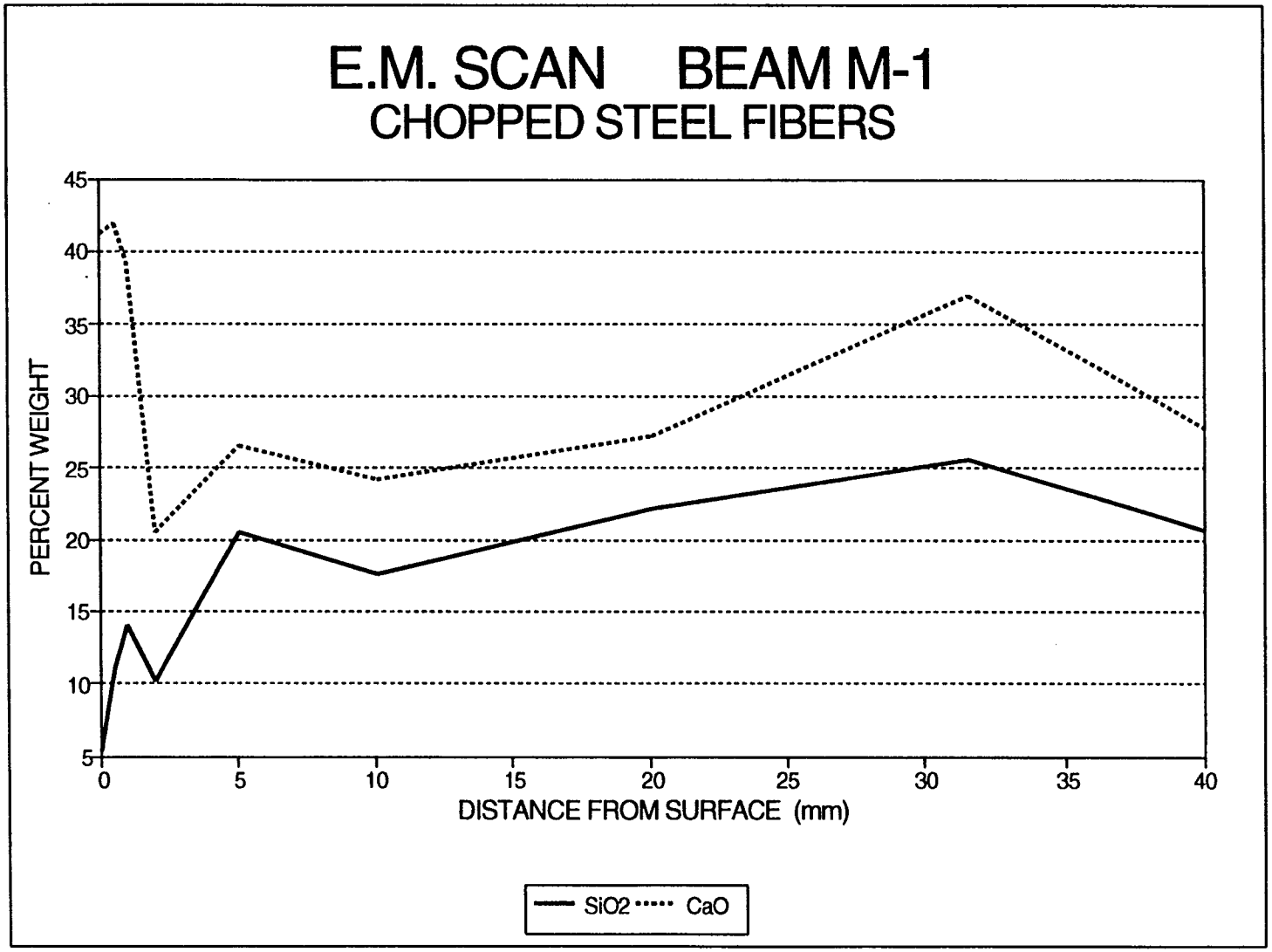
E.M. SCAN BEAM M-1
CHOPPED STEEL FIBERS
PERCENT WEIGHT
45
40
35
30
25
20
15
10
5
0
5
10
15
20
25
30
35
40
DISTANCE FROM SURFACE (mm)
SiO2
CaO

# E.M. SCAN BEAM N-1
## GLASS FIBERS

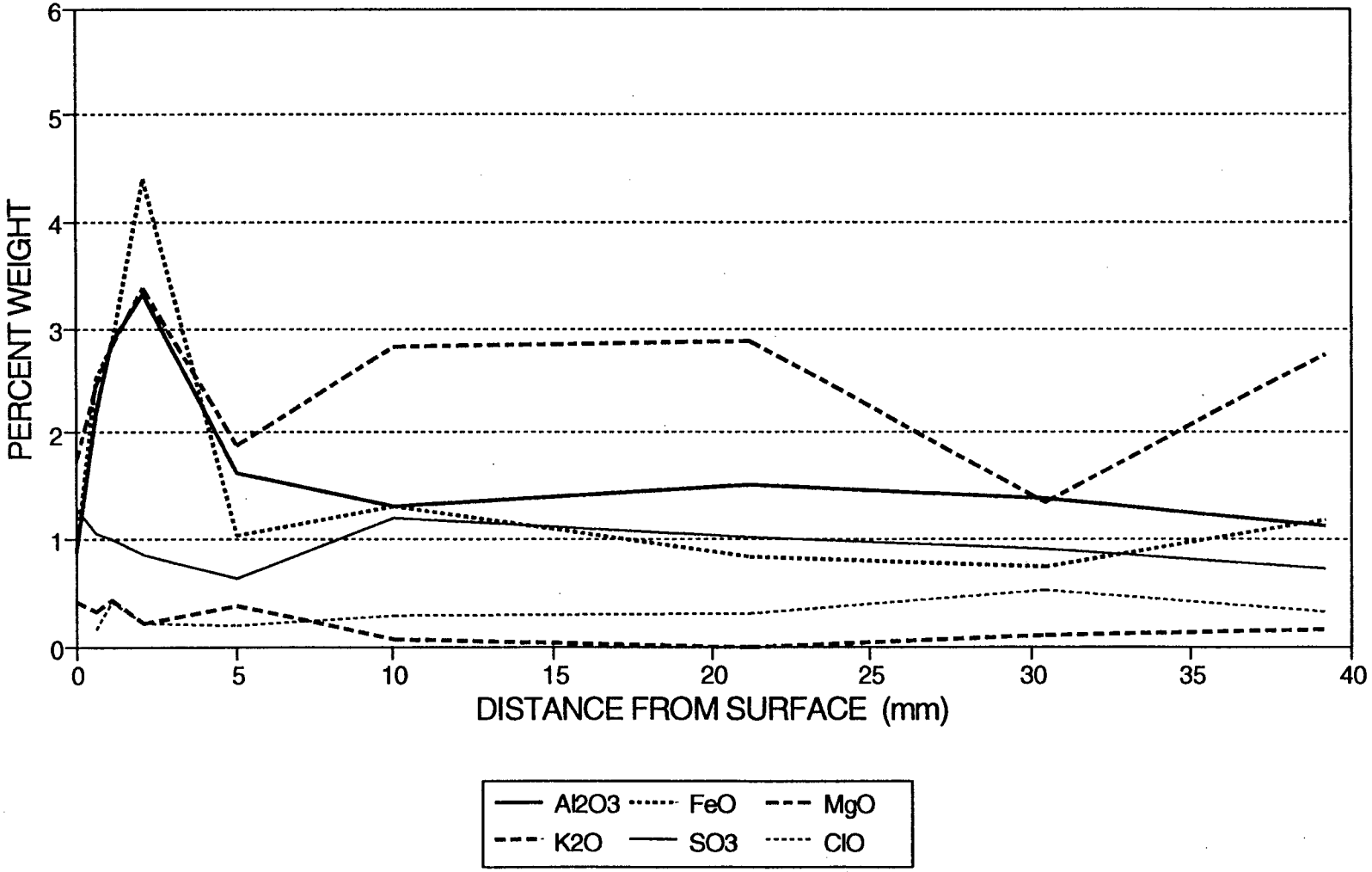

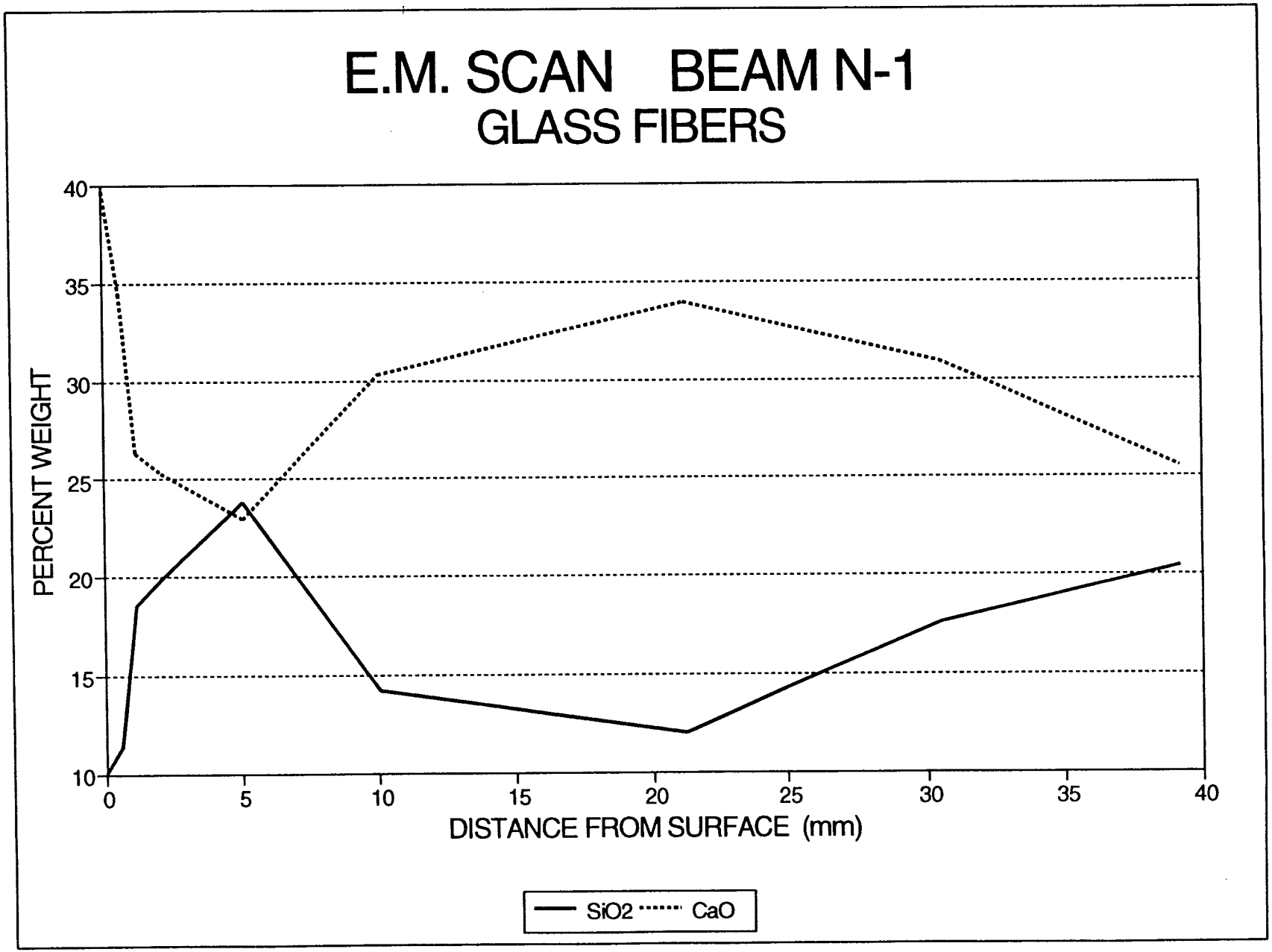
E.M. SCAN BEAM N-1
GLASS FIBERS
PERCENT WEIGHT
40
35
30
25
20
15
10
0
5
10
15
20
25
30
35
40
DISTANCE FROM SURFACE (mm)
SiO2
CaO

# E.M. SCAN BEAM O-3
## GLASS FIBERS

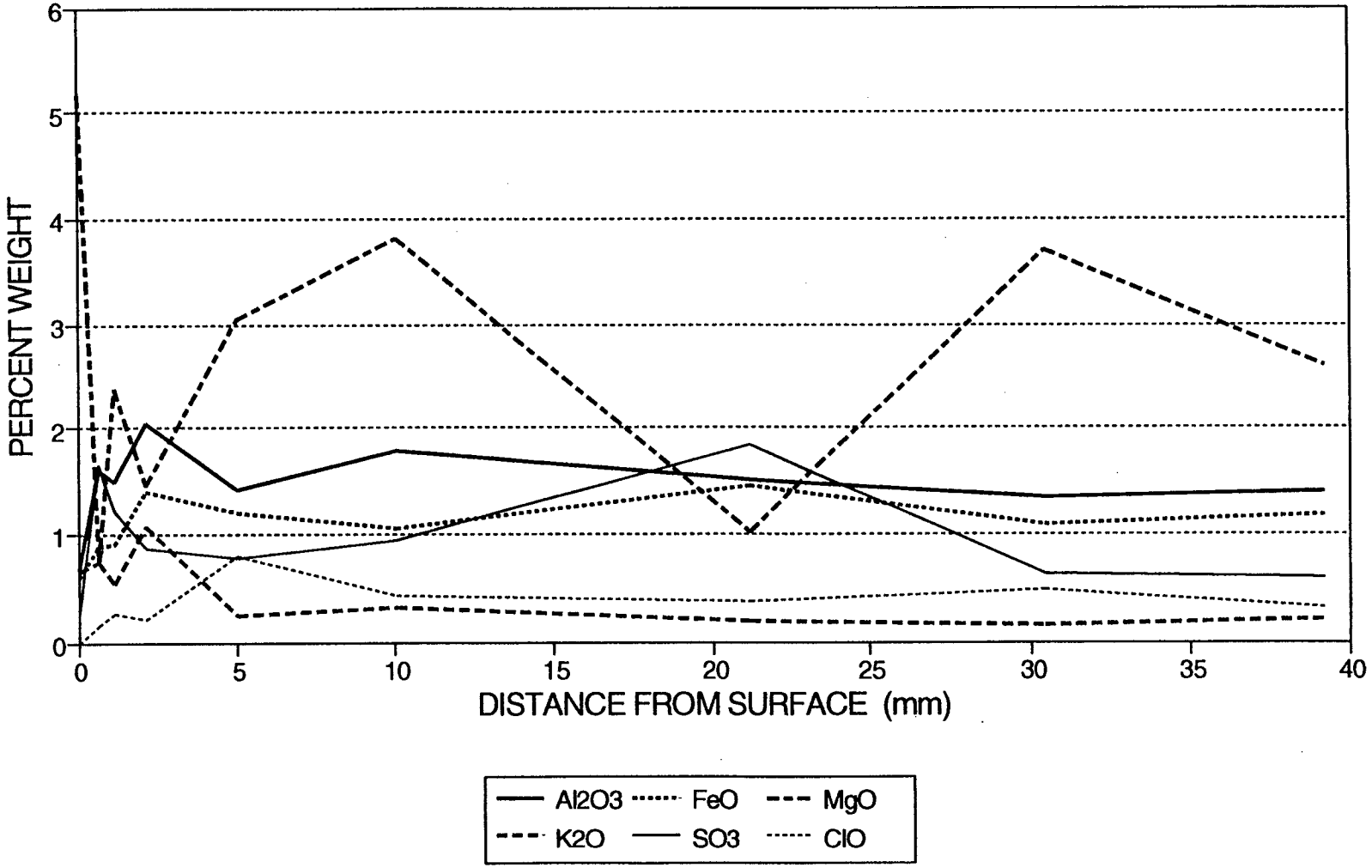

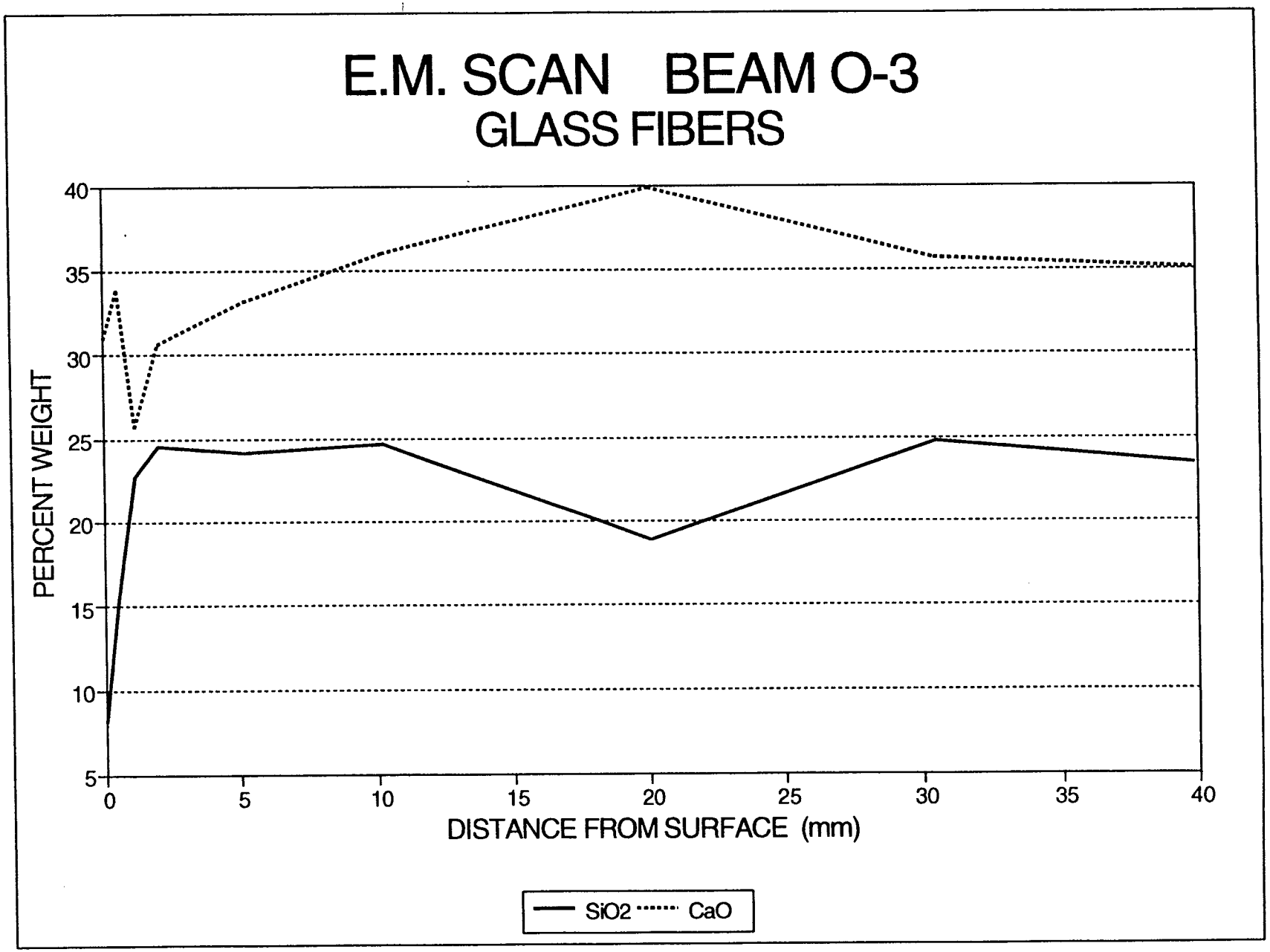
E.M. SCAN BEAM O-3
GLASS FIBERS
PERCENT WEIGHT
40
35
30
25
20
15
10
5
0
5
10
15
20
25
30
35
40
DISTANCE FROM SURFACE (mm)
SiO2
CaO

# E.M. SCAN BEAM P-2
## STAINLESS STEEL FIBERS

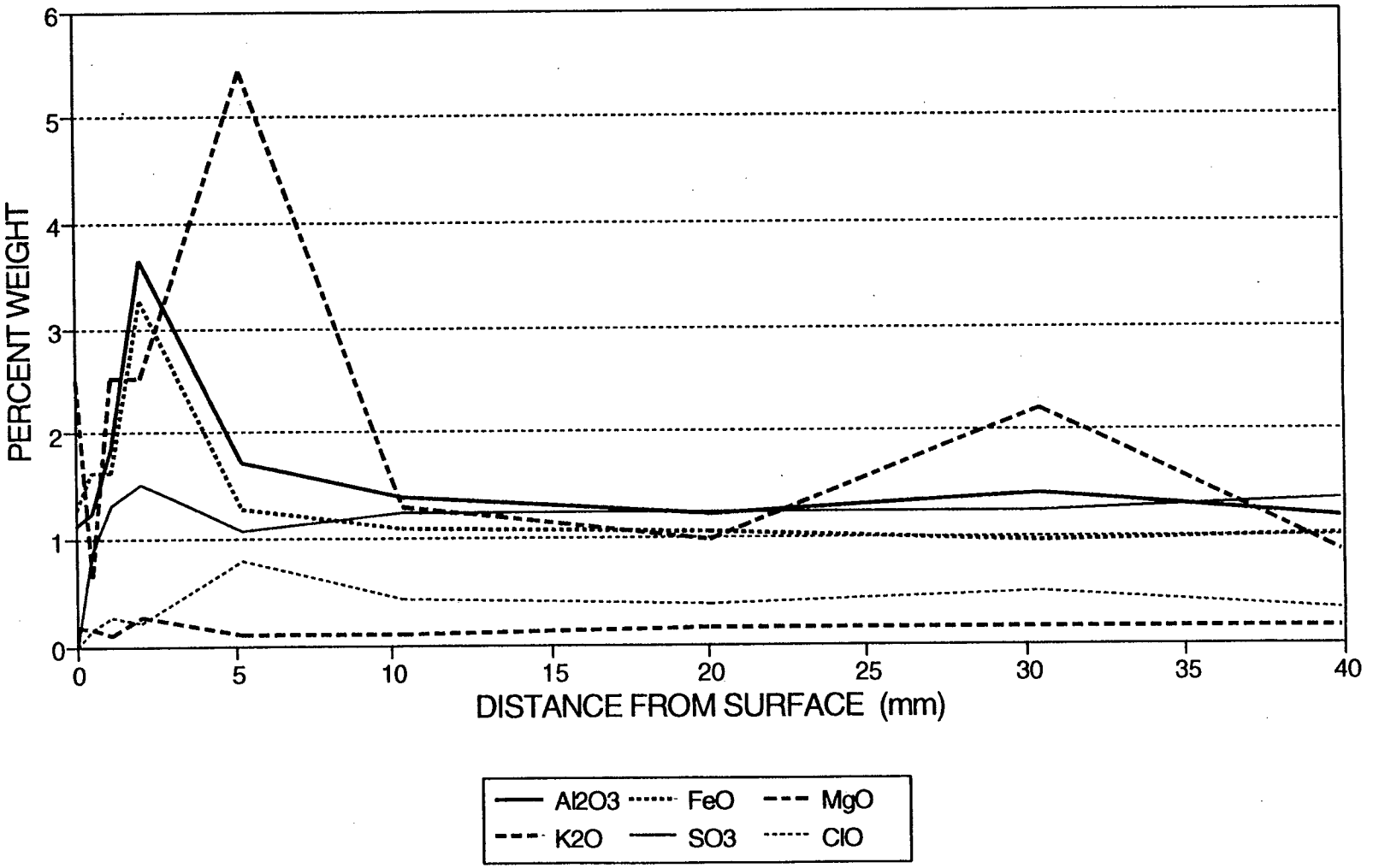

# E.M. SCAN BEAM P-2
## STAINLESS STEEL FIBERS

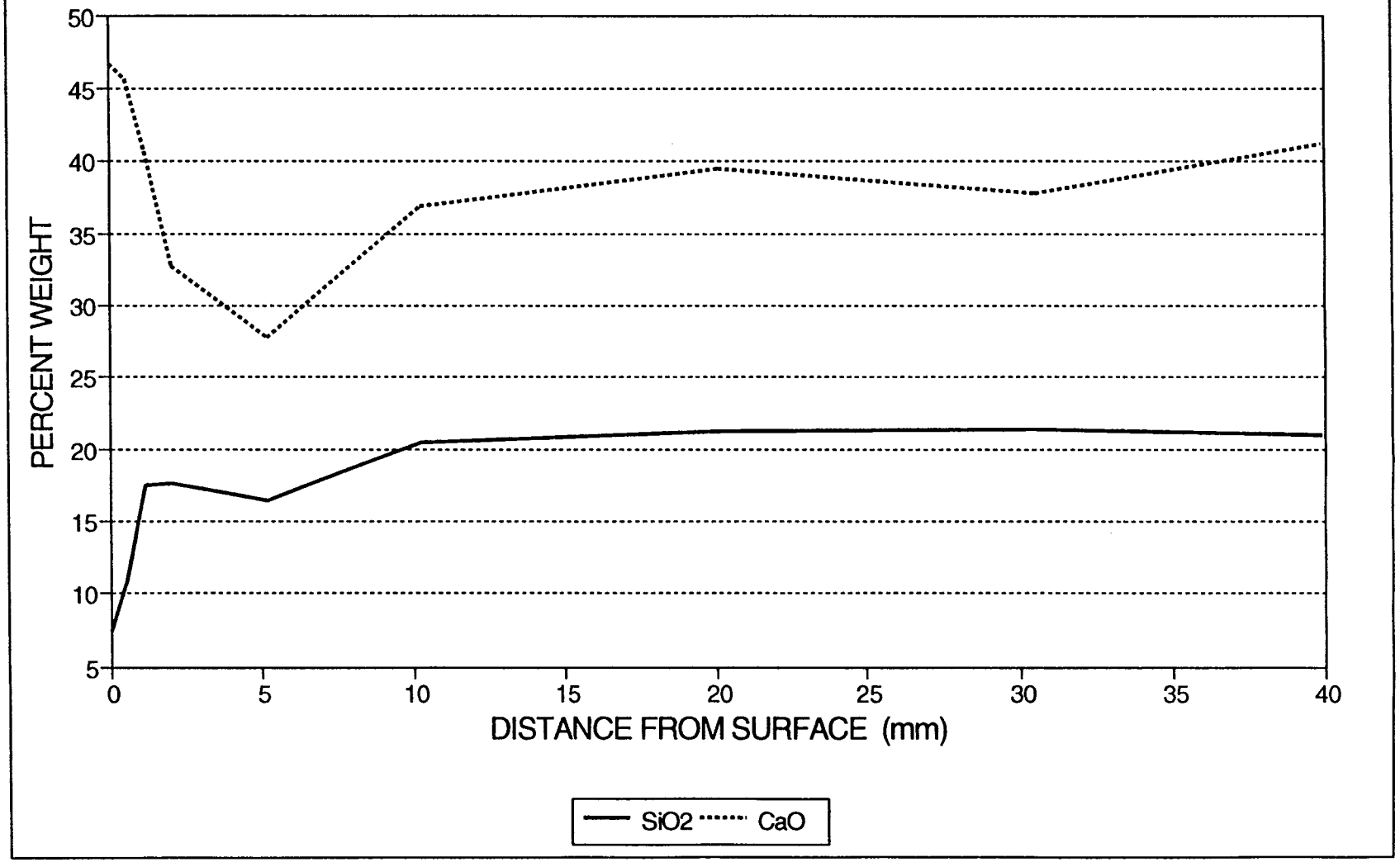

# REPORT DOCUMENTATION PAGE

*Form Approved*
*OMB No. 0704-0188*



| 1. AGENCY USE ONLY *(Leave blank)* | 2. REPORT DATE | 3. REPORT TYPE AND DATES COVERED |
|---|---|---|
| | September 1999 | Final report |

**4. TITLE AND SUBTITLE**
Durability of Fiber-Reinforced Concrete Under Flexural Stress in a Severe Marine Environment

**5. FUNDING NUMBERS**
Work Unit 31132

**6. AUTHOR(S)**
Edward F. O'Neil, Jack T. Devlin

**7. PERFORMING ORGANIZATION NAME(S) AND ADDRESS(ES)**
See reverse.

**8. PERFORMING ORGANIZATION REPORT NUMBER**
Technical Report SL-99-9

**9. SPONSORING/MONITORING AGENCY NAME(S) AND ADDRESS(ES)**
U.S. Army Corps of Engineers, Washington, DC 20314-1000;
Structures Laboratory, U.S. Army Engineer Research and Development Center
3909 Halls Ferry Road, Vicksburg, MS 39180-6199

**10. SPONSORING/MONITORING AGENCY REPORT NUMBER**

**11. SUPPLEMENTARY NOTES**

**12a. DISTRIBUTION/AVAILABILITY STATEMENT**
Approved for public release; distribution is unlimited.

**12b. DISTRIBUTION CODE**

**13. ABSTRACT** *(Maximum 200 words)*

In July 1975, the U.S. Army Engineer Research and Development Center (ERDC), initiated a long-term durability study of fiber-reinforced concrete exposed to a severe marine environment. Fifty concrete beams were constructed that were reinforced with various types and sizes of distributed fibers available on the market at the time (carbon-steel, stainless steel, and glass). The beams were then placed at midtide elevation on the exposure wharf at the ERDC Severe Weather Exposure Station, Treat Island, Maine. Sixteen of the beams were yoked and stressed to 35 percent of their flexural strength with third-point loading.

In 1993 there were twelve stressed beams which had survived 18 years of severe marine exposure. These were removed from exposure and subjected to a wide variety of destructive and nondestructive experiments under laboratory conditions. This report documents the investigation to determine the material properties of the fiber-reinforced concretes and evaluate the beams in their as-removed condition documenting flexural strength, toughness, and the effect of stress direction. The report also investigates material properties of the beams by use of a scanning electron microscope to investigate microstructural and microchemical changes that occurred.

(Continued)

**14. SUBJECT TERMS**
Brass-coasted fibers; Fiber-reinforced concrete; Durability; Marine exposure; Fiberglass fibers; Stainless-steel fibers

**15. NUMBER OF PAGES**
211

**16. PRICE CODE**

| 17. SECURITY CLASSIFICATION OF REPORT | 18. SECURITY CLASSIFICATION OF THIS PAGE | 19. SECURITY CLASSIFICATION OF ABSTRACT | 20. LIMITATION OF ABSTRACT |
|---|---|---|---|
| UNCLASSIFIED | UNCLASSIFIED | | |

7. (Concluded).

U.S. Army Engineer Research and Development Center
Waterways Experiment Station
3909 Halls Ferry Road, Vicksburg, MS 39180-6199;
University of New Brunswick,
P.O. Box 4400,
Fredericton, N.B. Canada E3B 5A3

13. (Concluded).

Test results document the tensile, compressive, and flexural properties of the beams and show the superiority of carbon-steel-fiber reinforcement over glass fiber, stainless-steel fiber, or no-fiber reinforcement in concrete. Results also indicate that the direction of stress in uncracked fiber-reinforced concrete does not affect its durability and performance in a severe environment.

Destroy this report when no longer needed. Do not return it to the originator.